

Global halocarbon emissions for the recent past and future

Dissertation
zur Erlangung des Doktorgrades
der Mathematisch-Naturwissenschaftlichen Fakultät
der Christian-Albrechts-Universität
zu Kiel

vorgelegt von
Dipl.- Meteorologin Franziska Ziska

Kiel 2014

Referent: Prof. Dr. Arne Körtzinger

Co-Referent: Prof. Dr. Christa Marandino

Tag der mündlichen Prüfung: 14. November 2014

Die vorliegende Arbeit wurde am GEOMAR Helmholtz-Zentrum für Ozeanforschung Kiel an der Christian-Albrechts-Universität zu Kiel von Februar 2010 bis November 2014 unter der Anleitung von Dr. Birgit Quack durchgeführt.

„Sei Du selbst die Veränderung, die Du Dir wünschst für diese Welt.“

Mahatma Gandhi

This thesis based on the following manuscripts:

- I. **Manuscript 1:** Ziska F., Quack B., Abrahamsson K., Archer, S. D., Atlas, E., Bell, T., Butler, J. H., Carpenter, L. J., Jones, C. E., Harris, N. R. P., Hepach, H., Heumann, K. G., Hughes, C., Kuss, J., Krüger, K., Liss, P., Moore, R. M., Orlikowska, A., Raimund, S., Reeves, C. E., Reifenhäuser, W., Robinson, A. D., Schall, C., Tanhua, T., Tegtmeier, S., Turner, S., Wang, L., Wallace, D., Williams, J., Yamamoto, H., Yvon-Lewis, S. and Yokouchi, Y.: Global sea-to-air flux climatology of bromoform, dibromomethane and methyl iodide, *Atmos. Chem. Phys.*, 13, 8915-8934, 10.5194/acp-13-8915-2013, 2013.

Contribution: Franziska Ziska collected the measurements into a database and evaluated them, made the calculations, and wrote the manuscript. Birgit Quack started collecting and helped evaluating the data, and assisted in the manuscript preparation and the review process. K. Abrahamsson, S. D. Archer, E. Atlas, T. Bell, J. H. Butler, L. J. Carpenete, C. E. Jones, N. R. P. Harris, H. Hepach, K. G. Heumann, C. Hughes, J. Kuss, P. Liss, R. M. Moore, A. Orlikowska, S. Raimund, C. E. Reeves, W. Reifenhäuser, A. D. Robinson, C. Schall, T. Tanhua, S. Turner, L. Wang, D. Wallace, J. Williams, H. Yamamoto, S. Yvon-Lewis and Y. Yokouchi supplied water and atmospheric halocarbon measurements and helped revising the manuscript. S. Tegtmeier and K. Krüger provided input during writing the manuscript and the review process.

- II. **Manuscript 2:** Hossaini, R., Mantle H., Chipperfield, M. P., Montzka, S. A., Hamer, P., Ziska, F., Quack, B., Krüger, K., Tegtmeier, S., Atlas, E., Sala, S., Engel, A., Bönisch, H., Keber, T., Oram, D., Millis, G., Ordóñez, C., Saiz-Lopez, A., Warwick, N., Liang, Q., Feng, W., Moore, E., Miller, B. R., Marécal, V., Richards, N. A. D., Dorf, M., and Pfeilsticker, K.: Evaluating global emission inventories of biogenic bromocarbons, *Atmos. Chem. Phys.*, 13, 11819-11838, 10.5194/acp-13-11819-2013, 2013.

Contribution: Ryan Hossaini collected and evaluated the data and wrote the paper. H. Mantle, M. Chipperfield, W. Feng and N. Richards run global simulations and evaluate the emissions. S. Montzka, B. Miller and E. Moore provided the long term observations and P. Halmer and V. Marécal contributed to implement the emissions. Franziska Ziska provided global halocarbon emission maps, wrote a part of the section 2.1 in the manuscript and helped revising the paper. E. Atlas provided aircraft measurements and S. Sala, A. Etlas, H. Bönisch, T. Keber, D. Oram and G. Millis contributed atmospheric data. C. Ordóñez, A. Saiz-Lopez, N. Warwick and Q. Liang supplied global halocarbon emission maps. M. Dorf and K. Pfeilsticker managed the project.

- III. **Manuscript 3:** Tegtmeier S., Krüger, K., Quack, B., Atlas, E., Blake, D. R., Bönisch, H., Engel, A., Hepach, H., Hossaini, R., Navarro M. A., Raimund, S., Sala, S., Shi, Q., and Ziska, F.: The contribution of oceanic methyl iodide to stratospheric iodine, *Atmos. Chem. Phys.*, 13, 11869-11886, 10.5194/acp-13-11869-2013, 2013.

Contribution: Susann Tegtmeier evaluated the data, made the calculations and wrote the paper. K. Krüger managed the project and helped revising the manuscript. Franziska Ziska took the air samples and provided global emission maps. B. Quack, H. Hepach, S. Raimund and Q. Shi measured oceanic halocarbon data during the campaigns and calculated the emissions. R. Hossaini provided the atmospheric lifetimes for methyl iodide and E. Atlas, E. Blake, D. R. Bönisch and M. A. Navarro contributed aircraft measurements. F. Ziska, B. Quack, H. Hepach, S. Raimund, R. Hossaini, M. A. Navarro S. Sala, H. Bönisch, A. Engel, D. R. Blake, E. Atlas and Q. Shi helped revising the manuscript.

- IV. **Manuscript 4:** Ziska F., Quack B., Tegtmeier S. and Krüger K., Future emissions of marine halocarbons, *in prep.*

Contribution: Franziska Ziska evaluated the data and wrote the paper. Birgit Quack, Susann Tegtmeier and Kirstin Krüger helped evaluating the data and assisted with input and revision of the manuscript.

- V. **Manuscript 5:** Tegtmeier, S., Ziska F., Pisso, I., Quack B., Velders, G., Krüger, K.: Oceanic bromine emissions weighted by their ozone depletion potential, *in prep.*

Contribution: Susann Tegtmeier developed and carried out analysis and wrote the paper. Franziska Ziska calculated future and present halogenated emission projections and provided global climatological emission maps of halogenated compounds. I. Pisso calculated the ozone depletion potential maps and G. Velders provided future emissions estimates of long-lived ozone depleting substances. B. Quack contributed to calculations of emission inventories and paper writing. K. Krüger contributed to paper writing and scientific discussion. F. Ziska, I. Pisso and G. Velders helped revising the manuscript.

- VI. **Manuscript 6:** Hepach, H., Quack, B., Ziska, F., Fuhlbrügge, S., Atlas, E., Krüger, K., Peeken, I., and Wallace, D. W. R.: Drivers of diel and regional variations of halocarbon emissions from the tropical North East Atlantic, *Atmos. Chem. Phys.*, 14, 1255-1275, 10.5194/acp-14-1255-2014, 2014.

Contribution: Helmke Hepach measured the oceanic halocarbon data, evaluated the data, made the calculations and wrote the manuscript. Birgit Quack contributed to the manuscript

preparation and review process. Franziska Ziska took the air samples and conducted the radio sonde launches during the campaign. Steffen Fuhlbrügge evaluated the meteorological data. Elliot Atlas analyzed the atmospheric samples and Ilka Peeken measured and calculated the phytoplankton pigments. F. Ziska, E. Atlas, I. Peeken, K. Krüger and D. W. R. Wallace helped revising the manuscript.

VII. Manuscript 7: Fuhlbrügge, S., Krüger, K., Quack, B., Atlas, E., Hepach, H., and Ziska, F.: Impact of the marine atmospheric boundary layer conditions on VSLs abundances in the eastern tropical and subtropical North Atlantic Ocean, *Atmos. Chem. Phys.*, 13, 6345-6357, 10.5194/acp-13-6345-2013, 2013.

Contribution: Steffen Fuhlbrügge evaluated the data and wrote the manuscript. Kirstin Krüger and Birgit Quack provided input during the manuscript preparation and the review process. E. Atlas measured and calculated the atmospheric samples and H. Hepach measured and evaluated the sea-water samples. Franziska Ziska took the atmospheric samples and conducted the radio sonde launches during the campaign. E. Atlas, H. Hepach and F. Ziska helped revising the manuscript.

In addition I have contributed to the following book chapter:

- I. Section "Perspectives and Integration in SOLAS Science" of the book "Ocean-Atmosphere Interactions of Gases and Particles" 2014 by P. S. Liss and M. T. Johnson

Table of contents

I.	Summary.....	3
II.	Zusammenfassung.....	9
III.	Introduction.....	15
1.	Halocarbons in the ocean.....	17
1.1.	Marine bromocarbons.....	17
1.1.1.	Anthropogenic sources.....	17
1.1.2.	Biological sources.....	18
1.2.	Marine methyl iodide.....	21
1.2.1.	Anthropogenic sources.....	21
1.2.2.	Biological and non-biological sources.....	21
1.3.	Ocean sinks.....	22
2.	Atmospheric bromocarbons and methyl iodide.....	24
2.1.	Atmospheric distribution and chemical fates.....	25
2.1.1.	Bromocarbons.....	25
2.1.2.	Methyl iodide.....	27
3.	Transport into the stratosphere.....	29
4.	(Chemical) transport models.....	30
5.	Global emission estimates.....	34
6.	Objectives and outline of this dissertation.....	35
IV.	Method.....	41
1.	HalOcAt database.....	41
1.1.	Extrapolation of the HalOcAt data.....	42
2.	Air-sea gas exchange.....	46
2.1.	The gas exchange velocity.....	47
3.	Earth under global warming.....	50
V.	Manuscripts.....	53
	Manuscript 1.....	55
	Manuscript 2.....	77
	Manuscript 3.....	99
	Manuscript 4.....	119
	Manuscript 5.....	139
VI.	Conclusions and future perspectives.....	157
VII.	References.....	165

VIII.	Abbreviations.....	179
IX.	Supplement.....	185
	Manuscript 6.....	187
	Manuscript 7.....	209
X.	Danksagung.....	225
XI.	Curriculum Vitae.....	227
XII.	Eidesstattliche Erklärung.....	231

SUMMARY

I. Summary

Very short lived substances (VSLs) as bromoform (CHBr_3), dibromomethane (CH_2Br_2) and methyl iodide (CH_3I) are formed in the ocean by biological, non-biological and anthropogenic processes. Marine CHBr_3 , CH_2Br_2 and CH_3I concentrations show strong geographical variability (vertical and horizontal) determined by their oceanic sources and sinks. After emitted into the atmosphere these halogenated compounds and their degradation products are involved in several chemical cycles, i.e. tropospheric and stratospheric ozone depletion. Although bromine is much less abundant than chlorine in the atmosphere, it is known to deplete stratospheric ozone 45 to 69 times more efficiently. CHBr_3 and CH_2Br_2 are the major carriers of organic bromine from the ocean to the atmosphere and CH_3I is a dominant source of organic iodine in the troposphere. Atmospheric concentrations of the three halogenated compounds are highly variable due to their heterogeneous distribution and seasonally varying natural sources. The tropical ocean is identified to be a key region for enhanced halogenated emissions and for transporting large amount of VSLs into the stratosphere.

Different calculation techniques derive sea-to-air flux estimates, including bottom-up and top-down approaches, as well as laboratory experiments. These estimates are used as input for atmospheric transport models i.e. chemical transport models (CTM). The global emission strength and distributions are highly variable as well as poorly quantified. Further, many uncertainties still exist in the production processes, dimension of sources and sinks and chemical fates of VSLs in both the ocean and the atmosphere. Due to that it is difficult to parameterize reliable global emission maps of halogenated compounds.

This thesis includes seven manuscripts and aims to reduce the uncertainties of global emission estimates based on in-situ measurements of the three VSLs and of their relevance on stratospheric ozone loss for the present and future.

The first manuscript (Ziska et al., 2013) presents the core and fundament of this thesis and contains the first data base for existing halogenated air and sea water measurements named **HalOcAt** (**Hal**ocarbons in the **O**cean and **A**tmosphere), as well as the calculation of global emission climatologies from a bottom-up approach (Ziska et al., 2013). Based on available surface data of the HalOcAt database global marine and atmospheric surface maps of CHBr_3 , CH_2Br_2 and CH_3I were calculated in order to finally derive global sea-to-air flux estimates. Due to low data density, the challenge was to find the best and most realistic way for inter- and extrapolation. Therefore, a new method was developed to fill the missing data in the global grid, combining extrapolation and classification techniques, by taking into account the biogeochemical character and distribution of the compound of interest. 'Hot spots' for global CHBr_3 and CH_2Br_2 emissions are located in the equatorial

belt, whereas CH_3I emissions are enhanced in the subtropical gyre regions. An important data source to the HalOcAt database are the sixth (Hepach et al., 2014) and seventh manuscripts (Fuhlbrügge et al., 2013) which contribute additional knowledge about the distribution and magnitude of VLSL concentrations in a tropical upwelling system in both the ocean and the atmosphere. Contrary to recent studies, negative fluxes (flux into the ocean) occur in each sea-to-air flux climatology, mainly in the Arctic (for CH_2Br_2) and in the Antarctic (for CHBr_3) region. Compared to earlier studies, Ziska et al. (2013) is at the lower end of estimates, especially for CHBr_3 . Additionally, a sensitivity study which demonstrates the changes of each input parameter (U, SST, SLP, SSS) onto the VLSL air-sea flux calculations, shows that the parameters U and SST have the strongest influence on the determination of global halogenated emissions.

The second manuscript (Hossaini et al., 2013) involves the simulation of Br_y loading into the stratosphere by comparing three top-down and one bottom-up (CHBr_3 and CH_2Br_2 emissions from Ziska et al. (2013)) approach in a model sensitivity study. Ziska et al. (2013) emissions match with the compilation of CHBr_3 surface observations in the tropics, but show a general overestimation of CH_2Br_2 . No single inventory gives the best agreement in all locations for CHBr_3 or CH_2Br_2 . An optimized estimate of bromine contribution of ~ 4 ppt was created based on the CHBr_3 emissions from Ziska et al. (2013) and of the CH_2Br_2 emissions from Liang et al. (2010). The second manuscript underlines the applicability and the importance of the Ziska et al. (2013) emissions for the model community.

Calculation of iodine transport from the tropical ocean surface into the stratosphere by using the CH_3I emission from Ziska et al. (2013) and a Lagrangian model is investigated in the third manuscript (Tegtmeier et al., 2013) for the first time. The results show that the transport of iodine in form of CH_3I into the tropical tropopause layer (TTL) and lowermost stratosphere are too low to be significant on a global scale for stratospheric ozone loss. However, on a regional scale, strong vertical transport combined with enhanced emission peaks are found in the West Pacific and appears considerable. The fourth manuscript (Ziska et al., *in prep.*) analyzes the effect of climate change on the oceanic emissions of CHBr_3 , CH_2Br_2 and CH_3I for the first time. The global maps of oceanic concentrations and atmospheric mixing ratios derived from the first manuscript and future physical input parameters of two different scenarios from three **IPCC (Intergovernmental Panel on Climate Change)** models are used to calculate halogenated future emission projections. Under low (RCP 2.6 scenario) and extreme (RCP 8.5 scenario) future conditions the halogenated emissions of CHBr_3 , CH_2Br_2 and CH_3I show an increase to 2100, however changes in ocean production are not considered in the calculations. Based on these results, the future impact of CHBr_3 on stratospheric ozone is determined in the fifth manuscript (Tegtmeier et al., *in prep.*). Calculation of future ozone-depleting-substances (ODP)-weighted emissions of CHBr_3 estimates an 80 % increase until 2100 for the extreme scenario

by taking into account changes of meteorological surface parameters and changes of convective activity results. The results of the manuscripts reduce some of the uncertainties, but there are still open questions, i.e. the quantification of the oceanic productivity under ongoing environmental changes in the future emission estimates. Enlarging the HalOcAt data base with more measurements, common calibration techniques and more basic research to understand source and sink mechanisms of the VSLS in the ocean and atmosphere are needed to improve Ziska et al. (2013) emissions and thus also the stratospheric budget of VSLS.

ZUSAMMENFASSUNG

II. Zusammenfassung

Flüchtige Substanzen (VSLs) mit kurzer atmosphärischer Lebenszeit (0-0.5 Jahre) wie Bromoform (CHBr_3), Dibrommethan (CH_2Br_2) und Methyljodid (CH_3I) werden im Ozean durch biologische, nicht biologische oder anthropogene Prozesse gebildet. Bedingt durch ihre ozeanischen Quellen und Senken weisen marine CHBr_3 , CH_2Br_2 und CH_3I Konzentrationen eine starke geographische Variabilität auf (vertikal und horizontal). Gelangen diese halogenierten Verbindungen sowie ihre Zerfallsprodukte in die Atmosphäre können sie in mehrere chemische Zyklen involviert sein, wie zum Beispiel beim troposphärischen und stratosphärischen Ozonabbau. Obwohl Brom in geringerer Konzentration als Chlor in der Atmosphäre vorhanden ist, wurde bewiesen, dass Brom 45- bis 69-mal effizienter im Abbau von stratosphärischem Ozon ist. CHBr_3 und CH_2Br_2 sind die wichtigsten Zulieferer zu atmosphärischem organischem Brom und CH_3I stellt eine bedeutende Quelle von organischem Jod in die Troposphäre dar. Die atmosphärischen Konzentrationen der drei halogenierten Verbindungen sind aufgrund ihrer unterschiedlichen Verteilung und zeitlich variierenden natürlichen Quellen sehr variabel. Der tropische Ozean wurde als Schlüsselregion für erhöhte halogenierte Emissionen und für den Transport großer Mengen von VSLs in die Stratosphäre identifiziert.

Es existieren verschiedene Verfahren wie Bottom-up oder Top-down, sowie Laborexperimente, die zur Berechnung von globalen Emissionskarten dienen. Sie werden als Inputdaten für atmosphärische Transportmodelle wie zum Beispiel chemische Transportmodelle (CTM) verwendet. Die globalen Emissionen variieren stark in ihrer Größenabschätzungen. Weiterhin existieren viele Unsicherheiten in den Bildungsprozessen, den Ausmaßen von Quellen und Senken und chemischen Prozessen der halogenierten VSLs im Ozean und der Atmosphäre. Daher ist es schwierig, aussagekräftige globale Emissionskarten von halogenierten Verbindungen zu berechnen. Die vorliegende Arbeit besteht aus sieben Manuskripten und zielt darauf ab, die existierenden Unsicherheiten der globalen Emissionsabschätzungen auf Grundlage von in-situ-Messungen der drei VSLs und ihre Relevanz auf den stratosphärischen Ozonverlust für die Gegenwart und Zukunft zu reduzieren.

Herzstück und Fundament dieser Arbeit ist das erste Manuskript (Ziska et al., 2013). Es beinhaltet die Veröffentlichung der ersten Datenbank **HalOcAt** (**Halocarbons in the Ocean and Atmosphere**), für halogenierte Luft- und Ozeanmessungen, sowie die Berechnung der globalen Emissionskarten nach einem Bottom-up-Ansatz (Ziska et al., 2013). Auf Grundlage der verfügbaren Oberflächenmessungen aus der HalOcAt Datenbank wurden globale ozeanische und atmosphärische Oberflächenkarten von CHBr_3 , CH_2Br_2 und CH_3I berechnet, um schließlich globale Emissionsabschätzungen abzuleiten. Aufgrund der zu geringen Datendichte bestand die Herausforderung darin, die beste und

realistischste Methode der Interpolation und Extrapolation zu finden. Dafür wurde eine neue Berechnung und Klassifizierungstechnik entwickelt, um fehlende Daten in die Gitterpunkte zu füllen. Dabei wurden der biogeochemische Charakter und die Verteilung der Verbindungen betrachtet. Alle drei Verbindungen weisen eine erhöhte Emissionsstärke in verschiedenen ozeanischen Regionen der Tropen auf. "Hot Spots" für die CHBr_3 und CH_2Br_2 Emissionen wurden im Äquatorband gefunden, während erhöhte CH_3I Emissionen in subtropischen Gürtel auftreten. Eine wichtige Datenquelle für die HalOcat Datenbank sind das sechste (Hepach et al., 2013) und siebte Manuskript (Fuhlbrügge et al., 2013). Sie tragen zusätzliche Kenntnisse zur Verteilung und Größe der ozeanischen und atmosphärischen VLSK Konzentrationen in tropischen Auftriebsregionen bei. Im Gegensatz zu bisherigen Studien enthalten die Ziska et al. (2013) Emissionen negativer Flüsse (Transport von der Atmosphäre in den Ozean), die vor allem in der Arktis (für CH_2Br_2) und in der Antarktis (für CHBr_3) vorkommen. Im Vergleich zu früheren Studien befinden sich die Ziska et al. (2013) Emissionen am unteren Ende der Abschätzungen, insbesondere für CHBr_3 . Zusätzlich zeigte eine Sensitivitätsstudie den Einfluss der einzelnen Eingangsparameter (Windgeschwindigkeit (U), Oberflächentemperatur (SST), Oberflächendruck (SLP) und Salzgehalt an der Wasseroberfläche (SSS) auf die VLSK Emissionsberechnung. Das Ergebnis zeigte, dass die Parameter U und SST den stärksten Einfluss auf die Ermittlung der globalen halogenierten Emissionen ausüben. Das zweite Manuskript (Hossaini et al., 2013) beinhaltet die Simulation des Transportes von anorganischem Brom (Br_y) in die Stratosphäre. Für den Vergleich wurden drei Top-down- und ein Bottom-up-Ansatz (CHBr_3 und CH_2Br_2 Emissionen von Ziska et al. (2013)) verwendet. Die Ziska et al. (2013) Emissionen weisen die beste Übereinstimmung für CHBr_3 mit den Oberflächendaten in den Tropen auf, gleichzeitig zeigen sie eine generelle Überschätzung der CH_2Br_2 Werte. Auf Grundlage der CHBr_3 Emissionen von Ziska et al. (2013) sowie der CH_2Br_2 Emissionen von Liang et al. (2010) wurde eine optimierte Abschätzung vom Brombeitrag in die Stratosphäre von ~ 4 ppt erstellt. Das zweite Manuskript bekräftigt die Anwendbarkeit und die Bedeutung der Ziska et al. (2013) Emissionen für die Modellierung. Die Berechnung des globalen Jodtransports aus dem tropischen Ozean in die Stratosphäre mit Hilfe der CH_3I Emission von Ziska et al. (2013) und einem Langrangigen-Modell wurde zum ersten Mal im dritten Manuskript durchgeführt (Tegtmeier et al., 2013). Die Ergebnisse zeigen, dass im globalen Kontext der Transport von Jod in Form von CH_3I in die tropische Tropopause und unterste Stratosphäre niedrig ist, um signifikant zum stratosphärischen Ozonverlust beizutragen. Auf regionaler Ebene jedoch, wurden starke vertikale Transporte in Verbindung mit erhöhten Emissionsspitzen im West-Pazifik gefunden. Das vierte Manuskript (Ziska et al., *in prep.*) analysierte zum ersten Mal die Wirkung des Klimawandels auf die ozeanischen Emissionen CHBr_3 , CH_2Br_2 und CH_3I . Für die Berechnung von zukünftigen halogenierten Emissionsprognosen wurden die globalen Ozeankonzentrationen und die atmosphärischen Mischungsverhältnisse aus dem ersten Manuskript verwendet, sowie die Zukunfts-

Input-Parameter von drei **IPCC** (Intergovernmental Panel on Climate Change) Modellen sowie von zwei unterschiedlichen Szenarien. Unter schwach (RCP 2.6 Szenario) und extrem (RCP 8.5 Szenario) ausgeprägten Zukunftsbedingungen zeigten die halogenierten Emissionen CHBr_3 , CH_2Br_2 und CH_3I einen Anstieg bis 2100. Die Änderungen der Produktion im Ozean wurden in den Berechnungen nicht mitberücksichtigt. Basierend auf diesen Ergebnissen wurde im fünften Manuskript (Tegtmeier et al., *in prep.*) die zukünftigen Auswirkungen von CHBr_3 auf das stratosphärische Ozon bestimmt. Eine Zunahme von 80 % bis zum Jahr 2100 für das extreme Szenario unter Berücksichtigung der Veränderungen der meteorologischen Parameter sowie der konvektiven Aktivität wurde für die zukünftigen ODP (Ozon zerstörendes Potential) - gewichteten Emissionen für CHBr_3 abgeschätzt.

Die Ergebnisse der Manuskripte haben dazu beigetragen, dass Unsicherheiten reduziert werden konnten, jedoch gibt es immer noch offene Fragen, wie die Quantifizierung des Einflusses der Ozeanproduktivität auf die Zukunftsemissionen.

Eine Vergrößerung der Datenmenge in der HalOcAt Datenbank, eine gemeinsame Kalibrierungstechnik für alle Messungen und mehr Grundlagenforschung für die Bestimmung der Quellen und Senken der VSLs im Ozean und Atmosphäre sind notwendig, um die Ziska et al. (2013) Emissionen und damit auch die Bestimmung des Halogenbudgets in der Stratosphäre zu verbessern.

INTRODUCTION

III. Introduction

Ozone (O_3) is a colorless gas and naturally present in the atmosphere (Figure III–1). Most (ca. 90 %) of the ozone is found in the stratosphere in 20 to 25 km height and enables life on earth by absorption of solar energy rich wavelengths (ultraviolet (UV) radiation: UV-C and most of UV-B). The physical and chemical processes of ozone formation in the stratosphere were discovered by Sydney Chapman in 1930 in the article ‘*Ozone-Oxygen-Cycle*’. UV-radiation splits oxygen molecules into two

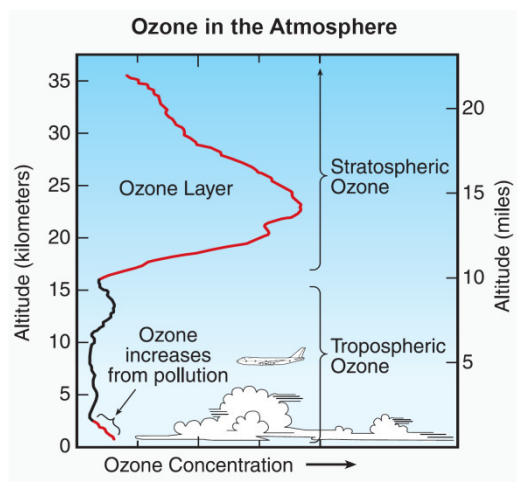


Figure III – 1. Vertical distribution of ozone concentrations in the atmosphere (Fahey and Hegglin, 2010).

oxygen atoms which form ozone together with other oxygen molecules. Stratospheric O_3 varies strongly with latitude and longitude (on average higher in the tropics and lower at the poles) and with seasons. Total ozone values are reported in Dobson units denoted as DU. Typical values vary between 200 and 500 DU. In 1950, David Bates found that free radicals like hydroxyl ($OH\cdot$) or nitric oxide ($NO\cdot$) reduce the amount of ozone. In 1956 scientists started to regularly measure ozone concentrations at the South Pole. One year later Gordon Dobson and two French scientists discovered the so-called ‘ozone hole’ (ozone values under 200

DU). In the late 1920, the industrial use of chlorofluorocarbons (CFCs) for refrigeration, air conditioning, foam blowing, aerosol propellants and cleaning of metals and electronic components started. They also occur as by-products of some chemical processes. CFCs including carbon, chlorine, and fluorine have long atmospheric life times (up to 130 years) and can be transported to the stratosphere. There, CFCs are dissociated by UV light to release chlorine atoms. The chlorine atoms act as catalysts and each can break down tens of thousands of ozone molecules before being removed. The connection between low ozone concentrations and CFC release was first published by Molina and Rowland (1974).

The impact of decreasing ozone concentration in the stratosphere is fatal for human beings, animals and plants all over the world, and decision-makers had to act fast. In order to protect the ozone layer 43 nations including most of the CFCs producers signed the Montreal Protocol in 1987. Stepwise the industrial production and the use of CFCs were limited, stagnated and banned worldwide through the Protocol, with success, since the ozone layer is slowly recovering (WMO, 2011).

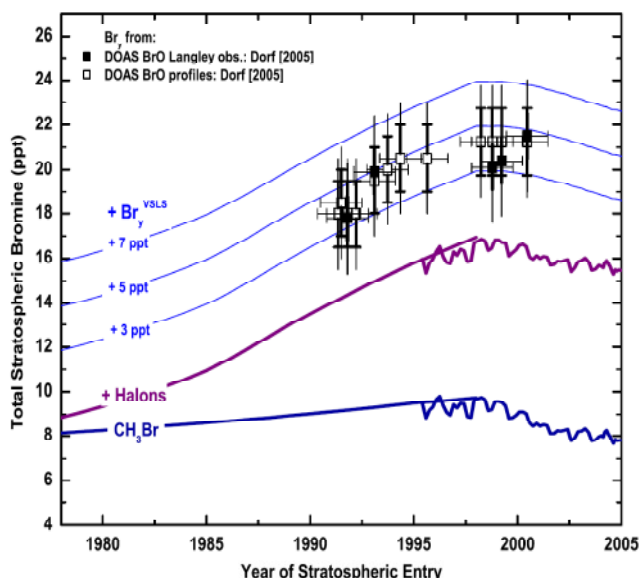


Figure III – 2. Trends for bromine (ppt) measured in the near surface (lines) and stratosphere (squares). Global tropospheric CH_3Br measured without and with halons (Butler et al., (1999) till 1998 and Montzka et al., (2003) after 1995). Total inorganic bromine derived from stratospheric measurements of BrO and photochemical modeling that accounts for BrO/Br_y by balloon experiments (filled squares) and lower most stratospheric BrO measurements (open squares). Assuming total contribution of 3, 5 and 7 ppt of Br_y from VLS to the total bromine budget of CH_3Br and halons (thin blue lines) (Dorf et al., 2006).

Although bromine is much less abundant than chlorine in the atmosphere, it is known to deplete stratospheric ozone 45 to 69 times more efficiently (Daniel et al., 1999). One human-made ozone depleting substance (ODS) including bromine is methyl bromide (CH_3Br). CH_3Br is used primarily as an agricultural and pre-shipping fumigant, but also has natural sources. Since 1990 this compound is regulated by the Montreal

Protocol. Balloon experiments measuring total stratospheric inorganic bromine (Br_y) for the time period of ten years showed that significantly more ozone-depleting bromine (4.1 ± 2.5 ppt) reaches the stratosphere than the transport of CH_3Br and halons can account for (Dorf et al., 2006) (Figure III–2).

Their idea was that very short lived

substances (VLS) like bromoform (CHBr_3) or dibromomethane (CH_2Br_2) could close the gap of the missing stratospheric Br_y . CHBr_3 and CH_2Br_2 are naturally produced in the ocean by macroalgae and phytoplankton (Quack and Wallace, 2003). Emitted into the marine boundary layer these bromocarbons have a short lifetime (2-3 weeks for CHBr_3 and 2-3 months for CH_2Br_2) and are mainly decomposed by photolysis and reaction with hydroxyl radicals (OH). Due to convective uplift of tropospheric air in the tropics, tropical sources of CHBr_3 and CH_2Br_2 and their breakdown products can reach the stratosphere (Dvortsov et al., 1999; Sinnhuber and Folkins, 2006) and can be involved in ozone depletion.

Methyl iodide (CH_3I) is the dominant gaseous organic iodine species in the troposphere where it is involved in several iodine cycles. CH_3I is mainly emitted from the ocean and is formed by biological and non-biological pathways. CH_3I has a short lifetime (several days) and if CH_3I is transported to the stratosphere it may take part in stratospheric chemical processes, including the destruction of ozone (Solomon et al., 1994). Global emission estimates of these halogenated compounds are poorly quantified (Hossaini et al., 2010), but are needed as input for (chemical) transport models, i.e. for explaining the missing Br_y in the stratosphere and to predict the recovery of the ozone layer (Yang et al., 2005). Many uncertainties still exist in the formation processes, sources, sinks and chemical fates

of VSLS in both the ocean and the atmosphere but have to be clarified to understand the past and future environment.

1. Halocarbons in the ocean

This thesis focuses on three halogenated compounds; the bromocarbons CHBr_3 and CH_2Br_2 and the iodinated methane CH_3I . They are formed in the ocean by biological, non-biological and human made processes. CHBr_3 , CH_2Br_2 and CH_3I show strong geographical variability (vertical and horizontal) characterized by their oceanic sources and sinks. On a global scale anthropogenic sources are negligible compared to the natural sources, however, this is not the case on a regional scale. Local sources, especially near coasts significantly impact the concentration of the compounds. Halocarbons are important in the global cycling of gaseous halogen species when they are transported to the atmosphere. In the following, different source and sink mechanisms forming and destroying marine CHBr_3 , CH_2Br_2 and CH_3I are described.

1.1. Marine bromocarbons

Enhanced marine CHBr_3 and CH_2Br_2 concentrations are found in coastal regions, continental shelves, around islands as well as in upwelling regions. Further outside these source regions, in the open ocean, lower and more homogenous concentrations are measured. Marine organisms such as macroalgae, phytoplankton and bacteria are involved in their production while air-sea gas exchange (from ocean to atmosphere) is the dominant loss process in the ocean. Additionally local anthropogenic processes lead to the formation of marine bromocarbons. CH_2Br_2 is formed as by-product of biological production of CHBr_3 in the ocean although it shows a different pattern in the deep ocean indicating its different cycling the marine environment (Quack et al., 2007a).

1.1.1. Anthropogenic sources

Large amounts of CHBr_3 and CH_2Br_2 entering the marine environment are formed as by-products of sea and fresh water disinfection (Quack and Wallace, 2003; Rook, 1974) and when chlorine is added to drinking water (Batjer et al., 1980) or swimming pools (Beech et al., 1980) to kill bacteria. Although chlorination has been used to treat drinking water almost 100 years, the production of CHBr_3 and CH_2Br_2 during the chlorination process was first identified by Rook (1974).

During chlorination hypochlorous acid (HOCl) reacts to hypobromous acid (HOBr) in the presence of Br^- (Jenner et al., 1997).



Further, HOBr reacts with dissolved organic matter (DOM) to form unstable brominated compounds which decay rapidly to CHBr_3 and CH_2Br_2 (Lin and Manley, 2012).



Compared to CHBr_3 the production of CH_2Br_2 by chlorination of waste water and drinking water is small (Perry et al., 1979). The discharge of chlorine into the marine environment will generally be

Table III – 1. CHBr_3 emissions in Mmol Br yr^{-1} from different anthropogenic sources (Quack and Wallace, 2003).

Anthropogenic source	CHBr_3 Emission [Mmol Br yr^{-1}]
Coastal power plants	34 (25-85)
Inland nuclear power	4 (1-85)
Coastal fossil fuel plants	280 (210-700)
Inland fossil fuel plants	14 (3-280)
Desalination/power plants	2*
Disinfection of waste water, drinking water and recreational water	12 (3-240)

*including atmospheric release from deaeration process

(Hamilton et al., 1977) the chlorination of seawater produces 6×10^8 g yr^{-1} of organic Br and 4×10^9 g yr^{-1} of organic Br by freshwater chlorination. Quack and Wallace (2003) and contributors within estimated a total anthropogenic Br amount of ~ 346 Mmol yr^{-1} (245 -1393 Mmol Br yr^{-1}), while the highest contaminant input is caused by coastal fossil fuel plants (Table III–1).

greatest in areas with high population density located in coastal regions where the use of waste treatment and power generation is large (Scott et al., 1990). A laboratory experiment showed that the dominant substance formed during water chlorination was CHBr_3 (96 to 98 %) (Padhi et al., 2012). Assuming the global chlorine usage is

twice that of the United States

1.1.2. Biological sources

Evidence has been provided for the production of volatile halogenated organic compounds by macroalgae and some marine microalgae (phytoplankton) (Gschwend et al., 1985; Sturges et al., 1992, Tokarczyk and Moore, 1994, Tait and Moore, 1995; Carpenter and Liss, 2000). Brown, green and red algae produce various amounts of the bromocarbons CHBr_3 and CH_2Br_2 (Gschwend et al., 1985;

Nightingale et al., 1995) and are abundant near coastal areas or near the sea surface, which may be transported to the atmosphere Dryssen and Fogelqvist (1981).

One formation process of marine bromocarbons CHBr_3 and CH_2Br_2 is the oxidation of bromine via hydrogen peroxide catalyzed by the enzymes bromo- and chloroperoxidase (e.g. Beissner et. al., 1981, Wever and van der Horst, 2013):



H₂O₂ is generated in plant cells during photosynthesis and photorespiration (Pedersén et al., 1996). Wever et al. (1991) proposed that the formation of HOBr by brown algae species is part of a host defense system against bacteria and viruses, a hypothesis which was later supported by other studies (Nightingale et al., 1995). Further, they investigated vanadium containing bromoperoxidase that could react to HBrO which is then released into the water. Two biosynthetic pathways of CHBr₃ and CH₂Br₂ formation from HOBr are possible. The first pathway was observed in the red algae species *Bonnemaisonia hannifera*. They contain ketones which are brominated by the peroxidase. These unstable ketones decay via the haloform reaction (Eq. 5) to form CHBr₃ and CH₂Br₂ (Theiler et al., 1978; Morrison and Boyd, 1992).



The second pathway is that HOBr is released into the seawater and reacts with dissolved organic matter (DOM) (Eq. 3) to form unstable brominated compounds which may produce e.g. CHBr₃ and CH₂Br₂ during decay (Eq. 4). In the Arctic Ocean DOM was identified as the key factor for production of bromocarbons (Karlsson et al., 2013). The link between halocarbons production and the cell excretion is not fully understood. Laboratory experiments showed that most of the brominated compounds formed by HOBr reaction with DOM are non-volatile, however, the dominant compound of the volatile fraction is bromoform (Hill and Manley, 2009). In brown seaweeds the maximum activity of bromoperoxidase enzymes is detected during winter and spring (Wever et al., 1988). The release rates are species-specific and sensitive to external physical conditions (e.g. light) (Carpenter et al., 2000).

Additionally, phytoplankton is a source of bromocarbons, especially in the open ocean (Carpenter et al., 2003, Quack and Wallace, 2003). Its main production pathway might be bromoperoxidase outside of the cell (Lin and Manley, 2012). Marine phytoplankton and sea-ice algae, especially diatoms are known as CHBr₃ and CH₂Br₂ producers (Moore et al., 1996; Sturges et al., 1997). Locations with high primary production, e.g. the tropical oceans, constitute a major source of bromocarbons. Laboratory experiments showed HOBr production by arctic, subtropical and tropical diatom species (Hewson and Hager 1980; Fenical et al., 1982; Moore et al., 1996; Hill and Manley, 2009). Temperate species appear to be poor producers (Moore et al., 1995b). However, it is controversial how much of the HOBr is converted to bromocarbons under different environmental conditions. Studies showed that changes in light, pH value, tides (Mtolera et al., 1996) and temperature or injuries distresses the macroalgae or phytoplankton organism and influences the bromocarbon production (Hewson and Hager 1980; Moore et al., 1996; Carpenter 2003; Quack and Wallace, 2003; Hill and Manley, 2009). High solar irradiance is generally reported to enhance CHBr₃ production (Moore et al., 1996; Ekdahl et al., 1998; Carpenter et al., 2000). However, Antarctic algae species showed higher CHBr₃

production in the dark and a temperature-dependent release (Laturnus, 1996). A field study of Abrahamsson et al. (2004b) showed diurnal cycles of CHBr_3 and CH_2Br_2 from microalgae. CHBr_3 and CH_2Br_2 concentrations in the ocean might be influenced by seasonal changes in biomass production and varying solar radiation. For example, in the Baltic Sea increased CHBr_3 and CH_2Br_2 concentrations have been observed during summer (Orlikowska and Schulz-Bull, 2009).

Globally, planktonic and macroalgae sources of bromocarbons are extrapolated to be of comparable magnitude (Quack and Wallace, 2003). Global macroalgae biomass is estimated to be $60 \cdot 10^{12}$ g total global fresh weight, two-thirds thereof from kelp (DeVooy et al., 1979). The macroalgae release rates of volatile bromine-containing compounds is estimated to be $\sim 10^{10} - 2 \cdot 10^{11}$ g yr^{-1} (Gschwend et al., 1985, Manley et al., 1992). Further, estimation of ice algae release are $1 \cdot 10^{10} - 1.5 \cdot 10^{11}$ g yr^{-1} organic Br (Sturges et al., 1992).

Bacteria as sources for bromocarbons are poorly investigated yet, but have to be considered in future work. Results of Granfors et al. (2013) suggest bacterial halocarbon production in Arctic sea ice, while experiments with metabolic inhibitors showed that ice algae rather than bacteria are responsible for bromoform formation (Sturges et al., 1992). Field incubations studies of microalgae communities in surface sea ice have shown that CHBr_3 and CH_2Br_2 are being produced and indicated that the CHBr_3 rate was 30-100 higher compared to CH_2Br_2 (Abrahamsson et al., 1995; Karlsson et al., 2013).

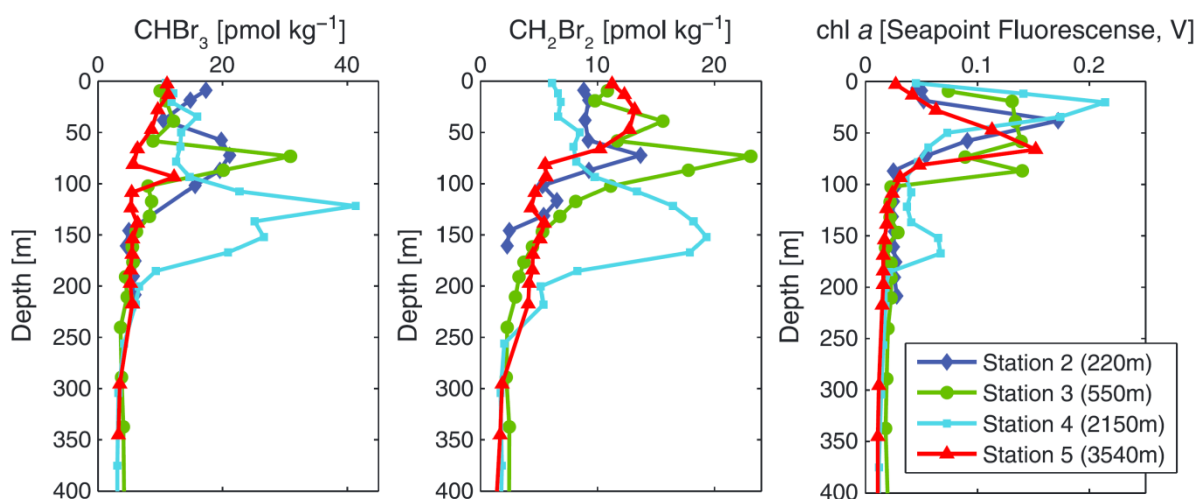


Figure III – 3. Depth profiles of CHBr_3 , CH_2Br_2 and $\text{Chl } a$ for stations on the continental shelf (station 2), over the continental slope to offshore (station 5) in Alaska (Karlsson et al., 2013).

A direct correlation between chlorophyll a ($\text{chl } a$) and the bromocarbons is not apparent (Abrahamsson et al., 2004; Quack et al., 2007b). The depth profiles in figure III-3 show the vertical distribution of CHBr_3 and CH_2Br_2 oceanic concentrations from continental shelf (station 2-dark blue) to offshore (station 5-red). $\text{Chl } a$ is a proxy indicator for biological production. The bromocarbons

maximum is identical to the $\text{CHl } \alpha$ maximum in station 2 and 3, but not in station 4. The vertical distribution of CHBr_3 and CH_2Br_2 is an interaction between production and sink mechanisms and transport (advection and diapycnal mixing).

1.2. Marine methyl iodide

The production processes of CH_3I are not fully understood. There is an ongoing debate whether the formation by biological organisms or photochemical degradation is the main source. CH_3I has low solubility and thus the ocean water can easily become supersaturated (Manley and Dastoor, 1988)

1.2.1. Biological and non-biological sources

The first sea water measurements of CH_3I is made by Lovelock (1973) and indicated that this compound was the main carrier of iodine in the atmosphere. Macroalgae, phytoplankton and bacteria can form CH_3I (e.g. Manley and Dastoor, 1987; Manley and de la Cuesta, 1997; Amachi et al., 2001; Hughes et al., 2011) as well as non-biological processes like photochemical degradation of organic matter (e.g., Moore and Zafiriou, 1994; Happell and Wallace, 1996; Richter and Wallace, 2004; Chuck et al., 2005; Butler et al., 2007; Yokouchi et al., 2008).

Several biological mechanisms have been identified for CH_3I production in seawater:

- i) White et al. (1982) suggest CH_3I formation by reaction of halides with dimethylsulfonium ions (e.g. DMSP) concentrated in the algae, but no evidence for this production pathway could be found in Antarctic macro-algae (Manley and Dastoor, 1988).
- ii) Moore and Zafiriou (1994) proposed that CH_3I is formed by reductive dehalogenation (similar to CHBr_3 and CH_2Br_2 (Eq. 2))
- iii) Manley and Dastoor, (1988) illustrated CH_3I production by microbes derived from decomposing kelp and estimated a global production of $2.4 \text{ Gmol } (\text{CH}_3\text{I}) \text{ I yr}^{-1}$ by enzymatic activity of methyltransferases (e.g. Ohsawa et al., 2001). The reaction includes the transfer of iodide via S-adenosyl-L-methionine (SAM).



In vitro experiments showed CH_3I formation by methylation in 13 of 20 terrestrial bacterial strains. The reaction depends strongly on the iodine level and the oxygen conditions (occur best in oxic and anoxic environments (Amachi et al., 2001).

- iv) An additional possible marine source of CH_3I is the reaction of the vitamin B12 derivate methylcobalamin ($\text{CH}_3\text{-B}_{12}$) with iodide-atoms (I) or molecules (I_2) (Manley, 1994). This process is more effective in seawater with lower ph ($\text{ph} < 7$):



At coastal areas CH_3I is formed by macroalgae. Global estimates show a wide range ($4.7 \cdot 10^7$ to $1.3 \cdot 10^{12} \text{ g yr}^{-1}$) of CH_3I production by macroalgae (Rasmussen et al., 1982; Manley and Dastoor, 1988; Nightingale et al., 1991; Nightingale, 1995).

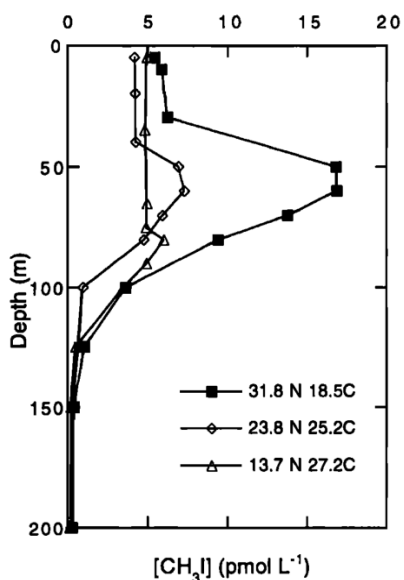


Figure III – 4. Vertical profiles of CH_3I concentrations in pmol L^{-1} at three different stations in the Pacific Ocean with temperatures in $^{\circ}\text{C}$ at the depth of each CH_3I maximum (Moore and Groszko et al., 1999).

In addition, biological pathway by phytoplankton, i.e. diatom species (Manleyq and de la Cuesta, 1997) and the cyanobacterium *Prochlorococcus* (Abrahamsson et al., 2008; Brownell et al., 2010), have been identified as CH_3I sources in the open ocean. Examples of depth profiles of CH_3I are shown in Figure III–4. Two profiles show a subsurface maximum at the base of the oceanic mixed layer which is identical with the chlorophyll a (indicator for biological production) maximum. Rasmussen et al. (1982) estimated a global CH_3I production by phytoplankton of $10^{12} \text{ g yr}^{-1}$. Under stress conditions (e.g. increasing solar irradiation (Abrahamson et al., 2008)) enhanced production rates of CH_3I by an order of magnitude have been documented (Hughes et al, 2011).

The open ocean sources and origin of CH_3I are controversial. Laboratory experiments of Richter and Wallace (2004) found a photochemical production pathway of CH_3I in sea water. Moore and Zafiriou (1994) suggested a photochemical source for CH_3I involving a radical recombination pathway:



The methyl radicals ($\text{CH}_3\bullet$) are formed by photolysis of humic material from DOM and has a lifetime of $\sim 1 \text{ ms}$. The main sink for methyl radicals is the reaction with oxygen (Zafiriou et al., 1990). Enhanced production of CH_3I occurs under low oxygen and high iodine conditions.

1.3. Ocean sinks

The dominant ocean sink process of CHBr_3 , CH_2Br_2 and CH_3I is the air-sea gas exchange and is discussed separately in section IV–2. Hydrolysis, halogen-substitution and photolysis constitute degradation pathways for the three halocarbons in sea water. Biotic and abiotic reductive dehalogenation represents an additional sink mechanism for the bromocarbons.

Hydrolysis is the cleavage of chemical bonds by the addition of water and is highly temperature dependent. The colder the sea water the slower are the reaction rate. At 2–4 °C marine bromocarbons lifetime is ~680–1000 years and at 25 °C the lifetime decreases to 30-50 years (Mabey and Hill, 1978).

Further, halogen substitution is 1-2 orders of magnitude faster than hydrolysis. Halogenated compounds can be biodegraded (by enzyme) via reductive removal of halogen substituents. Class and Ballschmiter (1988) suggest nucleophilic substitution in sea water according to:



The end product of this reaction chain might be chloroform (CHCl_3). For the conversion the lifetime of bromoform to dibromochloromethane is reported to vary from 5 (25 °C) to 74 (2 °C) years (Geen, 1992). Marine CH_3I also reacts with chloride via halogen substitution to produce methyl chloride (Zafiriou et al., 1975):



The reductive dechlorination of CH_3I (to CH_3Cl) is the most common nucleophilic substitution in seawater (Zika et al., 1984; Moore and Zafiriou, 1994). Zafiriou et al (1975) reported a marine CH_3I lifetime of 19.7 days at 19.2 °C and 58.4 days at 10.8 °C. Because of temperature dependence, the Cl^- substitution varies strongly by latitude and depth. Between the temperature range 5–25 °C, the half-life of CH_3I varies from thousands of days for cold water to 6 days for the warmest water (Zika et al., 1984).

Near the ocean surface layer solar photolysis is an important sink mechanism for halocarbons. The C–Br bond of CHBr_3 is broken down by 380 nm light (Betterton et al., 1995) and CH_3I is degraded by light of <340 nm wave length. Zika et al. (1984) predicted a lifetime for CH_3I in tropical surface water of 2.7 days and suggest that photolysis reaction might be a major sink for CH_3I , especially in warm waters. Reductive dehalogenation of brominated compounds has been found primarily in syntrophic anaerobic communities and occurs through microbial activity (Bouwer et al., 1981). Goodwin et al (1997) have demonstrated that bacteria are able to oxidize CH_2Br_2 in sea water. Further, CH_2Br_2 concentrations in the Black Sea decrease through the suboxic and into the anoxic zone (Tanhua et al., 1996). They suggest that CH_2Br_2 and other halogenated compounds are removed by means of reduction. The higher the redox-potential of a halocarbon is the higher is the rate of reduction.

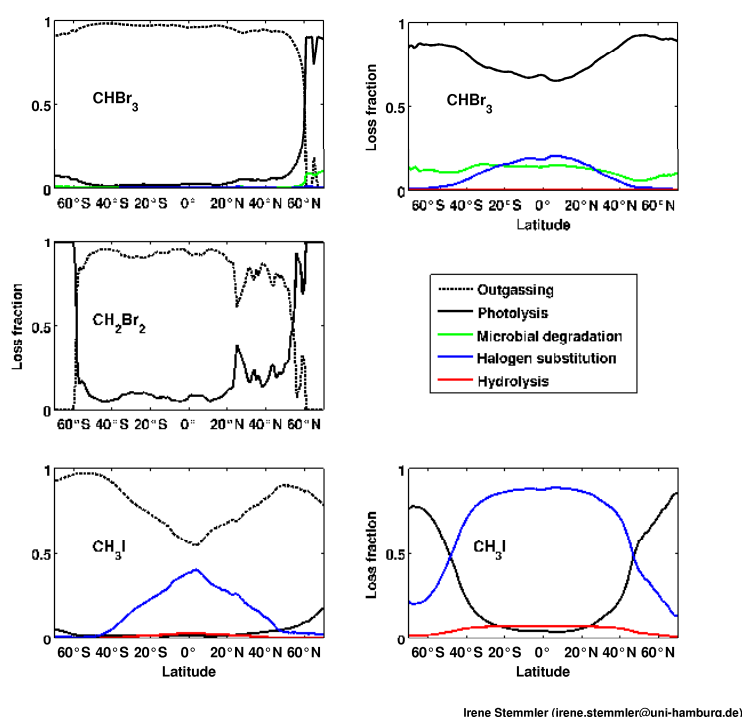


Figure III – 5. Left: Annual zonal mean of the ocean loss fraction outgassing (black dashed), photolysis (black), microbial degradation (green), halogen substitution (blue) and hydrolysis (red) from the compounds CHBr_3 , CH_2Br_2 and CH_3I calculated with the global 3D general ocean circulation model MIOPM with coupled ecosystem model HAMOCC (Stemmler et al., 2014). Right: the same as shown left only for CHBr_3 and CH_3I without outgassing.

reaction time of hydrolysis, this sink process is a minor part compared to the other ones. CHBr_3 and CH_2Br_2 show similar features, photolysis is the second dominant surface sink. Microbial degradation of CHBr_3 shows no latitudinal trend whereas halogen substitution is temperature dependent and presents a stronger influence in lower latitudes. Identical features are seen for the degradation processes of CH_3I . Cl^- substitution is a dominant sink for CH_3I in the tropics while photolysis is dominant in higher colder latitudes.

2. Atmospheric bromocarbons and methyl iodide

Bromoform and dibromomethane are the major carriers of bromine from the ocean to the atmosphere (Penkett et al., 1985). CH_3I is a dominant source of organic iodine in the troposphere and is involved in several atmospheric chemical cycles (Saiz-Lopez et al. 2012). After emitted into the marine boundary layer, the halogens and their breakdown products are involved in chemical processes in the troposphere and stratosphere (WMO, 2011). The compounds and their degradation products can be transported by vertical deep convection (Aschmann et al., 2009) into the tropical tropopause layer (TTL) and even reach the stratosphere where there are involved in ozone depletion.

A model study calculated the loss fraction of the four degradation pathways on a global scale and shows the dominant sink process for each halogenated compound (Figure III–5, I. Stemmler personal communication). The fractions are calculated by the sum of each pathway for a climatological year. Further each sink was zonal averaged and fractionated. The sea-to-air flux is zero if there is uptake from the atmosphere to the ocean such as in the Arctic/Antarctic regions for the bromocarbons. The major sink for all three compounds is the air-sea gas exchange. Due to the long

Bromine is about 45-69 times more efficient than chlorine in destroying stratospheric ozone (Sinnhuber et al., 2006). Atmospheric concentrations of the three halogenated compounds are highly variable due to their heterogeneous distribution and time varying natural sources.

2.1. Atmospheric distribution and chemical fates

2.1.1. Bromocarbons

Short-lived brominated organic compounds such as CHBr_3 and CH_2Br_2 have life times of $\sim 2-3$ weeks and $\sim 2-3$ months, respectively (Montzka and Reimann, 2011). Mean background concentrations of CHBr_3 in the MBL (<1000 m height) in the Tropical Pacific were 0.58 to 0.85 ppt and 0.5 ppt in the open ocean (Fischer et al., 2000). Highest concentrations were measured at coastal areas (i.e. Mace Head 1.0 to 22.7 ppt (Carpenter et al., 1999)). Also, higher mean background concentrations were measured in the Northern Hemisphere (0.85 to 0.94 ppt (Penkett et al., 1985; Atlas et al., 1993)) compared to the Southern Hemisphere (0.58 to 0.74 ppt). Khalil and Rasmussen (1999) reported that the Arctic has more alkanobromine as bromoform compared to the Antarctic (57 % versus 15 %). A seasonal cycle of bromoform was measured in the Arctic and over Hawaii (Cicerone et al., 1988; Yokouchi et al., 1996).

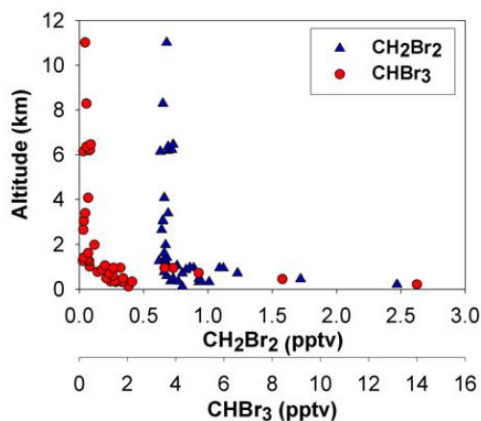


Figure III - 6. Tropospheric vertical distribution of CHBr_3 and CH_2Br_2 at the coastal region of the Gulf of Maine (aircraft measurements between $42.0-43.5^\circ \text{ N}$ and $69.5-71.0^\circ \text{ W}$) (Zhou et al., 2008).

Both compounds show a rapid decrease with altitude whereas CHBr_3 concentrations decline faster than those of CH_2Br_2 due to vertical mixing and/or chemical loss (Figure III-6) (Zhou et al., 2008). Mean mixing ratios range from 2.9 ppt and 1.0 ppt of CHBr_3 and CH_2Br_2 , respectively, below 1km altitude to 0.4 ppt and 0.7 ppt above 1km height (Zhou et al., 2008). Quack and Wallace, (2003) estimate ~ 0.02 Gmol of CHBr_3 in the MBL. Due to common sources atmospheric CHBr_3 and CH_2Br_2 mixing ratios show strong linear correlations. To identify similar pathways of either biological or chemical production $\text{CH}_2\text{Br}_2/\text{CHBr}_3$ ratios are used to characterize the origin of the air mass (Carpenter et al., 2003, Yokouchi et al., 2005). The lower the ratio value the higher is the CHBr_3 concentration towards CH_2Br_2 which indicates a strong local source. Zhou et al. (2008) found atmospheric concentration ratios $\text{CH}_2\text{Br}_2/\text{CHBr}_3$ ranges from 0.13 to 0.16 from coastal measurements.

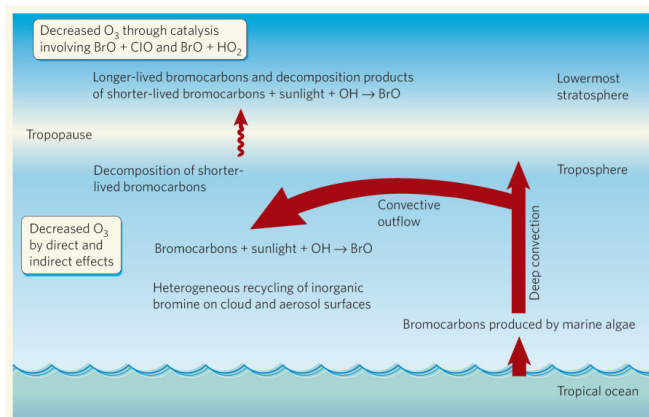


Figure III – 7. Bromine chemical reactions and transport through the atmosphere. The bromocarbons CHBr_3 and CH_2Br_2 are naturally produced in the ocean. Emitted into the troposphere they are decomposed by the reaction with OH and sunlight (Salawitch, (2006). Most of CHBr_3 decayed to BrO which could take part in stratospheric ozone depletion.

(Hönninger and Platt, 2002).

Once emitted into the atmosphere, CHBr_3 and CH_2Br_2 are degraded either via reactions with hydroxyl radicals (OH), Cl (chloride), NO (nitrous monoxide) or photolysis in the atmosphere resulting in inorganic bromine Br_y ($\text{Br}_y = \text{Br} + \text{BrO} + \text{HOBr} + \text{BrCl} + \text{HBr} + \text{BrONO}_2$). The dominant loss process for CH_2Br_2 is the reaction with OH while for CHBr_3 it is photolysis. Both react rapidly with oxygen (O_2) and are assumed to be removed via reaction with NO and HO_2 . The major end products of atmospheric bromoform are CBr_2O and CHBrO which degrade to Br-atoms via photolysis. CHBrO and Br_y are expected to be the major end products for atmospheric CH_2Br_2 . Br_y are removed from the troposphere by washout (Ko and Poulet et al., 2003; Yang et al., 2005; Hoassaini et al., 2010), oxidation of mercury, reaction with ozone or particle formation (aerosols) (Saiz-Lopez et al., 2012a). Measurements at the weather station in Alert (Canada) showed the seasonal fluctuation of surface ozone via tropospheric bromine atoms (Figure III–8). The most rapid decrease in bromine is observed during polar sunrise (Barrie et al., 1988). It has been shown that the destruction is caused by Br_y compounds such as Br_2 , BrCl and HOBr that originate from bromide in sea salt particles (Finlayson-Pitts, 2010).

A simple diagram from Salawitch (2006) summarizes the most important pathways of bromocarbons in the troposphere and lower stratosphere (Figure III–7). Including bromine chemistry in model simulation showed that bromine influences 5-30 % of the global tropospheric ozone budget depending on location and season (von Glasow et al. 2004, Yang et al. 2005). Tropospheric ozone can be destroyed by direct (catalytic loss initiated by the reaction of BrO with HO_2) and indirect (NO_x removal via bromine nitrate hydrolysis) effects

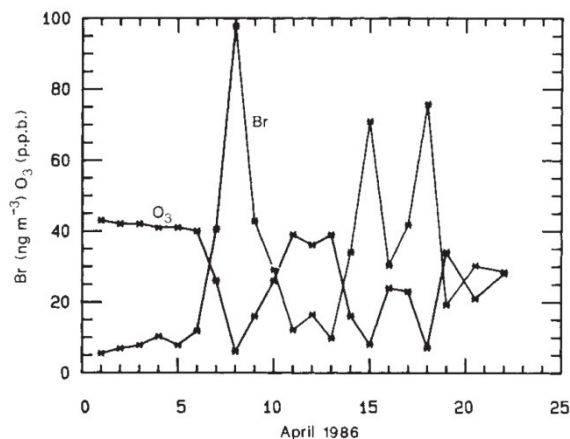


Figure III – 8. Reduction of tropospheric ozone via filterable Br-atoms at Alert (Canada) (Barrie et al., 1988).

Anthropogenic emissions account for approximately 75 % of the total bromine in the stratosphere. The remainder is thought to arise from biogenic VSLS such as CHBr_3 and CH_2Br_2 . Modeling studies and field measurements suggest that bromoform contributes significantly (30 to >60 %) to inorganic bromine within the upper troposphere and lower stratosphere (Law and Sturges et al., 1997; Schauffler et al., 1998; Dvortsov et al. 1999). In the stratosphere bromine is involved in several catalytic cycles effectively destroying stratospheric ozone (cycles 2, 4, 6 and 8 including bromine are listed below) (Table III–2):

Table III – 2. Stratospheric catalytic ozone destroying cycles including bromine according to Daniel et al. (1999). M indicates a catalyzer.

<p><u>Primary cycle during polar springtime in lower stratosphere (Cycle 2):</u></p> $\text{Br} + \text{O}_3 \rightarrow \text{BrO} + \text{O}_2$ $\text{Cl} + \text{O}_3 \rightarrow \text{ClO} + \text{O}_2$ $\text{ClO} + \text{BrO} \rightarrow \text{Br} + \text{ClO}_2$ $\text{ClO}_2 + \text{M} \rightarrow \text{Cl} + \text{O}_2 + \text{M}$ <p><i>Net: $2\text{O}_3 \rightarrow 3\text{O}_2$</i></p>	<p><u>Lower stratosphere in midlatitudes (Cycle 6):</u></p> $\text{NO} + \text{O}_3 \rightarrow \text{NO}_2 + \text{O}_2$ $\text{Br} + \text{O}_3 \rightarrow \text{BrO} + \text{O}_2$ $\text{BrO} + \text{NO}_2 + \text{M} \rightarrow \text{BrONO}_2 + \text{M}$ $\text{BrONO}_2 + \text{h}\nu \rightarrow \text{Br} + \text{NO}_3$ $\text{NO}_3 + \text{h}\nu \rightarrow \text{NO} + \text{O}_2$ <p><i>Net: $2\text{O}_3 \rightarrow 3\text{O}_2$</i></p>
<p><u>Lower stratosphere in midlatitudes (Cycle 4):</u></p> $\text{OH} + \text{O}_3 \rightarrow \text{HO}_2 + \text{O}_2$ $\text{Br} + \text{O}_3 \rightarrow \text{BrO} + \text{O}_2$ $\text{BrO} + \text{HO}_2 \rightarrow \text{HOBr} + \text{O}_2$ $\text{HOBr} + \text{h}\nu \rightarrow \text{Br} + \text{OH}$ <p><i>Net: $2\text{O}_3 \rightarrow 3\text{O}_2$</i></p>	<p><u>Middle and upper stratosphere: (Cycle 8):</u></p> $\text{Br} + \text{O}_3 \rightarrow \text{BrO} + \text{O}_2$ $\text{BrO} + \text{O} \rightarrow \text{Br} + \text{O}_2$ <p><i>Net: $\text{O}_3 + \text{O} \rightarrow 2\text{O}_2$</i></p>

2.1.2. Methyl iodide

CH_3I mixing ratios range from 0.2 to 3 ppt in the boundary layer varying from pole to pole with enhanced concentrations in the tropics and subtropics (Rasmussen et al., 1982; Yokouchi et al., 2010). Near coastal areas or over biologically productive oceans higher CH_3I concentrations were found in the atmosphere. Oram and Penkett (1994) measured CH_3I mixing ratios of 43 ppt at the Atlantic coast (eastern England). Seasonal variation in atmospheric CH_3I with maxima in summer/autumn was found by Rasmussen et al. (1982) and Yokouchi et al (2001).

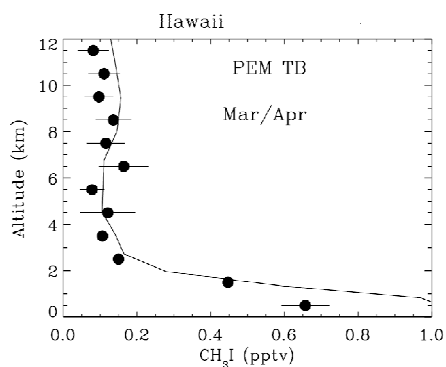


Figure III – 9. Vertical profile of CH_3I measured from aircraft (black dot) near Hawaii. Horizontal bars indicate the standard deviations calculated from individual measurements. Corresponding modeled profile is shown in solid black line (Bell et al., 2002)

Most of the CH_3I concentration is concentrated in the marine boundary layer (MBL) (Bell et al., 2002). Only a small fraction of CH_3I reaches the stratosphere (Aschmann et al., 2009; Gettelman et al., 2009). Modeling results from Donner et al., 2007 indicated CH_3I concentrations of 0.1 ppt in the TTL at 15 km altitude and drop below at the cold point tropopause of 0.05 ppt.

Atmospheric methyl iodide has a much shorter lifetime (few days (~ 7 days)) compared to the bromocarbons CHBr_3 and CH_2Br_2 (weeks to months) and is very reactive. CH_3I is involved in several chemical reaction processes and is one main carrier of iodine from the ocean to the atmosphere (Lovelock et al., 1973).

Figure III–10 shows among others an overview over the currently known chemical reaction pathways of methyl iodide in the troposphere. Upon volatilization to the atmosphere it is rapidly decomposed into reactive iodine species and impacts the tropospheric chemistry, such as the oxidative capacity and ozone depletion (e.g. Chameides and Davis, 1980; Solomon et al., 1994; Vogt et al., 1999).

CH_3I and other short-lived iodocarbons are photodissociated to generate iodine atoms (I) which mostly react with ozone to form IO-radicals. Further, IO reacts rapidly with NO_x and HO_x or with elemental mercury into gaseous reactive mercury follow. IO is also involved in the oxidation of DMS to DMSO (dimethylsulfoxid) or takes part in particle formation (Saiz-Lopez and von Glasow, 2012).

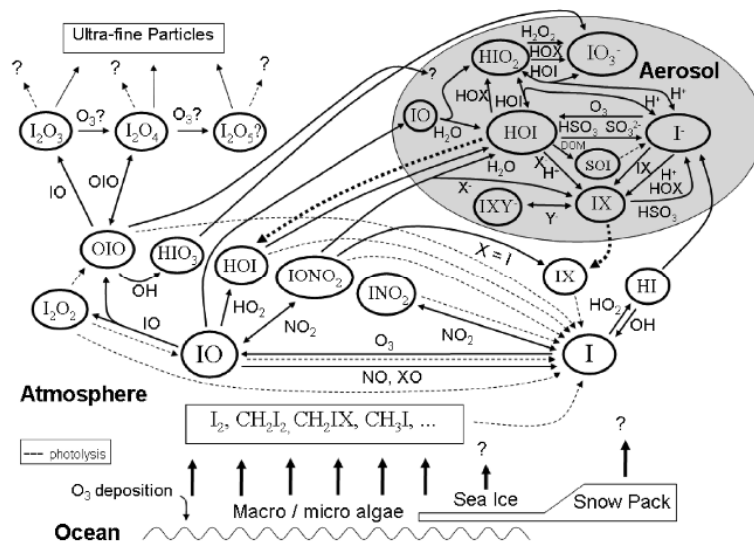
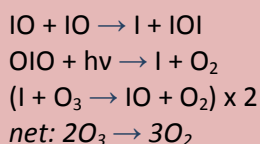


Figure III – 10. Simplified schematic of tropospheric iodine chemistry. Dashed lines illustrate photolysis and dotted lines represent phase equilibrium from aerosols. X and Y are halogen atoms, DOM is dissolved organic matter and SOI is soluble organic iodine (Saiz-Lopez et al., 2012b).

Three catalytic ozone depletion cycles in the troposphere including iodine are known (Liss and Johnson, 2014):

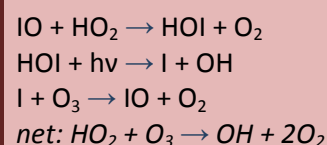
Cycle 1:



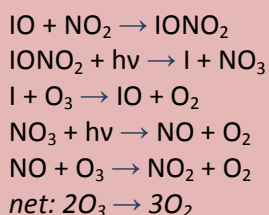
O₃ can be depleted by IO radicals through its self reaction to form IOI radicals (Cycle 1). This ozone depletion reaction becomes most important when IO concentration is more than several ppt. The reaction with HO₂ radicals (Cycle 2) takes place with lower iodine mixing ratios.

HOI is the most abundant inorganic gas and reaches maximum mixing ratios of 2 ppt at daytime. Cycle 3 describes the ozone depletion due to IONO₂ formation in semi-polluted regions, like industrial areas.

Cycle 2:



Cycle 3:



HOI and IONO₂ can also be removed to sea-salt aerosols (i.e. HOI reaction with Cl⁻ and Br⁻ to ICl and IBr), sulfate aerosols and/or IONO₂ is assumed to react with I-atoms to recycle back to I₂. Solomon et al. (1994) suggest that iodine could pass similar ozone destruction cycles in the stratosphere as chlorine and bromine with minor efficiency compared to BrO and ClO. Regarding its lower photochemical stability, CH₃I might only play a minor role in stratospheric ozone depletion (Zafiriou, 1977).

3. Transport into the stratosphere

Once emitted from the ocean the halogenated compounds CHBr₃, CH₂Br₂ and CH₃I are transported from the MBL into the free troposphere and can even reach the stratosphere. Due to the short lifetime of CH₃I the research community believed that this kind of VSLs and such of even shorter lifetimes might not reach the stratosphere (Montzka and Reimann, 2010). This is the case unless this compound is directly emitted into a deep convective cell in the tropics (Figure III–11). Tropical overshooting convection can rapidly inject surface air into the upper tropical tropopause layer (TTL) and to the stratosphere (e.g. Ricaud et al., 2007; Aschmann et al., 2011) which is also simulated by different models (Donner et al., 2007). The transport of VSLs through the troposphere depends on the region and season of VSLs emission, as well as on wash out, atmospheric losses (reaction with O₃, OH, photolysis) and duration of deep convective lifting in the tropics (Aschmann et al., 2009). The tropical Western Pacific is identified as a region where VSLs emissions can be efficiently transported

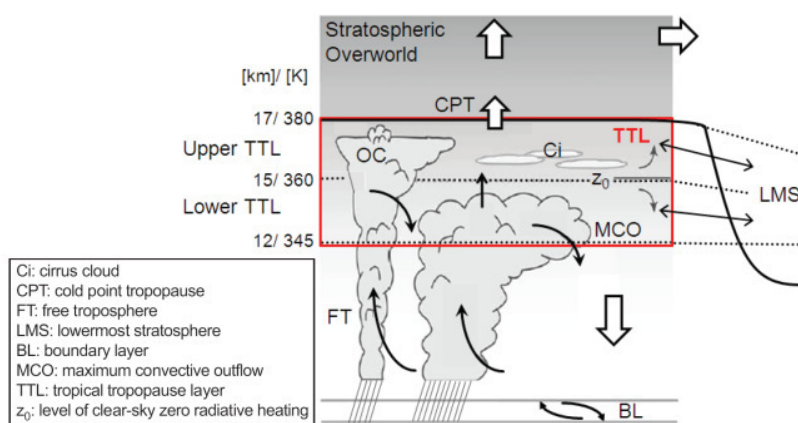


Figure III – 11. Schematic diagram showing the principals of dynamical pathways in the tropics transporting VSL source gases and their breakdown products into the stratosphere (modified from Fueglistaler et al., 2009a). The black bold line illustrate the tropopause.

the TTL is presented by Fueglistaler et al., (2009a) in figure III–11 which illustrates tropical deep convection reaching the altitudes of 10-15 km. The TTL is divided into two levels. The lower TTL is dominated by convection and is above the level of main convective outflow (12 km/345 K). However, cloud formation can even reach the stratosphere. The upper TTL is located between the level of clear-sky zero radiative heating (z_0) to the CPT (17 km/380 K). Sherwood and Dessler (2003) termed the z_0 level the “stagnation surface”. A particle has to be lifted above the z_0 to enter the stratosphere. The residence time through the upper TTL is estimated by 25 to 45 days (Krüger et al., 2009). Additionally, the transport through the TTL varies with season—highest VSL concentrations are found in the northern hemispheric (NH) winter due to higher convective cloud tops reaching the TTL (more for CHBr_3 than for CH_2Br_2) and higher vertical velocities within the TTL (Fueglistaler et al., 2009a).

After entering into the upper TTL vertical circulation driven by atmospheric waves transport upper trace gases from the tropics to the extratropics (Brewer Dobson Circulation). In the next section the amount of atmospheric CHBr_3 , CH_2Br_2 and CH_3I concentrations and their breakdown products entering the TTL is described.

4. (Chemical) transport models

There are different types of models which one can use to estimate the amount of total inorganic bromine (Br_y) and total inorganic iodine (I_y) transported into the stratosphere. Chemical transport models (CTM) focus on modeling atmospheric chemistry by solving the continuity equation for the compound of interest. CTMs include the whole chemical fate (emission strength, sources, sinks, reaction pathways) of the trace gas. General circulation models (GCM), on the other hand, simulate

to the TTL compared to other ocean regions (Aschmann et al., 2009). The TTL is the interface between the two different dynamical atmospheric regimes the troposphere and the stratosphere and is roughly defined as the level of temperature minimum (“cold point tropopause (CPT)”). A more detailed schematic of

the overall atmospheric dynamics by solving the primitive equations. Using output fields (e.g. temporally and spatially highly resolved meteorological fields) from GCMs for CTMs and vice versa can reduce computer costs and improve the model performance. CTMs are further classified according to their methodology into Eulerian or Lagrangian models (Jacob, 1999). The Eulerian method is based on solving the continuity equation for a fixed frame of reference, while the Lagrangian CTMs use a moving frame of reference.

Product gas (PGI) and source gas injection (SGI) efficiency reaching the TTL depends on chemical loss (OH and photolysis) and rate of removal (wet deposition). SGI describes the entering of a VSLS into the stratosphere in the same form as it is emitted from the surface and PGI represents the injection of their breakdown products into the stratosphere. The Br_y amount coming from natural VSLS like bromoform and dibromomethane or for I_y from methyl iodide emissions is a crucial and uncertain factor. Observations and modeling results estimate a total Br_y in the stratosphere of 19.5-24.5 ppt (Montzka and Reimann, 2011) which cannot be explained by CH_3Br and halones alone – a significant amount has to come from other sources, most likely from VSLS (Figure III-2). $CHBr_3$ and CH_2Br_2 account for >80 % VSL organic bromine in the MBL and free troposphere and are expected to account for a large fraction of stratospheric Br_y (WMO, 2007). Some studies suggest that the combination of more minor VSLS as CH_2BrCl , $CHBr_2Cl$, $CHBrCl_2$ or C_2H_5Br may contribute a significant amount of bromine. The amount of bromine reaching the stratosphere from VSLS is highly dependent on season and distribution of surface emissions (Bridgeman et al., 2000).

There are several kinds of (chemical) transport models calculating the total bromine entering the stratosphere where they are involved in ozone depletion (Liang et al., 2010). The model results vary substantially spanning a range of 0.8-7 ppt Br_y from VSLS reaching the stratosphere (Table III-3). Earlier studies range from 1.1 to 1.9 ppt Br from $CHBr_3$ (Dvorstov et al., 1999 and Nielsen and Douglas, 2001) using a uniform net global flux for this compound (3×10^8 kg yr^{-1} to 5×10^8 kg yr^{-1}). They found that convection is needed to transport $CHBr_3$ into the stratosphere. Sinnhuber and Folkins, (2006) assumed a varying lifetime of Br_y due to washout of 10 to 30 days in the TTL and estimate inorganic bromine of 0.8 to 2.1 ppt deriving from $CHBr_3$ of both SG and PG entering the stratosphere. A maximum of 6-7 ppt Br_y reaching the TTL is calculated by Warwick et al. (2006) including five brominated compounds (about 3.4 to 4 ppt Br deriving from $CHBr_3$). They were the first using a not uniform global sea-to-air flux fields as source for bromocarbons. Aschmann et al. (2009) indicate that the most effective region is the West Pacific accounting for 55 % of the stratospheric Br_y from $CHBr_3$. Hoassaini et al. (2010) calculated a total Br_y from $CHBr_3$ and CH_2Br_2 of 2.4 ppt (= $CHBr_3$ (0.72 ppt, ~53 % SG), CH_2Br_2 (1.69 ppt, 94 % SG)) using a constant washout life time of 10 days for Br_y resulting in 60 % loss of bromine from $CHBr_3$ and CH_2Br_2 . The later study of Hossaini et al. (2012) found that 10 days of washout is too short and updated convection by mass flux scheme,

detrainment rates and altitude dependent wet deposition of Br_y . Further they used tropical surface atmospheric mixing ratio fields as the bromocarbon source. Liang et al. (2010) used a detailed wet and dry deposition scheme to calculate Br_y loss and showed a removal of 85 % by wet deposition below 500 hPa. They calculated an injection of 5 ppt of Br_y deriving from CHBr_3 and CH_2Br_2 into the stratosphere. A model comparison study published in Aschmann et al. (2011) using on the one hand a full scheme state-of-the-art chemistry and on the other hand a simplified setup with idealized tracers presented similar bromine injection into the TTL for CHBr_3 and CH_2Br_2 (4.9-5 ppt Br_y calculated with the full chemistry model to 3.4-5 ppt Br_y determined with simple chemistry). They concluded that nearly all bromine from VLSL reaches the TTL in areas of deep convection. Further, they suggest that fluxes of VLSL into the TTL are controlled by the distribution of VLSL in the surface and the pathways by which VLSL enters deep convective lifting (Aschmann et al., 2011). Tegtmeier et al. (2012) used the Lagrangian particle dispersion model **FLEXPART** (**FLEX**ible **PART**icle dispersion model) to simulate the atmospheric transport of CHBr_3 and CH_2Br_2 from the oceanic surface into the upper troposphere and TTL. FLEXPART is an offline model driven by meteorological fields. It includes parameterizations for moist convection, dry deposition and in-cloud as well as below cloud scavenging and the simulation of chemical decay (Stohl et al., 2005). Compared to most Eulerian models the FLEXPART model resolves the MBL and free troposphere and connected local emissions with convection. CHBr_3 and CH_2Br_2 emissions from the West Pacific contribute to the stratospheric bromine budget with 0.4 ppt Br on average and 2.3 ppt Br for cases of maximum emissions. There are no model results for iodine loading from CH_3I into the stratosphere. Aircraft campaigns lead to the conclusion that no more than 0.05 ppt of iodine enters the stratosphere in the form of the source gas CH_3I (Montzka and Reimann, 2011).

As shown in this chapter there exist several model studies using different parameterizations of convection, transport and atmospheric sink processes as well as different sources which leads to a wide range of stratospheric bromine loading estimates (Table III–3). Strength and distribution of VLSL emissions are nearly always a significant source of uncertainty in any CTM system and constitute a main difference among the models (Section III.5).

Table III – 3. Summary of different kinds of models calculating the total bromine (Br_y) loading into the stratosphere under several initial conditions (more description in the text).

Reference	Short model discription	Method	VSLs	Br _y from VSLs [ppt]	Forcing
Dvorstov et al. (1999)	3D CTM	Eulerian	CHBr ₃	1.9	uniform, global flux: 3x10 ⁸ kg yr ⁻¹
Nielsen and Douglas (2001)	3D PCTM (parameterized chemistry and transport model), resolution: 2.5° x 2°	Semi-Lagrangian	CHBr ₃	1.1	uniform, global flux: 5x10 ⁸ kg yr ⁻¹
Sinnhuber and Folkins (2006)	2D mechanistic model	Eulerian	CHBr ₃	0.8 to 2.1	uniform, 1 ppt
Warwick et al. (2006)	3D CTM, resolution: 2.8° x 2.8°, simple chemistry	Eulerian	CHBr ₃ , CH ₂ Br ₂ , CH ₂ BrCl CHBr ₂ Cl, CHBrCl ₂	6 – 7	non uniform, global flux estimates
Gettleman et al. (2009)	1D model simple transport, convective source and parameterized loss	Eulerian	CHBr ₃ and CH ₂ Br ₂	1.1 to 4.1	mean boundary concentrations: 1.1 ppt for CHBr ₃ , 1.6 ppt for CH ₂ Br ₂
Aschmann et al. (2009)	3D CTM, chemistry included, resolution: 2.5° x 3.75°, 29 vertical level, (10-55 km)	Eulerian	CHBr ₃	1.6 to 3	uniform, 1 ppt in the MBL
Hoassaini et al. (2010)	3D CTM, resolution: 5.6° x 5.6°, 38 vertical levels	Eulerian	CHBr ₃ and CH ₂ Br ₂	2.4	mean mixing ratios 1.2 ppt for both
Liang et al. (2010)	CCM with coupled GCM , resolution: 2° x 2.5°, 72 vertical levels	Semi-Lagrangian	CHBr ₃ and CH ₂ Br ₂	5.0	non uniform, 425 Gg Br yr ⁻¹ (CHBr ₃), 57 Gg Br yr ⁻¹ (CH ₂ Br ₂)
Aschmann et al. (2011)	same as Aschmann et al. (2009) plus full scheme state of the art chemistry	Eulerian	CHBr ₃ and CH ₂ Br ₂	4.9 to 5	1 ppt mixing ratio for both
Hossaini et al. (2012)	same as Hossaini et al. (2010) plus additional mass flux scheme and altitude-dependent wet deposition	Eulerian	CHBr ₃ , CH ₂ Br ₂ , CH ₂ BrCl, CHBr ₂ Cl, CHBrCl ₂ , C ₂ H ₅ Br	4.9 to 5.2	tropical surface mixing ratios
Tegtmeier et al. (2012)	Lagrangian particle dispersion model FLEXPART, offline	Lagrangian	CHBr ₃ and CH ₂ Br ₂	0.4 to 2.3*	local measured emissions
Aschmann and Sinnhuber (2013)	same as Aschmann et al. (2009)	Eulerian	CHBr ₃ and CH ₂ Br ₂	4.5 to 6	1 ppt mixing ratio for both

* only West Pacific

5. Global emission estimates

A key problem for modeling marine bromine and iodine transport from the ocean to the stratosphere is a correct description of the halocarbon sources. As input for CTMs global halogen emission inventories are needed. Different sea-to-air flux estimates are found in the literature; including extrapolation methods (e.g. using emission ratios $\text{CHBr}_3/\text{CH}_2\text{Br}_2$), bottom-up and top-down approaches, as well as laboratory experiments. Their global emission magnitudes and distributions are strongly varying because of the high geographical and temporal variability.

The first global emission estimates focused on CHBr_3 being the largest single source of atmospheric bromine from bromocarbons. The results covered a wide range from 200 Gg yr^{-1} to over 1000 Gg $\text{CHBr}_3 \text{ yr}^{-1}$ and are all globally uniformly distributed (Penkett et al., 1985; WMO, 1998; Dvortstov et al., 1999; Carpenter and Liss, 2000; Nielsen and Douglass, 2001). In example, Carpenter and Liss (2000) made the first estimates from macroalgae and seaweed biomass leading to CHBr_3 production, added them with non kelp emission rates and extrapolate the combination onto a global scale.

Taking into account the geographical distribution of halocarbons global bottom-up emission estimates are calculated. Therefore, measured surface atmospheric and oceanic concentrations of halocarbons are interpolated onto a global scale and have yielded bottom-up emission estimates of between 2.8 and 10.3 Gmol Br yr^{-1} for CHBr_3 and between 0.8 and 3.5 Gmol Br yr^{-1} for CH_2Br_2 (Quack and Wallace, 2003; Yokouchi et al., 2005; Butler et al., 2007; O'Brien et al., 2009). Yokouchi et al. (2005) and O'Brien et al. (2009) extrapolated a measured coastal emission ratio $\text{CHBr}_3/\text{CH}_2\text{Br}_2$ to the globe whereas Quack and Wallace (2003) and Butler et al. (2007) interpolated oceanic and atmospheric in-situ measurements for global emission estimates.

With increasing knowledge of the compounds and computer capacity costly modeling studies of emission estimates which reproduce (measured) background atmospheric concentrations of halocarbons are provided ('top down' approach). These top-down emission estimates range between 5.4 and 7 Gmol Br yr^{-1} for bromoform and between 0.7 and 1.4 Gmol Br yr^{-1} for dibromomethane using different atmospheric transport models (Warwick et al., 2006; Kerkweg et al., 2008; Liang et al., 2010; Pyle et al., 2011; Ordonez et al., 2012). Warwick et al. (2006) modelled surface mixing ratios using e.g. the bottom-up scenario of Quack and Wallace (2003) and fitted them to available atmospheric measurements. Later, based on local measurements in Southeast Asia Pyle et al. (2011) reduced the emission scenario of Warwick et al. (2006) in that region. This study shows the importance of field measurements. A finer classification of the emission estimates is shown in Liang et al. (2010) and Ordonez et al. (2012) where especially the coastlines are considered with higher emission values. Ordonez et al. (2012) were the first who parameterized oceanic

polybromomethanes emissions based on a chl *a* dependent source in the tropical ocean (20° N and 20° S). Additionally, a parameterization for oceanic bromoform concentrations covered by a homogenous atmosphere estimates a flux of 1.45 Gmol yr⁻¹ for CHBr₃ between 30° N and 30° S (Palmer and Reason, 2009).

Model studies and data interpolations estimate global CH₃I emissions between 2.4 and 4.3 Gmol I yr⁻¹ (Bell et al., 2002; Butler et al., 2007; Ordonez et al., 2012). The first seasonal model simulations of global oceanic and atmospheric CH₃I surface concentrations is given by Bell et al. (2002).

Smythe-Wright et al. (2006) extrapolated a laboratory culture experiment with *Prochlorococcus marinus* to a global CH₃I emission estimate of 4.2 Gmol I yr⁻¹, whereas the study of Brownell et al. (2010) disputed the result of Smythe-Wright et al. (2006) and suggests that *P. marinus* is not significant on a global scale.

The wide spread of emission estimates illustrate a large uncertainty especially for CHBr₃. To determine the role in tropospheric and stratospheric chemistry highly resolved and measurement based emission maps of CHBr₃, CH₂Br₂ and CH₃I are needed.

6. Objectives and outline of this dissertation

In recent years, the interest on the distribution of very short lived halogenated substances (VSLS) in ocean and atmosphere and the magnitude of their sea-to-air flux has grown significantly in order to quantify their role in tropospheric and stratospheric ozone loss. As outlined above, many uncertainties exist in their formation processes, sources, sinks and chemical fates in both, the ocean and the atmosphere. Global emission magnitudes and distributions are not well constrained because of their high geographical and temporal variability, and the sparseness of available in-situ measurements which only allows to derive emission estimates at a coarse grid resolution. As a result, global emission estimates of halogenated VSLS are poorly quantified (Hossaini et al., 2010), but are needed as input for atmospheric modeling studies (Figure III–2) for calculating reliable bromine and iodine budgets in both the troposphere and the stratosphere. The tropical ocean was identified to be a key region for enhanced halogenated emissions (Butler et al., 2007) and for the transport of large amounts of VSLS into the stratosphere (Aschmann et al., 2009). The transport of halocarbons and their product gases into the stratosphere depends on several chemical and physical (e.g. wet scavenging and duration of convection) interactions (Liang et al., 2010), which are not fully understood. High uncertainties exist in the parameterization of convection in models (Tost et al., 2010) as well as in the knowledge of the atmospheric lifetime of inorganic iodine (e.g., Dix et al., 2013) or bromine. How and in which way the emissions will change in a future environment and how

they will affect the stratospheric ozone loss is also still unclear. Figure III–12 shows an overview of the present knowledge described above, the uncertainty in the estimates and the gaps.

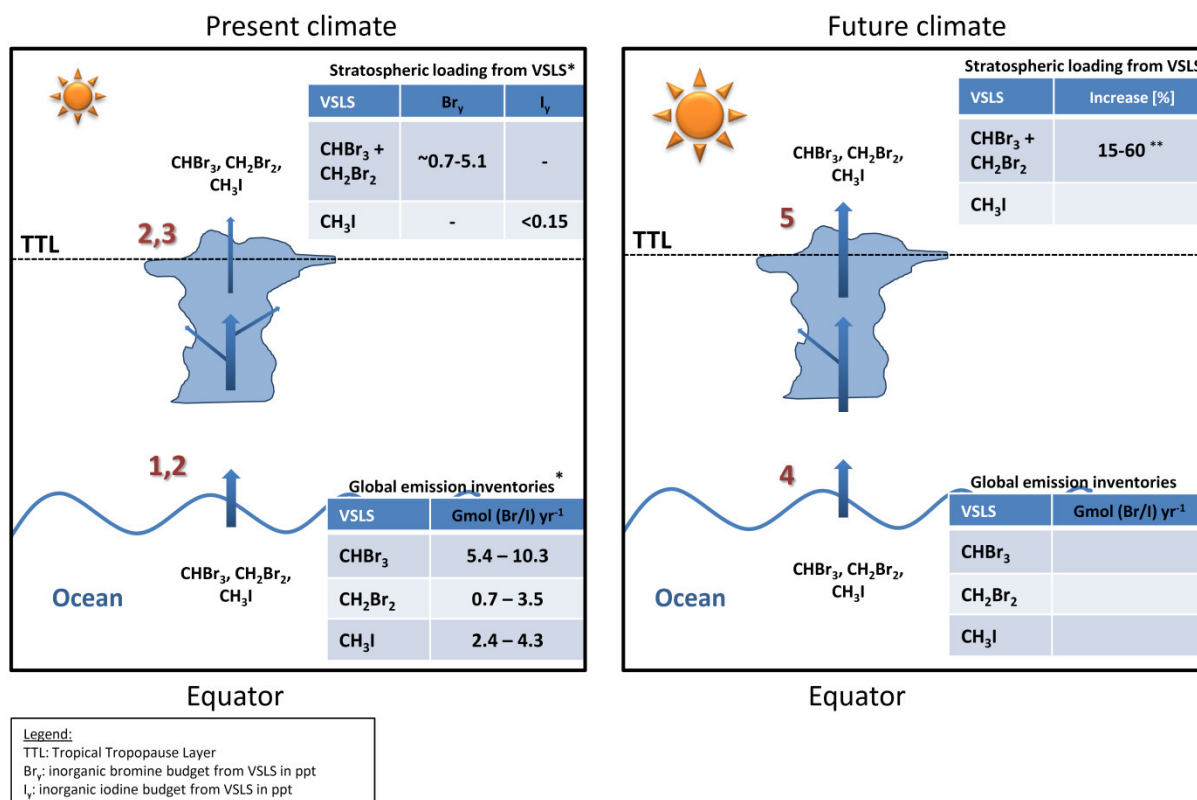


Figure III – 12. Schematic overview of the present knowledge and understanding of VSLs global emission inventories, transport into and loading in the TTL in a present and future climate. The numbers illustrate in which manuscript of the thesis the process is investigated.

* Montzka and Reimann (2011)

** Hossaini et al. (2012b)

This thesis includes the first compilation of existing air and sea water measurements into a data base for halocarbons, the calculation of global CHBr₃, CH₂Br₂ and CH₃I emission estimates based on this comprehensive data set, and an assessment of potential future changes of marine VSLs emissions. Furthermore, the relevance of oceanic CHBr₃, CH₂Br₂ and CH₃I emissions for recent past and future stratospheric ozone is investigated (Figure III–12). The work has been embedded into several projects: The Leibniz (WGL)-project TransBrom (Very short lived bromine compounds in the ocean and their transport pathways into the stratosphere), within the frame of the Pact for Research and Innovation 2009 the EU-project SHIVA (Stratospheric ozone: Halogen Impacts in a Varying Atmosphere SHIVA) supported by the European commission and the **SOPRAN** (Surface Ocean PRocesses in the ANthropocene) project supported by the German Federal Ministry of Education and Research (BMBF). Further, **SOLAS** Integration (Surface Ocean and Lower Atmosphere Study) helped to instigate the data base, also supported by **COST** (European COoperation in Science and

Technology) Action 735. The main research tasks with regard to five manuscripts are described in the next paragraphs.

- 1. Compilation of the global data base HalOcAt based on existing air and sea water measurements of halogenated compounds**
- 2. Production of best estimates of sea-to-air fluxes from a bottom-up approach of three important short-lived halocarbons CHBr_3 , CH_2Br_2 and CH_3I based on HalOcAt**

While global emissions of brominated volatile organic compounds with short atmospheric lifetimes have a significant influence on the bromine and iodine loading of the stratosphere, the magnitude and nature of their sources and oceanic emissions are poorly understood. Emissions estimates based on atmospheric modeling studies (top-down), parameterizations and bottom-up methods show large uncertainties (Section III.5). In order to improve previously derived global emission inventories of the halogenated compounds CHBr_3 , CH_2Br_2 and CH_3I it is necessary to include more measurements in critical regions (e.g., in upwelling and tropical waters). The core and fundament of this thesis is presented in the first manuscript *“Global sea-to-air flux climatology of bromoform, dibromomethane and methyl iodide”*, which includes the publication of the first database for halocarbons **HalOcAt** (**H**alocarbons in the **O**cean and **A**tmosphere) and the calculation of emission inventories of CHBr_3 , CH_2Br_2 and CH_3I on the basis of this new database. Filling the missing values in regions where no measurements are available in order to derive the global estimate is a large challenge, which has been met by finding the most reliable way for inter- and extrapolation based on our limited knowledge.

- 3. Contribution of CHBr_3 and CH_2Br_2 to the stratospheric bromine (Br_y) budget based on global emission inventories – a sensitivity study**

To simulate the inorganic bromine (Br_y) loading of the stratosphere in order to quantify its impact on ozone depletion (Figure III–2) it is necessary to include global emission inventories of the significant marine sources into atmospheric transport models (e.g. chemical transport models (CTM)). Several global emission estimates for CHBr_3 and CH_2Br_2 already exist (Section III.5), which are the results of different calculation techniques and lead to a wide range of stratospheric bromine loading estimates (Section III.4). Three top-down and one bottom-up (first manuscript) emission inventories of CHBr_3 and CH_2Br_2 are used as input for global CTM model runs and the derived atmospheric concentration are compared in both their magnitude and spatial distribution with measurements from aircraft campaigns and at long-term time series from ground based stations. The best agreement has been identified for a combination of different CHBr_3 and CH_2Br_2 emission inventories which are illustrated in the second manuscript *“Evaluating global emission inventories of biogenic bromocarbons”*.

4. Calculation of iodine transport from the tropical surface ocean into the stratosphere based on global CH₃I sea-to-air fluxes

Emission inventories and atmospheric transport of CH₃I are poorly constrained. Emitted into the troposphere, oceanic CH₃I is degraded and involved in several atmospheric iodine cycles or it can be transported into the TTL where it might contribute to ozone degradation. There are no model results for iodine transport from CH₃I in the stratosphere. Aircraft campaigns led to the conclusion that no more than 0.05 ppt of iodine enters the stratosphere in the form of the source gas CH₃I (Montzka and Reimann, 2011). A more significant contribution of oceanic CH₃I to the stratospheric iodine budget in the Western Pacific has been quantified in the third manuscript *“The contribution of oceanic methyl iodide to stratospheric iodine”* by using the emission inventory from the first manuscript and the Lagrangian transport model FLEXPART.

5. Estimating CHBr₃, CH₂Br₂ and CH₃I emissions in a future changing environment

A future increase of stratospheric bromine loading including CHBr₃ and CH₂Br₂ due to intensified vertical transport into the stratosphere has been projected (Pyle et al., 2007, Dessens et al., 2009, Hossaini et al., 2012b). However, the effect of climate change on the oceanic emissions of CHBr₃, CH₂Br₂ and CH₃I is still unknown. The global contemporary maps of oceanic concentrations and atmospheric mixing ratios from the first manuscript were combined with future physical input parameters of two different scenarios from the three CMIP 5 (fifth phase of the Climate Model Intercomparison Project, 2013) models; MPI-ESM-LR, CESM1-CAM5 and HadGEM2-ES (Collins and Knutti et al., 2013) to calculate emission projections of halogenated compounds in the fourth manuscript *“Future emissions of marine halocarbons”*.

6. Determination of future impact of CHBr₃ on stratospheric ozone

The natural ozone-depleting substances with chemical lifetimes of less than 6 months such as CHBr₃ are not controlled by the Montreal Protocol, while they are suggested to increase in the future. Ozone depletion potential (ODP)-weighted emissions illustrate a new possibility to estimate the overall impact on oceanic bromine emissions on stratospheric ozone loss in the future.

The global emission strength of CHBr₃ derived from the fourth manuscript and the ozone-destroying capabilities are combined to calculate ODP - weighted emissions. The ODP-weighted emissions of CHBr₃ were compared to the ODP of long-lived substances in the fifth manuscript *“Oceanic bromine emissions weighted by their ozone depletion potential”*.

METHOD

IV. Method

In the following sections the most complete compilation of existing air and sea water measurements into the first data base for halocarbons is introduced which is used to calculate global CHBr_3 , CH_2Br_2 and CH_3I emissions for the recent past and the future. The challenge is to fill all missing values for the global estimate. Due to low data coverage a new interpolation technique is developed in this thesis considering the biogeochemical character of the VSLs compounds (Section III.1). Further, the air-sea gas exchange flux theory and its conversion to the VSLs compounds with emphasizes on the air-sea gas exchange velocity is presented. The last section focuses on global ongoing environmental changes due to rising anthropogenic greenhouse gases emissions. Based on future model predictions emission estimates of CHBr_3 , CH_2Br_2 and CH_3I are calculated, based on the changing physical forcings of air- sea gas exchange.

1. HalOcAt database

The **HalOcAt** (**Halocarbons in the Ocean and Atmosphere**) database project (<http://halocat.geomar.de>) has been initiated to work with the research community to bring together global oceanic and atmospheric halocarbon data with an emphasis on short-lived brominated and iodinated trace gases from the surface ocean and lower atmosphere. The project aims to utilize data collected during numerous hydrographic cruises and from other relevant platforms and to assemble a global database which would represent a substantial resource that will be made available to the community.

The raw data, which is obtained from individual PI's and data bases, is filled into a predefined template MS EXCEL-sheet in order to extract them with an own MATLAB® script for further calculations. The template involves three parts;

- (i) meta data includes fields for: platform type and name, expedition name, cruise start and end, EXPOCODE, dataset creator, PI contact details, HOST data centre, relevant publications, sampling technique, method, detection limits, calibration technique, used standard, additional data (i. e. wind speed, SST, Chl α) and an extra table for detection limit and precision of every measured halogenated compound
- (ii) atmospheric data and
- (iii) seawater data involve: sample identifier, sampling gear, date, sample start and end, sample depth, bottom depth, water/air temperature, (salinity), quality control comments and the concentrations in ppt or pmol L^{-1} for each measured compound in the atmosphere or in the ocean (CH_3I , CH_2I_2 , $\text{C}_2\text{H}_5\text{I}$, $\text{C}_3\text{H}_7\text{I}$, $\text{C}_4\text{H}_9\text{I}$, CH_3Br , CHBr_3 , CH_2Br_2 , $\text{C}_2\text{H}_5\text{Br}$, CH_3Cl , CHCl_3 , CH_2Cl_2 , C_2HCl_3 , C_2Cl_4 , CH_2ICl , CH_2IBr , CHIBr_2 , CHBr_2Cl , CHBrCl_2)

The quality control is provided by the data set creator. Different analysis techniques and standardization techniques are used for measuring halogenated compounds. Currently, no robust criterion for quality check and data selection was identified and no overall intercalibration control exists due to sparse knowledge about the applied standards and the highly variable compound distributions. As an example, the oceanic and atmospheric measurements of CHBr_3 from the HalOcaT database are shown in figure IV–1.

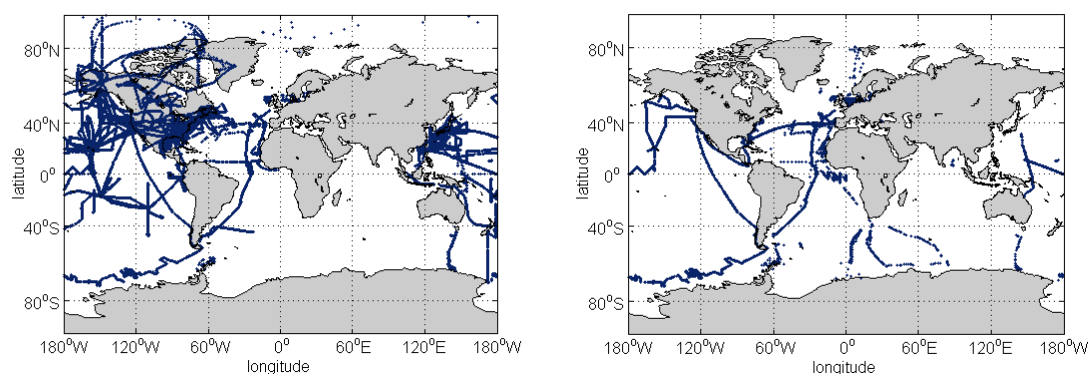


Figure IV – 1. Global distribution of bromoform measurements in the atmosphere (left panel) and in the ocean (right panel) of the HalOcaT database.

1.1. Extrapolation of the HalOcaT data

In this thesis the calculation of global emission fields of the three halogenated compounds bromoform, dibromomethane and methyl iodide started with the generation of global oceanic concentration and atmospheric mixing ratio maps. All available oceanic and atmospheric surface data of CHBr_3 , CH_2Br_2 and CH_3I from the HalOcaT database (Table IV–1) were used to first calculate global maps of the compound CHBr_3 . The global coverage of the surface seawater and atmospheric measurements of the three VSLs compounds are shown in the first manuscript (Ziska et al., 2013). The challenge of filling all missing values for a global estimate, based on limited knowledge, was to find the best and most realistic way for inter- and extrapolation.

Table IV – 1. Number of atmospheric and oceanic data of the halogenated compounds CHBr_3 , CH_2Br_2 and CH_3I from the HalOcaT database (data from 1989 to 2011).

Compound	Amount of atmospheric data	Amount of oceanic data
CHBr_3	5255	5305
CH_2Br_2	5227	4824
CH_3I	4580	4952

DMS (Kettle et al., 1999; Lana et al., 2011) and CO_2 (Takahashi et al., 2009) interpolation methods for the development of global data coverage were considered in our approach of the construction of climatological concentration maps. However, the conversion of the used technique for DMS or CO_2 to the halocarbon dataset was not possible due to less data coverage. The halocarbon database the total number of available

data relating to the mentioned two gases is only 11.2 %, respectively 0.08 % of the aforementioned. Thus the interpolation technique for the halocarbons had to include some further classification(s) and new biogeochemical parameterization to fill the missing data.

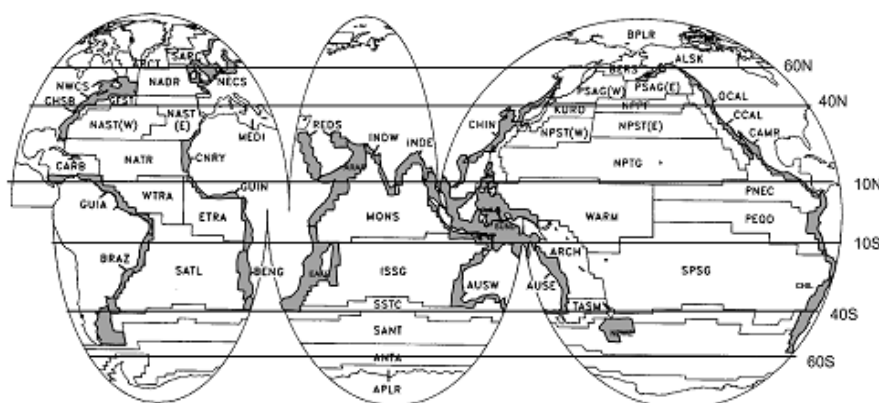


Figure IV – 2. The ocean classification into 57 biogeochemical regions after Longhurst et al. (1995).

As a first approach, the extrapolation of the data was tried applying the Longhurst et al. (1995) classification of the global ocean into biogeochemical regimes (Figure IV–2), as was done earlier with less data (Quack and Wallace, 2003). Longhurst et al. (1995) used information about the hydrographical conditions, oceanographic processes and marine and coastal ecosystems to classify the ocean into 57 biogeochemical provinces, since physical features often control the distribution of organisms, and there is a strong relationship between physical and biological parameters. However, the high resolved Longhurst et al. (1995) classification was discarded, since many regions couldn't be covered with data.

Important information on the biogeochemical distribution of the compound CHBr_3 could be extracted from the data sets, which are for instance higher concentrations in coastal and equatorial upwelling regions ($> 15 \text{ pmol L}^{-1}$), at coast lines ($> 100 \text{ pmol L}^{-1}$) and close to islands, while generally lower and more homogeneous surface concentrations are found in the open ocean ($< 5 \text{ pmol L}^{-1}$). Considering this, all data were divided into coast, shelf and open ocean regimes (coastal and shelf seas are neighboring $1^\circ \times 1^\circ$ each, rest is open ocean). To fill in the remaining gaps linear, cubic and thin-plate smoothing spline interpolation techniques were adapted to the original data in each of the regions and separate for each hemisphere. Figure IV–3 shows the first approach using the linear technique.

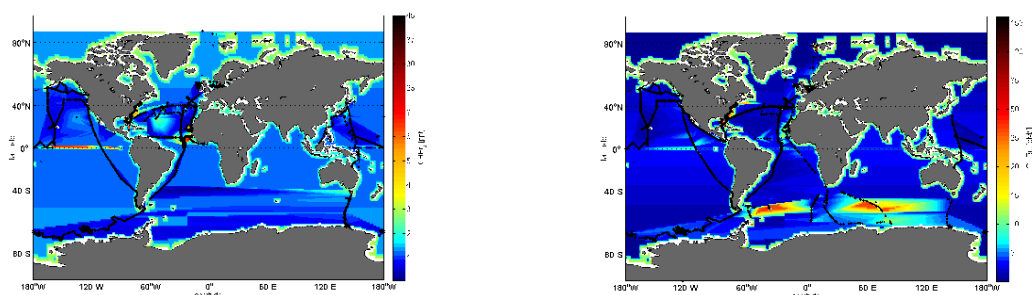


Figure IV – 3. A first assessment of an atmospheric in ppt (left panel) and marine interpolated CHBr₃ sea surface concentrations in pm L⁻¹ (=pmol L⁻¹) (right panel) from HalOcat data, based on a linear interpolation into Longhurst et al. (1995) biogeochemical regimes, including a regression analysis of open ocean, shelf and coastal latitudinal gradients.

Other extrapolation methods will be tested, since the regionally sharp boundaries and temporal homogeneity of regional data, seem unlikely (Figure IV–3). In fact, only 4 % of the global ocean is covered with existing data on the 1° x 1° grid, thus 96 % are inter-and extrapolated.

The data division into coast, shelf and open ocean data seemed plausible and was maintained for a next approach. Further, a Gauss-Marcow-Smoothing was used to transfer the data into the global 1° x 1° grid and to broaden the dataset. This technique calculates the grid point percentage of the surrounding data position, which is located in the discrete Gaussian bell area. Because of the homogeneity of the open ocean the Gaussian Bell area is wider (3°) than for the coast or shelf region (1°) (Figure IV–4).

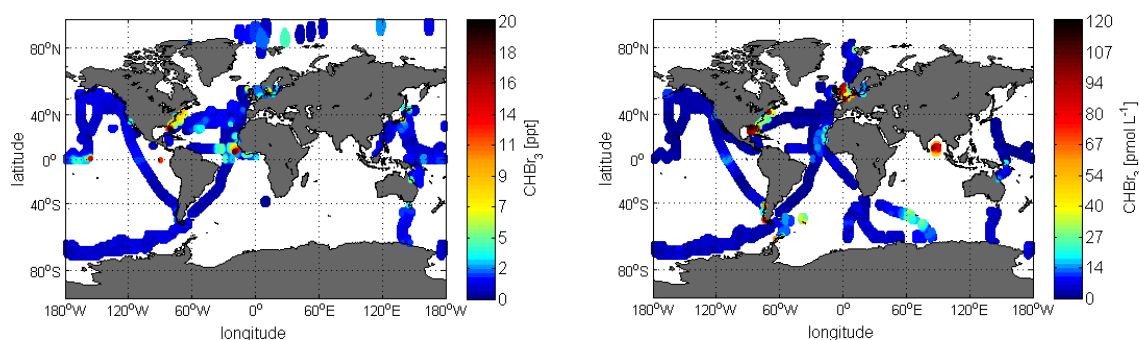


Figure IV – 4. Transferring the original data onto 1°x1° grid and boarding the data set with the Gauss-Marcow Smoothing technique to calculated global surface atmospheric CHBr₃ mixing ratios in ppt (left panel) and marine CHBr₃ concentration map in pmol L⁻¹ (right panel). A figure of the original data is shown in the first manuscript (Ziska et al., 2013).

Open ocean surface CHBr₃ concentrations in the ocean and atmosphere show a latitudinal and longitudinal variation. For the further extrapolation of the data, the open ocean data of the ocean and atmosphere were divided into four atmospheric and four oceanic latitudinal regions for each hemisphere (Figure IV–5) as well as into four ocean basins (Figure IV–6) in order to take the physical

and biogeochemical character of the marine surface waters into account (more details are described in the first manuscript Ziska et al. (2013)).

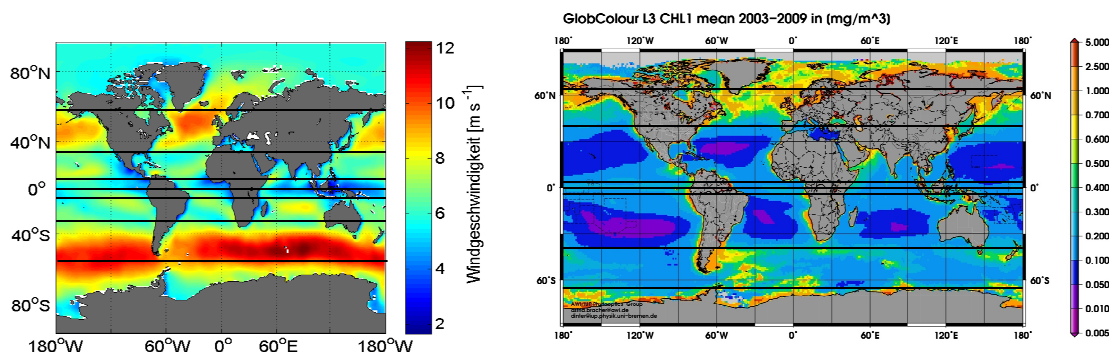


Figure IV – 5. Latitudinal classification of the atmosphere based on the global climatologically mean wind fields (1989-2011) and of the ocean based on the surface chl a climatology from 2003-2009 (right panel, T. Dinter, personal communication).

After the two classifications 21 *open ocean* regions exist in each atmosphere and ocean. Due to high variability of the open ocean data the use of multi linear regressions depending on the latitude and longitude is described in detail in the first manuscript (Ziska et al., 2013). Based on the produced regression equations every missing value was calculated. The fit for the coastal and shelf regions was calculated over both entire hemispheres. The gridded data from the Gauss-Marcow-Smoothing and the multi-linear regression extrapolation were combined to derive the global surface concentration maps of CHBr_3 in the ocean and atmosphere. Since the classifications were roughly related to biogeochemical and physical ocean regimes, the global maps of CH_3I and CH_2Br_2 were calculated and extrapolated in the same way.

Besides the above described extrapolation of the existing data, different parameterizations for the reproduction of the measured surface data were tested. However, correlations of biological, physical and chemical parameters of individual cruises

or the global data set yield until now no satisfying results. The marine bromoform parameterization of Palmer and Reason (2009) (Section III.5) was applied on cruise data and time series measured in different ocean basins (Quack and Wallace, 2003 and references therein, Ekdahl et al., 1998, Butler et al., 2007 and J. H. Butler, unpublished data from 1992–2001) and showed, negative concentrations above 30° north and south and is thus not useful for a global approach.

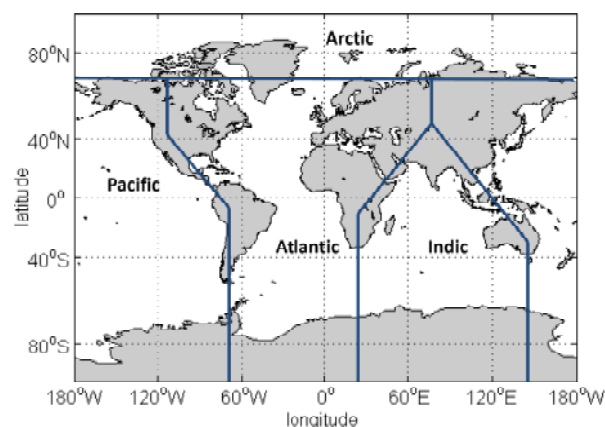


Figure IV – 6. Longitudinal classification of the ocean and atmosphere into the basins Arctic, Atlantic, Pacific and Indian Ocean

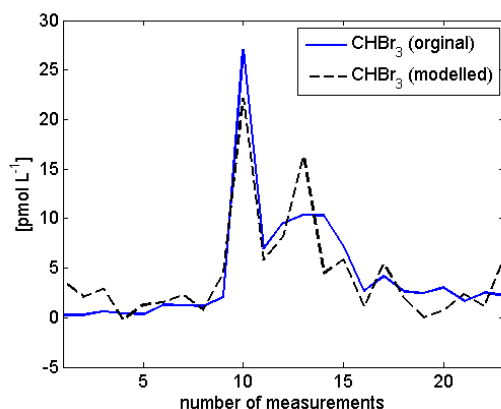


Figure IV – 7. First approach determining a parameterization of marine CHBr_3 based on the measured biological compounds chlorophyll c1+2, lutein and alpha carotene. Blue line indicates the original CHBr_3 data (transit cruise in the West Pacific) and the black dashed line the modeled CHBr_3 value.

Additionally, the (multiple) linear regression technique “stepwise fit” on different cruise parameters (e.g. longitude, latitude, mixed layer depth, Chl a , U, SST, SSS, pigments) was applied in order to parameterize oceanic CHBr_3 concentrations. The best parameterization of CHBr_3 was found as linear combination of three pigments chlorophyll c1+2, lutein and alpha carotene (Figure IV–7). However, this correlation was only seen for one cruise in the western Pacific (Krüger and Quack, 2012). Further, these parameters are not available for global fields for the past or the future.

2. Air-sea gas exchange

Air-sea gas exchange is important for the biogeochemical cycling of elements and for climate and weather. Increasing uptake of CO_2 (from the atmosphere to the ocean) due to anthropogenic pollution or the exchange of water vapor from the ocean to the atmosphere producing different types of clouds (regulation of radiation transfer), are only two processes illustrating the global relevance of the air-sea-gas exchange mechanism.

On regional and global scale the air-sea gas exchange is the most important sink mechanisms for CHBr_3 , CH_2Br_2 and CH_3I from the oceanic mixed layer (Section III.1). This process can also act as a source for the compound into the ocean, if the surface water is under saturated, which can be the case especially in colder regions due to the large variability of the compounds sources and concentrations (Garbe et al., 2014).

The theory of a two-layer model for the mechanism of air-sea gas exchange was introduced by

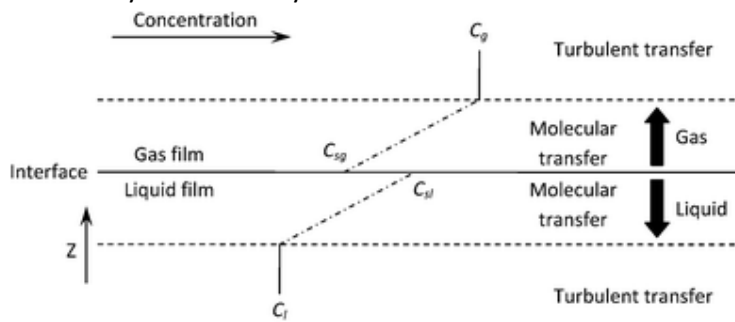


Figure IV – 8. Two-layer model of a gas-liquid interface (See text for further explanations) (Liss and Slater, 1974)

Whitman (1923) and is still used in modified form. A simplified schematic of the gas-liquid interface model to parameterize gas exchange is presented by Liss and Slater (1974) (Figure IV–8). Both medium the gas and the liquid are assumed to be turbulent well-mixed and

separated by a laminar interface. Since the transport near the interface takes place by molecular diffusion (Liss and Slater, 1974), Fick's first law in the one-dimensional form describes the flux F of a gas through the layer with thickness z and shows the common form of the air-sea gas exchange equation:

$$F = k (C_w - C_a H^1) \quad (\text{equation 1})$$

where k is the air - sea gas exchange velocity and C_w presents the measured concentration at the liquid phase and C_a at the gas phase.

Table IV - 2. Henry' law coefficients of CHBr_3 , CH_2Br_2 and CH_3I . SST is the sea surface temperature in Kelvin.

Compound	Henry's coefficient
CHBr_3	$\exp\left(13.16 - \frac{4973}{\text{SST}[\text{K}]}\right)$
CH_2Br_2	$\exp\left(11.7 - \frac{4418}{\text{SST}[\text{K}]}\right)$
CH_3I	$\exp\left(13.22 - \frac{4338}{\text{SST}[\text{K}]}\right)$

For the three compounds there exist several parameterizations for the dimensionless Henry's law constant (H) (e.g. Mackay and Shiu, 1981; Hunter et al., 1983; Staudinger and Roberts, 1996). In this thesis the parameterization calculated by Moore et al., (1995a, b) is used because they determined H by direct measurements. Henry' law coefficients of CHBr_3 , CH_2Br_2 and CH_3I are listed in table IV–2. H described the solubility of a (volatile) compound in the liquid phase and is highly

temperature dependent. The transfer of gases and particles across the air-sea interface depends not only on the concentration differences, but on the efficiency of the transfer process which is influenced by several factors which are described in the following section.

2.1. The gas transfer velocity

The gas transfer velocity k is a key variable in air-sea gas exchange calculation, but there still exist a lot of uncertainties in their determination.

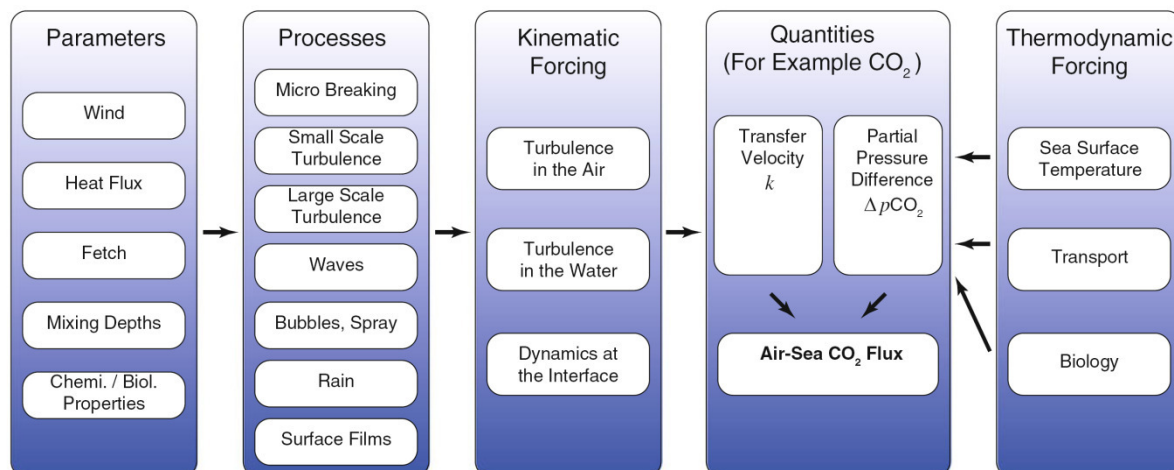


Figure IV – 9. Simplified schematic of environmental and thermodynamic forcing factors that affect air-sea CO₂ fluxes (Garbe et al., 2014).

A variety of techniques to measure the gas transfer velocity directly in the environment have established through the years. The most used types are: small scale measurements including particle-based (i.e. Siddiqui and Loewen, 2010; Garbe et al., 2012) and thermographic techniques (i. e. Haußecker and Jähne, 1995; Garbe et al., 2003, 2004), micrometeorological techniques (eddy-covariance and eddy accumulation method) and the mass balance technique (including inventory calculation of radiocarbon ¹⁴C (Sweeney et al., 2007; Wanninkhof, 1992), the radon deficit method by using the tracers ²²²Rn and ²²⁶Ra (Peng et al., 1979) and simultaneous injection of the two volatile tracers ³He and SF₆).

No direct flux measurements exist for CHBr₃, CH₂Br₂ and CH₃I since the analytical techniques are not developed yet, to determine halocarbons extremely rapid in their low concentrations.

Another possibility for determining the gas exchange velocity is the use of a parameterization. The major processes influencing the air-sea transfer velocity are shown in figure IV–9 (as example for CO₂). A lot of studies showed a strong relationship between gas exchange velocity and the wind speed/stress. The first wind speed dependent parameterization was presented by Liss and Slater (1974) by laboratory experiments. One key uncertainty is the functional relationship of the wind speed to the transfer velocity (linear, quadratic, cubic, polynomial).

A comparison of different wind speed relationships from mass balance techniques are shown in figure IV–10. The estimates present a wide range of uncertainties approximately a factor of 2 at an average wind speed of 7 m s⁻¹ (Garbe et al., 2014).

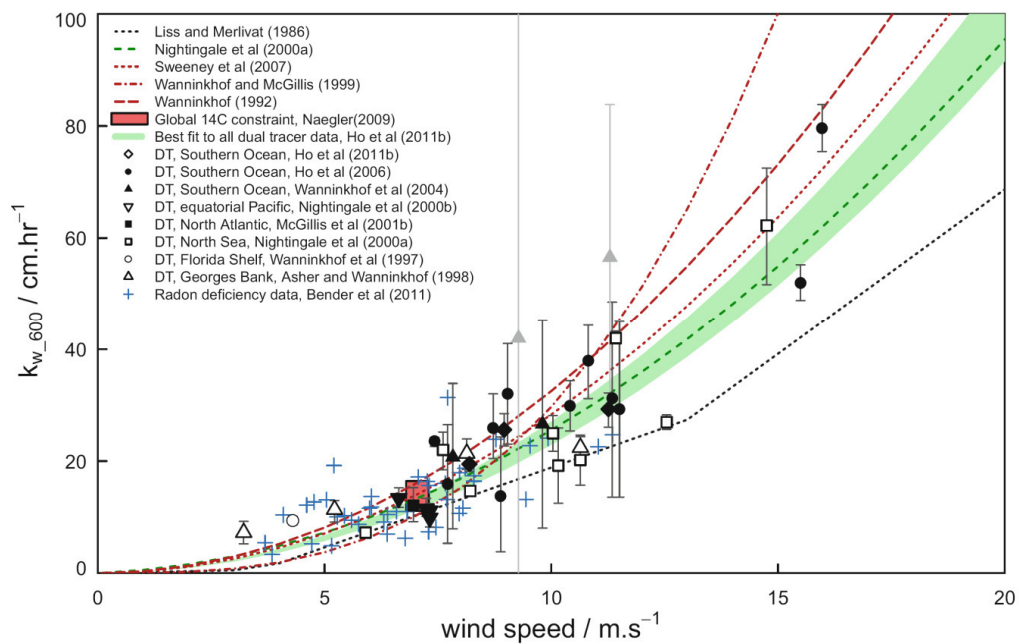


Figure IV – 10. Comparison of different wind speed relationships of the water-side transfer velocity from mass balance techniques (Ho et al., 2011b).

Compared to other mass balance techniques and parameterizations (Figure IV–10), the one of Nightingale et al. (2000) is within the “best fit” (95 % confidence interval) of Ho et al., (2011) over the wind speed range 5-17 m s⁻¹ and that’s why used in this thesis:

$$k_{600} = 0.222U^2 + 0.333U \quad (\text{equation 2})$$

Nightingale et al. (2000) injected two volatile tracers ³He and SF₆ containing very different diffusion coefficients in the North Sea (mass balance technique). The gas exchange of ³He is faster than SF₆ and so the ratio ³He/SF₆ will decrease with time, while dilution will not alter the ³He/SF₆ ratio.

More than the parameter wind speed has been taken into account to parameterize the gas exchange velocity, like the influence of bubbles, sea spray and waves by high wind speeds.

The dimensionless Schmidt number Sc describes the viscosity of sea water and is the ratio of the diffusion coefficient *D* of the compound and the kinematic viscosity *ν* of sea water, and depends mainly on the sea surface temperature (SST) and the salinity. The diffusion coefficients are not known for the halogens CHBr₃, CH₂Br₂ and CH₃I, therefore they have to be estimated from the common relation Sc = 600 for CO₂ (for freshwater at 20 °C) to their Sc with a power law dependent of n = - 0.5 (for wind speeds above 3.6 m s⁻¹ (Nightingale et al., 2000)) (according to Quack and Wallace, 2003):

$$k = k_{600} (600Sc^{-1})^n \quad (\text{equation 3})$$

The Schmidt numbers for the three halogenated compounds were calculated as a mean between the methods described in Hayduk and Laudie (1974) and Wilke and Chang (1955) and are listed in table IV–3.

Table IV – 3. Schmidt numbers for CHBr_3 , CH_2Br_2 and CH_3I

Compound	Schmidt number Sc
CHBr_3	$\frac{\nu}{193 \times 10^{-10} \times \text{SST}^2 + 1686 \times 10^{-10} \times \text{SST} + 403.42 \times 10^{-8}}$
CH_2Br_2	$\frac{\nu}{193 \times 10^{-10} \times \text{SST}^2 + 1686 \times 10^{-10} \times \text{SST} + 403.42 \times 10^{-8}}$
CH_3I	$\frac{\nu}{2.5 \times 10^{-9} \times \text{SST}^2 + 1.76 \times 10^{-7} \times \text{SST} + 4.2 \times 10^{-6}}$

3. Earth under global change

The Earth's climate system is balanced by several feedbacks and complex interaction between incoming shortwave radiation (SWR), outgoing longwave radiation (LWR) and atmospheric gases and aerosols (Figure IV–11). The Earth's energy budget ensures a global mean temperature of $\sim 14^\circ\text{C}$ and enables life in different forms.

On-going anthropogenic emissions of greenhouse gases, particularly CO_2 , and of large aerosols ($>2.5 \mu\text{m}$ in size), inhibit the outgoing of LWR to space by absorbing. Further, the human change of vegetation cover and land-use modify the amount of back scatter SWR (surface albedo). These combined processes led to an increase of the global mean surface air temperature over land and ocean by 0.3 to 0.6°C over the last 100 years (Cubasch and Wuebbles et al., 2013). The Earth's response in modifying the balance between SWR and LWR are complex internal feedbacks, which could strengthen (i.e. water vapor feedback) or weaken (i.e. blackbody radiation feedback) the change in climate forcing. The timescale of the feedbacks vary between fast and now to slow up to millennia. How, and in which way the environmental processes will change is unclear. Sea level rise and an oceanic pH decrease have been observed: Mesocosm experiments (Riebesell et al., 2007) which are used as tools to get a view into the future development of biological, physical and chemical processes in the ocean showed marginal effects of ocean acidification on marine CHBr_3 , CH_2Br_2 and CH_3I concentrations (Hopkins et al., 2013). However, future changes of oceanic production and its influence on VSLs production are poorly investigated. The ongoing environmental

changes will influence the production and destruction of marine compounds as well as their transport from the ocean to the stratosphere (Behrenfeld et al., 2006, Bopp et al., 2012).

Another possibility to determine environmental changes under various future scenarios is the use of modeling studies which allow a projection to the year 2300. The fifth phase of the Climate Model Intercomparison Project (CMIP 5) includes several state-of-the-art models and is part of the 5th IPCC (Intergovernmental Panel on Climate Change) report. Goals of the 5th IPCC report (Collins and Knutti et al., 2013) are to model realistic recent past simulations and to calculate and evaluate future projections. Different scenarios, *Representative Concentration Pathways*, (RCP 2.6, RCP 4.5 and RCP 8.5 (Figure IV–12)) are available for investigating varying future developments (van Vuuren et al., 2011).

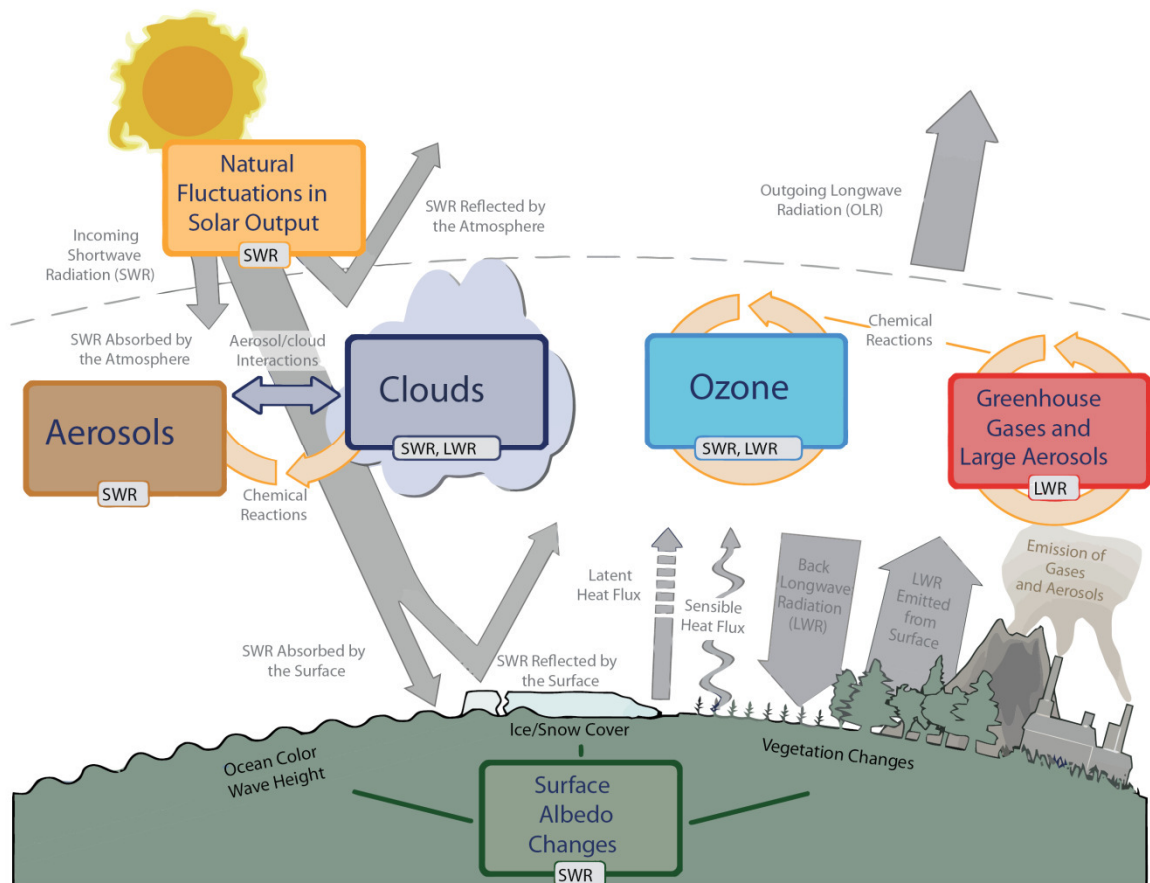


Figure IV - 11. Simple schematic of the main drivers of climate change (more description in the text). (Cubasch and Wuebbles et al., 2013).

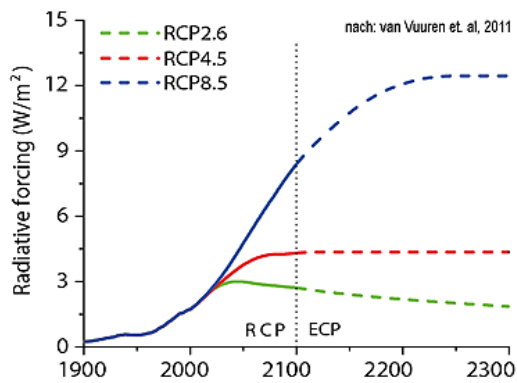


Figure IV - 12. Diagram of the three different Radiative forcings (RCPs) (van Vuuren et al., 2011).

Earlier model results using the IPCC scenarios IS92a (Leggrett et al., 1992), SRES A2 (Nakicenovic et al., 2000) and RCP 4.5 and 8.5 (van Vuuren et al., 2011) projected a future increase of stratospheric bromine loading including CHBr_3 and CH_2Br_2 due to higher atmospheric vertical transport into the tropical stratosphere (Pyle et al., 2007; Dessens et al., 2009; Hossaini et al., 2012b). However, these

models do not consider future changes in halogenated sea-to-air fluxes. In this thesis, the outputs of three CMIP 5 models are used, including

their historical runs (1979-2005) and their future RCP scenarios 2.6 and 8.5 for the years 2006-2100 to calculate emission projections of CHBr_3 , CH_2Br_2 and CH_3I , based on the changing physical forcings of air- sea gas exchange. The results and calculation techniques are described in detail in the fifth manuscript (Ziska et al., 2014, *in prep*)



MANUSCRIPTS

V. Manuscripts

1. Manuscript

Global sea-to-air flux climatology of bromoform, dibromomethane and methyl iodide

F. Ziska^{1*}, B. Quack¹, K. Abrahamsson², S. D. Archer³, E. Atlas⁴, T. Bell⁵, J. H. Butler⁶, L. J. Carpenter⁷, C. E. Jones^{7,21}, N. R. P. Harris⁸, H. Hepach¹, K. G. Heumann⁹, C. Hughes¹⁰, J. Kuss¹¹, K. Krüger¹, P. Liss¹², R. M. Moore¹³, A. Orlikowska¹¹, S. Raimund¹⁴, C. E. Reeves¹², W. Reifenhäuser¹⁵, A. D. Robinson⁸, C. Schall¹⁶, T. Tanhua¹, S. Tegtmeier¹, S. Turner¹², L. Wang¹⁷, D. Wallace¹³, J. Williams¹⁸, H. Yamamoto^{19,22}, S. Yvon-Lewis²⁰, Y. Yokouchi¹⁹

[1] GEOMAR, Helmholtz-Zentrum für Ozeanforschung Kiel, Kiel, Germany

[2] Department of Analytical and Marine Chemistry, Chalmers University of Technology and Gothenburg University, Gothenburg, Sweden

[3] Plymouth Marine Laboratory, Plymouth, PMI, Plymouth, United Kingdom now at Bigelow Laboratory of Ocean Sciences, USA

[4] Marine and Atmospheric Chemistry, Rosenstiel School of Marine and Atmospheric Science, University of Miami, MAC, Miami, USA

[5] Department of Earth System Science, University of California, UCI, Irvine, United States of America

[6] Earth System Research Laboratory, Global Monitoring Division, ESRL/NOAA, Boulder, USA

[7] Department of Chemistry, University of York, York, YO10 5DD, United Kingdom

[8] Department of Chemistry, University of Cambridge, Cambridge, CB2 1EW, UK, Cambridge, United Kingdom

[9] Institut für Anorganische Chemie und Analytische Chemie, Johannes Gutenberg-Universität, JGU, Mainz, Germany

[10] Laboratory for Global Marine and Atmospheric Chemistry, University of East Anglia, LGMAC/UEA, Norwich, United Kingdom

[11] Institut für Ostseeforschung Warnemünde, IOW, Rostock-Warnemünde, Germany

[12] School of Environmental Science, University of East Anglia, Norwich, United Kingdom

- [13] Department of Oceanography, Dalhousie University, Halifax, Canada B3H 4R2
- [14] CNRS, UMR 7144, Equipe Chim Marine, Stn Biol Roscoff, F-29680 Roscoff, France now at:
GEOMAR, Helmholtz-Zentrum für Ozeanforschung Kiel, Kiel, Germany
- [15] Bayerisches Landesamt für Umwelt, Augsburg, Germany
- [16] Fresenius Medical Care Deutschland GmbH, Frankfurterstrasse 6-8, 66606 St. Wendel
- [17] Rutgers State University of New Jersey, New Brunswick, USA
- [18] Max Planck Institute for Chemistry, Air Chemistry Department, MPI, Mainz, Germany
- [19] National Institute for Environmental Studies, Tsukuba, Ibaraki 305-0053, Japan
- [20] Department of Oceanography, Texas A&M University, College Station, United States of America
- [21] now at: Graduate School of Global Environmental Studies, Kyoto University, Yoshida-Honmachi,
Sakyo-ku, Kyoto 606-8501, Japan
- [22] now at: Marine Works Japan, Ltd., Oppamahigashi, Yokosuka 237-0063, Japan

Published in: Atmospheric Chemistry and Physics, 13, 8915-8934, doi: 10.5194/acp-13-8915-2013,
2013



Global sea-to-air flux climatology for bromoform, dibromomethane and methyl iodide

F. Ziska¹, B. Quack¹, K. Abrahamsson², S. D. Archer^{3,*}, E. Atlas⁴, T. Bell⁵, J. H. Butler⁶, L. J. Carpenter⁷, C. E. Jones^{7,**}, N. R. P. Harris⁸, H. Hepach¹, K. G. Heumann⁹, C. Hughes¹⁰, J. Kuss¹¹, K. Krüger¹, P. Liss¹², R. M. Moore¹³, A. Orlikowska¹¹, S. Raimund^{14,***}, C. E. Reeves¹², W. Reifenhäuser¹⁵, A. D. Robinson⁸, C. Schall¹⁶, T. Tanhua¹, S. Tegtmeier¹, S. Turner¹², L. Wang¹⁷, D. Wallace¹³, J. Williams¹⁸, H. Yamamoto^{19,****}, S. Yvon-Lewis²⁰, and Y. Yokouchi¹⁹

¹GEOMAR, Helmholtz-Zentrum für Ozeanforschung Kiel, Kiel, Germany

²Department of Analytical and Marine Chemistry, Chalmers University of Technology and Gothenburg University, Gothenburg, Sweden

³Plymouth Marine Laboratory, Plymouth, PMI, Plymouth, UK

⁴Marine and Atmospheric Chemistry, Rosenstiel School of Marine and Atmospheric Science, University of Miami, MAC, Miami, USA

⁵Department of Earth System Science, University of California, UCI, Irvine, USA

⁶Earth System Research Laboratory, Global Monitoring Division, ESRL/NOAA, Boulder, USA

⁷Department of Chemistry, University of York, York, YO10 5DD, UK

⁸Department of Chemistry, University of Cambridge, Cambridge, CB2 1EW, UK, Cambridge, UK

⁹Institut für Anorganische Chemie und Analytische Chemie, Johannes Gutenberg-Universität, JGU, Mainz, Germany

¹⁰Laboratory for Global Marine and Atmospheric Chemistry, University of East Anglia, LGMAC/UEA, Norwich, UK

¹¹Institut für Ostseeforschung Warnemünde, IOW, Rostock-Warnemünde, Germany

¹²School of Environmental Science, University of East Anglia, Norwich, UK

¹³Department of Oceanography, Dalhousie University, Halifax, B3H 4R2, Canada

¹⁴CNRS, UMR7144, Equipe Chim Marine, Stn Biol Roscoff, 29680 Roscoff, France

¹⁵Bayerisches Landesamt für Umwelt, Augsburg, Germany

¹⁶Fresenius Medical Care Deutschland GmbH, Frankfurterstraße 6–8, 66606 St. Wendel, Germany

¹⁷Rutgers State University of New Jersey, New Brunswick, USA

¹⁸Max Planck Institute for Chemistry, Air Chemistry Department, MPI, Mainz, Germany

¹⁹National Institute for Environmental Studies, Tsukuba, Ibaraki 305-0053, Japan

²⁰Department of Oceanography, Texas A&M University, College Station, USA

* now at: Bigelow Laboratory of Ocean Sciences, Maine, USA

** now at: Graduate School of Global Environmental Studies, Kyoto University, Yoshida-Honmachi, Sakyo-ku, Kyoto 606-8501, Japan

*** now at: GEOMAR, Helmholtz-Zentrum für Ozeanforschung Kiel, Kiel, Germany

**** now at: Marine Works Japan, Ltd., Oppamahigashi, Yokosuka 237-0063, Japan

Correspondence to: F. Ziska (fziska@geomar.de)

Received: 13 December 2012 – Published in Atmos. Chem. Phys. Discuss.: 27 February 2013

Revised: 14 July 2013 – Accepted: 21 July 2013 – Published: 6 September 2013

Abstract. Volatile halogenated organic compounds containing bromine and iodine, which are naturally produced in the ocean, are involved in ozone depletion in both the troposphere and stratosphere. Three prominent compounds transporting large amounts of marine halogens into the atmosphere are bromoform (CHBr_3), dibromomethane (CH_2Br_2) and methyl iodide (CH_3I). The input of marine halogens to the stratosphere has been estimated from observations and modelling studies using low-resolution oceanic emission scenarios derived from top-down approaches. In order to improve emission inventory estimates, we calculate data-based high resolution global sea-to-air flux estimates of these compounds from surface observations within the HalOCat (Halocarbons in the Ocean and Atmosphere) database (<https://halocat.geomar.de/>). Global maps of marine and atmospheric surface concentrations are derived from the data which are divided into coastal, shelf and open ocean regions. Considering physical and biogeochemical characteristics of ocean and atmosphere, the open ocean water and atmosphere data are classified into 21 regions. The available data are interpolated onto a $1^\circ \times 1^\circ$ grid while missing grid values are interpolated with latitudinal and longitudinal dependent regression techniques reflecting the compounds' distributions. With the generated surface concentration climatologies for the ocean and atmosphere, global sea-to-air concentration gradients and sea-to-air fluxes are calculated. Based on these calculations we estimate a total global flux of 1.5/2.5 Gmol Br yr^{-1} for CHBr_3 , 0.78/0.98 Gmol Br yr^{-1} for CH_2Br_2 and 1.24/1.45 Gmol Br yr^{-1} for CH_3I (robust fit/ordinary least squares regression techniques). Contrary to recent studies, negative fluxes occur in each sea-to-air flux climatology, mainly in the Arctic and Antarctic regions. "Hot spots" for global polybromomethane emissions are located in the equatorial region, whereas methyl iodide emissions are enhanced in the subtropical gyre regions. Inter-annual and seasonal variation is contained within our flux calculations for all three compounds. Compared to earlier studies, our global fluxes are at the lower end of estimates, especially for bromoform. An under-representation of coastal emissions and of extreme events in our estimate might explain the mismatch between our bottom-up emission estimate and top-down approaches.

1 Introduction

Halogen (fluorine, chlorine, bromine, iodine)-containing volatile organic compounds play an important role in tropospheric (Vogt et al., 1999; von Glasow et al., 2004) and stratospheric chemical cycles (Solomon et al., 1994; Salawitch et al., 2005). The ocean is the largest source of natural bromine- and iodine-containing halocarbons (Quack and Wallace, 2003; Butler et al., 2007; Montzka and Reimann, 2011). When emitted into the atmosphere, these compounds,

comprising mainly very short-lived species (VLSL) having an atmospheric lifetime of less than 0.5 yr, contribute to the pool of reactive halogen compounds via photochemical destruction and reaction with hydroxyl radicals (von Glasow, 2008). Deep convection, especially in the tropics, can transport VLSL above the tropical tropopause layer (Aschmann et al., 2009; Tegtmeier et al., 2012, 2013) and into the stratosphere, where they influence stratospheric ozone destruction (Salawitch et al., 2005; Sinnhuber et al., 2009). Reactive bromine and iodine are more efficient in destroying stratospheric ozone than chlorine (e.g. Chipperfield and Pyle, 1998).

The absence of global emission maps of VLSL as input for chemistry transport models and coupled chemistry climate models is a key problem for determining their role in stratospheric ozone depletion. The most widely reported short-lived halogenated compounds containing bromine in both the atmosphere and the ocean are bromoform (CHBr_3) and dibromomethane (CH_2Br_2). Together, they may contribute $\sim 15\text{--}40\%$ to stratospheric bromine (Montzka and Reimann, 2011), with CHBr_3 considered to be the largest single source of organic bromine (Penkett et al., 1985) to the atmosphere. Its production involves marine organisms such as macroalgae and phytoplankton (Gschwend et al., 1985; Nightingale et al., 1995; Carpenter and Liss, 2000; Quack et al., 2004). CH_2Br_2 is formed in parallel with biological production of CHBr_3 in seawater (Manley et al., 1992; Tokarczyk and Moore, 1994) and, therefore, generally correlates with oceanic and atmospheric bromoform (e.g. Yokouchi et al., 2005; O'Brien et al., 2009), although it occasionally shows a different pattern in the deeper ocean indicating its different cycling in the marine environment (Quack et al., 2007). Large variability in the $\text{CH}_2\text{Br}_2:\text{CHBr}_3$ ratio has been observed in sea water and atmosphere, while elevated concentrations of both compounds in air and water are found in coastal regions, close to macroalgae and around islands, as well as in oceanic upwelling areas (Yokouchi et al., 1997, 2005; Carpenter and Liss, 2000; Quack and Wallace, 2003; Quack et al., 2007). Seasonal variations have been observed in coastal regions (Archer et al., 2007; Orlikowska and Schulz-Bull, 2009), however the database is insufficient to resolve a global temporal dependence. Anthropogenic sources, such as water chlorination, are locally significant, but relatively small on a global scale (Quack and Wallace, 2003). There is uncertainty in the magnitude of the global emission flux, and the formation processes are poorly known. Recent studies have revealed a missing source of ~ 5 pptv inorganic bromine in the stratosphere, which could possibly be explained by the contribution of oceanic VLSL (Sturges et al., 2000; Sinnhuber and Folkins, 2006; Dorf et al., 2008).

Atmospheric modelling studies have derived top-down global estimates of between 5.4 and 7 Gmol Br yr^{-1} for bromoform and between 0.7 and 1.4 Gmol Br yr^{-1} for dibromomethane using different atmospheric transport models (Warwick et al., 2006; Kerkweg et al., 2008; Liang et al.,

2010; Ordonez et al., 2012). Global bottom-up emission estimates based on the interpolation of surface atmospheric and oceanic measurements have yielded emission estimates of between 2.8 and 10.3 Gmol Br yr⁻¹ for CHBr₃ and between 0.8 and 3.5 Gmol Br yr⁻¹ for CH₂Br₂ (Carpenter and Liss, 2000; Yokouchi et al., 2005; Quack and Wallace, 2003; Butler et al., 2007). Additionally, a parameterization for oceanic bromoform concentrations covered by a homogenous atmosphere estimates a flux of 1.45 Gmol yr⁻¹ for CHBr₃ between 30° N and 30° S (Palmer and Reason, 2009).

Methyl iodide is mainly emitted from the ocean and is characterized as a dominant gaseous organic iodine species in the troposphere (Carpenter, 2003; Yokouchi et al., 2008). This compound is involved in important natural iodine cycles, in several atmospheric processes such as the formation of marine aerosol (McFiggans et al., 2000), and has been suggested to contribute to stratospheric ozone depletion in case it reaches the stratosphere through deep convection (Solomon et al., 1994). Current model results of Tegtmeier et al. (2013) suggest an overall contribution of 0.04 ppt CH₃I mixing ratios at the cold point and a localized mixing ratio of 0.5 ppt. Enhanced oceanic concentrations of CH₃I are found in coastal areas where marine macroalgae have been identified as the dominant coastal CH₃I source (e.g. Manley and Dastoor, 1988, 1992; Manley and dela Cuesta, 1997; Laturus et al., 1998; Bondu et al., 2008). Phytoplankton, bacteria and non-biological pathways, such as photochemical degradation of dissolved organic carbon, are significant open ocean sources (Happell and Wallace, 1996; Amachi et al., 2001; Richter and Wallace, 2004; Hughes et al., 2011). Terrestrial sources, such as rice paddies and biomass burning, are suggested to contribute 30 % to the total atmospheric CH₃I budget (Bell et al., 2002). Modelling studies and data interpolation estimate global CH₃I emissions between 2.4 and 4.3 Gmol I yr⁻¹ (Bell et al., 2002; Butler et al., 2007; Ordonez et al., 2012). Smythe-Wright et al. (2006) extrapolated a laboratory culture experiment with *Prochlorococcus marinus* (kind of picoplankton) to a global CH₃I emission estimate of 4.2 Gmol I yr⁻¹, whereas the study of Brownell et al. (2010) disputed the result of Smythe-Wright et al. (2006) and suggests that *P. marinus* is not significant on a global scale.

This study presents the first global 1° × 1° climatological concentration and emission maps for the three important VLS bromoform, dibromomethane and methyl iodide based on atmospheric and oceanic surface measurements available from the HalOcAt (Halocarbons in the Ocean and Atmosphere) database project (<https://halocat.geomar.de/>). According to current knowledge of the compounds' distributions and possible sources, we classify the data based on physical and biogeochemical characteristics of the ocean and atmosphere. The interpolation of the missing values onto the 1° × 1° grid with two different regression techniques is analysed. Based on the generated marine and atmospheric surface concentration maps, global climatological emissions are

calculated with a commonly used sea-to-air flux parameterization applying temporally highly resolved wind speed, sea surface temperature, salinity and pressure data. The results are compared to estimates of other studies, and the temporal and spatial variability of the climatological sea-to-air flux are discussed. The aim of this study is to provide improved global sea-to-air flux maps based on in situ measurements and on known physical and biogeochemical characteristics of the ocean and atmosphere in order to reduce the uncertainties in modelling the contribution of VLS to the stratospheric halogen budget (Hamer et al., 2013; Hossaini et al., 2013; Tegtmeier et al., 2013).

2 Data

In this study, CHBr₃, CH₂Br₂ and CH₃I data are extracted from the HalOcAt database (<https://halocat.geomar.de/>, see Supplement for a list of all data). The database currently contains about 200 contributions, comprising roughly 55 400 oceanic and 476 000 atmospheric measurements from a range of oceanic depths and atmospheric heights of 19 different halocarbon compounds (mainly very short-lived brominated and iodinated trace gases) from 1989 to 2011. The dataset mainly consists of data from coastal stations, ship operations and aircraft campaigns. The individual datasets are provided by the dataset creators. Since the compound distribution is too variable and the current data are too sparse to identify a robust criterion for quality check and data selection, no overall quality and intercalibration control on the database exists. Future work is planned to use common standards and perform laboratory intercalibrations (Butler et al., 2010; Jones et al., 2011). Thus, we use all available surface ocean values to a maximum depth of 10 m (5300 data points) and atmospheric values to a maximum height of 20 m (4200 data points) from January 1989 until August 2011 (Fig. 1) for the calculation of the climatological concentrations. For sea-to-air flux calculations (see Sect. 3.5), 6-hourly means of wind speed (U), sea level pressure (SLP) and sea surface temperature (SST) are extracted from the ERA-Interim meteorological assimilation database (Dee et al., 2011) for the years 1989–2011 (1° × 1°), whereas salinity (SSS) is taken from the World Ocean Atlas 2009 (Antonov et al., 2010).

3 Methodology

3.1 Approach

The high variability of VLS (especially for CHBr₃) in both ocean and atmosphere is not explicable with any correlation to common parameterizations. Production pathways with associated production rates and reliable proxies for the compounds' distributions are not available. We tested correlations, multiple linear regressions and polynomial fits with biological and physical parameters (e.g. chlorophyll a , SST,

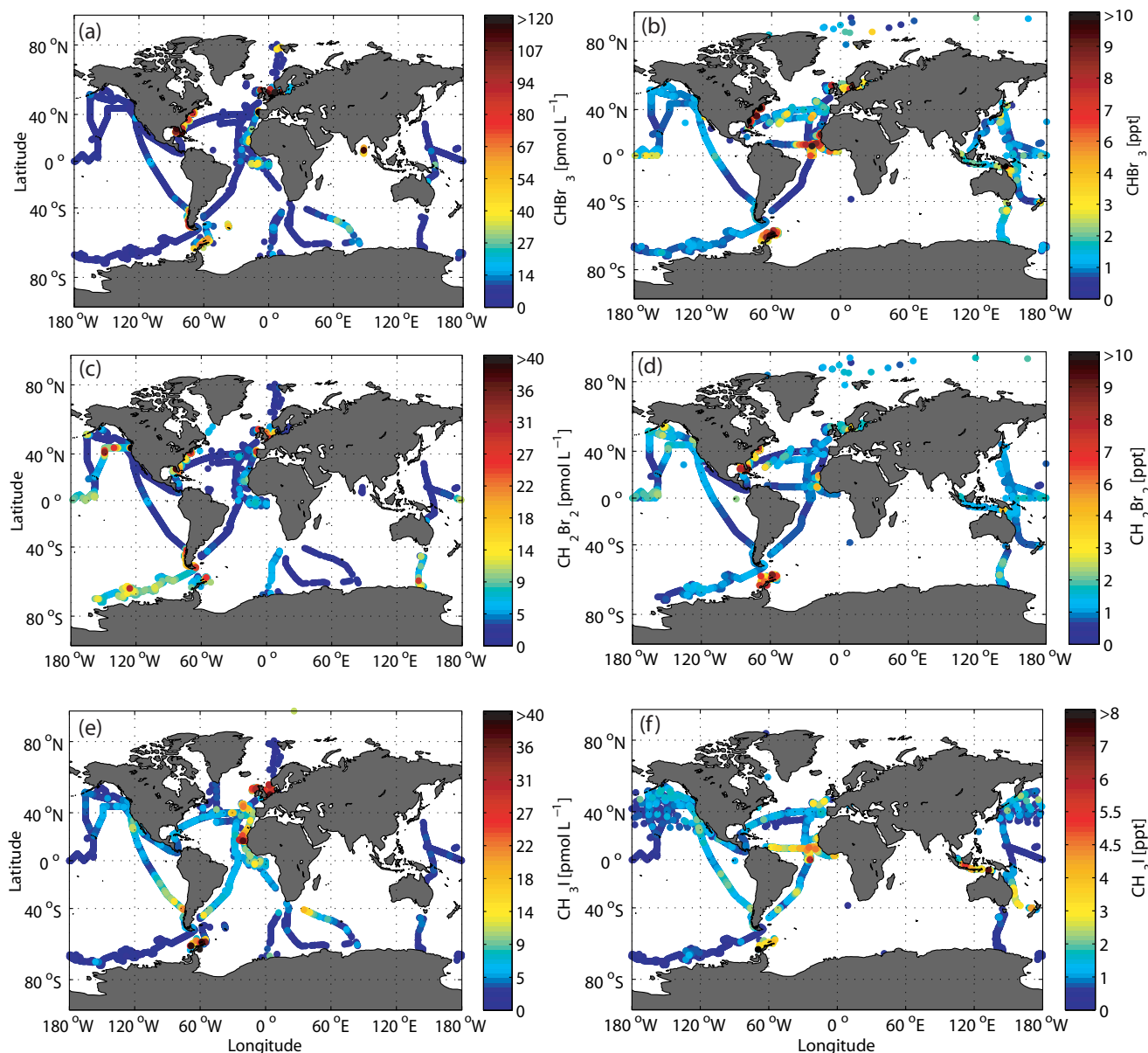


Fig. 1. Global coverage of available surface seawater measurements in pmol L^{-1} and atmospheric measurements in ppt for bromoform (a, b), dibromomethane (c, d) and methyl iodide (e, f) from the HalOcat database project (data from 1989 to 2011).

SSS, SLP, mixed layer depth) to interpolate the data. Since none of the techniques provided satisfying results, we choose to simplify our approach. In order to compute climatological concentration maps, information on the compounds' distributions is extracted from the existing datasets of the HalOcat database and the literature on source distributions. Both surface ocean and atmospheric CHBr_3 concentrations are generally higher in productive tropical regions, at coast lines and close to islands, while generally lower and more homogeneous concentrations are located in the open ocean (Fig. 1). The global ocean shows a latitudinal and longitudinal variation of biological regimes, driven by circula-

tion and regionally varying nutrient input as well as light conditions. Productive eastern boundary upwelling, equatorial and high latitudinal areas are separated by low productive gyre regions. We therefore separated the ocean in different latitudinal bands and applied (multiple) linear regressions between the compounds' distributions and latitude and longitude (see more details in Sect. 3.3). The linear regressions reflect the underlying coarse distribution of the data, and their longitudinal and latitudinal concentration dependence within different biogeochemical and physical regimes appears to be the current best available approach for data analysis and interpolation. This approach is independent of

additional variables, reasonably reflecting the current knowledge about the compounds' distributions considering different biogeochemical oceanic regions and minimizes the creation of non-causal characteristics. The existing data are interpolated onto a $1^\circ \times 1^\circ$ grid. The missing grid values are filled using the latitudinal and longitudinal dependent regression techniques. The climatological oceanic and atmospheric surface concentration maps are used to calculate global fields of concentration gradients and sea-to-air fluxes.

3.2 Classification

All data are divided into coastal, shelf and open ocean regimes. The coastal area is defined as all first $1^\circ \times 1^\circ$ grid points next to the land mask, while the shelf regime comprises all second grid points neighbouring the coastal one. The other grid points belong to the open ocean water and atmosphere regime. The data from coastal and shelf regions are very sparse. For this reason, they are only separated between Northern Hemisphere and Southern Hemisphere.

The open ocean water data are further divided into 4 regions for each hemisphere. The inner tropics (0 to 5°) include the equatorial upwelling regions with high biomass abundance and elevated CHBr_3 concentrations, especially in the eastern ocean basins. The subtropical gyres, with descending water masses and hence low biological production at the surface, are identified as the second region (5 to 40°). The third region comprises the temperate zones between 40 to 66° with higher climatological surface chlorophyll concentrations than in the gyre region and decreasing water temperature and increasing CHBr_3 concentrations towards higher latitudes. The fourth region (poleward of 66°) encompasses the polar Arctic and Antarctic with cold surface waters and occasional ice cover.

The open ocean atmosphere is classified in a slightly different way from that of the open ocean waters. The inner tropical region (here from 0 to 10°) is characterized by the intertropical convergence zone, upward motion, low pressure and deep convection. Additionally, each hemisphere is divided into 3 wind regimes: subtropics (10 to 30°), midlatitudes (30 to 60°) (westerlies, storm tracks) and polar regions (60 to 90°), characterized by distinctive air masses, wind directions and weather conditions.

The open ocean regimes (oceanic and atmospheric) are further subdivided into the Atlantic, Pacific, Indian and Arctic basins. Thus, the HalOcAt data is sorted into 21 different regions for surface open ocean water and atmosphere (see Tables S1 and S2 in the Supplement). Gridding the data and inserting missing values is described in the following section. Dibromomethane has been reported to have similar source regions as CHBr_3 , (Yokouchi et al., 2005; O'Brien et al., 2009), while methyl iodide is reported to also have coastal, planktonic and photochemical sources (Hughes et al., 2011; Moore et al., 1994; Richter and Wallace, 2004). Both compounds are also tight to unrevealed direct or indirect biolog-

ical processes. Thus, we divide the CH_2Br_2 and CH_3I data between the regions in the same way as we have classified the CHBr_3 data. The data density for dibromomethane and methyl iodide is equivalent to that of bromoform (Fig. 1).

3.3 Objective mapping

The original, irregular measurements from the HalOcAt database are transferred to a uniform global $1^\circ \times 1^\circ$ grid using a Gaussian interpolation. Based on this technique the value at each grid point is calculated with the measurements located in a defined Gaussian range. The Gaussian bell radius is 3° for the surface open ocean water and atmosphere data and 1° for the coast and shelf region. The wider radius for the open ocean regimes are caused by the higher homogeneity of the data in this region. This kind of interpolation takes the spatial variance of the measurements into account. The smaller the distance between a given data point and the grid point, the greater is its weighting in the grid point calculation (Daley, 1991) (see Supplement for a list of all calculated atmospheric and oceanic grid points based on objective mapping). For grid points where no measurements are available within the Gaussian bell area, no concentration data can be calculated directly and a linear regression needs to be applied.

3.4 Linear regression

Data gaps on the $1^\circ \times 1^\circ$ grid are filled based on a multiple linear regression technique using the original dataset, applying the functional relationship between latitude and longitude as predictor variables, x_1 and x_2 , and compound concentration as the response variable, y (Fig. 2, for specific details see Sect. 3.5).

The regression coefficients for each defined oceanic and atmospheric region are given in Tables S1 and S2 in the Supplement. For regions where the spatial coverage of the data is extremely poor, a first order regression based on the latitude variable only is used. For regions without data or in case the interpolation does not produce reasonable results (e.g. concentrations calculated with the regression are negative), the linear regression of neighbouring open ocean regions of the same latitudinal band is used to fill the data gaps, assuming similar physical and biogeochemical conditions. For example, no data exist for the tropical Indian Ocean (0 – 5° N), thus, open ocean data from the tropical Atlantic and Pacific (0 – 5° N) are used to determine the missing values. Since data coverage in coastal and shelf regions is low, the regression coefficients are calculated over each entire hemisphere. Additionally, we apply the root mean square error (RMSE), calculated as the difference between the predicted values and the observed data, as a measure of accuracy. A small RMSE reflects a low bias and variance of the predicted values, with zero indicating that the regression techniques predict the observations perfectly.

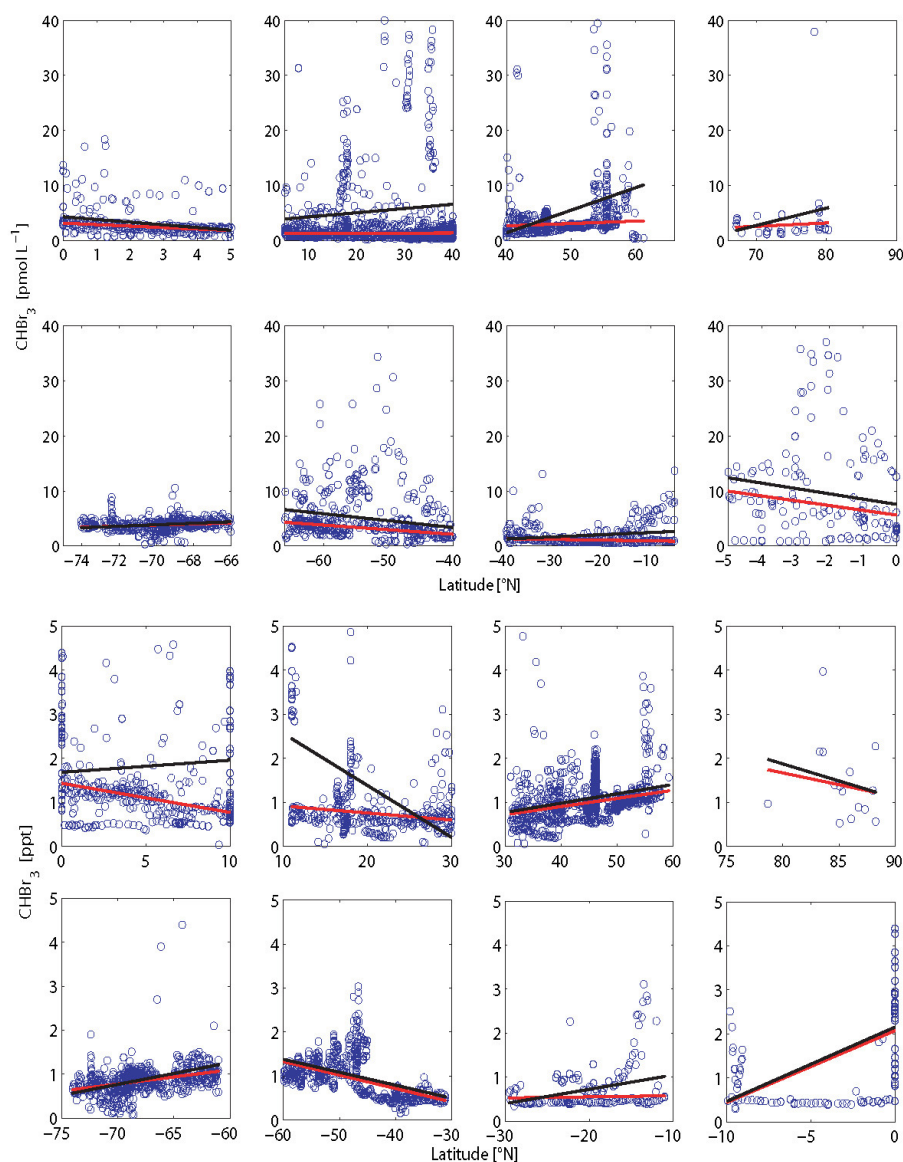


Fig. 2. Latitudinal distribution of open ocean water (a) (pmol L^{-1}) and atmosphere (b) (ppt) bromoform concentrations (blue circles) classified in eight different latitudinal bands. The robust fit (RF) (red line) and ordinary least squares (OLS) (black line) regression analyses are included.

3.5 Robust fit vs. ordinary least squares

In our study, two different regression techniques are applied. The ordinary least squares (OLS) technique contains the least squares method. This means that the sum of squared deviations between the empirical y values in the dataset and the predicted linear approximation is minimized.

The second method for calculating regression coefficients is the robust fit (RF) technique which is especially used for not normally distributed values. A regression analysis is *robust* if it is not sensitive to outliers. The calculation of the robust coefficients is based on the *iteratively reweighted least squares* process. In the first iteration each data point has

equal weight and the model coefficients are estimated using ordinary least squares. In the following iterations, the weighting of the data points is recalculated so that the distant data points from the model regression from the previous iteration are given lower weight. This process continues until the model coefficients are within a predefined range. Our calculations are based on the most common general method of robust regression, the “M-estimation” introduced by Huber (1964).

Both regression methods are shown in Fig. 2 for all latitudinal divided open ocean water and atmospheric measurements for bromoform. The RF regression lines (red) are lower than the OLS (black) and occasionally show different

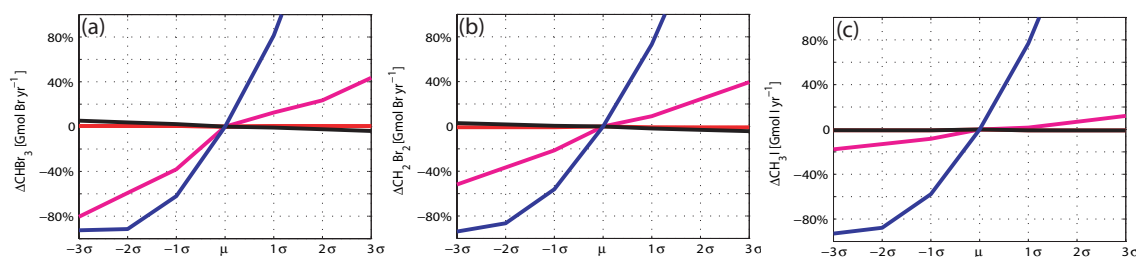


Fig. 3. The percentage change of the global oceanic emission for bromoform (a), dibromomethane (b), both in Gmol Br yr^{-1} , and methyl iodide (c), in Gmol I yr^{-1} , based on individual input parameters: wind speed (blue), sea surface temperature (magenta), sea surface salinity (red) and sea level pressure (black). The input parameters are individually increased and decreased by their multiple standard deviations (-3σ to 3σ) while the other input parameters remain fixed (μ presents the oceanic emission using the mean input parameters).

trends. The reason for the large deviation between the RF and OLS regression is the different weighting of outliers. Outliers crucially influence the value of the OLS slope, whereas the RF regression is located at the largest data density and reduces the influence of outliers. While the RF captures background values, the OLS technique indicates the variability of the data. Based on the obtained concentration maps, global fluxes are calculated and compared to literature values (see Supplement for a list of all calculated atmospheric and oceanic grid points based on linear regression and objective mapping as well as on linear regression only).

3.6 Air–sea gas exchange and input parameters

Fluxes (F in pmol cm h^{-1}) across the sea–air interface are generally calculated as the product of the sea-to-air concentration difference and a gas exchange velocity. The partitioning of a gas between the water and gas phase is described by the dimensionless Henry's law constant (H) which highly depends on temperature and the molecular structure of the species. For our calculations, the Henry's law constants of Moore et al. (1995a, b) are used. The atmospheric mixing ratios (C_m in ppt) are converted to equilibrium water concentrations (C_a in pmol L^{-1}) and the deviation from the actual measured water concentration (C_w in pmol L^{-1}) describes the driving concentration gradient. The sea-to-air flux is negative if the transport is from the atmosphere to the ocean.

$$F = k(C_w - C_a H^{-1}) \quad (1)$$

$$C_a = C_m \cdot \text{SLP} / (\text{SST} + 273.15) / 83.137 \quad (2)$$

$$H = \exp(-4973 / (\text{SST} + 273.15) + 13.16) \text{ for } \text{CHBr}_3 \quad (3)$$

Several parameterizations for the air–sea gas exchange exist in the literature, which express the relationship between the gas exchange velocity (k in cm h^{-1}) and wind speed (e.g. Liss and Merlivat, 1986; Wanninkhof, 1992; Wanninkhof and McGillis, 1999; Nightingale et al., 2000). Experiments have shown that the dominant parameter influencing k is the wind speed. We chose to calculate the transfer coefficients based on the parameterization from Nightingale et al. (2000) with

corrections for the water temperature and a Schmidt number (Sc) dependence for each gas (Quack and Wallace, 2003; Johnson, 2010).

$$k = (0.222U^2 + 0.333U)\text{sqrt}(660Sc^{-1}) \quad (4)$$

The dimensionless Schmidt number is the ratio of the diffusion coefficient of the compound (D in $\text{cm}^2 \text{s}^{-1}$) of interest and the kinematic viscosity (ν in $\text{cm}^2 \text{s}^{-1}$) of sea water, and depends mainly on the temperature and the salinity.

$$Sc = \nu / D \quad (5)$$

$$D = (193 \times 10^{-10} \times \text{SST}^2 + 1686 \times 10^{-10} \times \text{SST} + 403.42 \times 10^{-8}) \text{ for } \text{CHBr}_3 \quad (6)$$

The diffusion coefficients for the compounds were calculated according to Quack and Wallace (2003).

The gas exchange velocity and concentration gradient are dependent on SST, SSS, U and SLP as input parameters. During the initial stages of this study, we used climatological mean values (1989–2011) of the input parameters for our calculation of the global climatological emission estimates. A sensitivity study demonstrates how changes in the input parameters (climatological means) affect the global flux calculation for bromoform, dibromomethane and methyl iodide (Fig. 3). Each input parameter is individually increased and decreased by their multiple standard deviations (-3σ to 3σ) while the other input parameters remain fixed. The standard deviations are calculated for every grid point for the years 1989–2011. This study shows the importance of each input parameter for the flux variance. Sea surface salinity and sea level pressure affects the VSLs emission calculations least compared with the other parameters (Fig. 3). Changes in wind speed and sea surface temperature have strong influences on the bromoform sea-to-air flux. In general, a reduction/enhancement of the wind speed is directly accompanied by a decrease/increase in air–sea gas exchange coefficients, and higher/lower sea surface temperature leads to an increase/decrease of the concentration gradients as well as the air–sea gas exchange coefficients (Schmidt number).

The dependencies of the global dibromomethane emission variability on the individual input parameters are the same as described for bromoform. The global methyl iodide emissions are mainly influenced by variations of the wind speed, while the other parameters have less effect. The sensitivity study shows that marginal changes of the input parameters can lead to a significant variation of the global flux estimate.

Averaging over a long time period when producing climatological means involves smoothing extreme values, which is especially relevant for the wind speed (Bates and Merlivat, 2001). Since the air–sea gas exchange coefficient has a non-linear dependence on wind speed, the application of averaged data fields causes a bias towards a lower flux when compared to using instantaneous winds and averaging the emission maps afterwards (Chapman et al., 2002; Kettle and Merchant, 2005). To reduce the bias, we apply the highest available temporal resolution of the input parameters and calculate 6-hourly global emissions with 6-hourly means of U , SST, SLP and monthly means for the SSS (from January 1989 to December 2011). Finally, we sum the emissions for each month, calculate monthly average emissions over the twenty-one years and summarise these twelve averages to obtain the climatological annual emission.

4 Results and discussion

Marine (pmol L^{-1}) and atmospheric (ppt) global surface concentration maps of bromoform, dibromomethane and methyl iodide calculated with the RF regression are shown in Fig. 4 (surface ocean concentrations and mixing ratios calculated with the OLS technique are illustrated in the Supplement). Based on the RF and OLS marine and atmospheric concentration maps, global sea-to-air flux climatologies are calculated (Fig. 5).

4.1 Climatological concentration maps of CHBr_3 and CH_2Br_2

Marine surface concentrations of bromoform (Fig. 4) are higher in the equatorial region ($\sim 6 \text{ pmol L}^{-1}$), upwelling areas (e.g. the Mauritanian upwelling region $\sim 21 \text{ pmol L}^{-1}$), near coastal areas ($\sim 17\text{--}42 \text{ pmol L}^{-1}$) and in shelf regions ($\sim 8\text{--}32 \text{ pmol L}^{-1}$), consistent with macroalgal and anthropogenic sources along the coast lines as well as biological sources in upwelling areas (Carpenter and Liss, 2000; Quack and Wallace, 2003; Yokouchi et al., 2005; Quack et al., 2007; Liu et al., 2011). The coastal and shelf areas both show a positive latitudinal sea surface concentration gradient for bromoform and dibromomethane towards the polar regions. The coastal sea surface concentrations of bromoform are on average twice as high as in the shelf region. The open ocean generally has homogeneous concentrations between 0.5 and 4 pmol L^{-1} . Lower values are located especially in the sub-

tropical gyres ($\sim 0.5\text{--}1 \text{ pmol L}^{-1}$), most distinctly in the Atlantic, North Pacific and southern Indian Ocean.

Estimating global concentration maps based on an identified linear relationship is difficult in regions with sparse or missing data (e.g. Indian Ocean). Atlantic and Pacific Ocean data must be used to fill the data gap in the Indian Ocean, since no measurements exist there. Thus, we expect similar concentrations as in the other oceans. One dataset is available for the northern Indian Ocean (Yamamoto et al., 2001). The few measurements of bromoform in the Bay of Bengal are unusually high ($> 50 \text{ pmol L}^{-1}$) for an open ocean area. We decided to not include these outliers in our analysis, since our method would possibly overestimate water concentrations in the entire northern Indian Ocean using these data. The high concentrations in the equatorial region (the product of the other two basins) are approximately collocated with the upwelling season during the northeast monsoon, indicating higher productivity (Schott et al., 2002). The global ocean, and especially the Indian and Arctic, is data poor, and requires further sampling and evaluation to improve the predictions. Atmospheric surface mixing ratios of bromoform show similar distribution patterns. Higher atmospheric mixing ratios are located in the equatorial regions (1–3 ppt), around coastlines ($\sim 1\text{--}10$ ppt) and upwelling regions (10–17 ppt), as well as in the northern Atlantic ($\sim 12\text{--}21$ ppt), while lower mixing ratios are found above the subtropical gyres ($\sim 0.2\text{--}0.8$ ppt).

The global surface oceanic concentration map of dibromomethane shows similar patterns as bromoform. Enhanced oceanic surface concentrations are located around the equatorial region ($\sim 6\text{--}9 \text{ pmol L}^{-1}$), while low concentrations occur in the subtropical gyres ($1\text{--}2 \text{ pmol L}^{-1}$), similar to CHBr_3 in distribution, but with higher values. Dibromomethane concentrations in the coastal regions are significantly lower than those for bromoform. Distant from the coastal source regions CH_2Br_2 is mostly elevated in the atmosphere relative to CHBr_3 , because it has a longer atmospheric lifetime than CHBr_3 (e.g. Brinckmann et al., 2012) ($\text{CH}_2\text{Br}_2 = 0.33 \text{ yr}$, $\text{CHBr}_3 = 0.07 \text{ yr}$, (Warneck and Williams, 2012)).

Elevated marine dibromomethane concentrations are found in the Southern Ocean ($4\text{--}6 \text{ pmol L}^{-1}$). This area is characterized by several circumpolar currents separated by frontal systems, with seasonally varying ice coverage, and is known to experience enhanced biological production (Smith and Nelson, 1985). Sea-ice retreat and the onset of microalgae blooms have been related to an increase in marine surface bromocarbon concentrations (Hughes et al., 2009). However, this strong increase of CH_2Br_2 is currently not understood.

The climatological maps represent annual average values that may underestimate seasonal and short-term variations (Hepach et al., 2013; Fuhlbrügge et al., 2013). These variations currently cannot be reflected in the model, since knowledge about production processes and the influence of environmental values on the concentrations is incomplete.

4.2 Climatological concentration maps of CH₃I

The same classification and interpolation technique used for the bromocarbons reveal elevated marine and atmospheric concentrations of methyl iodide (2–9 pmol L⁻¹, 0.3–1.5 ppt) in the subtropical gyre regions of both hemispheres (Fig. 4). This is in contrast to the oceanic concentration maps of bromoform and dibromomethane, and is in agreement with reported production processes, such as photochemical oxidation of dissolved organic matter and iodide, as well as production from cyanobacteria (e.g. Richter and Wallace, 2004; Smythe-Wright et al., 2006).

Additionally, enhanced oceanic concentrations and atmospheric mixing ratios are found in the upwelling region off Mauritania and near the coastlines north of 40° (~9 pmol L⁻¹). Here in the region of offshore trade winds and dust export, the atmospheric methyl iodide from the ocean may be supplemented by input from land sources (Sive et al., 2007) as elevated air concentrations have been noted to be associated with dust events (Williams et al., 2007). The sharp concentration increase towards the coast, as observed for bromoform and dibromomethane, does not exist for methyl iodide. The open ocean concentrations are generally higher than the coastal values, except for the Northern Hemisphere. The elevated coastal oceanic concentrations might be due to the occurrence of macroalgae and anthropogenic land sources (e.g. Laturnus et al., 1998; Bondu et al., 2008) or to elevated levels of dissolved organic material (DOM) (e.g. Manley et al., 1992; Bell et al., 2002). The polar regions show generally homogenous and low concentrations of methyl iodide (Antarctic: ~0.3 ppt, ~1.5 pmol L⁻¹; Arctic: ~1 ppt and ~0.3 pmol L⁻¹).

4.3 Climatological emission maps of CHBr₃ and CH₂Br₂

Elevated bromoform fluxes from the ocean to the atmosphere are generally found close to coastlines, in equatorial and eastern boundary upwelling regions (e.g. the Mauritanian upwelling region) and a wide region of the southern Pacific (subtropical gyre). Very high sea-to-air fluxes (> 1500 pmol m⁻² h⁻¹) also occur in the Bay of Bengal, the Gulf of Mexico, the North Sea and the east coast of North America.

While they cover 16% of the world ocean area, the coastal and shelf regions, with their high biological productivity, have enhanced concentrations of bromoform and dibromomethane and account for 67/78(RF/OLS)% of total Br emission attributable to CHBr₃ and 22/24% of that attributable to CH₂Br₂. Most of the open ocean appears almost in equilibrium with the atmosphere, especially in the subtropical gyre regions. A CHBr₃ flux from the atmosphere to the ocean is seen in the entire Southern Ocean, the northern part of the Pacific and in some parts of the North Atlantic (e.g. east of North America).

Our open ocean flux of CHBr₃ is about 25% of the global sea-to-air flux estimate, which is in agreement with the 20% calculated by Butler et al. (2007) and the 33% of Quack and Wallace (2003). This underlines that the coast and shelf regions play a significant role in the global bromoform budget. The tropics (20° N to 20° S, including open ocean, shelf and coastal area) represent the region with the highest bromoform emissions of 44/55% (Table 3). This is in agreement with the top-down approach of 55.6% between 20° N to 20° S published by Ordonez et al. (2012) and of 37.7% for 10° N to 10° S from Liang et al. (2010). A decrease in the total emission towards the polar region is visible. Hence, the tropics are a “hot spot” for bromoform emissions.

Comparable with the sea-to-air fluxes based on the RF analysis, the emissions using the OLS method shows enhanced sea-to-air fluxes in the North Atlantic and all gyre regions, and an elevated sink in the Arctic region (Fig. 5). We estimate a global positive sea-to-air flux for CHBr₃ of ~2.06 Gmol Br yr⁻¹ (RF), ~2.96 Gmol Br yr⁻¹ (OLS); and a global sink, air-to-sea flux, for CHBr₃ of ~0.56 Gmol Br yr⁻¹ (RF), ~0.47 Gmol Br yr⁻¹ (OLS).

Differences between the distribution of source and sink regions and of CH₂Br₂ emissions calculated with the RF and OLS regression are less pronounced than those of CHBr₃ (Fig. 5). The Arctic Ocean acts mainly as a sink for atmospheric CH₂Br₂, most likely because of the low sea surface temperatures, low water concentrations and higher air concentrations. The Southern Ocean (south of 50° S) acts as a source to the atmosphere. The OLS based emissions show an enhanced source region in the southern Pacific due to elevated marine surface concentrations. We estimate a positive global CH₂Br₂ sea-to-air flux of ~0.89 Gmol Br yr⁻¹ (RF), ~1.09 Gmol Br yr⁻¹ (OLS); and an air-to-sea flux of ~0.12 Gmol Br yr⁻¹ (RF), ~0.11 Gmol Br yr⁻¹ (OLS).

Our total open ocean flux of 0.6–0.76 Gmol Br (CH₂Br₂) yr⁻¹ is in agreement with the estimates of ~0.7 Gmol Br yr⁻¹ given by Ko et al. (2003) and 0.6 Gmol Br yr⁻¹ given by Butler et al. (2007). The coast and shelf regions play a minor role for the global CH₂Br₂ budget compared to the open ocean, which contributes ~77% Gmol Br yr⁻¹. The global emission distribution for CH₂Br₂ and CHBr₃ is similar in the midlatitudes and the tropics. (Table 3). Enhanced source regions for the atmosphere are found in the tropical area contributing about 44/49% between 20° N and 20° S. This is lower compared with the study of Ordonez et al. (2012) who calculated a contribution of 63.1% from 20° N to 20° S. The CH₂Br₂ emissions decrease towards the polar regions.

4.4 Climatological emission maps of CH₃I

The global emissions of CH₃I reveal an opposite pattern compared with CHBr₃ and CH₂Br₂ (Fig. 5). The main difference is the enhanced emission in the subtropical gyre regions.

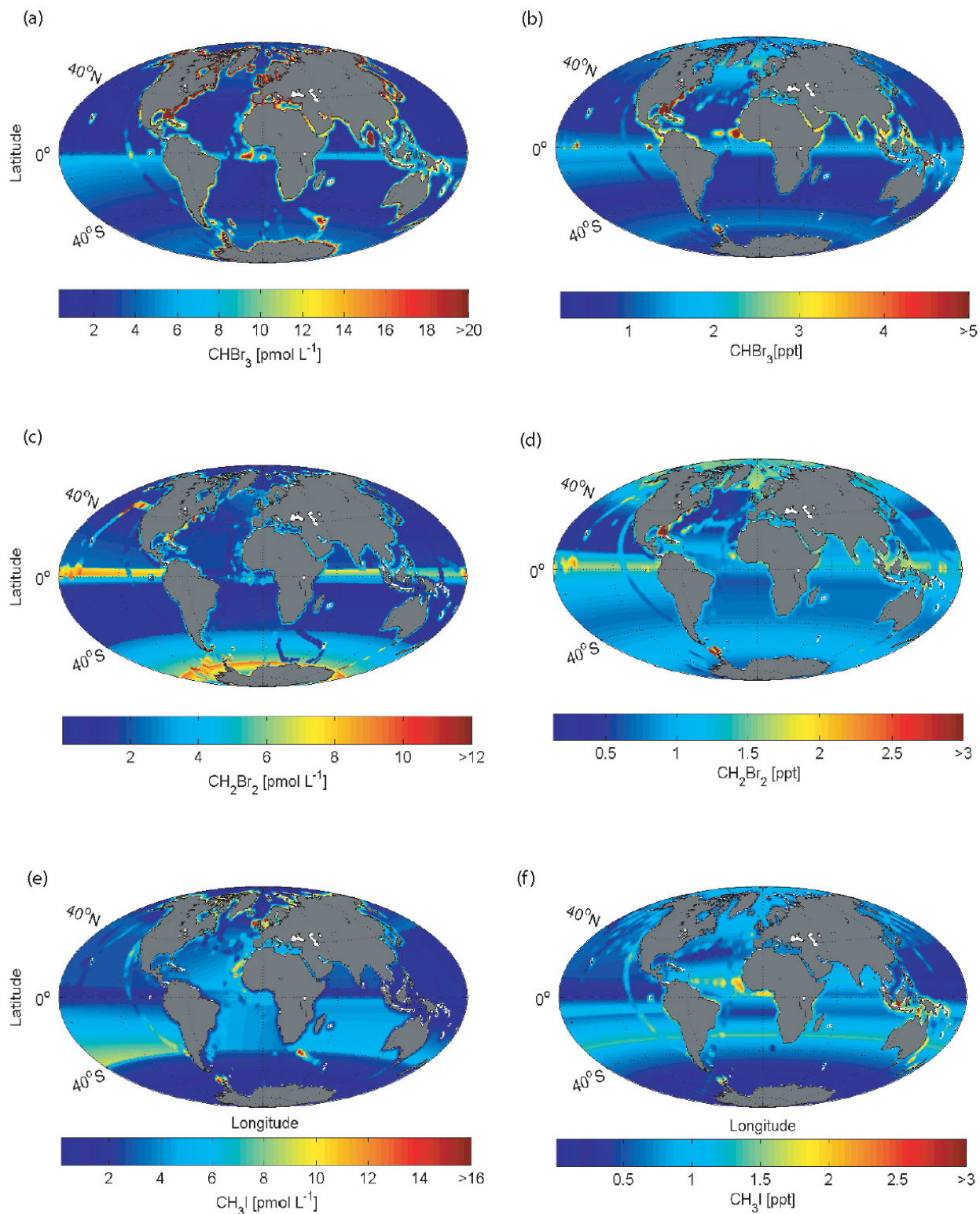


Fig. 4. Global maps of marine concentrations (pmol L^{-1}) and atmospheric mixing ratios (ppt) for bromoform (**a, b**), dibromomethane (**c, d**) and methyl iodide (**e, f**) based on the robust fit (RF) regression analyses. The concentration maps calculated with the OLS method are included in the Supplement (Fig. S3).

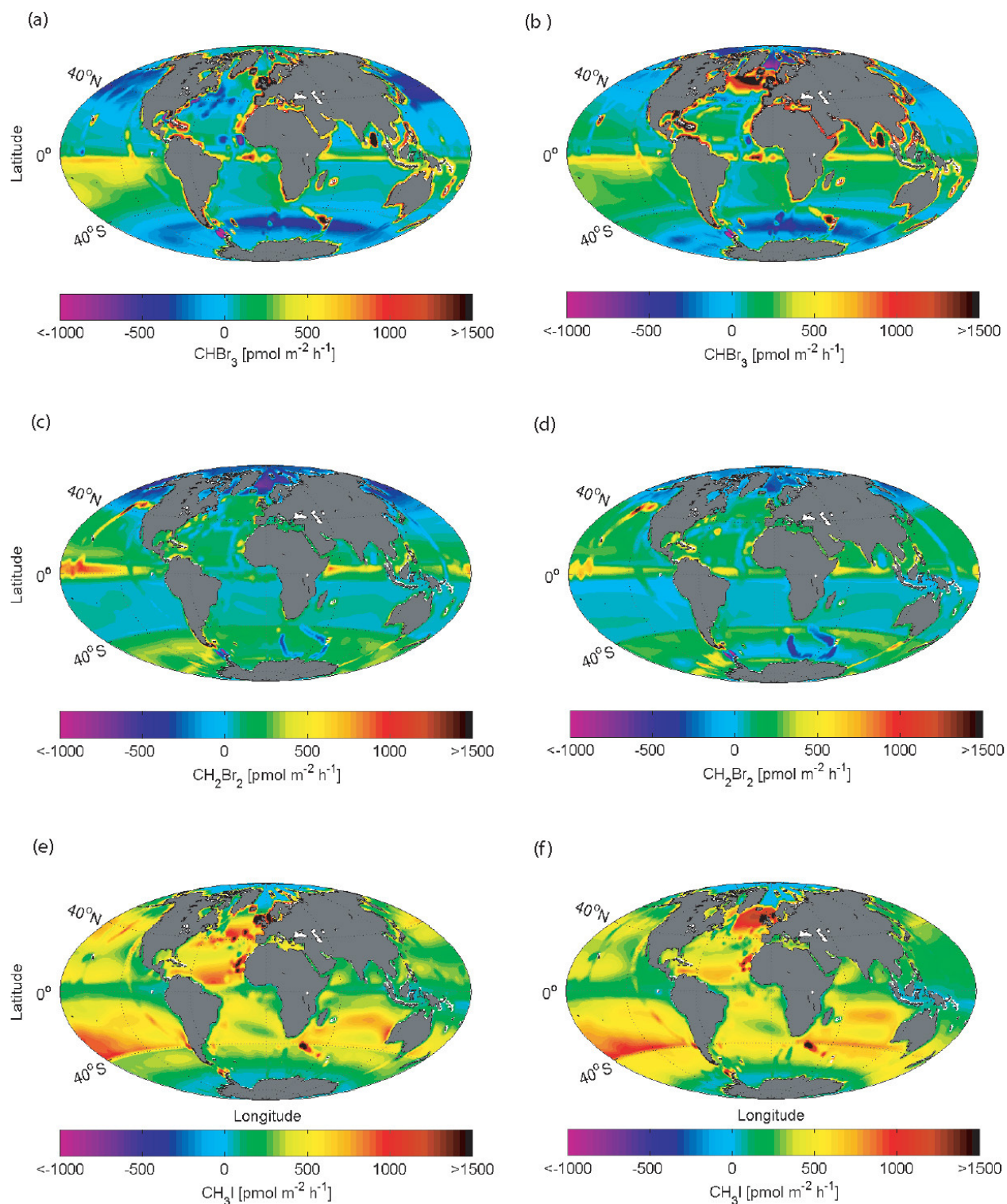


Fig. 5. Global sea-to-air flux climatology of bromoform (a, b), dibromomethane (c, d) and methyl iodide (e, f) in pmol m⁻² h⁻¹ based on the RF (a, c, e, left column) and OLS (b, d, f, right column) analyses.

Equatorial upwelling regions, as well as the Arctic and Antarctic polar regions, are mostly in equilibrium. In comparison with CHBr_3 and CH_2Br_2 , the global CH_3I sea-to-air fluxes are generally positive, indicating the larger supersaturations of the oceanic waters. The OLS regression shows the North Atlantic to be a very strong source region for atmospheric methyl iodide. Coast and shelf regions transport only $\sim 13\%$ of I (CH_3I) to the atmosphere. The open ocean contribution of 87% is more than the estimate from Butler et al. (2007) of 50% open ocean emissions of methyl iodide. Possibly, the subtropical gyre regions are more distinctive source areas in our climatology than in Butler et al. (2007). The southern tropics and subtropics represent the regions with the highest emission strength, decreasing towards the polar areas (Table 3). We calculate a global sea-to-air flux for CH_3I of $\sim 1.24 \text{ Gmol I yr}^{-1}$ (RF) and $\sim 1.45 \text{ Gmol I yr}^{-1}$ (OLS).

4.5 Evaluation of RF and OLS results

All subtropical regions, and especially the equator, show a large temporal and spatial variability in the data, which is reflected in the enhanced RMSE parameter (Tables S1 and S2 in the Supplement). The wide concentration ranges might be caused by real variations between sampling in different seasons, where the seasonally varying strength and expansion of upwelling (equatorial and coastal) (Minas et al., 1982; Hagen et al., 2001) and solar flux may cause different concentrations of the compounds.

The evaluation of the two regression methods shows that RF is more representative of a climatology, since it is calculating a regression independently of outliers and weighted by the data distribution. In comparison, the OLS regression weights outliers, and, hence considers extreme data and variability more than the RF method (Fig. 2). The global appearances of RF and OLS maps are not extremely different (see Supplement). Nevertheless, they introduce slight differences in the concentration gradients and in the sea-to-air flux climatologies.

The influence of the RF and the OLS regression for the global surface concentration distribution in atmosphere and ocean, which has consequences for the concentration gradient, is shown in Table 1 and Fig. 6. In general, the OLS technique calculates higher mean and median values, including the enhanced concentrations and outliers. Additionally, bromoform shows higher variance compared with the other compounds in both techniques and reflects the high data variability between coastal and open ocean bromoform concentrations. Further, the calculated concentration gradient from the OLS method exhibits stronger source (emission into the atmosphere) and weaker sink regions compared with RF, which is again most pronounced for bromoform (Fig. 6). The OLS and RF distribution (mean, median and standard deviation) for dibromomethane and methyl iodide are in closer agreement compared with bromoform. The reason for this

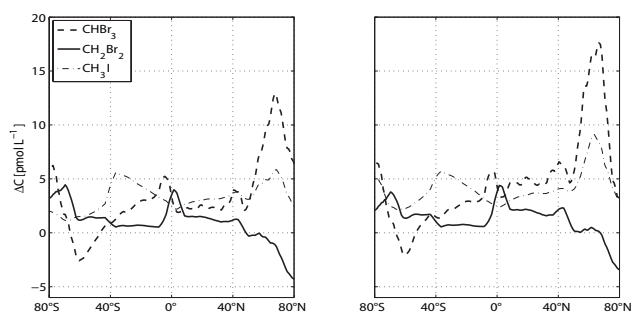


Fig. 6. Zonal mean concentration gradients for bromoform (dashed line), dibromomethane (solid line) and methyl iodide (dash-dotted line) in pmol L^{-1} , calculated with RF (left side) and OLS (right side) methods.

smaller difference between RF and OLS is the occurrence of less extreme values in the concentration gradients for CH_2Br_2 and CH_3I compared with CHBr_3 . The global surface emissions of bromoform, dibromomethane and methyl iodide yield a similar spatial distribution with both techniques (Table 2).

4.6 Comparison of estimation methods

In the following section we compare our emission climatology with recently published estimates, including different calculation techniques (i.e. bottom-up and top-down approaches), as well as laboratory experiments (Table 6). The global bromoform emission estimates show the largest difference between the studies.

Warwick et al. (2006) modelled surface mixing ratios using different emission scenarios and fitted them to the available atmospheric measurements. These scenarios applied different global emission estimates, e.g. the bottom-up estimate from Quack and Wallace (2003). The coarse resolution of $2.8^\circ \times 2.8^\circ$ used in the Warwick study does not well resolve the coastal areas, which are thought to be the main source for bromoform. In addition the applied uniform interpolations do not reflect the actual conditions. In the results of Warwick et al. (2006), the coastlines further north and south of the tropics exhibit no enhanced atmospheric bromoform concentrations or emission to the atmosphere compared to the open ocean. This does not reflect the in situ measurements from the HalOcAt database. Based on local bromoform measurements in Southeast Asia, Pyle et al. (2011) reduced the emission estimate of Warwick et al. (2006) in this coastal area. This study shows the importance of local measurements for the improvement of global estimates. Other model studies based on the ideas of Warwick et al. (2006), e.g. Kerkweg et al. (2008), show the same underestimation of coastal emissions in the extra tropics. In contrast, Liang et al. (2010) consider all coastlines with enhanced emissions in their scenario; furthermore the finer classification of their emission scenario compared with Warwick et al. (2006) is

Table 1. Statistical moments: mean (μ), median, standard deviation (σ), minimum and maximum values of atmospheric mixing ratio (ppt) and oceanic concentration (pmol L^{-1}) climatologies of CHBr_3 , CH_2Br_2 and CH_3I based on the RF and OLS regression analyses.

Compound	μ		Median		σ		Minimum		Maximum	
	RF	OLS	RF	OLS	RF	OLS	RF	OLS	RF	OLS
Atmosphere										
CHBr_3	0.9	1.1	1.0	1.6	1.2	1.6	0.01	0.03	53.1	53.1
CH_2Br_2	1.0	1.1	1.0	1.1	0.4	0.4	0.07	0.07	7.8	7.8
CH_3I	0.7	0.8	0.7	0.7	0.4	0.4	0.05	0.01	7.3	7.3
Ocean										
CHBr_3	5.9	9.3	3.1	4.4	9.8	14.6	0.29	0.19	823.0	823.0
CH_2Br_2	2.9	3.5	1.9	2.6	2.4	2.7	0.01	0.01	89.8	89.8
CH_3I	3.2	3.9	2.6	3.4	2.6	2.9	0.03	0.05	39.6	39.6

Table 2. Statistical moments: mean (μ), median, standard deviation (σ), minimum and maximum values for the calculated global sea-to-air flux climatologies of CHBr_3 , CH_2Br_2 and CH_3I based on the RF and OLS regression analyses, in $\text{pmol m}^{-2} \text{h}^{-1}$.

Global Sea-to-Air Flux Climatology	μ		Median		σ		Minimum		Maximum	
	RF	OLS	RF	OLS	RF	OLS	RF	OLS	RF	OLS
CHBr_3	154.9	236.2	47.1	89.7	549.7	749.6	-5339	-5230	19 618	19 618
CH_2Br_2	76.5	112.4	79.3	78.8	237.9	258.4	-1687	-1714	3978	3978
CH_3I	329.6	405.0	307.3	385.2	289.8	348.3	-49	-55	4895	4878

Table 3. The emission distribution of CHBr_3 , CH_2Br_2 and CH_3I calculated with two different regression methods (RF and OLS) for different latitudinal bands (see text for explanation), expressed as a percentage.

	CHBr_3		CH_2Br_2		CH_3I	
	RF	OLS	RF	OLS	RF	OLS
50–90° N	22.8	21.2	-9.7	-4.9	10.4	7.6
20–50° N	7.4	15.9	13.7	19.1	19.8	20.3
20° N–20° S	54.7	43.6	48.9	44.3	28.9	32.1
20–50° S	22.7	19.3	25.1	22.1	32.8	34.1
50–90° S	-7.6	0.007	22.0	19.5	8.2	5.9

similar to our study. Another comparable classification (latitudinal bands, higher emissions in coastal regions) is used in the model (top-down approach) by Ordonez et al. (2012), who parameterized oceanic polybromomethanes emissions based on a chlorophyll *a* (chl *a*) dependent source in the tropical ocean (20° N to 20° S). We also see the occurrence of enhanced bromoform, as well as dibromomethane emissions in tropical upwelling regions and in coastal regions, although a direct correlation between chl *a* and the VSLS compounds is not apparent from the observations (Abrahamsson et al., 2004; Quack et al., 2007b). Palmer and Reason (2009) developed a parameterization for CHBr_3 based on chl *a* (between 30° N and 30° S), including other parameters (mixed layer depth, sea surface temperature and salinity, wind speed). The

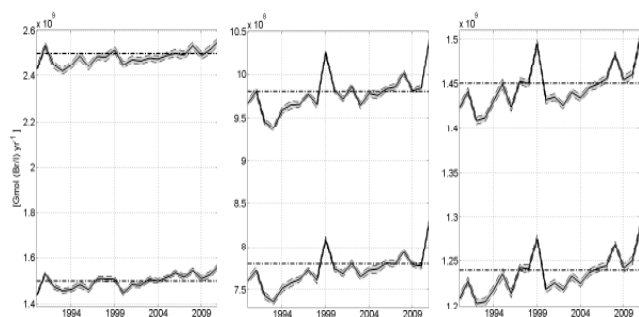
correlation between his modelled values and observations is, with $r^2 = 0.4$, low, which reveals the deficiency of this method (and chl *a*).

In some studies local emission estimates are extrapolated to a global scale. Extrapolating near-shore emissions may significantly overestimate the global sea-to-air fluxes, since they generally include elevated coastal concentrations, which are not representative of the global ocean. Yokouchi et al. (2005) applied a coastal emission ratio of $\text{CHBr}_3/\text{CH}_2\text{Br}_2$ of 9, and a global emission of $0.76 \text{ Gmol Br yr}^{-1}$ for CH_2Br_2 to infer a global CHBr_3 flux estimate of $10.26 \pm 3.88 \text{ Gmol Br yr}^{-1}$. O'Brien et al. (2009) followed the same method and extrapolated local near-shore measurements in the region surrounding Cape Verde to a global scale using an emission ratio of $\text{CHBr}_3/\text{CH}_2\text{Br}_2 = 13$. The global fluxes from these studies are nearly four times higher than those calculated in our study. However, since the emission ratios of CHBr_3 to CH_2Br_2 are generally higher in coastal regions than in the other areas (Hepach et al., 2013), the calculated global flux for CHBr_3 could be an overestimation.

Butler et al. (2007) and Quack and Wallace (2003) interpolated oceanic and atmospheric in situ measurements for global emission estimates. Butler et al. (2007) subdivided the ocean into the main basins and calculated the fraction of each compound for each region as a percentage. Coastal areas were not considered. The extrapolation by Quack and Wallace (2003) contained most of the currently available

Table 4. Fluxes of bromine from CHBr_3 and CH_2Br_2 in Gmol Br yr^{-1} , and iodine from CH_3I in Gmol I yr^{-1} .

References	CHBr_3 Flux (Gmol Br yr^{-1})		CH_2Br_2 Flux (Gmol Br yr^{-1})		CH_3I Flux (Gmol I yr^{-1})		Approach
	Global	Global	Global	Global	Source	Sink	
Butler et al. (2007)	10.01		3.50		4.33		bottom-up
Liang et al. (2010)	5.38		0.71				top-down
O'Brien et al. (2009)	10.26						bottom-up
Yokouchi et al. (2005)	10.26						bottom-up
Warwick et al. (2006)	7.01		1.25				top-down
Pyle et al. (2011)	4.78		1.25				top-down
Quack and Wallace (2003)	10.01						bottom-up
Smythe-Wright et al. (2006)					4.18		lab experiment
Bell et al. (2002)					2.4		model study
Ordonez et al. (2011)	6.67		0.84		2.39		top-down
Kerkweg et al. (2008)	7.45		1.41				top-down
	Source	Sink	Source	Sink	Source	Sink	
This study RF	2.06	-0.56	0.89	-0.12	1.24	-0.00008	bottom-up
This study OLS	2.96	-0.47	1.09	-0.11	1.45	-0.0001	bottom-up

**Fig. 7.** Inter-annual sea-to-air flux variability over 1989–2011 (bold solid line) of bromoform (left), dibromomethane (centre) and methyl iodide (right) calculated with the two regression techniques (RF (lower panels) and OLS (upper panels)), in $\text{Gmol (Br/I) yr}^{-1}$. Additionally, the respective climatological value is marked (dash-dotted line) as well as the standard deviation (grey shaded).

published measurements and used a finer area classification for shore, shelf and open ocean regions as well as for latitudinal bands. Both bottom-up approaches applied a coarse data interpolation compared to the classification and regression techniques used in this study and appear too high.

We calculate a global CH_2Br_2 sea-to-air flux of $0.77\text{--}0.98 \text{ Gmol Br yr}^{-1}$, which is also in the lower ($0.71\text{--}3.5 \text{ Gmol Br yr}^{-1}$) range of the other estimates (Table 4), but is in much closer agreement compared to the other compounds. Reasons for the good agreement with recent studies could be the longer atmospheric lifetime of CH_2Br_2 and the lower variance of sea water values which cause a more homogenous global distribution.

Some earlier emission estimations for CH_3I ($1.05\text{--}10.5 \text{ Gmol I yr}^{-1}$) are given by Bell et al. (2002), who produced the first seasonal model simulation of global oceanic and atmospheric CH_3I surface concentrations. A low correlation between observations and modelled data was obtained ($r = 0.4$). The authors assumed a missing biological sink of CH_3I in the ocean that would have reduced their computed concentrations to better match the observations. Sink and source mechanisms for the formation of CH_3I are not fully understood, making it difficult to model CH_3I emissions based on source and sink parameterizations. In our study a global sea-to-air flux of $1.24\text{--}1.45 \text{ Gmol I yr}^{-1}$ is estimated, which is within the lower range of earlier studies (Table 4). Our calculated climatology uses a larger dataset than the study of Bell et al. (2002). Ordonez et al. (2012) calculate a global CH_3I flux of the same magnitude as our study using a top-down approach with a modified global chemistry model that includes bromine and iodine chemistry. Smythe-Wright et al. (2006) calculated a global flux of iodine from *Prochlorococcus marinus* of $\sim 4.18 \text{ Gmol I yr}^{-1}$ based on measurements from two cruises. The latter study assumes that this phytoplankton species is the major marine source of atmospheric CH_3I . The assumption of Smythe-Wright et al. (2006) that the oceanic surface ($< 40^\circ \text{ N}$ and S) is covered with CH_3I -producing picoplankton might overestimate the global CH_3I sea-to-air flux. Calculations based on culture experiments from Brownell et al. (2010) demonstrate that *Prochlorococcus marinus* accounts only for 0.03 % of the global CH_3I budget and is not a globally significant source of CH_3I . Hughes et al. (2011) suggest different culture conditions as a possible explanation for the contradictory findings of the culture experiments. The bottle experiments of

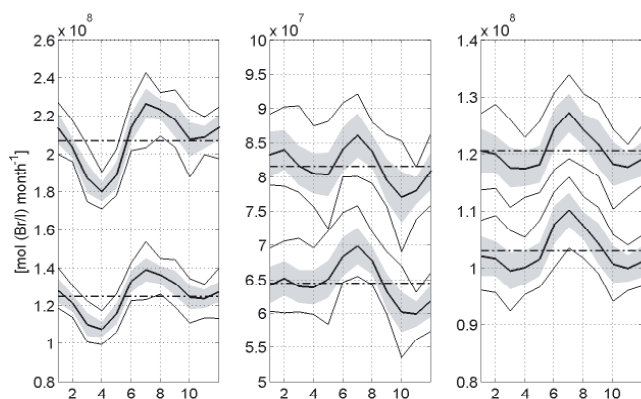


Fig. 8. Global monthly sea-to-air flux averages of bromoform (left), dibromomethane (centre) and methyl iodide (right) in mol (Br/I) month⁻¹ (bold solid line) from 1989 to 2011, including their standard deviation (grey shaded area) and their minimum and maximum value (solid line). Additionally, the respective annual mean value is marked (dash-dotted line). The upper graphs show the oceanic emissions using the OLS regression technique and the bottom graphs the RF calculated fluxes.

Richter and Wallace (2004) suggested a photochemical production pathway of CH₃I in open ocean water which might also explain our surface distribution (enhanced emissions in the subtropical gyre regions).

The comparison of our global sea-to-air fluxes with other global estimates reveals the greatest discrepancy for bromoform. We have shown that bromoform levels are the most variable in the ocean and atmosphere. Possibly, the underrepresentation of extreme values generates too small concentration gradients, which reduces our total emission estimate. Especially in coastal and shelf regions, the 1° × 1° grid resolution cannot resolve these extreme concentrations and very likely leads to underestimated emissions.

5 Variability of the climatological sea-to-air fluxes

We calculate global emission fields using fixed oceanic concentrations and atmospheric mixing ratios and the highest available temporal resolution of the input parameters over the time period 1989–2011: 6-hourly means of U , SST, SLP and monthly means for the SSS. The global emissions of every time step are averaged over each month and the average monthly emissions are summed to the annual climatological emission. The climatologies thus include annual, seasonal and short timescale temporal variability.

5.1 Variability of the concentration data

The calculated global 1° × 1° maps of oceanic concentrations and atmospheric mixing ratios include in situ measurements from 1989 to 2011, illustrating a climatological year and covering the entire globe. Seasonally changing condi-

tions, e.g. light and water temperature or biological species composition, which have an influence on the variability of the air and water concentrations in certain areas (Archer et al., 2007; Orlikowska and Schulz-Bull, 2009), are not considered because of the generally poor temporal data coverage. Fitting the in situ measurements onto our 1° × 1° grid (by using objective mapping) leads on average to a reduction of the initial atmospheric mixing ratios and oceanic concentrations of less than 1%. The accuracy of the interpolation is limited by the sparse data coverage and the regression technique used. Seasonal and spatial accuracy could be improved if a larger dataset was available. Thus we recommend more measurements, especially in the ocean, as well as a refinement of process understanding. The temporal variability of the SST is considered in the concentration gradient, used in the sea-to-air flux calculation, by computing a new equilibrium concentration for every 6 h time step from 1989 to 2011.

5.2 Annual and seasonal variability

The inter-annual variability of the global sea-to-air flux from 1989 to 2011 is small and generally less than 5% (Fig. 7). The halocarbons all show a positive trend towards 2011. Within a year, the global flux varies monthly for every halogenated compound (Fig. 8). The maximum global sea-to-air flux is most pronounced in July for all compounds, while the minimum is reached in March–April for CHBr₃ and CH₃I and in October for CH₂Br₂. The climatological monthly flux and the corresponding minimum and maximum monthly fluxes vary between 9 and 21%. CH₃I shows the smallest mean deviation with 9 and 11% for OLS and RF respectively, whereas the variation for CH₂Br₂ is between 14 and 17% and for CHBr₃ between 17 and 21%. Thus the seasonal variation of the global climatological flux is larger than the inter-annual variation, despite the shifting of the seasons (half a year) between the Northern Hemisphere and Southern Hemisphere. The global climatological fluxes, obtained from the sum of the monthly averages between 1989 and 2011, describe the current best possible estimates of the moderately varying annual and seasonal global emissions. However, the results do not consider a seasonally varying influence of either the water or the air concentration on the emission because the current sparse investigations do not allow a suitable parameterization of the VSL yet.

5.3 Short time variability of fluxes

In situ fluxes from a cruise (TransBrom) between Japan and Australia in October 2009 are compared to the nearest grid points of our climatology (Fig. 9) as an example for the influence of short time variability. The TransBrom data include 105 CHBr₃ and CH₂Br₂ measurements and 96 CH₃I measurements, and are included in the climatology. The cruise transited through different biogeochemical regions with varying meteorological conditions influencing

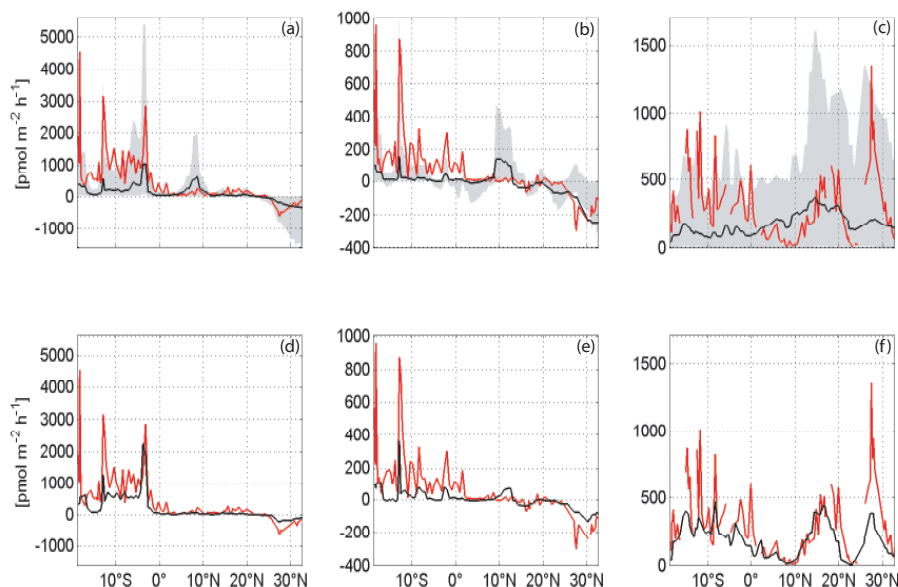


Fig. 9. The upper panels illustrate the comparison between our climatological estimate (black line) and the in situ sea-to-air fluxes from the TransBrom cruise (red line) for bromoform (a), dibromomethane (b) and methyl iodide (c) in $\text{pmol m}^{-2} \text{h}^{-1}$ (see more details in the text) including the climatological minimum and maximum values (grey shaded area). The lower panels represent the same in situ measurements compared to our model values using the nearest 6-hourly mean of SST, U and SLP and monthly mean of SSS with fixed mixing ratios and oceanic concentrations calculated with the RF method for bromoform (d), dibromomethane (e) and methyl iodide (f) (the emissions using OLS look similar).

the strength of VSLs emissions (Krüger and Quack, 2012). The in situ and climatological sea-to-air fluxes for bromoform and dibromomethane compare very well in the Northern Hemisphere, where small concentration gradients are found in the open oceans. The enhanced emissions in the Southern Hemisphere encountered during the cruise are under-represented in the climatology. Comparison of the methyl iodide in situ fluxes and the climatology shows a similar trend, although the extreme values of the in situ measurements are highly under-represented in the climatological mean flux value. Our climatology underestimates the short-term measured fluxes by smoothing the values of the varying input parameters. The mean deviation between the climatology and the in situ fluxes during October 2009 is $\sim 120\%$ for CHBr_3 , $\sim 20\%$ for CH_2Br_2 and $\sim 176\%$ for CH_3I , respectively.

We also calculate the sea-to-air fluxes using the nearest temporal and spatial 6-hourly means (highest available resolution) of SST, SLP and U , the monthly mean of the SSS and the climatological oceanic concentration and mixing ratios, and compare them to the measured fluxes (Fig. 9). The mean deviation between the 6-hourly means and the in situ fluxes for the three compounds is only $\sim 48\%$ for CHBr_3 , $\sim 15\%$ for CH_2Br_2 and 51% for CH_3I . These values show the good match between “modelled” and in situ measurements and validate the predictive capability of this approach. The climatological minimum and maximum values of the cruise

nearest data points (Fig. 9, upper panel) reveal how variable the “modelled” fluxes can be at a single location. While most in situ fluxes are included in the 6 h minimum and maximum range from 1989 to 2011, it is also noteworthy that even with this high temporal (6 h) resolution of input parameters, the “modelled” fluxes can neither match the extreme values of the encountered in situ fluxes, nor do they resolve the high variability of the in situ fluxes completely. An additional factor for the under-representation of the extreme in situ values is the mean concentration gradient ($1^\circ \times 1^\circ$ resolution) in our “model”. In the vicinity of source regions, e.g. coast lines, the water concentrations can vary by more than 100% over short distances (Butler et al., 2006), which strongly influences the in situ fluxes and is likely not resolved in the model due to poor data coverage.

6 Summary and conclusion

Global sea-to-air flux climatologies (considering the time span from 1989 to 2011 of the three important short-lived halocarbons, bromoform, dibromomethane and methyl iodide) are calculated based on surface oceanic and atmospheric measurements from the HalOcAt database. The physical and biogeochemical factors of the compounds’ distributions in ocean and atmosphere are also considered. Data are classified into coastal, shelf and open ocean regions, and are interpolated on a $1^\circ \times 1^\circ$ grid. The missing grid values are

filled with robust fit (RF) and ordinary least squares (OLS) regression techniques based on the latitudinal and longitudinal distribution of the compounds. The RF interpolation estimates background values, since it is weighted on the quantity of measurements, whereas the OLS regressions include extreme data and therefore represent our highest values. Global emission fields are calculated with a high temporal resolution of 6-hourly wind speed, sea surface temperature and sea level pressure data. The climatological annual global flux for 1989 to 2011 is obtained as sum of the monthly average fluxes. We estimate positive global sea-to-air fluxes of CHBr_3 , CH_2Br_2 and CH_3I of 2.06/2.96, 0.89/1.09 Gmol Br yr^{-1} and 1.24/1.45 Gmol I yr^{-1} , based on RF/OLS respectively, which are all at the lower end of earlier studies. Previous global climatological estimate studies have not determined negative fluxes (flux into the ocean). We estimate negative global sea-to-air fluxes of $-0.47/-0.56$, $-0.11/-0.12$ Gmol Br yr^{-1} and $-0.08/-0.1$ Mmol I yr^{-1} for CHBr_3 , CH_2Br_2 and CH_3I , respectively. The net oceanic emissions of our climatology are 1.5/2.5 Gmol Br yr^{-1} for CHBr_3 , 0.78/0.98 Gmol Br yr^{-1} for CH_2Br_2 , and 1.24/1.45 Gmol I yr^{-1} for CH_3I .

Our low bottom-up emission estimates, compared to recent top-down approaches, especially for bromoform, are most likely caused by an under-representation of extreme emissions. Observed high temporal and spatial in situ variances cannot be resolved in the $1^\circ \times 1^\circ$ grid climatology. It is still unclear how important extreme events are for the global bromoform budget, but we suggest that small spatial and temporal events of high oceanic bromoform emissions are important for the transport of bromine into the troposphere and lower stratosphere. The monthly variation of the global climatological flux (9–21 %) is contained within our calculations and it is larger than the inter-annual variability, which is generally less than 5 % for all three compounds.

Our global sea-to-air flux estimates can be used as input for different model calculations. The existing uncertainties can be reduced by enlarging of the HalOcat database with more measurements, especially in ocean waters, common calibration techniques and more basic research into the underlying source and sink processes.

Supplementary material related to this article is available online at: <http://www.atmos-chem-phys.net/13/8915/2013/acp-13-8915-2013-supplement.zip>.

Acknowledgements. We thank all contributors sending their data to the HalOcat database and for their helpful comments on the manuscript. We also thank our assisting student helpers Julian Kinzel, Christian Müller, Eike Hümpel, Anja Müller and Theresa Conradi who populated the database, which started in 2009. This work was financially supported by the WGL project TransBrom, the European commission under the project SHIVA

(grant no. 226 224) and by the German Federal Ministry of Education and Research (BMBF) during the project SOPRAN (grant no: 03F0611A). SOLAS Integration (Surface Ocean Lower Atmosphere Study; http://www.bodc.ac.uk/solas_integration/) helped instigate this project and Tom Bell and Peter Liss were supported in this by a NERC UK SOLAS Knowledge Transfer grant (NE/E001696/1). Part of this project was supported by COST (European Cooperation in Science and Technology) Action 735, a European Science Foundation-supported initiative. Additionally, we would like to thank the ECMWF for providing the ERA Interim reanalysis data. We thank two anonymous reviewers for their useful comments and advice.

The service charges for this open access publication have been covered by a Research Centre of the Helmholtz Association.

Edited by: R. Volkamer

References

- Abrahamsson, K., Bertilsson, S., Chierici, M., Fransson, A., Froneman, P. W., Loren, A., and Pakhomov, E. A.: Variations of biochemical parameters along a transect in the southern ocean, with special emphasis on volatile halogenated organic compounds, *Deep-Sea Res. Part II*, 51, 2745–2756, doi:10.1016/j.dsr2.2004.09.004, 2004.
- Amachi, S., Kamagata, Y., Kanagawa, T., and Muramatsu, Y.: Bacteria mediate methylation of iodine in marine and terrestrial environments, *Appl. Environ. Microbiol.*, 67, 2718–2722, doi:10.1128/aem.67.6.2718-2722.2001, 2001.
- Antonov, J. I., Seidov, D., Boyer, T. P., Locarnini, R. A., Mishonov, A. V., Garcia, H. E., Baranova, O. K., Zweng, M. M., and Johnson, D. R.: World ocean atlas 2009, Volume 2: Salinity. S. Levitus Ed. NOAA Atlas NESDIS 69, U.S. Government Printing Office, Washington, DC, 184 pp., 2010.
- Archer, S. D., Goldson, L. E., Liddicoat, M. I., Cummings, D. G., and Nightingale, P. D.: Marked seasonality in the concentrations and sea-to-air flux of volatile iodocarbon compounds in the western English Channel, *J. Geophys. Res.-Oceans*, 112, C08009, doi:10.1029/2006jc003963, 2007.
- Aschmann, J., Sinnhuber, B.-M., Atlas, E. L., and Schauffler, S. M.: Modeling the transport of very short-lived substances into the tropical upper troposphere and lower stratosphere, *Atmos. Chem. Phys.*, 9, 9237–9247, doi:10.5194/acp-9-9237-2009, 2009.
- Bates, N. R. and Merlivat, L.: The influence of short-term wind variability on air-sea CO_2 exchange, *Geophys. Res. Lett.*, 28, 3281–3284, doi:10.1029/2001gl012897, 2001.
- Bell, N., Hsu, L., Jacob, D. J., Schultz, M. G., Blake, D. R., Butler, J. H., King, D. B., Lobert, J. M., and Maier-Reimer, E.: Methyl iodide: Atmospheric budget and use as a tracer of marine convection in global models, *J. Geophys. Res.-Atmos.*, 107, 4340, doi:10.1029/2001jd001151, 2002.
- Bondu, S., Cocquempot, B., Deslandes, E., and Morin, P.: Effects of salt and light stress on the release of volatile halogenated organic compounds by *Solieria Chordalis*: A laboratory incubation study, *Bot. Mar.*, 51, 485–492, doi:10.1515/bot.2008.056, 2008.
- Brinckmann, S., Engel, A., Bönisch, H., Quack, B., and Atlas, E.: Short-lived brominated hydrocarbons – observations in the

- source regions and the tropical tropopause layer, *Atmos. Chem. Phys.*, 12, 1213–1228, doi:10.5194/acp-12-1213-2012, 2012.
- Brownell, D. K., Moore, R. M., and Cullen, J. J.: Production of methyl halides by *Prochlorococcus* and *Synechococcus*, *Glob. Biogeochem. Cy.*, 24, Gb2002, doi:10.1029/2009gb003671, 2010.
- Butler, J. H., King, D. B., Lobert, J. M., Montzka, S. A., Yvon-Lewis, S. A., Hall, B. D., Warwick, N. J., Mondeel, D. J., Aydin, M., and Elkins, J. W.: Oceanic distributions and emissions of short-lived halocarbons, *Glob. Biogeochem. Cy.*, 21, Gb1023, doi:10.1029/2006gb002732, 2007.
- Butler, J. H., Bell, T. G., Hall, B. D., Quack, B., Carpenter, L. J., and Williams, J.: Technical Note: Ensuring consistent, global measurements of very short-lived halocarbon gases in the ocean and atmosphere, *Atmos. Chem. Phys.*, 10, 327–330, doi:10.5194/acp-10-327-2010, 2010.
- Carpenter, L. J.: Iodine in the marine boundary layer, *Chem. Rev.*, 103, 4953–4962, doi:10.1021/cr0206465, 2003.
- Carpenter, L. J. and Liss, P. S.: On temperate sources of bromoform and other reactive organic bromine gases, *J. Geophys. Res.-Atmos.*, 105, 20539–20547, doi:10.1029/2000jd900242, 2000.
- Chapman, E. G., Shaw, W. J., Easter, R. C., Bian, X., and Ghan, S. J.: Influence of wind speed averaging on estimates of dimethylsulfide emission fluxes, *J. Geophys. Res.-Atmos.*, 107, 4672, doi:10.1029/2001jd001564, 2002.
- Chipperfield, M. P. and Pyle, J. A.: Model sensitivity studies of arctic ozone depletion, *J. Geophys. Res.-Atmos.*, 103, 28389–28403, doi:10.1029/98jd01960, 1998.
- Daley, R.: *Atmospheric data analysis*, Cambridge University Press, Cambridge, England, 457 pp., 1991.
- Dee, D. P., Uppala, S. M., Simmons, A. J., Berrisford, P., Poli, P., Kobayashi, S., Andrae, U., Balmaseda, M. A., Balsamo, G., Bauer, P., Bechtold, P., Beljaars, A. C. M., van de Berg, L., Bidlot, J., Bormann, N., Delsol, C., Dragani, R., Fuentes, M., Geer, A. J., Haimberger, L., Healy, S. B., Hersbach, H., Hólm, E. V., Isaksen, I., Kållberg, P., Köhler, M., Matricardi, M., McNally, A. P., Monge-Sanz, B. M., Morcrette, J.-J., Park, B.-K., Peubey, C., de Rosnay, P., Tavolato, C., Thépaut, J.-N., and Vitart, F.: The era-interim reanalysis: Configuration and performance of the data assimilation system, *Q. J. Roy. Meteorol. Soc.*, 137, 553–597, doi:10.1002/qj.828, 2011.
- Dorf, M., Butz, A., Camy-Peyret, C., Chipperfield, M. P., Kritten, L., and Pfeilsticker, K.: Bromine in the tropical troposphere and stratosphere as derived from balloon-borne BrO observations, *Atmos. Chem. Phys.*, 8, 7265–7271, doi:10.5194/acp-8-7265-2008, 2008.
- Fuhlbrügge, S., Krüger, K., Quack, B., Atlas, E., Hepach, H., and Ziska, F.: Impact of the marine atmospheric boundary layer conditions on VLS abundances in the eastern tropical and subtropical North Atlantic Ocean, *Atmos. Chem. Phys.*, 13, 6345–6357, doi:10.5194/acp-13-6345-2013, 2013.
- Gschwend, P. M., Mac Farlane, J. K., and Newman, K. A.: Volatile halogenated organic-compounds released to seawater from temperate marine macro algae, *Science*, 227, 1033–1035, doi:10.1126/science.227.4690.1033, 1985.
- Hagen, E., Feistel, R., Agenbag, J. J., and Ohde, T.: Seasonal and interannual changes in intense Benguela upwelling (1982–1999), *Oceanol. Acta.*, 24, 557–568, doi:10.1016/s0399-1784(01)01173-2, 2001.
- Hamer, P. D., Marécal, V., Hossaini, R., Pirre, M., Warwick, N., Chipperfield, M., Samah, A. A., Harris, N., Robinson, A., Quack, B., Engel, A., Krüger, K., Atlas, E., Subramaniam, K., Oram, D., Leedham, E., Mills, G., Pfeilsticker, K., Sala, S., Keber, T., Bönisch, H., Peng, L. K., Nadzir, M. S. M., Lim, P. T., Mujahid, A., Anton, A., Schlager, H., Catoire, V., Krysztofiak, G., Fühlbrügge, S., Dorf, M., and Sturges, W. T.: Modelling the chemistry and transport of bromoform within a sea breeze driven convective system during the SHIVA Campaign, *Atmos. Chem. Phys. Discuss.*, 13, 20611–20676, doi:10.5194/acpd-13-20611-2013, 2013.
- Happell, J. D. and Wallace, D. W. R.: Methyl iodide in the Greenland/Norwegian seas and the tropical Atlantic Ocean: Evidence for photochemical production, *Geophys. Res. Lett.*, 23, 2105–2108, doi:10.1029/96gl01764, 1996.
- Hepach, H., Quack, B., Ziska, F., Fuhlbrügge, S., Atlas, E. L., Peeken, I., Krüger, K., and Wallace, D. W. R.: Drivers of diel and regional variations of halocarbon emissions from the tropical North East Atlantic, *Atmos. Chem. Phys. Discuss.*, 13, 19701–19750, doi:10.5194/acpd-13-19701-2013, 2013.
- Hossaini, R., Mantle, H., Chipperfield, M. P., Montzka, S. A., Hamer, P., Ziska, F., Quack, B., Krüger, K., Tegtmeier, S., Atlas, E., Sala, S., Engel, A., Bönisch, H., Keber, T., Oram, D., Mills, G., Ordóñez, C., Saiz-Lopez, A., Warwick, N., Liang, Q., Feng, W., Moore, F., Miller, B. R., Marécal, V., Richards, N. A. D., Dorf, M., and Pfeilsticker, K.: Evaluating global emission inventories of biogenic bromocarbons, *Atmos. Chem. Phys. Discuss.*, 13, 12485–12539, doi:10.5194/acpd-13-12485-2013, 2013.
- Huber, P. J.: Robust estimation of location parameter, *Ann. Math. Stat.*, 35, 73–101, doi:10.1214/aoms/1177703732, 1964.
- Hughes, C., Chuck, A. L., Rossetti, H., Mann, P. J., Turner, S. M., Clarke, A., Chance, R., and Liss, P. S.: Seasonal cycle of seawater bromoform and dibromomethane concentrations in a coastal bay on the western Antarctic Peninsula, *Glob. Biogeochem. Cy.*, 23, Gb2024, doi:10.1029/2008gb003268, 2009.
- Hughes, C., Franklin, D. J., and Malin, G.: Iodomethane production by two important marine cyanobacteria: *Prochlorococcus marinus* (ccmp 2389) and *Synechococcus sp* (ccmp 2370), *Mar. Chem.*, 125, 19–25, doi:10.1016/j.marchem.2011.01.007, 2011.
- Johnson, M. T.: A numerical scheme to calculate temperature and salinity dependent air-water transfer velocities for any gas, *Ocean Sci.*, 6, 913–932, doi:10.5194/os-6-913-2010, 2010.
- Jones, C. E., Andrews, S. J., Carpenter, L. J., Hogan, C., Hopkins, F. E., Laube, J. C., Robinson, A. D., Spain, T. G., Archer, S. D., Harris, N. R. P., Nightingale, P. D., O'Doherty, S. J., Oram, D. E., Pyle, J. A., Butler, J. H., and Hall, B. D.: Results from the first national UK inter-laboratory calibration for very short-lived halocarbons, *Atmos. Meas. Tech.*, 4, 865–874, doi:10.5194/amt-4-865-2011, 2011.
- Kerkweg, A., Jöckel, P., Warwick, N., Gebhardt, S., Brenninkmeijer, C. A. M., and Lelieveld, J.: Consistent simulation of bromine chemistry from the marine boundary layer to the stratosphere – Part 2: Bromocarbons, *Atmos. Chem. Phys.*, 8, 5919–5939, doi:10.5194/acp-8-5919-2008, 2008.
- Kettle, H. and Merchant, C. J.: Systematic errors in global air-sea CO₂ flux caused by temporal averaging of sea-level pressure, *Atmos. Chem. Phys.*, 5, 1459–1466, doi:10.5194/acp-5-1459-2005, 2005.

- Ko, M. K. W., Poulet, G., Blake, D. R., Boucher, O., Burkholder, J. H., Chin, M., Cox, R. A., George, C., Graf, H.-F., Holton, J. R., Jacob, D. J., Law, K. S., Lawrence, M. G., Midgley, P. M., Seakins, P. W., Shallcross, D. E., Strahan, S. E., Wuebbles, D. J., and Yokouchi, Y.: Very short-lived halogen and sulfur substances, in: Scientific assessment of ozone depletion: 2002, Global Ozone Res. Monit. Proj. Rep.47, World Meteorol. Org., Geneva, 2.1–2.57, 2003.
- Krüger, K. and Quack, B.: Introduction to special issue: the Trans-Brom Sonne expedition in the tropical West Pacific, Atmos. Chem. Phys. Discuss., 12, 1401–1418, doi:10.5194/acpd-12-1401-2012, 2012.
- Laternus, F., Adams, F. C., and Wiencke, C.: Methyl halides from Antarctic macro algae, Geophys. Res. Lett., 25, 773–776, doi:10.1029/98gl00490, 1998.
- Liang, Q., Stolarski, R. S., Kawa, S. R., Nielsen, J. E., Douglass, A. R., Rodriguez, J. M., Blake, D. R., Atlas, E. L., and Ott, L. E.: Finding the missing stratospheric Br_y: a global modeling study of CHBr₃ and CH₂Br₂, Atmos. Chem. Phys., 10, 2269–2286, doi:10.5194/acp-10-2269-2010, 2010.
- Liss, P. S. and Merlivat, L.: Air-sea gas exchange rates: Introduction and synthesis, in: The role of air-sea exchange in geochemical cycling, edited by: Buat-Ménard, P., D. Reidel, Hingham, Mass., 113–129, 1986.
- Liu, Y., Yvon-Lewis, S. A., Hu, L., Salisbury, J. E., and O'Hern, J. E.: CHBr₃, CH₂Br₂, and CHClBr₂ in U.S. Coastal waters during the Gulf of Mexico and East Coast carbon cruise, J. Geophys. Res., 116, C10004, doi:10.1029/2010JC006729, 2011.
- Manley, S. L. and Dastoor, M. N.: Methyl-iodide (CH₃I) production by kelp and associated microbes, Mar. Biol., 98, 477–482, doi:10.1007/bf00391538, 1988.
- Manley, S. L. and dela Cuesta, J. L.: Methyl iodide production from marine phytoplankton cultures, Limnol. Oceanogr., 42, 142–147, 1997.
- Manley, S. L., Goodwin, K., and North, W. J.: Laboratory production of bromoform, methylene bromide, and methyl-iodide by macro algae and distribution in near-shore southern California waters, Limnol. Oceanogr., 37, 1652–1659, 1992.
- McFiggans, G., Plane, J. M. C., Allan, B. J., Carpenter, L. J., Coe, H., and O'Dowd, C.: A modeling study of iodine chemistry in the marine boundary layer, J. Geophys. Res.-Atmos., 105, 14371–14385, doi:10.1029/1999jd901187, 2000.
- Minas, H. J., Packard, T. T., Minas, M., and Coste, B.: An analysis of the production-regeneration system in the coastal upwelling area off NW Africa based on oxygen, nitrate and ammonium distributions, J. Mar. Res., 40, 615–641, 1982.
- Montzka, S. A. and Reimann, S.: Ozone-depleting substances and related chemicals, in: Scientific Assessment of Ozone Depletion: 2010, Global Ozone Research and Monitoring Project - Report No. 52, Chapt. 1, edited by: World Meteorological Project, Geneva Switzerland, 2011.
- Moore, R. M. and Zafiriou, O. C.: Photochemical production of methyl-iodide in seawater, J. Geophys. Res.-Atmos., 99, 16415–16420, doi:10.1029/94jd00786, 1994.
- Moore, R. M., Geen, C. E., and Tait, V. K.: Determination of Henry law constants for a suite of naturally-occurring halogenated methanes in seawater, Chemosphere, 30, 1183–1191, doi:10.1016/0045-6535(95)00009-w, 1995a.
- Moore, R. M., Tokarczyk, R., Tait, V. K., Poulin, M., and Geen, C. E.: Marine phytoplankton as a natural source of volatile organohalogens, in: Naturally-produced organohalogens, edited by: Grimvall, A., and deLeer, E. W. B., Kluwer Academic Publishers, D., 283–294, 1995b.
- Nightingale, P. D., Malin, G., and Liss, P. S.: Production of chloroform and other low-molecular-weight halocarbons by some species of macro algae, Limnol. Oceanogr., 40, 680–689, 1995.
- Nightingale, P. D., Malin, G., Law, C. S., Watson, A. J., Liss, P. S., Liddicoat, M. I., Boutin, J., and Upstill-Goddard, R. C.: In situ evaluation of air-sea gas exchange parameterizations using novel conservative and volatile tracers, Glob. Biogeochem. Cy., 14, 373–387, 2000.
- O'Brien, L. M., Harris, N. R. P., Robinson, A. D., Gostlow, B., Warwick, N., Yang, X., and Pyle, J. A.: Bromocarbons in the tropical marine boundary layer at the Cape Verde Observatory – measurements and modelling, Atmos. Chem. Phys., 9, 9083–9099, doi:10.5194/acp-9-9083-2009, 2009.
- Ordóñez, C., Lamarque, J.-F., Tilmes, S., Kinnison, D. E., Atlas, E. L., Blake, D. R., Sousa Santos, G., Brasseur, G., and Saiz-Lopez, A.: Bromine and iodine chemistry in a global chemistry-climate model: description and evaluation of very short-lived oceanic sources, Atmos. Chem. Phys., 12, 1423–1447, doi:10.5194/acp-12-1423-2012, 2012.
- Orlikowska, A. and Schulz-Bull, D. E.: Seasonal variations of volatile organic compounds in the coastal Baltic sea, Environ. Chem., 6, 495–507, doi:10.1071/en09107, 2009.
- Palmer, C. J. and Reason, C. J.: Relationships of surface bromoform concentrations with mixed layer depth and salinity in the tropical oceans, Glob. Biogeochem. Cy., 23, Gb2014, doi:10.1029/2008gb003338, 2009.
- Penkett, S. A., Jones, B. M. R., Rycroft, M. J., and Simmons, D. A.: An interhemispheric comparison of the concentrations of bromine compounds in the atmosphere, Nature, 318, 550–553, doi:10.1038/318550a0, 1985.
- Pyle, J. A., Ashfold, M. J., Harris, N. R. P., Robinson, A. D., Warwick, N. J., Carver, G. D., Gostlow, B., O'Brien, L. M., Manning, A. J., Phang, S. M., Yong, S. E., Leong, K. P., Ung, E. H., and Ong, S.: Bromoform in the tropical boundary layer of the Maritime Continent during OP3, Atmos. Chem. Phys., 11, 529–542, doi:10.5194/acp-11-529-2011, 2011.
- Quack, B. and Wallace, D. W. R.: Air-sea flux of bromoform: Controls, rates, and implications, Glob. Biogeochem. Cy., 17, 1023, doi:10.1029/2002gb001890, 2003.
- Quack, B., Atlas, E., Petrick, G., Stroud, V., Schauffler, S., and Wallace, D. W. R.: Oceanic bromoform sources for the tropical atmosphere, Geophys. Res. Lett., 31, L23s05, doi:10.1029/2004gl020597, 2004.
- Quack, B., Atlas, E., Petrick, G., and Wallace, D. W. R.: Bromoform and dibromomethane above the Mauritanian upwelling: Atmospheric distributions and oceanic emissions, J. Geophys. Res.-Atmos., 112, D09312, doi:10.1029/2006jd007614, 2007a.
- Quack, B., Peeken, I., Petrick, G., and Nachtigall, K.: Oceanic distribution and sources of bromoform and dibromomethane in the Mauritanian upwelling, J. Geophys. Res.-Oceans, 112, C10006, doi:10.1029/2006jc003803, 2007b.
- Richter, U. and Wallace, D. W. R.: Production of methyl iodide in the tropical Atlantic Ocean, Geophys. Res. Lett., 31, L23s03, doi:10.1029/2004gl020779, 2004.

- Salawitch, R. J., Weisenstein, D. K., Kovalenko, L. J., Sioris, C. E., Wennberg, P. O., Chance, K., Ko, M. K. W., and McLinden, C. A.: Sensitivity of ozone to bromine in the lower stratosphere, *Geophys. Res. Lett.*, 32, L05811, doi:10.1029/2004gl021504, 2005.
- Schott, F. A., Dengler, M., and Schoenefeldt, R.: The shallow overturning circulation of the Indian Ocean, *Prog. Oceanogr.*, 53, 57–103, doi:10.1016/s0079-6611(02)00039-3, 2002.
- Sinnhuber, B.-M. and Folkens, I.: Estimating the contribution of bromoform to stratospheric bromine and its relation to dehydration in the tropical tropopause layer, *Atmos. Chem. Phys.*, 6, 4755–4761, doi:10.5194/acp-6-4755-2006, 2006.
- Sinnhuber, B.-M., Sheode, N., Sinnhuber, M., Chipperfield, M. P., and Feng, W.: The contribution of anthropogenic bromine emissions to past stratospheric ozone trends: a modelling study, *Atmos. Chem. Phys.*, 9, 2863–2871, doi:10.5194/acp-9-2863-2009, 2009.
- Sive, B. C., Varner, R. K., and Mao, H.: A large terrestrial source of methyl iodide, *Geophys. Res. Lett.*, 34, L17808, doi:10.1029/2007GL030528, 2007.
- Smith, W. O. and Nelson, D. M.: Phytoplankton bloom produced by a receding ice edge in the Ross Sea – spatial coherence with the density field, *Science*, 227, 163–166, doi:10.1126/science.227.4683.163, 1985.
- Smythe-Wright, D., Boswell, S. M., Breithaupt, P., Davidson, R. D., Dimmer, C. H., and Diaz, L. B. E.: Methyl iodide production in the ocean: Implications for climate change, *Glob. Biogeochem. Cy.*, 20, Gb3003, doi:10.1029/2005gb002642, 2006.
- Solomon, S., Garcia, R. R., and Ravishankara, A. R.: On the role of iodine in ozone depletion, *J. Geophys. Res.-Atmos.*, 99, 20491–20499, doi:10.1029/94jd02028, 1994.
- Sturges, W. T., Oram, D. E., Carpenter, L. J., Penkett, S. A., and Engel, A.: Bromoform as a source of stratospheric bromine, *Geophys. Res. Lett.*, 27, 2081–2084, doi:10.1029/2000gl011444, 2000.
- Tegtmeier, S., Krüger, K., Quack, B., Atlas, E. L., Pisso, I., Stohl, A., and Yang, X.: Emission and transport of bromocarbons: from the West Pacific ocean into the stratosphere, *Atmos. Chem. Phys.*, 12, 10633–10648, doi:10.5194/acp-12-10633-2012, 2012.
- Tegtmeier, S., Krüger, K., Quack, B., Atlas, E., Blake, D. R., Boenisch, H., Engel, A., Hepach, H., Hossaini, R., Navarro, M. A., Raimund, S., Sala, S., Shi, Q., and Ziska, F.: The contribution of oceanic methyl iodide to stratospheric iodine, *Atmos. Chem. Phys. Discuss.*, 13, 11427–11471, doi:10.5194/acpd-13-11427-2013, 2013.
- Tokarczyk, R. and Moore, R. M.: Production of volatile organohalogen by phytoplankton cultures, *Geophys. Res. Lett.*, 21, 285–288, doi:10.1029/94gl00009, 1994.
- Vogt, R., Sander, R., Von Glasow, R., and Crutzen, P. J.: Iodine chemistry and its role in halogen activation and ozone loss in the marine boundary layer: A model study, *J. Atmos. Chem.*, 32, 375–395, doi:10.1023/a:1006179901037, 1999.
- von Glasow, R.: Atmospheric chemistry – sun, sea and ozone destruction, *Nature*, 453, 1195–1196, doi:10.1038/4531195a, 2008.
- von Glasow, R., von Kuhlmann, R., Lawrence, M. G., Platt, U., and Crutzen, P. J.: Impact of reactive bromine chemistry in the troposphere, *Atmos. Chem. Phys.*, 4, 2481–2497, doi:10.5194/acp-4-2481-2004, 2004.
- Wanninkhof, R.: Relationship between wind-speed and gas-exchange over the ocean, *J. Geophys. Res.-Oceans*, 97, 7373–7382, doi:10.1029/92jc00188, 1992.
- Wanninkhof, R. and McGillis, W. R.: A cubic relationship between air-sea CO₂ exchange and wind speed, *Geophys. Res. Lett.*, 26, 1889–1892, doi:10.1029/1999gl000363, 1999.
- Warneck, P. and Williams, J.: *The atmospheric chemist's companion-numerical data for use in the atmospheric sciences*, Springer Science+Business Media B.V., 2012.
- Warwick, N. J., Pyle, J. A., Carver, G. D., Yang, X., Savage, N. H., O'Connor, F. M., and Cox, R. A.: Global modeling of biogenic bromocarbons, *J. Geophys. Res.-Atmos.*, 111, D24305, doi:10.1029/2006jd007264, 2006.
- Williams, J., Gros, V., Atlas, E., Maciejczyk, K., Batsaikhan, A., Scholer, H. F., Forster, C., Quack, B., Yassaa, N., Sander, R., and Van Dingenen, R.: Possible evidence for a connection between methyl iodide emissions and Saharan dust, *J. Geophys. Res.-Atmos.*, 112, D07302, doi:10.1029/2005jd006702, 2007.
- Yamamoto, H., Yokouchi, Y., Otsuki, A., and Itoh, H.: Depth profiles of volatile halogenated hydrocarbons in seawater in the Bay of Bengal, *Chemosphere*, 45, 371–377, doi:10.1016/s0045-6535(00)00541-5, 2001.
- Yokouchi, Y., Mukai, H., Yamamoto, H., Otsuki, A., Saitoh, C., and Nojiri, Y.: Distribution of methyl iodide, ethyl iodide, bromoform, and dibromomethane over the ocean (east and Southeast Asian seas and the western Pacific), *J. Geophys. Res.-Atmos.*, 102, 8805–8809, doi:10.1029/96jd03384, 1997.
- Yokouchi, Y., Hasebe, F., Fujiwara, M., Takashima, H., Shiotani, M., Nishi, N., Kanaya, Y., Hashimoto, S., Fraser, P., Toom-Sauntry, D., Mukai, H., and Nojiri, Y.: Correlations and emission ratios among bromoform, dibromochloromethane, and dibromomethane in the atmosphere, *J. Geophys. Res.-Atmos.*, 110, D23309, doi:10.1029/2005jd006303, 2005.
- Yokouchi, Y., Osada, K., Wada, M., Hasebe, F., Agama, M., Murakami, R., Mukai, H., Nojiri, Y., Inuzuka, Y., Toom-Sauntry, D., and Fraser, P.: Global distribution and seasonal concentration change of methyl iodide in the atmosphere, *J. Geophys. Res.-Atmos.*, 113, D18311, doi:10.1029/2008jd009861, 2008.

2. Manuscript

Evaluating global emission inventories of biogenic bromocarbons

R. Hossaini¹, H. Mantle¹, M. P. Chipperfield¹, S. A. Montzka², P. Hamer, F. Ziska⁴, B. Quack⁴, K. Krüger^{4,*}, S. Tegtmeier⁴, E. Atlas⁵, S. Sala⁶, A. Engel⁶, H. Bönisch⁶, T. Keber⁶, D. Oram⁷, G. Mills⁷, C. Ordóñez⁸, A. Saiz-Lopez⁹, N. Warwick¹⁰, Q. Liang¹¹, W. Feng¹, F. Moore², B. R. Miller², V. Marécal, N. A. D. Richards¹, M. Dorf¹², and K. Pfeilsticker¹²

[1] Institute for Climate and Atmospheric Science (ICAS), School of Earth and Environment, University of Leeds, Leeds, UK

[2] National Oceanic and Atmospheric Administration, Boulder, USA

[4] GEOMAR Helmholtz Centre for Ocean Research Kiel, Kiel, Germany

[5] Rosenstiel School of Marine and Atmospheric Science, University of Miami, Miami, USA

[6] Institute for Atmospheric and Environmental Sciences, Universität Frankfurt/Main, Germany

[7] School of Environmental Sciences, University of East Anglia, Norwich, UK

[8] Met Office, Exeter, UK

[9] Atmospheric Chemistry and Climate Group, Institute for Physical Chemistry Rocasolano, CSIC, Madrid, Spain

[10] National Centre for Atmospheric Science (NCAS), University of Cambridge, Cambridge, UK

[11] Universities Space Research Association, GESTAR, Columbia, Maryland, USA

[12] Institute for Environmental Physics, University of Heidelberg, Heidelberg, Germany

[*] now at: Department of Geosciences, University of Oslo, Oslo, Norway

Published in: Atmospheric Chemistry and Physics, 13, 11819-11838, 10.5194/acp-13-11819-2013, 2013.



Evaluating global emission inventories of biogenic bromocarbons

R. Hossaini¹, H. Mantle¹, M. P. Chipperfield¹, S. A. Montzka², P. Hamer³, F. Ziska⁴, B. Quack⁴, K. Krüger^{4,*}, S. Tegtmeier⁴, E. Atlas⁵, S. Sala⁶, A. Engel⁶, H. Bönisch⁶, T. Keber⁶, D. Oram⁷, G. Mills⁷, C. Ordóñez⁸, A. Saiz-Lopez⁹, N. Warwick¹⁰, Q. Liang¹¹, W. Feng¹, F. Moore², B. R. Miller², V. Maréchal³, N. A. D. Richards¹, M. Dorf¹², and K. Pfeilsticker¹²

¹Institute for Climate and Atmospheric Science (ICAS), School of Earth and Environment, University of Leeds, Leeds, UK

²National Oceanic and Atmospheric Administration, Boulder, USA

⁴GEOMAR Helmholtz Centre for Ocean Research Kiel, Kiel, Germany

⁵Rosenstiel School of Marine and Atmospheric Science, University of Miami, Miami, USA

⁶Institute for Atmospheric and Environmental Sciences, Universität Frankfurt/Main, Germany

⁷School of Environmental Sciences, University of East Anglia, Norwich, UK

⁸Met Office, Exeter, UK

⁹Atmospheric Chemistry and Climate Group, Institute for Physical Chemistry Rocasolano, CSIC, Madrid, Spain

¹⁰National Centre for Atmospheric Science (NCAS), University of Cambridge, Cambridge, UK

¹¹Universities Space Research Association, GESTAR, Columbia, Maryland, USA

¹²Institute for Environmental Physics, University of Heidelberg, Heidelberg, Germany

* now at: Department of Geosciences, University of Oslo, Oslo, Norway

Correspondence to: R. Hossaini (r.hossaini@see.leeds.ac.uk)

Received: 9 April 2013 – Published in Atmos. Chem. Phys. Discuss.: 14 May 2013

Revised: 18 September 2013 – Accepted: 4 November 2013 – Published: 6 December 2013

Abstract. Emissions of halogenated very short-lived substances (VSLS) are poorly constrained. However, their inclusion in global models is required to simulate a realistic inorganic bromine (Br_y) loading in both the troposphere, where bromine chemistry perturbs global oxidising capacity, and in the stratosphere, where it is a major sink for ozone (O_3). We have performed simulations using a 3-D chemical transport model (CTM) including three *top-down* and a single *bottom-up* derived emission inventory of the major brominated VSLS bromoform (CHBr_3) and dibromomethane (CH_2Br_2). We perform the first concerted evaluation of these inventories, comparing both the magnitude and spatial distribution of emissions. For a quantitative evaluation of each inventory, model output is compared with independent long-term observations at National Oceanic and Atmospheric Administration (NOAA) ground-based stations and with aircraft observations made during the NSF (National Science Foundation) HIAPER Pole-to-Pole Observations (HIPPO) project. For CHBr_3 , the mean absolute deviation between model and surface observation ranges from 0.22 (38 %) to 0.78 (115 %) parts per trillion (ppt) in the trop-

ics, depending on emission inventory. For CH_2Br_2 , the range is 0.17 (24 %) to 1.25 (167 %) ppt. We also use aircraft observations made during the 2011 Stratospheric Ozone: Halogen Impacts in a Varying Atmosphere (SHIVA) campaign, in the tropical western Pacific. Here, the performance of the various inventories also varies significantly, but overall the CTM is able to reproduce observed CHBr_3 well in the free troposphere using an inventory based on observed sea-to-air fluxes. Finally, we identify the range of uncertainty associated with these VSLS emission inventories on stratospheric bromine loading due to VSLS ($\text{Br}_y^{\text{VSLS}}$). Our simulations show $\text{Br}_y^{\text{VSLS}}$ ranges from ~ 4.0 to 8.0 ppt depending on the inventory. We report an optimised estimate at the lower end of this range (~ 4 ppt) based on combining the CHBr_3 and CH_2Br_2 inventories which give best agreement with the compilation of observations in the tropics.

1 Introduction

On regional to global scales, bromine (Br) chemistry plays an important role in atmospheric composition. In the stratosphere, through coupling with analogous chlorine radicals, active bromine ($\text{Br}_x = \text{Br} + \text{BrO}$) takes part in catalytic cycles (e.g. $\text{BrO}-\text{ClO}$) which cause large seasonal ozone (O_3) loss during polar spring (e.g. Solomon, 1999, and references therein). At midlatitudes, a cycle involving hydroperoxyl radicals (HO_2) (e.g. Lary, 1996) is also significant, particularly during periods of elevated stratospheric aerosol when heterogeneous halogen activation is enhanced (Salawitch et al., 2005; Feng et al., 2007). Reduced column O_3 increases the transmission of potentially harmful ultraviolet (UV) radiation to the surface, in addition to impacting surface temperature and climate both directly and indirectly (e.g. WMO, 2011, and references therein).

In the troposphere, where understanding of halogen impacts is evolving rapidly (e.g. Saiz-Lopez and von Glasow, 2012), Br-mediated O_3 loss is also significant (von Glasow et al., 2004; Yang et al., 2005), such as in the marine boundary layer (MBL) (e.g. Read et al., 2008) where biogenic emissions of halogenated species can be large (e.g. Carpenter and Liss, 2000; Quack and Wallace, 2003). Modelling work has also highlighted the importance of halogen-driven O_3 loss in the mid–upper troposphere (Saiz-Lopez et al., 2012). Through reactions involving HO_x (OH and HO_2) and NO_x (NO and NO_2), bromine chemistry may indirectly perturb oxidising capacity and thus impact the lifetime of greenhouse gases (GHGs) such as methane (CH_4) (e.g. Lary and Toumi, 1997). Bromine chemistry may also impact other climate-relevant species; e.g. bromine monoxide (BrO) is a significant sink for dimethyl sulfide (DMS) – a precursor for cloud condensation nuclei (CCN) (Breider et al., 2010).

Sources of organic bromine include anthropogenic emissions of long-lived halons (e.g. CBrF_3 , Halon 1301) and also methyl bromide (CH_3Br), whose emissions are mostly biogenic (>70%) (e.g. WMO, 2011). As their production is regulated under the Montreal Protocol (and amendments), the total tropospheric bromine burden from these gases is now declining, from a peak observed towards the end of the 20th century (Montzka et al., 2003). Given their long tropospheric lifetimes, these gases are a relatively minor source of total inorganic bromine (Br_y) below the tropopause. However, in the stratosphere they account for ~75% of the total Br_y budget. The remainder is thought to arise from so-called very short-lived substances (VSLS) of predominately natural oceanic origin (e.g. Sturges et al., 2000; Pfeilsticker et al., 2000). In recent years, both observational (e.g. Sioris et al., 2006; Dorf et al., 2006, 2008; Salawitch et al., 2010; Brinckmann et al., 2012) and modelling (e.g. Schofield et al., 2011; Hossaini et al., 2012b; Tegmeier et al., 2012; Aschmann and Sinnhuber, 2013) studies have constrained their contribution to stratospheric Br_y ($\text{Br}_y^{\text{VSLS}}$) – currently estimated at 1–8 parts per trillion (ppt) (Montzka and Reimann, 2011).

The most abundant Br-containing VSLS are bromoform (CHBr_3) and dibromomethane (CH_2Br_2) with mean MBL mixing ratios of ~1.1 and 1.5 ppt. As their nominal surface lifetimes are short (~26 and 120 days, assuming $[\text{OH}] = 1 \times 10^6 \text{ molecules cm}^{-3}$ and a global/seasonal mean photolysis rate), and their emissions exhibit significant spatial and temporal inhomogeneity, tropospheric gradients can be large (Montzka and Reimann, 2011). Localised *hot-spots*, where emissions are relatively strong, have been identified; for example Mace Head (Ireland) (e.g. Carpenter et al., 2005). At present, the total global source strength of these VSLS are poorly constrained and range from 430 to 1400 Gg Br yr^{-1} and 57–280 Gg Br yr^{-1} for CHBr_3 and CH_2Br_2 (Montzka and Reimann, 2011). For global-scale models, a sound treatment of the magnitude and spatial distribution of VSLS emissions is required in order to simulate a reasonable Br_y budget in both the troposphere and the stratosphere. As recent chemistry–climate model (CCM) studies suggest $\text{Br}_y^{\text{VSLS}}$ in the lower stratosphere may increase in response to climate change (Dessens et al., 2009; Hossaini et al., 2012a), validation of VSLS emission inventories is particularly important.

Here, we use a three-dimensional (3-D) chemical transport model (CTM) to investigate global CHBr_3 and CH_2Br_2 emission inventories. We perform the first concerted evaluation of three *top-down* and a single *bottom-up* derived inventory using a combination of long-term ground-based observations and aircraft observations. A case study for the period of the 2011 Stratospheric Ozone: Halogen Impacts in a Varying Atmosphere (SHIVA) campaign, in which aircraft VSLS observations were obtained over the poorly sampled tropical western Pacific, is also performed. Finally, we update our previous model estimate of stratospheric $\text{Br}_y^{\text{VSLS}}$ based on these new emission data sets. Section 2 provides a description of the CTM and the emission inventories. Section 3 contains a quantitative comparison of the CTM with ground-based data. Section 4 contains a comparison of the CTM with observations from the recent HIAPER Pole-to-Pole Observation (HIPPO) campaigns. Section 5 highlights results from the SHIVA western Pacific case study. Section 6 examines the sensitivity of $\text{Br}_y^{\text{VSLS}}$ to emission inventories. A summary and conclusions are given in Sect. 7.

2 Model and experiments

TOMCAT is a global 3-D CTM described in Chipperfield (2006). The CTM runs *offline* and uses prescribed 6 h wind, temperature and humidity fields from the European Centre for Medium-Range Weather Forecasts (ECMWF) ERA Interim reanalysis. The CTM includes a treatment of convection, described in Stockwell and Chipperfield (1999) and further validated in Feng et al. (2011), based on the mass flux scheme of Tiedtke (1989). Vertical winds are diagnosed from divergence. In the boundary layer, turbulent mixing follows the non-local scheme of Holtslag and Boville (1993). For

tracer advection, the CTM uses the conservation of 2nd-order moments scheme of Prather (1986). The CTM was run with a resolution of $\sim 2.8^\circ$ longitude $\times \sim 2.8^\circ$ latitude and with 60 hybrid sigma-pressure (σ - p) levels (surface to ~ 60 km).

The CTM configuration here is similar to that of Hossaini et al. (2012b) and includes 5 brominated very short-lived (VSL) source gases (SGs): CHBr_3 , CH_2Br_2 , dibromochloromethane (CHBr_2Cl), bromodichloromethane (CHBrCl_2) and bromochloromethane (CH_2BrCl). Loss of these SGs occurs via oxidation with the hydroxyl radical (OH) or by photolysis, calculated using the recommended rate constants/absorption cross-section data of Sander et al. (2011). For simulations here, the CTM used a prescribed monthly mean OH field which was used in TransCom- CH_4 (Patra et al., 2011) and produced reasonable simulations of methyl chloroform (CH_3CCl_3) and CH_4 .

2.1 Biogenic emissions from the ocean

Given the significant uncertainty in global VSLs emissions, TOMCAT was run for the period 1 January 1997 to 31 December 2011 with 4 previously published oceanic CHBr_3 and CH_2Br_2 emission inventories. Run S_{Liang} used the top-down emission fluxes of Liang et al. (2010) (hereafter “Liang-2010”). Run S_{Warwick} used the top-down estimates described in Warwick et al. (2006) and updated in Pyle et al. (2011) (hereafter “Warwick-2011”). Run $S_{\text{Ordóñez}}$ used the top-down estimates of Ordóñez et al. (2012) (“Ordóñez-2012”). Finally, run S_{Ziska} used the bottom-up emission fluxes proposed by Ziska et al. (2013) (“Ziska-2013”). The global total emissions for each source gas under each scenario is given in Table 1.

The top-down inventories described below rely on aircraft observations of CHBr_3 and CH_2Br_2 to constrain surface fluxes using a global model. Assumptions regarding the latitudinal distribution and the relative importance of open ocean versus coastal emissions are made and vary between inventories. Therefore, some of the most significant uncertainty in the top-down approach is due to the lack of available CHBr_3 and CH_2Br_2 observations in the free troposphere over certain regions and due to the lack of understanding of emission distribution. An iterative modelling approach is used whereby the magnitude of emissions within a given latitude band is adjusted, in a sequential set of simulations, to yield the optimised agreement with observations. Model parameters, such as coarse horizontal resolution, may add further uncertainty as strong local emissions, such as those from coastal regions, are smeared over a relatively large grid box. The use of observations representative of the background tropospheric CHBr_3 and CH_2Br_2 loading may also lead to an under-representation of particularly strong local emissions or *hot-spots* in the top-down approach.

The Warwick-2011 scenario is a top-down estimate based on the original work of Warwick et al. (2006). Aircraft observations of CHBr_3 and CH_2Br_2 , collected during the 1999

Table 1. Summary of 14 yr CTM runs and the global total source strength ($\text{Gg source gas yr}^{-1}$) of CHBr_3 and CH_2Br_2 .

Run	Scenario	Derivation	CHBr_3	CH_2Br_2
S_{Liang}	Liang-2010	Top-down	450	62
S_{Warwick}	Warwick-2011	Top-down	380	113
$S_{\text{Ordóñez}}$	Ordóñez-2012	Top-down	533	67
S_{Ziska}	Ziska-2013	Bottom-up	183	64

National Aeronautics and Space Administration (NASA) Pacific Exploratory Mission (PEM) Tropics B, were used to constrain surface emissions. The updated scenario used here is based on scenario 5 outlined in Warwick et al. (2006), however South-east Asian CHBr_3 emissions have been scaled down to give agreement with surface observations collected at Danum Valley, Borneo. This updated scenario is further described in Pyle et al. (2011).

The Liang-2010 scenario is also a model top-down estimate constrained by aircraft observations. These observations were mostly concentrated around the Pacific and North America between 1996 and 2008 and include the following campaigns: PEM-Tropics, TRACE-P, INTEX, TC4, ARCTAS, STRAT, Pre-AVE and AVE (Liang et al., 2010). The emissions were formulated using a baseline scenario from Warwick et al. (2006), which was adjusted in both magnitude and location, so that modelled CHBr_3 and CH_2Br_2 gave good agreement with observations in the mid-troposphere, and the observed vertical gradient was well represented. The spatial distribution of emissions is assumed to be equal for CHBr_3 and CH_2Br_2 .

The Ordóñez-2012 scenario is the third top-down estimate. It is formulated using the same aircraft observations as Liang-2010 but also includes those obtained during the NASA POLARIS and SOLVE missions. This scenario is relatively sophisticated as, in the tropics ($\pm 20^\circ$), VSLs emissions are weighted towards the concentration of chlorophyll *a* (chl *a*); a potential proxy for oceanic bio-productivity. A monthly-varying satellite chl *a* climatology was used which allows some seasonality in the magnitude of the CHBr_3 and CH_2Br_2 emission fields. This is the only inventory to consider such seasonality. Outside of tropical latitudes the sea-air flux is constant with coastal emissions assumed to be a factor of 2.5 larger than the open ocean.

Finally, the Ziska-2013 scenario is a bottom-up estimate of emissions. Based on data of the HalOcat database project (<https://halocat.geomar.de/>), global surface marine and atmospheric concentration maps of CHBr_3 and CH_2Br_2 (and CH_3I) were calculated in order to derive global sea-to-air flux estimates. The available in situ measurements were classified according to current knowledge about the distribution and possible sources of each compound, as well as the physical and biogeochemical characteristics of ocean and atmosphere. Missing $1^\circ \times 1^\circ$ grid values were extrapolated with

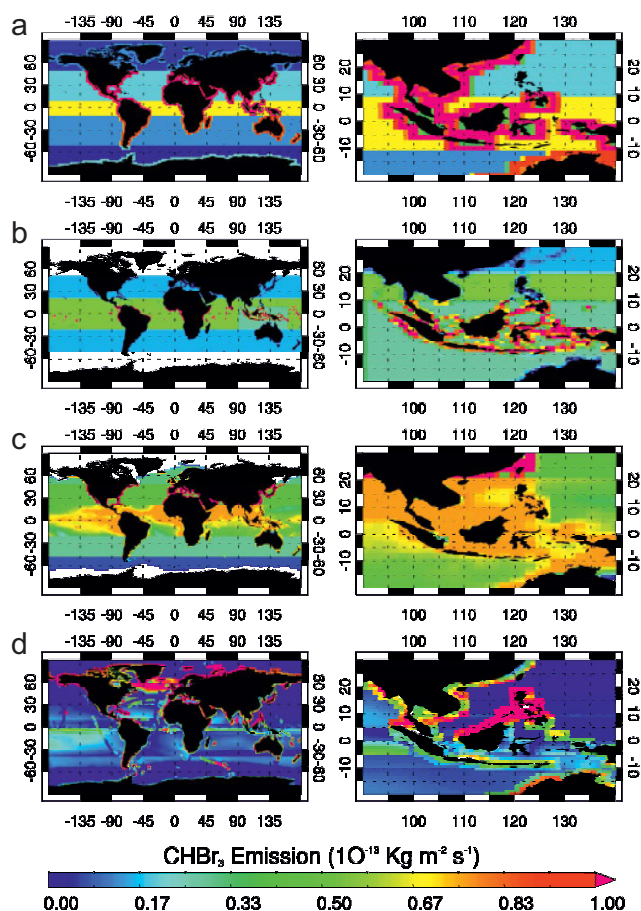


Fig. 1. Bromoform emission field ($10^{-13} \text{ kg m}^{-2} \text{ s}^{-1}$) on $1^\circ \times 1^\circ$ grid for global (left) and western Pacific (right) regions. Emissions from the (a) Liang-2010, (b) Warwick-2011, (c) Ordóñez-2012 and (d) Ziska-2013 scenarios.

the ordinary least square (OLS) regression technique depending on longitude and latitude. The OLS method includes outliers and thus represents the spread and variable concentration distribution well. Based on the generated marine and atmospheric surface concentration maps, global climatological emission maps were calculated with a commonly used sea-to-air flux parameterisation. This applied highly temporal (6 h) resolved wind speed, sea surface temperature, salinity and pressure data (Ziska et al., 2013).

Global emission maps for CHBr_3 and CH_2Br_2 are shown in Figs. 1 and 2, respectively. All scenarios differ significantly over the tropical western Pacific – an important region for the troposphere–stratosphere transport of VSLS (e.g. Aschmann et al., 2009), where observations of these species are limited. The latitudinal-dependence of emissions is shown in Fig. 3. For CHBr_3 , significant variation between the top-down derived estimates (Warwick-2011, Liang-2010, Ordóñez-2012) and the bottom-up estimate (Ziska-2013) is apparent – particularly in the tropics ($\pm 20^\circ$) and at high latitudes ($> 60^\circ$) in the Northern Hemisphere (NH). For CH_2Br_2 ,

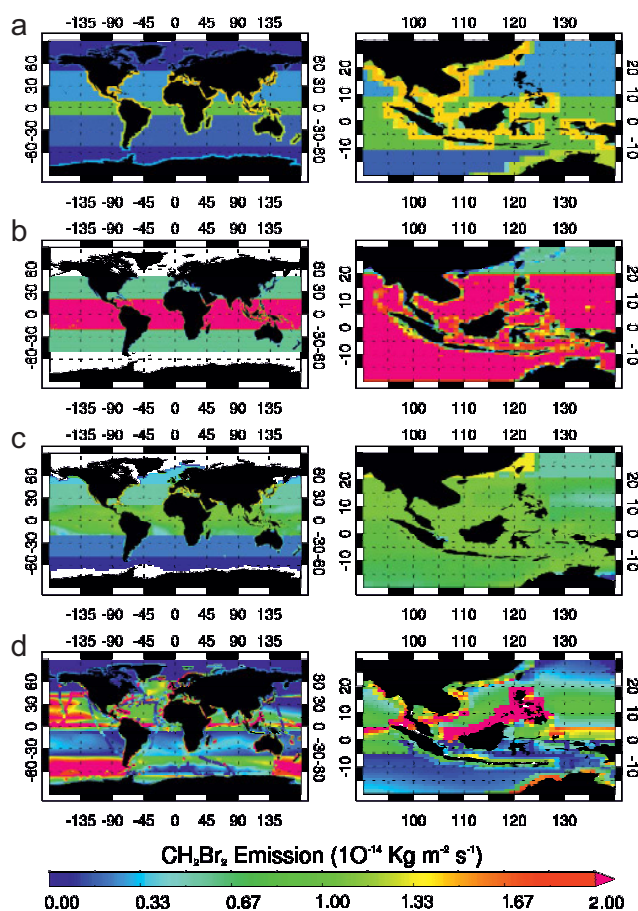


Fig. 2. As Fig. 1 but for dibromomethane ($10^{-14} \text{ kg m}^{-2} \text{ s}^{-1}$). Note the change in scale.

the total global source strength between inventories is more consistent (Table 1), with the exception of Warwick-2011 in which it is $\sim 1.7\times$ larger than the others. Both Warwick-2011 and Ziska-2013 exhibit a significantly stronger CH_2Br_2 emission in the tropics relative to Liang-2010 and Ordóñez-2012. The Ziska-2013 inventory also contains particularly strong emissions in the Southern Hemisphere (see Ziska et al., 2013).

For minor VSLS (CHBr_2Cl , CHBrCl_2 & CH_2BrCl), emissions are not specified, rather their surface abundance is constrained using an assumed uniform volume mixing ratio (0.3, 0.3, 0.5 ppt) based on compiled observations in the tropical MBL (Montzka and Reimann, 2011). Note, Warwick et al. (2006) and Ordóñez et al. (2012) reported emissions for these species but they are not available at present from the other inventories considered. While these minor VSLS are not the focus of this work, they are included in the calculation of $\text{Br}_y^{\text{VSLS}}$ in Sect. 6. As their nominal lifetime is relatively long-lived at the surface (59, 78 and 137 days) (Montzka and Reimann, 2011), the spatial distribution of emission is less important for their troposphere–stratosphere transport (relative to CHBr_3).

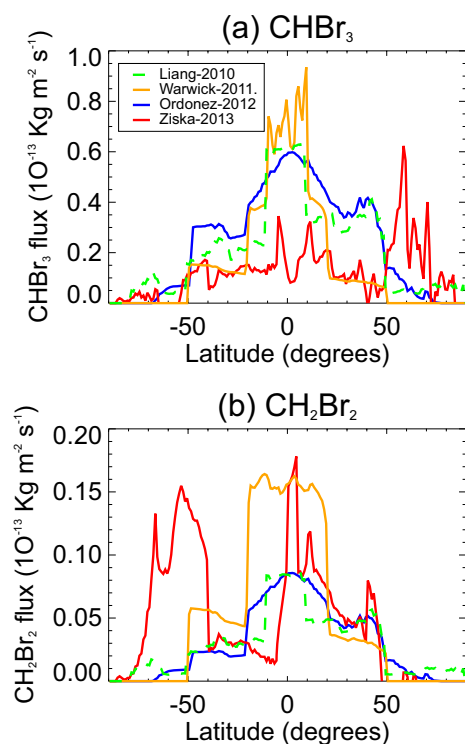


Fig. 3. Zonally averaged global emission source strength ($10^{-13} \text{ kg m}^{-2} \text{ s}^{-1}$) for (a) CHBr_3 and (b) CH_2Br_2 .

3 Evaluation of emission inventories with long-term ground-based observations

Previous model studies have used aircraft observations to validate simulated VLSL profiles in the upper troposphere (e.g. Liang et al., 2010; Ashfold et al., 2012; Hossaini et al., 2012b; Ordóñez et al., 2012). Ideally, global models should be evaluated against observations from multiple platforms. For VLSL, whose emissions are poorly constrained and represent a significant uncertainty in global-scale models, a robust validation of available emission inventories with ground-based observations is desirable. As the troposphere–stratosphere transport of VLSL is highly dependant on the location of emissions (Aschmann et al., 2009), validation of both the spatial distribution and magnitude of emissions is needed. However, to date an evaluation of published emission inventories has yet to be performed.

In this study, multi-annual observations of CHBr_3 and CH_2Br_2 at 14 ground-based stations (Table 2) have been used to validate modelled fields and test emission estimates. The observed data are from an ongoing cooperative flask sampling program of the National Oceanic and Atmospheric Administration/Earth System Research Laboratory (NOAA/ESRL). Figure 4 shows the location of observations. Whole air samples (WAS) were collected approximately weekly into paired steel or glass flasks and were analysed using gas chromatography/mass spectrometry (GC-MS)

Table 2. Summary and location of NOAA/ESRL ground-based stations arranged from north to south. * Stations SUM, MLO and SPO elevated at ~ 3210 , 3397 and 2810 m respectively.

Station	Name	Lat	Lon
ALT	Alert, NW Territories, Canada	82.5° N	62.3° W
SUM*	Summit, Greenland	72.6° N	38.4° W
BRW	Pt. Barrow, Alaska, USA	71.3° N	156.6° W
MHD	Mace Head, Ireland	53.0° N	10.0° W
LEF	Wisconsin, USA	45.6° N	90.2° W
HFM	Massachusetts, USA	42.5° N	72.2° W
THD	Trinidad Head, USA	41.0° N	124.0° W
NWR	Niwot Ridge, Colorado, USA	40.1° N	105.6° W
KUM	Cape Kumukahi, Hawaii, USA	19.5° N	154.8° W
MLO*	Mauna Loa, Hawaii, USA	19.5° N	155.6° W
SMO	Cape Matatula, American Samoa	14.3° S	170.6° W
CGO	Cape Grim, Tasmania, Australia	40.7° S	144.8° E
PSA	Palmer Station, Antarctica	64.6° S	64.0° W
SPO*	South Pole	90.0° S	–

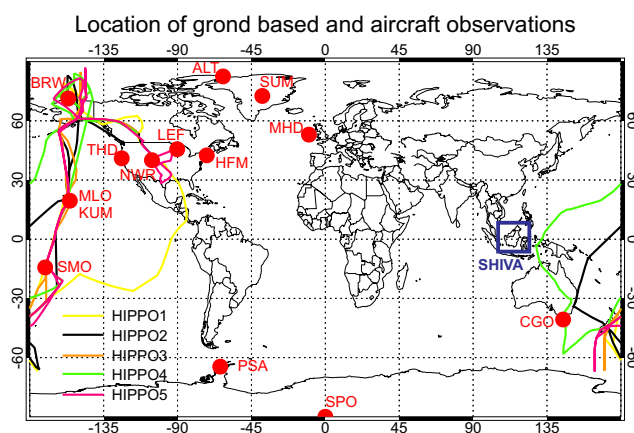


Fig. 4. Location of NOAA/ESRL ground-based monitoring stations. Note, the close proximity of stations MLO and KUM (see Table 2). In this work we group the stations into 5 latitude bands; high NH ($\geq 60^\circ$ N), midlatitude NH ($30\text{--}60^\circ$ N), tropical ($\pm 30^\circ$), midlatitude SH ($30\text{--}60^\circ$ S) and high SH ($\geq 60^\circ$ S). Also shown are the flight tracks from the NSF HIPPO aircraft campaigns (1–5) which took place between 2009 and 2011 (see Sect. 4). The location of the SHIVA aircraft campaign (see Sect. 5) that took place in the tropical western Pacific during Nov–Dec 2011 is also indicated.

(Montzka et al., 2003). NOAA data from flasks collected at surface sites and also on the HIPPO aircraft campaign are presented relative to the NOAA-2003 scale for CH_2Br_2 and the NOAA-2004 scale for CHBr_3 . These scales consist of 2–4 standards prepared with gravimetric techniques at 3–20 ppt in high-pressure (900 psi initially) 30 L, electropolished stainless steel canisters.

Figure 5 shows the NOAA/ESRL observed CHBr_3 mixing ratio at these stations (north–south). The observed data points are monthly mean fields that have been calculated from a 14 yr monthly mean data set (i.e. we have taken the mean of

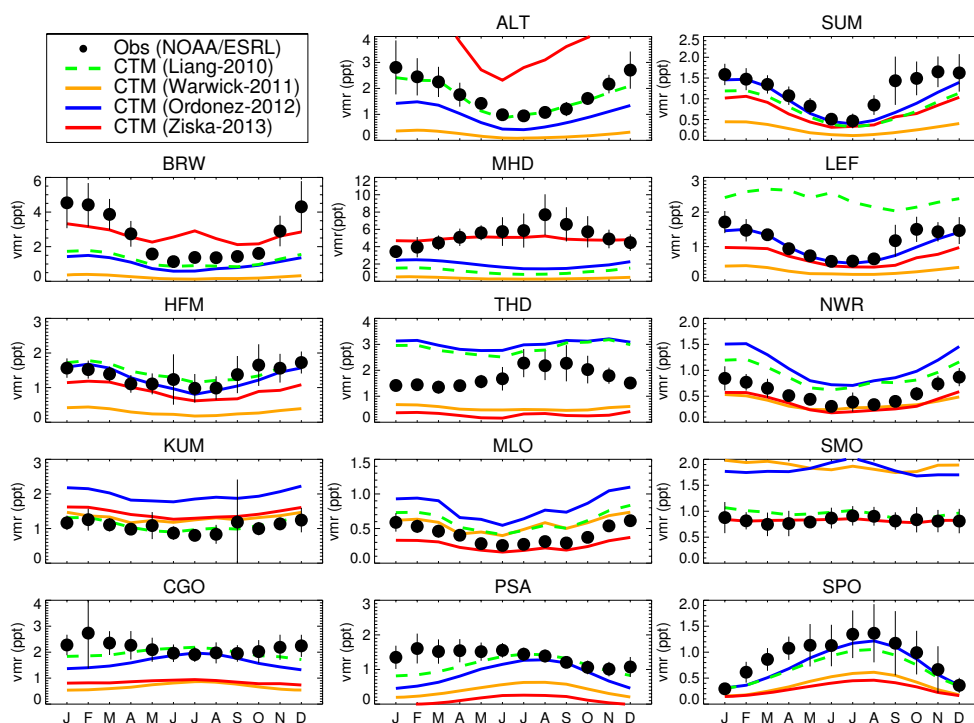


Fig. 5. Comparison of observed monthly mean CHBr_3 mixing ratio (ppt) at 14 NOAA/ESRL ground stations with output from TOMCAT runs S_{Liang} (Liang-2010 emissions), S_{Warwick} (Warwick-2011 emissions), $S_{\text{Ordóñez}}$ (Ordóñez-2012 emissions) and S_{Ziska} (Ziska-2013 emissions). The vertical bars denote ± 1 standard deviation on the observed mean (see text for details).

monthly mean fields). This approach smooths intra-monthly variability but can give a clear signal of seasonal variations. The observations spanned the period 1 January 98 to 1 January 2012 at all stations except SPO, THD, and SUM, which are shorter records. Also shown in Fig. 5 is the corresponding modelled CHBr_3 mixing ratio from runs S_{Liang} , S_{Warwick} , $S_{\text{Ordóñez}}$ and S_{Ziska} . The CTM was run for the same (14 yr) period following 3 yr of spin-up. Monthly mean data was output allowing a like-for-like comparison between model and observation.

At NH high-latitude ($\geq 60^\circ$) stations (ALT, SUM and BRW), observed CHBr_3 exhibits a pronounced seasonal cycle with elevated mixing ratios during NH winter (DJF). This seasonality, likely due to the enhanced photochemical sink of CHBr_3 during summer (JJA) months (or potentially transport), has been previously observed (at ALT) by Yokouchi et al. (1996). The CTM captures this seasonality, particularly at ALT and SUM, where the bias between model and observation is highly dependent on the emission inventory used. The top-down inventories (Liang-2010, Warwick2011 and Ordóñez-2012) on average underestimate observed CHBr_3 at these high-latitude NH stations (Fig. 5). The calculated mean bias (model minus observation) for the entire 14 yr monthly-mean data set is -0.65 , -1.61 and -0.88 ppt for these inventories, respectively. The bottom-up estimate of Ziska-2013 overestimates with a positive mean bias of $+0.54$ ppt. This is

skewed by the significant overestimation of CHBr_3 at ALT. It was previously shown in Fig. 3 that Ziska-2013 exhibits a significantly larger CHBr_3 source at high NH latitudes over the other inventories considered.

At NH midlatitude ($30\text{--}60^\circ$ N) stations (MHD, LEF, HFM, THD and NWR), the agreement between model and observation varies significantly with emission inventory. At Mace Head (MHD), the top-down inventories underestimate the large background CHBr_3 (up to ~ 8 ppt). However, the larger bottom-up emissions of Ziska-2013 in this region lead to a reasonable agreement between model and observation. Note, here the seasonal cycle is out of expected phase, as a CHBr_3 minimum is observed during winter months and a maximum during summer. Carpenter et al. (2005) observed a similar seasonality and deduced that strong local emissions (during summer) dominate over enhanced photochemical loss to control the local CHBr_3 abundance at MHD.

For VLSL, transport to the stratosphere is most efficient in tropical regions where convection can rapidly loft boundary layer air into the mid/upper troposphere (e.g. Aschmann et al., 2009). At tropical ($\pm 30^\circ$) stations KUM and MLO there is also noticeable seasonality in observed CHBr_3 . This is in phase with most other NH stations and indicative of larger-scale processes (likely the photochemical sink) controlling the seasonality. The bias between the model and observation is again varied and strongly dependent on emission

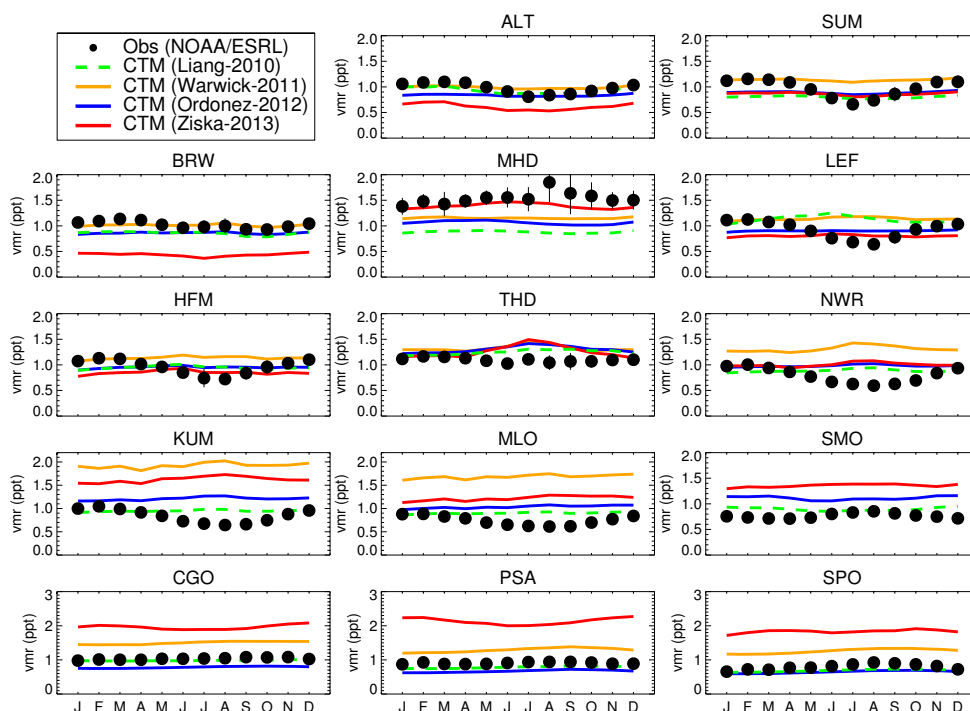


Fig. 6. As Fig. 5 but for CH_2Br_2 .

inventory. The Ordóñez-2012 emissions, which are weighted towards a seasonal climatology of chlorophyll *a* in the tropics, lead to an overestimate of CHBr_3 at each tropical station (KUM, MLO and SMO), and for all months. For these stations the mean bias is 0.12, 0.48, 0.76 and 0.07 ppt for runs S_{Liang} , S_{Warwick} , $S_{\text{Ordóñez}}$ and S_{Ziska} , respectively. This indicates that the Liang-2010 (top-down) and the Ziska-2013 (bottom-up) derived CHBr_3 emissions perform particularly well at these locations in the tropical Pacific.

In the SH, long-term observations of VSLs are particularly sparse. In the SH midlatitude ($30\text{--}60^\circ\text{S}$) band, data from just one station is available (CGO). Here, CHBr_3 is generally underestimated but reasonable agreement is obtained with the Liang-2010 and Ordóñez-2012 inventories. This is also the case at the two high-latitude SH stations ($60\text{--}90^\circ\text{S}$) PSA and SPO. Here, a clear seasonal cycle is apparent at the latter with a CHBr_3 maximum occurring during SH winter (JJA), consistent with Swanson et al. (2004) and Beyersdorf et al. (2010) who note a similar seasonality. The CTM is able to reproduce this seasonality well, which is likely driven by photochemistry, and again the Liang-2010 and Ordóñez-2012 scenarios provide the best agreement.

For CH_2Br_2 , a similar comparison between the observations and the model has been performed (Fig. 6). Photolysis is a minor tropospheric sink for CH_2Br_2 , which has a nominal surface lifetime of ~ 120 days (Montzka and Reimann, 2011), and whose dominant sink is by reaction with OH. As its lifetime is significantly longer than that of CHBr_3

(~ 26 days), horizontal gradients are expected to be less pronounced. The observations show background mixing ratios in the range of $\sim 0.5\text{--}1.5$ ppt at all stations (excluding MHD) with generally low variability. Seasonality is apparent at most sites in the NH (e.g. ALT, SUM, LEF, NWR, KUM, MLO etc.), and is likely due to seasonal changes to the $\text{CH}_2\text{Br}_2 + \text{OH}$ loss rate. The magnitude of relative variation is smaller than that for CHBr_3 due to the significantly longer lifetime of CH_2Br_2 .

The global CH_2Br_2 source strength is relatively similar for 3 out of the 4 inventories considered: $62\text{--}67\text{ Gg yr}^{-1}$, among Liang-2010, Ordóñez-2012 and Ziska-2013. However, it is significantly larger (113 Gg yr^{-1}) in the Warwick-2011 inventory. Also, the latitudinal distribution of emissions, including in the tropics, varies significantly between inventories (e.g. Fig. 3). At tropical stations KUM, MLO and SMO, CH_2Br_2 is overestimated when using Warwick-2011 and Ziska-2013 emissions. At these stations, improved agreement is obtained using Ordóñez-2012 and good agreement using Liang-2010. In the SH, between ~ 40 and 75°S , the Ziska-2013 inventory exhibits a particularly strong CH_2Br_2 source (see Fig. 3), not featured in the other inventories. Comparison of modelled CH_2Br_2 with observations within this latitude range (i.e. CGO and PSA sites) show a significant overestimation of CH_2Br_2 , by an approximate factor of 2, when using the Ziska-2013 inventory.

For a more quantitative evaluation of the modelled CHBr_3 and CH_2Br_2 fields with these long-term surface observations,

Table 3. Summary of calculated error metrics between NOAA/ESRL observed surface CHBr₃ with analogous fields from CTM runs S_{Liang} , S_{Ziska} , S_{Warwick} and S_{Ordonez} . Shown is the mean bias (MB) and the mean absolute deviation (MAD) both in units of ppt. Also shown is the mean absolute percentage error (MAPE, see text). These fields were calculated for the entire 14 yr period of available observation (1 January 1998–1 January 2012) and for the 5 latitudinal bands shown in Fig. 4. The global values shown are a comparison for all 14 stations.

Latitude	Run S_{Liang}			Run S_{Warwick}			Run S_{Ordonez}			Run S_{Ziska}		
	MB	MAD	MAPE	MB	MAD	MAPE	MB	MAD	MAPE	MB	MAD	MAPE
≥ 60° N	−0.65	0.73	33 %	−1.61	1.61	84 %	−0.88	0.91	42 %	0.54	1.24	79 %
30–60° N	−0.25	1.45	84 %	−1.64	1.64	67 %	−0.35	1.15	59 %	−0.57	0.77	42 %
±30°	0.12	0.22	38 %	0.48	0.52	77 %	0.76	0.78	115 %	0.07	0.26	36 %
30–60° S	−0.20	0.45	19 %	−1.48	1.48	67 %	−0.54	0.63	26 %	−1.32	1.32	59 %
≥ 60° S	−0.24	0.32	28 %	−0.75	0.75	61 %	−0.32	0.40	33 %	−0.93	0.93	77 %
Global	−0.25	0.80	50 %	−1.04	1.25	72 %	−0.24	0.87	61 %	−0.30	0.82	55 %

Table 4. As Table 3 but for CH₂Br₂.

Latitude	Run S_{Liang}			Run S_{Warwick}			Run S_{Ordonez}			Run S_{Ziska}		
	MB	MAD	MAPE	MB	MAD	MAPE	MB	MAD	MAPE	MB	MAD	MAPE
≥ 60° N	−0.11	0.15	15 %	0.08	0.14	16 %	−0.11	0.15	15 %	−0.34	0.36	36 %
30–60° N	−0.03	0.28	27 %	0.18	0.33	37 %	−0.00	0.24	24 %	0.02	0.21	22 %
±30°	0.14	0.17	24 %	1.25	1.25	167 %	0.35	0.35	49 %	0.63	0.63	85 %
30–60° S	−0.05	0.10	10 %	0.47	0.49	48 %	−0.25	0.25	23 %	0.93	0.94	92 %
≥ 60° S	−0.11	0.12	13 %	0.43	0.45	55 %	−0.19	0.19	21 %	1.14	1.14	137 %
Global	−0.02	0.19	20 %	0.44	0.52	64 %	0.00	0.24	27 %	0.30	0.52	60 %

three error metrics were calculated (Tables 3, 4); the mean bias (MB) (ppt), calculated using Eq.(1), the mean absolute deviation (MAD) (ppt), calculated using Eq.(2), and the mean absolute percentage error (MAPE), using Eq.(3), for the 5 latitudinal bands considered. Here, M and O denote the monthly modelled and observed fields for the entire 14 yr period of comparison, respectively. The total number of comparison points (n) is 168.

$$\text{MB} = \frac{1}{n} \sum_{t=1}^n (M_t - O_t) \quad (1)$$

$$\text{MAD} = \frac{1}{n} \sum_{t=1}^n |M_t - O_t| \quad (2)$$

$$\text{MAPE} = \frac{100}{n} \sum_{t=1}^n \left| \frac{M_t - O_t}{O_t} \right| \quad (3)$$

Based on the reported error metrics it is clear the performance of each inventory varies significantly by region. Focusing on the important tropical latitude band, for CHBr₃ the MAPE between model and observation ranges between 36 % and 115 %. The best agreement, diagnosed by the lowest MAPE (36 %), is obtained from run S_{Ziska} (bottom-up emissions). S_{Liang} also performs well in the tropics with a

similar MAPE of 38 %, which is significantly lower than runs S_{Warwick} and S_{Ordonez} . Note, small values of observed CHBr₃ can cause large skew in the calculated MAPE (see Eq. 3). For CH₂Br₂, MAPE ranges from 24 to 166 % in the tropics. The best agreement is obtained from run S_{Liang} (24 %), using the Liang-2010 inventory which has the lowest total emissions in the tropics and also the lowest global total (see Fig. 3 also). The calculated mean bias presented in Table 4 confirms the significant overestimation of CH₂Br₂ by runs S_{Warwick} and S_{Ziska} suggesting a significant overestimate of the tropical CH₂Br₂ source in these emissions inventories.

Overall, the global performance (all stations) of each scenario can be assessed based on the error metrics in Table 3. Globally, the best agreement between model and observation, for both CHBr₃ and CH₂Br₂, is obtained for run S_{Liang} ; the global MAPE using the Liang-2010 inventory is 50 and 20 % for these species, respectively. To support this conclusion, further long-term observations of VLSL would be desirable, particularly in the tropics and in the poorly sampled Southern Hemisphere. While the NOAA/ESRL observations are a valuable long-term record, the spatial distribution of sampling is limited in these regions. Therefore, we also consider recent aircraft observations of CHBr₃ and CH₂Br₂ made during the HIPPO aircraft campaigns over the Pacific Basin that spanned global latitudes (Sect. 4). Observations of VLSL made in the poorly sampled tropical western Pacific during

the SHIVA campaign are also considered in a case study (Sect. 5).

The error metrics presented in Tables 3 and 4 were computed for all months. To examine any potential systematic seasonal bias between the model and the observations, probability density functions (PDF) have been computed by season and latitude band (see supplementary material). For both CHBr_3 and CH_2Br_2 , no clear systematic seasonal bias is apparent. The skill of the model in reproducing the observations is highly dependent on the magnitude/distribution of emissions, which were previously shown to vary significantly. The seasonality of these gases, observed at numerous ground-based stations, is generally well captured by aseasonal emissions (3 of the 4 inventories). This suggests at these sites the seasonality is largely driven by photochemistry; i.e. sinks that are well represented in the model.

4 Evaluation of emission inventories with HIPPO aircraft data

The HIAPER Pole-to-Pole Observations (HIPPO) project consisted of a series of aircraft campaigns between 2009 and 2011 supported by the National Science Foundation (NSF). Five missions were conducted (January 2009, November 2009, March/April 2010, June 2011 and August/September 2011). The aim of HIPPO was to make global measurements of various trace gases, including greenhouse gases CO_2 , CH_4 , N_2O and also CO , SF_6 , CFCs and bromine-containing VSLs (Wofsy et al., 2011). Sampling spanned a range of latitudes, from near the North Pole to coastal Antarctica, on board the NSF Gulfstream V aircraft and from the surface to ~ 14 km over the Pacific Basin. As such, these comprehensive data complement the long-term observations of VSLs discussed in Sect. 3 and allow for further evaluation of the model with varying emission inventories of CHBr_3 and CH_2Br_2 . The HIPPO data is particularly valuable for this analysis as it is independent, i.e. has not been used in constructing the emission inventories considered. The data is archived at the following web address: <http://www.eol.ucar.edu/projects/hippo/>.

Figures 7 and 8 compare mean observed profiles of CHBr_3 and CH_2Br_2 , made during HIPPO 1–5, with modelled TOMCAT profiles for the 5 latitude bands considered in this work. The observations here were collected using whole air samples, in stainless steel and glass flasks, and analysed by two different laboratories by gas chromatography/mass spectrometry (GC-MS); NOAA/ESRL and the University of Miami. Mixing ratios from HIPPO are reported on the same calibration scale as the NOAA/ESRL ground-based station results. The model has here been sampled for each flight track to match the observations and allowing a point-by-point comparison throughout the profiles. To assess the skill of the model against the HIPPO observations, three error metrics were again computed; the MB (ppt), calculated using Eq.(1),

the MAD (ppt), calculated using Eq.(2), and the MAPE, using Eq.(3), for the 5 latitudinal bands considered. These are summarised in Tables 5 and 6 for CHBr_3 and CH_2Br_2 , respectively.

In general, the model is able to reproduce the observed vertical distribution of CHBr_3 well in all latitude bands. The overall skill of the model is highly dependent on the given emission inventory. At high latitudes in the NH ($\geq 60^\circ$ N), the MAPE between the model and observation ranges from ~ 31 to 63% across HIPPO 1–5. As was reported in Sect. 3 using ground-based data, the best agreement, diagnosed by the lowest MAPE, is obtained from S_{Liang} . We find run S_{Liang} also gives the best agreement with observed CHBr_3 within the 30 – 60° N latitude band, where MAPE ranges between 28 and 51% . In the tropics ($\pm 30^\circ$), it was previously shown in Sect. 3 that run S_{Ziska} , with bottom-up derived emissions from sea-to-air fluxes, performed particularly well against long-term NOAA/ESRL ground-based observations. Based on the comparison with HIPPO observations here, run S_{Ziska} , which contains the lowest CHBr_3 source in the tropics (e.g. Fig. 3), is again found to give the best agreement in the tropics. Here, the MAPE ranges from ~ 35 to 102% with runs S_{Ziska} and S_{Ordonez} accounting for this lower and upper limit, respectively. The significant overestimate of CHBr_3 from S_{Ordonez} , along with the similar reported overestimate found from the ground-based analysis, suggests that CHBr_3 emissions from the Ordóñez-2012 inventory may be too large within the $\pm 30^\circ$ latitude band.

In the SH, where the coverage provided from the ground-based stations is limited, HIPPO made a number of observations. Within the 30 – 60° S band, the model performs reasonably well with the MAPE ranging from ~ 39 to 69% . The lower and upper limit is given by runs S_{Warwick} and S_{Ordonez} , respectively. At high latitudes in the SH (60 – 90° S), observations are limited relative to other latitude bands, however some profiles are available for analysis. Note, the exception being for HIPPO-4, during which observations $\geq 60^\circ$ S were particularly sparse. Nevertheless, in this region the model performs reasonably well with MAPE ranging from ~ 42 to 62% with the best agreement from run S_{Liang} .

To determine which CHBr_3 emission inventory gives best agreement globally, i.e. spanning the range of latitudes covered by HIPPO, we have also calculated a global MAPE (Table 5). Globally, the best agreement (lowest MAPE) between the model and observation is obtained from runs S_{Liang} and S_{Ziska} , where MAPE is $\sim 40\%$ for both. This supports the findings in Sect. 3, where it was also shown that the Liang-2010 and Ziska-2013 emission inventories give the best agreement with long-term NOAA/ESRL ground-based observations of CHBr_3 . Note, while the global MAPE happens to be similar for these two runs, differences within the 5 latitudes bands are apparent. For example, in the tropics ($\pm 30^\circ$), as noted, the better agreement is obtained from the lower (Ziska-2013) bottom-up emissions (MAPE $\sim 35\%$). In fact, this is the only inventory that results in a MAPE $< 50\%$ for

Table 5. Summary of calculated error metrics between CHBr_3 observed in the free troposphere during the HIPPO project (2009–2011) with analogous fields from CTM runs S_{Liang} , S_{Warwick} , S_{Ordonez} and S_{Ziska} . Shown are the MB and the MAD both in units of ppt. Also shown is the MAPE (see text). These fields were calculated for all observations made during HIPPO missions 1–5 for the 5 latitudinal bands shown in Fig. 4. A global value is also quoted for comparisons at all latitudes.

Latitude	Run S_{Liang}			Run S_{Warwick}			Run S_{Ordonez}			Run S_{Ziska}		
	MB	MAD	MAPE	MB	MAD	MAPE	MB	MAD	MAPE	MB	MAD	MAPE
$\geq 60^\circ \text{ N}$	−0.16	0.23	31 %	−0.55	0.55	63 %	−0.03	0.24	37 %	−0.25	0.26	38 %
$30\text{--}60^\circ \text{ N}$	0.04	0.12	28 %	−0.27	0.29	42 %	0.22	0.23	51 %	−0.25	0.25	42 %
$\pm 30^\circ$	0.30	0.31	63 %	0.32	0.33	68 %	0.51	0.51	102 %	−0.19	0.20	35 %
$30\text{--}60^\circ \text{ S}$	0.09	0.13	45 %	−0.07	0.13	39 %	0.19	0.21	69 %	−0.18	0.19	42 %
$\geq 60^\circ \text{ S}$	−0.12	0.21	42 %	−0.37	0.40	60 %	0.06	0.28	62 %	−0.40	0.41	54 %
Global	0.04	0.20	42 %	−0.17	0.34	54 %	0.21	0.30	65 %	−0.24	0.25	41 %

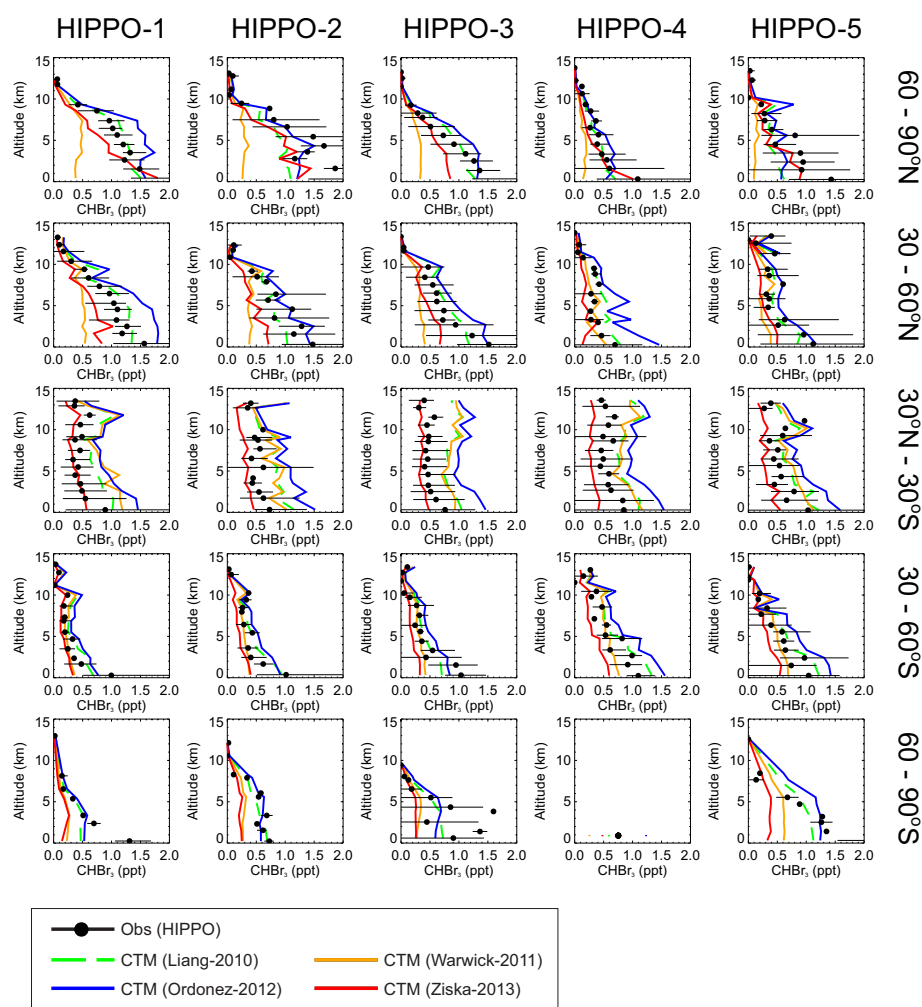
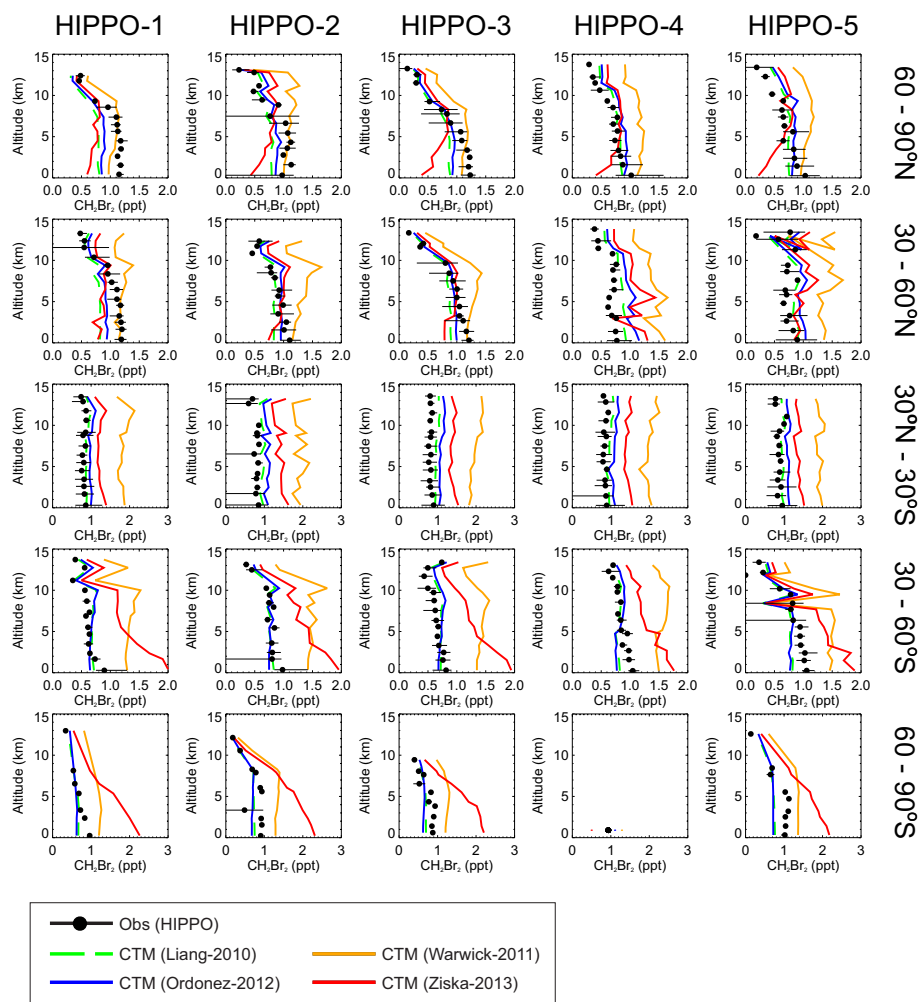


Fig. 7. Comparison of observed CHBr_3 profiles (ppt) made during the NSF HIPPO project (campaigns 1–5, 2009–2011) with analogous modelled profiles from TOMCAT runs S_{Liang} , S_{Warwick} , S_{Ordonez} and S_{Ziska} . All profiles shown are the average for the 5 latitudinal bands considered in this work and are also averaged vertically in ~ 1 km bins. The horizontal lines on the observed data denote the min–max variability from the mean. Note, very few observations were made during HIPPO-4 between 60 and 90° S .

Table 6. As Table 5 but for CH_2Br_2 .

Latitude	Run S_{Liang}			Run S_{Warwick}			Run S_{Ordonez}			Run S_{Ziska}		
	MB	MAD	MAPE	MB	MAD	MAPE	MB	MAD	MAPE	MB	MAD	MAPE
$\geq 60^\circ \text{N}$	-0.10	0.17	23 %	0.25	0.29	57 %	-0.02	0.16	24 %	-0.12	0.28	39 %
30–60° N	-0.02	0.15	19 %	0.47	0.47	75 %	0.08	0.17	25 %	0.11	0.25	37 %
$\pm 30^\circ$	0.12	0.13	16 %	1.11	1.11	134 %	0.24	0.24	29 %	0.54	0.54	66 %
30–60° S	-0.01	0.09	13 %	0.67	0.67	101 %	0.01	0.12	18 %	0.55	0.55	77 %
$\geq 60^\circ \text{S}$	-0.09	0.13	18 %	0.43	0.43	69 %	-0.06	0.17	23 %	0.55	0.73	96 %
Global	-0.01	0.13	18 %	0.60	0.61	88 %	0.06	0.17	24 %	0.30	0.45	60 %

Fig. 8. As Fig. 7 but for CH_2Br_2 .

CHBr_3 in the tropics, suggesting overestimated emissions in this region from the top-down inventories.

The model is also able to reproduce the observed distribution of CH_2Br_2 well. Again, the overall skill of the model is highly dependent on the given emission inventory. For each of the 5 latitude bands considered, the best agreement between the model and observation is obtained from run S_{Liang} . The calculated MAPE for this run is $< 25\%$ within each lat-

itude band and globally is $\sim 18\%$. This supports the findings of the ground-based analysis presented in Sect. 3, where the Liang-2010 emission inventory, which has the lowest total emissions of $62 \text{ Gg } \text{CH}_2\text{Br}_2 \text{ yr}^{-1}$ (Table 1), was shown to perform particularly well. Note, the Ordóñez-2012 inventory also performs well for CH_2Br_2 with a global MAPE of $\sim 24\%$. This is a significantly better agreement than obtained from the Warwick-2011 (87 %) and Ziska-2013

inventories (63 %) that generally lead to overestimation of CH_2Br_2 . Overall, for both CHBr_3 and CH_2Br_2 the calculated biases between the model and the HIPPO aircraft data are consistent with, and support the findings of, the comparisons with the NOAA/ESRL ground-based observations.

5 A case study in the tropical western Pacific

The tropical western Pacific is a region of frequent and intense convection resulting in efficient transport of boundary layer air into the tropical tropopause layer (TTL) (e.g. Fueglistaler et al., 2009; Kruiger et al., 2009). A number of model studies have reported the importance of the tropical western Pacific for the transport of VLS into the stratosphere (e.g. Levine et al., 2007; Aschmann et al., 2009). The region is poorly sampled and local emissions, including those from farmed seaweed species (Leedham et al., 2013), are uncertain. Previous regional observations of VLS include those made during the OP3 campaign on Borneo (Pyle et al., 2011). Background CHBr_3 was reported at ~ 1 ppt inland (Danum Valley) with a larger background (2–5 ppt) reported along the coast (Kunak).

Figure 9 shows the modelled 2011 mean surface mixing ratio of CHBr_3 over the tropical western Pacific. Different emission inventories lead to significant variation between the modelled CHBr_3 abundance. The largest modelled CHBr_3 in this region is from S_{Liang} and $S_{\text{Ordóñez}}$ with ~ 3.25 and 3.0 ppt around the northern coast of Borneo. These emission inventories were derived with little or no observations in the tropical western Pacific (see Liang et al., 2010; and Ordóñez et al., 2012). Runs S_{Warwick} and S_{Ziska} show significantly lower CHBr_3 (~ 2 ppt) and this is likely due to the use of regional observations in the formulation of these inventories. Warwick-2011 was derived with regional scaling to give good agreement with observations made during OP3 on Borneo, while Ziska-2013, the bottom-up estimate, included CHBr_3 sea–air flux data measured in this region during the Trans-Brom cruise (Krüger and Quack, 2013). For surface CH_2Br_2 (also Fig. 9), the modelled mixing ratio is typically between ~ 1.0 and 1.5 ppt in the region of Borneo for all runs. The exception is run S_{Warwick} , where it is ~ 1 ppt greater (i.e. ~ 2.0 – 2.5 ppt) due to the larger regional emissions in the Warwick-2011 inventory. The remainder of Sect. 5 evaluates the CTM and emission inventories in this region using recent aircraft observations made in the free troposphere during the 2011 SHIVA campaign.

5.1 The 2011 SHIVA campaign

The SHIVA campaign is a European Union (EU) funded research project (<http://shiva.iup.uni-heidelberg.de/>). A primary SHIVA objective is to investigate biogenic emissions of VLS, their atmospheric transformation, transport to the stratosphere and ultimately their impact on O_3 . A field cam-

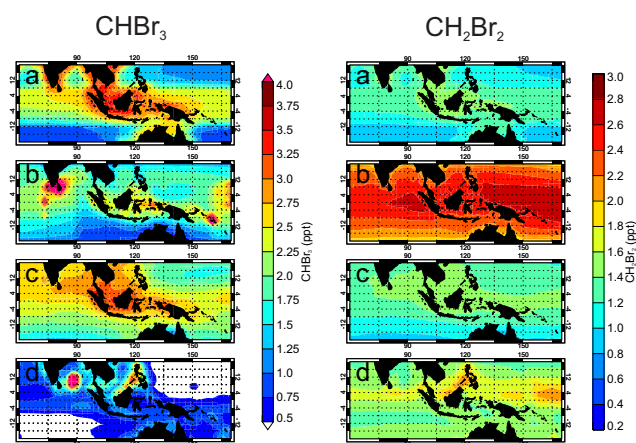


Fig. 9. Modelled mean surface mixing ratio (ppt) of CHBr_3 (left column) and CH_2Br_2 (right column) over the tropical western Pacific during 2011 for CTM runs (a) S_{Liang} , (b) S_{Warwick} , (c) $S_{\text{Ordóñez}}$ and (d) S_{Ziska} .

paign was conducted during November–December 2011 in the tropical western Pacific region based on Malaysian Borneo. An overview of the campaign is given in Pfeilsticker and the SHIVA consortium (2013).

5.1.1 Aircraft observations

Aircraft observations of VLS in the tropical western Pacific region are extremely limited. Within the framework of SHIVA, aircraft observations of brominated VLS were made during 14 flights on board the Deutschen Zentrums für Luft- und Raumfahrt (DLR) Falcon aircraft around Borneo. The flight tracks and location of sampling is shown in Fig. 10. Here we consider observations of major VLS CHBr_3 and CH_2Br_2 made by the University of Frankfurt (UOF) and the University of East Anglia (UEA). These data are used to further evaluate the performance of the model, and top-down/bottom-up emission inventories, in the free troposphere within this poorly sampled region.

Observations made by the UOF group used the Gas chromatograph for Observation of Stratospheric Tracers-Mass Spectrometer (GhOST-MS) instrument – a fully automated GC/MS system for airborne (in situ) observations of halogenated hydrocarbons. Observed mixing ratios for CHBr_3 and CH_2Br_2 from the GhOST-MS are reported on the NOAA-2003 calibration scale (see Sects. 3 and 4). The determined accuracy of the working standard gas is estimated at 16.5 and 9.0 % for these species, respectively. The precision of the instrument varies between flights but is typically < 4 % for both species. For further details of the SHIVA aircraft observations see Sala et al. (2013).

Observations by UEA used the Falcon’s whole air sampler (WASP) that consisted of 30 glass flasks (approximately 700 mL internal volume) which were filled to a pressure of 2.5 Bar using a diaphragm pump. The samples were analysed

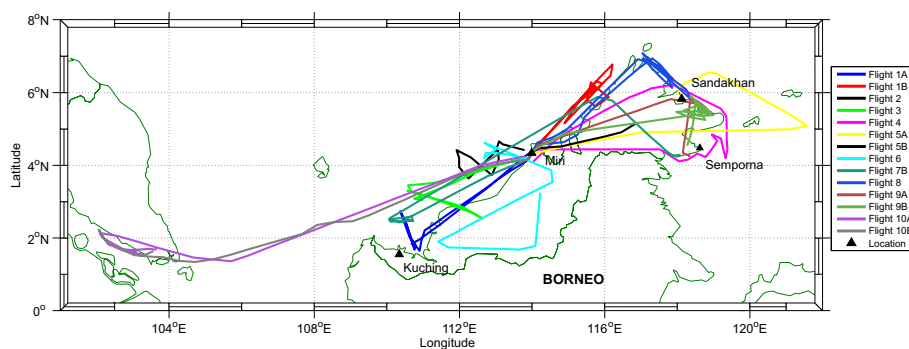


Fig. 10. Flight tracks of the DLR Falcon aircraft during November and December 2011 as part of the 2011 SHIVA campaign.

for halocarbons within 48 h of collection using a GC/MS (Agilent 6973) operating in negative ion, chemical ionisation mode (Worton et al., 2008). Because of a limitation of the sampling pump, WASP samples were only collected at altitudes below ~ 3 km. WASP data for CHBr_3 and CH_2Br_2 are also reported on the most recent NOAA scales. Typical analytical precision (750 mL sample) was $< 4\%$ for both compounds, with a calibration uncertainty of 7.1 and 6.5 % for CHBr_3 and CH_2Br_2 , respectively. The two bromocarbon data sets will be examined in further detail in Sala et al. (2013).

Figure 11 shows the modelled mixing ratio of CHBr_3 sampled along the flight track of the Falcon aircraft during SHIVA. Also shown is the observed CHBr_3 mixing ratio from the GhOST-MS and WASP instruments. The observations show that during most flights, CHBr_3 rarely exceed 1.0–1.5 ppt. A notable exception is flight 4, during which CHBr_3 was elevated (> 2 ppt) near the surface. Large quantities of seaweed were visible from the aircraft during this flight, suggesting a large and localised emission source. Note, within the framework of SHIVA, emissions of halocarbons from both naturally occurring, and farmed tropical macroalgae, has been investigated (Leedham et al., 2013).

The agreement between modelled and observed CHBr_3 is highly dependent on the emission inventory. As before, we have calculated the MB (ppt), the MAD (ppt) and the MAPE (%) between the model and observation for all flights considered. For CHBr_3 , a summary of these metrics is given in Table 7. In general, the top-down inventories (Liang-2010, Warwick-2011, and Ordóñez-2012) overestimate the observations. This is particularly the case for runs S_{Liang} and $S_{\text{Ordóñez}}$ where CHBr_3 is overestimated, from the surface up to ~ 12 km, during numerous flights (e.g. flights 2a, 7, 10b). The MB between model and observation for these flights is 1.67, 1.32 and 0.96 ppt for S_{Liang} and 1.61, 1.19 and 0.99 ppt for $S_{\text{Ordóñez}}$. Whilst also overestimating, an improved agreement is obtained from run S_{Warwick} in this region. For example, for the same flights the MB is smaller (i.e. $\text{MB} < 1$ ppt) at 0.82, 0.78, and 0.47 ppt. Overall, the best agreement is obtained from S_{Ziska} (bottom-up emissions), which for some

flights exhibits a small negative bias. For the above flights, the MB from this run is 0.31, 0.06 and 0.07 ppt, respectively.

Across all the flights considered, the MAPE between the model and observed CHBr_3 is 117, 68, 125 and 37 % for runs S_{Liang} , S_{Warwick} , $S_{\text{Ordóñez}}$ and S_{Ziska} , respectively – highlighting the significant variation in the performance of the inventories in this region. The bottom-up CHBr_3 emissions proposed by Ziska et al. (2013) perform particularly well as this is the only inventory that gives rise to a $\text{MAPE} < 50\%$ in this region. This inventory was also shown to perform well against the NOAA/ESRL ground-based observations (Sect. 3) and HIPPO aircraft observations (Sect. 4) in the tropical Pacific Basin. The Ziska-2013 inventory is constrained by local sea-to-air fluxes obtained in the tropical western Pacific during ship cruises; e.g. Trans-Brom (Krüger and Quack, 2013). This is the likely explanation as to why the MAPE is significantly lower for this inventory, over Liang-2010 and Ordóñez-2012, that are based on limited or no regional (aircraft) observations. The same is true of the Warwick-2011 inventory, which also performs relatively well in this region, and is constrained by local (ground-based) observations. This further highlights the need for more local observations of VSLs, particularly in poorly sampled regions, in order to improve VSLs emission inventories at the regional scale.

Figure 12 shows the modelled versus observed CH_2Br_2 during SHIVA flights. The observations show CH_2Br_2 typically in the range of 0.5–1.5 ppt during most flights and with a relatively small vertical gradient. The performance of each emission inventory is assessed using the error metrics summarised in Table 8. Across all flights, the MAPE is relatively low (compared with that for CHBr_3) at 25, 119, 34 and 56 % for runs S_{Liang} , S_{Warwick} , $S_{\text{Ordóñez}}$ and S_{Ziska} , respectively. Consistent with the NOAA/ESRL ground-based analysis (Sect. 3) and also the HIPPO aircraft analysis (Sect. 4), the best agreement (diagnosed by lowest MAPE) between modelled and observed CH_2Br_2 , is obtained by S_{Liang} . For run S_{Warwick} , which was previously shown to overestimate surface CH_2Br_2 at NOAA/ESRL stations in the Pacific Basin (e.g. Fig. 6), we again find an overestimate against SHIVA

Table 7. Summary of calculated error metrics between CHBr_3 observed in the free troposphere during 14 flights of the SHIVA aircraft campaign (November–December 2011) with analogous fields from CTM runs S_{Liang} , S_{Warwick} , S_{Ordonez} and S_{Ziska} . Shown is the MB and the MAD both in units of ppt. Also shown is the MAPE (see text). These fields were calculated for all observations from both instruments deployed during SHIVA (i.e. GhOST-MS and WASP, see text). A mean value for all 14 flights is also reported.

Flight	Run S_{Liang}			Run S_{Warwick}			Run S_{Ordonez}			Run S_{Ziska}		
	MB	MAD	MAPE	MB	MAD	MAPE	MB	MAD	MAPE	MB	MAD	MAPE
2a	1.67	1.67	192 %	0.82	0.82	99 %	1.61	1.61	187 %	0.31	0.39	46 %
2b	0.58	0.58	101 %	0.43	0.43	77 %	0.70	0.70	122 %	−0.08	0.16	24 %
3	0.49	0.61	40 %	−0.20	0.34	22 %	0.55	0.62	44 %	0.34	0.58	35 %
4	0.70	0.70	82 %	0.25	0.31	42 %	0.84	0.85	101 %	0.13	0.27	32 %
5	0.43	0.53	67 %	0.04	0.41	51 %	0.55	0.63	80 %	−0.76	0.79	48 %
6a	0.42	0.57	122 %	0.18	0.42	84 %	0.48	0.59	127 %	−0.28	0.35	39 %
6b	0.62	0.75	113 %	0.26	0.43	65 %	0.73	0.87	127 %	−0.07	0.27	28 %
7	1.32	1.32	308 %	0.78	0.78	186 %	1.19	1.19	277 %	0.06	0.20	39 %
8b	0.81	0.81	120 %	0.33	0.35	62 %	0.86	0.86	128 %	−0.08	0.20	28 %
9	0.56	0.59	91 %	0.36	0.43	68 %	0.70	0.71	109 %	−0.23	0.28	34 %
10a	1.01	1.01	150 %	0.40	0.41	74 %	1.03	1.03	155 %	0.18	0.29	40 %
10b	0.96	0.96	172 %	0.47	0.49	106 %	0.99	0.99	178 %	0.07	0.25	40 %
11a	0.45	0.57	77 %	−0.02	0.43	47 %	0.65	0.71	92 %	−0.50	0.54	37 %
11b	0.49	0.59	78 %	−0.01	0.38	43 %	0.70	0.74	95 %	−0.42	0.46	34 %
All	0.76	0.81	117 %	0.28	0.46	68 %	0.84	0.87	125 %	−0.12	0.39	37 %

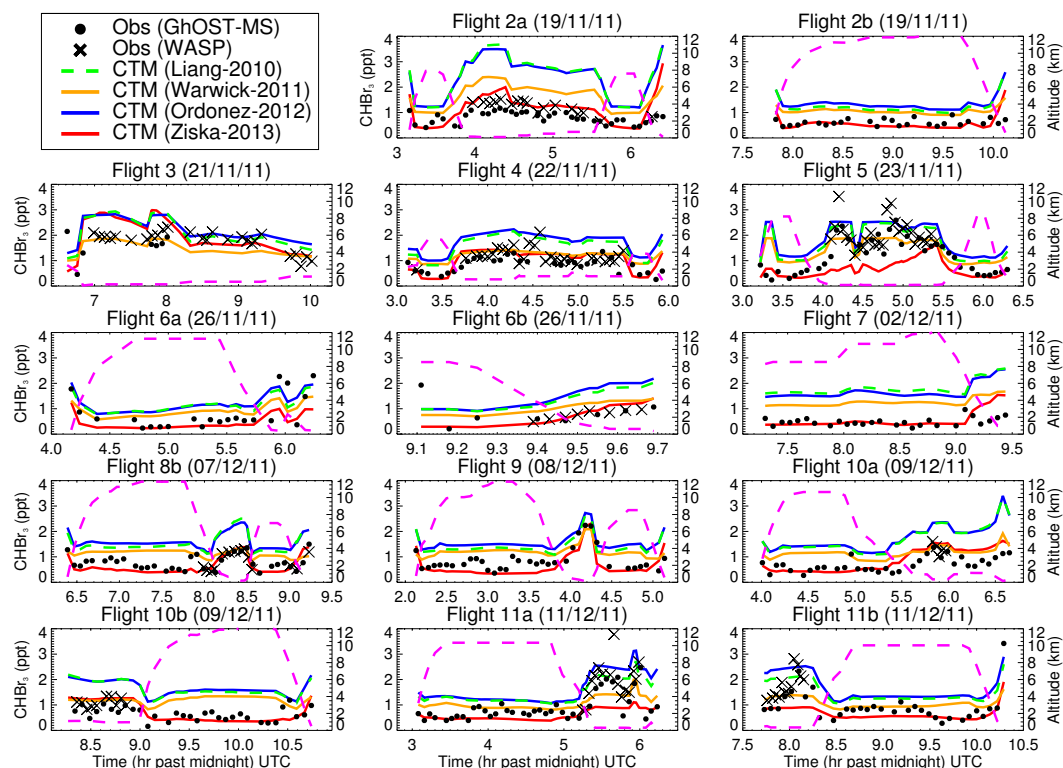
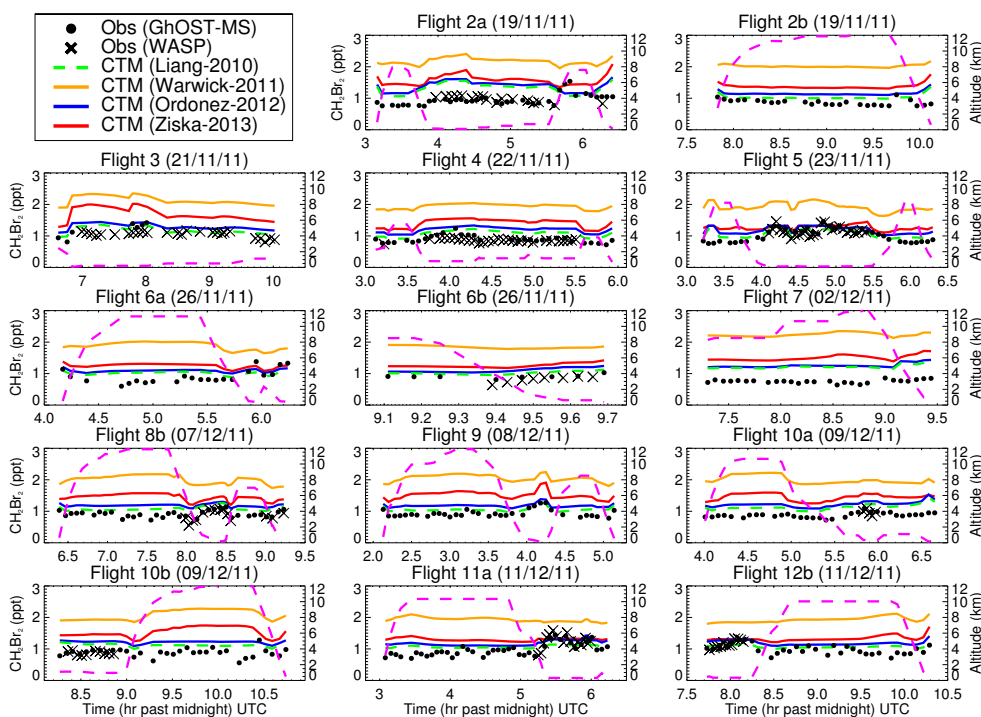


Fig. 11. Comparison between modelled and observed CHBr_3 mixing ratio (ppt) along the flight tracks of the DLR Falcon aircraft during the 2011 SHIVA campaign. Model output is from CTM runs S_{Liang} , S_{Warwick} , S_{Ordonez} and S_{Ziska} and observed data from the GhOST in situ GC/MS system and the WASP whole air sampler (Sala et al., 2013). The dashed pink line denotes the altitude of the aircraft.

Table 8. As Table 7 but for CH_2Br_2 .

Flight	Run S_{Liang}			Run S_{Warwick}			Run S_{Ordonez}			Run S_{Ziska}		
	MB	MAD	MAPE	MB	MAD	MAPE	MB	MAD	MAPE	MB	MAD	MAPE
2a	0.38	0.42	45 %	1.23	1.23	134 %	0.45	0.48	52 %	0.64	0.65	70 %
2b	0.16	0.16	20 %	1.14	1.14	133 %	0.27	0.27	32 %	0.49	0.49	58 %
3	0.12	0.13	13 %	1.08	1.08	102 %	0.23	0.23	23 %	0.66	0.66	62 %
4	0.22	0.22	26 %	1.08	1.08	125 %	0.34	0.34	40 %	0.57	0.57	65 %
5	0.04	0.12	12 %	0.90	0.90	89 %	0.15	0.17	18 %	0.22	0.24	25 %
6a	0.13	0.20	25 %	1.00	1.00	124 %	0.21	0.25	31 %	0.37	0.38	49 %
6b	0.17	0.17	21 %	0.97	0.97	115 %	0.27	0.27	32 %	0.41	0.41	49 %
7	0.46	0.46	62 %	1.49	1.49	200 %	0.50	0.50	68 %	0.75	0.75	101 %
8b	0.20	0.20	24 %	1.07	1.07	125 %	0.30	0.30	35 %	0.52	0.52	61 %
9	0.12	0.13	15 %	1.13	1.13	125 %	0.25	0.25	29 %	0.59	0.59	65 %
10a	0.26	0.26	29 %	1.10	1.10	126 %	0.35	0.35	40 %	0.57	0.57	65 %
10b	0.25	0.26	32 %	1.18	1.18	139 %	0.35	0.35	42 %	0.65	0.65	77 %
11a	0.05	0.18	18 %	0.88	0.88	94 %	0.17	0.21	23 %	0.27	0.30	34 %
11b	0.06	0.13	14 %	0.89	0.89	92 %	0.19	0.19	21 %	0.30	0.31	33 %
All	0.18	0.22	25 %	1.07	1.07	119 %	0.28	0.29	34 %	0.49	0.49	56 %

Fig. 12. As Fig. 11 but for CH_2Br_2 .

observations (approximate factor of 2). Therefore, it seems highly likely that the CH_2Br_2 emission strength is significantly overestimated in the tropics by the Warwick-2011 inventory.

6 Sensitivity of stratospheric bromine loading to emission inventory

In our previous modelling work, emissions of major VLSLs CHBr_3 and CH_2Br_2 were not specified in the TOMCAT CTM (Hossaini et al., 2010, 2012b). Rather, a uniform surface mixing ratio (~ 1.2 ppt) was imposed in the tropics ($\pm 20^\circ$) based on compiled aircraft observations. Using this

approach, Hossaini et al. (2012b) quantified stratospheric $\text{Br}_y^{\text{VLSL}}$ as ~ 5 ppt; i.e. within the compiled range of 1–8 ppt outlined in WMO (2011), and in general agreement with balloon-borne estimates (Dorf et al., 2006, 2008). The CTM performed reasonably well against aircraft observations in the TTL. However, this approach meant regional *hot-spots*, where emissions may be large and background concentrations elevated, were not captured. Any dependence of stratospheric $\text{Br}_y^{\text{VLSL}}$ on the spatial distribution of surface emissions was also not modelled. Here, using the CTM runs presented in this paper (i.e. multiple emission inventories for CHBr_3 and CH_2Br_2), we revise our estimate of $\text{Br}_y^{\text{VLSL}}$ based on these spatially varying, and seasonally varying in the case of Ordóñez-2012, emission inventories.

It is thought that VLSL contribute to the stratospheric bromine budget via both source gas injection (SGI) and also product gas injection (PGI). The SGI pathway is quantified by summing the total organic bromine from VLSL reaching the lower stratosphere. For PGI, which refers to the troposphere–stratosphere transport of inorganic product gases (e.g. BrO , HBr), the tropospheric partitioning of Br_y among soluble and non-soluble species needs consideration. As this involves complex heterogeneous and multi-phase processes (e.g. Aschmann and Sinnhuber, 2013), which are crudely treated in global models, Br_y speciation and recycling represents a significant uncertainty in the quantification of PGI with models. The approach used here is identical to that described in Hossaini et al. (2012b). Once Br_y is released from source gases it is partitioned between soluble and non-soluble form according to a mean altitude-dependent $\text{HBr}:\text{Br}_y$ ratio. This was taken from a previous CTM integration in which detailed partitioning of tropospheric Br_y was considered.

Figure 13 shows the modelled tropical mean profile of $\text{Br}_y^{\text{VLSL}}$ in the stratosphere at the end of the 14 yr simulation. We find $\text{Br}_y^{\text{VLSL}}$ ranges from ~ 5 to 8 ppt (above ~ 30 km) depending on the choice of emission inventory. Runs S_{Ziska} and S_{Warwick} account for the lower limit and upper limit, respectively. However, as S_{Warwick} overestimated both CHBr_3 and CH_2Br_2 significantly in the tropics, it seems likely that the upper limit of ~ 8 ppt reported here is also an overestimate. We have therefore now identified a range of uncertainty with regard to emissions of major VLSL CHBr_3 and CH_2Br_2 on stratospheric $\text{Br}_y^{\text{VLSL}}$ loading. Note, here $\text{Br}_y^{\text{VLSL}}$ also includes the contribution from minor VLSL CHBr_2Cl , CHBrCl_2 and CH_2BrCl . Their total contribution to $\text{Br}_y^{\text{VLSL}}$ is ~ 1 ppt and is consistent between each model run.

The modelled stratospheric $\text{Br}_y^{\text{VLSL}}$ ranges from ~ 5 to 8 ppt when both CHBr_3 and CH_2Br_2 are taken from the same inventory. However, in the tropics, where the troposphere–stratosphere transport of VLSL is most rapid, it was shown using ground-based (Sect. 3) and aircraft (Sect. 4) observations that a single inventory does not provide the simultaneous best agreement for both VLSL in this region. For CHBr_3 ,

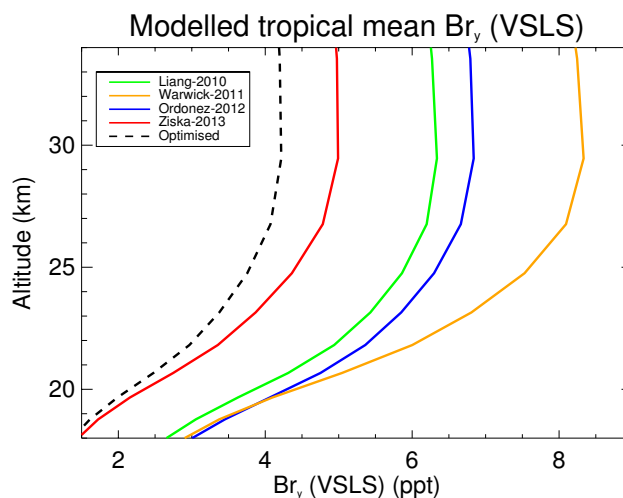


Fig. 13. Modelled 2011 tropical ($\pm 30^\circ$) mean profile of total inorganic bromine (ppt) from CHBr_3 , CH_2Br_2 , CHBr_2Cl , CH_2BrCl and CHBrCl_2 ($\text{Br}_y^{\text{VLSL}}$) in the stratosphere. Profiles are shown for CTM runs S_{Liang} , S_{Warwick} , $S_{\text{Ordóñez}}$, and S_{Ziska} . An optimised estimate, calculated by combining CHBr_3 from S_{Ziska} and CH_2Br_2 from S_{Liang} , is also shown.

the best agreement was obtained from run S_{Ziska} and similarly, for CH_2Br_2 , run S_{Liang} gave the best agreement. Therefore, we also report an *optimised* estimate of stratospheric $\text{Br}_y^{\text{VLSL}}$ based on a combination of these two fields; ~ 4 ppt (also shown in Fig. 13). From the 4 inventories considered, the CHBr_3 and CH_2Br_2 source strengths are the lowest in Ziska-2013 and Liang-2010, respectively. Therefore, the optimised estimate reported here is lower than the range obtained when considering emissions of both species from the same inventory.

Our optimised $\text{Br}_y^{\text{VLSL}}$ estimate of ~ 4 ppt is lower than that reported in our previous work (~ 5 ppt) (Hossaini et al., 2012b), which did not use spatially varying emission fluxes. The use of a fixed mixing ratio as a surface boundary condition for CHBr_3 and CH_2Br_2 in Hossaini et al. (2012b) may have overestimated their abundance in the boundary layer. However, our modelled optimised estimate is in good agreement with $\text{Br}_y^{\text{VLSL}}$ derived from observations of stratospheric BrO (the so-called *inorganic method*). For example, using differential optical absorption spectroscopy (DOAS) to obtain BrO profiles, combined with photochemical modelling, Dorf et al. (2006) reported a $\text{Br}_y^{\text{VLSL}}$ contribution of $4.1(\pm 2.5)$ ppt. However, given the recent findings of Kreygy et al. (2013) on the ratio of $J(\text{BrONO}_2)/k(\text{BrO}+\text{NO}_2)$, this estimate may need to be revised downward. Overall, our model calculations are consistent with the broad $\text{Br}_y^{\text{VLSL}}$ range of 1–8 ppt reported by WMO (2011).

7 Summary and conclusions

Global models require a realistic treatment of biogenic bromine emissions in order to simulate a reasonable Br_y budget in both the troposphere and the stratosphere. At present, oceanic emissions of brominated VSLs are poorly constrained and represent a significant uncertainty in global models (WMO, 2007, 2011). Given suggestions that stratospheric VSLs loading may increase in response to climate change (Dessens et al., 2009; Hossaini et al., 2012a), constraining both the magnitude and spatial distribution of contemporary emissions is important. In this study we have used a global model to perform the first concerted evaluation of previously published global CHBr_3 and CH_2Br_2 emission inventories. We have evaluated three top-down and a bottom-up derived inventory by comparing the simulated abundance of these VSLs with independent observations – i.e. the observed data was not included in the formulation of the emission inventories. The observed data have included long-term observations at various NOAA/ESRL ground-based stations, aircraft observations made during the NSF HIPPO campaigns (1–5) and also novel aircraft observations made during the 2011 SHIVA campaign over the poorly sampled tropical western Pacific. We have also updated our previous model estimate of $\text{Br}_y^{\text{VSLs}}$ based on these available emission scenarios.

Our comparisons reveal the TOMCAT CTM is able to reproduce a variety of global CHBr_3 and CH_2Br_2 observations. The agreement between the model and the observation is highly dependent on the choice of emission inventory, which differ significantly in terms of magnitude and spatial distribution. All the inventories considered give good agreement in some locations. However, to accurately diagnose the source gas injection of VSLs into the stratosphere, simulating their abundance in the tropics, where transport to the stratosphere is rapid, is most important. Comparison of the model with observations at NOAA/ESRL surface sites and also with aircraft observations obtained during HIPPO, shows a consistent pattern on the performance of individual emission inventories. Based on these comparisons, along with the results from the SHIVA case study, our main findings are the following.

- Current global emission inventories of CHBr_3 and CH_2Br_2 , which are used in global models, vary significantly. Evaluating these inventories is challenging due to the limited spatial coverage of long-term observations, particularly in the tropics and in the Southern Hemisphere. Averaged globally, the best agreement between modelled CHBr_3 and CH_2Br_2 with long-term surface observations made by NOAA/ESRL is obtained using the top-down emissions proposed by Liang et al. (2010). Globally, the mean absolute percentage error between the model and NOAA/ESRL observations for this inventory is ~ 50 and ~ 20 % for

CHBr_3 and CH_2Br_2 over a 14 yr period, respectively. Comparison of the model with aircraft observations made during the HIPPO project, which spanned global latitudes over the Pacific Basin, also support these findings. Globally, the mean absolute percentage error between the model and HIPPO observations is similar at 42 and 18 %, for CHBr_3 and CH_2Br_2 respectively, when using the Liang et al. (2010) emissions. Globally, we also find the CH_2Br_2 emissions of Ordóñez et al. (2012) perform particularly well with a mean absolute percentage error of less than ~ 30 % between model and observations.

- For CHBr_3 , within the tropics only, the best agreement between the model and observations is obtained using the bottom-up emission fluxes proposed by Ziska et al. (2013). Using this inventory, the mean absolute percentage error between the model and long-term NOAA/ESRL surface observations is ~ 36 %. Against the HIPPO observations it is ~ 35 %, with the other inventories considered giving a significantly larger bias (> 60 %). For CH_2Br_2 , in the tropics the model is able to reproduce observations well using the Liang et al. (2010) emissions. The mean absolute percentage error is 24 and 16 % when the model is compared with the NOAA/ESRL and HIPPO observations, respectively. Therefore, our results show the bias between model and observations is lowest when using the inventories that have the lowest tropical (and also total global) CHBr_3 and CH_2Br_2 emission strength (i.e. Ziska and Liang, respectively).
- In the tropical western Pacific, where rapid troposphere–stratosphere transport coincides with relatively large VSLs emissions, the model is able to reproduce novel aircraft observations of CHBr_3 and CH_2Br_2 made during the 2011 SHIVA campaign. The skill of the model is highly dependant on the choice of emission inventory. Good agreement is obtained for CHBr_3 using the bottom-up emissions of Ziska et al. (2013). These emissions, along with the Warwick-2011 inventory, were formulated using local observations around Borneo and as such perform significantly better than inventories based on limited aircraft observations alone. Therefore, this further highlights the need for more observations of VSLs, particularly at a finer spatial resolution, in order to improve current regional emission estimates. For CH_2Br_2 , which is a longer-lived source gas, the Liang et al. (2010) emissions were again found to give the best agreement with the observations.
- The modelled contribution of VSLs to stratospheric inorganic bromine varies significantly depending on the CHBr_3 and CH_2Br_2 inventory used. We find $\text{Br}_y^{\text{VSLs}}$ ranges from ~ 5.0 to 8.0 ppt when using

CHBr₃ and CH₂Br₂ from the same inventory. However, we find no single inventory provides the simultaneous best agreement with observations in the tropics. Therefore, we also report an optimised estimate, calculated by combining the inventories which perform the best in this region. A combination of CHBr₃ emissions from Ziska et al. (2013) and CH₂Br₂ emissions from Liang et al. (2010) lead to our (lower) optimised estimate of ~4 ppt. These inventories were found to consistently perform the best in the tropics using three independent sets of observations (i.e. NOAA/ESRL surface, HIPPO aircraft and SHIVA aircraft data). Both the modelled range and optimised estimate are within the compiled 1–8 ppt range reported by WMO (2011). Therefore, in this study we have now identified the range of uncertainty associated with emissions of major VLSL CHBr₃ and CH₂Br₂ on stratospheric Br_y^{VLSL} loading. Although, model estimates of the product gas injection contribution to Br_y^{VLSL} remain a significant uncertainty (e.g. Salawitch et al., 2010; Aschmann and Sinnhuber, 2013).

Our study has shown that in recent years understanding of oceanic VLSL emissions has improved significantly and that current inventories used in global models are reasonable. Based on the results of this work, it would be useful to revise current inventories and/or combine them to improve the treatment of CHBr₃ and CH₂Br₂ emissions in global models. Furthermore, it would be useful for the analysis performed in this study to be repeated by other modelling groups, in order to determine the extent to which our results are model dependent. For example, to assess the role of differences in model transport, such as mixing in the boundary layer and convection, which are parameterised and likely to vary between models. A related exercise examining inter-model variability on the tropospheric distribution and the troposphere–stratosphere transport of VLSL is planned, within the framework of the ongoing Atmospheric Tracer Transport Model Inter comparison (TransCom) project (e.g. Patra et al., 2011). This project, TransCom-VLSL, will examine the performance of a number of global models against existing VLSL observations and also assess the variability between data sets, including the impact of temporal sampling and systematic biases on the agreement between models and observations. Finally, future work will examine emissions of relatively minor VLSL (e.g. CHBr₂Cl, CH₂BrCl) along with a more detailed examination of emission seasonality.

Acknowledgements. This work was supported by the UK Natural Environment Research Council (NERC) and the EU Stratospheric Ozone: Halogen Impacts in a Varying Atmosphere (SHIVA) project (SHIVA-226224-FP7-ENV-2008-1). TOMCAT work is supported by the National Centre for Atmospheric Science (NCAS). NOAA measurements were supported in part by NOAA's Atmospheric Chemistry, Carbon Cycle and Climate Program of its Climate

Program Office. Technical assistance, standardisation, and programmatic support for NOAA flask measurements was provided by C. Siso, B. Hall, and J. W. Elkins. The HIPPO project was supported by the National Science Foundation (NSF).

Edited by: J. Williams

References

- Aschmann, J. and Sinnhuber, B.-M.: Contribution of very short-lived substances to stratospheric bromine loading: uncertainties and constraints, *Atmos. Chem. Phys.*, 13, 1203–1219, doi:10.5194/acp-13-1203-2013, 2013.
- Aschmann, J., Sinnhuber, B.-M., Atlas, E. L., and Schauffler, S. M.: Modeling the transport of very short-lived substances into the tropical upper troposphere and lower stratosphere, *Atmos. Chem. Phys.*, 9, 9237–9247, doi:10.5194/acp-9-9237-2009, 2009.
- Ashfold, M. J., Harris, N. R. P., Atlas, E. L., Manning, A. J., and Pyle, J. A.: Transport of short-lived species into the Tropical Tropopause Layer, *Atmos. Chem. Phys.*, 12, 6309–6322, doi:10.5194/acp-12-6309-2012, 2012.
- Beyersdorf, A. J., Blake, D. R., Swanson, A., Meinardi, S., Rowland, F. S., and Davis, D.: Abundances and variability of tropospheric volatile organic compounds at the South Pole and other Antarctic locations, *Atmos. Environ.*, 44, 4565–4574, doi:10.1016/j.atmosenv.2010.08.025, 2010.
- Breider, T. J., Chipperfield, M. P., Richards, N. A. D., Carslaw, K. S., Mann, G. W., and Spracklen, D. V.: Impact of BrO on dimethylsulfide in the remote marine boundary layer, *Geophys. Res. Lett.*, 37, L02807, doi:10.1029/2009GL040868, 2010.
- Brinckmann, S., Engel, A., Bönisch, H., Quack, B., and Atlas, E.: Short-lived brominated hydrocarbons – observations in the source regions and the tropical tropopause layer, *Atmos. Chem. Phys.*, 12, 1213–1228, doi:10.5194/acp-12-1213-2012, 2012.
- Carpenter, L. and Liss, P.: On temperate sources of bromoform and other reactive organic bromine gases, *J. Geophys. Res.-Atmos.*, 105, 20539–20547, doi:10.1029/2000JD900242, 2000.
- Carpenter, L. J., Wevill, D. J., O'Doherty, S., Spain, G., and Simmonds, P. G.: Atmospheric bromoform at Mace Head, Ireland: seasonality and evidence for a peatland source, *Atmos. Chem. Phys.*, 5, 2927–2934, doi:10.5194/acp-5-2927-2005, 2005.
- Chipperfield, M. P.: New version of the TOMCAT/SLIMCAT offline chemical transport model: Intercomparison of stratospheric tracer experiments, *Q. J. Roy. Meteorol. Soc.*, 132, 1179–1203, doi:10.1256/qj.05.51, 2006.
- Dessens, O., Zeng, G., Warwick, N., and Pyle, J.: Short-lived bromine compounds in the lower stratosphere; impact of climate change on ozone, *Atmos. Sci. Lett.*, 10, 201–206, doi:10.1002/asl.236, 2009.
- Dorf, M., Butler, J. H., Butz, A., Camy-Peyret, C., Chipperfield, M. P., Kritten, L., Montzka, S. A., Simmes, B., Weidner, F., and Pfeilsticker, K.: Long-term observations of stratospheric bromine reveal slow down in growth, *Geophys. Res. Lett.*, 33, L24803, doi:10.1029/2006GL027714, 2006.
- Dorf, M., Butz, A., Camy-Peyret, C., Chipperfield, M. P., Kritten, L., and Pfeilsticker, K.: Bromine in the tropical troposphere and stratosphere as derived from balloon-borne BrO observations, *Atmos. Chem. Phys.*, 8, 7265–7271, doi:10.5194/acp-8-7265-2008, 2008.

- Feng, W., Chipperfield, M. P., Dorf, M., Pfeilsticker, K., and Ricaud, P.: Mid-latitude ozone changes: studies with a 3-D CTM forced by ERA-40 analyses, *Atmos. Chem. Phys.*, 7, 2357–2369, doi:10.5194/acp-7-2357-2007, 2007.
- Feng, W., Chipperfield, M. P., Dhomse, S., Monge-Sanz, B. M., Yang, X., Zhang, K., and Ramonet, M.: Evaluation of cloud convection and tracer transport in a three-dimensional chemical transport model, *Atmos. Chem. Phys.*, 11, 5783–5803, doi:10.5194/acp-11-5783-2011, 2011.
- Fueglistaler, S., Dessler, A. E., Dunkerton, T. J., Folkins, I., Fu, Q., and Mote, P. W.: Tropical tropopause layer, *Reviews Geophys.*, 47, RG1004, doi:10.1029/2008RG000267, 2009.
- Holtslag, A. and Boville, B.: Local versus nonlocal boundary-layer diffusion in a global climate model, *J. Climate*, 6, 1825–1842, 1993.
- Hossaini, R., Chipperfield, M. P., Monge-Sanz, B. M., Richards, N. A. D., Atlas, E., and Blake, D. R.: Bromoform and dibromomethane in the tropics: a 3-D model study of chemistry and transport, *Atmos. Chem. Phys.*, 10, 719–735, doi:10.5194/acp-10-719-2010, 2010.
- Hossaini, R., Chipperfield, M. P., Dhomse, S., Ordonez, C., Saiz-Lopez, A., Abraham, N. L., Archibald, A., Braesicke, P., Telford, P., Warwick, N., Yang, X., and Pyle, J.: Modelling future changes to the stratospheric source gas injection of biogenic bromocarbons, *Geophys. Res. Lett.*, 39, L20813, doi:10.1029/2012GL053401, 2012a.
- Hossaini, R., Chipperfield, M. P., Feng, W., Breider, T. J., Atlas, E., Montzka, S. A., Miller, B. R., Moore, F., and Elkins, J.: The contribution of natural and anthropogenic very short-lived species to stratospheric bromine, *Atmos. Chem. Phys.*, 12, 371–380, doi:10.5194/acp-12-371-2012, 2012b.
- Kreycey, S., Camy-Peyret, C., Chipperfield, M. P., Dorf, M., Feng, W., Hossaini, R., Kritten, L., Werner, B., and Pfeilsticker, K.: Atmospheric test of the $J(\text{BrONO}_2)/k\text{BrO}+\text{NO}_2$ ratio: implications for total stratospheric bromine and bromine-mediated ozone loss, *Atmos. Chem. Phys.*, 13, 6263–6274, doi:10.5194/acp-13-6263-2013, 2013.
- Krüger, K. and Quack, B.: Introduction to special issue: the Trans-Brom Sonne expedition in the tropical West Pacific, *Atmos. Chem. Phys.*, 13, 9439–9446, doi:10.5194/acp-13-9439-2013, 2013.
- Krüger, K., Tegtmeier, S., and Rex, M.: Variability of residence time in the Tropical Tropopause Layer during Northern Hemisphere winter, *Atmos. Chem. Phys.*, 9, 6717–6725, doi:10.5194/acp-9-6717-2009, 2009.
- Lary, D.: Gas phase atmospheric bromine photochemistry, *J. Geophys. Res.-Atmos.*, 101, 1505–1516, doi:10.1029/95JD02463, 1996.
- Lary, D. and Toumi, R.: Halogen-catalyzed methane oxidation, *J. Geophys. Res.-Atmos.*, 102, 23421–23428, doi:10.1029/97JD00914, 1997.
- Leedham, E. C., Hughes, C., Keng, F. S. L., Phang, S.-M., Malin, G., and Sturges, W. T.: Emission of atmospherically significant halocarbons by naturally occurring and farmed tropical macroalgae, *Biogeosciences*, 10, 3615–3633, doi:10.5194/bg-10-3615-2013, 2013.
- Levine, J. G., Braesicke, P., Harris, N. R. P., Savage, N. H., and Pyle, J. A.: Pathways and timescales for troposphere-to-stratosphere transport via the tropical tropopause layer and their relevance for very short lived substances, *JOURNAL OF Geophys. Res.-Atmos.*, 112, D04308, doi:10.1029/2005JD006940, 2007.
- Liang, Q., Stolarski, R. S., Kawa, S. R., Nielsen, J. E., Douglass, A. R., Rodriguez, J. M., Blake, D. R., Atlas, E. L., and Ott, L. E.: Finding the missing stratospheric bromine: a global modeling study of CHBr_3 and CH_2Br_2 , *Atmos. Chem. Phys.*, 10, 2269–2286, doi:10.5194/acp-10-2269-2010, 2010.
- Montzka, S. and Reimann, S.: Ozone-depleting substances (ODSs) and related chemicals, in: Scientific Assessment of Ozone Depletion: 2010, Global Ozone Research and Monitoring Project, Report No. 52, Chapt. 1, World Meteorological Organization, Geneva, 2011.
- Montzka, S., Butler, J., Hall, B., Mondeel, D., and Elkins, J.: A decline in tropospheric organic bromine, *Geophys. Res. Lett.*, 30, 1826, doi:10.1029/2003GL017745, 2003.
- Ordóñez, C., Lamarque, J.-F., Tilmes, S., Kinnison, D. E., Atlas, E. L., Blake, D. R., Sousa Santos, G., Brasseur, G., and Saiz-Lopez, A.: Bromine and iodine chemistry in a global chemistry-climate model: description and evaluation of very short-lived oceanic sources, *Atmos. Chem. Phys.*, 12, 1423–1447, doi:10.5194/acp-12-1423-2012, 2012.
- Patra, P. K., Houweling, S., Krol, M., Bousquet, P., Belikov, D., Bergmann, D., Bian, H., Cameron-Smith, P., Chipperfield, M. P., Corbin, K., Fortems-Cheiney, A., Fraser, A., Gloor, E., Hess, P., Ito, A., Kawa, S. R., Law, R. M., Loh, Z., Maksyutov, S., Meng, L., Palmer, P. I., Prinn, R. G., Rigby, M., Saito, R., and Wilson, C.: TransCom model simulations of CH_4 and related species: linking transport, surface flux and chemical loss with CH_4 variability in the troposphere and lower stratosphere, *Atmos. Chem. Phys.*, 11, 12813–12837, doi:10.5194/acp-11-12813-2011, 2011.
- Pfeilsticker, K. and the SHIVA consortium: Overview on the project SHIVA (Stratospheric Ozone: Halogen Impacts in a Varying Atmosphere): Achievements and key results, in preparation, 2013.
- Pfeilsticker, K., Sturges, W., Bosch, H., Camy-Peyret, C., Chipperfield, M., Engel, A., Fitzenberger, R., Müller, M., Payan, S., and Sinnhuber, B.: Lower stratospheric organic and inorganic bromine budget for the Arctic winter 1998/99, *Geophys. Res. Lett.*, 27, 3305–3308, doi:10.1029/2000GL011650, 2000.
- Prather, M.: Numerical advection by conservation of 2nd-order moments, *J. Geophys. Res.-Atmos.*, 91, 6671–6681, doi:10.1029/JD091iD06p06671, 1986.
- Pyle, J. A., Ashfold, M. J., Harris, N. R. P., Robinson, A. D., Warwick, N. J., Carver, G. D., Gostlow, B., O'Brien, L. M., Manning, A. J., Phang, S. M., Yong, S. E., Leong, K. P., Ung, E. H., and Ong, S.: Bromoform in the tropical boundary layer of the Maritime Continent during OP3, *Atmos. Chem. Phys.*, 11, 529–542, doi:10.5194/acp-11-529-2011, 2011.
- Quack, B. and Wallace, D.: Air-sea flux of bromoform: Controls, rates, and implications, *Global Biogeochem. Cy.*, 17, 1023, doi:10.1029/2002GB001890, 2003.
- Read, K. A., Mahajan, A. S., Carpenter, L. J., Evans, M. J., Faria, B. V. E., Heard, D. E., Hopkins, J. R., Lee, J. D., Moller, S. J., Lewis, A. C., Mendes, L., McQuaid, J. B., Oetjen, H., Saiz-Lopez, A., Pilling, M. J., and Plane, J. M. C.: Extensive halogen-mediated ozone destruction over the tropical Atlantic Ocean, *Nature*, 453, 1232–1235, doi:10.1038/nature07035, 2008.
- Saiz-Lopez, A. and von Glasow, R.: Reactive halogen chemistry in the troposphere, *Chem. Soc. Rev.*, 41, 6448–6472, doi:10.1039/c2cs35208g, 2012.

- Saiz-Lopez, A., Lamarque, J.-F., Kinnison, D. E., Tilmes, S., Ordóñez, C., Orlando, J. J., Conley, A. J., Plane, J. M. C., Mahajan, A. S., Sousa Santos, G., Atlas, E. L., Blake, D. R., Sander, S. P., Schauffler, S., Thompson, A. M., and Brasseur, G.: Estimating the climate significance of halogen-driven ozone loss in the tropical marine troposphere, *Atmos. Chem. Phys.*, 12, 3939–3949, doi:10.5194/acp-12-3939-2012, 2012.
- Sala, S., Bönnisch, H., Keber, T., and Engel, A.: A Budget of total organic bromine from airborne VLSL measurements during SHIVA, in preparation, 2013.
- Salawitch, R., Weisenstein, D., Kovalenko, L., Sioris, C., Wennberg, P., Chance, K., Ko, M., and McLinden, C.: Sensitivity of ozone to bromine in the lower stratosphere, *Geophys. Res. Lett.*, 32, L05811, doi:10.1029/2004GL021504, 2005.
- Salawitch, R. J., Canty, T., Kurosu, T., Chance, K., Liang, Q., da Silva, A., Pawson, S., Nielsen, J. E., Rodriguez, J. M., Bhartia, P. K., Liu, X., Huey, L. G., Liao, J., Stickel, R. E., Tanner, D. J., Dibb, J. E., Simpson, W. R., Donohoue, D., Weinheimer, A., Flocke, F., Knapp, D., Montzka, D., Neuman, J. A., Nowak, J. B., Ryerson, T. B., Oltmans, S., Blake, D. R., Atlas, E. L., Kinnison, D. E., Tilmes, S., Pan, L. L., Hendrick, F., Van Roozendaal, M., Kreher, K., Johnston, P. V., Gao, R. S., Johnson, B., Bui, T. P., Chen, G., Pierce, R. B., Crawford, J. H., and Jacob, D. J.: A new interpretation of total column BrO during Arctic spring, *Geophys. Res. Lett.*, 37, L21805, doi:10.1029/2010GL043798, 2010.
- Sander, S., Friedl, R., Barker, J., Golden, D., Kurylo, M., Wine, P., Abbatt, J., Burkholder, J., Kolb, C., Moortgat, G., Huie, R., and Orkin, V.: Chemical Kinetics and Photochemical Data for Use in Atmospheric Studies., Evaluation Number 17, JPL Publication 10-6, Jet Propulsion Laboratory, 2011.
- Schofield, R., Fueglistaler, S., Wohltmann, I., and Rex, M.: Sensitivity of stratospheric Br₂ to uncertainties in very short lived substance emissions and atmospheric transport, *Atmos. Chem. Phys.*, 11, 1379–1392, doi:10.5194/acp-11-1379-2011, 2011.
- Sioris, C. E., Kovalenko, L. J., McLinden, C. A., Salawitch, R. J., Van Roozendaal, M., Goutail, F., Dorf, M., Pfeilsticker, K., Chance, K., von Savigny, C., Liu, X., Kurosu, T. P., Pommereau, J. P., Boesch, H., and Frerick, J.: Latitudinal and vertical distribution of bromine monoxide in the lower stratosphere from Scanning Imaging Absorption Spectrometer for Atmospheric Chartography limb scattering measurements, *J. Geophys. Res.-Atmos.*, 111, D14301, doi:10.1029/2005JD006479, 2006.
- Solomon, S.: Stratospheric ozone depletion: a review of concepts and history, *Rev. Geophys.*, 37, 275–316, 1999.
- Stockwell, D. and Chipperfield, M.: A tropospheric chemical-transport model: Development and validation of the model transport schemes, *Q. J. Roy. Meteorol. Soc.*, 125, 1747–1783, doi:10.1256/smsqj.55713, 1999.
- Sturges, W., Oram, D., Carpenter, L., Penkett, S., and Engel, A.: Bromoform as a source of stratospheric bromine, *Geophys. Res. Lett.*, 27, 2081–2084, doi:10.1029/2000GL011444, 2000.
- Swanson, A., Davis, D., Arimoto, R., Robert, P., Atlas, E., Flocke, F., Meinardi, S., Rowland, F., and Blake, D.: Organic trace gases of oceanic origin observed at South Pole during ISCAT 2000, *Atmos. Environ.*, 38, 5463–5472, doi:10.1016/j.atmosenv.2004.03.072, 2004.
- Tegtmeier, S., Krüger, K., Quack, B., Atlas, E. L., Pisso, I., Stohl, A., and Yang, X.: Emission and transport of bromocarbons: from the West Pacific ocean into the stratosphere, *Atmos. Chem. Phys.*, 12, 10633–10648, doi:10.5194/acp-12-10633-2012, 2012.
- Tiedtke, M.: A comprehensive mass flux scheme for cumulus parameterization in large-scale models, *Mon. Weather Rev.*, 117, 1779–1800, doi:10.1175/1520-0493(1989)117<1779:ACMFSF>2.0.CO;2, 1989.
- von Glasow, R., von Kuhlmann, R., Lawrence, M. G., Platt, U., and Crutzen, P. J.: Impact of reactive bromine chemistry in the troposphere, *Atmos. Chem. Phys.*, 4, 2481–2497, doi:10.5194/acp-4-2481-2004, 2004.
- Warwick, N. J., Pyle, J. A., Carver, G. D., Yang, X., Savage, N. H., O'Connor, F. M., and Cox, R. A.: Global modeling of biogenic bromocarbons, *J. Geophys. Res.-Atmos.*, 111, D24305, doi:10.1029/2006JD007264, 2006.
- WMO: Scientific Assessment of Ozone Depletion: 2006, Global Ozone Research and Monitoring Project, Report No. 50, World Meteorological Organization, Geneva, Switzerland, 2007.
- WMO: Scientific Assessment of Ozone Depletion: 2010, Global Ozone Research and Monitoring Project, Report No. 52, World Meteorological Organization, Geneva, Switzerland, 2011.
- Wofsy, S. C., Team, H. S., Team, C. M., and Team, S.: HIPPO Pole-to-Pole Observations (HIPPO): fine-grained, global-scale measurements of climatically important atmospheric gases and aerosols, *Philos. T. Roy. Soc. A*, 369, 2073–2086, doi:10.1098/rsta.2010.0313, 2011.
- Worton, D. R., Mills, G. P., Oram, D. E., and Sturges, W. T.: Gas chromatography negative ion chemical ionization mass spectrometry: Application to the detection of alkyl nitrates and halocarbons in the atmosphere, *J. Chromatogr. A*, 1201, 112–119, doi:10.1016/j.chroma.2008.06.019, 2008.
- Yang, X., Cox, R., Warwick, N., Pyle, J., Carver, G., O'Connor, F., and Savage, N.: Tropospheric bromine chemistry and its impacts on ozone: A model study, *JOURNAL OF Geophys. Res.-Atmos.*, 110, D23311, doi:10.1029/2005JD006244, 2005.
- Yokouchi, Y., Barrie, L., Toom, D., and Akimoto, H.: The seasonal variation of selected natural and anthropogenic halocarbons in the Arctic troposphere, *Atmos. Environ.*, 30, 1723–1727, doi:10.1016/1352-2310(95)00393-2, 1996.
- Ziska, F., Quack, B., Abrahamsson, K., Archer, S. D., Atlas, E., Bell, T., Butler, J. H., Carpenter, L. J., Jones, C. E., Harris, N. R. P., Hepach, H., Heumann, K. G., Hughes, C., Kuss, J., Krüger, K., Liss, P., Moore, R. M., Orlikowska, A., Raimund, S., Reeves, C. E., Reifenhäuser, W., Robinson, A. D., Schall, C., Tanhua, T., Tegtmeier, S., Turner, S., Wang, L., Wallace, D., Williams, J., Yamamoto, H., Yvon-Lewis, S., and Yokouchi, Y.: Global sea-to-air flux climatology for bromoform, dibromomethane and methyl iodide, *Atmos. Chem. Phys.*, 13, 8915–8934, doi:10.5194/acp-13-8915-2013, 2013.

3. Manuscript

The contribution of oceanic methyl iodide to stratospheric iodine

S. Tegtmeier¹, K. Krüger^{1,*}, B. Quack¹, E. Atlas², D. R. Blake³, H. Boenisch⁴, A. Engel⁴, H. Hepach¹, R. Hossaini⁵, M. A. Navarro², S. Raimund¹, S. Sala⁴, Q. Shi¹, and F. Ziska¹

[1] GEOMAR Helmholtz Centre for Ocean Research Kiel, Kiel, Germany

[2] Rosenstiel School of Marine and Atmospheric Science, University of Miami, Miami, Florida, USA

[3] University of California, Irvine, USA

[4] Goethe University Frankfurt am Main, Frankfurt, Germany

[5] Institute for Climate and Atmospheric Science, School of Earth and Environment, University of Leeds, Leeds, UK

[*] now at: University of Oslo, Oslo, Norway

Published in: Atmospheric Chemistry and Physics, 13, 11869-11886, doi:10.5194/acp-13-11869-2013, 2013.



The contribution of oceanic methyl iodide to stratospheric iodine

S. Tegtmeier¹, K. Krüger^{1,*}, B. Quack¹, E. Atlas², D. R. Blake³, H. Boenisch⁴, A. Engel⁴, H. Hepach¹, R. Hossaini⁵, M. A. Navarro², S. Raimund¹, S. Sala⁴, Q. Shi¹, and F. Ziska¹

¹GEOMAR Helmholtz Centre for Ocean Research Kiel, Kiel, Germany

²Rosenstiel School of Marine and Atmospheric Science, University of Miami, Miami, Florida, USA

³University of California, Irvine, USA

⁴Goethe University Frankfurt am Main, Frankfurt, Germany

⁵Institute for Climate and Atmospheric Science, School of Earth and Environment, University of Leeds, Leeds, UK

* now at: University of Oslo, Oslo, Norway

Correspondence to: S. Tegtmeier (stegtmeier@geomar.de)

Received: 4 April 2013 – Published in Atmos. Chem. Phys. Discuss.: 30 April 2013

Revised: 14 October 2013 – Accepted: 6 November 2013 – Published: 9 December 2013

Abstract. We investigate the contribution of oceanic methyl iodide (CH₃I) to the stratospheric iodine budget. Based on CH₃I measurements from three tropical ship campaigns and the Lagrangian transport model FLEXPART, we provide a detailed analysis of CH₃I transport from the ocean surface to the cold point in the upper tropical tropopause layer (TTL). While average oceanic emissions differ by less than 50 % from campaign to campaign, the measurements show much stronger variations within each campaign. A positive correlation between the oceanic CH₃I emissions and the efficiency of CH₃I troposphere–stratosphere transport has been identified for some cruise sections. The mechanism of strong horizontal surface winds triggering large emissions on the one hand and being associated with tropical convective systems, such as developing typhoons, on the other hand, could explain the identified correlations. As a result of the simultaneous occurrence of large CH₃I emissions and strong vertical uplift, localized maximum mixing ratios of 0.6 ppt CH₃I at the cold point have been determined for observed peak emissions during the SHIVA (Stratospheric Ozone: Halogen Impacts in a Varying Atmosphere)-Sonne research vessel campaign in the coastal western Pacific. The other two campaigns give considerably smaller maxima of 0.1 ppt CH₃I in the open western Pacific and 0.03 ppt in the coastal eastern Atlantic. In order to assess the representativeness of the large local mixing ratios, we use climatological emission scenarios to derive global upper air estimates of CH₃I abundances. The model results are compared with available upper air measurements, including data from the recent ATTREX and HIPPO2

aircraft campaigns. In the eastern Pacific region, the location of the available measurement campaigns in the upper TTL, the comparisons give a good agreement, indicating that around 0.01 to 0.02 ppt of CH₃I enter the stratosphere. However, other tropical regions that are subject to stronger convective activity show larger CH₃I entrainment, e.g., 0.08 ppt in the western Pacific. Overall our model results give a tropical contribution of 0.04 ppt CH₃I to the stratospheric iodine budget. The strong variations in the geographical distribution of CH₃I entrainment suggest that currently available upper air measurements are not representative of global estimates and further campaigns will be necessary in order to better understand the CH₃I contribution to stratospheric iodine.

1 Introduction

It is currently believed that organic iodine compounds are not important for stratospheric ozone chemistry as a result of their very short lifetimes that allow only small fractions of the emitted iodine to reach the stratosphere (Aschmann et al., 2009; Montzka and Reimann, 2011). Emissions of iodinated compounds from the ocean into the atmosphere and subsequent strongly localized vertical transport in convective systems determines if and how much of the short-lived iodinated gases reach the upper tropical tropopause layer (TTL) and lower stratosphere. Both processes are highly variable in time and space and reliable global estimates should, if possible, be derived from frequent upper air observations and from model

studies based on high resolution emission maps. In addition to the unknown variability of CH_3I in the TTL, uncertainties in the knowledge of the atmospheric lifetime of inorganic iodine (e.g., Dix et al., 2013) pose a major challenge for the quantification of the stratospheric iodine budget. If iodinated species reach the upper troposphere and lower stratosphere (UTLS), they might enhance ozone destruction due to the possible role of active iodine in rapid interhalogen reactions (Solomon et al., 1994).

Methyl iodide (CH_3I) is an important carrier of iodine from the surface to the free troposphere, where it plays an important role for ozone chemistry and oxidizing capacities (Chameides and Davis, 1980; Davis et al., 1996; McFiggans et al., 2000; O'Dowd et al., 2002; Saiz-Lopez et al., 2012; Vogt et al., 1999). CH_3I is emitted mainly from the ocean where biological sources in form of algae and phytoplankton (e.g., Hughes et al., 2011; Manley and Dastoor, 1987, 1988; Manley and de la Cuesta, 1997; Smythe-Wright et al., 2006) and non-biological sources in form of photochemical production (e.g., Butler et al., 2007; Chuck et al., 2005; Happell and Wallace, 1996; Moore and Zafriou, 1994; Richter and Wallace, 2004; Yokouchi et al., 2008) have been identified. Note that current studies suggest that organic sources of iodine cannot explain iodine oxide concentrations in the lower troposphere over the tropical oceans (Jones et al., 2010; Mahajan et al., 2010) and that emissions of inorganic iodine following heterogeneous reactions at the ocean surface can account for a primary source of oceanic iodine emissions (Carpenter et al., 2013).

Global emission estimates are based on oceanic and atmospheric CH_3I concentrations obtained during ship cruises (*bottom-up*) and on model studies which are adjusted to CH_3I upper-air observations (*top-down*) (Montzka and Reimann, 2011). Oceanic and atmospheric surface CH_3I is characterized by a large spatial (e.g., Ziska et al., 2013) and temporal (e.g., Fuhlbrügge et al., 2013) variability. Additionally, differences between calibration scales, applied during past campaigns, might exist (Butler et al., 2007). Estimating local fluxes from observations and extrapolating them to a larger scale in order to derive global estimates may thus result in large uncertainties. Atmospheric modeling studies, on the other hand, prescribe global emissions with the emission strength chosen so as to reproduce atmospheric aircraft observations and might miss the importance of localized sources. As a result, emissions are poorly constrained and available global oceanic flux estimates based on the different approaches (*top-down*, *bottom-up* and laboratory experiments) range widely from 180 to 1163 Gg I yr^{-1} . An overview of available global oceanic emission estimates in the literature is given in Table 1 in Gg I yr^{-1} and, for a better comparability with the ship campaign emissions presented in Sect. 3, in $\text{pmol CH}_3\text{I m}^{-2} \text{h}^{-1}$. Additionally, terrestrial sources such as rice paddies, wetlands, and biomass burning, which are not well quantified yet, are assumed to contribute

80–110 Gg I yr^{-1} (Bell et al., 2002; Redeker et al., 2000; Sive et al., 2007).

Atmospheric mixing ratios of CH_3I in the marine boundary layer have been reported by a large number of measurement campaigns, and background values range between 0.4 and 1.6 ppt (Saiz-Lopez et al., 2012 and references therein). With increasing altitude the CH_3I abundance decreases and measurements from two aircraft campaigns reveal very little CH_3I in the TTL, with mean values of 0.01 ppt above 14 km (Montzka and Reimann, 2011). The two campaigns were conducted with the NASA WB57 high-altitude aircraft over Central America and the Gulf of Mexico, but due to the horizontal limitations of the campaign area, the results might not be representative of global CH_3I estimates in the TTL. The observational data obtained during the aircraft campaigns, combined with the outcome of model studies (Aschmann et al., 2009; Donner et al., 2007; Gettelman et al., 2009), lead to the conclusion that no more than 0.05 ppt of iodine enters the stratosphere in the form of the source gas CH_3I (Montzka and Reimann, 2011). If CH_3I is photolyzed before reaching the stratosphere, the generated inorganic iodine can be removed from the atmosphere by washout. It has been suggested recently that heterogeneous recycling of inorganic iodine on aerosol surfaces can occur (Dix et al., 2013), which could enable a longer atmospheric lifetime and possibly the direct entrainment of inorganic iodine into the stratosphere.

Once in the lower stratosphere, CH_3I will contribute to the inorganic iodine (I_y) budget, which is of interest due to the suggested efficiency of active iodine in destroying ozone (Davis et al., 1996; Solomon et al., 1994; WMO, 2007). Stratospheric iodine exists mostly in the form of free radicals (iodine atoms and iodine monoxide), so that the partitioning of free radicals to total halogen content is much higher for iodine than for chlorine or bromine (Brasseur and Solomon, 2005). Investigations of inorganic iodine species, in the form of iodine monoxide (IO) or iodine dioxide (OIO), in the lower stratosphere give an upper limit of IO of 0.3 ppt based on ground-based measurements (Wennberg et al., 1997) and 0.2 ppt based on solar-occultation balloon-borne measurements (Pundt et al., 1998). Other balloon campaigns in the upper TTL, however, detected no IO or OIO in the upper TTL above the detection limit at 0.1 ppt (Bösch et al., 2003; Butz et al., 2009). As a result, the total amount of stratospheric I_y is currently estimated to be below 0.15 ppt (Montzka and Reimann, 2011), arising from the detection limit of inorganic iodine (0.1 ppt) given by the latter studies and the iodine supply in form of CH_3I (0.05 ppt).

Due to its short lifetime of around 7 days (given in Montzka and Reimann, 2011), one expects CH_3I in the troposphere and TTL to exhibit significantly large variability. The amount of CH_3I transported from the ocean into the stratosphere is determined by oceanic emissions and the efficiency of atmospheric transport. In order to quantify the contribution of CH_3I to the stratospheric I_y budget, observations of CH_3I and IO with a good global coverage would be

Table 1. Global CH₃I emission estimates in the literature given in Gg I yr⁻¹ and additionally in pmol CH₃I m⁻² h⁻¹.

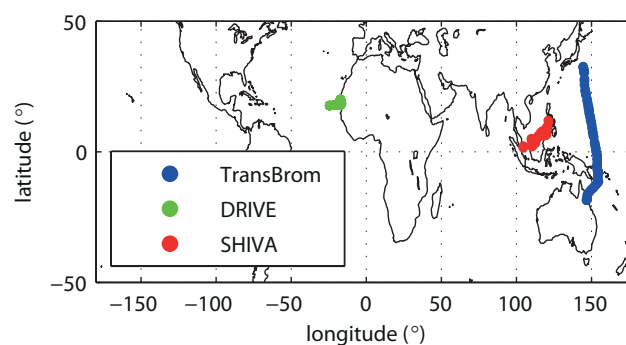
CH ₃ I emission (Gg I yr ⁻¹)	CH ₃ I emission (pmol CH ₃ I m ⁻² h ⁻¹)	Reference	Approach
241	593	Liss and Slater (1974)	Bottom up
1163	2862	Rasmussen et al. (1982)	Bottom up
270–450	665–1107	Singh et al. (1983)	Bottom up
134	330	Campos et al. (1996)	Bottom-up
254	625	Moore and Groszko (1999)	Bottom up
272	670	Bell et al. (2002)	Bottom-up
180	443	Chuck et al. (2005)	Bottom up
531	1307	Smythe-Wright et al. (2006)	Lab-experiment
550	1354	Butler et al. (2007)	Bottom-up
272	748	Ordóñez et al. (2012)	Top-down
184	453	Ziska et al. (2013)	Bottom-up

necessary. While in the UTLS such observational evidence of global iodine abundances does not exist so far, recent measurements in the free troposphere over the Canary Islands (Puentedura et al., 2012) and the Pacific Ocean (Dix et al., 2013) report significant amounts of IO of up to 0.4 ppt and suggest that IO occurs in the lower troposphere on a global scale. At the surface, a variety of CH₃I data originating from ship campaigns and the resulting first global emission climatology (Ziska et al., 2013) are available. Here, we use in situ CH₃I measurements from three tropical ship campaigns, one in the eastern Atlantic and two in the western Pacific, and a Lagrangian transport model to analyze the characteristics and the variability of CH₃I transport from the ocean surface into the upper TTL. Furthermore, we derive upper air estimates of CH₃I abundances based on the global emission climatology and compare them to available upper air measurements that include new data from various aircraft campaigns. The ship and aircraft campaigns as well as the atmospheric transport model are introduced in Sect. 2. Estimates of atmospheric CH₃I abundances based on the individual ship campaigns are given in Sect. 3, while the model results based on global emissions, including their comparison to aircraft campaign data, are discussed in Sect. 4. We present the contribution of oceanic CH₃I to stratospheric iodine in the form of the model estimated CH₃I mixing ratios at the cold point. The summary and discussion of the key results can be found in Sect. 5.

2 Data and model

2.1 Ship campaigns

Oceanic CH₃I emissions from three tropical ship campaigns (Table 2), calculated from measurements of CH₃I mixing ratios in the surface water and atmosphere, are used in this study. The two ship campaigns TransBrom-Sonne and SHIVA-Sonne took place in the open and coastal western Pacific while the DRIVE campaign was located in the north-

**Fig. 1.** Map of ship campaigns used in this study.

eastern Atlantic (Fig. 1). During each cruise, surface air samples were collected every 1 to 3 h in pressurized stainless steel canisters and analyzed subsequently for CH₃I at the Rosenstiel School of Marine and Atmospheric Sciences (RS-MAS) at the University of Miami by the group lead by Elliot Atlas. Surface water samples were collected simultaneously by a submersible pump at 5 m depth and analyzed on board using a purge-and-trap gas chromatography/mass spectrometry (GC/MS) analytical system (Quack et al., 2004). Both data sets were calibrated with a NOAA standard (Butler et al., 2007). The instantaneous CH₃I sea-to-air fluxes were calculated from the measured sea surface concentration and local atmospheric mixing ratios applying Henry's law constant from Moore et al. (1995) and the instantaneous 10 min average wind speed. Henry's law constant was calculated as a function of the 10 min average water temperature. The flux calculations are based on the transfer coefficient parameterization of Nightingale et al. (2000) adapted to CH₃I. For the parameterization, the transfer velocity at Schmidt number 660, which corresponds to CO₂ at 20 °C in seawater (Wanninkhof, 1992), was corrected by the CH₃I Schmidt number at the temperature of measurement. The ratio of the diffusion coefficients from CH₃Br (De Bruyn and Saltzman, 1997) and

Table 2. Recent ship campaigns providing oceanic and atmospheric CH₃I measurements.

Campaign (R/V)	Full name	Route	Time period	References
TransBrom-Sonne (Sonne)	Very short lived bromine compounds in the ocean and their transport pathways into the stratosphere – Sonne	Western Pacific: Tomakomai, Japan – Townsville, Australia	2009 October	Krüger and Quack (2013)
DRIVE (Poseidon)	Diurnal and Regional Variability of Halogen Emissions	Atlantic: Las Palmas, Spain – Vigo, Spain	2010 May/June	Bange et al. (2011)
SHIVA-Sonne (Sonne)	Stratospheric Ozone: Halogen Impacts in a Varying Atmosphere – Sonne	Western Pacific: Singapore – Manila, Philippines	2011 November	Quack and Krüger (2013)

CH₃I, estimated according to Wilke and Chang (1955), was used as a function of temperature for the Schmidt-number correction (e.g., Richter and Wallace, 2004).

2.2 Aircraft campaigns

CH₃I measurements in the upper troposphere and TTL are currently available from seven aircraft campaigns. Three campaigns provide data from the surface up to the upper troposphere/lower TTL: the TC4-DC8 over Central America and the HIPPO and SHIVA campaigns which took place in the Pacific and western Pacific area, respectively. Note that SHIVA is a combined aircraft-, ship- and ground-based campaign with measurements both from the ship and from the aircraft used in this study. From the HIPPO mission, we use here the measurements obtained during the HIPPO2 campaign in 2009. CH₃I measurements in the upper TTL are available from Pre-AVE and TC4 campaigns. These two campaigns have been used to derive recent estimates of the upper air CH₃I abundance (Montzka and Reimann, 2011). In addition to the data used for the current upper TTL CH₃I estimate, observations from the ACCENT campaign in 1999 and from the ATTREX campaign in 2011 are included in our study. All four campaigns, which provide CH₃I measurements in the upper TTL, took place over the southern US and Central America. Detailed information about the aircraft missions, including location and time period, are presented in Table 3.

2.3 Global emission climatology

The global emission scenario from Ziska et al. (2013) is a bottom-up estimate of the oceanic CH₃I fluxes. Atmospheric and oceanic surface in situ measurements from the HalOcat (Halocarbons in the ocean and atmosphere) database project (<https://halocat.geomar.de>) were used to generate global surface concentration maps. In a first step the surface measurements were classified based on physical and biogeochemi-

cal characteristics of the ocean and atmosphere important for the CH₃I distribution and sources. Within each classified region, the global 1° × 1° grid was filled through the extrapolation of the in situ measurements based on the ordinary least square (OLS) regression technique. The estimated surface concentration maps do not provide any information on temporal variability, but represent climatological fields of a 20 yr time period. Based on the global concentration maps, the oceanic emissions were calculated with the transfer coefficient parameterization of Nightingale et al. (2000), adapted to CH₃I. The emission parameterization is based on 6 hourly meteorological ERA-Interim data (Dee et al., 2011), taking into account emission peaks related to maxima in the horizontal wind fields. The final emission climatology product is calculated as the 20 yr-average emission field. Emission peaks related to 6 hourly wind maxima are not present any more in the final 20 yr mean climatology; however, their existence in the temporally resolved emission fields counteracts a possible underestimation introduced by smoothing effects of the climatological approach.

2.4 Modeling atmospheric transport

The atmospheric transport of CH₃I from the oceanic surface into the upper troposphere and TTL is simulated with the Lagrangian particle dispersion model, FLEXPART (Stohl et al., 2005). This model has been validated based on comparisons with measurement data from three large-scale tracer experiments (Stohl et al., 1998) and on intercontinental air pollution transport studies (e.g., Forster et al., 2001; Spichtinger et al., 2001; Stohl and Trickl, 1999). FLEXPART is driven by meteorological fields from the ECMWF (European Centre for Medium-Range Weather Forecasts) numerical weather prediction model and includes parameterizations for moist convection (Forster et al., 2007), turbulence in the boundary layer and free troposphere (Stohl and Thomson, 1999), dry

Table 3. Aircraft campaigns with CH₃I measurements used in the study.

Campaign (Aircraft)	Full name	Max. altitude	Location	Time period	References
ACCENT (WB57)	Atmospheric Chemistry of Combustion Emissions Near the Tropopause	19 km	Southern US Central America	1999 April, September	http://espoarchive.nasa.gov/archive/browse/accent
Pre-AVE (WB57)	Pre-Aura Validation Experiment	19 km	Southern US Central America	2004 January–February	http://espoarchive.nasa.gov/archive/browse/pre_ave
TC4 (DC 8)	Tropical Composition, Cloud and Climate Coupling	12 km	Southern US Central America	2007 July–August	Toon et al. (2010)
TC4 (WB57)	Tropical Composition, Cloud and Climate Coupling	19 km	Southern US Central America	2007 August	Toon et al. (2010)
HIPPO2 (HIAPER)	HIAPER Pole-to-Pole Observations 2	14 km	Pacific	2009 November	Wofsy et al. (2011)
ATTREX (Global Hawk)	Airborne Tropical Tropopause Experiment	19 km	Eastern Pacific	2011 October–November	http://espo.nasa.gov/missions/attrex
SHIVA (Falcon)	Stratospheric ozone: Halogen Impacts in a Varying Atmosphere	14 km	Western Pacific (Maritime Continent)	2011 November	http://shiva.iup.uni-heidelberg.de/index.html

deposition and in-cloud as well as below-cloud scavenging, and the simulation of chemical decay.

We perform two different kinds of studies based on the different model setups, one using in situ emissions observed during individual ship campaigns and one using a global emission climatology. For the in situ experiments, the transport of CH₃I is simulated with a multitude of trajectories launched for each emission data point, as described in detail by Tegtmeier et al. (2012). The trajectories are assigned the amounts of CH₃I emitted from a 0.0002° × 0.0002° grid box (~ 500 m²) at the measurement location over one hour, as calculated from the observation-derived flux. Atmospheric mixing ratio profiles resulting from in situ emissions have been determined following the method described in Tegtmeier et al. (2012). The calculation of global CH₃I estimates is based on the emission climatology from Ziska et al. (2013). The oceanic sea-to-air flux is given globally on a 1° × 1° grid. From each grid box 10 trajectories are released per day, carrying the according amount of CH₃I as prescribed by the emission scenario. While the simulations based on the in situ ship campaign data are carried out for the time period of the respective ship campaigns (see Table 2), the global simulations are run for the year 2009. Additionally, the global simulations are carried out for the time periods of the aircraft campaigns (see Table 3) in order to allow for a direct comparison between aircraft measurements and model results. The FLEXPART runs are driven by the ECMWF reanalysis product ERA-Interim (Dee et al., 2011), given at a horizontal

resolution of 1° × 1° on 60 model levels. Transport, dispersion and convection of the air parcels are calculated from the 6-hourly fields of horizontal and vertical wind, temperature, specific humidity, convective, and large scale precipitation and others. The vertical wind is calculated in hybrid coordinates mass consistently from spectral data by the pre-processor, which retrieves the meteorological fields from the ECMWF archives.

The atmospheric lifetime of CH₃I was assumed to be constant in the troposphere and set to 7 days according to current estimates (Montzka and Reimann, 2011). Trajectories were terminated after 20 days. For a sensitivity study, an altitude-dependent lifetime of CH₃I, derived by the TOMCAT chemical transport model (CTM) (Chipperfield, 2006), was also used. The CTM calculated tropospheric loss of CH₃I through photolysis, the major tropospheric sink, using the recommended absorption cross section data of Sander et al. (2011). The modeled CH₃I lifetime diagnosed by the CTM is relatively short (~ 2–3 days) in the tropical troposphere and thus this experiment is useful for examining the sensitivity of CH₃I loading in the upper troposphere to a range of lifetimes. Previously, CH₃I profiles from TOMCAT have been shown to agree well with aircraft observations in the tropical troposphere (Hossaini et al., 2012). The mass of the CH₃I carried by each air parcel is reduced at a rate corresponding to its chemical lifetime.

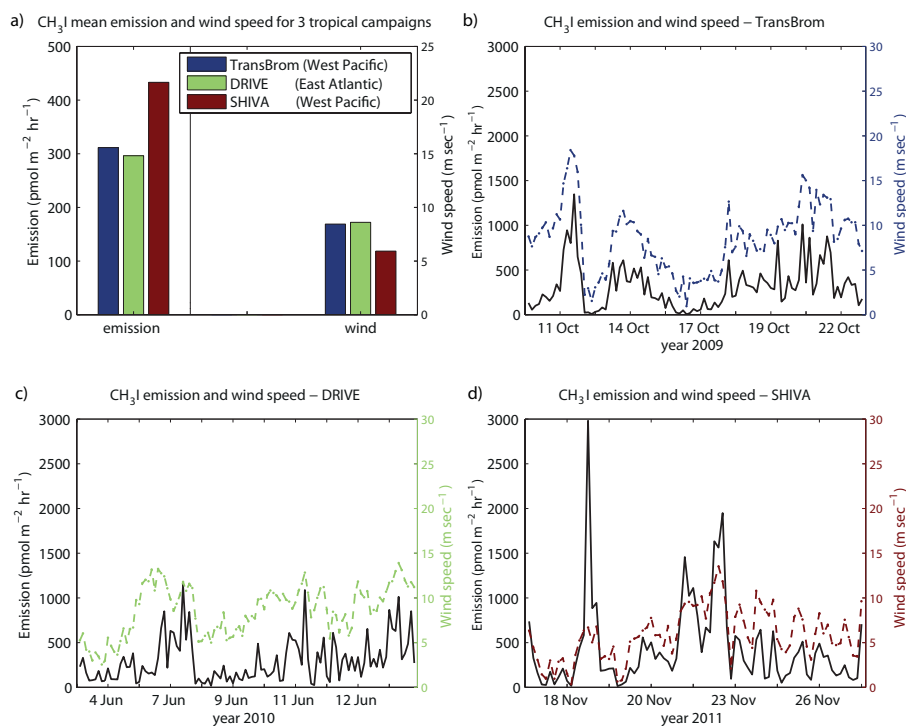


Fig. 2. Campaign-averaged CH₃I emissions and wind speed are shown for three tropical campaigns (a). CH₃I emissions (black line), as well as the wind speed (colored line) are displayed as a function of time along the cruise track for TransBrom (b), DRIVE (c), and SHIVA (d).

3 Atmospheric CH₃I transport based on individual ship campaigns

3.1 Comparison of three tropical campaigns

CH₃I emissions observed during the tropical ship cruises vary substantially from campaign to campaign. Figure 2a shows the campaign-averaged emissions for all three cruises, with stronger emissions for the coastal western Pacific campaign SHIVA-Sonne (referred to as SHIVA hereinafter) compared to the northeastern Atlantic campaign DRIVE and the open western Pacific campaign TransBrom-Sonne (referred to as TransBrom hereinafter). In contrast to global estimates (Table 1), the emissions observed during the three campaigns are small with mean values of 310 (DRIVE), 320 (TransBrom) and 430 (SHIVA) pmol m⁻² h⁻¹ just below the minimum global estimate (443 pmol m⁻² h⁻¹, Chuck et al., 2005) and three times smaller than the maximum global estimate (1354 pmol m⁻² h⁻¹, Butler et al., 2007).

Black lines in Fig. 2b–d give the emission strength along the cruise tracks and demonstrate the large variability of sea-to-air fluxes during the campaigns, with the measurement locations often about less than 100 km apart. CH₃I is generally oversaturated in oceanic surface waters. As a result, emission flux is primarily controlled by concentrations in water (rather than air) and the water–air exchange rate, which is in turn driven by the wind speed (Ziska et al., 2013). In ad-

dition to the emission time series, the wind speed along the cruise track (colored dashed lines) for the individual campaigns is presented in Fig. 2b–d. Particularly high emissions occur for the TransBrom cruise during times of high wind speeds, e.g., emissions of up to 1364 and 600 pmol m⁻² h⁻¹ were observed during the tropical storms Nepartak and Lupit on 12 October and 14 October 2009, respectively (Quack et al., 2013).

Among the different existing parameterizations, the here applied sea-to-air flux parameterization of Nightingale et al. (2000) predicts transfer velocities in the middle range (e.g., Carpenter et al., 2012) for wind speeds below 20 m s⁻¹. All parameterizations gain uncertainty for wind speeds above 20 m s⁻¹ and a possible overestimation of sea-to-air fluxes at these very high wind speeds has been suggested (McNeil and D’Asaro, 2007). While this needs to be kept in mind when fluxes at higher wind speeds are considered, for the here discussed cruises wind speeds are always below 20 m s⁻¹ and the Nightingale parameterization has been applied throughout. CH₃I emissions during the DRIVE campaign are also determined by the large supersaturation in combination with varying wind speeds, with the largest emissions of up to 1146 pmol m⁻² h⁻¹ observed on 7 June 2010. For SHIVA, relatively high oceanic concentrations and warm water temperatures lead to very high supersaturations of methyl iodide in the coastal western Pacific and trigger large CH₃I emissions due to elevated wind speeds. Local peak emissions

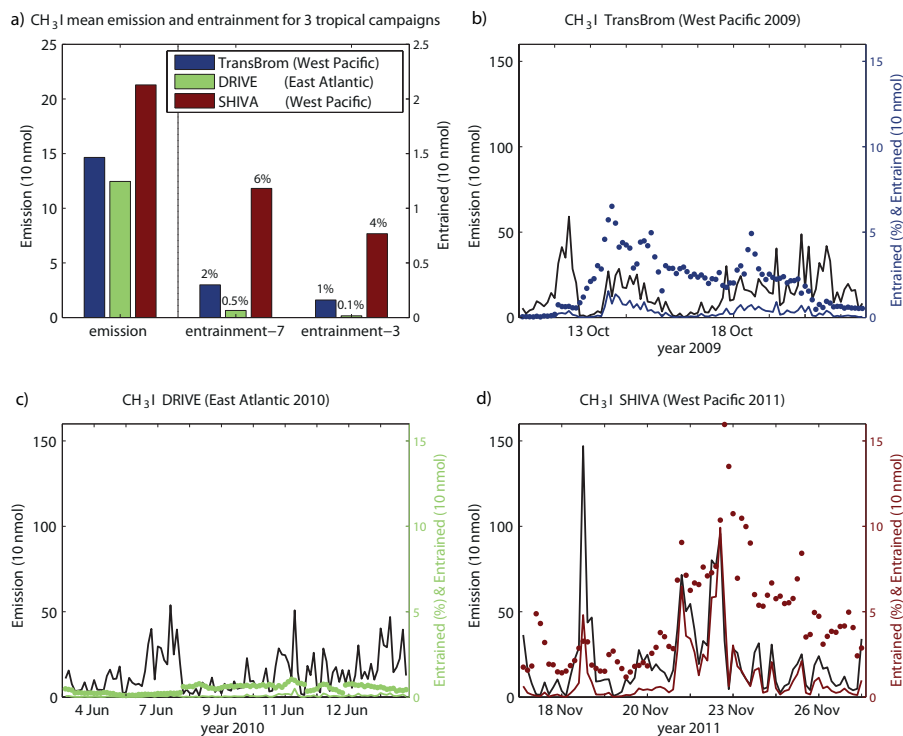


Fig. 3. Campaign-averaged CH₃I emissions and modeled entrainment above 17 km are shown for three tropical campaigns (a). CH₃I emissions (black line) as well as the relative (colored dots) and total (colored line) amount of CH₃I entrained above 17 km are displayed as a function of time along the cruise track for TransBrom (b), DRIVE (c), and SHIVA (d). Emissions are calculated from the observed flux for a time period of one hour and an area of 500 m² for each observation. CH₃I lifetime is prescribed with 7 days (entrainment-7 in panel a and all results in b–d) or with 2–3 days (entrainment-3 in a).

during SHIVA of up to 2980 pmol m⁻² h⁻¹ (19 November 2011) exceed the maximum emissions observed during the other two campaigns and are among the largest local emissions observed so far (Ziska et al., 2013).

The amount of CH₃I that reaches the stratosphere has been estimated based on Lagrangian transport calculations with FLEXPART. CH₃I emissions in the FLEXPART runs are calculated from the observed flux for a time period of one hour and an area of 500 m² for each observation, presented in Fig. 3 as campaign averages (Fig. 3a) and as time series over the length of each individual campaign (Fig. 3b–d). The level above which no significant washout is expected is particularly important for stratospheric iodine chemistry, since all CH₃I which reaches this level before being photolyzed can be expected to contribute to the stratospheric I_y budget. While the exact altitude of the “no-washout level” is still under debate (Fueglistaler et al., 2009), we have chosen the cold point altitude as an upper estimate since no dehydration is expected to occur above. Based on evaluations of regular radiosonde measurements during the ship campaigns, the cold point is found at 17 km (Fuhlbrügge et al., 2013; Krüger and Quack, 2012). We quantify the contribution of CH₃I to stratospheric iodine based on the amount of CH₃I entrained above 17 km, which is calculated as the sum of CH₃I carried

by all the computational particles across this altitude. Note that the altitude of the level above which no washout occurs is a source of uncertainty regarding our results of the CH₃I contribution to stratospheric iodine. If, for instance, heterogeneous recycling of iodine from aerosols back to the gas phase were to occur (Dix et al., 2013), the “no-washout level” would be lower than the cold point and, as a consequence, the CH₃I contribution to stratospheric iodine would be larger than estimated below. A simple sensitivity study reveals that approximately twice as much CH₃I is found to contribute to the stratospheric iodine if the “no-washout level” is set at 16 km instead of 17 km.

For all three campaigns the average amount of CH₃I being entrained above 17 km is shown in Fig. 3a. For the scenario of a uniform atmospheric lifetime of 7 days (WMO, 2011), about 0.5 % (DRIVE), 2 % (TransBrom) and 6 % (SHIVA) of the emitted CH₃I reaches the upper TTL and is projected to be entrained into the stratosphere. In order to investigate the sensitivity of our results to the prescribed atmospheric lifetime of CH₃I, we repeat the same calculation but using an altitude dependent CH₃I lifetime from the TOMCAT CTM. When the considerably shorter profile lifetime (2–3 days) is assumed, only 0.1 % (DRIVE), 1 % (TransBrom) and 4 % (SHIVA) of the emitted CH₃I are transported into the upper

TTL. The entrainment of CH₃I above 17 km based on the two different lifetimes reveals considerable differences, as one would expect, and illustrates the need for a better understanding of tropospheric CH₃I chemistry. While all the following results are based on assuming a CH₃I atmospheric lifetime of 7 days, the case study above provides an estimate of the sensitivity of our results (30–80 % less entrainment) to variations of the atmospheric lifetime (2.5–3 days instead of 7 days).

The efficiency of atmospheric CH₃I transport from the surface to the cold point (given by the percentage value of CH₃I reaching 17 km) during SHIVA (western Pacific) is 12 to 40 times larger than the efficiency of CH₃I transport during DRIVE (Atlantic). While these results are derived from model runs based on local campaign data, it is known from previous studies that the western Pacific is in general an important region for troposphere–stratosphere transport of short-lived compounds (e.g., Aschmann et al., 2009; Krüger et al., 2009; Levine et al., 2007) due to active deep convection (Fueglistaler et al., 2009 and references therein). For SHIVA, the large emissions together with the very efficient vertical transport lead to an overall large amount of CH₃I reaching the stratosphere. The absolute amounts of CH₃I being entrained above the cold point at 17 km are given in Fig. 3a for all campaigns, illustrating that 20 times more CH₃I is entrained for SHIVA compared to DRIVE and 4 times more when compared to TransBrom.

3.2 Possible connection between CH₃I emissions and atmospheric transport

Oceanic emissions and atmospheric transport vary from campaign to campaign but also considerably within each campaign. Dotted lines in Fig. 3b, c, and d give the transport efficiency along the cruise track and demonstrate its large variability from measurement side to measurement side. During DRIVE, the CH₃I troposphere–stratosphere transport is weak for the whole campaign and less than 1 % reaches the stratosphere (Fig. 3c). However, for the two western Pacific campaigns, the vertical transport is more efficient, lifting 1–16 % of emitted CH₃I from the surface to 17 km for SHIVA, and 0–6 % for TransBrom. While both ship campaigns took place in the western Pacific and encountered periods of strong convective activity, the amount of overshooting convection responsible for the transport of the short-lived CH₃I up to 17 km differs between the campaigns. An overall stronger vertical transport is predicted for the SHIVA campaign, which took place in the coastal regions of the maritime continent, an area well known for deep cumulus convection and heavy precipitation systems during boreal winter (Chang et al., 2005). For TransBrom, convection above the open ocean including tropical storm systems dominates the vertical transport from the surface to the cold point at 17 km. The total amount of CH₃I entrained above 17 km shows maximum values for cases when both variables, emission and

transport efficiency, are large. For the SHIVA campaign, this coincidence is found for the event of the second largest emission on 22 November 2011, where the transport model estimates that around 10 % CH₃I could reach 17 km. For TransBrom, the largest total entrainment takes place on 14 October 2009 and is based on an average emission value during times of maximum efficiency of vertical transport.

In order to further analyze possible coincidences of strong emissions and efficient vertical transport, a correlation analysis has been applied to the two time series. For the entire time series covering the whole cruise length, no correlation exists for any of the three campaigns. However, when parts of the time series are analyzed, high correlations are found. For the TransBrom campaign, correlations between emissions and vertical atmospheric transport reach a maximum for two individual campaign sections (Fig. 4a). A very high correlation of 0.89 is found for the first section, comprising 16 data points collected over 2 days (red lines). A high correlation ($r = 0.69$) also exists for the subsequent cruise section extending from 13 October 2009 to 18 October 2009 based on 39 data points. All correlation coefficients are statistically significant at the 95 % confidence level based on the Student's t test. Scatter plots of the emissions versus vertical atmospheric transport show different relationships for the two periods, with linear fits resulting in slopes of 54 and 5, respectively.

Understanding the two different regimes occurring during TransBrom, which show correlations if analyzed separately, but lead to uncorrelated data sets when combined, requires some background information on the meteorological situation during the cruise (Krüger and Quack, 2012). The first cruise section extends north of the Intertropical Convergence Zone (ITCZ) from 32° N to 24° N, and model results suggest that vertical transport from the surface to 17 km is weak with less than 1 % of CH₃I being lifted by deep convection into the upper TTL. At the end of the first cruise section (12 October 2009, 27° N), the ship crossed the track of the tropical storm Nepartak and large horizontal wind speeds reaching values of 20.4 m s⁻¹ were observed. Measurements were increased to an hourly frequency and peak emissions of oceanic CH₃I were reported during periods of maximum horizontal winds. Note that during the influence of Nepartak, the transport model shows strong convective activity, reaching only main convective outflow regions around 12 km and not the upper TTL, resulting in the weak transport efficiency discussed above. At the beginning of the second cruise section, the ship crossed the ITCZ and came close to the tropical storm Lupit (14 October 2009, 18° N), which developed into a super typhoon a couple of days later (Krüger and Quack, 2012). Similar to the situation during Nepartak, the strong horizontal wind speeds are accompanied by increased atmospheric trace gas concentrations and emissions. As opposed to the first cruise track section, atmospheric transport into the upper TTL is very efficient during the second cruise section, in accordance with its location within the ITCZ.

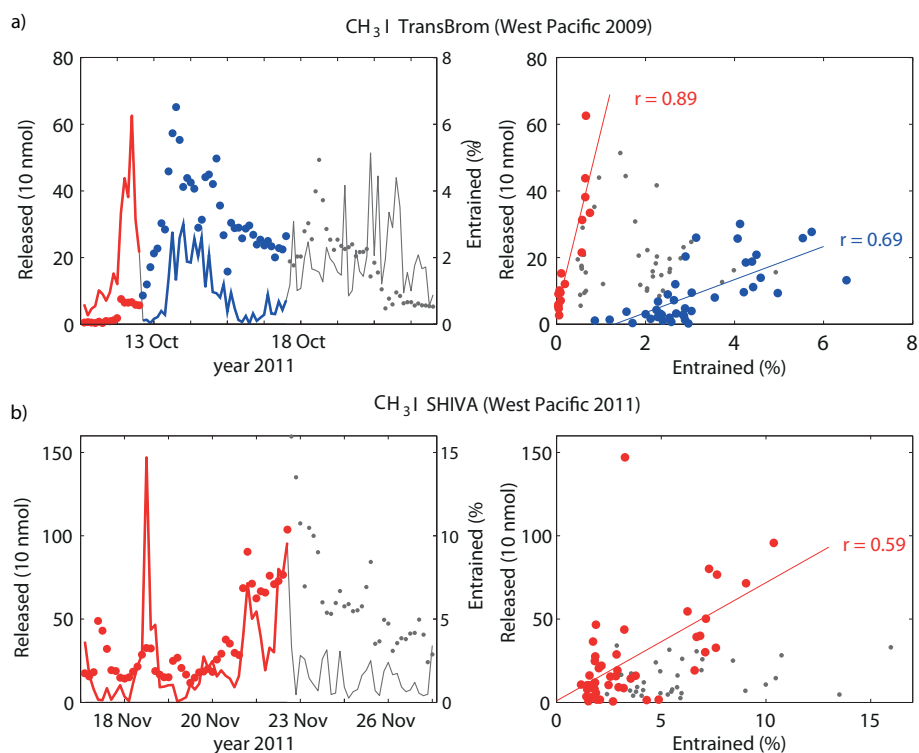


Fig. 4. The CH₃I observed emissions (line) and the modeled relative amount entrained above 17 km (dots) are shown for TransBrom (a) and SHIVA (b) as a function of time (left panels) and as a scatter plot (right panels). The subsets, for which correlations between the two functions have been identified, are color-coded in red and blue. The correlation coefficients (r) are given in the right panel.

Table 4. Correlation coefficients between CH₃I emission, horizontal wind speed and vertical transport efficiency (given by the relative amount of CH₃I entrained above 17 km). The coefficients are given for the entire TransBrom and SHIVA campaigns as well as for the subsets where correlations between the CH₃I emissions and vertical transport efficiency have been identified (TransBrom section 1 and 2, SHIVA section 1).

Correlation coefficients for various cruise sections	TransBrom section 1	TransBrom section 2	TransBrom entire	SHIVA section 1	SHIVA entire
CH ₃ I emission and horizontal wind speed	0.93	0.93	0.82	0.70	0.62
Horizontal wind speed and vertical transport	0.87	0.74	-0.29	0.73	0.49
CH ₃ I emission and vertical transport	0.89	0.69	-0.05	0.59	0.28

For the SHIVA campaign, the correlation between oceanic emissions and atmospheric transport reaches a maximum for the cruise section in the South China Sea from 17 November to 23 November 2011, comprising 47 data points. Figure 4b shows the two time series, oceanic emissions and troposphere–stratosphere transport efficiency, with the data during the respective cruise section displayed in red. The correlation ($r = 0.59$) results mostly from the fact that the large emissions on 21–22 November 2011 are accompanied by fast vertical transport. Note that for these two days high

horizontal wind speeds of up to 13 m s^{-1} occurred, while the horizontal winds during the time period before were moderate, around 5 m s^{-1} . After 23 November 2011, the horizontal winds and also the vertical transport continued to be large; however, due to lower oceanic concentrations and saturation anomalies the emissions are small compared with the first cruise section.

Based on two tropical campaigns in the western Pacific, three cruise sections have been identified that show a correlation between the amount of CH₃I emitted from the ocean

and the fraction of emitted CH_3I transported from the surface to the cold point at 17 km. In general, CH_3I shows relatively uniform oceanic concentrations over the various cruise sections (Quack et al., 2013). Emission rates are mainly determined by the wind speed variations with high wind speeds resulting in a fast atmospheric outflow and an immediate replacement of the gas from the oceanic source. Such correlations between emissions and horizontal wind speeds have also been observed for other short-lived halogenated gases such as CHBr_3 and CH_2Br_2 in supersaturated coastal waters during tropical storm activities (Zhou et al., 2008). We find the strongest CH_3I emissions during tropical storms, which on the other hand can lead to intense vertical transport associated with developing tropical cyclones. It has been suggested that tropical cyclones could play an important role for troposphere–stratosphere exchange due to associated frequent convective overshooting (Rossow and Pearl, 2007) and due to contributing a disproportional large amount of the convection that penetrates the stratosphere (Romps and Kuang, 2009). The mechanism of strong horizontal winds triggering large emissions, on the one hand, and being associated with tropical convective systems, on the other hand, could provide a possible explanation of the identified correlations. Such a mechanism could also explain why data over longer time periods are uncorrelated if the meteorological or oceanic regime changes. Examples are the change in oceanic CH_3I concentration gradients during SHIVA on 23 November 2011 coinciding with the end of the correlation time period and the change of meteorological conditions during TransBrom on 14 October, across the ITCZ, coinciding with the switch between the two correlation regimes.

Correlation coefficients between all three quantities are presented in Table 4 for different sections of the two cruises. Evidently, in all cases there is a strong correlation between CH_3I emissions and the horizontal wind speed. When the horizontal surface wind is also strongly correlated with the efficiency of vertical transport, we find the above discussed correlation between CH_3I emissions and vertical transport. The fact that for these cases both quantities are highly correlated with the horizontal wind further strengthens the above suggested mechanism. For the entire TransBrom cruise, no correlation of the horizontal winds with the vertical transport can be found, probably due to the very different meteorological regimes. For the entire SHIVA campaign, the correlation between CH_3I emission and horizontal winds is somewhat weaker than for the other cases, probably because of a switch in the oceanic regime.

For the cruise sections where a correlation between emission and vertical transport could be identified, one also finds the overall largest amounts of CH_3I being transported into the stratosphere. For TransBrom, the maximum amount of 0.1 ppt CH_3I at 17 km (Fig. 5) is associated with emissions on 14 October 2009 and subsequent atmospheric transport influenced by the tropical storm Lupit. Atmospheric CH_3I abundance at 17 km averaged over the whole campaign amounts

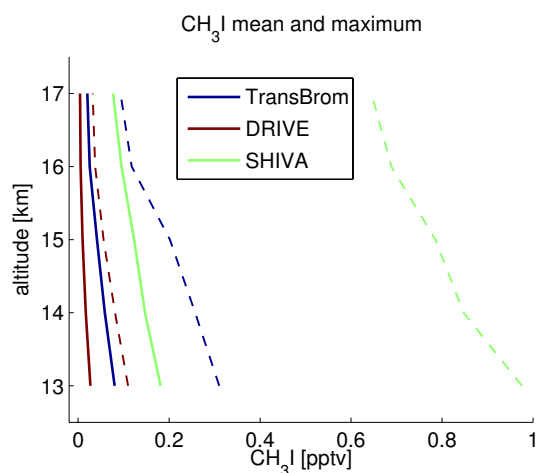


Fig. 5. Modeled CH_3I profiles based on observed emissions during the TransBrom, DRIVE and SHIVA ship campaigns. For all three campaigns mean values (solid lines) and maximum values (dashed lines) are given.

to 0.02 ppt. During SHIVA, very large peak emissions as well as very intense vertical transport result in model estimates of 0.6 ppt CH_3I at 17 km (Fig. 5), which is much larger than any values reported by high reaching aircraft measurements so far (Montzka and Reimann, 2011). The campaign average mixing ratio at 17 km is considerably lower, amounting to 0.07 ppt. During DRIVE, the maximum values at 17 km range around 0.03 ppt and mean values are in the order of 0.01 ppt (Fig. 5). Note that in the free troposphere, the CH_3I estimates are of similar order of magnitude as recent observations of inorganic iodine (Puentedura et al., 2012; Dix et al., 2013). In order to investigate whether the relatively large mixing ratios in the upper TTL estimated for the western Pacific emissions are isolated cases, strongly deviating from otherwise low CH_3I abundances, or if they occur frequently enough to impact global CH_3I , we analyze global model runs in the next section.

4 Global atmospheric CH_3I transport

4.1 Comparison with aircraft measurements in the lower TTL

The global contribution of CH_3I to the stratospheric iodine budget is estimated from FLEXPART model runs using a global emission climatology provided by Ziska et al. (2013) as input data. The emission maps have been derived from individual campaign measurements; however, as a result of the averaging process they do not represent the full spread of the original data. Furthermore, they do not include instantaneous peak emissions that might be correlated to the subsequent atmospheric transport, as illustrated above for individual campaigns. Figure 6 presents the 40°S – 40°N section of

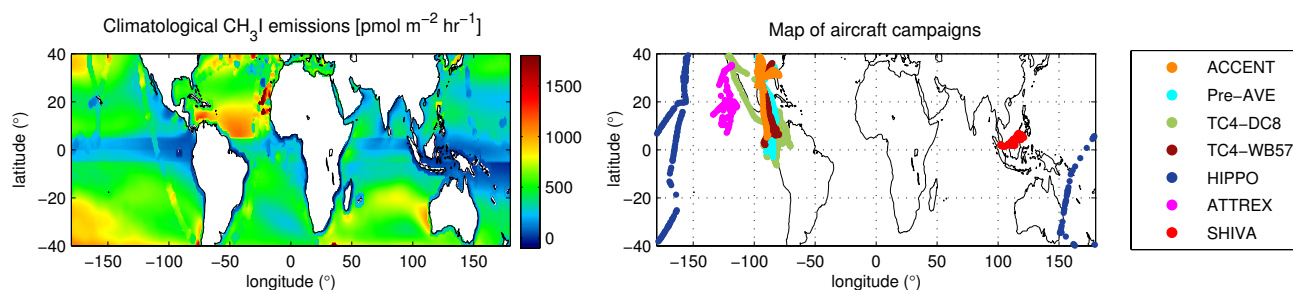


Fig. 6. Climatological CH_3I emissions [$\text{pmol m}^{-2} \text{h}^{-1}$] visualized between 40°S and 40°N on a $1^\circ \times 1^\circ$ grid from Ziska et al. (2013) (a). Locations of aircraft campaign measurements for the ACCENT, Pre-AVE, TC4, HIPPO2, ATTREX, and SHIVA missions (b).

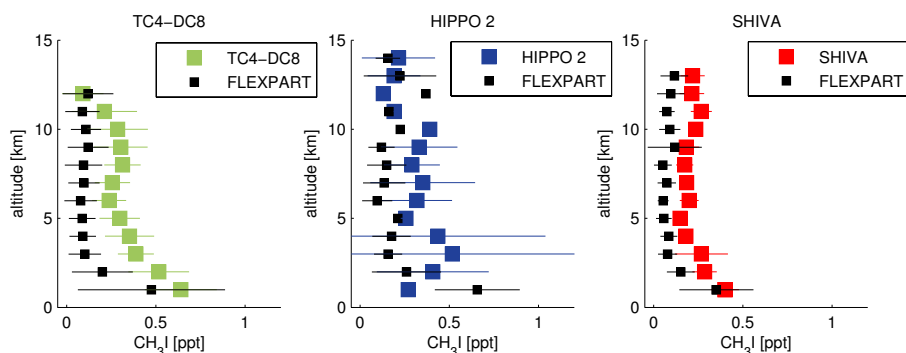


Fig. 7. Comparison between observed and modeled vertical profiles of CH_3I in the troposphere and lower TTL. Observations from all tropical flight sections of each aircraft campaign are used to find coincident model output. Observations and model results are averaged over all coincident data points in 1 km wide vertical intervals for TC4-DC8 (left panel), HIPPO2 (middle panel), and SHIVA (right panel). Horizontal bars indicate ± 1 standard deviation.

the emission climatology. Due to supersaturated oceans the climatological emissions are nearly everywhere positive and only a very few grid points denote CH_3I sinks. Large oceanic sources are found in the subtropical gyre regions as well as in North Atlantic. The tropical western Pacific region shows particularly low CH_3I emissions. Recent observations in this region during the SHIVA ship campaign, which have not been included in the climatology compilation so far, suggest the climatology might underestimate western Pacific emissions.

We compare modeled CH_3I abundances to available aircraft measurements in the free troposphere and TTL region. A special focus is on the model-measurement comparison in the upper TTL and on the question whether the aircraft measurements available here are representative of existing global estimates. The comparison is based on model runs carried out for the time period of the respective campaign and uses global emission climatologies as input data. As a result we expect the modeled atmospheric transport to represent the atmospheric conditions during the campaign, even though the climatological emissions might deviate from the true local emissions present at the time. A geographic map of the flight tracks is shown in Fig. 6. In a first step, coincident data points for observations and model output are identified

if they are less than 12 h apart and if their distance is less than 0.5° horizontally and less than 0.5 km vertically. Profile comparisons are determined for each campaign by taking the mean and standard deviation over all coincidences identified for the particular campaign data and for the corresponding model output.

The profile comparison for the three aircraft campaigns, which provide data in the free troposphere and lower UTLS, show in general a good agreement between the observations and the model results, with the latter being consistently lower (Fig. 7). For TC4-DC8, the modeled profile shows a steeper vertical gradient between 1 and 3 km than the observations, leading to some disagreement below 5 km. Above this level, model output and observations agree within their respective standard deviations. The HIPPO2 flight tracks extend over all tropical latitudes and campaign averaged profiles show a large variability below 10 km and around 13–14 km, which is also displayed although somewhat weaker by the model results. Mean values agree very well on some levels (e.g., above 10 km) but show larger discrepancies on other levels (e.g., 3–4 km). For SHIVA, the variability over all flight sections is small for observations and model results. In general, observed and modeled profiles show a very similar shape with FLEXPART results being slightly smaller consistently

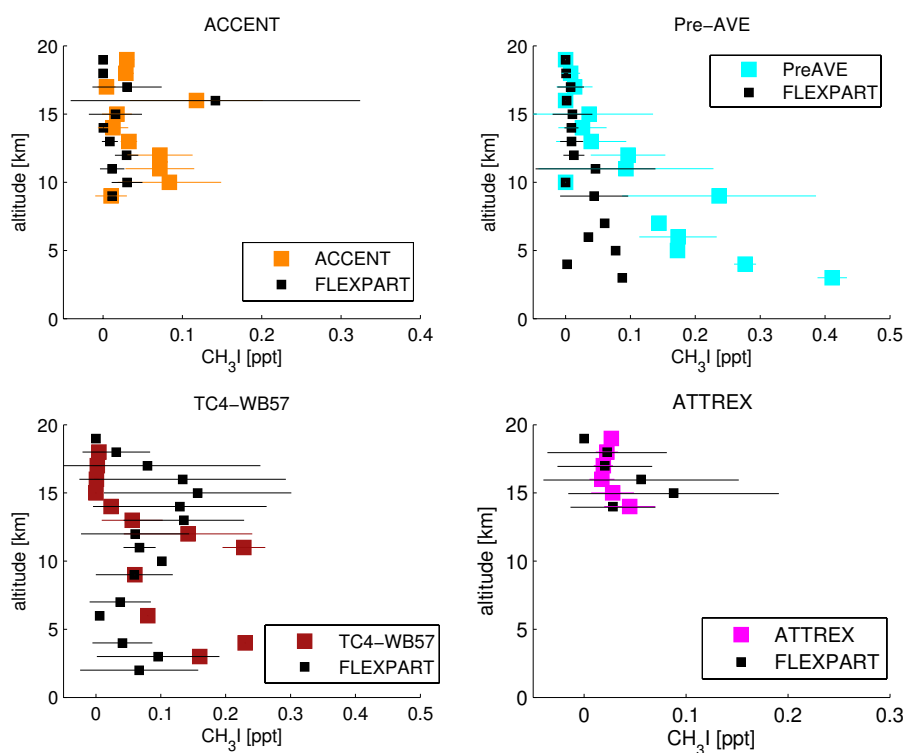


Fig. 8. Same as Fig. 7 for vertical profiles of CH_3I in the troposphere and TTL for the aircraft campaigns ACCENT, Pre-AVE, TC4-WB57, and ATTREX.

over the whole altitude range. The largest differences are found around 11 km. For some individual flights, convective outflow leads to observations of enhanced CH_3I between 10 and 12 km that result in a “C-shape” profile, a characteristic which is well captured by the model results (not shown here).

4.2 Comparison with aircraft measurements in the upper TTL

Model-measurement comparisons for the four campaigns conducted with the high-altitude aircraft sampling in the upper TTL and lower stratosphere are shown in Fig. 8. For three out of four campaigns, the modeled abundances above 10 km agree very well with the observations. For all three cases, the mixing ratios in the upper TTL are below 0.1 ppt, with the exception of the strongly enhanced mixing ratios at 16 km during ACCENT, which are reported by the observations and the model results. Largest discrepancies are found for the TC4-WB57 campaign, where basically no CH_3I was observed above 15 km while FLEXPART simulates mixing ratios around 0.1 ppt for the levels 13–17 km. Only below 10 and above 17 km does the model output agree well with the TC4-WB57 observations. A summary of the model-measurement comparison in the TTL is displayed in Fig. 9, where the modeled and observed profiles averaged over all four campaigns are displayed. FLEXPART overestimates the amount of CH_3I observed at 17–18 km (0.01 ppt) simulating

a too strong CH_3I entrainment. However, the model results underestimate CH_3I at 19 km, which observations suggest to be around 0.02 ppt. Since CH_3I has no source in the atmosphere, one would expect to find lower values at higher altitudes. A horizontally moving aircraft, however, will probe different air masses at the different altitude levels, and a positive vertical gradient, as noted between 17 and 19 km, can occur. The overall comparison of the 17–19 km region gives a good agreement between observations (0.011–0.019 ppt) and model results (0.006–0.032 ppt).

4.3 Global CH_3I in the upper TTL

It is also of interest to estimate CH_3I abundances in regions where no in situ measurements in the upper TTL are available. The projected amount of CH_3I entrained into the stratosphere depends on various FLEXPART model parameters and their associated uncertainties such as in the convective parameterization and in the vertical transport driven by the vertical wind fields. The accurate representation of convection has been validated with tracer experiments and ^{222}Rn measurements (Forster et al., 2007). The application of transport timescales based on vertical heating rates instead of vertical wind fields in the TTL between 15 and 17 km results in only minor differences of VLSL entrainment (Tegtmeier et al., 2012). As discussed earlier, our results are also constrained by the prescribed CH_3I lifetime, which can

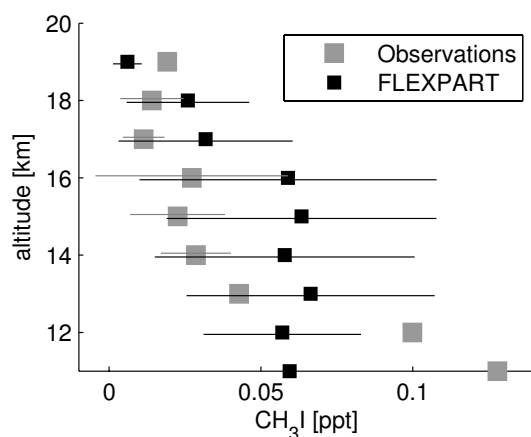


Fig. 9. Comparison between observed and modeled vertical profiles of CH_3I in the upper troposphere and TTL. Observations and model results are averaged over all data campaign-averaged profiles that include measurements in the upper TTL (ACCENT, Pre-AVE, TC4-WB57, and ATTREX). Horizontal bars indicate ± 1 standard deviation.

cause variations of CH_3I entrainment into the stratosphere of around 50%. However, the overall good agreement between model and observations in the eastern Pacific encourages the use of the FLEXPART model results for further analysis.

The western Pacific region is of particular interest for the troposphere–stratosphere transport, and we will evaluate how the FLEXPART results in this area compare to the model results and observations in the eastern Pacific. Such a comparison will allow speculations of how representative global estimates are of existing aircraft measurements. In Fig. 10a observations averaged over four tropical campaigns that crossed the eastern Pacific are displayed together with FLEXPART results averaged over three regions: the whole tropical belt (30°N – 30°S), the tropical western Pacific, and the tropical eastern Pacific aircraft campaign area. While for the western Pacific and the tropical belt the 2009 annual mean is displayed, the eastern Pacific average is based on the months when aircraft measurements are available (see Table 3) in order to allow for a comparison of the modeled eastern Pacific mean values with the in situ observations. The observations and model results for the eastern Pacific agree quite well, as discussed above for the comparisons based on coincidences. While observations suggest 0.01 ppt CH_3I at 17 km, the modeled profile shows slightly larger values of 0.02 ppt. Overall, the comparison indicates that the available in situ measurements provide representative estimates of the mean CH_3I abundance in the eastern Pacific region. FLEXPART results for the western Pacific region show considerably larger mixing ratios, especially between 14 and 18 km with 0.08 ppt CH_3I at 17 km. The geographical distribution of the mixing ratios is displayed in Fig. 10b, indicating that the western Pacific region between 100°W and 150°E shows the largest CH_3I abundances. Our model does not take into account ter-

restrial CH_3I emissions and therefore the very-short lived CH_3I is projected to reach the cold point and enter the stratosphere mostly above the oceans.

The average entrainment of CH_3I into the stratosphere amounts to 0.04 ppt, as demonstrated by the tropical mean (30°S – 30°N) CH_3I profile (Fig. 10a). In the annual mean distribution the entrainment is focused on the inner tropical latitude bands, mainly between 20°S and 20°N where the mean mixing ratio is about 0.05 ppt. Figure 11 provides information on the frequency occurrence of CH_3I mixing ratios at 17 km between 20°S and 20°N . As already evident from the geographical distribution of CH_3I abundances (Fig. 10), most values range between 0 and 0.1 ppt (82%). However, a small amount of air is projected to carry larger amounts of CH_3I , with 5.5% of air having mixing ratios larger than 0.2 ppt. Mixing ratios above 0.4 ppt occur only very rarely (0.6%), while mixing ratios above 0.6 ppt occur only in less than 0.1% of all air masses. The results from the global CH_3I model run show that the estimates from ship campaigns for TransBrom and SHIVA (0.02 and 0.07 ppt, respectively) are in the general range of values found in the western Pacific. Some in situ peak emissions observed during SHIVA combined with subsequent strong vertical transport lead to extremely high CH_3I abundances at 17 km (~ 0.6 ppt), which are expected to occur in less than 0.1% of all events based on global model projections.

5 Summary and discussion

Our study follows a two-way approach for modeling upper air CH_3I abundances. One method uses highly localized CH_3I emissions estimated during three ship campaigns to study the detailed characteristics of CH_3I transport from the ocean surface through the TTL up to the cold point. The second approach uses global climatological emissions to estimate the global strength and geographical distribution of CH_3I entrainment into the tropical stratosphere. Model results are compared to measurements from high-altitude aircraft campaigns currently available in the eastern Pacific region.

The detailed analysis of CH_3I emissions and transport for three individual ship campaigns reveals that the emissions vary by about 50% from campaign to campaign, but show much larger variations within one campaign. The large variability between measurements is supposedly related to the varying meteorological conditions, in particular to the variations of the horizontal winds. It is of interest to estimate to what degree one needs to know this variability in order to realistically simulate the CH_3I transport from the surface into the stratosphere. Especially if the CH_3I emissions and the intensity of vertical transport are correlated, coarse model simulations could potentially over- or underestimate atmospheric CH_3I abundances. While such correlations have not been observed over the entire length of one ship campaign,

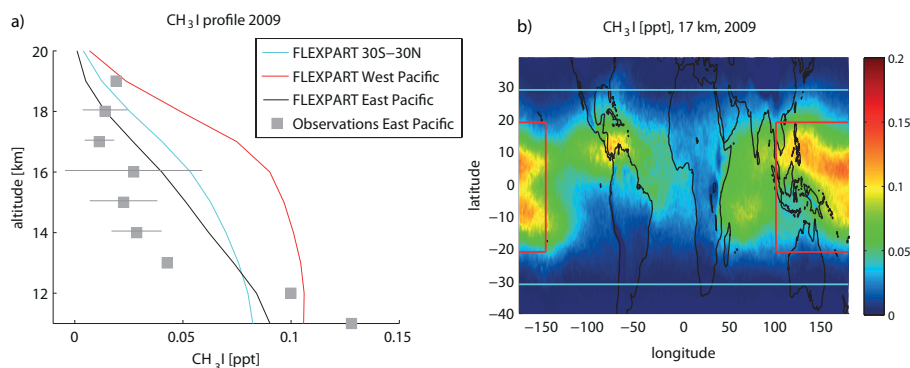


Fig. 10. Comparison between observed and modeled vertical profiles of CH_3I in the upper troposphere and TTL (a). Observations are as in Fig. 7. Model output is averaged over the tropics (blue, 30°S – 30°N) and the western Pacific (red, 100°W – 150°E , 20°S – 20°N) for 2009 and the eastern Pacific aircraft campaign region (green, 70 – 130°E , 6°S – 30°N) for the months of available measurements. Modeled tropical distribution of CH_3I at 17 km for 2009 (b).

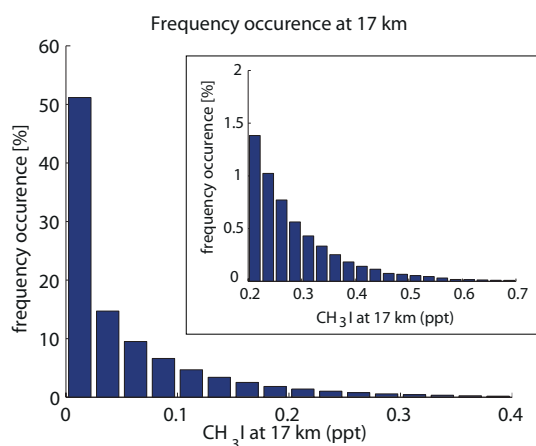


Fig. 11. Frequency occurrence of CH_3I abundances at 17 km in the tropics for 2009 based on climatological emissions. The inset panel provides a zoom-in for the range of larger mixing ratios 0.2–0.7 ppt.

individual sections with high correlations between emission and vertical transport have been identified. The analysis of the meteorological conditions during the campaigns leads to the hypothesis that the horizontal surface winds act as a connecting link between emission and transport. On the one hand, horizontal wind strength directly determines the emission strength by diluting CH_3I rich air and thereby controlling the uptake capacities of the atmosphere. Note that such mechanism works only for short-lived gases that are strongly supersaturated, as it is the case for CH_3I in most regions. Elevated oceanic concentrations and larger concentration gradients between sea water and air in source regions support this effect. On the other hand, horizontal wind variations depend on the meteorological conditions, such as convective systems or storm events. In particular, strong horizontal winds associated with tropical cyclones (i.e., typhoons) can indicate efficient vertical uplift possibly penetrating the stratosphere

and thereby complete the line of argument connecting CH_3I emission strength and CH_3I troposphere–stratosphere transport. Note that for the DRIVE campaign with very little uplift of CH_3I into the upper TTL, emission and vertical transport are found to be uncorrelated. Determining the conditions that are required in order for the proposed mechanism to hold would require further analysis, ideally based on campaign data obtained during various meteorological situations.

The importance of the identified coincidences of strong emissions and efficient vertical transport for model simulations can be investigated with a simple test. For the campaign sections where a correlation between emission and transport was found, a considerable difference (of up to 70 %) would result when the transport simulations would have been initiated with one average emission instead of the highly variable emission time series. The opposite is true for campaign sections where emissions and vertical transport are uncorrelated. Here, model runs using one average emission lead to approximately the same amount of CH_3I at the cold point level as model runs using the spatially resolved emissions. If such correlations, as identified for parts of the tropical campaigns, were a more general phenomena, than global modeling studies should be based on highly resolved emissions scenarios instead of uniform background mixing ratios. However, CH_3I emission maps derived from observations can only be compiled in a climatological sense due to the low data density and cannot include information on the temporarily highly variable emission peaks. As a result, modeling studies based on climatological emission maps cannot fully take into account the simultaneous occurrence of large CH_3I emissions and strong vertical uplift and might therefore lead to an underestimation of stratospheric CH_3I . Model simulations could benefit from using the climatological surface concentration maps in order to calculate the emissions instantaneously. Parameterizations of CH_3I oceanic concentrations based on biogeochemical modeling (e.g., Stemmler et al., 2013) could help to further improve the modeling approach.

Our results indicate that a realistic simulation of current and future iodine loading in the troposphere and stratosphere requires, among many other factors, highly resolved and well constrained CH₃I emission scenarios. In particular, the simultaneous occurrence of large CH₃I emissions and strong vertical uplift during the developing tropical typhoon suggest that future changes in tropical cyclone activity (Murakami et al., 2011) might influence the contribution of CH₃I to stratospheric iodine in a changing climate.

Comparisons of aircraft measurements in the upper TTL with coincident model output give a good agreement with slightly larger CH₃I abundances in the model. In the eastern Pacific region, where aircraft campaigns are available, the observations and the model indicate that around 0.01 to 0.02 ppt of CH₃I enter the stratosphere. However, other tropical regions, which are subject to stronger convective activity, are suggested to have larger CH₃I entrainment, e.g., 0.08 ppt in the western Pacific. Note that our global climatological approach cannot account for any link between strong local emissions and vertical transport, which could lead to even larger entrainment, as discussed earlier. One example of such large entrainment is given by the peak emission and simultaneous strong vertical uplift during the SHIVA campaign, which results in a localized mixing ratio of 0.6 ppt, a magnitude larger than area-average mixing ratios. While our current understanding of the CH₃I contribution to stratospheric iodine is mostly based on above-mentioned measurements and on model results (Aschmann et al., 2009; Ordóñez et al., 2012), which range around 0.01 ppt, our model results suggest an overall tropical contribution of 0.04 ppt. This is in good agreement with a model study from Donner et al. (2007), who derived similar CH₃I mixing ratios at the cold point. Differences between existing model results can arise from different treatment of CH₃I emissions, convection and photochemistry in the models. Note that in addition to our insufficient knowledge of the direct CH₃I entrainment into the stratosphere, the atmospheric lifetime of inorganic iodine is a major uncertainty for the quantification of the stratospheric iodine budget. Our results show strong variations in the geographical distribution of CH₃I entrainment, suggesting that currently available upper air measurements are not representative of global estimates. Further aircraft campaigns for different emission regions and especially for different convective transport regimes will be necessary in order to better understand the CH₃I contribution to stratospheric iodine.

Acknowledgements. We thank the TransBrom, DRIVE and SHIVA team for collecting the samples and providing the oceanic VLSL measurements. The authors would also like to thank X. Zhu and L. Pope for their technical support in the analysis of the whole air samples, and R. Lueb, R. Hendershot, and S. Gabbard for support of the ATTREX and HIPPO airborne sample collections. We thank Ben Miller, Steve Montzka, and Fred Moore for contributing the CH₃I measurements from the HIPPO2 aircraft campaign. The authors are grateful to the ECMWF for making the reanalysis

product ERA-Interim available. This study is carried out within the WGL project TransBrom and the EU project SHIVA (FP7-ENV-2007-1-226224) and contributes to the BMBF ROMIC grant THREAT 01LG1217A.

The service charges for this open access publication have been covered by a Research Centre of the Helmholtz Association.

Edited by: W. T. Sturges

References

- Aschmann, J., Sinnhuber, B.-M., Atlas, E. L., and Schauffler, S. M.: Modeling the transport of very short-lived substances into the tropical upper troposphere and lower stratosphere, *Atmos. Chem. Phys.*, 9, 9237–9247, doi:10.5194/acp-9-9237-2009, 2009.
- Bange, H. W.: FS Poseidon cruise report P399 legs 2 and 3, IFM-GEOMAR report no. 48 Rep. 48, 74 pp., IFM-GEOMAR, Kiel, 2011.
- Bell, N., Hsu, L., Jacob, D. J., Schultz, M. G., Blake, D. R., Butler, J. H., King, D. B., Lobert, J. M., and Maier-Reimer, E.: Methyl iodide: Atmospheric budget and use as a tracer of marine convection in global models, *J. Geophys. Res.*, 107, 4340, doi:10.1029/2001JD001151, 2002.
- Bösch, H., Camy-Peyret, C., Chipperfield, M. P., Fitzenberger, R., Harder, H., Platt, U., and Pfeilsticker, K.: Upper limits of stratospheric IO and OIO inferred from center-to-limb-darkening-corrected balloon-borne solar occultation visible spectra: Implications for total gaseous iodine and stratospheric ozone, *J. Geophys. Res.*, 108, 4455, doi:10.1029/2002JD003078, D15, 2003.
- Brasseur, G. and Solomon, S.: *Aeronomy of the Middle Atmosphere*, 2nd ed., Springer, New York, 2005.
- Butler, J. H., King, D. B., Lobert, J. M., Montzka, S. A., Yvon-Lewis, S. A., Hall, B. D., Warwick, N. J., Mondeel, D. J., Aydin, M., and Elkins, J. W.: Oceanic distributions and emissions of short-lived halocarbons, *Global Biogeochem. Cy.*, 21, GB1023, doi:10.1029/2006GB002732, 2007.
- Butz, A., Bösch, H., Camy-Peyret, C., Chipperfield, M. P., Dorf, M., Kreygy, S., Kritten, L., Prados-Román, C., Schwärzle, J., and Pfeilsticker, K.: Constraints on inorganic gaseous iodine in the tropical upper troposphere and stratosphere inferred from balloon-borne solar occultation observations, *Atmos. Chem. Phys.*, 9, 7229–7242, doi:10.5194/acp-9-7229-2009, 2009.
- Campos, M. L. A. M., Nightingale, P. D., and Jickells, T. D.: A comparison of methyl iodide emissions from seawater and wet depositional fluxes of iodine over the southern North Sea, *Tellus B*, 48, 106–114, doi:10.1034/j.1600-0889.1996.00010.x, 1996.
- Carpenter, L. J., Archer, S. D., and Beale, R.: Ocean-atmosphere trace gas exchange, *Chem. Soc. Rev.*, 41, 6473–6506, 2012.
- Carpenter, L. J., MacDonald, S. M., Shaw, M. D., Kumar, R., Saunders, R. W., Parthipan, R., Wilson, J., and Plane, J. M. C.: Atmospheric iodine levels influenced by sea surface emissions of inorganic iodine, *Nature Geosci.*, 6, 108–111, doi:10.1038/ngeo1687, 2013.
- Chameides, W. L. and Davis, D. D.: Iodine: Its possible role in tropospheric photochemistry, *J. Geophys. Res.*, 85, 7383, doi:10.1029/JC085iC12p07383, 1980.

- Chang, C.-P., Harr, P. A., and Chen, H.-J.: Synoptic Disturbances over the Equatorial South China Sea and Western Maritime Continent during Boreal Winter, *Mon. Weather Rev.*, 133, 489–503, doi:10.1175/MWR-2868.1, 2005.
- Chipperfield, M. P.: New version of the TOMCAT/SLIMCAT offline chemical transport model: Intercomparison of stratospheric tracer experiments, *Q. J. Roy. Meteorol. Soc.*, 132, 1179–1203, doi:10.1256/qj.05.51, 2006.
- Chuck, A. L., Turner, S. M., and Liss, P. S.: Oceanic distributions and air-sea fluxes of biogenic halocarbons in the open ocean, *J. Geophys. Res.*, 110, C10022, doi:10.1029/2004JC002741, 2005.
- Davis, D., Crawford, J., Liu, S., McKeen, S., Bandy, A., Thornton, D., Rowland, F., and Blake, D.: Potential impact of iodine on tropospheric levels of ozone and other critical oxidants, *J. Geophys. Res.*, 101, 2135, doi:10.1029/95JD02727, 1996.
- De Bruyn, W. J. and Saltzman, E. S.: Diffusivity of methyl bromide in water, *Mar. Chem.*, 57, 55–59, 1997.
- Dee, D. P., Uppala, S. M., Simmons, A. J., Berrisford, P., Poli, P., Kobayashi, S., Andrae, U., Balmaseda, M. A., Balsamo, G., Bauer, P., Bechtold, P., Beljaars, A. C. M., van de Berg, L., Bidlot, J., Bormann, N., Delsol, C., Dragani, R., Fuentes, M., Geer, A. J., Haimberger, L., Healy, S. B., Hersbach, H., Hólm, E. V., Isaksen, I., Kållberg, P., Köhler, M., Matricardi, M., McNally, A. P., Monge-Sanz, B. M., Morcrette, J.-J., Park, B.-K., Peubey, C., de Rosnay, P., Tavolato, C., Thépaut, J.-N. and Vitart, F., The ERA-Interim reanalysis: configuration and performance of the data assimilation system, *Q. J. Roy. Meteorol. Soc.*, 137, 553–597, 2011.
- Dix, B., Baidar, S., Bresch, J. F., Hall, S. R., Schmidt, K. S., Wang, S., and Volkamer, R.: Detection of iodine monoxide in the tropical free troposphere, *P. Natl. Acad. Sci. USA*, 110, 2035–2040, doi:10.1073/pnas.1212386110, 2013.
- Donner, L. J., Horowitz, L. W., Fiore, A. M., Seman, C. J., Blake, D. R., and Blake, N. J.: Transport of radon-222 and methyl iodide by deep convection in the GFDL Global Atmospheric Model AM2, *J. Geophys. Res.*, 112, D17303, doi:10.1029/2006JD007548, 2007.
- Forster, C., Wandinger, U., Wotawa, G., James, P., Mattis, I., Althausen, D., Simmonds, P., O'Doherty, S., Jennings, S. G., Kleefeld, C., Schneider, J., Trickl, T., Kreipl, S., Jäger, H., and Stohl, A.: Transport of boreal forest fire emissions from Canada to Europe, *J. Geophys. Res.*, 106, 22887, doi:10.1029/2001JD900115, 2001.
- Forster, C., Stohl, A., and Seibert, P.: Parameterization of Convective Transport in a Lagrangian Particle Dispersion Model and Its Evaluation, *J. Appl. Meteorol. Climatol.*, 46, 403–422, doi:10.1175/JAM2470.1, 2007.
- Fueglistaler, S., Dessler, A. E., Dunkerton, T. J., Folkins, I., Fu, Q., and Mote, P. W.: Tropical tropopause layer, *Rev. Geophys.*, 47, RG1004, doi:10.1029/2008RG000267, 2009.
- Fuhlbrügge, S., Krüger, K., Quack, B., Atlas, E., Hepach, H., and Ziska, F.: Impact of the marine atmospheric boundary layer conditions on VSLS abundances in the eastern tropical and subtropical North Atlantic Ocean, *Atmos. Chem. Phys.*, 13, 6345–6357, doi:10.5194/acp-13-6345-2013, 2013.
- Gottelman, A., Lauritzen, P. H., Park, M., and Kay, J. E.: Processes regulating short-lived species in the tropical tropopause layer, *J. Geophys. Res.*, 114, D1330, doi:10.1029/2009JD011785, 2009.
- Happell, J. D. and Wallace, D. W. R.: Methyl iodide in the Greenland/Norwegian Seas and the tropical Atlantic Ocean: Evidence for photochemical production, *Geophys. Res. Lett.*, 23, 2105–2108, doi:10.1029/96GL01764, 1996.
- Hossaini, R., Chipperfield, M. P., Feng, W., Breider, T. J., Atlas, E., Montzka, S. A., Miller, B. R., Moore, F., and Elkins, J.: The contribution of natural and anthropogenic very short-lived species to stratospheric bromine, *Atmos. Chem. Phys.*, 12, 371–380, doi:10.5194/acp-12-371-2012, 2012.
- Hughes, C., Franklin, D. J., and Malin, G.: Iodomethane production by two important marine cyanobacteria: *Prochlorococcus marinus* (CCMP 2389) and *Synechococcus* sp. (CCMP 2370), *Marine Chem.*, 125, 19–25, doi:10.1016/j.marchem.2011.01.007, 2011.
- Jones, C. E., Hornsby, K. E., Sommariva, R., Dunk, R. M., von Glasow, R., McFiggans, G., and Carpenter, L. J.: Quantifying the contribution of marine organic gases to atmospheric iodine, *Geophys. Res. Lett.*, 37, L18804, doi:10.1029/2010GL043990, 2010.
- Krüger, K. and Quack, B.: Introduction to special issue: the Trans-Brom Sonne expedition in the tropical West Pacific, *Atmos. Chem. Phys.*, 13, 9439–9446, doi:10.5194/acp-13-9439-2013, 2013.
- Krüger, K., Tegtmeier, S., and Rex, M.: Variability of residence time in the Tropical Tropopause Layer during Northern Hemisphere winter, *Atmos. Chem. Phys.*, 9, 6717–6725, doi:10.5194/acp-9-6717-2009, 2009.
- Levine, J. G., Braesicke, P., Harris, N. R. P., Savage, N. H., and Pyle, J. A.: Pathways and timescales for troposphere-to-stratosphere transport via the tropical tropopause layer and their relevance for very short lived substances, *J. Geophys. Res.*, 112, D04308, doi:10.1029/2005JD006940, 2007.
- Liss, P. S. and Slater, P. G.: Flux of Gases across the Air-Sea Interface, *Nature*, 247, 181–184, doi:10.1038/247181a0, 1974.
- Mahajan, A. S., Plane, J. M. C., Oetjen, H., Mendes, L., Saunders, R. W., Saiz-Lopez, A., Jones, C. E., Carpenter, L. J., and McFiggans, G. B.: Measurement and modelling of tropospheric reactive halogen species over the tropical Atlantic Ocean, *Atmos. Chem. Phys.*, 10, 4611–4624, doi:10.5194/acp-10-4611-2010, 2010.
- Manley, S. L. and Dastoor, M. N.: Methyl halide production from the giant kelp, *Macrocystis* and estimates of global CH₃X production by kelp, *Limnol. Oceanogr.*, 32, 709–715, 1987.
- Manley, S. L. and Dastoor, M. N.: Methyl iodide (CH₃I) production by kelp and associated microbes, *Marine Biol.*, 98, 477–482, doi:10.1007/BF00391538, 1988.
- Manley, S. L. and De la Cuesta, J. L.: Methyl iodide production from marine phytoplankton cultures, *Limnol. Oceanogr.*, 41, 142–147, 1997.
- McFiggans, G., Plane, J. M. C., Allan, B. J., Carpenter, L. J., Coe, H., and O'Dowd, C.: A modeling study of iodine chemistry in the marine boundary layer, *J. Geophys. Res.*, 105, 14371, doi:10.1029/1999JD901187, 2000.
- McNeil, C. L. and D'Asaro, E. A.: Parameterization of air-sea gas fluxes at extreme wind speeds, *J. Mar. Syst.*, 66, 110–121, 2007.
- Montzka, S. A. and Reimann, S.: Ozone-depleting substances and related chemicals, in *Scientific Assessment of Ozone Depletion: 2010, Global Ozone Research and Monitoring Project – Report No. 52*, Geneva, Switzerland, 2011.
- Moore, R. M. and Groszko, W.: Methyl iodide distribution in the ocean and fluxes to the atmosphere, *J. Geophys. Res.*, 104, 11163, doi:10.1029/1998JC900073, 1999.

- Moore, R. M. and Zafiriou, O. C.: Photochemical production of methyl iodide in seawater, *J. Geophys. Res.*, 99, 16415, doi:10.1029/94JD00786, 1994.
- Moore, R. M., Geen, C. E., and Tait, V. K.: Determination of Henry's Law constants for a suite of naturally occurring halogenated methanes in seawater, *Chemosphere*, 30, 1183–1191, doi:10.1016/0045-6535(95)00009-W, 1995.
- Murakami, H., Wang, B., and Kitoh, A.: Future Change of Western North Pacific Typhoons: Projections by a 20-km-Mesh Global Atmospheric Model*, *J. Climate*, 24, 1154–1169, doi:10.1175/2010JCLI3723.1, 2011.
- Nightingale, P. D., Malin, G., Law, C. S., Watson, A. J., Liss, P. S., Liddicoat, M. I., Boutin, J., and Upstill-Goddard, R. C.: In situ evaluation of air-sea gas exchange parameterizations using novel conservative and volatile tracers, *Global Biogeochem. Cy.*, 14(1), 373–387, doi:10.1029/1999GB900091, 2000.
- Ordóñez, C., Lamarque, J.-F., Tilmes, S., Kinnison, D. E., Atlas, E. L., Blake, D. R., Sousa Santos, G., Brasseur, G., and Saiz-Lopez, A.: Bromine and iodine chemistry in a global chemistry-climate model: description and evaluation of very short-lived oceanic sources, *Atmos. Chem. Phys.*, 12, 1423–1447, doi:10.5194/acp-12-1423-2012, 2012.
- O'Dowd, C. D., Jimenez, J. L., Bahreini, R., Flagan, R. C., Seinfeld, J. H., Hämeri, K., Pirjola, L., Kulmala, M., Jennings, S. G., and Hoffmann, T.: Marine aerosol formation from biogenic iodine emissions, *Nature*, 417, 632–636, 2002.
- Puentedura, O., Gil, M., Saiz-Lopez, A., Hay, T., Navarro-Comas, M., Gómez-Pelaez, A., Cuevas, E., Iglesias, J., and Gomez, L.: Iodine monoxide in the north subtropical free troposphere, *Atmos. Chem. Phys.*, 12, 4909–4921, doi:10.5194/acp-12-4909-2012, 2012.
- Pundt, I., Pommereau, J. P., Phillips, C., and Lateltin, E.: Upper limits of iodine oxide in the lower stratosphere, *J. Atmos. Chem.*, 30, 173–185, 1998.
- Quack, B. and Krüger, K. (Eds.): RV SONNE Fahrtbericht/Cruise Report SO218 SHIVA 15.–29.11.2011 Singapore – Manila, Philippines Stratospheric Ozone: Halogens in a Varying Atmosphere Part 1: SO218 – SHIVA Summary Report (in German) Part 2: SO218 – SHIVA English reports of participating groups GEOMAR Report, N. Ser. 012, GEOMAR Helmholtz-Zentrum für Ozeanforschung, Kiel, Germany, 112 pp., doi:10.3289/GEOMAR_REP_NS_12_2013 (<http://oceanrep.geomar.de/22284/>), 2013.
- Quack, B., Atlas, E., Petrick, G., Stroud, V., Schauffler, S., and Wallace, D. W. R.: Oceanic bromoform sources for the tropical atmosphere, *Geophys. Res. Lett.*, 31, L23S05, doi:10.1029/2004GL020597, 2004.
- Quack, B., Atlas, E., Krüger, K., Taylor, B., Dinter, T., Bracher, A., Petrick, G., Stange, K., Fuhlbrügge, S., Tegtmeier, S., Wache, S., and Wallace, D.: Distribution and air-sea fluxes of halocarbons through the Western Pacific, *Atmos. Chem. Phys. Discuss.*, in preparation, 2013.
- Rasmussen, R. A., Khalil, M. A. K., Gunawardena, R., and Hoyt, S. D.: Atmospheric methyl iodide (CH_3I), *J. Geophys. Res.*, 87, 3086, doi:10.1029/JC087iC04p03086, 1982.
- Redeker, K. R., Wang, N.-Y., Low, J. C., McMillan, A., Tyler, S. C., and Cicerone, R. J.: Emissions of Methyl Halides and Methane from Rice Paddies, *Science*, 290, 966–969, doi:10.1126/science.290.5493.966, 2000.
- Richter, U. and Wallace, D. W. R.: Production of methyl iodide in the tropical Atlantic Ocean, *Geophys. Res. Lett.*, 31, L23S03, doi:10.1029/2004GL020779, 2004.
- Romps, D. M. and Kuang, Z.: Overshooting convection in tropical cyclones, *Geophys. Res. Lett.*, 36, L09804, doi:10.1029/2009GL037396, 2009.
- Rossow, W. B. and Pearl, C.: 22-Year survey of tropical convection penetrating into the lower stratosphere, *Geophys. Res. Lett.*, 34, L04803, doi:10.1029/2006GL028635, 2007.
- Saiz-Lopez, A., Plane, J. M. C., Baker, A. R., Carpenter, L. J., Von Glasow, R., Martín, J. C. G., McFiggans, G. and Saunders, R. W.: Atmospheric chemistry of iodine, *Chem. Rev.*, 112, 1773–804, doi:10.1021/cr200029u, 2012.
- Sander, S., Friedl, R., Barker, J., Golden, D., Kurylo, M., Wine, P., Abbatt, J., Burkholder, J., Kolb, C., Moortgat, G., Huie, R., V. L. Orkin, “Chemical Kinetics and Photochemical Data for Use in Atmospheric Studies, Evaluation No. 17”, JPL Publication 10-6, Jet Propulsion Laboratory, Pasadena, 2011.
- Singh, H. B., Salas, L. J., and Stiles, R. E.: Methyl halides in and over the eastern Pacific (40°N – 32°S), *J. Geophys. Res.*, 88, 3684, doi:10.1029/JC088iC06p03684, 1983.
- Sive, B. C., Varner, R. K., Mao, H., Blake, D. R., Wingenter, O. W., and Talbot, R.: A large terrestrial source of methyl iodide, *Geophys. Res. Lett.*, 34, L17808, doi:10.1029/2007GL030528, 2007.
- Smythe-Wright, D., Boswell, S. M., Breithaupt, P., Davidson, R. D., Dimmer, C. H., and Eiras Diaz, L. B.: Methyl iodide production in the ocean: Implications for climate change, *Global Biogeochem. Cy.*, 20, GB3003, doi:10.1029/2005GB002642, 2006.
- Solomon, S., Garcia, R. R., and Ravishankara, A. R.: On the role of iodine in ozone depletion, *J. Geophys. Res.*, 99, 20491, doi:10.1029/94JD02028, 1994.
- Spichtinger, N., Wenig, M., James, P., Wagner, T., Platt, U., and Stohl, A.: Satellite detection of a continental-scale plume of nitrogen oxides from boreal forest fires, *Geophys. Res. Lett.*, 28, 4579–4582, doi:10.1029/2001GL013484, 2001.
- Stemmler, I., Rothe, M., Hense, I., and Hepach, H.: Numerical modelling of methyl iodide in the eastern tropical Atlantic, *Biogeosciences*, 10, 4211–4225, doi:10.5194/bg-10-4211-2013, 2013.
- Stohl, A. and Thomson, D. J.: A density correction for Lagrangian particle dispersion models, *Boundary-Lay. Meteorol.*, 90, 155–167, doi:10.1023/A:1001741110696, 1999.
- Stohl, A. and Trickl, T.: A textbook example of long-range transport: Simultaneous observation of ozone maxima of stratospheric and North American origin in the free troposphere over Europe, *J. Geophys. Res.*, 104, 30445, doi:10.1029/1999JD900803, 1999.
- Stohl, A., Hittenberger, M., and Wotawa, G.: Validation of the lagrangian particle dispersion model FLEXPART against large-scale tracer experiment data, *Atmos. Environ.*, 32, 4245–4264, doi:10.1016/S1352-2310(98)00184-8, 1998.
- Stohl, A., Forster, C., Frank, A., Seibert, P., and Wotawa, G.: Technical note: The Lagrangian particle dispersion model FLEXPART version 6.2, *Atmos. Chem. Phys.*, 5, 2461–2474, doi:10.5194/acp-5-2461-2005, 2005.
- Tegtmeier, S., Krüger, K., Quack, B., Atlas, E. L., Pisso, I., Stohl, A., and Yang, X.: Emission and transport of bromocarbons: from the West Pacific ocean into the stratosphere, *Atmos. Chem. Phys.*, 12, 10633–10648, doi:10.5194/acp-12-10633-2012, 2012.

- Toon, O. B., Starr, D. O., Jensen, E. J., Newman, P. A., Platnick, S., Schoeberl, M. R., Wennberg, P. O., Wofsy, S. C., Kurylo, M. J., Maring, H., Jucks, K. W., Craig, M. S., Vasques, M. F., Pfister, L., Rosenlof, K. H., Selkirk, H. B., Colarco, P. R., Kawa, S. R., Mace, G. G., Minnis, P., and Pickering, K. E.: Planning, implementation, and first results of the Tropical Composition, Cloud and Climate Coupling Experiment (TC4), *J. Geophys. Res.*, 115, D00J04, doi:10.1029/2009JD013073, 2010.
- Vogt, R., Sander, R., Von Glasow, R., and Crutzen, P. J.: Iodine Chemistry and its Role in Halogen Activation and Ozone Loss in the Marine Boundary Layer?: A Model Study, *J. Atmos. Chem.*, 32, 375–395, 1999.
- Wanninkhof, R.: Relationship between wind speed and gas exchange over the ocean, *J. Geophys. Res.*, 97, 7373–7382, 1992.
- Wennberg, P. O., Brault, J. W., Hanisco, T. F., Salawitch, R. J., and Mount, G. H.: The atmospheric column abundance of IO: Implications for stratospheric ozone, *J. Geophys. Res.*, 102, 8887–8898, doi:10.1029/96JD03712, 1997.
- Wilke, C. R. and Chang, P.: Correlation of diffusion coefficients in dilute solutions, *AIChE (Am. Inst. Chem. Eng.) J.*, 1, 264–270, 1955.
- WMO (World Meteorological Organization): Scientific Assessment of Ozone Depletion: 2006, Global Ozone Research and Monitoring Project – Report No. 50, Geneva., 2007.
- Wofsy, S. C., HIPPO Sci Team, Cooperating Modellers Team and Satellite Team: HIAPER Pole-to-Pole Observations (HIPPO): fine-grained, global-scale measurements of climatically important atmospheric gases and aerosols., *Philosophical Transactions Series A, Mathematical, physical, and engineering sciences*, 369, 2073–2086, doi:10.1098/rsta.2010.0313, 2011.
- Yokouchi, Y., Osada, K., Wada, M., Hasebe, F., Agama, M., Murakami, R., Mukai, H., Nojiri, Y., Inuzuka, Y., Toom-Saunty, D., and Fraser, P.: Global distribution and seasonal concentration change of methyl iodide in the atmosphere, *J. Geophys. Res.*, 113, D18311, doi:10.1029/2008JD009861, 2008.
- Zhou, Y., Mao, H., Russo, R. S., Blake, D. R., Wingenter, O. W., Haase, K. B., Ambrose, J., Varner, R. K., Talbot, R., and Sive, B. C.: Bromoform and dibromomethane measurements in the sea-coast region of New Hampshire, 2002–2004, *J. Geophys. Res.*, 113, D08305, doi:10.1029/2007JD009103, 2008.
- Ziska, F., Quack, B., Abrahamsson, K., Archer, S. D., Atlas, E., Bell, T., Butler, J. H., Carpenter, L. J., Jones, C. E., Harris, N. R. P., Hepach, H., Heumann, K. G., Hughes, C., Kuss, J., Krüger, K., Liss, P., Moore, R. M., Orlikowska, A., Raimund, S., Reeves, C. E., Reifenhäuser, W., Robinson, A. D., Schall, C., Tanhua, T., Tegtmeier, S., Turner, S., Wang, L., Wallace, D., Williams, J., Yamamoto, H., Yvon-Lewis, S., and Yokouchi, Y.: Global sea-to-air flux climatology for bromoform, dibromomethane and methyl iodide, *Atmos. Chem. Phys.*, 13, 8915–8934, doi:10.5194/acp-13-8915-2013, 2013.

4. Manuscript

Future emissions of marine halocarbons

Franziska Ziska¹, Birgit Quack¹, Susann Tegtmeier¹ and Kirstin Krüger²

[1] GEOMAR Helmholtz-Zentrum für Ozeanforschung Kiel, Germany

[2] University of Oslo, Department of Geosciences, Norway

Corresponding author: F. Ziska, GEOMAR Helmholtz-Zentrum für Ozeanforschung Kiel, Germany,
Research Division 2: Marine Biogeochemistry, Chemical Oceanography Düsternbrooker Weg 20,
24105 Kiel, Germany, (fziska@geomar.de)

to be submitted

Abstract

Very short lived organic compounds containing halogens, as bromoform (CHBr_3), dibromomethane (CH_2Br_2) and methyl iodide (CH_3I) are naturally produced in the oceans and are involved in ozone depletion in both the troposphere and the stratosphere. The effect of climate change on the oceanic emissions of these compounds is unknown. Based on present global oceanic and atmospheric concentrations and future sea surface wind speed, temperature and salinity and sea level pressure from three CMIP 5 (fifth phase of the Climate Model Intercomparison Project) models past and future sea-to-air fluxes of CHBr_3 , CH_2Br_2 and CH_3I are simulated. The output fields from the model runs of CESM1-CAM5, MPI-ESM-LR and HadGEM2-ES for the time period 1979-2100 from the historical scenario and the RCP scenarios 2.6 and 8.5 are used as input data for emission calculations. Globally, the sea surface temperatures show a steady increase during the 21th century, while the modeled changes of sea surface wind speed vary from a small positive trend at the beginning to a negative trend at the end of the century. The emissions based on the historical model runs of CESM1-CAM5 and MPI-ESM-LR (1979-2005) agree well with the emissions based on ERA-Interim data as driving forces, while the HadGEM2-ES model output is much lower, likely caused by the different temporal resolutions of the input parameters. The future sea-to-air fluxes of the halogenated compounds generally increase during the 21th century. The global emissions of CHBr_3 increase by 29.4% (9.0%) between the time periods 1986-2005 and 2081-2100 for the RCP 8.5 (2.6) scenario. The future CH_2Br_2 and CH_3I emissions increase by 23.3% (6.4%) and by 5.5% (1.5%) for the RCP 8.5 (2.6) scenario. Possible uncertainties of the future emission estimates, such as the role of oceanic productivity under ongoing environmental changes are discussed.

1. Introduction

The very short-lived halogenated compounds bromoform (CHBr_3), dibromomethane (CH_2Br_2) and methyl iodide (CH_3I) are naturally produced by biological and non-biological pathways in the ocean (Quack and Wallace, 2003; Richter and Wallace, 2004; Hopkins et al., 2013). The emission strength of these halocarbons from the ocean into the atmosphere can be estimated, based on their concentration gradient between sea water and atmosphere, wind speed, sea surface temperature and sea surface salinity (Quack and Wallace, 2004; Ziska et al., 2013; Hepach et al., 2014). Emitted into the marine boundary layer, the halocarbons are oxidized or photo dissociated to reactive halogen species which play an important role for tropospheric and stratospheric chemistry (Montzka and Reimann, 2011; Saiz-Lopez and von Glasow, 2012). Model studies revealed that the inorganic bromine (Br_y) influence on the global tropospheric ozone budget is about 5-30% (Yang et al., 2005; von Glasow et al., 2004). CH_3I is the dominant source of organic iodine in the troposphere, which is

involved in several atmospheric chemical cycles, e.g. the tropospheric ozone cycle and aerosol formation (Saiz-Lopez et al., 2012; Dix et al., 2013). The three halogenated compounds and their degradation products can be transported by deep convection (Aschmann et al., 2009; Tegtmeier et al., 2012) into the tropical tropopause layer (TTL) and even reach the stratosphere where they can also be involved in ozone depletion. Bromine is about 45-69 times more efficient than chlorine in destroying stratospheric ozone (Sinnhuber and Folkins, 2006) while iodine is even much more efficient in the catalytic cycles (Solomon, et al. 1994)

Environmental processes are expected to change due to the ongoing anthropogenic emissions of greenhouse gases, particularly CO₂, which leads to global warming and ocean acidification (Bopp et al., 2013; Doney, 2010). Field experiments (Riebesell et al., 2007) and modelling studies (Collins and Knutti, 2013) are used as tools to estimate future changes of biological, physical and chemical processes both in the ocean and in the atmosphere until the year 2300.

The fifth phase of the Climate Model Intercomparison Project (CMIP 5) includes a large number of different state-of-the-art climate models and is part of the 5th IPCC report. Goals of the 5th IPCC report are to provide realistic model simulations of the recent past, as well as to calculate and evaluate future projections. Climate model runs vary global warming from 2.6 to 8.5W m⁻² and predict the future changes for different scenarios (Taylor et al., 2012). Multi model means of the 5th IPCC report project an increase in sea surface temperature, apparently strongest in the tropics and subtropics for the end of the century (Collins and Knutti, 2013). The ongoing environmental changes might also have an influence on the oceanic production of the marine derived compounds (Behrenfeld et al., 2006; Bopp et al., 2013). Biological future changes influencing very short lived substances (VSLs) production in the ocean have been poorly investigated so far. During a mesocosm experiment in the Arctic Ocean the effects of ocean acidification on halocarbon concentrations were marginal (Hopkins et al., 2013).

A future increase of stratospheric bromine loading including CHBr₃ and CH₂Br₂ due to intensified vertical transport into the tropical stratosphere is predicted (Pyle et al., 2007; Dessens et al., 2009). An increase in stratospheric source gas injection of the biogenic VSLs CH₂Br₂ and CHBr₃ of ~60% until 2100 under extreme (RCP scenario 8.5) conditions is projected due to enhanced convection as demonstrated by Hossaini et al. (2012b). Further, the study suggests that CH₂Br₂ will be more sensitive to the predicted future increase in tropospheric hydroxyl radicals which is the major sink for CH₂Br₂ compared to CHBr₃ which main tropospheric reduction is photolysis. Under future climate, longer lived species like CH₂Br₂ with an atmospheric lifetime of several months might contribute more to total stratospheric bromine compared to shorter lived species like CHBr₃ (Dessens et al., 2009). However, none of these models consider future changes in halogenated sea-to-air fluxes. Thus

future emission estimates are needed to reduce the uncertainties of model studies projecting halogen contribution of VLS into the future stratosphere (Hossaini et al., 2012).

Our study estimates first future oceanic emissions of bromoform, dibromomethane and methyl iodide to the year 2100, based on the projected change of physical driving forces. We use the model output fields from two RCP scenarios (2.6 and 8.5) of the three different CMIP 5 models CESM1-CAM5, MPI-ESM-LR and HadGEM2-ES (IPCC). Model based sea surface salinity (SSS), temperature (SST), wind speed (U) and sea level pressure (SLP) from 1979-2100 are used for the sea-to-air flux calculation together with the observation based climatological oceanic concentration and atmospheric mixing ratios of Ziska et al. (2013). Emissions based on the historical CMIP 5 model runs are compared to the emission climatology calculated with ERA-Interim data (Ziska et al., 2013) for the time period 1979-2005 and to future emissions projections (2006-2100). Finally, possible uncertainties of the future halogenated emissions are discussed.

2. Data and Method

2.1. Concentration maps

Based on surface measurements from the HalOcAt database (<https://halocat.geomar.de>) global marine and atmospheric maps of CHBr_3 , CH_2Br_2 and CH_3I were calculated on a common $1^\circ \times 1^\circ$ grid (Ziska et al., 2013). All available data were classified into coastal, shelf and open ocean region and were interpolated onto the grid. Furthermore, based on the observed biogeochemical distribution of the VLS the oceanic and atmospheric open ocean regions were divided into four different ocean basins and into five latitudinal bands. In each region missing grid values were extrapolated with the ordinary least square regression technique. The thus derived oceanic and atmospheric concentration fields are considered climatological data covering 1989-2011 since all measurements over this time period were included (Ziska et al., 2013).

2.2. Meteorological input parameters

For the time period 1979-2013 the marine halogenated emissions were calculated with 6 hourly input parameters U, SST and SLP from the ECMWF meteorological reanalysis product ERA-Interim (Dee et al., 2011), and a monthly mean SSS from the World Ocean Atlas 2009 (Antonov et al., 2010).

From three CMIP 5 models, MPI-ESM-LR, CESM1-CAM5 and HadGEM2-ES, monthly model output fields of U, SST, SLP and SSS of two Representative Concentration Pathways (RCP) 2.6 (less warming) and 8.5 (extreme warming) (van Vuuren et al., 2011) were used as input parameters for the calculation of oceanic emissions for the time period 2006-2100. Additionally, for the years 1979-2005 historical model runs were determined. Our goal was to use several model parameterizations as well as models from different modeling centers sharing individual model components to cover a wide

range of possible future variability. The models had to include the four input parameters for both scenarios. Finally, we chose the two models which agree best with the ERA-Interim emissions and one exemplary model which shows an offset (section 3.3) to the ERA-Interim sea-to-air fluxes. The physical parameters supplied by the three Earth System Models vary in horizontal and vertical resolution in ocean and atmosphere (Table 1). For further calculations, all variables were interpolated onto a common $1^\circ \times 1^\circ$ grid. We use the first ensemble run of the historical model runs and all available ensemble runs of the future projections for further calculations.

2.3. Emission calculation

Based on the global oceanic and atmospheric concentration climatologies from Ziska et al. (2013) and the input parameters of the CMIP 5 models and ERA-Interim sea-to-air fluxes estimates were determined. The sea-to-air flux (F in $\text{pmol m}^{-2} \text{h}^{-1}$) was calculated as the product of the air-sea gas exchange coefficient (k in cm h^{-1}) and the sea-to-air concentration gradient (ΔC in pmol L^{-1}):

$$F = k \Delta C. \quad (1)$$

The parameterization of Nightingale et al. (2000) was used to determine k , which was adapted to the compounds of interest applying the same underlying equations described in the publication of Ziska et al. (2013) in order to be consistent and comparable with the present day estimates from that study. For the time period 1979-2013 we calculated 6-hourly global emission maps based on 6-hourly ERA-Interim U, SST, SLP monthly mean of SSS and the climatological global oceanic concentrations and atmospheric mixing ratios from Ziska et al. (2013). Monthly means, yearly means and the long term mean of the 35-year time period (ERA-Interim time series) were calculated for each grid point. For the time period 1979-2100 we determined global monthly mean emissions based on the monthly mean input parameters U, SST, SLP and SSS of the three CMIP 5 models with fixed atmospheric and oceanic concentrations from Ziska et al. (2013). The monthly CMIP 5 global emissions were added upto annual values.

3. Results and discussion

We compare the past and present emissions determined with the historical CMIP 5 model runs and those based on ERA-Interim data. Further, the sea-to-air flux projections using the extreme and low (RCP 8.5 and 2.6) scenarios are analyzed to the year 2100.

3.1. ERA-Interim

Time series of the calculated global annual mean sea-to-air flux of CHBr_3 , CH_2Br_2 and CH_3I over three decades based on the ERA-Interim dataset as well as the corresponding input parameters U, SST and SLP for the time period 1979-2013 are shown in Figure 1. The emissions determined for the years 1989-2011 from Ziska et al. (2013) are included and extended for the complete available time period

of the ERA-Interim dataset (1979-2013). A trend was calculated based on the linear regression method for each time series. Except for the SLP, all time series show significant trends with $p < 0.01$ and the linear regression term is included in Figure 1. The three sea-to-air flux time series show a similar increase from 1979 to 2013 of 7.9% for CHBr_3 , 6.7% for CH_2Br_2 and 6.3% for CH_3I , respectively. The inter-annual variability (calculated as standard deviation over the annual mean time series) of the VSLs emission for the time period 1979-2013 is less than 5% showing no significant changes compared to the publication of Ziska et al. (2013). The sea-to-air fluxes show a minimum to maximum range within the years 1979-2013 from 2.3 to 2.6 Gmol Br yr^{-1} , 0.9 to 1.1 Gmol Br yr^{-1} and 1.3 to 1.5 Gmol I yr^{-1} for CHBr_3 , CH_2Br_2 and CH_3I respectively. The positive trend of the emission time series is a result of the 2.5% and 1% increase of the input parameters U and SST (Figure 1) showing an inter-annual variability of less than 1%. The input parameter SLP illustrates a slight increase of 0.02% for the time period 1979-2013, however, the trend is not significant.

3.2. CMIP5

We compare the output fields from the three different CMIP 5 models that are used for the future sea-to-air flux calculations of CHBr_3 , CH_2Br_2 and CH_3I . The global 1979-2100 time series of the parameters U and SST are shown in Figure 2. The temporal changes of global SLP and SSS (not shown) are negligible compared to U and SST. All three historical (1979-2005) SST fields are in good agreement with the ERA-Interim dataset regarding absolute values as well as a linear significant ($p < 0.01$) increase from 1979-2005 (Figure 2). The global annual mean values are 13.5°C, 13.4°C and 13.3°C for HadGEM2-ES, CESM1-CAM5 and MPI-ESM-LR, respectively and 13.5°C for the ERA-Interim data set. A future increase in sea surface temperature is seen for all three model runs. HadGEM2-ES, CESM1-CAM5 and MPI-ESM-LR project a 4.4%, 5.7% and 2.0% increase for the RCP 2.6 scenario and 24.8%, 18.7% and 17.4% for the RCP 8.5 scenario from the years 2006-2100, respectively. The SST in the low scenario shows a steady increase up to the year 2060. Afterwards a significant ($p < 0.01$) weak (~ 1%) decrease is shown for MPI-ESM-LR and HadGEM2-ES (Meehl et al., 2013).

The global historical sea surface wind speed time series of the three CMIP 5 models show a similar linear trend ($p < 0.05$) as the ERA-Interim dataset, however the annual mean of the wind speed time series over the time period 1979-2005 range between 7.5 m s^{-1} (MPI-ESM-LR), 7.4 m s^{-1} (CESM1-CAM5), 6.9 m s^{-1} (HadGEM2-ES) and 7.1 m s^{-1} (ERA-Interim). For the extreme scenario the future model runs show an increase of 0.6% (MPI-ESM-LR), 1.1% (CESM1-CAM5) and a reduction of -0.2% (HadGEM2-ES) from 2006-2100 for the mean global wind speed. While the trend in the global wind field is significant ($p < 0.01$) for CESM1-CAM5 and MPI-ESM-LR, it is not significant for the HadGEM2-ES model. The low scenario shows a weak changes of the global wind from 2006 to 2100 for all model runs of -0.09% (MPI-ESM-LR), 0.28% (CESM1-CAM5) and -0.78% (HadGEM2-ES), but the trend

($p < 0.05$) is only significant for the MPI-ESM-LR model. Compared to the other two models, the HadGEM2-ES model has the lowest global wind speed and an equal long-term change for both scenarios from 2006–2100. More distinct developments of future wind speeds are illustrated on a spatial scale. For further investigations, we divided the globe into five latitudinal bands (Figure 3) and analyze the regional variations of the four input parameters from the three models for the RCP 8.5 scenario from 2010 to 2100. In more than 60% of the spatial parameter development, the model runs agree in long-term changes and magnitude of the parameters. Significant linear trends ($p < 0.01$) in the time series U, SST, SLP and SSS generally exist for at least one model in every latitudinal band. In the northern and southern high latitudinal bands of 50° – 90° U and SST are increasing whereas SLP and SSS are decreasing. The tropical area from 20° N– 20° S is characterized by a U and SSS decline and a SST and SLP increase to the year 2100. In the extra tropics, north and south of 20° – 50° U and SSS are marginally reduced from 2010–2100 while the SST strongly increases. The SST increase of 2 – 4° C is shown in all latitudinal bands as also seen from Bopp et al. (2013). The fact that the 2010–2100 long-term changes of the wind are of opposite sign between the latitude bands likely causes the low overall global increase of the surface wind speed projections.

3.3. Sea-to-air fluxes

Based on the historical model outputs of U, SST, SLP and SSS from the three CMIP 5 models MPI-ESM-LR, CESM1-CAM5 and HadGEM2-ES, halocarbon sea-to-air fluxes were calculated (Equation 1) and compared to the ERA-Interim emissions for the time period 1979–2005 (Figure 4).

The annual mean emissions of CHBr_3 , CH_2Br_2 and CH_3I calculated with the historical MPI-ESM-LR and CESM1-CAM5 model output fields from 1979–2005 are in good agreement with the ERA-Interim average emissions for the same time period (Table 2). In comparison, the annual mean emissions determined with the HadGEM2-ES output fields are much lower for the three compounds compared to the ERA-Interim averaged time series, especially for CHBr_3 .

The highest available temporal resolution for the historical and future model output fields (is monthly means whereas it is 6 hourly means for the ERA-Interim dataset). In order to analyze if the temporal resolution of the input data has an impact on the observed high offset between ERA-Interim and HadGEM2-ES emissions (Figure 4), we look in detail into the methods for the emission calculations based on historical and ERA-Interim data.

Therefore, the sea-to-air fluxes were newly calculated with ERA-Interim input parameters averaged from 6 hourly to monthly and compared with the historical model runs and the 6 hourly ERA-Interim emissions (Figure 5). The annual mean ERA-Interim emissions over the time period 1979–2005 calculated with the 6 hourly input data are always higher by 11%, 10.9% and 11.1% for CHBr_3 , CH_2Br_2 and CH_3I , respectively than the monthly fluxes. It is already known for other gases as CO_2 , that global monthly averaged emissions can be about 5% lower compared to emissions calculated with 6 hourly

wind speeds if applying a quadratic dependent parameterization (Wanninkhof, 2002). Our determined offset between hourly and monthly ERA-Interim emissions is higher than that estimated by Wanninkhof, (2002) which could be due to the averaging of three more parameters in our calculations. MPI-ESM-LR and CESM1-ESM-LR annual mean emissions of CHBr_3 , CH_2Br_2 and CH_3I are in good agreement to ERA-Interim 6 hourly emissions for the three compounds, whereas the HadGEM2-ES is equal to the monthly ERA-Interim emissions, which are about 11% lower. Compared to the HadGEM2-ES model the MPI-ESM-LR and CESM1-CAM5 models showed higher mean global and regional U and seem to compensate the averaging bias by a larger regional variability in wind speed. Internal variability has been found to play a large role in uncertainties of future projections (Deser et al., 2012), which has to be investigated further. Although the HadGEM2-ES emissions show lower absolute values compared to the ERA-Interim sea-to-air fluxes (6 hourly) and the MPI-ESM-LR and CESM1-ESM-LR models they have a similar long-term change (Table 3).

For the time period 2006-2100 halocarbon sea-to-air fluxes were calculated based on the future model outputs of U, SST, SLP and SSS from the three CMIP 5 models MPI-ESM-LR, CESM1-CAM5 and HadGEM2-ES (Figure 5).

The modeled future sea-to-air fluxes for both scenarios (RCP 2.6 and 8.5) show an increase from 2006 to 2100 for all three halocarbons with a steeper slope for the RCP 8.5 scenario. The long-term change of the modeled emissions over the time period from 1986-2005 to 2081-2100 given by the three different models ranges from 25.9% to 31.3% for CHBr_3 , from 21.7% to 24.3% for CH_2Br_2 and from 4.8% to 5.9% for CH_3I for the RCP 8.5 scenario. For the 2.6 scenario the predicted emission increase over the next century is much smaller ranging from 5.7 to 12.0%, from 3.9 to 8.2% and from 1.2 to 1.9% for CHBr_3 , CH_2Br_2 and CH_3I , respectively (Table 4). The lowest increase is seen for the MPI-ESM-LR model for both the RCP 2.6 and 8.5 scenarios which is possibly due to its lower global SST (Figure 2 and 3).

The spatial halocarbon future emissions calculated with the RCP 2.6 and 8.5 scenarios from the time period 1989-2005 (historical) to 2081-2100 show a reduction of CHBr_3 and CH_2Br_2 emissions in the tropical band from 20°N-20°S (Table 5). The largest increases are seen for CHBr_3 and CH_3I in the southern high latitudes between 50°S-90°S and for CH_2Br_2 in the northern high latitudes between 50°N-90°N. The emission increase in the high latitudes might be due to the combined increase of U and SST in these regions. In the extra tropics between 20°N-50°N the models simulate a reduction of CH_2Br_2 and CH_3I emissions and illustrate a slight increase of CHBr_3 sea-to-air fluxes. While little changes in the emission rates are seen for CH_3I and CHBr_3 between 20°S-50°S, the CH_2Br_2 emission shows a clear increase in that region.

3.4. Uncertainties in ocean concentration changes

We calculated emission fields based on the temporal varying physical input parameters U, SST, SLP and SSS and fixed global oceanic concentration and atmospheric mixing ratio maps derived from observations from the years 1989-2011. Due to sparse data resolution and a lack in process understanding, marine concentration changes due to biological or chemical changes in the ocean are not taken into account in the future flux calculation. Indeed the increased future fluxes assume an increased halocarbon production in the ocean due to the fixed concentrations. However, although the oceanic emissions may increase significantly, the changes of the oceanic production are minor and will not be measurable with current instrumentation, since the oceanic concentrations are influenced by many factors and the change is occurring in the entire mixed layer, leading to an unmeasurable dilution of the assumed increased production (Quack et al., 2007b; Hepach et al., 2014). Thus the assumption of a naturally unvarying oceanic concentration for the time period of 120 years is justifiable for this study. Future productivity changes and their actual influence on the oceanic halocarbon concentrations need to be assessed in follow-up studies.

Projected ocean biology changes to the 21th century are e.g. analyzed in the study of Bopp et al. (2013). There, the trend of the most important drivers for oceanic ecosystems as SST, oxygen, net primary production (net production of organic matter by phytoplankton, NPP) and pH (Fischlin and Midgley, 2007) of 10 different CMIP 5 models based on two scenarios (RCP 2.6 and 8.5) were compared (MPI-ESM-LR and HadGEM2-ES are included). On a global scale all models showed a consistent warming, acidification, deoxygenation and a NPP decrease. However the results are spatially different. E.g. tropical oceans will be influenced by a high increase of SST, decreasing acidification and NPP rates and inconsistent changes in subsurface oxygen under the RCP 8.5 scenario. The three ocean basins, North Atlantic, Southern Ocean and North Pacific, are instead characterized by high acidification, lower oxygen, inconsistent warming and decreasing to consistent NPP. The future decrease of NPP on a global scale is confirmed in the study of Steinacher et al. (2010) which implicates a decrease of the marine production and emissions of the biologically related halocarbons such as CHBr_3 , since a model study by Stemmler et al (2014) suggests that bulk primary production might be a good proxy for simulating global bromoform production in the open ocean. The projected future increase of SST could lead to enhanced oceanic production of CH_3I in the oligotrophic tropical oceans (Hepach et al., 2014), although a link to oceanic biological production also may exist (Stemmler et al., 2014) However, since it is not revealed which production processes influence the oceanic halocarbon concentrations at present, also their future development remains obscure, which needs further investigation.

4. Summary and conclusion

In this study, the existing emission time series of bromoform, dibromomethane and methyl iodide from the publication of Ziska et al. (2013) are extended to the years 1979-2013. We find an overall increase of the annual oceanic emissions of 7.9% for CHBr_3 , 6.7% for CH_2Br_2 and 6.3% for CH_3I , respectively over these last 34 years due to rising global sea surface wind speed and temperature.

Additionally, first future emission estimates of CHBr_3 , CH_2Br_2 and CH_3I based on present day concentration fields and on monthly U, SST, SLP and SSS output fields of three different CMIP 5 model (MPI-ESM-LR, CESM1-CAM5 and HadGEM2-ES), from two RCP (2.6 and 8.5) scenarios were calculated and compared. The global halocarbon emissions based on the projected input parameters show an increase from 2006-2100 for both scenarios, which is most pronounced in high latitudes due to increasing temperature and wind. The long-term change of the determined emissions over the time period from 1986-2005 to 2081-2100 given by the three different models shows a mean increase of 29.4% for CHBr_3 , of 23.3% for CH_2Br_2 and of 5.5% for CH_3I based on the 8.5 scenario. For the 2.6 scenario the predicted emission increase over the next century is much smaller presenting a model mean of 9.0%, 6.4% and 1.5% for CHBr_3 , CH_2Br_2 and CH_3I , respectively.

We suggest that the calculated increase in CHBr_3 , CH_2Br_2 and CH_3I emissions will lead to enhanced reduction of tropospheric ozone due to higher amount of atmospheric Br_y and I_y concentrations. Further, the stratospheric ozone depletion might be intensified by the combination of rising halocarbon emissions and the postulated increase of vertical transport into the tropical stratosphere (Pyle et al., 2007; Dessens et al., 2009; Hossaini et al., 2012).

The historical HadGEM2-ES model shows a distinct offset towards the ERA-Interim emission time series, which might be due to its low projected sea surface wind speeds which is the most important driving factor in sea-to-air flux calculations on a global (Ziska et al., 2013) and region scale. In addition it was found, that averaging of 6 hourly input parameters to monthly means reduce the annual mean halocarbon emissions by about 11%. For a reduction of the averaging bias higher temporal resolution of model output fields is needed.

More measurements in data sparse regions and time series in hot spot regions are needed to gain further knowledge and process understanding about sources and sinks mechanisms of natural halogenated compounds. This is also necessary as input for biogeochemical ocean models and parameterizations, which also requires an understanding of the future development of oceanic primary productivity. Additionally other halocarbon sources in the ocean due to water pollution have to be further investigated and also to be taken into account (Werschkun et al., 2012). The derived future emission maps of the two scenarios can be used as input for chemistry climate models to estimate the injection of entrainment of biogenic halogens into the stratosphere and their influence on the future ozone layer chemistry.

Acknowledgements We like to thank Irene Stemmler and Ryan Hossaini for helpful comments during the writing process. This work was financially supported by the European commission under the project SHIVA (grant no. 226 224) and the German Federal Ministry of Education and Research (BMBF) during the project SOPRAN (grant no: 03F0611A). We acknowledge the World Climate Research Programme's Working Group on Coupled Modelling, which is responsible for CMIP, and we thank the climate modeling groups (listed in Table 1 of this paper) for producing and making available their model output. Additionally, we would like to thank the ECMWF for providing the ERA Interim reanalysis data.

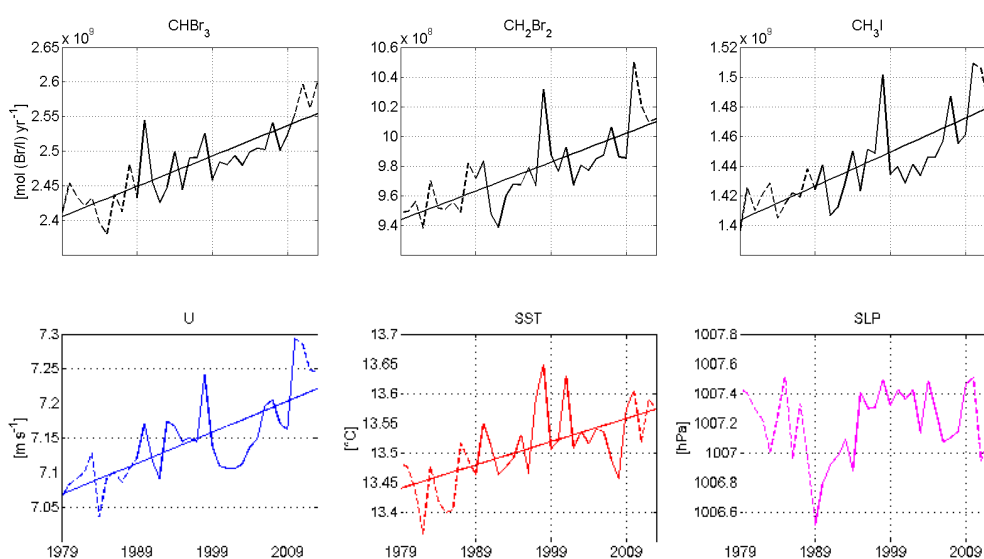


Figure 1. Time series of the sea-to-air flux of CHBr_3 , CH_2Br_2 and CH_3I (in $\text{mol (Br/I) yr}^{-1}$) and of the input parameters SLP in hPa, SST in $^\circ\text{C}$ and U in m s^{-1} for the time period 1979-2013 based on the ERA-Interim dataset. The solid lines indicate the dataset used in Ziska et al. (2013) (1989-2011) and the dashed lines show the extension of the available time period of ERA-Interim. Further, a significant linear regressions trend with $p < 0.01$ is included.

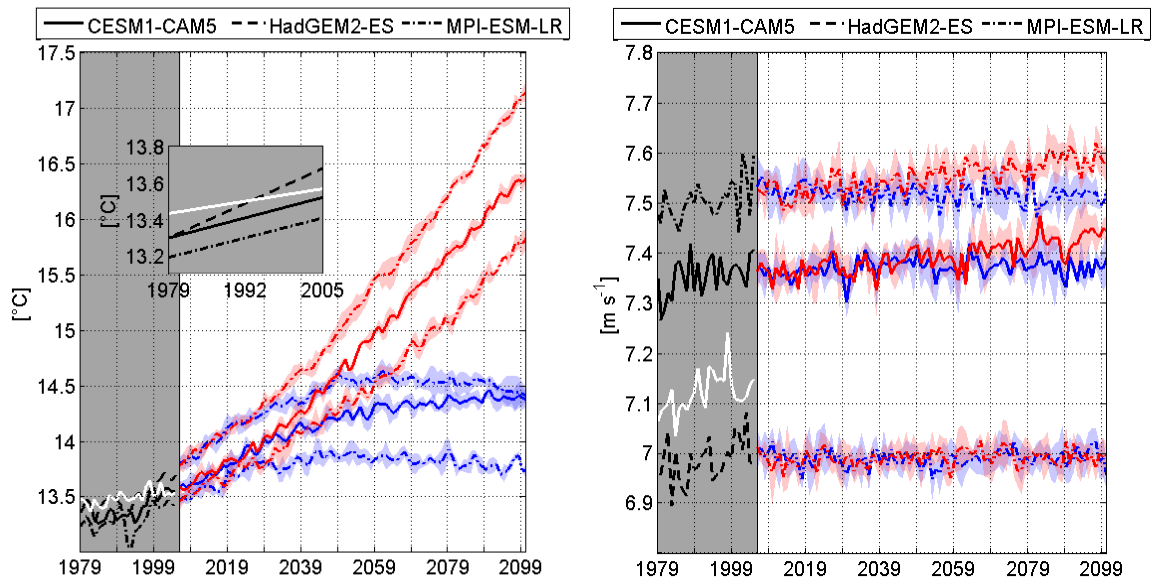


Figure 2. Time series from 1979-2100 of the input parameters SST in $^{\circ}\text{C}$ (left panel) and U in m s^{-1} (right panel) from the CMIP5 models CESM1-CAM5 (solid line), HadGEM2-ES (dashed line) and MPI-ESM-LR (dashed dotted line) for the past from 1979-2005 (historical runs in black) and for the future from 2006-2100 (RCP 2.6 scenario in blue and 8.5 scenario in red) are shown, as well as the standard deviation of the ensemble means (shaded area). The ERA-Interim dataset from 1979-2005 is included for both parameters (white line). Additionally, the calculated linear regression of the three historical and the ERA-Interim SST time series from 1979 to 2005 are plotted in a separate figure in the left panel.

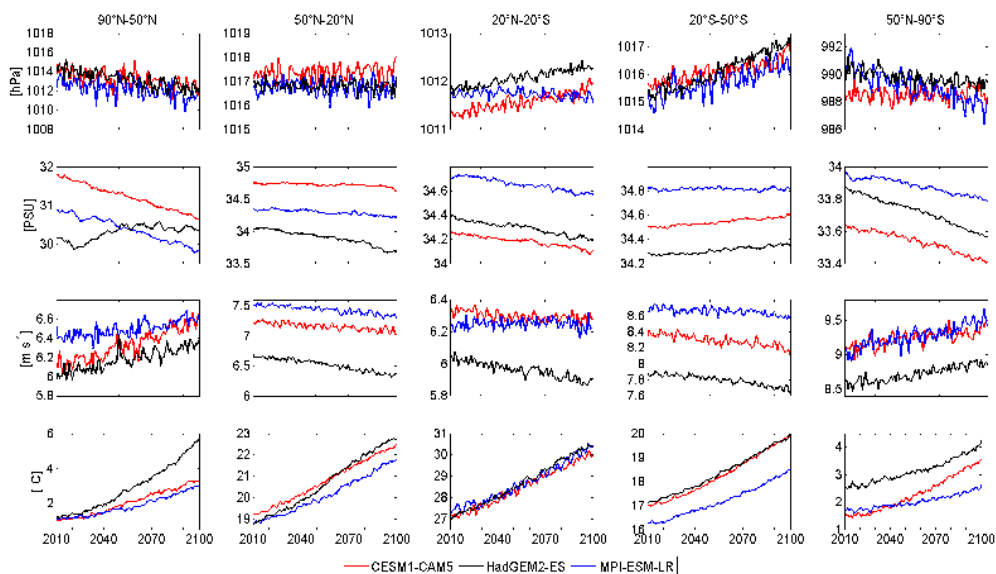


Figure 3. Model output time series (from top to bottom); sea level pressure in hPa, sea surface salinity in PSU, sea surface wind speed in $m s^{-1}$ and sea surface temperature in °C from MPI-ESM-LR (blue line), CESM1-CAM5 (red line) and HadGEM2-ES (black line) for the time period 2010-2100 divided into five latitudinal bands.

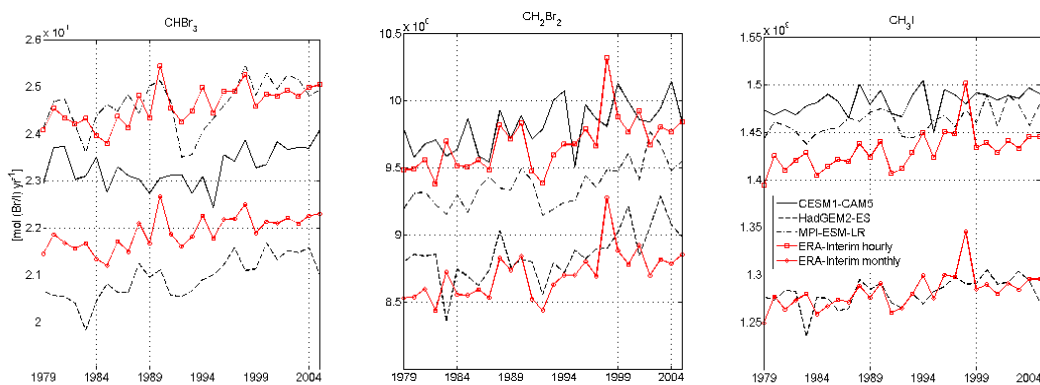


Figure 4. Emission time series of the halogenated compounds bromoform (right), dibromomethane (middle) and methyl iodide (left) calculated with the output fields of the models MPI-ESM-LR (dashed dotted line), CESM1-CAM5 (solid line) and HadGEM2-ES (dashed line) as well as with the ERA-Interim data 6 hourly (red line with squares) and monthly (red line with circles) for the time period 1979-2005.

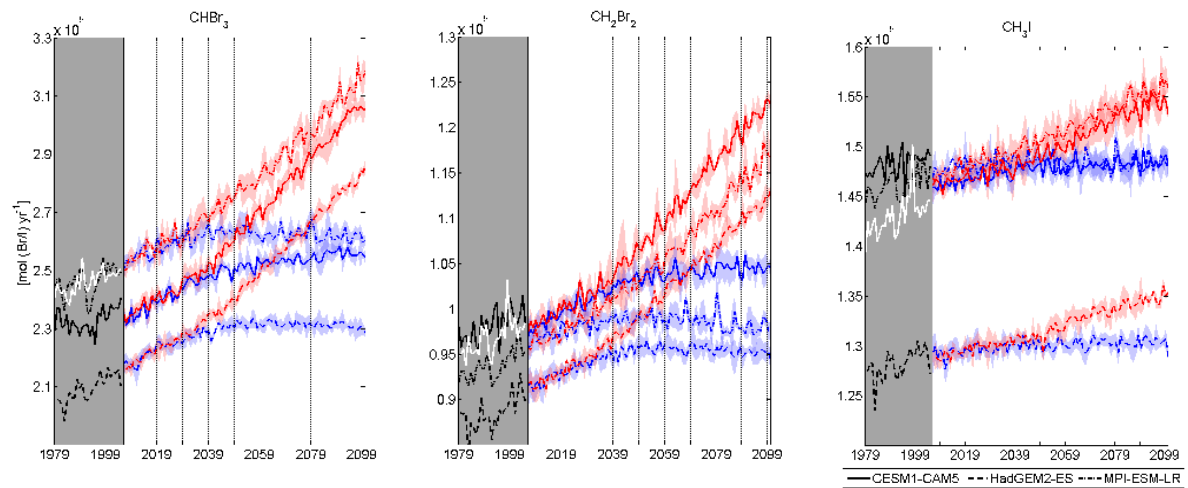


Figure 5. Modeled global sea-to-air fluxes time series of bromoform (left), dibromomethane (middle) and methyl iodide (right) in $\text{pmol m}^{-2} \text{h}^{-1}$ calculated with the CMIP 5 model output fields of MPI-ESM-LR (dashed dotted lines), CEM1-CAM5 (solid line) and HadGEM2-ES (dashed line) using the historical runs from 1979-2005 (black line), the RCP 2.6 scenario (blue lines) and RCP 8.5 scenario (red lines) both for the time period 2006-2100. Additionally, the standard deviation of the ensemble means (shaded area) and the ERA-Interim dataset from 1979-2005 is included for both parameters (white line) are included.

Table 1. A brief description of the CMIP 5 models, including atmospheric and oceanic resolution (lev is number of vertical levels and the horizontal resolution is in degree) as well as the number of ensembles of the historical (1979-2005) model runs and the number of the ensemble of the RCP scenarios (2.6 and 8.5) (2006-2100) used in this study.

Model	Model Centre (or Group)	Atmosphere	Ocean	Number of ensemble (1979-2005)	Number of ensemble (2006 -2100)	Reference
MPI-ESM-LR	Max Planck Institute for Meteorology	47 lev, 1.9°	40 lev, 1.5°	1	3	Giorgetta et al. 2013
CESM1-CAM5	Community Earth System Model Contributors	30 lev, 0.9°x1.25°	60 lev, 1.1°-0.27°	1	3	Neale et al., 2010
HadGEM2-ES	Met Office Hadley Centre*	38 lev, 1.2°x1.9°	40 lev, 0.3°-1°	1	4	Jones et al. 2011

* additional HadGEM2-ES realizations contributed by Instituto Nacional de Pesquisas Espaciais

Table 2. Global annual mean CHBr_3 , CH_2Br_2 and CH_3I emissions calculated with the historical MPI-ESM-LR, CESM1-CAM5 and HadGEM2-ES model as well as with the ERA-Interim dataset in $\text{Gmol (Br/I) yr}^{-1}$ for the time period 1979-2005.

compound	ERA-Interim	MPI-ESM-LR	CESM1-CAM5	HadGEM2-ES
CHBr_3	2.50	2.46	2.33	2.09
CH_2Br_2	0.98	0.94	0.98	0.89
CH_3I	1.45	1.46	1.48	1.28

Table 3. Percentage increase per year of the linear regressions determined for the historical emission time series using the MPI-ESM-LR, CESM1-CAM5 and HadGEM2-ES model output fields over the time period 1979-2005 as well as for the ERA-Interim emissions (based on the 6 hourly mean input parameters).

	CHBr ₃ [% yr ⁻¹]	CH ₂ Br ₂ [% yr ⁻¹]	CH ₃ I [% yr ⁻¹]
MPI-ESM-LR	0.13	0.15	0.07
CESM1-CAM5	0.09	0.14	0.04
HadGEM2-ES	0.21	0.17	0.08
ERA-Interim	0.14	0.16	0.11

Table 4. Percentage increases of future global VSLs emissions from the years 1986-2005 (historical) to the years 2081-2100 (a) RCP 2.6 and b) RCP 8.5 scenario).

a)	MPI-ESM-LR	HadGEM2-ES	CESM1-CAM5
CHBr ₃	5.7	9.4	12.0
CH ₂ Br ₂	3.9	7.1	8.2
CH ₃ I	1.2	1.5	1.9
b)			
CHBr ₃	25.9	31.1	31.3
CH ₂ Br ₂	21.7	23.9	24.3
CH ₃ I	5.9	4.8	5.8

Table 5. Spatial distribution of CHBr₃, CH₂Br₂ and CH₃I emissions calculated with the MPI-ESM-LR, CESM1-CAM5 and HadGEM2-ES model output fields for the years 1986-2005 (a) historical) and the years 2081-2100 (b) the RCP 2.6 scenario and c) the RCP 8.5 scenario) for different latitudinal bands, expressed as percentage.

a) historical	CHBr ₃			CH ₂ Br ₂			CH ₃ I		
	MPI-ESM-LR	HadGEM2-ES	CESM1-CAM5	MPI-ESM-LR	HadGEM2-ES	CESM1-CAM5	MPI-ESM-LR	HadGEM2-ES	CESM1-CAM5
50°N-90°N	16.08	14.85	17.17	-3.05	-2.42	-2.49	7.10	6.82	7.20
20°N-50°N	21.33	17.01	18.72	19.88	18.46	18.35	16.50	14.87	15.77
20°N-20°S	46.99	50.00	49.16	42.71	44.10	44.19	30.10	32.17	31.55
20°S-50°S	17.51	18.75	18.85	20.94	20.84	20.76	37.90	37.34	36.70
50°S-90°S	-1.93	-0.72	-3.90	19.52	19.02	19.19	8.40	8.79	8.77
b) 2.6 Scenario									
50°N-90°N	16.33	14.64	16.92	-2.42	-2.43	-1.89	7.11	6.64	7.30
20°N-50°N	21.13	18.02	19.11	19.79	16.62	18.53	16.40	15.07	15.77
20°N-20°S	46.26	48.62	46.51	42.36	43.69	41.99	30.19	32.24	31.24
20°S-50°S	17.65	18.66	18.97	21.31	21.07	21.32	38.02	37.21	36.78
50°S-90°S	-1.38	0.08	-1.51	18.96	21.06	20.06	8.27	8.84	8.91
c) 8.5 Scenario									
50°N-90°N	16.24	15.49	16.17	-1.08	-0.79	-1.14	7.11	6.83	7.23
20°N-50°N	21.40	17.96	18.94	19.26	16.10	17.79	16.18	14.72	15.56
20°N-20°S	44.65	45.19	44.46	40.57	40.24	39.77	30.56	32.02	31.52
20°S-50°S	17.82	18.56	18.87	21.40	21.36	21.48	37.20	36.79	36.25
50°S-90°S	-0.11	2.83	1.56	19.86	23.10	22.10	8.97	9.42	9.41

References

- Antonov, J. I., D. Seidov, T. P. Boyer, R. A. Locarnini, A. V. Mishonov, H. E. Garcia, O. K. Baranova, M. M. Zweng, and D. R. Johnson, 2010. *World Ocean Atlas 2009, Volume 2: Salinity*. S. Levitus, Ed. NOAA Atlas NESDIS 69, U.S. Government Printing Office, Washington, D.C., 184 pp.
- Aschmann, J., Sinnhuber, B. M., Atlas, E. L., and Schauffler, S. M.: Modeling the transport of very short-lived substances into the tropical upper troposphere and lower stratosphere, *Atmos. Chem. Phys.*, 9, 9237-9247, 2009.
- Behrenfeld, M. J., O'Malley, R. T., Siegel, D. A., McClain, C. R., Sarmiento, J. L., Feldman, G. C., Milligan, A. J., Falkowski, P. G., Letelier, R. M., and Boss, E. S.: Climate-driven trends in contemporary ocean productivity, *Nature*, 444, 752-755, 10.1038/nature05317, 2006.
- Bopp, L., Resplandy, L., Orr, J. C., Doney, S. C., Dunne, J. P., Gehlen, M., Halloran, P., Heinze, C., Ilyina, T., Seferian, R., Tjiputra, J., and Vichi, M.: Multiple stressors of ocean ecosystems in the 21st century: projections with CMIP5 models, *Biogeosciences*, 10, 6225-6245, 10.5194/bg-10-6225-2013, 2013.
- Collins, M., R. Knutti, J. Arblaster, J.-L. Dufresne, T. Fichet, P. Friedlingstein, X. Gao, W.J. Gutowski, T. Johns, G. Krinner, M. Shongwe, C. Tebaldi, A.J. Weaver and M. Wehner, 2013: Long-term Climate Change: Projections, Commitments and Irreversibility. In: *Climate Change 2013: The Physical Science Basis. Contribution of Working Group I to the Fifth Assessment Report of the Intergovernmental Panel on Climate Change* [Stocker, T.F., D. Qin, G.-K. Plattner, M. Tignor, S.K. Allen, J. Boschung, A. Nauels, Y. Xia, V. Bex and P.M. Midgley (eds.)]. Cambridge University Press, Cambridge, United Kingdom and New York, NY, USA.
- Dee, D. P., Uppala, S. M., Simmons, A. J., Berrisford, P., Poli, P., Kobayashi, S., Andrae, U., Balmaseda, M. A., Balsamo, G., Bauer, P., Bechtold, P., Beljaars, A. C. M., van de Berg, L., Bidlot, J., Bormann, N., Delsol, C., Dragani, R., Fuentes, M., Geer, A. J., Haimberger, L., Healy, S. B., Hersbach, H., Holm, E. V., Isaksen, L., Kallberg, P., Koehler, M., Matricardi, M., McNally, A. P., Monge-Sanz, B. M., Morcrette, J. J., Park, B. K., Peubey, C., de Rosnay, P., Tavolato, C., Thepaut, J. N., and Vitart, F.: The ERA-Interim reanalysis: configuration and performance of the data assimilation system, *Quarterly Journal of the Royal Meteorological Society*, 137, 553-597, 10.1002/qj.828, 2011.
- Deser, C., Phillips, A., Bourdette, V., and Teng, H.: Uncertainty in climate change projections: the role of internal variability, *Climate Dynamics*, 38, 527-546, 10.1007/s00382-010-0977-x, 2012.
- Dessens, O., Zeng, G., Warwick, N., and Pyle, J.: Short-lived bromine compounds in the lower stratosphere; impact of climate change on ozone, *Atmospheric Science Letters*, 10, 201-206, 10.1002/asl.236, 2009.
- Dix, B., Baidar, S., Bresch, J. F., Hall, S. R., Schmidt, K. S., Wang, S., and Volkamer, R.: Detection of iodine monoxide in the tropical free troposphere, *P. Natl. Acad. Sci. USA*, 110, 2035-2040, doi:10.1073/pnas.1212386110, 2013
- Doney, S. C.: The Growing Human Footprint on Coastal and Open-Ocean Biogeochemistry, *Science*, 328, 1512-1516, 10.1126/science.1185198, 2010.
- Fischlin, A., G.F. Midgley, J.T. Price, R. Leemans, B. Gopal, C. Turley, M.D.A. Rounsevell, O.P. Dube, J. Tarazona, A.A. Velichko, 2007: Ecosystems, their properties, goods, and services. *Climate Change*

2007: *Impacts, Adaptation and Vulnerability. Contribution of Working Group II to the Fourth Assessment Report of the Intergovernmental Panel on Climate Change*, M.L. Parry, O.F. Canziani, J.P. Palutikof, P.J. van der Linden and C.E. Hanson, Eds., Cambridge University Press, Cambridge, 211-272.

Hepach, H., Quack, B., Ziska, F., Fuhlbrügge, S., Atlas, E. L., Krüger, K., Peeken, I., and Wallace, D. W. R.: Drivers of diel and regional variations of halocarbon emissions from the tropical North East Atlantic, *Atmos. Chem. Phys.*, 14, 1255-1275, 10.5194/acp-14-1255-2014, 2014.

Hopkins, F. E., Kimmance, S. A., Stephens, J. A., Bellerby, R. G. J., Brussaard, C. P. D., Czerny, J., Schulz, K. G., and Archer, S. D.: Response of halocarbons to ocean acidification in the Arctic, *Biogeosciences*, 10, 2331-2345, 10.5194/bg-10-2331-2013, 2013.

Hossaini, R., Chipperfield, M. P., Dhomse, S., Ordonez, C., Saiz-Lopez, A., Abraham, N. L., Archibald, A., Braesicke, P., Telford, P., Warwick, N., Yang, X., and Pyle, J.: Modelling future changes to the stratospheric source gas injection of biogenic bromocarbons, *Geophys. Res. Lett.*, 39, 10.1029/2012gl053401, 2012.

Meehl, G. A., Washington, W. M., Arblaster, J. M., Hu, A., Teng, H., Kay, J. E., Gettelman, A., Lawrence, D. M., Sanderson, B. M., and Strand, W. G.: Climate Change Projections in CESM1(CAM5) Compared to CCSM4, *J. Clim.*, 26, 6287-6308, 10.1175/jcli-d-12-00572.1, 2013.

Montzka, S. A., and Reimann, S.: Ozone-depleting substances and related chemicals, Chapter 1 in *Scientific Assessment of Ozone Depletion: 2010*, Global Ozone Research and Monitoring Project, World Meteorological Organization (WMO), Geneva, Report No. 52, 2011.

Nightingale, P. D., Malin, G., Law, C. S., Watson, A. J., Liss, P. S., Liddicoat, M. I., Boutin, J., and Upstill-Goddard, R. C.: In situ evaluation of air-sea gas exchange parameterizations using novel conservative and volatile tracers, *Glob. Biogeochem. Cycle*, 14, 373-387, 10.1029/1999gb900091, 2000.

Pyle, J. A., Warwick, N., Yang, X., Young, P. J., and Zeng, G.: Climate/chemistry feedbacks and biogenic emissions, *Philos. Trans. R. Soc. A-Math. Phys. Eng. Sci.*, 365, 1727-1740, 10.1098/rsta.2007.2041, 2007.

Quack, B., and Wallace, D. W. R.: Air-sea flux of bromoform: Controls, rates, and implications, *Glob. Biogeochem. Cycle*, 17, 102310.1029/2002gb001890, 2003.

Quack, B., Atlas, E., Petrick, G., and Wallace, D. W. R.: Bromoform and dibromomethane above the Mauritanian upwelling: Atmospheric distributions and oceanic emissions, *J. Geophys. Res.-Atmos.*, 112, D0931210.1029/2006jd007614, 2007b.

Richter, U., and Wallace, D. W. R.: Production of methyl iodide in the tropical Atlantic Ocean, *Geophys. Res. Lett.*, 31, L23s0310.1029/2004gl020779, 2004.

Riebesell, U., Schulz, K. G., Bellerby, R. G. J., Botros, M., Fritsche, P., Meyerhoefer, M., Neill, C., Nondal, G., Oschlies, A., Wohlers, J., and Zoellner, E.: Enhanced biological carbon consumption in a high CO₂ ocean, *Nature*, 450, 545-U510, 10.1038/nature06267, 2007.

Saiz-Lopez, A., and von Glasow, R.: Reactive halogen chemistry in the troposphere, *Chemical Society Reviews*, 41, 6448-6472, 10.1039/c2cs35208g, 2012.

Saiz-Lopez, A., Plane, J. M. C., Baker, A. R., Carpenter, L. J., von Glasow, R., Martin, J. C. G., McFiggans, G., and Saunders, R. W.: Atmospheric Chemistry of Iodine, *Chem. Rev.*, 112, 1773-1804, 10.1021/cr200029u, 2012.

Sinnhuber, B. M., and Folkins, I.: Estimating the contribution of bromoform to stratospheric bromine and its relation to dehydration in the tropical tropopause layer, *Atmos. Chem. Phys.*, 6, 4755-4761, 2006.

Solomon, S., R. R. Garcia, and A. R. Ravishankara (1994), On the role of iodine in ozone depletion, *J. Geophys. Res.*, 99(D10), 20491–20499, doi:10.1029/94JD02028.

Steinacher, M., Joos, F., Froelicher, T. L., Bopp, L., Cadule, P., Cocco, V., Doney, S. C., Gehlen, M., Lindsay, K., Moore, J. K., Schneider, B., and Segschneider, J.: Projected 21st century decrease in marine productivity: a multi-model analysis, *Biogeosciences*, 7, 979-1005, 2010.

Stemmler, I., Hense, I., Quack, B., and Maier-Reimer, E.: Methyl iodide production in the open ocean, *Biogeosciences*, 11, 4459-4476, 10.5194/bg-11-4459-2014, 2014.

Taylor, K. E., Stouffer, R. J., and Meehl, G. A.: AN OVERVIEW OF CMIP5 AND THE EXPERIMENT DESIGN, *Bulletin of the American Meteorological Society*, 93, 485-498, 10.1175/bams-d-11-00094.1, 2012.

Tegtmeier, S., Krüger, K., Quack, B., Atlas, E. L., Pisso, I., Stohl, A. and Yang, X.: Emission and transport of bromocarbons: from the West Pacific ocean into the stratosphere, *Atmospheric Chemistry and Physics*, 12(22), 10633–10648, doi:10.5194/acp-12-10633-2012, 2012.

van Vuuren, D. P., Edmonds, J., Kainuma, M., Riahi, K., Thomson, A., Hibbard, K., Hurtt, G. C., Kram, T., Krey, V., Lamarque, J.-F., Masui, T., Meinshausen, M., Nakicenovic, N., Smith, S. J., and Rose, S. K.: The representative concentration pathways: an overview, *Clim. Change*, 109, 5-31, 10.1007/s10584-011-0148-z, 2011.

von Glasow, R., von Kuhlmann, R., Lawrence, M. G., Platt, U., and Crutzen, P. J.: Impact of reactive bromine chemistry in the troposphere, *Atmos. Chem. Phys.*, 4, 2481-2497, 2004.

Wanninkhof, R.: The effect of using time-averaged winds on regional air-sea CO₂ fluxes, in: *Gas Transfer at Water Surface*, American Geophysical Union, 351-357, 2002.

Werschkun, B., Sommer, Y., and Banerji, S.: Disinfection by-products in ballast water treatment: An evaluation of regulatory data, *Water Research*, 46, 4884-4901, 10.1016/j.watres.2012.05.034, 2012.

Yang, X., Cox, R. A., Warwick, N. J., Pyle, J. A., Carver, G. D., O'Connor, F. M., and Savage, N. H.: Tropospheric bromine chemistry and its impacts on ozone: A model study, *J. Geophys. Res.-Atmos.*, 110, D2331110.1029/2005jd006244, 2005.

Ziska, F., Quack, B., Abrahamsson, K., Archer, S. D., Atlas, E., Bell, T., Butler, J. H., Carpenter, L. J., Jones, C. E., Harris, N. R. P., Hepach, H., Heumann, K. G., Hughes, C., Kuss, J., Krüger, K., Liss, P., Moore, R. M., Orlikowska, A., Raimund, S., Reeves, C. E., Reifenhäuser, W., Robinson, A. D., Schall, C., Tanhua, T., Tegtmeier, S., Turner, S., Wang, L., Wallace, D., Williams, J., Yamamoto, H., Yvon-Lewis, S., and Yokouchi, Y.: Global sea-to-air flux climatology for bromoform, dibromomethane and methyl iodide, *Atmos. Chem. Phys.*, 13, 8915-8934, 10.5194/acp-13-8915-2013, 2013.

5. Manuscript

Oceanic bromine emissions weighted by their ozone depletion potential

S. Tegtmeier¹, F. Ziska¹, I. Pisso², B. Quack¹, G. J. M. Velders³ and K. Krüger⁴

[1] GEOMAR Helmholtz Centre for Ocean Research Kiel, Kiel, Germany

[2] Norwegian Institute for Air Research (NILU), Kjeller, Norway

[3] National Institute for Public Health and the Environment, Bilthoven, the Netherlands

[4] University of Oslo, Oslo, Norway

Corresponding author: S. Tegtmeier, GEOMAR Helmholtz-Zentrum für Ozeanforschung Kiel, Germany, Research Division 1: Maritime Meteorology, Ocean circulation and Climate dynamics
Düsternbrooker Weg 20, 24105 Kiel, Germany, (stegtmeier@geomar.de)

to be submitted

Abstract

The comparison of the Ozone Depletion Potential (ODP)-weighted emissions of short and long-lived halocarbons provides a new concept for assessing the overall impact of oceanic bromine emissions on stratospheric ozone depletion. Seasonally and spatially dependent distributions are derived exemplary for CHBr_3 . ODP-weighted emissions of CHBr_3 amount up to 50% of ODP-weighted anthropogenic emissions of CFC-11 and to 9% of all long-lived ozone depleting substances. CHBr_3 ODP-weighted emissions show pronounced peaks at the equator and the coasts with largest contributions from the Maritime Continent and West Pacific. Variations of convective activity lead to seasonal shifts in the spatial distribution of the ODP with the updraught mass flux explaining 71% of the variance of the ODP distribution. Projections based on mass-flux derived ODP suggest an 80% increase of the ODP-weighted CHBr_3 emissions until 2100 compared to present values. This increase is related to climate change causing larger convective activity and increasing emissions.

1. Introduction

The overall abundance of ozone-depleting substances in the atmosphere has been decreasing since the beginning of the 21 century as a result of the successful implementation of the 1987 Montreal Protocol and its later Adjustments and Amendments (*Montzka et al.*, 2011). In contrast to the long-lived halocarbons, the so-called Very Short-Lived Substances (VSLs) with chemical lifetimes of less than 6 months are not controlled by the Montreal Protocol and are even suggested to increase in the future (*Hepach et al.*, 2014). VSLs are known to have large natural sources; however increasing evidence arises that their oceanic production and emission is enhanced by anthropogenic activities which are expected to increase in the future (*Leedham et al.*, 2013; *Ziska et al.*, in prep.). At present, oceanic VSLs provide a significant contribution to the stratospheric bromine budget (*Montzka et al.*, 2011). In the future, the decline of anthropogenic chlorine and bromine will increase the relative impact of oceanic VSLs on stratospheric chemistry. Furthermore, the impacts of climate change on surface emissions, troposphere-stratosphere transport and the role of deep convection, stratospheric chemistry and residence time will change the role of VSLs (*Pyle et al.*, 2007; *Hossaini et al.*, 2012). While stratospheric ozone depletion due to long-lived halocarbons is expected to level off and reverse (*Austin and Butchart*, 2003), it remains an important challenge to assess the role of oceanic VSLs on stratospheric ozone in a future changing climate.

Over the last years there has been increasing evidence from observational (e.g., *Dorf et al.*, 2006, *Sioris et al.*, 2006) and modelling (e.g., *Warwick et al.* 2006, *Liang et al.*, 2010; *Tegtmeier et al.*, 2012) studies that VSLs provide a significant contribution to stratospheric total bromine (Br_y). Previous estimates ranging between 1 and 8 ppt (*Montzka et al.*, 2011) recently seem to converge to a

narrower range of 4-6.5 ppt (e.g., *Aschmann and Sinnhuber, 2013, Hossaini et al., 2013*). The most abundant bromine containing VSLs are dibromomethane (CH_2Br_2) and bromoform (CHBr_3) with potentially important source regions in tropical, subtropical and shelf waters (*Quack et al., 2007*). The contribution of VSLs to stratospheric bromine in form of source gases or inorganic product gases depends strongly on the efficiency of troposphere-stratosphere transport compared to the photochemical loss of the source gases and to the wet deposition of the product gases.

The relative contribution of individual halogens to stratospheric ozone depletion is often quantified by the Ozone Depletion Potential (ODP) defined as the time-integrated ozone depletion resulting from a unit mass emission of that substance relative to that resulting from a unit mass emission of CFC-11 (CCl_3F) (*Wuebbles, 1983*). The ODP is independent of the total amount of the substance emitted and describes only the potential and not the actual damaging effect of the substance to the ozone layer, The ODP is independent of the total amount of the substance emitted and describes only the potential and not the actual damaging effect of the substance to the ozone layer, relative to that of CFC-11. While the ODP of long-lived halocarbons is a well-established and extensively used measure and plays an important role in the Montreal Protocol for control measures and reporting of emissions, the same concept can not easily be applied to VSLs. Depending on the meteorological conditions, only fractions of the originally released VSLs are injected into the stratosphere. As a consequence the ODP of a VSLs cannot be given by one number as for long-lived halocarbons but needs to be estimated as a function of time and location of emission. So far ODPs of VSLs have been estimated based on Eulerian (*Wuebbles et al., 2001*) and Lagrangian (*Brioude et al., 2010; Pisso et al., 2010*) studies, showing strong geographical and seasonal variations, in particular within the tropics. The studies demonstrated that the ODPs of VSLs are to a large degree determined by the efficiency of vertical transport from the surface to the stratosphere and that uncertainties in the ODPs arise mainly from uncertainties associated with the representation of convection.

Combining the emission strength and the ozone-destroying capabilities in a meaningful way can be achieved by calculating the ODP-weighted emissions, which provides a strong metric for the contribution of a specific compound to ozone depletion and has been applied to long-lived substances such as the CFCs and N_2O (e.g., *Velders et al., 2007; Ravishankara et al., 2009*). For the long-lived halocarbons, the global ODP-weighted emissions are calculated as the product of two numbers, their mean global emission and their ODP. For the VSLs, however, the concept of ODP-weighted emissions has not been applied yet and will require weighting the spatially and temporally highly variable emissions with the also highly variable ODPs. Such a quantity will provide inside in where and when the VSLs are emitted that impact stratospheric ozone. Furthermore, in a globally averaged framework the ODP-weighted emissions will allow to compare the impact of past, present

and future long- and short-lived halocarbon emissions. Note that ideally the ODP-weighted emissions would be calculated only for the anthropogenic component of the VSLS emissions; however, no such estimates are available at the moment.

Here, we compile the first ODP-weighted emissions of CHBr_3 in form of the seasonal and annual mean distribution in order to assess the overall impact of oceanic CHBr_3 emissions on stratospheric ozone. This new approach provides a powerful tool for an assessment of future growing VSLS and declining chlorine emissions in form of a direct comparison of the global-averaged ODP-weighted emissions of short- and long-lived halocarbons.

2. Method

The present-day global emission scenario from Ziska et al. (2013) is a bottom-up estimate of the oceanic CHBr_3 fluxes. Emissions are estimated using global surface concentration maps generated from the atmospheric and oceanic in-situ measurements of the HalOcAt (Halocarbons in the ocean and atmosphere) database project (<https://halocat.geomar.de>). The in-situ measurements for 1989-2011 were classified based on physical and biogeochemical characteristics of the ocean and atmosphere and extrapolated to a global $1^\circ \times 1^\circ$ grid with the Ordinary Least Square regression technique. Based on the concentration maps the oceanic emissions were calculated with the transfer coefficient parameterization of Nightingale et al. (2000) adapted to CHBr_3 (Quack and Wallace, 2003). While the concentration maps represent in a first step climatological fields covering 1989-2011, the emissions are calculated based on 6-hourly meteorological ERA-Interim data (Dee et al., 2011) for 1979-2013 assuming constant concentrations over the complete time period.

Future emission estimates are calculated based on the present day climatological concentration maps and future estimates of global sea surface temperature, pressure, winds and salinity (Ziska et al., in prep.). The meteorological parameters are model output from the Community Earth System Model version 1 - Community Atmospheric Model version 5 (CESM1-CAM5) (Neale et al., 2010) runs based on the Representative Concentration Pathways (RCP) 8.5 scenarios conducted within phase 5 of the Coupled Model Intercomparison Project (CMIP5) (Taylor et al., 2012). Thus the derived changes of the future VSLS emissions are only driven by projected changes in the meteorological surface parameters, but do not take into account possible changes of the oceanic concentrations which will be assessed in follow-up studies.

ODPs of long-lived halogen compounds can be calculated using atmospheric chemistry-transport models or can be estimated by a semi-empirical approach (Solomon et al., 1992). In contrary to the long-lived halocarbons, for VSLS the tropospheric transport time scales play a dominant role for the calculation of their ODP. Following a method previously developed specifically for VSLS, the ODP of

CHBr_3 is calculated as a function of location and time of emission based on ERA-Interim driven FLEXPART trajectories (Pisso *et al.*, 2010). Owing to the different timescales and processes in the troposphere and stratosphere, the estimates are based on separate ensembles of trajectories quantifying the fraction of VSLs reaching the tropopause and their subsequent residence time in the stratosphere.

The concept of ODP-weighted emissions combines information on the emission strength and on the relative ozone-destroying capability of a substance. Its application to VSLs has been recently rendered possible by the availability of observation-based VSLs emission maps (Ziska *et al.*, 2013). We calculate the present-day ODP-weighted emissions for CHBr_3 for four months (March, June, September and December) from 1999 to 2006 by multiplying the CHBr_3 emissions with the ODP at each grid point.

While present day ODP estimates for VSLs based on ERA-Interim are available (Pisso *et al.*, 2010), so far the trajectory-based method has not been applied to future model scenarios due to the lack of suitable Lagrangian modeling tools associated with global models. Therefore we attempt to determine an ODP proxy easily available from Climate Model output, which can be used to derive future estimates of the ODP fields. Due to the pronounced relationship between the ODP and the deep convective activity we are able to develop a proxy based on the ERA-Interim convective upward mass flux. For the available trajectory-based ODP fields (26 months of data) we determine a polynomial fit in a least-square sense to reconstruct the ODP from the convective mass flux fields. The fitted ODP fields explain 71% of the variance of the original fields. By applying the polynomial fit function to the convective upward mass flux from ERA-Interim and from the CESM1-CAM5 RCP8.5 runs we estimate observational (1979-2013) as well as model historical (1979-2005) and future (2006-2100) ODP fields.

3. Results

We will introduce the concept of the ODP-weighted emissions of CHBr_3 exemplarily for March 2005 and discuss how the ODP-weighted emissions of this very short-lived compound compare to those of long-lived ODSs. The CHBr_3 emissions (Ziska *et al.*, 2013) for March 2005 are shown in Figure 1a with highest emissions in coastal regions, in the upwelling equatorial waters and the NH mid-latitude Atlantic. Apart from the gradients between coastal, shelf and deep ocean waters the emissions show no pronounced longitudinal variations. The potentially damaging effect of CHBr_3 on the stratospheric ozone layer is displayed in Figure 1b in form of the CHBr_3 ODP distribution defined as a function of time and location of the emission but independent of its strength. Overall, the ODP of CHBr_3 is largest in the tropics (tropical ODP belt) and has low values (mostly below 0.1) north and south of 20°. The

ODP depends strongly on the efficiency of rapid transport from the surface to the stratosphere which is in turn determined by the intensity of high reaching convection. In the NH winter/spring, the strongest convection and therefore the highest ODP values of up to 0.85 are found over the equatorial West Pacific region (*Pisso et al.*, 2010). In contrast to the CHBr_3 emission estimates, the ODP shows pronounced longitudinal variations linked to the distribution of convection and low-level flow patterns.

The ODP-weighted CHBr_3 emissions for March 2005 are displayed in Figure 1c. While the emissions itself describe the strength of the CHBr_3 sea-to-air flux, the ODP-weighted emissions cannot be interpreted directly as a physical quantity but only relative to ODP-weighted emissions of long-lived halocarbons. The spatial distribution of the ODP-weighted emissions combines information on where large amounts of CHBr_3 are emitted from the ocean and where strong convective transport enables CHBr_3 to reach the stratosphere. Only for regions where both quantities are large, strong ODP-weighted emissions will be found, whereas regions with one of the quantities is close to zero will not be important, such as the mid-latitude North Atlantic. Negative ODP-weighted emissions occur in regions where negative emissions indicate a CHBr_3 flux from the atmosphere into the ocean. Since negative ODP-weighted emissions are not a meaningful quantity and occur in regions where the ODP is small they will not be displayed in the following figures and are not taken into account for the calculations of the global mean values. The ODP-weighted emissions are in general largest between 20°S and 20°N (72% of the overall global amount) as a result of the tropical ODP belt and peak at the equator and coasts as a result of the emission distribution. Of particular importance for the stratospheric ozone chemistry are emissions from the Maritime Continent (South-East Asia), the tropical Pacific and the Indian Ocean.

The global annual mean ODP-weighted emissions of CHBr_3 are about 41 GgCFC-11-eq/year for 2005 (Figure 1d). The concept of ODP-weighted emissions becomes particularly useful when comparing this quantity for CHBr_3 with the ones of human-made halocarbons. For the year 2005, ODP-weighted emissions of CHBr_3 amount up to 50% of the ODP-weighted emissions of CH_3Br (natural and anthropogenic), of CFC-11, or of CFC-12 and are of similar magnitude as the ODP-weighted emissions of CCl_4 and the individual halons. While the ODP of CHBr_3 exceeds the value of 0.5 only in less than 10% over the globe, the relatively large CHBr_3 emissions make up for the mostly small ODP. Current estimates of global CHBr_3 emissions range between 249 Gg/year and 864 Gg/year (*Ziska et al.*, 2013 and references therein). Even the lower boundary of this range, which is at the same time the emission inventory used in this study, exceeds the combined emissions of the most abundant CFCs. Still more important than the overall CHBr_3 emission strength is the fact that emission and ODP show the same latitudinal gradients with both fields having higher values at the low latitudes. This spatial

coincidence of large sources and efficient transport causes the relatively large global mean value of CHBr_3 ODP-weighted emissions.

The CHBr_3 ODP-weighted emissions vary with season as demonstrated in Figure 2a for June and December 2001. In the NH summer 57% of the ODP-weighted emissions stem from the NH tropical belt (30°N - 0°N) with largest contributions from the Maritime Continent and Asian coastal areas. In the NH winter, the ODP-weighted emissions shift to the SH tropical belt (48%) with strongest contributions from the equatorial upwelling in the West Pacific. While the Maritime Continent is an important source region all-year around, emissions from the southern coast line of Asia during NH winter are not important for stratospheric ozone depletion. The emissions reveal slight seasonal variations (not shown here) due to varying surface wind and temperature; however, it is the seasonality of the ODP (Figure 2b) that causes the pronounced shift of the ODP-weighted emissions from one hemisphere to the other. The ODP distributions for the months June and December 2001 have their maxima between 0°N and 20°N for the NH summer and 5°N and 15°S for the NH winter consistent with the main patterns of tropical convection.

A detailed picture of the high reaching convective activities within these two months is given in Figure 2c in form of the ERA-Interim monthly mean updraught mass flux between 250 and 80 hPa. The rapid updraughts transporting air masses from the boundary layer into the tropical tropopause layer (TTL) are part of the ascending branch of the tropospheric circulation constituted by the position of the intertropical convergence zone (ITCZ). The updraught convective mass fluxes are largest in and near the summer monsoon driven circulations close to the equator. Over the West Pacific and Maritime Continent the region of intense convection is quite broad compared to the other ocean basins due to strong monsoon flow and the oceanic warm pool. In addition to the overall annual north-south migration pattern, large seasonal changes of the updraught mass flux can be observed over South America and the Maritime Continent consistent with the climatological distribution of the ITCZ. The obvious strong correlations of the CHBr_3 ODP and the TTL convective mass flux indicate that variations in chemistry or stratospheric residence time do not have a strong impact on the ODP variability. Based on the polynomial fit determined between the updraught mass flux and the trajectory-derived ODP we calculate ERA-Interim mass flux-derived ODP estimates (Figure 2d) which explain 76% and 81% of the variance of the original trajectory-based ODP fields (Figure 2b). Largest disagreement is found over South America; however, the CHBr_3 ODP values over the continents are not important due to the very low to non-existent emissions over land and are not used in our study. The ODP proxy provides a cost-efficient method to derive ODP fields for past (ERA-Interim) and future (climate model output) meteorological conditions.

The global mean CHBr_3 ODP-weighted emissions are compared for the trajectory- and mass flux-derived ODP fields for the years 1999-2006 (black and green line in Figure 3a). While individual months can show strong deviations (e.g., for December 1999 the mass-flux derived ODP-weighted emissions are about 30% smaller), there is an overall good agreement between the two time series. In particular, the pronounced seasonal cycle with maximum values in the NH summer and autumn is captured by both methods. In addition to ODP-weighted emissions based on the Reanalysis data (observation-derived), we calculate the same quantity from the CESM1-CAM5 historical model run (red line in Figure 3a). The model-derived ODP-weighted emissions show slightly larger deviations than the two observation-derived time series among themselves. However, the overall magnitude as well as the phase and amplitude of the seasonal cycle are reasonably well captured by the model indicating the meteorological surface variables (in order to derive the model-based emissions) as well as the convective mass flux (in order to derive the model-based ODP) are realistic. Recent improvements have been reported in the regional cloud representation in the deep convective tropical Pacific (*Kay et al., 2012*) and in the parameterization of deep convection and ENSO simulation (*Neale et al., 2008*).

The comparison of the annual mean time series of the mass-flux derived ODP-weighted emissions (Figure 3b) for 1979-2013 (observations) and 1979-2005 (model) shows an offset with the model results being about 12% smaller but give similar interannual variations for some years. The offset between the observational and model-derived long term mean of the ODP-weighted emissions stems mostly from less deep convective activity in the model. Future estimates of the CHBr_3 ODP-weighted emissions are calculated based on the meteorological surface variables and convective mass flux from the CESM1-CAM5, RCP8.5 runs (Figure 3b). Note that there is an offset in 2005/2006 between the ODP-weighted CHBr_3 emissions based on the historical and future runs of about 14%. If both quantities, emissions and ODP, are based on the future model predictions (red line), strong interannual variations of up to 20% occur. Overall, in the scenario the ODP-weighted emissions increase steadily until 2100 by nearly 80% of the 2006-2015 mean value. This increase is driven by increasing emissions and increasing convective transport as evident from sensitivity studies where one of the two parameters is kept constant at the 2006-2015 mean value. If the ODP is kept constant (light grey) the weighted emissions increase by 17% and if the emissions are kept constant (dark grey) they increase by 40%. In addition to the stronger increase the ODP cause the pronounced interannual variations. Note that for the RCP2.6 scenario only a moderate increase of around 15% is predicted.

The comparison of the model-derived CHBr_3 ODP-weighted emissions with the ones of other long-lived substances shows that CHBr_3 emissions can be expected to have a larger impact on

stratospheric ozone than all other individual gases except for CH₃Br after approximately 2025 except for ODP-weighted emissions of anthropogenic N₂O (*Ravishankara et al.*, 2009) not shown in our plot. The CH₃Br emission scenario suggests constant emissions from natural and anthropogenic sources. Taking into account possible changes in anthropogenic CH₃Br emissions and in oceanic CHBr₃ production would further change the balance between the ODP-weighted emissions of these two gases.

4. Summary and Discussion

The ODP-weighted emissions of CHBr₃ give a detailed picture on where and when oceanic CHBr₃ emissions take place that will later impact stratospheric ozone. Furthermore, they provide a useful tool of comparing the emission strength of CHBr₃ with the ones of long-lived anthropogenic gases in an ozone depletion framework. Since currently no information is available on the strength of anthropogenic VSLs emissions, the ODP concept is applied to the complete emission budget. While the ODP-weighted emissions are an important step towards assessing the current and future effects of VSLs on the ozone layer, one needs to keep in mind that the absolute values are subject of large uncertainties arising from uncertainties in the emission inventories and in the parameterization of the convective transport. This sensitivity is demonstrated by applying the ODP fields calculated from FLEXPART trajectories without convective parameterization (*Pisso et al.*, 2010) which results in roughly 50% lower global mean ODP-weighted emissions. Additionally, uncertainties may arise from the simplified tropospheric and stratospheric chemistry schemes. Further detailed studies including different convective parameterization schemes, more detailed representation of tropospheric chemistry, product gas impacts and various emission inventories are required in order to obtain reliable uncertainty ranges which need to be included in any communication of ODPs to policy makers.

Future ODP-weighted emission estimates have been derived taking into account changing meteorological surface parameters and changing convective activity, but neglecting changes in tropospheric and stratospheric chemistry (including changes of the alpha value of bromine) and stratospheric residence time. While our methodology is somewhat limited by these simplifications, CHBr₃ delivery from the surface to the tropopause in a future changing climate is expected to be mostly related to changes in transport rather than changes in the chemistry (*Hossaini et al.*, 2013) suggesting that we include the important processes. Furthermore, we do not account for changes in oceanic sources which are not well enough understood yet to derive future estimates. While there are discrepancies between the observation and model derived present estimates, our focus is on the future projections which suggest an 80% increase of the ODP-weighted CHBr₃ emissions until 2100

for the RCP8.5 scenario. Given the decreasing chlorine levels such significant anthropogenically driven increase will make CHBr_3 an important ozone destroying substance.

Acknowledgements The authors are grateful to the ECMWF for making the reanalysis product ERA-Interim available. This study is carried out within the EU project SHIVA (FP7-ENV-2007-1-226224) and the BMBF project ROMIC THREAT. We thank Steve Montzka for helpful discussions. Data used to generate the figures is available from the corresponding author.

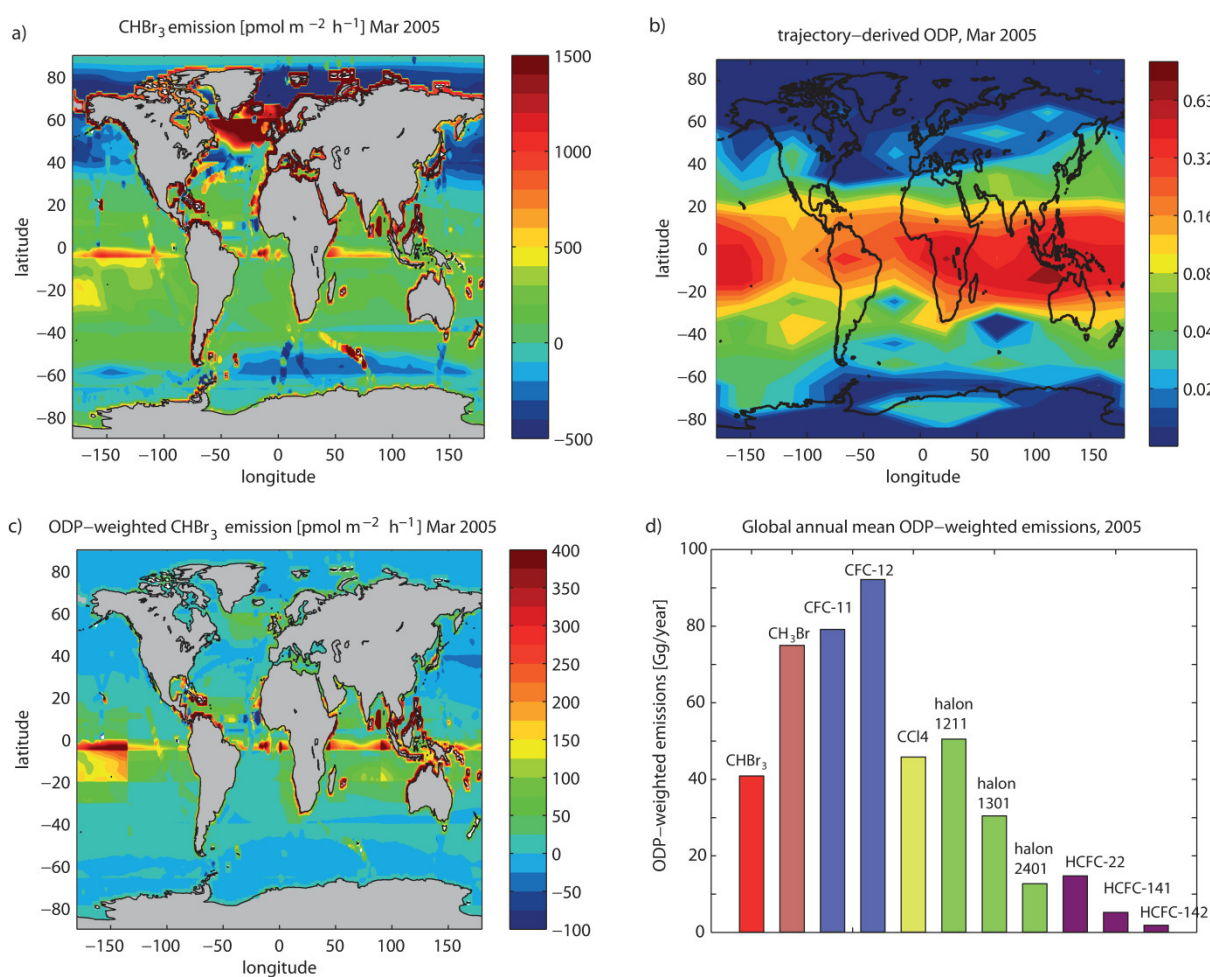


Figure 1. CHBr_3 emissions (a), ODP (b) and the ODP-weighted emissions (c) are given for March 2005. A comparison of the global annual mean ODP-weighted emissions of CHBr_3 and long-lived halocarbons is shown

for 2005 (d). Emissions of long-lived halocarbons being derived from NOAA and AGAGE global sampling network measurements (Montzka *et al.*, 2011).

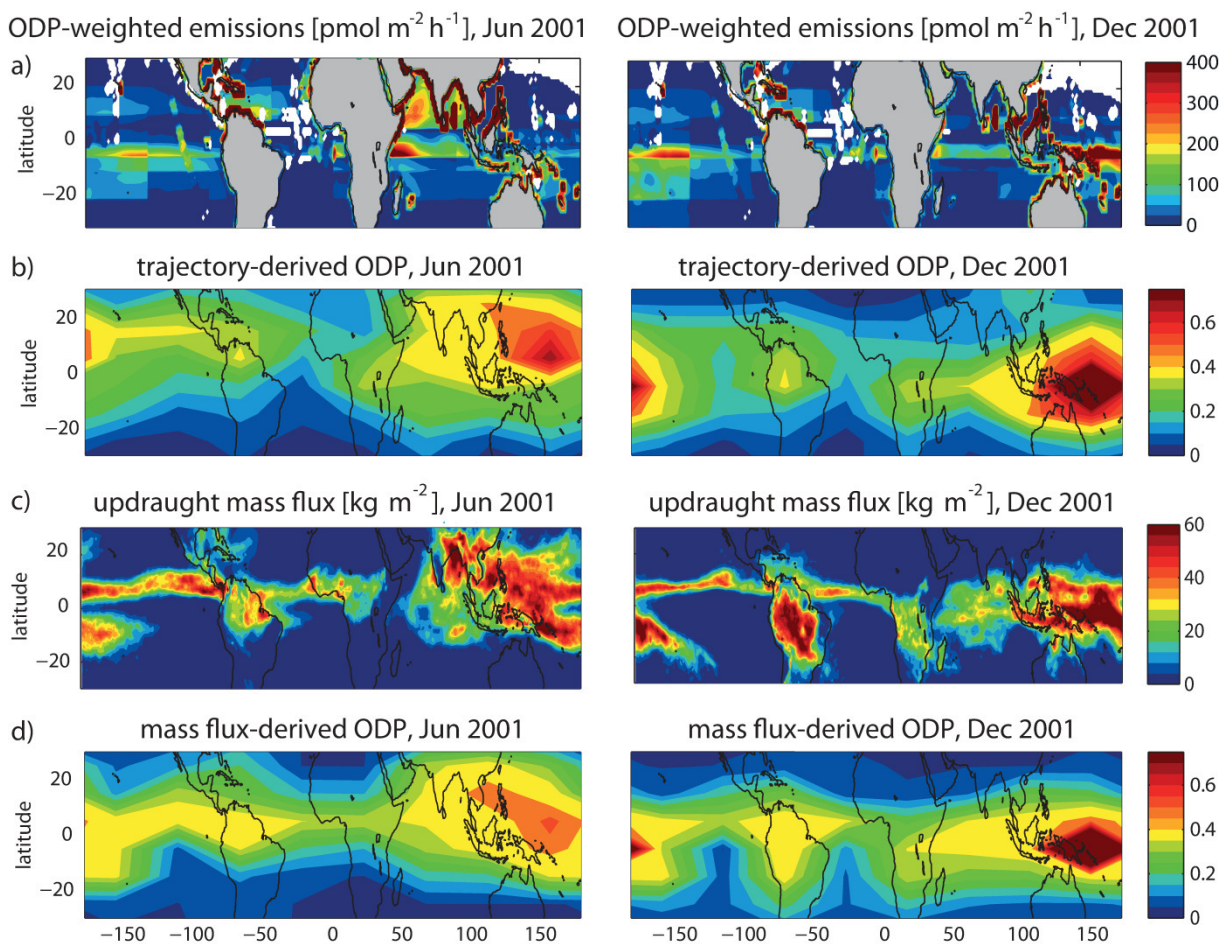


Figure 2. ODP-weighted emissions (a) calculated as the product of the emissions maps (not show here) and the trajectory-based ODP fields (b) are displayed for June and December 2001. The monthly mean ERA-Interim updraught mass flux between 250 and 80 hPa (c) and the mass flux-derived ODP (d) are also shown.

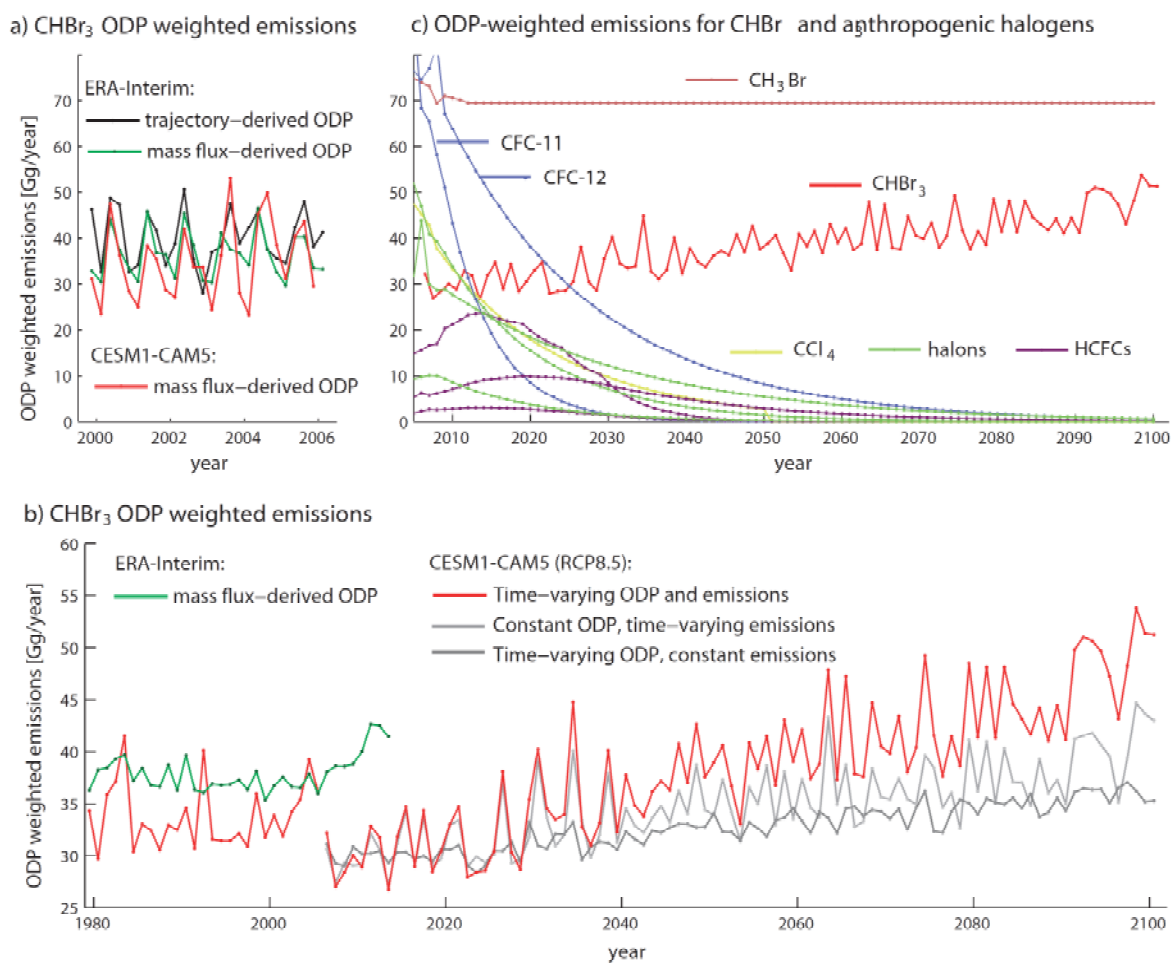


Figure 3. Time series of CHBr₃ ODP-weighted emissions based on ERA-Interim (black and green line) and on historical and future (RCP 8.5 scenario) CESM1-CAM5 runs (red lines) are shown (a and b). Additionally, the future time series are displayed for either constant (2006-2015 mean value) ODP (light grey) or constant emissions (dark grey). Future ODP-weighted emission estimates for long-lived halocarbons (halons: halon 1211, 1301, 2402; HCFCs: HCFC-22, -141, -142) are shown (c).

References

- Aschmann, J. and B.-M. Sinnhuber (2013), Contribution of very short-lived substances to stratospheric bromine loading: uncertainties and constraints, *Atmos. Chem. Phys.*, 13, 1203-1219, doi:10.5194/acp-13-1203-2013.
- Austin, J., N., Butchart (2003), Coupled chemistry-climate model simulations for the period 1980 to 2020: ozone depletion and the start of ozone recovery, *Quarterly Journal of the Royal Meteorological Society*, 129: 3225–3249.
- Brioude, J., R. W. Portmann, J. S. Daniel, O. R. Cooper, G. J. Frost, K. H. Rosenlof, C. Granier, A. R. Ravishankara, S. A. Montzka, and A. Stohl (2010), Variations in ozone depletion potentials of very short-lived substances with season and emission region. *Geophys. Res. Lett.*, 37, L19804, doi:10.1029/2010GL044856.
- Dee, D. P., et al. (2011), The ERA-Interim reanalysis: configuration and performance of the data assimilation system, *Quarterly Journal of the Royal Meteorological Society*, 137(656), 553–597, doi:10.1002/qj.828.
- Dorf, M., J.H. Butler, A. Butz, C. Camy-Peyret, M.P. Chipperfield, L. Kritten, S.A. Montzka, B. Simmes, F. Weidner, and K. Pfeilsticker (2006), Long-term observations of stratospheric bromine reveal slow down in growth, *Geophys. Res. Lett.*, 33, L24803, doi: 10.1029/2006GL027714.
- Hepach, H., B. Quack, F. Ziska, S. Fuhlbrügge, E. L. Atlas, K. Krüger, I. Peeken, and D. W. R. Wallace (2014), Drivers of diel and regional variations of halocarbon emissions from the tropical North East Atlantic, *Atmos. Chem. Phys.*, 14, 1255-1275, doi:10.5194/acp-14-1255-2014.
- Hossaini, R., et al. (2012), Modelling future changes to the stratospheric source gas injection of biogenic bromocarbons, *Geophys. Res. Lett.*, 39, L20813, doi:10.1029/2012GL053401.
- Hossaini, R., et al., (2013), Evaluating global emission inventories of biogenic bromocarbons, *Atmos. Chem. Phys.*, 13, 11819-11838.
- Leedham, E. C., C. Hughes, F. S. L. Keng, S.-M. Phang, G. Malin, and W. T. Sturges (2013), Emission of atmospherically significant halocarbons by naturally occurring and farmed tropical macroalgae, *Biogeosciences*, 10, 3615–3633, doi:10.5194/bg-10-3615-2013.
- Kay, J. E., et al. (2012), Exposing global cloud biases in the Community Atmosphere Model (CAM) using satellite observations and their corresponding instrument simulators, *J. Climate*, 25, 5190–5207.
- Liang, Q., R. S. Stolarski, S. R. Kawa, J. E. Nielsen, A. R. Douglass, J. M. Rodriguez, D. R. Blake, E. L. Atlas, and L. E. Ott (2010), Finding the missing stratospheric Br₂: a global modeling study of CHBr₃ and CH₂Br₂, *Atmos. Chem. Phys.*, 10, 2269–2286, doi:10.5194/acp-10-2269-2010.
- Montzka, S., et al. (2011), Ozone-depleting substances (ODSs) and related chemicals, in *Scientific Assessment of Ozone Depletion: 2010, Rep. 52*, chap. 1, pp. 1–112, Global Ozone Res. and Monit. Proj., World Meteorol. Organ., Geneva, Switzerland.
- Neale, R. B., J. H. Richter, and M. Jochum (2008), The impact of convection on ENSO: From a delayed oscillator to a series of events. *J. Climate*, 21, 5904–5924.
- Neale, R. B., and Coauthors, 2010: Description of the NCAR Community Atmosphere Model (CAM5.0). NCAR Tech. Rep. NCAR/TN-486+STR, 268 pp.
- Nightingale, P. D., Malin, G., Law, C. S., Watson, A. J., Liss, P. S., Liddicoat, M. I., Boutin, J. and Upstill-Goddard, R. C.: In situ evaluation of air-sea gas exchange parameterizations using novel conservative and volatile tracers, *Global Biogeochemical Cycles*, 14(1), 373–387, doi:10.1029/1999GB900091, 2000.

Pisso, I., P. H. Haynes, and K. S. Law (2010), Emission location dependent ozone depletion potentials for very short-lived halogenated species, *Atmos. Chem. Phys.*, 10, 12025-12036.

Pyle, J. A., N. Warwick, X. Yang, P. J. Young, and G. Zeng (2007), Climate/chemistry feedbacks and biogenic emissions, *Philos. Trans. R. Soc. A*, 365(1856), 1727–1740, doi:10.1098/rsta.2007.2041.

Quack, B., E. Atlas, G. Petrick, and D. W. R. Wallace (2007), Bromoform and dibromomethane above the Mauritanian upwelling: Atmospheric distributions and oceanic emissions, *J. Geophys. Res.*, 112(D9), D09312, doi:10.1029/2006JD007614.

Ravishankara, A.R., J. S. Daniel, R. W. Portmann (2009), Nitrous oxide (N₂O): The dominant ozone-depleting substance emitted in the 21st century. *Science* 326:123–125.

Sioris, C. E., et al. (2006), Latitudinal and vertical distribution of bromine monoxide in the lower stratosphere from Scanning Imaging Absorption Spectrometer for Atmospheric Cartography limb scattering measurements, *J. Geophys. Res.*, 111, D14301, doi: 10.1029/2005JD006479.

Solomon, S., M. Mills, L. E. Heidt, W. H. Pollock, and A. F. Tuck (1992), On the evaluation of ozone depletion potentials, *J. Geophys. Res.*, 97, 825–842.

Tegtmeier, S., Krüger, K., Quack, B., Atlas, E. L., Pisso, I., Stohl, A. and Yang, X.: Emission and transport of bromocarbons: from the West Pacific ocean into the stratosphere, *Atmospheric Chemistry and Physics*, 12(22), 10633–10648, doi:10.5194/acp-12-10633-2012, 2012.

Taylor, K. E., R. J. Stouffer, and G. A. Meehl, 2012: The CMIP5 experiment design. *Bull. Amer. Meteor. Soc.*, **93**, 485–498.

Velders, G. J. M., S. O. Andersen, J. S. Daniel, D. W. Fahey and M. McFarland (2007), The Importance of the Montreal Protocol in Protecting Climate, *PNAS*, 104:4814 – 4819, doi: 10.1073/pnas.0610328104.

Warwick, N. J., J. A. Pyle, G. D. Carver, X. Yang, N. H. Savage, F. M. O'Connor, and R. A. Cox (2006), Global modeling of biogenic bromocarbons, *J. Geophys. Res.*, 111, D24305, doi:10.1029/2006JD007264.

Wuebbles, D. J. (1983), Chlorocarbon emission scenarios: Potential impact on stratospheric ozone, *J. Geophys. Res.*, 88, 1433–1443.

Wuebbles, D. J., K. Patten, M. Johnson, and R. Kotamarthi (2001), New methodology for ozone depletion potentials of short-lived compounds: n-propyl bromide as an example, *J. Geophys. Res.*, 106, 14551–14571.

Ziska, F., Quack, B., Abrahamsson, K., Archer, S. D., Atlas, E., Bell, T., Butler, J. H., Carpenter, L. J., Jones, C. E., Harris, N. R. P., Hepach, H., et al.: Global sea-to-air flux climatology for bromoform, dibromomethane and methyl iodide, *Atmospheric Chemistry and Physics Discussions*, 13(2), 5601–5648, doi:10.5194/acpd-13-5601-2013, 2013.

CONCLUSIONS
AND
FUTURE PERSPECTIVES

VI. Conclusions and future perspectives

The objectives of this thesis were to reduce the uncertainties in global emission estimates of CHBr_3 , CH_2Br_2 and CH_3I on basis of a novel halocarbon database and in their impact on stratospheric bromine and iodine loading for the past and future (Figure III–12) and they were summarized in six research tasks in section III.6. Each task has been carefully processed and the results have been evaluated with recent results in the literature. The six research tasks were addressed in seven manuscripts and will be discussed in the below paragraphs. The first manuscript presents the basis of the following manuscripts.

1. Compilation of the global data base HalOcAt based on existing air and sea water measurements of halogenated compounds

The novel HalOcAt (**H**alocarb**o**ns in the **O**cean and **A**tmosphere database project) database was initiated in June 2009 with about 200 contributions adding up to in total 554000 oceanic and 47600 atmospheric measurements of 19 different halogenated compounds (Figure VI–1) covering the time period of 1989–2011. The majority of the submitted data is atmospheric data taken from land based stations (mostly coastal), from airborne missions and research cruises.

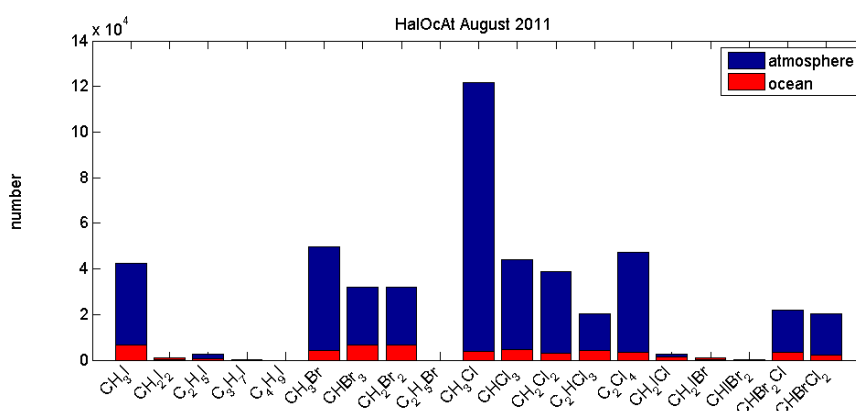


Figure VI – 1. Number of halocarbons measurements in the ocean (red) and atmosphere (blue) included in the HalOcAt database (August 2012).

The data is available online for the research community (<https://halocat.geomar.de/>). The database is a useful source for the comparison of individual data sets and a tool to predict surface ocean/lower atmosphere halocarbon concentrations and fluxes.

Important contributions of air and water measurements in the tropical oligotrophic ocean and upwelling region to the HalOcAt database have been provided in the sixth manuscript “*Drivers of diel and regional variations of halocarbon emissions from the tropical North East Atlantic*” and in the seventh manuscript “*Impact of the marine atmospheric boundary layer conditions on VLSL abundances in the eastern tropical and subtropical North Atlantic Ocean*” (Supplement).

2. Production of best estimates of sea-to-air flux climatologies from a bottom-up approach of three important short-lived halocarbons CHBr_3 , CH_2Br_2 and CH_3I based on HalOcat

The first global bottom-up emission inventory based on the so far most comprehensive available dataset has been determined and made publicly available. Based on the HalOcat database, global marine and atmospheric surface maps of bromoform (CHBr_3), dibromomethane (CH_2Br_2) and methyl iodide (CH_3I) concentrations were calculated in order to finally derive global sea-to-air flux estimates from a bottom-up approach. Due to low data density, the challenge was to find the best and most realistic way for inter- and extrapolation. Therefore, a new method was developed to fill the missing data in the global grid, combining extrapolation and classification techniques, by taking into account the biogeochemical character and distribution of the compound of interest. Note that this method can also be applied to other trace gases (e.g., N_2O or CH_4).

First, the data were interpolated onto a $1^\circ \times 1^\circ$ grid, while missing grid values were interpolated with latitudinal and longitudinal dependent regression techniques reflecting the distribution of the VSLs. Resulting from this, global sea-to-air fluxes were calculated using physical forcing fields with a high temporal resolution of 6 hours. Based on these calculations a total global flux of (Robust Fit/ Ordinary Least Square regression techniques) of 1.5/ 2.5 Gmol Br yr^{-1} for CHBr_3 , 0.78/ 0.98 Gmol Br yr^{-1} for CH_2Br_2 and 1.24/ 1.45 Gmol I yr^{-1} for CH_3I was derived. Contrary to recent studies, negative fluxes (flux into the ocean) occurred in each sea-to-air flux climatology, mainly in the Arctic (for CH_2Br_2) and in the Antarctic (for CHBr_3) region. "Hot spots" of CHBr_3 and CH_2Br_2 emissions are located in the equatorial belt, whereas CH_3I emissions are enhanced in the subtropical gyre regions. The seasonal variation of the global climatological flux (9-21 %) of the three compounds is larger than the inter-annual variability, which is generally less than 5 %. Compared to earlier studies, our global fluxes are at the lower end of estimates, especially for CHBr_3 . A possible explanation might be the underrepresentation of coastal emissions and of extreme events, which cannot be resolved for the $1^\circ \times 1^\circ$ resolution. Additionally, a sensitivity study which demonstrates the changes of each input parameter (U, SST, SLP, SSS) onto the VSLs air-sea flux calculation, shows that the parameters U and SST have the strongest influence on the determination of global halogenated emissions. The results show that marginal changes of the input parameters can lead to variation of the global flux estimate.

3. Contribution of CHBr_3 and CH_2Br_2 to the stratospheric bromine (Br_y) budget based on global emission inventories – a sensitivity study

The global bottom-up estimates derived from the first manuscript (Ziska et al., 2013) improves the quantification of the impact of brominated VSLs on the stratospheric Br_y budget.

Three different top-down estimates and one bottom-up emission scenario were evaluated in a model sensitivity study using a combination of long-term ground-based observations and aircraft

observations. Further, the different emission estimates were used as input layer for a CTM to simulate stratospheric bromine loading.

The global emission inventories of CHBr_3 and CH_2Br_2 vary significantly. Zonal averages of the four global emission source strengths revealed that Ziska et al. (2013) show enhanced emission values in the Arctic (for CHBr_3) and Antarctic (for CH_2Br_2) which are not seen in the three top-down emissions. Ziska et al. (2013) is at the lower end of published halocarbon emission estimates and shows the best agreement with CHBr_3 atmospheric surface observations in the tropics, but a general overestimation of CH_2Br_2 .

The aircraft measurements in the tropical Western Pacific, which is identified as a region where VLSL emissions can be efficiently transported to the TTL (Aschmann et al., 2009), were well reproduced by the model using the emission inventory of Ziska et al. (2013). Opposed to two of the other estimates, the Ziska et al. (2013) included local measurements in that area. This indicates the need for more observations of VLSL in the ocean and atmosphere at a finer spatial grid in order to improve current regional VLSL emission estimates.

Furthermore, an optimized estimate of stratospheric bromine contribution of ~ 4 ppt was created as a combination of the CHBr_3 sea-to-air fluxes from Ziska et al. (2013) and top down CH_2Br_2 emissions derived from Liang et al. (2010). The bottom-up Ziska et al. (2013) estimate is the current most detailed global emission estimate and serves as an important basis for the model community.

4. Calculation of iodine transport from the tropical surface ocean into the stratosphere based on global CH_3I sea-to-air fluxes

For the first time, the stratospheric iodine loading from CH_3I was modeled using the Lagrangian model FLEXPART. A major uncertainty for the quantification of the stratospheric iodine budget is the insufficient knowledge of the amount of direct CH_3I entrainment into the stratosphere and the atmospheric lifetime of inorganic iodine. The results of the third manuscript indicate that iodine in form of CH_3I is not transported in significant amounts into the stratosphere on a global scale but on a regional scale. Using the global (tropical) emission inventory of Ziska et al. (2013) (30°N – 30°S), the averaged CH_3I entrainment above 17 km height is about 0.04 ppt which is in agreement to the estimates of Montzka and Reimann (2011). However, strong vertical transport combined with enhanced local emission peaks which were found in the West Pacific could lead to a significant CH_3I entrainment of ~ 0.6 ppt. Ziska et al. (2013) do not include terrestrial sources, hence the ocean is the single source of CH_3I . This study identified the need for high-reaching aircraft campaigns in the West Pacific.

5. Estimating CHBr_3 , CH_2Br_2 and CH_3I emissions in a future changing environment

For the first time the effect of climate change on the oceanic emissions of CHBr_3 , CH_2Br_2 and CH_3I was analyzed. Based on the global oceanic and atmospheric concentrations from Ziska et al. (2013) and the future modeled output fields of U, SST, SLP and SSS from three CMIP 5 (fifth phase of the Climate Model Intercomparison Project) models past and future sea-to-air fluxes of CHBr_3 , CH_2Br_2 and CH_3I were determined. Therefore, the output fields from the historical scenario and the RCP scenarios 2.6 and 8.5 of the models CESM1-CAM5, MPI-ESM-LR and HadGEM2-ES for the time period 1979-2100 were compared and used for emission calculations. The modeled sea-to-air fluxes generally increase during the 21st century. The global emissions of the halogenated compounds rise between 9.0 % and 29.4 % for the RCP 2.6, respectively 8.5 scenarios for CHBr_3 between the time periods 1986-2005 and 2081-2100. The future CH_2Br_2 emissions increase from 6.4 % to 23.3 % and from 1.5% to 5.5 % for CH_3I . The emissions based on the historical model runs of CESM1-CAM5 and MPI-ESM-LR (1979-2005) agree well with the emissions based on ERA-Interim data, while emissions based on the HadGEM2-ES model are much lower. The different temporal resolutions of input parameters of the ERA-Interim (6 hourly averaged) and the CMIP 5 models (monthly averaged) might be the reason for this discrepancy. Scaling the ERA-Interim input parameters from 6 hourly to monthly averages reduces the global halogenated emissions by about 11 %. Consequently, the emission estimates based on monthly mean meteorological fields from the three models are likely about 11 % too low. Compared to the ERA-Interim data set, the MPI-ESM-LR and CESM1-CAM5 models show higher global and regional winds, a fact which seems to compensate the bias introduced by the monthly resolution of the input fields. For eliminating the averaging bias, a higher temporal resolution of model output fields is needed. The role of oceanic productivity under ongoing environmental changes is not considered in the future emission estimations.

6. Determination of future impact of CHBr_3 on stratospheric ozone

Historical (1979-2005) and future (2006-2100) CHBr_3 ODP-weighted emissions were calculated based on the meteorological surface parameters and convective mass flux from the CESM1-CAM5, RCP 8.5 runs. The historical CHBr_3 ODP-weighted emissions showed an offset of 12 % to the ERA-Interim derived ODP, but gave similar inter-annual variation for some years. In the scenario, the CHBr_3 ODP-emissions increased steadily until 2100 by 80 %. The increase is driven by the increase of global CHBr_3 emissions and an increase of convective transport. Compared to longer-lived substances (e.g. CCl_4) CHBr_3 emissions can be expected to have a larger impact on stratospheric ozone in the future. While changes in tropospheric and stratospheric chemistry, stratospheric residence time and changes in oceanic sources are neglected, earlier study results showed that future climate

differences are expected to be mostly related to changes in transport rather than changes in the chemistry.

With the obtained knowledge of the manuscripts, Figure III–12 can be filled with additional information (red highlighted).

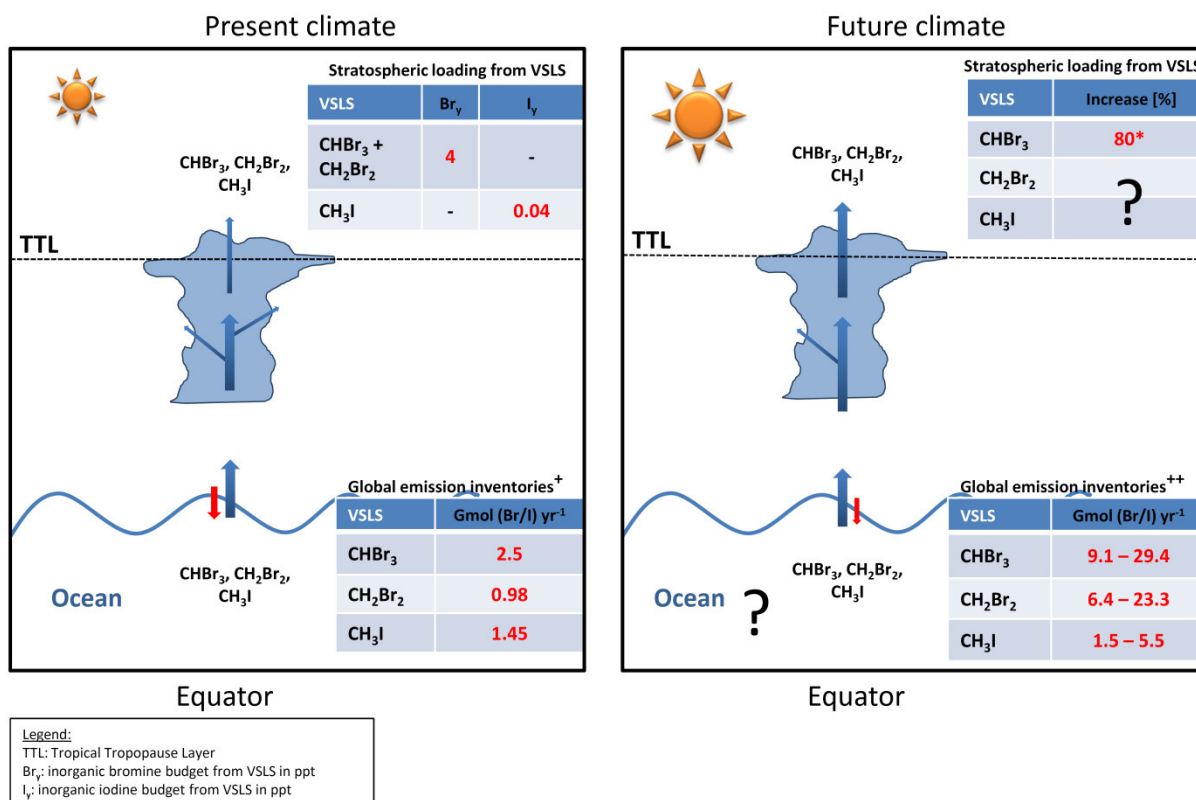


Figure V – 2. Same schemata as in Figure III–12 updated with the findings of the five manuscripts. Each result is afflicted with a certain uncertainty. Some question marks still exist and will be discussed in the text.

⁺Total (including sources and sinks) global emission estimates based on the OLS regression technique

⁺⁺Percentage increases of future global VSLs emission from the year 1986–2005 to 2081–2100. The first number illustrates the low scenario and the second the extreme scenario. The numbers are an average of the three future model results.

*Ozone depleting emissions of CHBr₃ increase steadily until 2100 by nearly 80% of the 2006-2015 (mean value).

The results of the manuscripts have closed gaps in the existing knowledge about past and future VSLs emission estimates as well as their stratospheric bromine and iodine loading, but there are still open questions, e.g. in the future stratospheric impact of CH₂Br₂ and CH₃I (Figure V–2). The findings illustrated that the uncertainties in the results of the research tasks are limited by the accuracy of the emission scenarios. The bottom-up estimates from Ziska et al. (2013) are a respectable and useful beginning for global VSLs emission estimates, but the following next steps have to be done to improve the global emission scenarios and their impact on stratospheric bromine and iodine loading in a past and future environment:

- Migration of the MS EXCEL based HalOcat database to a SQL database for easier usage
- Increasing the temporal (monthly) and spatial resolution (especially in the polar zones) of the dataset by collecting more measurements into the HalOcat database in order to update the

bottom-up emission estimates and to determine seasonal climatologically concentration fields

- Identification of a robust criterion for quality check and data selection of the HalOcat data as well as an overall quality and intercalibration control
- Reducing the grid size of the inventories to represent the coastline better
- Including the changes of oceanic productivity under ongoing environmental changes in the future emission estimations

The VSLs emissions and the global ocean concentration and atmospheric mixing ratio maps (determined in the first manuscript (Ziska et al., 2013)) are used in further calculations in different institutes and working groups (e.g. Max-Planck Institute in Hamburg, Germany; Karlsruher Institute for Technology, Germany; Helmholtz Centre for Ocean Research, GEOMAR in Kiel, Germany; University of Leeds, Great Britain; University of York, Great Britain). Future cooperation's will focus on the comparison of the projected future VSLs emission scenarios and other models, currently under development, including changes in ocean production and their future impact on VSLs concentrations and emissions and the impact on ozone destruction in the stratosphere. It is further necessary to reduce the uncertainties in process understanding such as decoding the production and destruction pathways for the three VSLs in the ocean. This should be done by well-planned in situ studies in different environments, thorough evaluation of existing cruise data and developing incubation experiments. Further, the knowledge (technical implementation) and understanding of the air-sea gas exchange parameterization for halogenated compounds have to be progressed. Time series including depth profiles in different ocean basins and productive areas, atmospheric measurements (aircraft campaigns) as well as additional parameters (Chl *a*, SST, U, SLP, SSS, pH, pigments, phytoplankton groups, production rates, radio sounds) will help to understand the variability of the ocean and its emission of VSLs to the atmosphere.

REFERENCES

VII. References

Abrahamsson, K., Ekdahl, A., Collén, J., and Pedersén, M.: Formation and distribution of halogenated volatile organics in sea water, in: *Naturally-Produced Organohalogen Environment & Chemistry 1*, Springer Netherlands, pp 317-326, 1995.

Abrahamsson, K., Bertilsson, S., Chierici, M., Fransson, A., Froneman, P. W., Loren, A., and Pakhomov, E. A.: Variations of biochemical parameters along a transect in the Southern Ocean, with special emphasis on volatile halogenated organic compounds, *Deep-Sea Res. Part II-Top. Stud. Oceanogr.*, 51, 2745-2756, 10.1016/j.dsr2.2004.09.004, 2004a.

Abrahamsson, K., Lorén, A., Wulff, A., and Wangberg, S. A.: Air-sea exchange of halocarbons: the influence of diurnal and regional variations and distribution of pigments, *Deep-Sea Res. Part II-Top. Stud. Oceanogr.*, 51, 2789-2805, 10.1016/j.dsr2.2004.09.005, 2004b.

Amachi, S., Kamagata, Y., Kanagawa, T., and Muramatsu, Y.: Bacteria Mediate Methylation of Iodine in Marine and Terrestrial Environments, *Applied and Environmental Microbiology*, 67, 2718-2722, 10.1128/aem.67.6.2718-2722.2001, 2001.

Aschmann, J., Sinnhuber, B. M., Atlas, E. L., and Schauffler, S. M.: Modeling the transport of very short-lived substances into the tropical upper troposphere and lower stratosphere, *Atmos. Chem. Phys.*, 9, 9237-9247, 2009.

Aschmann, J., Sinnhuber, B. M., Chipperfield, M. P., and Hossaini, R.: Impact of deep convection and dehydration on bromine loading in the upper troposphere and lower stratosphere, *Atmos. Chem. Phys.*, 11, 2671-2687, 10.5194/acp-11-2671-2011, 2011.

Aschmann, J., and Sinnhuber, B. M.: Contribution of very short-lived substances to stratospheric bromine loading: uncertainties and constraints, *Atmos. Chem. Phys.*, 13, 1203-1219, 10.5194/acp-13-1203-2013, 2013.

Atlas, E., Pollock, W., Greenberg, J., Heidt, L., and Thompson, A. M.: Alkyl Nitrates, Nonmethane Hydrocarbons, and Halocarbon Gases over the Equatorial Pacific-Ocean during SAGA-3, *J. Geophys. Res.-Atmos.*, 98, 16933-16947, 1993.

Barrie, L. A., Bottenheim, J. W., Schnell, R. C., Crutzen, P. J., and Rasmussen, R. A.: OZONE DESTRUCTION AND PHOTOCHEMICAL-REACTIONS AT POLAR SUNRISE IN THE LOWER ARCTIC ATMOSPHERE, *Nature*, 334, 138-141, 10.1038/334138a0, 1988.

Batjer, K., Gabel, B., Koschorrek, M., Lahl, U., Lierse, K. W., Stachel, B., and Thiemann, W.: DRINKING-WATER IN BREMEN - TRIHALOMETHANES AND SOCIAL COSTS - A CASE-STUDY OF BROMOFORM FORMATION DURING CHLORINATION OF RIVER WATER HIGHLY CONTAMINATED WITH BROMIDE IONS, *Science of the Total Environment*, 14, 287-291, 10.1016/0048-9697(80)90030-3, 1980.

Beech, J. A., Diaz, R., Ordaz, C., and Palomeque, B.: NITRATES, CHLORATES AND TRIHALOMETHANES IN SWIMMING POOL WATER, *American Journal of Public Health*, 70, 79-82, 10.2105/ajph.70.1.79, 1980.

Behrenfeld, M. J., O'Malley, R. T., Siegel, D. A., McClain, C. R., Sarmiento, J. L., Feldman, G. C., Milligan, A. J., Falkowski, P. G., Letelier, R. M., and Boss, E. S.: Climate-driven trends in contemporary ocean productivity, *Nature*, 444, 752-755, 10.1038/nature05317, 2006.

- Beissner, R. S., Guilford, W. J., Coates, R. M., and Hager, L. P.: SYNTHESIS OF BROMINATED HEPTANONES AND BROMOFORM BY A BROMOPEROXIDASE OF MARINE ORIGIN, *Biochemistry*, 20, 3724-3731, 10.1021/bi00516a009, 1981.
- Bell, N., Hsu, L., Jacob, D. J., Schultz, M. G., Blake, D. R., Butler, J. H., King, D. B., Lobert, J. M., and Maier-Reimer, E.: Methyl iodide: Atmospheric budget and use as a tracer of marine convection in global models, *J. Geophys. Res.-Atmos.*, 107, 434010.1029/2001jd001151, 2002.
- Betterton, E. A., Arnold, R. G., Kuhler, R. J., and Santo, G. A.: Reductive dehalogenation of bromoform in aqueous solution, *Environmental Health Perspectives*, 103, 89-91, 10.2307/3432487, 1995.
- Bridgeman, C. H., J. A. Pyle, and D. E. Shallcross (2000), A three-dimensional model calculation of the ozone depletion potential of 1-bromopropane (1-C₃H₇Br), *J. Geophys. Res.*, 105, 26,493– 26,502.
- Bopp, L., Resplandy, L., Orr, J. C., Doney, S. C., Dunne, J. P., Gehlen, M., Halloran, P., Heinze, C., Ilyina, T., Seferian, R., Tjiputra, J., and Vichi, M.: Multiple stressors of ocean ecosystems in the 21st century: projections with CMIP5 models, *Biogeosciences*, 10, 6225-6245, 10.5194/bg-10-6225-2013, 2013.
- Bouwer, E. J., Rittmann, B. E., and McCarty, P. L.: Anaerobic degradation of halogenated 1- and 2-carbon organic compounds, *Environ. Sci. Technol.*, 15, 596-599, 10.1021/es00087a012, 1981.
- Brownell, D. K., Moore, R. M., and Cullen, J. J.: Production of methyl halides by *Prochlorococcus* and *Synechococcus*, *Glob. Biogeochem. Cycle*, 24, 10.1029/2009gb003671, 2010.
- Butler, J. H., King, D. B., Lobert, J. M., Montzka, S. A., Yvon-Lewis, S. A., Hall, B. D., Warwick, N. J., Mondeel, D. J., Aydin, M., and Elkins, J. W.: Oceanic distributions and emissions of short-lived halocarbons, *Glob. Biogeochem. Cycle*, 21, Gb102310.1029/2006gb002732, 2007.
- Carpenter, L. J., Sturges, W. T., Penkett, S. A., Liss, P. S., Alicke, B., Hebestreit, K., and Platt, U.: Short-lived alkyl iodides and bromides at Mace Head, Ireland: Links to biogenic sources and halogen oxide production, *J. Geophys. Res.-Atmos.*, 104, 1679-1689, 1999.
- Carpenter, L. J., and Liss, P. S.: On temperate sources of bromoform and other reactive organic bromine gases, *J. Geophys. Res.-Atmos.*, 105, 20539-20547, 2000.
- Carpenter, L. J., Liss, P. S., and Penkett, S. A.: Marine organohalogens in the atmosphere over the Atlantic and Southern Oceans, *J. Geophys. Res.-Atmos.*, 108, 425610.1029/2002jd002769, 2003.
- Chameides, W. L., and Davis, D. D.: IODINE - ITS POSSIBLE ROLE IN TROPOSPHERIC PHOTOCHEMISTRY, *Journal of Geophysical Research-Oceans and Atmospheres*, 85, 7383-7398, 10.1029/JC085iC12p07383, 1980.
- Chuck, A. L., Turner, S. M., and Liss, P. S.: Oceanic distributions and air-sea fluxes of biogenic halocarbons in the open ocean, *J. Geophys. Res.-Oceans*, 110, C1002210.1029/2004jc002741, 2005.
- Cicerone, R. J., Heidt, L. E., and Pollock, W. H.: MEASUREMENTS OF ATMOSPHERIC METHYL-BROMIDE AND BROMOFORM, *J. Geophys. Res.-Atmos.*, 93, 3745-3749, 10.1029/JD093iD04p03745, 1988.
- Class, T., and Ballschmiter, K.: Chemistry of Organic Traces in Air VIII: Sources and Distribution of Bromo- and Bromochloromethanes in Marine Air and Surfacewater of the Atlantic Ocean, *J. Atmos. Chem.*, 6, 35-46, 1988.

Collins, M., R. Knutti, J. Arblaster, J.-L. Dufresne, T. Fichet, P. Friedlingstein, X. Gao, W.J. Gutowski, T. Johns, G. Krinner, M. Shongwe, C. Tebaldi, A.J. Weaver and M. Wehner, 2013: Long-term Climate Change: Projections, Commitments and Irreversibility. In: *Climate Change 2013: The Physical Science Basis. Contribution of Working Group I to the Fifth Assessment Report of the Intergovernmental Panel on Climate Change* [Stocker, T.F., D. Qin, G.-K. Plattner, M. Tignor, S.K. Allen, J. Boschung, A. Nauels, Y. Xia, V. Bex and P.M. Midgley (eds.)]. Cambridge University Press, Cambridge, United Kingdom and New York, NY, USA.

Cubasch, U., D. Wuebbles, D. Chen, M.C. Facchini, D. Frame, N. Mahowald, and J.-G. Winther, 2013: Introduction. In: *Climate Change 2013: The Physical Science Basis. Contribution of Working Group I to the Fifth Assessment Report of the Intergovernmental Panel on Climate Change* [Stocker, T.F., D. Qin, G.-K. Plattner, M. Tignor, S.K. Allen, J. Boschung, A. Nauels, Y. Xia, V. Bex and P.M. Midgley (eds.)]. Cambridge University Press, Cambridge, United Kingdom and New York, NY, USA

Daniel, J. S., Solomon, S., Portmann, R. W., and Garcia, R. R.: Stratospheric ozone destruction: The importance of bromine relative to chlorine, *J. Geophys. Res.-Atmos.*, 104, 23871-23880, 10.1029/1999jd900381, 1999.

Dessens, O., Zeng, G., Warwick, N., and Pyle, J.: Short-lived bromine compounds in the lower stratosphere; impact of climate change on ozone, *Atmospheric Science Letters*, 10, 201-206, 10.1002/asl.236, 2009.

Devoys, C. G. N.: ANAEROBIC METABOLISM IN SUBLITTORAL LIVING MYTILUS GALLOPROVINCIALIS IN THE MEDITERRANEAN .1. PARTIAL ADAPTATION OF ANAEROBIC ENERGY-METABOLISM, *Netherlands Journal of Sea Research*, 13, 192-202, 10.1016/0077-7579(79)90002-4, 1979.

Dix, B., Baidar, S., Bresch, J. F., Hall, S. R., Schmidt, K. S., Wang, S., and Volkamer, R.: Detection of iodine monoxide in the tropical free troposphere, *P. Natl. Acad. Sci. USA*, 110, 2035–2040, doi:10.1073/pnas.1212386110, 2013

Donner, L. J., Horowitz, L. W., Fiore, A. M., Seman, C. J., Blake, D. R., and Blake, N. J.: Transport of radon-222 and methyl iodide by deep convection in the GFDL Global Atmospheric Model AM2, *J. Geophys. Res.-Atmos.*, 112, 10.1029/2006jd007548, 2007.

Dorf, M., Butler, J. H., Butz, A., Camy-Peyret, C., Chipperfield, M. P., Kritten, L., Montzka, S. A., Simmes, B., Weidner, F., and Pfeilsticker, K.: Long-term observations of stratospheric bromine reveal slow down in growth, *Geophys. Res. Lett.*, 33, 10.1029/2006gl027714, 2006.

Dvortsov, V. L., Geller, M. A., Solomon, S., Schauffler, S. M., Atlas, E. L., and Blake, D. R.: Rethinking reactive halogen budgets in the midlatitude lower stratosphere, *Geophys. Res. Lett.*, 26, 1699-1702, 10.1029/1999gl900309, 1999.

Dyrssen, D., and Fogelqvist, E.: BROMOFORM CONCENTRATIONS OF THE ARCTIC OCEAN IN THE SVALBARD AREA, *Oceanol. Acta*, 4, 313-317, 1981.

Ekdahl, A., Pedersén, M., and Abrahamsson, K.: A study of the diurnal variation of biogenic volatile halocarbons, *Mar. Chem.*, 63, 1-8, 1998.

Fahey, D.W., and M.I. Hegglin (Coordinating Lead Authors), *Twenty Questions and Answers About the Ozone Layer: 2010 Update, Scientific Assessment of Ozone Depletion: 2010*, 72 pp., World Meteorological Organization, Geneva, Switzerland, 2011. Reprinted from *Scientific Assessment of*

Ozone Depletion: 2010, Global Ozone Research and Monitoring Project-Report No. 52, 516 pp., World Meteorological Organization, Geneva, Switzerland, 2011.

Fenical, W.: Natural halogenated organics, in: *Marine Organic Chemistry*, edited by: Duursma, E. K., and Dawson, R., Elsevier, New York, 375-393, 1981.

Finlayson-Pitts, B. J.: Halogens in the Troposphere, *Analytical Chemistry*, 82, 770-776, 10.1021/ac901478p, 2010.

Fischer, R. G., Kastler, J., and Ballschmiter, K.: Levels and pattern of alkyl nitrates, multifunctional alkyl nitrates, and halocarbons in the air over the Atlantic Ocean, *J. Geophys. Res.-Atmos.*, 105,14473-14494, 2000.

Fueglistaler, S., Dessler, A. E., Dunkerton, T. J., Folkins, I., Fu, Q., and Mote, P. W.: TROPICAL TROPOPAUSE LAYER, *Rev. Geophys.*, 47, 10.1029/2008rg000267, 2009a.

Fuhlbrügge, S., Krüger, K., Quack, B., Atlas, E. L., Hepach, H., and Ziska, F.: Impact of the marine atmospheric boundary layer on VLS abundances in the eastern tropical and subtropical North Atlantic Ocean, *Atmos. Chem. Phys.*, 13, 6345-6357, 10.5194/acp-13-6345-2013, 2013.

Garbe, C., Voss, B., and Stapf, J.: Plenoptic particle streak velocimetry (ppsv): 3d3c fluid flow measurement from light fields with a single plenoptic camera, 16th international symposium on applications of laser techniques to fluid mechanics, Instituto Superior Técnico, Lisbon, 2012, 1-12,

Garbe, C. S., Spies, H., and Jähne, B.: Estimation of surface flow and net heat flux from infrared image sequences, *Journal of Mathematical Imaging and Vision*, 19, 159-174, 2003.

Garbe, C. S., Schimpf, U., and Jähne, B.: A surface renewal model to analyze infrared image sequences of the ocean surface for the study of air-sea heat and gas exchange, *Journal of Geophysical Research: Oceans (1978–2012)*, 109, 2004.

Garbe, C. S., Rutgersson, A., Boutin, J., de Leeuw, G., Delille, B., Fairall, C. W., Gruber, N., Hare, J. E., Ho, D. T., Johnson, M. T., Nightingale, P. D., Pettersson, H., Piskozub, J., Sahlée, E., Tsai, W.-T., Ward, B., Woolf, D. K., and Zappa, C. J.: Transfer Across the Air-Sea Interface, in: *Ocean-Atmosphere Interactions of Gases and Particles*, edited by: Liss, P. S., and Johnson, M. T., Springer Earth System Sciences, Norwhich, UK, 55-112, 2014.

Geen, C. E.: Selected marine sources and sinks of bromoform and other low molecular weight organobromines, PhD, Dalhousie University, Halifax, Halifax, Nova Scotia, 1992.

Gettelman, A., Lauritzen, P. H., Park, M., and Kay, J. E.: Processes regulating short-lived species in the tropical tropopause layer, *J. Geophys. Res.-Atmos.*, 114, 10.1029/2009jd011785, 2009.

Goodwin, K. D., Lidstrom, M. E., and Oremland, R. S.: Marine Bacterial Degradation of Brominated Methanes, *Environ. Sci. Technol.*, 31, 3188-3192, 10.1021/es970165g, 1997b.

Granfors, A., Andersson, M., Chierici, M., Fransson, A., Gardfeldt, K., Torstensson, A., Wulff, A., and Abrahamsson, K.: Biogenic halocarbons in young Arctic sea ice and frost flowers, *Mar. Chem.*, 155, 124-134, 10.1016/j.marchem.2013.06.002, 2013.

- Gschwend, P. M., Macfarlane, J. K., and Newman, K. A.: Volatile halogenated organic compounds released to seawater from temperate marine macroalgae, *Science*, 227, 1033-1035, 10.1126/science.227.4690.1033, 1985.
- Happell, J. D., and Wallace, D. W. R.: Methyl iodide in the Greenland/Norwegian Seas and the tropical Atlantic Ocean: Evidence for photochemical production, *Geophys. Res. Lett.*, 23, 2105-2108, 10.1029/96gl01764, 1996.
- Haußecker, H., and Jähne, B.: In situ measurements of the air-sea gas transfer rate during the MBL/CoOP west coast experiment, *Air-Water Gas Transfer*, AEON Verlag & Studio, Hanau, Germany, 775-784, 1995.
- Hayduk, W., and Laudie, H.: PREDICTION OF DIFFUSION-COEFFICIENTS FOR NONELECTROLYTES IN DILUTE AQUEOUS-SOLUTIONS, *Aiche J.*, 20, 611-615, 10.1002/aic.690200329, 1974.
- Hepach, H., Quack, B., Ziska, F., Fuhlbrügge, S., Atlas, E. L., Krüger, K., Peecken, I., and Wallace, D. W. R.: Drivers of diel and regional variations of halocarbon emissions from the tropical North East Atlantic, *Atmos. Chem. Phys.*, 14, 1255-1275, 10.5194/acp-14-1255-2014, 2014.
- Hewson, W. D., and Hager, L. P.: BROMOPEROXIDASES AND HALOGENATED LIPIDS IN MARINE-ALGAE, *J. Phycol.*, 16, 340-345, 1980.
- Hill, V. L., and Manley, S. L.: Release of reactive bromine and iodine from diatoms and its possible role in halogen transfer in polar and tropical oceans, *Limnol. Oceanogr.*, 54, 812-822, 10.4319/lo.2009.54.3.0812, 2009.
- Ho, D. T., Sabine, C. L., Hebert, D., Ullman, D. S., Wanninkhof, R., Hamme, R. C., Strutton, P. G., Hales, B., Edson, J. B., and Hargreaves, B. R.: Southern Ocean Gas Exchange Experiment: Setting the stage, *J. Geophys. Res.-Oceans*, 116, 10.1029/2010jc006852, 2011.
- Honninger, G., and Platt, U.: Observations of BrO and its vertical distribution during surface ozone depletion at Alert, *Atmos. Environ.*, 36, 2481-2489, 10.1016/s1352-2310(02)00104-8, 2002.
- Hopkins, F. E., Kimmance, S. A., Stephens, J. A., Bellerby, R. G. J., Brussaard, C. P. D., Czerny, J., Schulz, K. G., and Archer, S. D.: Response of halocarbons to ocean acidification in the Arctic, *Biogeosciences*, 10, 2331-2345, 10.5194/bg-10-2331-2013, 2013.
- Hossaini, R., Chipperfield, M. P., Monge-Sanz, B. M., Richards, N. A. D., Atlas, E., and Blake, D. R.: Bromoform and dibromomethane in the tropics: a 3-D model study of chemistry and transport, *Atmos. Chem. Phys.*, 10, 719-735, 2010.
- Hossaini, R., Chipperfield, M. P., Feng, W., Breider, T. J., Atlas, E., Montzka, S. A., Miller, B. R., Moore, F., and Elkins, J.: The contribution of natural and anthropogenic very short-lived species to stratospheric bromine, *Atmos. Chem. Phys.*, 12, 371-380, 10.5194/acp-12-371-2012, 2012a.
- Hossaini, R., Chipperfield, M. P., Dhomse, S., Ordonez, C., Saiz-Lopez, A., Abraham, N. L., Archibald, A., Braesicke, P., Telford, P., Warwick, N., Yang, X., and Pyle, J.: Modelling future changes to the stratospheric source gas injection of biogenic bromocarbons, *Geophys. Res. Lett.*, 39, 10.1029/2012gl053401, 2012b.
- Hossaini, R., Mantle, H., Chipperfield, M. P., Montzka, S. A., Hamer, P., Ziska, E., Quack, B., Krueger, K., Tegtmeier, S., Atlas, E., Sala, S., Engel, A., Boenisch, H., Keber, T., Oram, D., Mills, G., Ordonez, C.,

Saiz-Lopez, A., Warwick, N., Liang, Q., Feng, W., Moore, E., Miller, B. R., Marecal, V., Richards, N. A. D., Dorf, M., and Pfeilsticker, K.: Evaluating global emission inventories of biogenic bromocarbons, *Atmos. Chem. Phys.*, 13, 11819-11838, 10.5194/acp-13-11819-2013, 2013.

Hughes, C., Franklin, D. J., and Malin, G.: Iodomethane production by two important marine cyanobacteria: *Prochlorococcus marinus* (CCMP 2389) and *Synechococcus* sp (CCMP 2370), *Mar. Chem.*, 125, 19-25, 10.1016/j.marchem.2011.01.007, 2011.

Hunter, M., Smith, P. A., and Case, R. M.: THE DEPENDENCE OF FLUID SECRETION BY MANDIBULAR SALIVARY-GLAND AND PANCREAS ON EXTRACELLULAR CALCIUM, *Cell Calcium*, 4, 307-317, 10.1016/0143-4160(83)90007-6, 1983.

Jacob, Daniel (1999). *Introduction to Atmospheric Chemistry* (1st Edition ed.). Princeton University Press. pp. 75–85. ISBN 0-691-00185-5

Jenner, H. A., Taylor, C. J. L., vanDonk, M., and Khalanski, M.: Chlorination by-products in chlorinated cooling water of some European coastal power stations, *Mar. Environ. Res.*, 43, 279-293, 10.1016/s0141-1136(96)00091-8, 1997.

Khalil, M. A. K., R. M. Moore, D. B. Harper, J. M. Lorbert, D. J. Erickson, V. Koropalov, W. T. Sturges, and W. C. Keene, Natural emissions of chlorine-containing gases: Reactive Chlorine Emissions Inventory, *J. Geophys. Res.*, 104, 8333–8346, 1999

Karlsson, A., Theorin, M., and Abrahamsson, K.: Distribution, transport, and production of volatile halocarbons in the upper waters of the ice-covered high Arctic Ocean, *Glob. Biogeochem. Cycle*, 2012GB004519, 10.1002/2012gb004519, 2013.

Kerkweg, A., Jockel, P., Warwick, N., Gebhardt, S., Brenninkmeijer, C. A. M., and Lelieveld, J.: Consistent simulation of bromine chemistry from the marine boundary layer to the stratosphere - Part 2: Bromocarbons, *Atmos. Chem. Phys.*, 8, 5919-5939, 2008.

Kettle, A. J., Andreae, M. O., Amouroux, D., Andreae, T. W., Bates, T. S., Berresheim, H., Bingemer, H., Boniforti, R., Curran, M. A. J., DiTullio, G. R., Helas, G., Jones, G. B., Keller, M. D., Kiene, R. P., Leck, C., Lévassieur, M., Malin, G., Maspero, M., Matrai, P., McTaggart, A. R., Mihalopoulos, N., Nguyen, B. C., Novo, A., Putaud, J. P., Rapsomanikis, S., Roberts, G., Schebeske, G., Sharma, S., Simo, R., Staubes, R., Turner, S., and Uher, G.: A global database of sea surface dimethylsulfide (DMS) measurements and a procedure to predict sea surface DMS as a function of latitude, longitude, and month, *Glob. Biogeochem. Cycle*, 13, 399-444, 10.1029/1999gb900004, 1999.

Khalil, M. A. K., and Rasmussen, R. A.: Atmospheric methyl chloride, *Atmos. Environ.*, 33, 1305-1321, 10.1016/s1352-2310(98)00234-9, 1999.

Ko, M. K. W., and Poulet, G.: Very Short-Lived Halogen and Sulfur Substances, Chapter 2 in *Scientific Assessment of Ozone Depletion: 2002*, Global Ozone Research and Monitoring Project, World Meteorological Organization (WMO), Geneva, Report No. 47, 2002.

Krueger, K., Tegtmeier, S., and Rex, M.: Variability of residence time in the Tropical Tropopause Layer during Northern Hemisphere winter, *Atmos. Chem. Phys.*, 9, 6717-6725, 2009.

Lana, A., Bell, T. G., Simó, R., Vallina, S. M., Ballabrera-Poy, J., Kettle, A. J., Dachs, J., Bopp, L., Saltzman, E. S., Stefels, J., Johnson, J. E., and Liss, P. S.: An updated climatology of surface

dimethylsulfide concentrations and emission fluxes in the global ocean, *Glob. Biogeochem. Cycle*, 25, GB1004, 10.1029/2010gb003850, 2011.

Laternus, F.: Volatile halocarbons released from Arctic macroalgae, *Mar. Chem.*, 55, 359-366, 1996.
Law, K., Sturges, W., Blake, D., Blake, N., Burkholder, J., Butler, J., Cox, R., Haynes, P., Ko, M., and Kreher, K.: Halogenated very short-lived substances, Chapter 2 in: *Scientific Assessment of Ozone Depletion: 2006*, Global Ozone Research and Monitoring Project–Report No. 50, World Meteorological Organization, Geneva, Switzerland, 572, 2007.

Leggett, J., Pepper, W.J., Swart, Edmonds, R.J. J., Meira Filho, L.G., Mintzer, I., Wang, M.X. and Watson, J., 1992. "Emissions Scenarios for the IPCC: an Update", *Climate Change 1992: The Supplementary Report to The IPCC Scientific Assessment*, Cambridge University Press, UK, pp. 68-95

Liang, Q., Stolarski, R. S., Kawa, S. R., Nielsen, J. E., Douglass, A. R., Rodriguez, J. M., Blake, D. R., Atlas, E. L., and Ott, L. E.: Finding the missing stratospheric Br-y: a global modeling study of CHBr₃ and CH₂Br₂, *Atmos. Chem. Phys.*, 10, 2269-2286, 2010.

Lin, C. Y., and Manley, S. L.: Bromoform production from seawater treated with bromoperoxidase, *Limnol. Oceanogr.*, 57, 1857-1866, 10.4319/1o.2012.57.06.1857, 2012.

Liss, P. S., and Slater, P. G.: Flux of Gases Across Air-Sea Interface, *Nature*, 247, 181-184, 1974.

Liss, P. S., and Johnson, M. T.: *Ocean-Atmosphere Interactions of Gases and Particles*, Springer, 2014.

Longhurst, A., Sathyendranath, S., Platt, T., and Caverhill, C.: AN ESTIMATE OF GLOBAL PRIMARY PRODUCTION IN THE OCEAN FROM SATELLITE RADIOMETER DATA, *J. Plankton Res.*, 17, 1245-1271, 10.1093/plankt/17.6.1245, 1995.

Lovelock, J. E., Maggs, R. J., and Wade, R. J.: Halogenated Hydrocarbons in and over the Atlantic, *Nature*, 241, 194-196, 10.1038/241194a0, 1973.

Mabey, W., and Mill, T.: Critical-review of hydrolysis of organic compounds in water under environmental-conditions, *J. Phys. Chem. Ref. Data*, 7, 383-415, 1978.

Mackay, D., and W. Y. Shiu, A critical review of Henry's law constants for chemicals of environmental interest, *J. Phys. Ref. Data*, 10, 1175–1199, 1981.

Manley, S. L., and Dastoor, M. N.: METHYL HALIDE (CH₃X) PRODUCTION FROM THE GIANT-KELP, MACROCYSTIS, AND ESTIMATES OF GLOBAL CH₃X PRODUCTION BY KELP, *Limnol. Oceanogr.*, 32, 709-715, 1987.

Manley, S. L., and Dastoor, M. N.: Methyl-Iodide (CH₃I) production by kelp and associated microbes, *Mar. Biol.*, 98, 477-482, 1988.

Manley, S. L., Goodwin, K., and North, W. J.: Laboratory production of bromoform, methylene bromide, and methyl-iodide by macroalgae and distribution in nearshore southern California waters, *Limnol. Oceanogr.*, 37, 1652-1659, 1992.

Manley, S. L.: The possible involvement of methylcobalamin in the production of methyl-iodide in the marine environment, *Mar. Chem.*, 46, 361-369, 10.1016/0304-4203(94)90032-9, 1994.

- Manley, S. L., and de la Cuesta, J. L.: Methyl iodide production from marine phytoplankton cultures, *Limnol. Oceanogr.*, 42, 142-147, 1997.
- Marandino, C. A., De Bruyn, W. J., Miller, S. D., and Saltzman, E. S.: Eddy correlation measurements of the air/sea flux of dimethylsulfide over the North Pacific Ocean, *J. Geophys. Res.-Atmos.*, 112, 10.1029/2006jd007293, 2007.
- McGillis, W. R., Edson, J. B., Hare, J. E., and Fairall, C. W.: Direct covariance air-sea CO₂ fluxes, *J. Geophys. Res.-Oceans*, 106, 16729-16745, 10.1029/2000jc000506, 2001.
- Miller, S., Marandino, C., de Bruyn, W., and Saltzman, E. S.: Air-sea gas exchange of CO₂ and DMS in the North Atlantic by eddy covariance, *Geophys. Res. Lett.*, 36, 10.1029/2009gl038907, 2009.
- Molina, M. J., and Rowland, F. S.: Stratospheric sink for chlorofluoromethanes - chlorine atomic-catalysed destruction of ozone, *Nature*, 249, 810-812, 10.1038/249810a0, 1974.
- Montzka, S. A., and Reimann, S.: Ozone-depleting substances and related chemicals, Chapter 1 in *Scientific Assessment of Ozone Depletion: 2010*, Global Ozone Research and Monitoring Project, World Meteorological Organization (WMO), Geneva, Report No. 52, 2011.
- Moore, R. M., and Zafiriou, O. C.: Photochemical production of methyl-iodide in seawater, *J. Geophys. Res.-Atmos.*, 99, 16415-16420, 10.1029/94jd00786, 1994.
- Moore, R. M., C. E. Geen, and V. K. Tait, Determination of Henry's law constants for a suite of naturally occurring halogenated methanes in seawater, *Chemosphere*, 30, 1183-1191, 1995a.
- Moore, R. M., Tokarczyk, R., Tait, V. K., Poulin, M., and Geen, C. E.: Marine phytoplankton as a natural source of volatile organohalogenes, in: *Naturally-Produced Organohalogenes*, edited by: Grimvall, A., and deLeer, E. W. B., Kluwer Academic Publishers, Dordrecht, 283-294, 1995b.
- Moore, R. M., Webb, M., Tokarczyk, R., and Wever, R.: Bromoperoxidase and iodoperoxidase enzymes and production of halogenated methanes in marine diatom cultures, *J. Geophys. Res.-Oceans*, 101, 20899-20908, 10.1029/96jc01248, 1996.
- Moore, R. M., and Groszko, W.: Methyl iodide distribution in the ocean and fluxes to the atmosphere, *J. Geophys. Res.-Oceans*, 104, 11163-11171, 10.1029/1998jc900073, 1999.
- Mtolera, M. S. P., Collén, J., Pedersén, M., Ekdahl, A., Abrahamsson, K., and Semesj, A. K.: Stress-induced production of volatile halogenated organic compounds in *Eucheuma denticulatum* (Rhodophyta) caused by elevated pH and high light intensities, *Eur. J. Phycol.*, 31, 89-95, 10.1080/09670269600651241, 1996.
- Nielsen, J. E., and A. R. Douglass (2001), A simulation of bromoform's contribution to stratospheric bromine, *J. Geophys. Res.*, 106, 8089-8100.
- Nakicenovic, N., Alcamo, J., Davis, G., de Vries, B., Fenhann, J., Gaffin, S., Gregory, K., Grübler, A., Jung, T. Y., Kram, T., La Rovere, E. L., Michaelis, L., Mori, S., Morita, T., Pepper, W., Pitcher, H., Price, L., Riahi, K., Roehrl, A., Rogner, H. H., Sankovski, A., Schlesinger, M., Shukla, P., Smith, S., Swart, R., van Rooijen, S., Victor, N., and Dadi, Z.: *Special Report on Emissions Scenarios. A Special Report of Working Group III of the Intergovernmental Panel on Climate Change*, Cambridge University Press: Cambridge, 599 pp., 2000

- Nightingale, P. D. 1991. *Low molecular weight halocarbons in seawater*. PhD Thesis. U. East Anglia, Norwich, UK
- Nightingale, P. D., Malin, G., and Liss, P. S.: Production of chloroform and other low-molecular-weight halocarbons by some species of macroalgae *Limnol. Oceanogr.*, 40, 680-689, 1995.
- Nightingale, P. D., Malin, G., Law, C. S., Watson, A. J., Liss, P. S., Liddicoat, M. I., Boutin, J., and Upstill-Goddard, R. C.: In situ evaluation of air-sea gas exchange parameterizations using novel conservative and volatile tracers, *Glob. Biogeochem. Cycle*, 14, 373-387, 10.1029/1999gb900091, 2000.
- O'Brien, L. M., Harris, N. R. P., Robinson, A. D., Gostlow, B., Warwick, N., Yang, X., and Pyle, J. A.: Bromocarbons in the tropical marine boundary layer at the Cape Verde Observatory - measurements and modelling, *Atmos. Chem. Phys.*, 9, 9083-9099, 10.5194/acp-9-9083-2009, 2009.
- Oram, D. E., and Penkett, S. A.: OBSERVATIONS IN EASTERN ENGLAND OF ELEVATED METHYL-IODIDE CONCENTRATIONS IN AIR OF ATLANTIC ORIGIN, *Atmos. Environ.*, 28, 1159-1174, 10.1016/1352-2310(94)90293-3, 1994.
- Ordóñez, C., Lamarque, J. F., Tilmes, S., Kinnison, D. E., Atlas, E. L., Blake, D. R., Santos, G. S., Brasseur, G., and Saiz-Lopez, A.: Bromine and iodine chemistry in a global chemistry-climate model: description and evaluation of very short-lived oceanic sources, *Atmos. Chem. Phys.*, 12, 1423-1447, 10.5194/acp-12-1423-2012, 2012.
- Orlikowska, A., and Schulz-Bull, D. E.: Seasonal variations of volatile organic compounds in the coastal Baltic Sea, *Environ. Chem.*, 6, 495-507, 10.1071/en09107, 2009.
- Padhi, R. K., Sowmya, M., Mohanty, A. K., Bramha, S. N., and Satpathy, K. K.: Formation and Speciation Characteristics of Brominated Trihalomethanes in Seawater Chlorination, *Water Environment Research*, 84, 2003-2009, 10.2175/106143012x13415215906735, 2012.
- Palmer, C. J., and Reason, C. J.: Relationships of surface bromoform concentrations with mixed layer depth and salinity in the tropical oceans, *Glob. Biogeochem. Cycle*, 23, 10.1029/2008gb003338, 2009.
- Pedersen, M., Collen, J., Abrahamsson, K., and Ekdahl, A.: Production of halocarbons from seaweeds: An oxidative stress reaction?, *Sci. Mar.*, 60, 257-263, 1996.
- Peng, T. H., Broecker, W. S., Mathieu, G. G., and Li, Y. H.: RADON EVASION RATES IN THE ATLANTIC AND PACIFIC OCEANS AS DETERMINED DURING THE GEOSECS PROGRAM, *Journal of Geophysical Research-Oceans and Atmospheres*, 84, 2471-2486, 10.1029/JC084iC05p02471, 1979.
- Penkett, S. A., Jones, B. M. R., Rycroft, M. J., and Simmons, D. A.: AN INTERHEMISPHERIC COMPARISON OF THE CONCENTRATIONS OF BROMINE COMPOUNDS IN THE ATMOSPHERE, *Nature*, 318, 550-553, 10.1038/318550a0, 1985.
- Perry, D. L., Chuang, C. C., Jungclaus, G. A., and Warner, J. S.: Identification of organic compounds in industrial effluent discharges, U.S. Environmental Protection Agency, Columbus, Ohio, 1-72, 1979.
- Pyle, J. A., Warwick, N., Yang, X., Young, P. J., and Zeng, G.: Climate/chemistry feedbacks and biogenic emissions, *Philos. Trans. R. Soc. A-Math. Phys. Eng. Sci.*, 365, 1727-1740, 10.1098/rsta.2007.2041, 2007.
- Pyle, J. A., Ashfold, M. J., Harris, N. R. P., Robinson, A. D., Warwick, N. J., Carver, G. D., Gostlow, B., O'Brien, L. M., Manning, A. J., Phang, S. M., Yong, S. E., Leong, K. P., Ung, E. H., and Ong, S.:

- Bromoform in the tropical boundary layer of the Maritime Continent during OP3, *Atmos. Chem. Phys.*, 11, 529-542, 10.5194/acp-11-529-2011, 2011.
- Quack, B., and Wallace, D. W. R.: Air-sea flux of bromoform: Controls, rates, and implications, *Glob. Biogeochem. Cycle*, 17, 102310.1029/2002gb001890, 2003.
- Quack, B., Peeken, I., Petrick, G., and Nachtigall, K.: Oceanic distribution and sources of bromoform and dibromomethane in the Mauritanian upwelling, *J. Geophys. Res.-Oceans*, 112, C1000610.1029/2006jc003803, 2007a.
- Quack, B., Atlas, E., Petrick, G., and Wallace, D. W. R.: Bromoform and dibromomethane above the Mauritanian upwelling: Atmospheric distributions and oceanic emissions, *J. Geophys. Res.-Atmos.*, 112, D0931210.1029/2006jd007614, 2007b.
- Rasmussen, R. A., Khalil, M. A. K., Gunawardena, R., and Hoyt, S. D.: ATMOSPHERIC METHYL-IODIDE (CH₃I), *Journal of Geophysical Research-Oceans and Atmospheres*, 87, 3086-3090, 10.1029/JC087iC04p03086, 1982.
- Ricaud, P., Barret, B., Attie, J. L., Motte, E., Le Flochmoeen, E., Teyssedre, H., Peuch, V. H., Livesey, N., Lambert, A., and Pommereau, J. P.: Impact of land convection on troposphere-stratosphere exchange in the tropics, *Atmos. Chem. Phys.*, 7, 5639-5657, 2007.
- Richter, U., and Wallace, D. W. R.: Production of methyl iodide in the tropical Atlantic Ocean, *Geophys. Res. Lett.*, 31, L23s0310.1029/2004gl020779, 2004.
- Riebesell, U., Schulz, K. G., Bellerby, R. G. J., Botros, M., Fritsche, P., Meyerhoefer, M., Neill, C., Nondal, G., Oschlies, A., Wohlers, J., and Zoellner, E.: Enhanced biological carbon consumption in a high CO₂ ocean, *Nature*, 450, 545-U510, 10.1038/nature06267, 2007.
- Rook, J. J.: Formation of haloforms during chlorination of natural waters, *Water Treat. Exam.*, 23, 234-243, 1974.
- Saiz-Lopez, A., Lamarque, J. F., Kinnison, D. E., Tilmes, S., Ordonez, C., Orlando, J. J., Conley, A. J., Plane, J. M. C., Mahajan, A. S., Santos, G. S., Atlas, E. L., Blake, D. R., Sander, S. P., Schauffler, S., Thompson, A. M., and Brasseur, G.: Estimating the climate significance of halogen-driven ozone loss in the tropical marine troposphere, *Atmos. Chem. Phys.*, 12, 3939-3949, 10.5194/acp-12-3939-2012, 2012a.
- Saiz-Lopez, A., Plane, J. M. C., Baker, A. R., Carpenter, L. J., von Glasow, R., Martin, J. C. G., McFiggans, G., and Saunders, R. W.: Atmospheric Chemistry of Iodine, *Chem. Rev.*, 112, 1773-1804, 10.1021/cr200029u, 2012b.
- Saiz-Lopez, A., and von Glasow, R.: Reactive halogen chemistry in the troposphere, *Chem. Soc. Rev.*, 41, 6448-6472, 10.1039/c2cs35208g, 2012.
- Salawitch, R. J.: Atmospheric chemistry - Biogenic bromine, *Nature*, 439, 275-277, 10.1038/439275a, 2006.
- Schauffler, S. M., Atlas, E. L., Flocke, F., Lueb, R. A., Stroud, V., and Travnicek, W.: Measurements of bromine containing organic compounds at the tropical tropopause, *Geophys. Res. Lett.*, 25, 317-320, 1998.

- Sherwood, S. C., and Dessler, A. E.: Convective mixing near the tropical tropopause: Insights from seasonal variations, *Journal of the Atmospheric Sciences*, 60, 2674-2685, 10.1175/1520-0469(2003)060<2674:cmnttt>2.0.co;2, 2003.
- Siddiqui, K., and Loewen, M. R.: Phase-Averaged Flow Properties Beneath Microscale Breaking Waves, *Boundary-Layer Meteorology*, 134, 499-523, 10.1007/s10546-009-9447-6, 2010.
- Sinnhuber, B. M., and Folkins, I.: Estimating the contribution of bromoform to stratospheric bromine and its relation to dehydration in the tropical tropopause layer, *Atmos. Chem. Phys.*, 6, 4755-4761, 2006.
- Smythe-Wright, D., Boswell, S. M., Breithaupt, P., Davidson, R. D., Dimmer, C. H., and Diaz, L. B. E.: Methyl iodide production in the ocean: Implications for climate change, *Glob. Biogeochem. Cycle*, 20, Gb300310.1029/2005gb002642, 2006.
- Solomon, S., Garcia, R. R., and Ravishankara, A. R.: On the role of iodine in ozone depletion, *J. Geophys. Res.-Atmos.*, 99, 20491-20499, 10.1029/94jd02028, 1994.
- Staudinger, J., and Roberts, P. V.: A critical review of Henry's law constants for environmental applications, *Critical Reviews in Environmental Science and Technology*, 26, 205-297, 1996.
- Stemmler, I., Hense, I., Quack, B., and Maier-Reimer, E.: Methyl iodide production in the open ocean, *Biogeosciences*, 11, 4459-4476, 10.5194/bg-11-4459-2014, 2014.
- Stohl, A., Forster, C., Frank, A., Seibert, P., and Wotawa, G.: Technical note: The Lagrangian particle dispersion model FLEXPART version 6.2, *Atmos. Chem. Phys.*, 5, 2461-2474, 2005.
- Sturges, W. T., Cota, G. F., and Buckley, P. T.: Bromoform Emission from Arctic Ice Algae, *Nature*, 358, 660-662, 1992.
- Sweeney, C., Gloor, E., Jacobson, A. R., Key, R. M., McKinley, G., Sarmiento, J. L., and Wanninkhof, R.: Constraining global air-sea gas exchange for CO₂ with recent bomb C-14 measurements, *Glob. Biogeochem. Cycle*, 21, 10.1029/2006gb002784, 2007.
- Tait, V. K., and Moore, R. M.: METHYL-CHLORIDE (CH₃CL) PRODUCTION IN PHYTOPLANKTON CULTURES, *Limnol. Oceanogr.*, 40, 189-195, 1995.
- Takahashi, T., Sutherland, S. C., Wanninkhof, R., Sweeney, C., Feely, R. A., Chipman, D. W., Hales, B., Friederich, G., Chavez, F., and Sabine, C.: Climatological mean and decadal change in surface ocean pCO₂, and net sea-air CO₂ flux over the global oceans, *Deep Sea Research Part II: Topical Studies in Oceanography*, 56, 554-577, 2009.
- Tanhua, T., Fogelqvist, E., and Bastürk, Ö.: Reduction of volatile halocarbons in anoxic seawater, results from a study in the Black Sea, *Mar. Chem.*, 54, 159-170, 1996.
- Tegtmeier, S., Kruger, K., Quack, B., Atlas, E. L., Pisso, I., Stohl, A., and Yang, X.: Emission and transport of bromocarbons: from the West Pacific ocean into the stratosphere, *Atmos. Chem. Phys.*, 12, 10633-10648, 10.5194/acp-12-10633-2012, 2012.
- Tegtmeier, S., Krüger, K., Quack, B., Atlas, E., Blake, D. R., Boenisch, H., Engel, A., Hepach, H., Hossaini, R., Navarro, M. A., Raimund, S., Sala, S., Shi, Q., and Ziska, F.: The contribution of oceanic

methyl iodide to stratospheric iodine, *Atmos. Chem. Phys.*, 13, 11869-11886, 10.5194/acp-13-11869-2013, 2013.

Tegtmeier, S., Ziska F., Pisso, I., Quack B., Velders, G., Krüger, K.: Oceanic bromine emissions weighted by their ozone depletion potential, *in prep.*

Theiler, R., Cook, J. C., and Hager, L. P.: HALOHYDROCARBON SYNTHESIS BY BROMOPEROXIDASE, *Science*, 202, 1094-1096, 10.1126/science.202.4372.1094, 1978.

Tokarczyk, R., and Moore, R. M.: Production of volatile organohalogens by phytoplankton cultures, *Geophys. Res. Lett.*, 21, 285-288, 1994.

Tost, H., Lawrence, M. G., Brühl, C., Jöckel, P., The GABRIEL Team, and The SCOUT-O3-DARWIN/ACTIVE Team: Uncertainties in atmospheric chemistry modelling due to convection parameterisations and subsequent scavenging, *Atmos. Chem. Phys.*, 10, 1931-1951, doi:10.5194/acp-10-1931-2010, 2010.

van Vuuren, D. P., Edmonds, J., Kainuma, M., Riahi, K., Thomson, A., Hibbard, K., Hurtt, G. C., Kram, T., Krey, V., Lamarque, J.-F., Masui, T., Meinshausen, M., Nakicenovic, N., Smith, S. J., and Rose, S. K.: The representative concentration pathways: an overview, *Clim. Change*, 109, 5-31, 10.1007/s10584-011-0148-z, 2011.

Vogt, R., Sander, R., Von Glasow, R., and Crutzen, P. J.: Iodine chemistry and its role in halogen activation and ozone loss in the marine boundary layer: A model study, *J. Atmos. Chem.*, 32, 375-395, 10.1023/a:1006179901037, 1999.

von Glasow, R., von Kuhlmann, R., Lawrence, M. G., Platt, U., and Crutzen, P. J.: Impact of reactive bromine chemistry in the troposphere, *Atmos. Chem. Phys.*, 4, 2481-2497, 2004.

Wanninkhof, R.: Relationship Between Wind-Speed and Gas-Exchange Over the Ocean, *J. Geophys. Res.-Oceans*, 97, 7373-7382, 1992.

Wanninkhof, R.: The effect of using time-averaged winds on regional air-sea CO₂ fluxes, in: *Gas Transfer at Water Surface*, American Geophysical Union, 351-357, 2002.

Warwick, N. J., Pyle, J. A., Carver, G. D., Yang, X., Savage, N. H., O'Connor, F. M., and Cox, R. A.: Global modeling of biogenic bromocarbons, *J. Geophys. Res.-Atmos.*, 111, D2430510.1029/2006jd007264, 2006.

Wever, R.: Ozone destruction by algae in the arctic atmosphere, *Nature*, 335, 501-501, 10.1038/335501b0, 1988.

Wever, R., Tromp, M. G. M., Krenn, B. E., Marjani, A., and Vantol, M.: Brominating Activity of the Seaweed *Ascophyllum Nodosum*: Impact on the Biosphere, *Environ. Sci. Technol.*, 25, 446-449, 1991.

Wever, R., and van der Horst, M. A.: The role of vanadium haloperoxidases in the formation of volatile brominated compounds and their impact on the environment, *Dalton Transactions*, 42, 11778-11786, 10.1039/c3dt50525a, 2013.

White, R. H.: ANALYSIS OF DIMETHYL SULFONIUM COMPOUNDS IN MARINE-ALGAE, *J. Mar. Res.*, 40, 529-536, 1982.

Whitman, W. G.: The two-film theory of gas absorption, *Chemical and Metallurgical*

Engineering 29, 146-148 (1923). Reprinted with permission from *Chemical Engineering*, Copyright 1923, McGraw-Hill Publishing Co.

Wilke, C. R., and Chang, P.: CORRELATION OF DIFFUSION COEFFICIENTS IN DILUTE SOLUTIONS, *Aiche J.*, 1, 264-270, 10.1002/aic.690010222, 1955.

World Meteorological Organization, *Scientific Assessment of Ozone Depletion: 1998*, WMO Global Ozone Research and Monitoring Project - Report No. 44, Geneva, 1998

WMO (World Meteorological Organization) *Scientific Assessment of Ozone Depletion: 2006*, Global Ozone Research and Monitoring Project - Report No. 50, 572pp., Geneva, 2007

WMO: (World Meteorological Organization), *Scientific Assessment of Ozone Depletion: 2010*, Global Ozone Research and Monitoring Project-Report No. 52, Geneva, Switzerland, 516 pp. pp., 2011.

Yang, X., Cox, R. A., Warwick, N. J., Pyle, J. A., Carver, G. D., O'Connor, F. M., and Savage, N. H.: Tropospheric bromine chemistry and its impacts on ozone: A model study, *J. Geophys. Res.-Atmos.*, 110, D2331110.1029/2005jd006244, 2005.

Yokouchi, Y., Barrie, L. A., Toom, D., and Akimoto, H.: The seasonal variation of selected natural and anthropogenic halocarbons in the Arctic troposphere, *Atmos. Environ.*, 30, 1723-1727, 10.1016/1352-2310(95)00393-2, 1996.

Yokouchi, Y., Nojiri, Y., Barrie, L. A., Toom-Sauntry, D., and Fujinuma, Y.: Atmospheric methyl iodide: High correlation with surface seawater temperature and its implications on the sea-to-air flux, *J. Geophys. Res.-Atmos.*, 106, 12661-12668, 10.1029/2001jd900083, 2001.

Yokouchi, Y., Hasebe, F., Fujiwara, M., Takashima, H., Shiotani, M., Nishi, N., Kanaya, Y., Hashimoto, S., Fraser, P., Toom-Sauntry, D., Mukai, H., and Nojiri, Y.: Correlations and emission ratios among bromoform, dibromochloromethane, and dibromomethane in the atmosphere, *J. Geophys. Res.-Atmos.*, 110, D2330910.1029/2005jd006303, 2005.

Yokouchi, Y., Osada, K., Wada, M., Hasebe, F., Agama, M., Murakami, R., Mukai, H., Nojiri, Y., Inuzuka, Y., Toom-Sauntry, D., and Fraser, P.: Global distribution and seasonal concentration change of methyl iodide in the atmosphere, *J. Geophys. Res.-Atmos.*, 113, 10.1029/2008jd009861, 2008.

Yokouchi, Y., Nagashima, Y., Saito, T., and Mukai, H.: Identification of coastal emissions of methyl chloride and methyl bromide based on high-frequency measurements on Hateruma Island, *Geochemical Journal*, 44, 173-179, 2010.

Zafiriou, O. C.: REACTION OF METHYL HALIDES WITH SEAWATER AND MARINE AEROSOLS, *J. Mar. Res.*, 33, 75-81, 1975.

Zafiriou, O. C.: MARINE ORGANIC-PHOTOCHEMISTRY PREVIEWED, *Mar. Chem.*, 5, 497-522, 10.1016/0304-4203(77)90037-8, 1977.

Zafiriou, O. C., Blough, N. V., Micinski, E., Dister, B., Kieber, D., and Moffett, J.: MOLECULAR PROBE SYSTEMS FOR REACTIVE TRANSIENTS IN NATURAL-WATERS, *Mar. Chem.*, 30, 45-70, 10.1016/0304-4203(90)90061-g, 1990.

Zhou, Y., Mao, H. T., Russo, R. S., Blake, D. R., Wingenter, O. W., Haase, K. B., Ambrose, J., Varner, R. K., Talbot, R., and Sive, B. C.: Bromoform and dibromomethane measurements in the seacoast region of New Hampshire, 2002-2004, *J. Geophys. Res.-Atmos.*, 113, D08305/10.1029/2007jd009103, 2008.

Zika, R. G., Gidel, L. T., and Davis, D. D.: A COMPARISON OF PHOTOLYSIS AND SUBSTITUTION DECOMPOSITION RATES OF METHYL-IODIDE IN THE OCEAN, *Geophys. Res. Lett.*, 11, 353-356, 10.1029/GL011i004p00353, 1984.

Ziska, F., Quack, B., Abrahamsson, K., Archer, S. D., Atlas, E., Bell, T., Butler, J. H., Carpenter, L. J., Jones, C. E., Harris, N. R. P., Hepach, H., Heumann, K. G., Hughes, C., Kuss, J., Krüger, K., Liss, P., Moore, R. M., Orlikowska, A., Raimund, S., Reeves, C. E., Reifenhäuser, W., Robinson, A. D., Schall, C., Tanhua, T., Tegtmeier, S., Turner, S., Wang, L., Wallace, D., Williams, J., Yamamoto, H., Yvon-Lewis, S., and Yokouchi, Y.: Global sea-to-air flux climatology for bromoform, dibromomethane and methyl iodide, *Atmos. Chem. Phys.*, 13, 8915-8934, 10.5194/acp-13-8915-2013, 2013.

Ziska F., Quack B., Tegtmeier S. and Krüger K., Future emissions of halocarbons based on CMIP 5 model output fields, *in prep.*

VIII. Abbreviations

BMBF	German Federal Ministry of Education and Research
Br ⁻	Bromide
BrCl	Bromine monochloride
BrO	Bromine oxide
BrONO ₂	Bromine nitrate
Br _y	Inorganic bromine
C ₂ Cl ₄	Tetrachloroethylene
C ₂ H ₅ Br	Bromoethane
C ₂ H ₅ I	Ethyl iodide
C ₂ HCl ₃	Trichloroethylene
C ₃ H ₇ I	Propyl iodide
C ₄ H ₉ I	2-iodo-2-methylpropane
C _a	measured concentration at gas phase
CBr ₂ O	Carbonyl bromide
CCM	Chemical climate model
CFC	Chlorofluorocarbons
CH ₂ Br ₂	Dibromomethane
CH ₂ BrCl	Dibromochloromethane
CH ₂ Cl ₂	Dichloromethane
CH ₂ I ₂	Diiodomethane
CH ₂ IBr	Bromodiiodomethane
CH ₂ ICl	Chloroiodomethane
CH ₃	Methyl radical
CH ₃ B ₁₂	Methylcobalamin
CH ₃ Cl	Methyl chloride

CH ₃ I	Methyl iodide
CH ₃ O ₂	Methyldioxy radical
CH ₄	Methane
CHBr ₂ Cl	Dibromchloromethane
CHBr ₃	Bromoform
CHBrCl ₂	Bromodichloromethane
CHCl ₃	Chloroform
CHIBr ₂	Bromochloriodomethane
Chl <i>a</i>	Chlorophyll <i>a</i>
Cl ⁻	Chloride
ClO	Chlorine monoxide
CMIP 5	fifth phase of the Climate Model Intercomparison Project
CO	Carbon monoxide
CO ₂	Carbon dioxide
COO ⁻	Carboxylate
COST	European COoperation in Science and Technology
CPT	Cold point tropopause
CTM	Chemical transport model
C _w	measured concentration at the liquid phase
DMS	Dimethylsulfid
DMSO	Dimethylsulfoxid
DOM	Dissolved organic matter
DU	Dobson unit
F	Air-sea flux
FLEXPART	FLEXible PARTicle dispersion model
GCM	General circulation model

H	Henry's law constant
H ⁺	Hydrogen ions
Halocarbons	Halogenated hydrocarbons
HalOcat	Halocarbons in the Ocean and Atmosphere
HAMOCC	Hamburg ocean carbon cycle model
HBr	Hydrogen bromide
HO ₂	Hydroperoxyl radicals
HOBr	Hypobromous acid
HOCl	Hypochlorous acid
HOI	Hypoiodous acid
H ₂ O ₂	hydrogen peroxide
I ⁻	Iodide
IBr	Iodine monobromide
ICl	Iodine monochloride
INO ₂	Nitryl iodide
IO ₃ ⁻	Iodate
IO _x	Active iodine
IPPC	Intergovernmental Panel of Climate Change
I _y	Inorganic iodine
K	Air-sea gas exchange velocity
k ₆₀₀	Air-sea gas exchange velocity at Sc=600
LWR	Longwave radiation
MBL	Marine boundary layer
MIOPM	The Max Planck Institute ocean model
N ₂ O	Nitrous oxide
NH	Northern hemisphere

NO	Nitric oxide
NO ₂	Nitrogen dioxide
O ₂	Oxygen
O ₃	Ozone
ODP	Tropical tropopause layer
OH	Hydroxyl radicals
PG(I)	Product gases (injection)
RCP	Representative Concentration Pathways
SAH	S-adenosyl-L-homocysteine
SAM	S-adenosyl-L-methionine
Sc	Schmidt number
SF ₆	Sulfur hexafluoride
SG(I)	Source gases (injection)
SH	Southern hemisphere
SHIVA	Stratospheric Ozone: Halogen Impacts in a Varying Atmosphere
SLP	Sea level pressure
SOI	Soluble organic iodine
SOLAS	S urface O cean and L ower A tmosphere S tudy
SOPRAN	Surface Ocean P R ocesses in the A Nthropocene
SSS	Sea surface salinity
SST	Sea surface temperature
SWR	Short wave radiation
TransBrom	Very short lived bromine compounds in the ocean and their transport pathways into the stratosphere
TTL	Tropical tropopause layer
U	Sea surface wind speed
UV	Ultra violet

VSLs	Very short lived substances
z ₀	level of clear-sky zero radiative heating

SUPPLEMENT

IX. Supplement

6. Manuscript

Drivers of diel and regional variations of halocarbon emissions from the tropical North East Atlantic

H. Hepach¹, B. Quack¹, F. Ziska¹, S. Fuhlbrügge¹, E. L. Atlas², K. Krüger^{1,*}, I. Peeken^{3,4}, and D. W. R. Wallace^{1,}**

[1] GEOMAR Helmholtz-Zentrum für Ozeanforschung Kiel, Germany

[2] Rosenstiel School of Marine and Atmospheric Science (RSMAS), University of Miami, USA

[3] Alfred-Wegener-Institut für Polar und Meeresforschung (AWI), Bremerhaven, Germany

[4] MARUM – Center for Marine Environmental Sciences, University Bremen, Bremen, Germany

[*]now at: Department of Geosciences, University of Oslo (UiO), Oslo, Norway

[**]now at: Department of Oceanography, Dalhousie University, Halifax, Canada

Published in: Atmospheric Chemistry and Physics, 14, 1255-1275, doi:10.5194/acp-14-1255-2014, 2014.



Drivers of diel and regional variations of halocarbon emissions from the tropical North East Atlantic

H. Hepach¹, B. Quack¹, F. Ziska¹, S. Fuhlbrügge¹, E. L. Atlas², K. Krüger^{1,*}, I. Peeken^{3,4}, and D. W. R. Wallace^{1,**}

¹GEOMAR Helmholtz-Zentrum für Ozeanforschung Kiel, Germany

²Rosenstiel School of Marine and Atmospheric Science (RSMAS), University of Miami, USA

³Alfred-Wegener-Institut für Polar und Meeresforschung (AWI), Bremerhaven, Germany

⁴MARUM – Center for Marine Environmental Sciences, University Bremen, Bremen, Germany

* now at: Department of Geosciences, University of Oslo (UiO), Oslo, Norway

** now at: Department of Oceanography, Dalhousie University, Halifax, Canada

Correspondence to: H. Hepach (hhepach@geomar.de)

Received: 15 July 2013 – Published in Atmos. Chem. Phys. Discuss.: 25 July 2013

Revised: 9 December 2013 – Accepted: 10 December 2013 – Published: 3 February 2014

Abstract. Methyl iodide (CH₃I), bromoform (CHBr₃) and dibromomethane (CH₂Br₂), which are produced naturally in the oceans, take part in ozone chemistry both in the troposphere and the stratosphere. The significance of oceanic upwelling regions for emissions of these trace gases in the global context is still uncertain although they have been identified as important source regions. To better quantify the role of upwelling areas in current and future climate, this paper analyzes major factors that influenced halocarbon emissions from the tropical North East Atlantic including the Mauritanian upwelling during the DRIVE expedition. Diel and regional variability of oceanic and atmospheric CH₃I, CHBr₃ and CH₂Br₂ was determined along with biological and physical parameters at six 24 h-stations. Low oceanic concentrations of CH₃I from 0.1–5.4 pmol L⁻¹ were equally distributed throughout the investigation area. CHBr₃ and CH₂Br₂ from 1.0 to 42.4 pmol L⁻¹ and to 9.4 pmol L⁻¹, respectively were measured with maximum concentrations close to the Mauritanian coast. Atmospheric CH₃I, CHBr₃, and CH₂Br₂ of up to 3.3, 8.9, and 3.1 ppt, respectively were detected above the upwelling, as well as up to 1.8, 12.8, and 2.2 ppt at the Cape Verdean coast. While diel variability in CH₃I emissions could be mainly ascribed to oceanic non-biological production, no main driver was identified for its emissions over the entire study region. In contrast, biological parameters showed the greatest influence on the regional distribution of sea-to-air fluxes of bromocarbons. The diel impact of wind speed on bromocarbon emissions increased

with decreasing distance to the coast. The height of the marine atmospheric boundary layer (MABL) influenced halocarbon emissions via its influence on atmospheric mixing ratios. Oceanic and atmospheric halocarbons correlated well in the study region, and in combination with high oceanic CH₃I, CHBr₃ and CH₂Br₂ concentrations, local hot spots of atmospheric halocarbons could solely be explained by marine sources. This conclusion is in contrast to previous studies that hypothesized elevated atmospheric halocarbons above the eastern tropical Atlantic to be mainly originated from the West-African continent.

1 Introduction

Volatile halogenated hydrocarbons (halocarbons) occur naturally in the oceans from where they are emitted into the atmosphere. Bromine and iodine atoms released from these compounds by photolysis and oxidation can take part in catalytic ozone destroying cycles in both the troposphere and stratosphere (McGivern et al., 2000; Salawitch et al., 2005; Montzka and Reimann, 2011) with iodine also participating in aerosol formation (O'Dowd et al., 2002). Halocarbons comprise brominated and iodinated methanes such as bromoform (CHBr₃) and dibromomethane (CH₂Br₂), methyl iodide (CH₃I) and diiodomethane, as well as longer chained and mixed halogenated compounds such as iodoethane, chloriodomethane, and dibromochloromethane.

While CHBr_3 and CH_2Br_2 represent the largest contributors to atmospheric organic bromine from the ocean to the atmosphere (Hossaini et al., 2012a), methyl iodide (CH_3I), originating mostly from marine sources, is the most abundant organoiodine in the atmosphere (Saiz-Lopez et al., 2012). Although these three halocarbons are among those that receive the most attention due to their large contributions to atmospheric organic halogens, many uncertainties remain regarding their formation pathways, influences on their emissions, and their fate in the ocean and the atmosphere.

Elevated halocarbon concentrations, particularly of CHBr_3 and CH_2Br_2 , occur in coastal regions where macroalgae are thought to be the most dominant sources (Carpenter and Liss, 2000; Laturnus, 2001). Elevated concentrations of halocarbons are often observed in upwelling regions with large phytoplankton activity, where cold, nutrient rich water is brought up to the sea surface (Tokarczyk and Moore, 1994; Quack et al., 2004). Abiotic production such as photochemical processes could be of high significance for the marine formation of iodinated organic trace gases (Martino et al., 2009), e.g. CH_3I . Hence, its distribution in the ocean may depend on physical parameters such as insolation (Moore and Groszko, 1999; Richter and Wallace, 2004; Yokouchi et al., 2008; Stemmler et al., 2013).

The subtropical and tropical regions represent the largest contributors to global emission budgets of CH_3I , CHBr_3 and CH_2Br_2 (Ziska et al., 2013). The compounds and their degradation products can be carried into the stratosphere in significant quantities (Solomon et al., 1994; Hossaini et al., 2010; Aschmann et al., 2011; Montzka and Reimann, 2011; Tegtmeyer et al., 2013), since deep tropical convection can lift surface air very rapidly into the tropical tropopause layer (Tegtmeyer et al., 2012). Studies by Pyle et al. (2007) and Hossaini et al. (2012b) projected considerable changes in future inorganic bromine in the tropical troposphere and to the stratosphere from biogenic halocarbon emissions due to strengthening of convection, increasing their importance in the tropics. Coastal upwelling systems might play a crucial role in a changing climate. The tropical Mauritanian upwelling is an example of a recently intensified coastal eastern boundary upwelling (McGregor et al., 2007). Primary production could increase with enhanced entrainment of nutrient rich deep water into the surface ocean leading to amplified production of halocarbons. Increasing wind speeds, caused by enhanced pressure gradients (Bakun, 1990), would also directly influence the sea-to-air fluxes of all trace gases via a faster transfer coefficient (e.g. Nightingale et al., 2000). Thus the identification of factors impacting halocarbon sea-to-air fluxes is crucial for assessing possible effects of climate change on future emissions from coastal upwelling systems.

This paper reports on oceanic and atmospheric halocarbon distributions and sea-to-air fluxes from the DRIVE (Diurnal and Regional Variability of halogen Emissions) campaign of RV *Poseidon* in the eastern tropical North Atlantic and the Mauritanian upwelling in June 2010. We present re-

sults from six 24 h-stations in different distances from the Mauritanian coast and from two simultaneous diel stations on the Cape Verde island Sao Vicente. We aim at describing and quantifying significant factors that control the concentrations and emission fluxes of CH_3I , CHBr_3 , and CH_2Br_2 both on a diel and a regional scale, including biological production, wind speed, and atmospheric transport. Previous studies have hypothesized that elevated atmospheric mixing ratios of CHBr_3 and CH_2Br_2 above the Mauritanian upwelling area were mainly of continental origin, since sea-to-air fluxes of these compounds appeared not sufficient to explain the observations (Quack et al., 2007a; Carpenter et al., 2009). In contrast, the investigation by Fuhlbrügge et al. (2013) revealed high atmospheric mixing ratios of CH_3I , CHBr_3 and CH_2Br_2 close to the coast also in air masses transported from the open ocean, with a significant anticorrelation between the atmospheric mixing ratios and the height of MABL. We therefore examine how oceanic emissions contribute to the mixing ratios of atmospheric halocarbons taking the height of the marine atmospheric boundary layer (MABL) into account. Meteorological constraints on the atmospheric distributions during the cruise are investigated in the accompanying paper by Fuhlbrügge et al. (2013).

2 Methods

The cruise P399/2 (Poseidon 399 leg 2) named DRIVE (Diurnal and Regional Variability of halogen Emissions) of RV *Poseidon* took place from May 31 to June 17 in 2010 in the eastern tropical North Atlantic and the Mauritanian upwelling. The ship followed a course from Las Palmas (Canary Islands, 28.1° N and 15.4° W) back to Las Palmas with a short stop at Mindelo (Sao Vicente, Cape Verde, 16.9° N and 25.0° W). The cruise track included six stations located at 17.6° N and 24.3° W (S1), 18.0° N and 21.0° W (S2), 18.0° N and 18.0° W (S3), 18.5° N and 16.5° W (S4), 19.0° N and 16.6° W (S5), and 20.0° N and 17.3° W (S6) where the ship remained at its position for 24 h (Fig. 1). Samples for dissolved halocarbons in sea water, atmospheric halocarbons and phytoplankton pigments were taken at all 24h-stations in parallel, and additionally four radio sonde launches per 24h-station were accomplished to determine the MABL properties. More details on the campaign and the meteorological conditions can be found in Bange et al. (2011) and Fuhlbrügge et al. (2013).

Related to the ship expedition a land-based operation took place from 3 to 8 June 2010 at the Cape Verde Atmospheric Observatory (CVAO) on Sao Vicente close to Mindelo at 17.6° N and 24.3° W (Fig. 1) where samples of atmospheric halocarbons were taken during two days.

Atmospheric halocarbon mixing ratios and meteorological conditions were also determined during a second cruise leg P399/3 from Las Palmas, Spain to Vigo, Spain and are covered in Fuhlbrügge et al. (2013). In contrast, this manuscript

focuses only on results from leg P399/2. The words “whole cruise” will refer to leg 2 and “whole campaign” includes leg 2 and the land-based operation at Cape Verde.

2.1 Sampling and analysis of halocarbons in sea surface water and air

Dissolved halocarbons were sampled in 500 mL amber glass bottles from a continuously working pump from the ships moon pool at a depth of 4.4 m. This allowed for nearly hourly sampling of sea surface water at every diel station. In between 24h-stations, the samples were taken every 3 h. The water was analyzed for halocarbons using a purge and trap system attached to a gas chromatograph with mass spectrometric detection (GC-MS). 80 mL of water were purged at 70 °C for 60 min with a stream of helium at 30 mL min⁻¹ in a glass chamber with a purge efficiency of more than 98 % for all three halocarbons. The volatilized trace gases were desiccated with a Nafion[®] dryer and were trapped on glass beads at -100 °C. After purging, the compounds were desorbed at 100 °C onto a deactivated capillary in liquid nitrogen as second trap. After three minutes, the sample was injected into the GC-MS, where the trace gases were separated on a Rtx-VGC capillary column with a length of 60 m, a diameter of 0.25 mm and a film thickness of 1.40 μm, and were detected in single ion mode. Quantification was achieved with volumetrically prepared standards in methanol. Four calibration curves were performed using different dilutions, each injected in triplicate. One standard was injected once a day in triplicate to monitor the internal drift of the instrumental set up which was low during the whole cruise. Precision for these measurements lay within 16 % for CH₃I, and 6 % for CHBr₃ and CH₂Br₂, determined only from duplicates due to time constraints.

Air samples were taken hourly at the diel stations. They were pumped into stainless steel canisters on the compass deck at a height of 13.7 m with a metal bellows pump. Samples were analyzed within a month at the Rosenstiel School of Marine and Atmospheric Science in Miami with a precision of approximately 5 % using GC-MS (Schauffler et al., 1999). Previous campaigns show that stability of the measured compounds in the canisters is not an issue over this time period. Additionally, air samples were taken at CVAO on an hourly basis parallel to the first two diel stations of the ship. Samples were taken according to the method onboard the RV *Poseidon* in approximately 3 m height above ground and then analyzed along with the other canisters collected during the cruise. Oceanic and atmospheric measurements were intercalibrated against whole air working-standards obtained from the NOAA Global Monitoring Division (Boulder, USA).

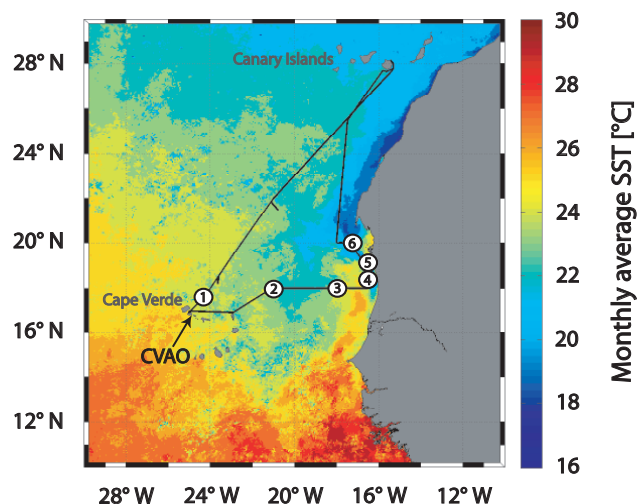


Fig. 1. Cruise track (black line) during DRIVE on SST derived from the monthly composite of June 2010 of MODIS-Aqua level 3 data. White circles with black numbers indicate 24-h-stations. Also marked is the location of the CVAO (Cape Verde Atmospheric Observatory).

2.2 Phytoplankton pigment analysis and flow cytometry

Samples for pigment analysis were taken approximately every 2 h at every diel station. 1 L of sea surface water from the continuously working pump in the ships moon pool was filtered through 25 mm Whatman GF/F filters and stored at -80 °C until analysis. Back in the lab, phytoplankton pigments were analyzed according to Tran et al. (2013) using a Waters high-performance liquid chromatography (HPLC) system at the Alfred Wegener Institute for Polar and Marine Research Bremerhaven (AWI). Apart from chlorophyll *a* (Chl *a*), the 27 marker pigments for which samples were analyzed include various chlorophyll type pigments such as chlorophyll *c1*, *c2* and *c3*, divinyl chlorophyll *b*, chlorophyll *b*, divinyl chlorophyll *a*, and phaeophytin *a*. The following carotenoids were detected: peridinin, predinin derivative, 19-butanoyloxyfucoxanthin, fucoxanthin, neoxanthin, 19-hexanoyloxyfucoxanthin, violaxanthin, astaxanthin, prasinoxanthin, diadinoxanthin, alloxanthin, diatloxanthin, anthreoxanthin, zeaxanthin, lutein, α -carotene, and β -carotene. Marker pigments and their relative abundance are indicative for different phytoplankton groups.

For flow cytometry, 4 mL of water from the underway pump system were preserved with glutaraldehyde with a final concentration of 0.1 %, shock frozen in liquid nitrogen and stored at -80 °C. Flow cytometry samples were analyzed for nanoplankton, picoplankton, *Prochlorococcus*, and *Synechococcus* at the AWI according to Taylor et al. (2011). Potential cell loss associated with the sample fixation has not been taken into account.

Table 1. Means and ranges (minimum – maximum) of ambient parameters (SST, salinity, Chl *a*, wind speed, MABL height) during DRIVE for open ocean stations S1–S2 and coastal stations S3–S6.

		S1	S2	S3	S4	S5	S6
Parameter	Unit	17.6° N and 24.3° W	18.0° N and 21.0° W	18.0° N and 18.0° W	18.5° N and 16.5° W	19.0° N and 16.6° W	20.0° N and 17.3° W
SST	°C	24.5 (24.4–24.7)	23.2 (23.0–23.6)	21.7 (21.6–21.8)	23.3 (23.1–23.4)	20.4 (20.2–21.0)	18.6 (18.4–18.7)
Salinity		36.7 (36.7–36.7)	36.4 (36.4–36.5)	35.9 (35.9–35.9)	35.9 (35.9–35.9)	35.8 (35.8–35.8)	35.9 (35.8–35.9)
Chl <i>a</i>	µg L ⁻¹	0.05 (0–0.08)	0.30 (0.10–0.43)	1.00 (0.58–1.79)	1.63 (0.81–3.01)	4.50 (1.69–8.12)	4.80 (7.40–6.70)
Wind speed	m s ⁻¹	4.6 (2.0–7.1)	11.0 (7.8–14.8)	6.0 (3.9–9.0)	9.7 (6.7–12.9)	8.9 (4.3–13.7)	11.0 (6.8–14.2)
MABL height	m	950 (850–1100)	540 (400–700)	290 (200–400)	120 (50–200)	25 (surface–100)	190 (100–350)

2.3 Calculation of sea-to-air fluxes and saturation anomaly

Sea-to-air fluxes (F) of CH₃I, CHBr₃ and CH₂Br₂ were calculated using the air-sea gas exchange parameterization of Nightingale et al. (2000). Schmidt number (Sc) corrections for the compound specific transfer coefficients k_w derived with the transfer coefficient k_{CO_2} of CO₂ as reported by Quack and Wallace (2003) were applied.

$$\frac{k_w}{k_{CO_2}} = \frac{Sc^{-\frac{1}{2}}}{660} \quad (1)$$

The air-sea concentration gradient was derived from all simultaneous water (c_w) and air (c_{atm}) measurements calculated with the Henry's law constants H of Moore and co-workers (Moore et al., 1995a, b) to obtain the theoretical equilibrium concentration c_{atm}/H .

$$F = k_w \cdot \left(c_w - \frac{c_{atm}}{H} \right) \quad (2)$$

The saturation anomaly S was calculated from the concentration gradient as the percentage of the equilibrium concentration.

$$S = \left(\left(c_w - \frac{c_{atm}}{H} \right) \cdot 100 \right) \cdot \left(\frac{c_{atm}}{H} \right)^{-1} \quad (3)$$

Water temperature and salinity were continuously recorded using the ships' thermosalinograph. Air pressure and wind speed were determined by sensors on the compass deck and in 25.5 m height, respectively. Ten minute averages of these four parameters were included in the calculations, and wind speed was corrected to 10 m values.

3 Hydrography and environmental parameters during DRIVE

High SST values between 23.0 and 24.7 °C and high salinities from 36.4 to 36.7 observed at S1 and S2 close to Cape Verde (Figs. 1–2a, Table 1) were consistent with tropical surface water characteristics (Tsuchiya et al., 1992). Low Chl *a* concentrations between 0.00 and 0.43 µg L⁻¹ were a sign of low primary production there. Stations S1 and S2 are hence defined as open ocean. Wind speed had the lowest mean of the whole cruise at S1 with 4.6 m s⁻¹ and was highest at S2 with a mean of 11.0 m s⁻¹. The MABL height in this region determined by Fuhlbrügge et al. (2013) ranged between 400 and 1100 m (Table 1). With decreasing distance to the Mauritanian coast, a decrease in SST and salinity and an increase in Chl *a* concentrations were observed. This is a sign of the North West African upwelling system on the African shelf as part of the wind-driven Canary Current extending from 30° N to 10° N (Fedoseev, 1970). South Atlantic Central Water (SACW), characterized as a straight T-S curve between 5 °C and 34.3 and 20 °C and 36.0 (Tomczak and Godfrey, 2005), is transported to the Mauritanian coast by a poleward directed undercurrent. Between 12° N and 20° N upwelling of the cold nutrient rich SACW takes place from late fall to late spring (Minas et al., 1982; Tomczak, 1982; Hagen, 2001) after which the upwelling starts to cease due to changing atmospheric conditions induced by the shift of the Intertropical Convergence Zone (Mittelstaedt, 1982). Although the upwelling already began to cease during our cruise, stations S3–S6 are defined as upwelling and coastal stations (further on called coastal stations) due to the lower SSTs observed there. The lowest SST with 18.4 °C as well as the highest daily mean Chl *a* concentration of 4.80 µg L⁻¹ were found at the northernmost station (S6), while the overall maximum Chl *a* concentration of 8.12 µg L⁻¹ was observed at S5. MABL heights generally ranged between surface and 400 m

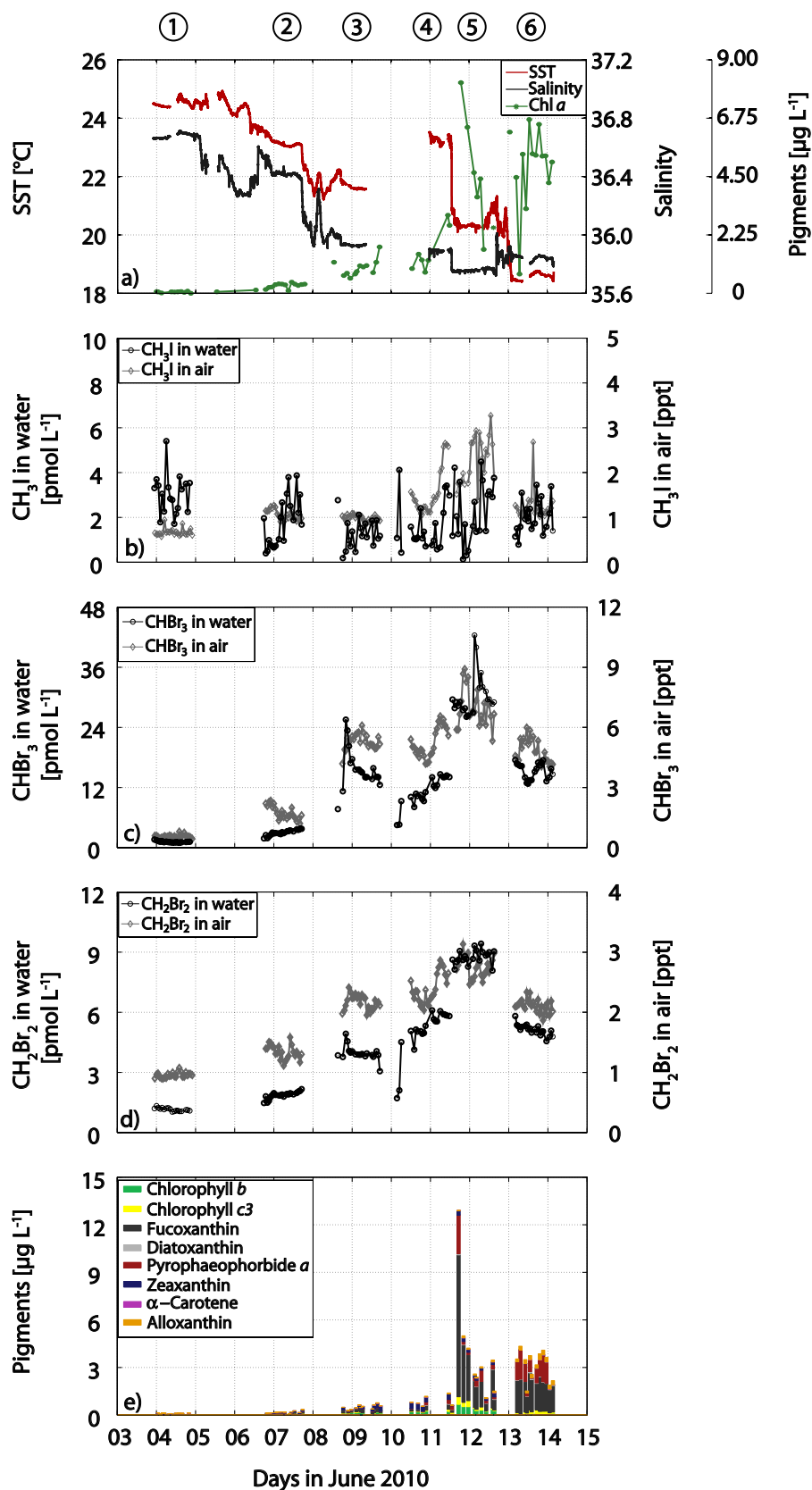


Fig. 2. SST, salinity and Chl *a* (a) along with halocarbon concentrations in water and atmospheric mixing ratios of CH₃I (b), CHBr₃ (c) and CH₂Br₂ (d) and pigments significant for the regional distribution of CHBr₃ and CH₂Br₂ (e) during the DRIVE campaign.

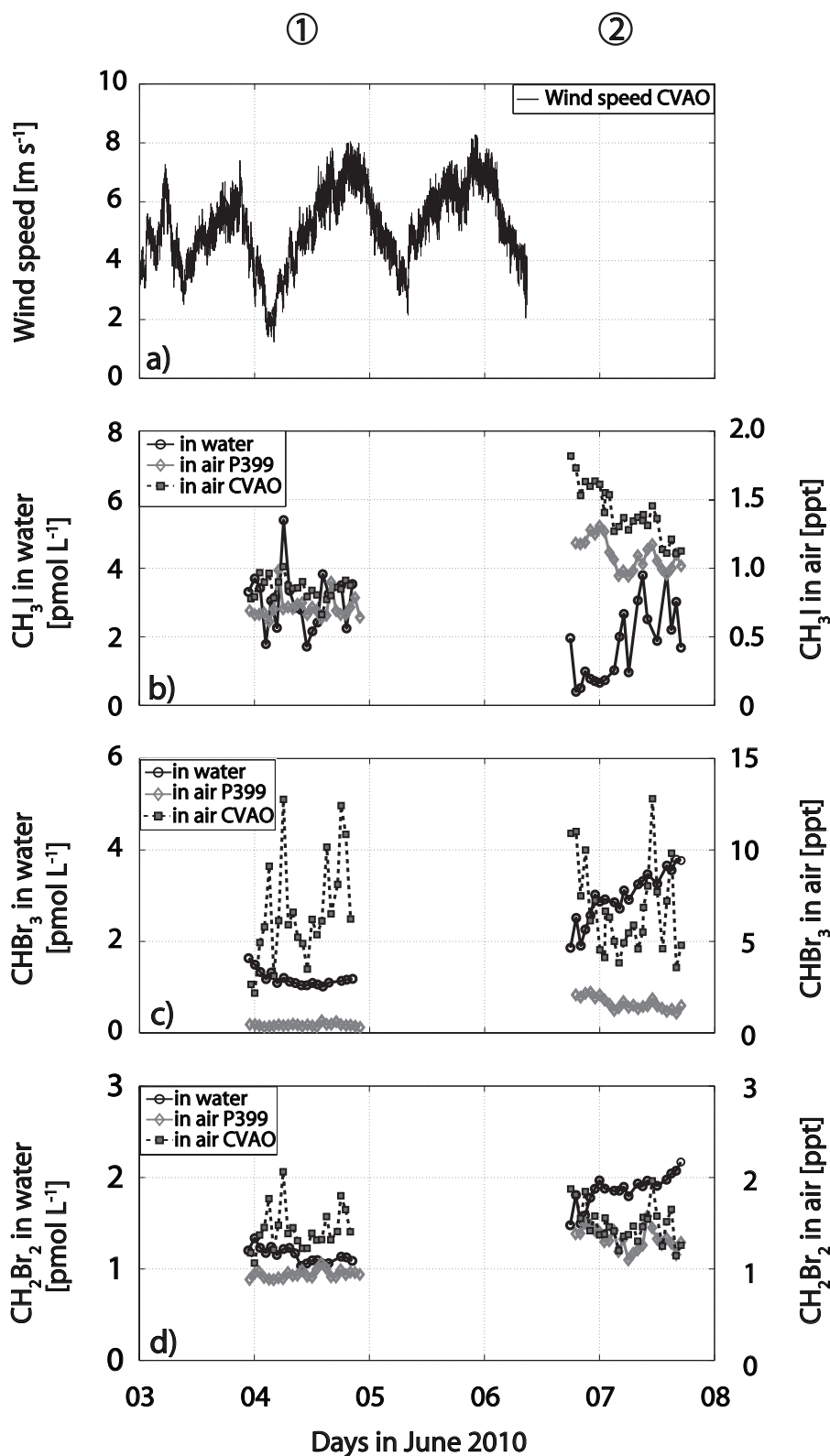


Fig. 3. Open ocean surface water and atmospheric halocarbons during stations S1 and S2 and atmospheric halocarbons measured parallel at CVAO as well as wind speed (wind speed in **a**, CH₃I in **b**, CHBr₃ in **c**, and CH₂Br₂ in **d**). Wind speed data for 7 and 8 June in 2010 was not available.

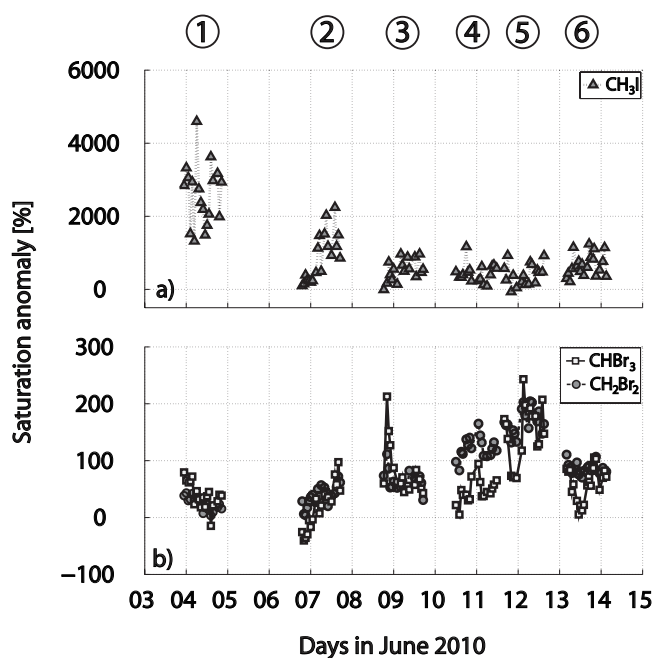


Fig. 4. Saturation anomalies of CH_3I (a) and CHBr_3 and CH_2Br_2 (b) throughout the RV *Poseidon* cruise.

at S3–S6, while wind speeds varied between 3.9 (S3) and 14.2 m s^{-1} (S6). At S5, the lowest MABL heights (close to the surface) together with the highest relative standard deviation (further on referred to as variability) in wind speed with a mean of 8.9 m s^{-1} and a variability of 27 % was observed at one station in the course of 24 h (Table 1). Due to the classification of the stations into two regions, average values of both open ocean stations together are based on fewer measurements than average values of the four coastal stations.

4 Results

4.1 Methyl iodide (CH_3I)

4.1.1 Regional distribution

At the open ocean stations S1 and S2 higher mean oceanic CH_3I of 2.4 pmol L^{-1} was found than at coastal stations S3–S6 with a mean of 1.8 pmol L^{-1} (Fig. 2b, Table 2). The maximum mean oceanic CH_3I of 3.0 (1.7 – 5.4) pmol L^{-1} was observed at S1, while S3 showed the lowest mean of 1.2 (0.2 – 2.1) pmol L^{-1} during 24 h. In total, the regional variability of CH_3I , which is the relative standard deviation between the means of the individual stations, was the lowest of all three halocarbons with 56 %. Correlations to neither phytoplankton pigments nor to picoplankton abundances were found for CH_3I in sea surface water (Table 3).

Atmospheric CH_3I with an overall mean of 1.3 (0.6 – 3.3) ppt revealed a different distribution in comparison to

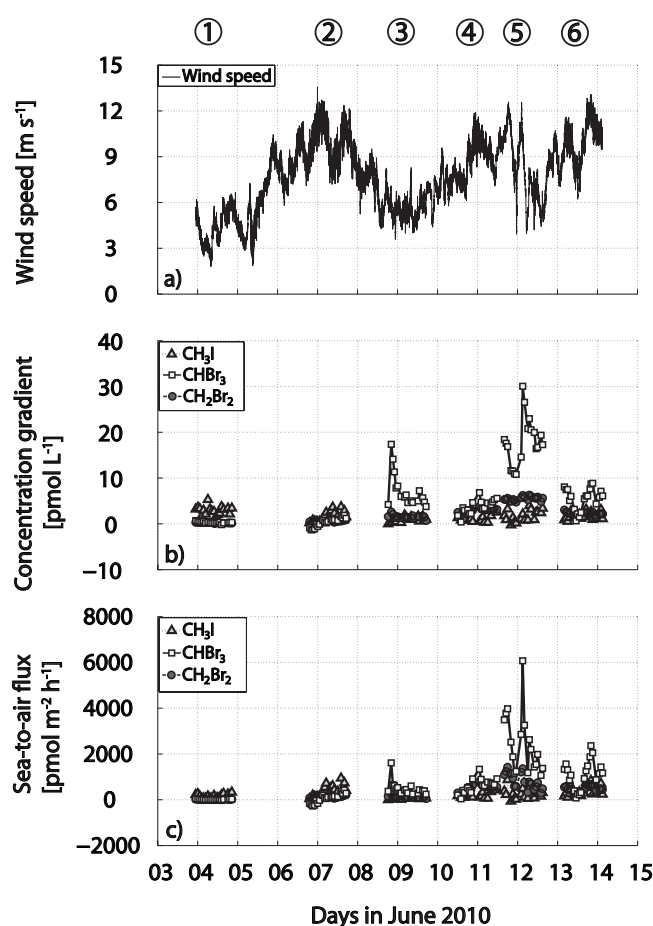


Fig. 5. Wind speed (a), concentration gradients (b) and sea-to-air fluxes (c) of CH_3I , CHBr_3 and CH_2Br_2 during DRIVE.

oceanic CH_3I (Fig. 2a). It was generally lower above the open ocean with 0.9 (0.6 – 1.3) ppt on average and increased towards the coast with a mean (range) of 1.6 (0.9 – 3.3) ppt (see also Fuhlbrügge et al., 2013). In total, atmospheric CH_3I had a lower regional variability of 44 % than oceanic CH_3I .

4.1.2 Diel variations

Of all three halocarbons, oceanic CH_3I showed the largest diel variability which was also larger than its regional variability. The lowest and the highest mean variability during 24 h were found at the open ocean stations S1 with 29 % and at S2 with 62 %. At the coastal stations oceanic CH_3I varied between 37 % (S6) and 60 % (S4). While at four stations maxima of CH_3I in the surface water were found in the morning hours, elevations in the afternoon were observed at open ocean station S2 and coastal station S6. Hence, no overall diurnal cycle could be detected.

Low relative diel variability between 9 % (S2) and 11 % (S1) was observed in atmospheric CH_3I above the open ocean. The variability at CVAO at the same time ranged

Table 2. Results of halocarbon measurements (water and air) and calculations (saturation anomalies and sea-to-air fluxes) for all six diel stations and parallel air sampling at CVAO.

			S1	S2	S3	S4	S5	S6
			17.6° N and 24.3° W	18.0° N and 21.0° W	18.0° N and 18.0° W	18.5° N and 16.5° W	19.0° N and 16.6° W	20.0° N and 17.3° W
Compound	Parameter	Unit						
CH ₃ I	Water	pmol L ⁻¹	3.0 (1.7–5.4)	1.8 (0.4–3.9)	1.2 (0.2–2.1)	1.6 (0.6–3.4)	2.2 (0.1–4.5)	2.0 (0.8–3.5)
	Air	ppt	0.7 (0.6–1.0)	1.1 (1.0–1.3)	1.0 (0.9–1.1)	1.6 (1.1–2.7)	2.3 (1.4–3.3)	1.3 (1.1–2.7)
	CVAO air	ppt	0.9 (0.7–1.0)	1.4 (1.1–1.8)	–	–	–	–
	Saturation anomaly	%	2606.3 (1321.1–4597.1)	870.2 (99.4–2243.7)	532.2 (–8.5–967.1)	445.6 (90.8–1167.4)	410.8 (–65.8–928.7)	672.1 (210.1–1242.3)
	Sea-to-air flux	pmol m ⁻² h ⁻¹	158.3 (59.3–330.4)	372.6 (39.6–941.6)	79.0 (–1.7–212.2)	227.7 (61.4–500.5)	259.6 (–64.6–871.6)	382.5 (106.1–837.9)
	CHBr ₃	Water	pmol L ⁻¹	1.2 (1.0–1.6)	3.0 (1.9–3.8)	16.2 (11.3–25.5)	11.9 (8.1–14.7)	30.6 (26.1–42.4)
Air		ppt	0.6 (0.5–0.8)	1.8 (1.2–2.4)	5.3 (4.2–6.1)	5.3 (4.2–6.6)	7.0 (5.4–8.9)	4.9 (4.1–6.0)
CVAO air		ppt	6.7 (2.3–12.8)	6.8 (3.7–12.8)	–	–	–	–
Saturation anomaly		%	39.6 (–14.7–79.3)	17.7 (–40.3–97.3)	80.6 (43.0–212.7)	46.1 (5.2–94.4)	148.0 (69.4–243.1)	59.4 (5.4–105.5)
Sea-to-air flux		pmol m ⁻² h ⁻¹	15.5 (–8.5–45.0)	65.6 (–273.4–426.7)	489.1 (241.4–1610.9)	611.7 (41.7–1333.8)	2423.0 (1063.3–6068.9)	1098.2 (77.8–2360.2)
CH ₂ Br ₂		Water	pmol L ⁻¹	1.2 (1.0–1.3)	1.9 (1.5–2.2)	4.0 (3.1–4.9)	5.4 (4.1–6.1)	8.8 (8.1–9.4)
	Air	ppt	1.0 (0.9–1.1)	1.4 (1.1–1.6)	2.2 (2.0–2.4)	2.4 (2.0–2.9)	2.8 (2.5–3.1)	2.1 (1.9–2.3)
	CVAO air	ppt	1.4 (1.1–2.1)	1.5 (1.2–2.0)	–	–	–	–
	Saturation anomaly	%	24.7 (3.4–43.2)	37.7 (4.1–72.2)	64.7 (30.9–111.5)	122.0 (82.7–165.0)	169.0 (131.8–204.3)	86.1 (70.1–110.6)
	Sea-to-air flux	pmol m ⁻² h ⁻¹	10.6 (1.8–27.9)	118.5 (14.5–214.3)	115.7 (50.0–260.3)	511.8 (207.9–801.0)	815.4 (285.6–1429.4)	470.4 (295.5–671.6)

between 9 % (4 June, parallel to S1) and 14 % (June 6 and 7, parallel to S2) (Fig. 3a, Table 2) with mean mixing ratios of 1.2 ppt (0.7 ppt, 4 June–1.8 ppt, 6 June). At the coastal stations S3–S6, diel variability of 7 (S3) – 33 % (S4) was observed. The highest mean atmospheric variability at S4 coincides with the largest oceanic variability. Similarly to oceanic CH₃I, there is no overall diurnal cycle in atmospheric mixing ratios. Maxima and minima occurred in both day and night hours.

4.1.3 Saturation anomaly, sea-air concentration gradient and sea-to-air fluxes

Saturation anomalies (Fig. 4), concentration gradient (Fig. 5b) as well as sea-to-air fluxes (Fig. 5c) were calculated according to Eqs. (1)–(3) (Table 2). To constrain the atmospheric influence on the concentration gradient, thus on the sea-to-air fluxes, the fraction of the equilibrium concentration c_{atm}/H of the oceanic concentration c_w was calculated (Fig. 6a). This is the relative reduction of the sea-to-air flux by the atmospheric mixing ratios compared to an empty atmosphere, which will be referred to as “flux reducing effect” further on.

For CH₃I the highest saturation anomalies with means of 931 (–66–4597) % (Fig. 4a, Table 2) and the lowest concentration gradients of 1.7 (–0.3–5.3) pmol L⁻¹ (Fig. 5b) of the three halocarbons were calculated for CH₃I for the whole cruise. Both were consistent with the oceanic distribution: they were highest in the open ocean with maxima at S1 where however no high emissions of this compound were calculated because of the prevailing low wind speeds during that time (Fig. 5c). The open ocean was generally highly supersaturated with mean anomalies of 1715 % on average, decreasing towards the coastal stations to a mean of 522 %. The reducing effect of atmospheric CH₃I on the sea-to-air flux was low, usually less than 50 %. One exception was S5 where low oceanic CH₃I coincided with high atmospheric mixing ratios, and the flux reducing effect reached 300 % leading to a flux into the water. Mainly positive sea-to-air fluxes of CH₃I could be observed with a mean of 254 pmol m⁻² h⁻¹ for the whole cruise (–65 at coastal station S5 to 942 pmol m⁻² h⁻¹ at open ocean station S2) (Fig. 5c, Table 2). Open ocean and mean coastal fluxes of 268 and 246 pmol m⁻² h⁻¹, respectively were in a similar range though with potentially higher fluxes in the open ocean due to its large supersaturation there.

Table 3. Correlation coefficients R^2 of halocarbons to nano- and picoplankton abundances as well as to phytoplankton pigment data (MLR – Multiple Linear Regression). The correlations to *Prochlorococcus* are all significant on the $p < 0.05$ level. Negative correlations are printed in italic.

		<i>n</i>	CH ₃ I	CHBr ₃	CH ₂ Br ₂
Nano- and picoplankton	<i>Prochlorococcus</i>	72	0.10	0.39	0.26
	Others	72	<0.08	<0.09	<0.10
Phytoplankton pigments	Chl <i>a</i>	61	0.00	0.38	0.49
	MLR	61	None	0.79	0.77

4.1.4 Impact of oceanic CH₃I and wind speed on fluxes

The sea-to-air flux of CH₃I showed significant but low regional correlations with sea surface concentrations ($R^2 = 0.37$) and wind speed ($R^2 = 0.24$) for the whole cruise (Fig. 7a, d, Table 4). Considering each station individually, high significant correlations of oceanic CH₃I and sea-to-air flux were found at open ocean station S2 and at all coastal stations with R^2 ranging between 0.57 and 0.91. Significant correlations of wind speed to the CH₃I sea-to-air flux only existed at coastal station S3 and open ocean station S1 ($R^2 = 0.24$ and 0.76).

4.2 Bromoform (CHBr₃) and dibromomethane (CH₂Br₂)

4.2.1 Regional distribution

CHBr₃ and CH₂Br₂ were both lower in the open ocean with means of 2.3 (1.0–3.8) pmol L⁻¹ for CHBr₃ and 1.6 (1.0–2.2) pmol L⁻¹ for CH₂Br₂ with minimum concentrations occurring at S1 (Fig. 2c, d, Table 2). Both compounds had higher coastal concentrations of 18.3 (8.1–42.4) pmol L⁻¹ for CHBr₃ and 5.8 (3.1–9.4) pmol L⁻¹ for CH₂Br₂ with maxima at S5 and a much more pronounced increase in oceanic CHBr₃ than in CH₂Br₂. CHBr₃ and CH₂Br₂ in sea surface water demonstrated much higher relative regional variability of 78 % (CHBr₃) and 59 % (CH₂Br₂) than oceanic CH₃I.

Atmospheric CHBr₃ and CH₂Br₂ increased towards the coast similarly to their oceanic counterparts (Fig. 2c, d, Table 2). The highest mean regional variability was found for CHBr₃ (56 %), while atmospheric CH₂Br₂ showed the lowest (33 %) of the three halocarbons.

4.2.2 Diel variations

Diel variations of both CHBr₃ and CH₂Br₂ in sea surface water were generally lower than their regional variations. The variability of CHBr₃ ranged between 14 % (S1) and 19 % (S2) in the open ocean, while the variability of CH₂Br₂ was even lower with 7 % (S1) and 9 % (S2). At most of the coastal stations CHBr₃ and CH₂Br₂ revealed similar distributions throughout 24 h with maxima in the evening and night hours with the exception of S5 where maxima

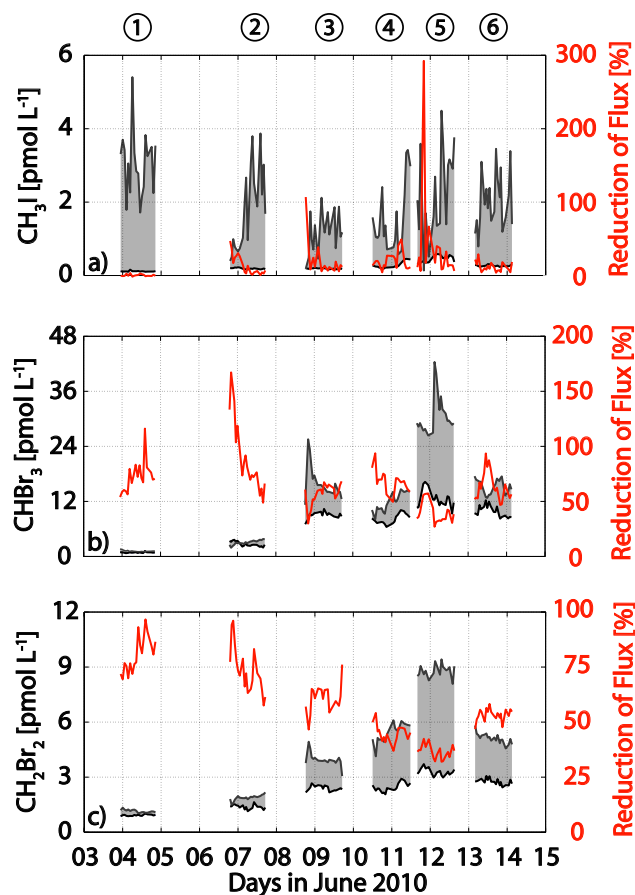


Fig. 6. Influence of atmospheric mixing ratios on the amount of oceanic halocarbons emitted for CH₃I (a), CHBr₃ (b), and CH₂Br₂ (c). Oceanic concentrations are plotted in grey (left axis), the equilibrium concentration is delineated in black, and the concentration gradient is shaded in grey. The percentaged reduction of the concentration gradient by the equilibrium concentration (flux reducing effect) derived from the atmospheric measurements (equilibrium concentration in percent in relation to the water concentrations) is shown in red (right axis). Values above 100 % refer to fluxes from the atmosphere into the ocean.

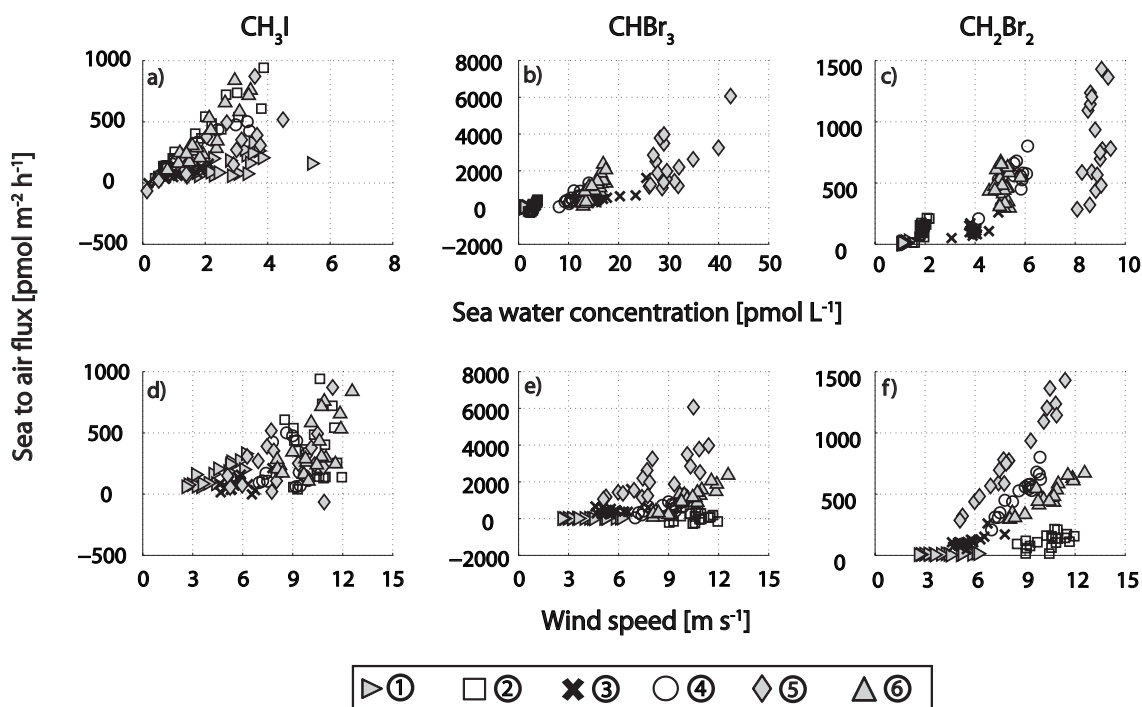


Fig. 7. Sea-to-air fluxes versus sea water concentrations of CH₃I (a), CHBr₃ (b) and CH₂Br₂ (c) and wind speed (d–f) during DRIVE.

of 42.4 pmol L⁻¹ (CHBr₃) and 9.4 pmol L⁻¹ (CH₂Br₂) were found in the morning hours. The highest diel variation of 23 % was found at coastal station S3 for oceanic CHBr₃, while CH₂Br₂ was generally less variable ranging from 4 (S5) to 10 % (S4).

Atmospheric mixing ratios of bromocarbons were low at the open ocean stations S1–S2 with means between 0.6 and 1.78 ppt and relative standard deviations of 13–19 % for CHBr₃ and atmospheric CH₂Br₂ ranging on average between 1.0 and 1.4 ppt with a relative standard deviation of 5–9 %. At CVAO mean mixing ratios of 6.7–6.8 ppt CHBr₃ and of 1.4–1.5 ppt CH₂Br₂ were higher than at S1–S2, as was their diel variability ranging from 35–43 % for CHBr₃ and 14–16 % for CH₂Br₂ (Fig. 3b, c, Table 2). The highest atmospheric CHBr₃ during the whole campaign of 12.8 ppt was measured at CVAO on 7 June. The diel variability of atmospheric CHBr₃ at the coastal stations S3–S6 was generally lower than what was observed above the open ocean with 7 (S3)–14 % (S4) and means of 4.8 (S6)–7.0 ppt (S5). The diel variability of atmospheric CH₂Br₂ at the coast was similar to the open ocean with 5 (S6)–10 % (S4) and means of 2.1 (S6)–2.8 ppt (S5). Atmospheric CHBr₃ and CH₂Br₂ showed no overall diurnal cycles above neither open ocean nor coastal stations with maxima during both day and night hours.

4.2.3 Correlations of CHBr₃ and CH₂Br₂ with phytoplankton pigments

Surface water concentrations of CHBr₃ and CH₂Br₂ correlated significantly with Chl *a* at the 95 % level with correlation coefficients R^2 of 0.38 and 0.49 (Table 3, Figure 2a). Multiple linear regressions (MLR) of brominated halocarbons to all phytoplankton marker pigments were carried out for the whole cruise. All pigment data related to CHBr₃ or CH₂Br₂ with $p < 0.05$ was regarded as significant. The six pigments chlorophyll *b*, chlorophyll *c3*, fucoxanthin, diatoxanthin, pyropheophorbide *a* and zeaxanthin were found to describe the regional distribution of CHBr₃ best (Fig. 2e, Table 3). Chlorophyll *b*, fucoxanthin, α -carotene (negatively correlated) and alloxanthin were important for CH₂Br₂ in the order of explanatory power. Additionally, significant but low correlations of CHBr₃ and CH₂Br₂ were found to *Prochlorococcus* with $R^2 = 0.39$ and $R^2 = 0.26$ (negatively correlated).

4.2.4 Saturation anomaly, sea-air concentration gradients and sea-to-air fluxes

The ocean was generally supersaturated with CHBr₃ and CH₂Br₂ (Fig. 4, Table 2). The overall saturation anomaly of 65 (–40 – 243) % for CHBr₃ was slightly lower than the mean of CH₂Br₂ with 84 (3–204) % (Fig. 4b). Both displayed similar trends opposite to CH₃I: lower anomalies of around 30 % in the open ocean stations, increasing towards the coastal stations S3 – S6 with means of

83 % for CHBr_3 and 110 % for CH_2Br_2 . Maximum saturation anomalies coincided with maximum oceanic and atmospheric bromocarbons at S5 with daily means of 148 % for CHBr_3 and 169 % for CH_2Br_2 . The concentration gradient $c_w - c_{\text{atm}}/H$ of CHBr_3 was the highest of all three halocarbons with a total mean of 5.8 (−1.3–30.0) pmol L^{-1} , followed by CH_2Br_2 with a mean of 2.2 (0–6.3) pmol L^{-1} and minima in the open ocean region (Fig. 5b). The reducing effect of atmospheric CHBr_3 and CH_2Br_2 on the sea-to-air flux was >75 % in the open ocean where both compounds were close to equilibrium and decreases simultaneously with the strongly increasing concentration gradient towards the coast (Fig. 6b, c). For CHBr_3 and CH_2Br_2 the flux reducing effect was around 50 % at the four coastal stations (S3–S6). Sea-to-air fluxes of CHBr_3 and CH_2Br_2 for the whole cruise were on average higher than CH_3I fluxes with 787 (−273–6069) $\text{pmol m}^{-2} \text{h}^{-1}$ and 341 (2–1429) $\text{pmol m}^{-2} \text{h}^{-1}$, respectively (Fig. 5c, Table 2). Fluxes of both compounds were low in the open ocean region with means of 41 $\text{pmol m}^{-2} \text{h}^{-1}$ for CHBr_3 and of 66 $\text{pmol m}^{-2} \text{h}^{-1}$ for CH_2Br_2 . Higher sea-to-air fluxes of CHBr_3 and CH_2Br_2 with means of 1171 and 483 $\text{pmol m}^{-2} \text{h}^{-1}$ were observed at the coastal stations S3–S6. The maximum fluxes of both compounds were found at coastal station 5.

4.2.5 Impact of oceanic CHBr_3 and CH_2Br_2 and wind speed on fluxes

Sea surface water concentrations of CHBr_3 and CH_2Br_2 correlated regionally to sea-to-air fluxes with $R^2 = 0.68$ (CHBr_3) and 0.71 (CH_2Br_2) for the whole cruise (Fig. 7, Table 4). Significant correlations of CHBr_3 fluxes with sea surface water concentrations were found at all 24h-stations (R^2 from 0.34 to 0.78). The highest correlations of sea surface CH_2Br_2 to its sea-to-air fluxes were found at open ocean station S2 (0.64) and coastal stations S3 and S4 (0.42, 0.53). No significant correlations could be observed at coastal stations S5 and S6. In contrast, wind speed showed low but regionally significant correlations to the overall sea-to-air fluxes with $R^2 = 0.14$ (CHBr_3) and $R^2 = 0.29$ (CH_2Br_2). Considering the stations individually, CHBr_3 and CH_2Br_2 revealed high correlations of wind speed with sea-to-air flux at coastal stations S4–S6 with R^2 from 0.56 to 0.95.

5 Discussion

5.1 Sea-to-air fluxes of CH_3I

5.1.1 Oceanic and atmospheric CH_3I as drivers of the regional and diel variability of the concentration gradient

The ocean was highly supersaturated with CH_3I throughout most of the cruise which is underlined by the low impact of atmospheric CH_3I on its concentration gradient (Fig. 6a).

Table 4. Correlation coefficients for water concentrations of halocarbons and wind speed with sea-to-air fluxes of halocarbons for the whole cruise and for the individual stations. Coefficients printed in bold represent significant correlations with $p < 0.05$.

Station	R^2 of	with F of			n
		CH_3I	CHBr_3	CH_2Br_2	
Whole cruise	Water conc.	0.37	0.68	0.71	109
	Wind speed	0.24	0.14	0.29	
S1	Water conc.	0.24	0.66	0.35	18
	Wind speed	0.73	0.28	0.21	
S2	Water conc.	0.89	0.78	0.64	19
	Wind speed	0.00	0.00	0.15	
S3	Water conc.	0.67	0.66	0.42	17
	Wind speed	0.24	0.21	0.56	
S4	Water conc.	0.91	0.60	0.53	17
	Wind speed	0.02	0.67	0.93	
S5	Water conc.	0.57	0.34	0.09	18
	Wind speed	0.02	0.55	0.95	
S6	Water conc.	0.79	0.70	0.00	20
	Wind speed	0.06	0.82	0.78	

Regional and diel variability in the concentration gradient was primarily a result of varying oceanic CH_3I . The oceanic concentrations during DRIVE (0.1 to 5.4 pmol L^{-1} , Table 2) compare well to the measurements by Schall et al. (1997) of 0–3 pmol L^{-1} in the Atlantic, north of 42° N during boreal wintertime. In contrast, Richter and Wallace (2004) measured 3–5 times higher oceanic CH_3I with 7.1–16.4 pmol L^{-1} in boreal fall south of 15° N, and Jones et al. (2010) reported even 6 times higher concentrations (total range from min to max: 1.0–36.5 pmol L^{-1} , data from Jones et al., 2010; Ziska et al., 2013) in the same region and season. Similarly to DRIVE, Jones et al. (2010) found no significant difference between open ocean and coastal regions which was ascribed to photochemical sources supported by the incubation experiments of Richter and Wallace (2004) from the equatorial Atlantic. Richter (2004) found a relationship of oceanic CH_3I with wind speed within this data which was not found during DRIVE: lower wind speeds led to elevated oceanic CH_3I . The much more elevated oceanic CH_3I of Jones et al. (2010) was measured in our study region and season. A possible explanation for their largely elevated CH_3I concentrations compared to our and other open ocean values (Ziska et al., 2013) might be enhanced photochemistry, but more detailed information is not given in the study of Jones et al. (2010). Smythe-Wright et al. (2006) measured CH_3I as high as 45 pmol L^{-1} in the Atlantic region south of 40° N in late summer which was accompanied by high *Prochlorococcus* abundance. In contrast, no outstanding relationship of CH_3I with picoplankton including *Prochlorococcus* or the marker pigment divinyl chlorophyll *a* indicative of these species was found during DRIVE. Additionally, no correlation with diatom pigments as suggested by Lai et al. (2011) for the production of open ocean CH_3I was

observed, supporting photochemistry as important production pathway for its formation as suggested by Moore and Zafriou (1994). The likely non-biological formation of CH_3I also leads to high saturation anomalies in open ocean surface waters. The lower saturation anomalies in the coastal zone might likely be a result of upwelled water diluting the more concentrated surface water (Happell and Wallace, 1996) combined with the elevated atmospheric CH_3I above the upwelling. The large supersaturation of CH_3I in surface water of the open ocean region indicates their potential for largely elevated sea-to-air fluxes in contrast to the coastal area. However, CH_3I production may not be completely independent of biological parameters. Lacking correlations of CH_3I concentrations with pigment and flow cytometry data does not necessarily allow for excluding a biological source completely. The concentrations are a result of production and loss processes, which may partly be temporally and spatially decoupled. Another possible source for CH_3I involves bacteria (Manley and Dastoor, 1998; Amachi et al., 2001; Fuse et al., 2003) which has not been taken into account during DRIVE. Additionally, Bell et al. (2002) suggested that organic precursors from phytoplankton production could be involved in the photochemical formation of CH_3I in the surface ocean.

Atmospheric CH_3I (0.6 to 3.3 ppt) measured during DRIVE falls well within the range of tropical Atlantic values reported by Williams et al. (2007) of 1.4 (0.6–3.0) ppt. Air mass back trajectory analysis and similar ranges of atmospheric CH_3I at open ocean station S1 and parallel at CVAO on Cape Verde indicate open ocean air masses at both locations on 4 June (Fuhlbrügge et al., 2013). Wind speed at Cape Verde was highly variable on June 6 (Fig. 3d) leading to high variations in local sea-to-air fluxes likely causing the observed higher mean variability in atmospheric CH_3I at CVAO parallel to open ocean station S2 (Sect. 4.1.2, Fig. 3a). Atmospheric CH_3I during DRIVE at CVAO (0.7–1.8 ppt) was generally lower than the 1.2–13.8 ppt detected by O'Brien et al. (2009) in a similar season.

Non-biological or indirect biological formation mechanisms in the surface water seem likely since the variability in oceanic CH_3I was not correlated to the measured biological variables. Although a biological source cannot completely be excluded, the abiotic formation thus appears as main driver for variations of its concentration gradient across the air-sea interface with negligible influence from atmospheric CH_3I on oceanic concentrations.

5.1.2 The relative influence of concentration gradient and wind speed on sea-to-air fluxes of CH_3I

Applying the parameterization of Nightingale et al. (2000), sea water concentrations and wind speed were almost equally important as driving factors for the variations in the CH_3I sea-to-air flux for the whole cruise region (Fig. 7) based on their similar regional variability (see the scatter in Fig. 8a

and similar error bars at the plot that includes all data points in Figure 8b). Diel variability in fluxes could be mainly ascribed to variations in oceanic CH_3I , since they were much higher than the diel variability in wind speed (Fig. 8a, b). Significant correlations of wind speed with sea-to-air fluxes of CH_3I were only found at two 24h-station. The high correlation to wind speed at S1 was caused by the large variability of the generally low speeds in combination with a relatively constant high concentration gradient. Here we note that although the parameterization of Nightingale et al. (2000) is a commonly applied parameterization for k_w in oceanic trace gas emissions, it might not include all factors influencing sea-to-air fluxes. Stability of the atmosphere and the ocean, sea state, bubble transfer, as well as surfactants might influence the transfer across the air-sea interface as well. Some of these factors are included in the TOGA COARE algorithm representing an alternative method for deriving transfer coefficients, which involves an additional set of meteorological parameters such as air temperature and specific humidity profiles, solar irradiance, downwelling longwave irradiance, and precipitation (Fairall et al., 2003).

Our mean (10^{th} – 90^{th} percentile) fluxes of 268 (64–550) in the open ocean and 246 (42–523) $\text{pmol m}^{-2} \text{h}^{-1}$ in the coastal region are 7.5 and 8.7 lower than the fluxes of Jones et al. (2010) of 2021 (417–4046) and 2154 (321–4096) $\text{pmol m}^{-2} \text{h}^{-1}$. Although the spatial resolution of the measurements by Jones et al. (2010) in the same region was higher than during DRIVE, the difference in emission strength can be mainly explained by their large sea water concentrations and very low atmospheric mixing ratios compared to our study. The fluxes reported here were 3.8 times lower than fluxes reported by Richter and Wallace (2004) ($958.3 \pm 750.0 \text{ pmol m}^{-2} \text{h}^{-1}$) using a similar flux parameterization which are a result of higher oceanic CH_3I as well.

5.2 Sea-to-air fluxes of CHBr_3 and CH_2Br_2

5.2.1 Oceanic and atmospheric CHBr_3 and CH_2Br_2 as drivers of regional and diel variability of the concentration gradient

The oceanic concentrations of both compounds were generally driving factors for their concentration gradients during DRIVE. Only in the open ocean atmospheric CHBr_3 and CH_2Br_2 reduced the sea-to-air fluxes significantly (Fig. 6) where the low oceanic concentrations were close to equilibrium with the atmosphere and even led to undersaturation of CHBr_3 at S2. The concentration gradient increased towards the Mauritanian upwelling with a much more pronounced increase in oceanic CHBr_3 and CH_2Br_2 than in the atmosphere. The oceanic and atmospheric concentrations as well as the concentration gradients of both bromocarbons peaked simultaneously at coastal station S5. Open ocean CHBr_3 (1.0 – 3.8 pmol L^{-1}) and CH_2Br_2 (1.0 – 2.2 pmol L^{-1}), increasing towards the coast of Mauritania to 8.1 – 42.4 pmol L^{-1} and

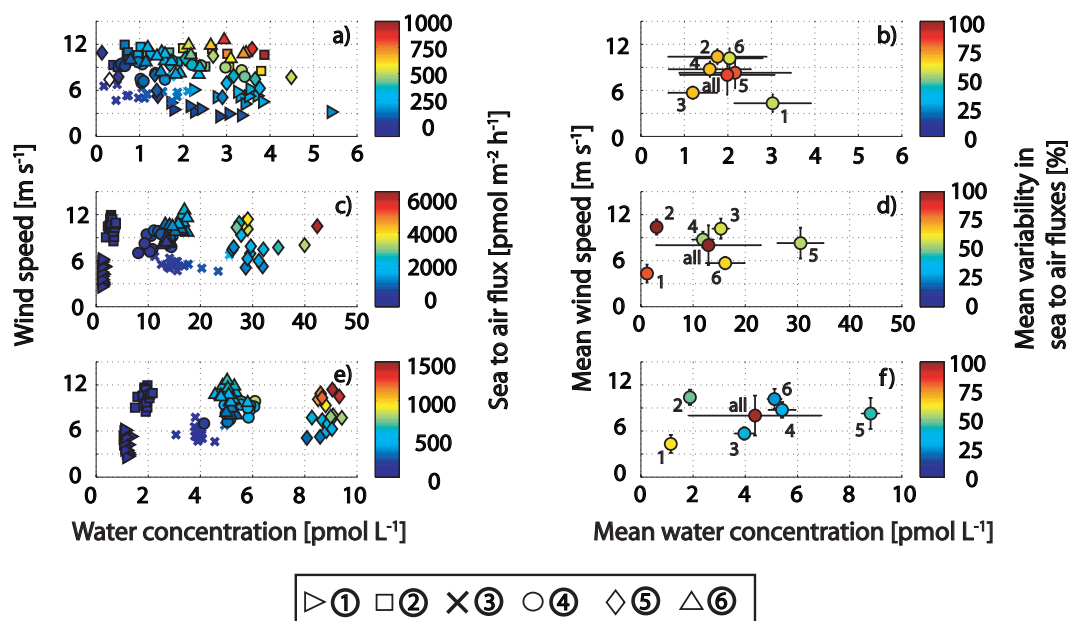


Fig. 8. Left side – wind speed versus CH_3I (a), CHBr_3 (c) and CH_2Br_2 (e) water concentrations. Symbols are filled according to their sea-to-air flux (see color bars). Right side – mean wind speed versus mean CH_3I (b), CHBr_3 (d) and CH_2Br_2 (f) water concentrations with their standard deviations which is expressed in error bars (horizontal for water concentrations and vertical for wind speed) for each diel station (S1–S6) and for all stations together. Symbols are filled with the relative standard deviations of the sea-to-air fluxes (see color bars).

Table 5. Phytoplankton pigments that were found to be significant at $p < 0.05$ and what they are indicative for.

Pigment	Indicative for	CHBr_3	CH_2Br_2
Chlorophyll <i>b</i>	Chlorophytes	x	x
Chlorophyll <i>c3</i>	Haptophytes	x	
Fucoxanthin		x	x
Diatoxanthin	Diatoms	x	
Zeaxanthin	Cyanobacteria	x	
α -carotene			x
Alloxanthin	Cryptophytes		x
Pyropheophorbide <i>a</i>	Grazing	x	

3.1–9.4 pmol L^{-1} , respectively were in good agreement to earlier studies conducted in the oligotrophic tropical and subtropical Atlantic. Class and Ballschmiter (1988) reported 3.2–23.7 pmol L^{-1} for CHBr_3 and 1.7–5.8 pmol L^{-1} for CH_2Br_2 in March, Schall et al. (1997) found 3.2–8.0 for CHBr_3 and 1.0–1.8 pmol L^{-1} for CH_2Br_2 in boreal wintertime, while Carpenter et al. (2009) published values from the same season as DRIVE of 2.1–43.6 for CHBr_3 and 0.7–8.7 pmol L^{-1} for CH_2Br_2 with the highest values in the Mauritanian upwelling and close to the coast. In contrast to oceanic CH_3I during DRIVE, oceanic CHBr_3 and CH_2Br_2 was elevated in the biological active regions and correlated with phytoplankton pigments.

Possible biological sources during DRIVE were identified by using pigments indicative for various phytoplank-

ton groups which were investigated with MLR more thoroughly. However it should be noted that, for example, fucoxanthin, which mainly occurs in diatoms, is also present in other phytoplankton groups to a certain extent (Jeffrey and Vesk, 1997). Production of halocarbons and the occurrence of the phytoplankton pigments may also take place on different time scales, which may obscure or stimulate a correlation. CHBr_3 and CH_2Br_2 showed a relationship to *Chlorophytes* and *Diatoms* while CHBr_3 also correlated significantly with *Cyanobacteria* and CH_2Br_2 with *Cryptophytes* (Tables 3, 5). Similar biological sources for both bromocarbons are in agreement to previous studies (Manley et al., 1992; Tokarczyk and Moore, 1994). The regional distribution of *Chlorophytes* and CHBr_3 and CH_2Br_2 were in best agreement to each other. *Diatoms*, although they were the dominant species in the Mauritanian upwelling and have been shown to produce halocarbons in the laboratory (Moore et al., 1996), appeared not as major contributors to bromocarbons which is in agreement to Quack et al. (2007b). Additionally, pyropheophorbide *a* was shown to be significant for the CHBr_3 distribution. This chlorophyll degradation product is specific for grazing which could lead to release of bromocarbons (Nightingale et al., 1995) produced within the algae (Moore et al., 1996). The correlations with phytoplankton pigments indicate a potential biological production of CHBr_3 and CH_2Br_2 , which is also supported by their regional distribution. However, these correlations can neither resolve the rates of production and loss processes of bromocarbons in the ocean, nor their temporal and spatial distribution. Thus,

the correlations found during DRIVE only represent indicators to possible source organisms.

Diel variability in the open ocean for both bromocarbons was very low and increased towards the coast. No relationship of halocarbons to either light, SST or salinity was found during 24 h. Elevated CHBr_3 and CH_2Br_2 were usually observed during evening (S3, S4 and S6) and night hours (S5). In contrast, many laboratory and field studies with both macroalgae and phytoplankton have shown maxima of CHBr_3 and CH_2Br_2 during the day which was attributed to light induced oxidative stress on the organisms (Ekdahl et al., 1998; Carpenter et al., 2000; Abrahamsson et al., 2004). Bromocarbon production from phytoplankton is still poorly characterized. Elevated bromocarbon production during night may indicate formation during respiration in contrast to light linked production during photosynthesis (Ekdahl et al., 1998; Abrahamsson et al., 2004) or other stress factors such as grazing. Alternatively, CHBr_3 and CH_2Br_2 could also be stored in the algal cells during light production and released later during the night time (Ekdahl et al., 1998) which would obscure a correlation to light in the field.

In conclusion, the regional variability of the concentration gradients of both bromocarbons was probably a result of the regional differences in primary production supported by their relationship to SST and phytoplankton pigment data (Sect. 4.2.3).

5.2.2 The relative influence of concentration gradient and wind speed on sea-to-air fluxes of CHBr_3 and CH_2Br_2

The regional distribution of sea-to-air fluxes of both bromocarbons was strongly determined by the most likely biologically produced oceanic CHBr_3 and CH_2Br_2 . The regional variability in oceanic bromocarbons was much larger than the regional variations in wind speed (Fig. 8c–f). However, within individual stations, the variability in oceanic CHBr_3 and CH_2Br_2 was mostly lower than the variations in wind speed. At the open ocean stations, only very low oceanic bromocarbons were measured leading to very low concentration gradients and thus to very low sea-to-air fluxes, since the wind speed did not have a large impact on the variability of sea-to-air fluxes. With increasing oceanic CHBr_3 and CH_2Br_2 concentrations, the diel impact of changes in wind speed on the sea-to-air flux variability increased which is expressed in high correlation coefficients (Table 4, Fig. 8c, e). This effect was most pronounced for CH_2Br_2 which showed the lowest diel concentration variability of all three halocarbons (see the scatter in Fig. 8e). The influences of wind speed and concentration gradient on the emissions of bromocarbons are discussed based on the parameterization of Nightingale et al. (2000), which may not include all control factors similarly to our discussions concerning CH_3I emissions (Sect. 5.1.2).

Carpenter et al. (2009) derived 8.9 times higher CHBr_3 fluxes in the open ocean and 1.3 times higher in the coastal region of mean (10th–90th percentile) 367 (42–625) and 1483 (421–3504) $\text{pmol m}^{-2} \text{h}^{-1}$ in comparison to our study with 41 (–150 – 222) and 1171 (300 – 2463) $\text{pmol m}^{-2} \text{h}^{-1}$. Sea-to-air fluxes of CH_2Br_2 calculated by Carpenter et al. (2009) were 2.4 times higher in the open ocean and in a similar range in the coastal region with 158 (17–288) and 554 (204–917) $\text{pmol m}^{-2} \text{h}^{-1}$ in comparison to 66 (5–155) and 483 (109–809) $\text{pmol m}^{-2} \text{h}^{-1}$ (this study) analyzing the same season and region although with higher spatial resolution. This resulted from larger concentration gradients due to their lower atmospheric mixing ratios and comparable ambient parameters.

5.3 Other impact factors on sea-to-air fluxes: MABL height and SST

Wind speed and concentration gradients are direct factors that influence sea-to-air fluxes. Some more indirect factors that could possibly impact the emissions include SST and the MABL through their intensifying or decreasing effect on the concentration gradient. Possible effects of the changes in SST on the solubility of oceanic halocarbons and therewith their concentration gradients were small during DRIVE compared to the variability in sea water concentrations (Fig. 2).

The MABL height has implications for the atmospheric mixing ratios of halocarbons and their sea-to-air fluxes via the concentration or dilution of atmospheric halocarbons, emitted from the oceans, within a decreasing or increasing MABL height (Fuhlbrügge et al., 2013). In order to understand the possible effect of MABL variations, sea-to-air fluxes of all three halocarbons were calculated with minimum and maximum atmospheric mixing ratios associated with high (S1) and low MABL heights (S5) to cover the range of potential fluxes in the study region (Fig. 9). A different concentration distribution caused by other atmospheric conditions can change the CHBr_3 and CH_2Br_2 sea-to-air fluxes on average between 19 % (S5) and 4160 % (S1) for CHBr_3 and between 7 % (S5) and 1337 % (S1) for CH_2Br_2 (see the lower and upper limits in Fig. 9b–c; the shading implicates the potential range). The effect on the CH_3I fluxes is from 1 % (S1) to 42 % (S4) (Fig. 9a) lower due to its high supersaturation (Fig. 4a). Considering the large MABL height changes occurring within one day above coastal stations, e.g. from 100 to 350 m at S6, the effect of the entailing varying atmospheric mixing ratios on local emissions has to be taken into account when assessing halocarbon sea-to-air fluxes from coastal upwelling regions.

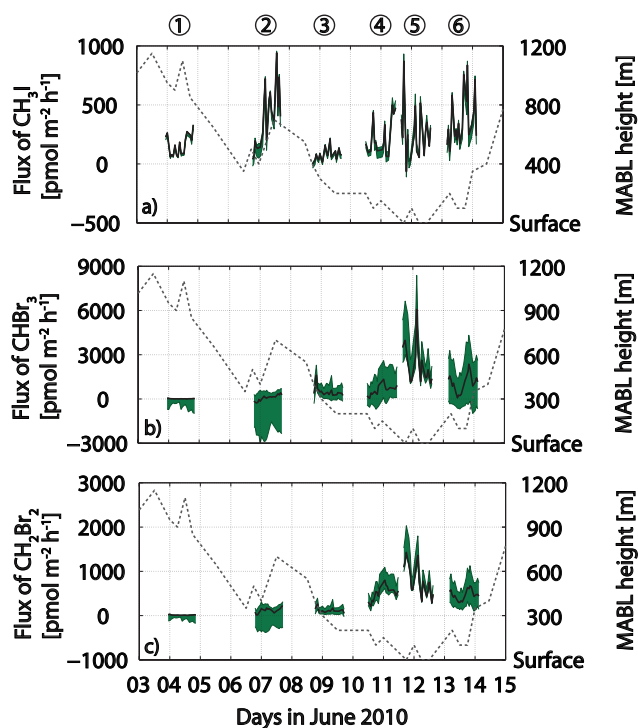


Fig. 9. Sea-to-air fluxes for CH_3I (a), CHBr_3 (b) and CH_2Br_2 (c) during DRIVE and the MABL height, determined by Fuhlbrügge et al. (2013) as the dashed grey line are shown on the right side. The upper and lower value of potential sea-to-air fluxes assuming the lowest MABL (lower range, 3.0 ppt for CH_3I , 3.1 ppt for CH_2Br_2 and 8.9 ppt for CHBr_3) and the highest MABL (upper range, 0.6 ppt for CH_3I , 0.9 ppt for CH_2Br_2 and 0.5 ppt for CHBr_3) valid for the whole region are shaded in green.

5.4 Oceanic influence on atmospheric mixing ratios of CH_3I , CHBr_3 and CH_2Br_2

5.4.1 The contribution of the oceanic emissions to the atmospheric mixing ratios

We have shown in the last sections that the sea-to-air fluxes of halocarbons are dominated by the oceanic production and that the sea water concentrations of bromocarbons are increasing towards the coast. In order to understand the importance of sea-to-air fluxes for the atmospheric halocarbon distribution, we calculated their relative contributions to the atmospheric mixing ratios at the individual 24-h-stations. Previous studies assigned the high CHBr_3 and CH_2Br_2 mixing ratios above the coastal upwelling to air masses originating from the North West African continent (Quack et al., 2007a) and very low atmospheric bromocarbons to air masses from the northern open ocean (Carpenter et al., 2009; Lee et al., 2010). Air masses during coastal station S5 also arrived from the northern open ocean (Fuhlbrügge et al., 2013) which contradicts the hypothesis that high atmospheric halocarbons could only be accounted for by continental sources.

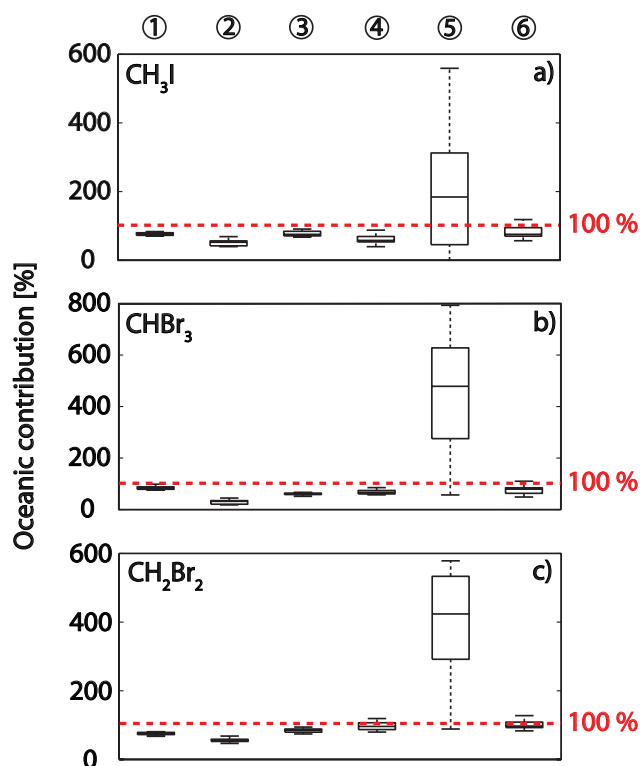


Fig. 10. Oceanic contributions to atmospheric halocarbons assuming a mean distance of 200 km, mean wind speeds, mean sea-to-air fluxes and background mixing ratios for the open ocean ($\text{CH}_3\text{I} = 0.50$ ppt, $\text{CHBr}_3 = 0.50$ ppt, $\text{CH}_2\text{Br}_2 = 0.75$ ppt) and the coastal region ($\text{CH}_3\text{I} = 0.75$ ppt, $\text{CHBr}_3 = 3.00$ ppt, $\text{CH}_2\text{Br}_2 = 1.80$ ppt), and the MABL heights determined by Fuhlbrügge et al. (2013) at every measurement point for CH_3I (a), for CHBr_3 (b) and for CH_2Br_2 (c), outliers are excluded. The red dashed line marks 100 % in every plot.

For our calculations, we apply a fetch of 200 km (the mean distance between the diel stations), sea-to-air fluxes from Sects. 4.1.5 and 4.2.6, according wind speeds and MABL heights (Table 1). The sea-to-air fluxes and the height of the MABL have numerically the same influence on atmospheric mixing ratios since bromocarbons in the atmosphere are within the calculations a product of both. Applying a fetch of 200 km, the air mass travels approximately 7 h until it arrives at the diel stations. Open ocean background values for S1 and S2 were set to 0.50 ppt for CH_3I and CHBr_3 , and 0.75 ppt for CH_2Br_2 , while higher background values of 0.75 ppt for CH_3I , 1.80 ppt for CH_2Br_2 and 3.00 ppt for CHBr_3 were assigned to coastal stations S3–S6. We did not include the tropical atmospheric lifetimes of the three halocarbons (7, 24, 123 days for CH_3I , CHBr_3 , CH_2Br_2 ; Montzka and Reimann, 2011) since the degradation during the short-term box-calculation has no substantial influence on the results. The oceanic emissions are nearly sufficient to explain most of the atmospheric halocarbons (Fig. 10a–c). Oceanic halocarbon contributions at S1–S6 (except for S5)

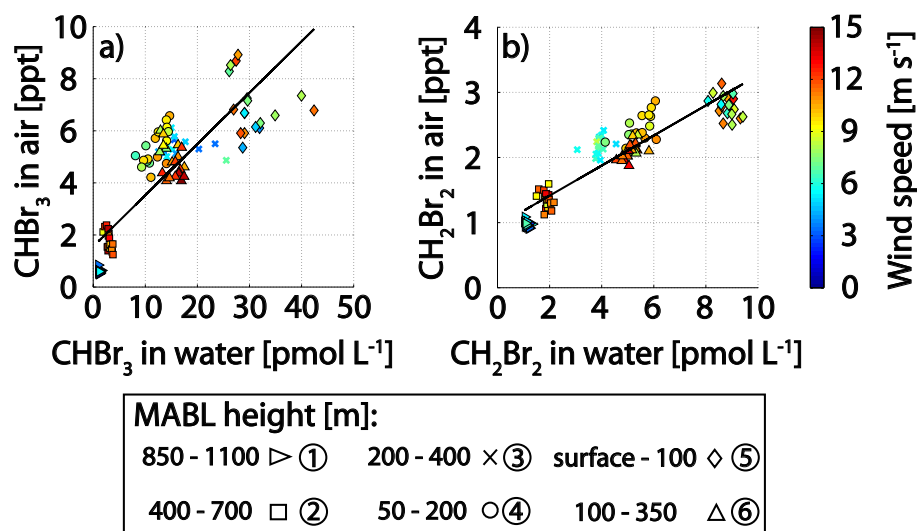


Fig. 11. Correlations of oceanic versus atmospheric halocarbons (CHBr_3 in **a** and CH_2Br_2 in **b**) filled with wind speed (see color coding). The black line indicates the regression line for the whole cruise. For the individual correlation coefficients see Table 6.

ranged from 39 to 135 % for CH_3I , between 18 and 126 % for CHBr_3 and from 47 to 148 % for CH_2Br_2 with generally lowest contributions at S2 (40–69 % for CH_3I , 18–45 % for CHBr_3 and 47–68 % for CH_2Br_2). At S5, the emissions from the assumed 200 km fetch contributed 560 (CH_3I)–800 % (CHBr_3) to the observed mixing ratios. At this station high oceanic and atmospheric CHBr_3 and CH_2Br_2 coincided with very low MABL heights. These results suggest that (1) atmospheric mixing ratios over the open ocean S1–S2 are derived from regional emissions and distant sources, (2) the source strength in combination with the observed MABL height can nearly maintain the medium range of atmospheric mixing ratios found at S3, S4, and S6, and (3) the high sea-to-air fluxes and low MABL heights leading to the highly elevated atmospheric mixing ratios at S5 are a very local phenomenon, constrained to the boundaries of this station. The large overestimation of mixing ratios within the box model is then a result of the extrapolation of the high sea-to-air fluxes to the fetch of 200 km. Vertical transport has been neglected in this simple model approach, which likely introduces only small errors since the top of the MABL was very stable and isolated above all coastal stations (Fuhlbrügge et al., 2013).

While the Mauritanian upwelling has been identified to contribute to the high atmospheric abundances of all halocarbons in the region, the elevated and highly variable atmospheric mixing ratios of CHBr_3 and CH_2Br_2 at Cape Verde can be attributed to local sources. O'Brien et al. (2009) suggested high atmospheric halocarbons at CVAO originating from the coastal region off Mauritania. However, back trajectory analysis revealed air masses at CVAO originating from the open ocean during our investigation (Fuhlbrügge et al., 2013). This together with the considerably lower atmospheric mixing ratios measured at the open ocean sta-

tions (0.5–2.4 ppt for CHBr_3 and 0.9–1.6 ppt for CH_2Br_2) and around the upwelling contradicts upwelling originated halocarbons at Cape Verde during DRIVE. In addition, CHBr_3 reached its highest value of the whole campaign at CVAO. Hence, the high and variable atmospheric CHBr_3 and CH_2Br_2 at Cape Verde in combination with comparably variable wind speeds suggest local coastal sources for both compounds.

5.4.2 Correlations between oceanic and atmospheric CHBr_3 and CH_2Br_2

In contrast to the observations presented in Quack et al. (2007a) and Carpenter et al. (2009), atmospheric CHBr_3 and CH_2Br_2 followed the same regional distribution as their oceanic counterparts. Water concentrations and atmospheric mixing ratios of CHBr_3 ($R^2=0.74$) and CH_2Br_2 ($R^2=0.85$) correlated regionally very well during DRIVE (Fig. 11a–b) which has not been observed during the other cruises. This is likely caused by a combination of the stable and isolated marine boundary layer observed over the upwelling, the coinciding high productivity and concentration of the bromocarbons in the upwelling, and the combined effects of air-sea exchange as slowest process (over a considerable fetch) and advection as the fastest (diluting with background air), both influencing the atmospheric signals. We assume biological production of bromocarbons and mixing within the water column also as rapid processes (Ekdahl et al., 1998). Correlations between atmospheric mixing ratios and oceanic concentrations within the individual 24h-stations were only significant at open ocean station S2 for CHBr_3 and at coastal stations S4 and S6 for both compounds (Table 6). A diel anti-correlation of atmospheric mixing ratios with water concentrations was also observed at several diel stations (S1, S2, S5,

Table 6. Correlation coefficients R^2 and number of data points n of oceanic versus atmospheric bromocarbons for the whole cruise and each individual station. Bold numbers indicate significant correlations with $p < 0.05$. Italic numbers mark negative correlations.

	Whole cruise	S1 (17.6° N and 24.3° W)	S2 (18.0° N and 21.0° W)	S3 (18.0° N and 18.0° W)	S4 (18.5° N and 16.5° W)	S5 (19.0° N and 16.6° W)	S6 (20.0° N and 17.3° W)
CHBr ₃	0.74	<i>0.01</i>	0.52	0.01	0.45	<i>0.05</i>	0.20
CH ₂ Br ₂	0.85	<i>0.19</i>	<i>0.09</i>	0.01	0.40	<i>0.18</i>	0.28
n	109	18	19	17	17	18	20

and S6). An explanation for this observation (see Table 6) between the atmospheric and oceanic concentrations on a diel scale is still lacking, since neither wind direction, including land-sea breeze circulation (Fuhlbrügge et al., 2013), nor MABL height variations led to clear correlations.

Positive and negative deviations from the overall good regional correlation of sea water concentrations and atmospheric mixing ratios could also be observed at the individual stations. Atmospheric concentrations can increase with wind speed due to increasing sea-to-air fluxes, while elevated wind speeds also dilute local emissions with background air and vice versa. Thus, low wind speeds in the open ocean led to lower atmospheric mixing ratios at S1 while the higher wind speeds at S2 triggered average mixing ratios (Fig. 11). This may not only be a result of increasing sea-to-air flux and fetch, but may also be partly a result of the reduction of the MABL height. While coastal stations S3, S4 and S6 have similar mean CHBr₃ surface water concentrations, S6 showed the largest sea-to-air fluxes of these three stations due to the largest prevailing wind speeds (see Fig. 5), but on average relatively low atmospheric mixing ratios (Fig. 11a, b). We interpret this as intense transport phenomenon and possible dilution of the large sea-to-air fluxes with background air masses due to intensifying winds and increasing MABL height. Although atmospheric mixing ratios for CHBr₃ and CH₂Br₂ were highest at S5, they are on average much lower as could be expected from the overall regional correlation and the large sea water concentrations (see the data points below the correlation line in Fig. 11a, b in contrast to most of the data points from other stations that are above the line). We hypothesize regional mixing with background air masses as cause for the lower than average correlation of sea surface CHBr₃ and CH₂Br₂ and atmospheric bromocarbons, which supports that the high atmospheric mixing ratios at S5, the high sea-to-air fluxes, and low MABL height are very local phenomena. The good overall correlation between atmospheric and oceanic bromocarbons shows the dominance of sea water production for the atmosphere. The co-correlation of increased productivity and production of bromocarbons during upwelling of cold and nutrient rich water and the high atmospheric mixing ratios in a low and stable MABL over the low sea surface temperature of the upwelled water (Fuhlbrügge et al., 2013) can be explained within the

known concepts of wind driven air-sea exchange, advection and MABL variations on a regional scale.

6 Summary and conclusions

We have discussed the temporal and spatial influence of biological productivity, wind speed, MABL height and SST on oceanic emissions and atmospheric mixing ratios of halocarbons in the tropical North East Atlantic.

During DRIVE, oceanic CH₃I neither showed a relationship to phytoplankton pigments nor to cyanobacteria, and its distribution appeared mainly as a result of abiotic or indirect biological formation which seemed to be the main driver of the CH₃I concentration gradient between sea water and air. On a regional scale, neither wind speed nor oceanic CH₃I were dominating the sea-to-air flux, while diel variations in emissions were a result of varying oceanic CH₃I concentrations almost throughout the whole cruise. On the contrary, the oceanic distribution of CHBr₃ and CH₂Br₂ and their emissions correlated with phytoplankton pigments which implies a biological source, albeit with no clear diurnal cycles unlike observed in previous studies. The variability in wind speed gained increasing impact on the diel bromocarbon emissions with decreasing distance to the coast, because the diel variability in oceanic CHBr₃ and even more pronounced in oceanic CH₂Br₂ was low in comparison to large diel wind speed variations.

MABL height was identified as an additional factor impacting oceanic emissions of halocarbons in the upwelling through its influence on atmospheric halocarbon abundances. Sea-to-air fluxes of CH₃I were hardly influenced by the varying MABL due to its high supersaturation in sea surface water. The sea-to-air fluxes of CHBr₃ and CH₂Br₂ however were substantially influenced by atmospheric conditions. High atmospheric CH₃I, CHBr₃ and CH₂Br₂ mixing ratios at a coastal site on the Cape Verde islands (CVAO) could be attributed to local coastal sources. Regional oceanic bromocarbon emissions from the upwelling, probably driven by biological production, could in combination with varying and low MABL heights and air mass transport explain most of the observed atmospheric halocarbons, contrasting previous hypotheses regarding additional continental bromo-

carbon sources above the upwelling. As a result, the atmospheric bromocarbons showed significant and high overall correlations with the oceanic concentrations, which is caused by the coincidence of oceanic production in upwelled water and low and stable MABLs over the cold upwelled water. We therefore hypothesize that low MABL heights and high sea-to-air fluxes coinciding with high atmospheric mixing ratios could be a common feature in coastal upwelling systems (this study; Fuhlbrügge et al., 2013).

The temporal and spatial development of biological production, wind speed, SST and changes in atmospheric mixing ratios with MABL height will influence the future sea-to-air fluxes and their corresponding atmospheric mixing ratios, as well as their contribution to atmospheric chemical processes. Surface air and water temperature could play a crucial role in the future development of wind speed via the potentially increased land-sea pressure gradients. A potential future increase of SST in the tropical oligotrophic Atlantic (Hoerling et al., 2001) could lead to enhanced oceanic production of CH₃I (Richter, 2004) and in combination with reduced solubility to elevated emissions of CH₃I. An elevation of atmospheric CH₃I with increasing SST and accompanying physical-biological phenomena on a decadal scale has already been shown by Yokouchi et al. (2012) in the tropical and temperate Pacific region. At the same time, the enhancement of eastern boundary upwelling systems accompanied by increasing primary production (Lachkar and Gruber, 2012) could result in higher production of oceanic bromocarbons. Combined with elevated wind speeds (Bakun, 1990), increased emissions of brominated compounds would be the consequence. Hence, the relevance of the tropical upwelling systems with respect to halocarbon emissions will likely increase and the influence of the diel and regional drivers on the emissions may be intensified. To better understand the current and future roles of halocarbon emissions from marine upwelling regions on global ozone changes and atmospheric chemistry, it is important to continue to better quantify the relative roles and interactions of oceanic halocarbon production, wind speed and MABL height, SST and seasonal variations, as well as other relevant forcings in oceanic upwelling regions around the global ocean.

Acknowledgements. The authors would like to thank the chief scientist of the cruise P399/2 Prof Dr Hermann W. Bange, as well as the captain and the crew of the RV *Poseidon* during P399/2 for all their help and support. We are also very grateful to Karen Stange and Gert Petrick for their technical support before and during the campaign. We would like to acknowledge Carolin Löscher for her help with water sampling for pigment analysis and Bettina Taylor for analysis of the flow cytometry samples. The authors thank Christian Müller and Julian Kinzel for their assistance with air sampling at CVAO. We thank Xiaorong Zhu and Leslie Pope for technical assistance in the air canister analyses. Furthermore, we would like to thank Christa Marandino and Susann Tegmeier for their helpful input. We acknowledge the National Centre

for Atmospheric Science (NCAS) for providing the Cape Verde Atmospheric Observatory wind speed data. Additionally, the authors would like to acknowledge NASA for providing satellite MODIS-Aqua data. We thank the anonymous reviewers for very helpful input and corrections. This work was part of the German research project SOPRAN II (grant no. FKZ 03F0611A) funded by the Bundesministerium für Bildung und Forschung (BMBF), and was also supported by the EU project SHIVA (grant no. FP7-ENV-2007-1-226224), as well as NASA UARP Grant NNX09AJ25G.

The service charges for this open access publication have been covered by a Research Centre of the Helmholtz Association.

Edited by: W. T. Sturges

References

- Abrahamsson, K., Lorén, A., Wulff, A., and Wangberg, S. A.: Air-sea exchange of halocarbons: The influence of diurnal and regional variations and distribution of pigments, *Deep-Sea Res. Part II-Top. Stud. Oceanogr.*, 51, 2789–2805, doi:10.1016/j.dsr2.2004.09.005, 2004.
- Amachi, S., Kamagata, Y., Kanagawa, T., and Muramatsu, Y.: Bacteria mediate methylation of iodine in marine and terrestrial environments, *Appl. Environ. Microbiol.*, 67, 2718–2722, doi:10.1128/aem.67.6.2718-2722.2001, 2001.
- Aschmann, J., Sinnhuber, B. M., Chipperfield, M. P., and Hosaini, R.: Impact of deep convection and dehydration on bromine loading in the upper troposphere and lower stratosphere, *Atmos. Chem. Phys.*, 11, 2671–2687, doi:10.5194/acp-11-2671-2011, 2011.
- Bakun, A.: Global climate change and intensification of coastal ocean upwelling, *Science*, 247, 198–201, doi:10.1126/science.247.4939.198, 1990.
- Bange, H. W., Atlas, E. L., Bahlmann, E., Baker, A. R., Bracher, A., Cianca, A., Dengler, M., Fuhlbrügge, S., Großmann, K., Hepach, H., Lavric, J., Löscher, C., Krüger, K., Orlikowska, A., Peeken, I., Quack, B., Schafstall, J., Steinhoff, T., Williams, J., and Wittke, F.: Fs poseidon fahrtbericht/cruise report p399 – 2 & 3, Leibniz-Institut für Meereswissenschaften IFM-GEOMAR, Kiel, 74, 2011.
- Bell, N., Hsu, L., Jacob, D. J., Schultz, M. G., Blake, D. R., Butler, J. H., King, D. B., Lobert, J. M., and Maier-Reimer, E.: Methyl iodide: Atmospheric budget and use as a tracer of marine convection in global models, *J. Geophys. Res.-Atmos.*, 107, 4340, doi:10.1029/2001jd001151, 2002.
- Carpenter, L. J. and Liss, P. S.: On temperate sources of bromoform and other reactive organic bromine gases, *J. Geophys. Res.-Atmos.*, 105, 20539–20547, 2000.
- Carpenter, L. J., Malin, G., Liss, P. S., and Kupper, F. C.: Novel biogenic iodine-containing trihalomethanes and other short-lived halocarbons in the coastal east atlantic, *Glob. Biogeochem. Cy.*, 14, 1191–1204, 2000.
- Carpenter, L. J., Jones, C. E., Dunk, R. M., Hornsby, K. E., and Woeltjen, J.: Air-sea fluxes of biogenic bromine from the tropical and north atlantic ocean, *Atmos. Chem. Phys.*, 9, 1805–1816, doi:10.5194/acp-9-1805-2009, 2009.

- Class, T., and Ballschmiter, K.: Chemistry of organic traces in air viii: Sources and distribution of brom- and bromochloromethanes in marine air and surfacewater of the atlantic ocean, *J. Atmos. Chem.*, 6, 35–46, 1988.
- Ekdahl, A., Pedersén, M., and Abrahamsson, K.: A study of the diurnal variation of biogenic volatile halocarbons, *Mar. Chem.*, 63, 1–8, 1998.
- Fairall, C. W., Bradley, E. F., Hare, J. E., Grachev, A. A., and Edson, J. B.: Bulk parameterization of air–sea fluxes: Updates and verification for the coare algorithm, *J. Clim.*, 16, 571–591, doi:10.1175/1520-0442(2003)016<0571:bpoasf>,2.0.co;2, 2003.
- Fedoseev, A.: Geostrophic circulation of surface waters on the shelf of north-west africa, *Rapp. Proc. Verb. Reun. Cons. Inst. Expl. Mer.*, 159, 32–37, 1970.
- Fuhlbrügge, S., Krüger, K., Quack, B., Atlas, E. L., Hepach, H., and Ziska, F.: Impact of the marine atmospheric boundary layer on vsls abundances in the eastern tropical and subtropical north atlantic ocean, *Atmos. Chem. Phys.*, 13, 6345–6357, doi:10.5194/acp-13-6345-2013, 2013.
- Fuse, H., Inoue, H., Murakami, K., Takimura, O., and Yamaoka, Y.: Production of free and organic iodine by roseovarius spp, *FEMS Microbiology Letters*, 229, 189–194, doi:10.1016/s0378-1097(03)00839-5, 2003.
- Hagen, E.: Northwest african upwelling scenario, *Oceanol. Acta*, 24, S113–S128, 2001.
- Happell, J. D. and Wallace, D. W. R.: Methyl iodide in the greenland/norwegian seas and the tropical atlantic ocean: Evidence for photochemical production, *Geophys. Res. Lett.*, 23, 2105–2108, doi:10.1029/96gl01764, 1996.
- Hoerling, M. P., Hurrell, J. W., and Xu, T. Y.: Tropical origins for recent north atlantic climate change, *Science*, 292, 90–92, doi:10.1126/science.1058582, 2001.
- Hossaini, R., Chipperfield, M. P., Monge-Sanz, B. M., Richards, N. A. D., Atlas, E., and Blake, D. R.: Bromoform and dibromomethane in the tropics: A 3-d model study of chemistry and transport, *Atmos. Chem. Phys.*, 10, 719–735, doi:10.5194/acp-10-719-2010, 2010.
- Hossaini, R., Chipperfield, M. P., Feng, W., Breider, T. J., Atlas, E., Montzka, S. A., Miller, B. R., Moore, F., and Elkins, J.: The contribution of natural and anthropogenic very short-lived species to stratospheric bromine, *Atmos. Chem. Phys.*, 12, 371–380, doi:10.5194/acp-12-371-2012, 2012a.
- Hossaini, R., Chipperfield, M. P., Dhomse, S., Ordonez, C., Saiz-Lopez, A., Abraham, N. L., Archibald, A., Braesicke, P., Telford, P., Warwick, N., Yang, X., and Pyle, J.: Modelling future changes to the stratospheric source gas injection of biogenic bromocarbons, *Geophys. Res. Lett.*, 39, L20813, doi:10.1029/2012gl053401, 2012b.
- Jeffrey, S. W. and Vesik, M.: Introduction to marine phytoplankton and their pigment signatures, in: *Phytoplankton pigments in oceanography: Guideline to modern methods.*, edited by: Jeffrey, S. W., Mantoura, R. F. C., and Wright, S. W., 10, UNESCO Publishing, Paris, 37–84, 1997.
- Jones, C. E., Hornsby, K. E., Sommariva, R., Dunk, R. M., Von Glasow, R., McFiggans, G., and Carpenter, L. J.: Quantifying the contribution of marine organic gases to atmospheric iodine, *Geophys. Res. Lett.*, 37, L18804, doi:10.1029/2010gl043990, 2010.
- Lachkar, Z. and Gruber, N.: A comparative study of biological production in eastern boundary upwelling systems using an artificial neural network, *Biogeosciences*, 9, 293–308, doi:10.5194/bg-9-293-2012, 2012.
- Lai, S. C., Williams, J., Arnold, S. R., Atlas, E. L., Gebhardt, S., and Hoffmann, T.: Iodine containing species in the remote marine boundary layer: A link to oceanic phytoplankton, *Geophys. Res. Lett.*, 38, L20801, doi:10.1029/2011gl049035, 2011.
- Laturnus, F.: Marine macroalgae in polar regions as natural sources for volatile organohalogenes, *Environ. Sci. Pollut. Res.*, 8, 103–108, doi:10.1007/bf02987302, 2001.
- Lee, J. D., McFiggans, G., Allan, J. D., Baker, A. R., Ball, S. M., Benton, A. K., Carpenter, L. J., Commane, R., Finley, B. D., Evans, M., Fuentes, E., Furneaux, K., Goddard, A., Good, N., Hamilton, J. F., Heard, D. E., Herrmann, H., Hollingsworth, A., Hopkins, J. R., Ingham, T., Irwin, M., Jones, C. E., Jones, R. L., Keene, W. C., Lawler, M. J., Lehmann, S., Lewis, A. C., Long, M. S., Mahajan, A., Methven, J., Moller, S. J., Muller, K., Muller, T., Niedermeier, N., O'Doherty, S., Oetjen, H., Plane, J. M. C., Pszenny, A. A. P., Read, K. A., Saiz-Lopez, A., Saltzman, E. S., Sander, R., von Glasow, R., Whalley, L., Wiedensohler, A., and Young, D.: Reactive halogens in the marine boundary layer (rhamble): The tropical north atlantic experiments, *Atmos. Chem. Phys.*, 10, 1031–1055, doi:10.5194/acp-10-1031-2010, 2010.
- Manley, S. L. and Dastoor, M. N.: Methyl-iodide (CH₃I) production by kelp and associated microbes, *Mar. Biol.*, 98, 477–482, 1988.
- Manley, S. L., Goodwin, K., and North, W. J.: Laboratory production of bromoform, methylene bromide, and methyl-iodide by macroalgae and distribution in nearshore southern california waters, *Limnol. Oceanogr.*, 37, 1652–1659, 1992.
- Martino, M., Mills, G. P., Woeltjen, J., and Liss, P. S.: A new source of volatile organoiodine compounds in surface seawater, *Geophys. Res. Lett.*, 36, L01609, doi:10.1029/2008GL036334, 2009.
- McGivern, W. S., Sorkhabi, O., Suits, A. G., Derecskei-Kovacs, A., and North, S. W.: Primary and secondary processes in the photodissociation of chbr₃, *J. Phys. Chem. A*, 104, 10085–10091, doi:10.1021/jp0005017, 2000.
- McGregor, H. V., Dima, M., Fischer, H. W., and Mulitza, S.: Rapid 20th-century increase in coastal upwelling off northwest africa, *Science*, 315, 637–639, doi:10.1126/science.1134839, 2007.
- Minas, H. J., Codispoti, L. A., and Dugdale, R. C.: Nutrients and primary production in the upwelling region off northwest africa, *Rapp. Proc. Verb. Reun. Cons. Inst. Expl. Mer.*, 180, 148–183, 1982.
- Mittelstaedt, E.: Large-scale circulation along the coast of north-west africa, *Rapp. Proc. Verb. Reun. Cons. Inst. Expl. Mer.*, 180, 50–57, 1982.
- Montzka, S. A. and Reimann, S.: Ozone-depleting substances and related chemicals, Chapter 1 in *Scientific Assessment of Ozone Depletion: 2010*, Global Ozone Research and Monitoring Project, World Meteorological Organization (WMO), Geneva, Report No. 52, 2011.
- Moore, R. M. and Zafiriou, O. C.: Photochemical production of methyl-iodide in seawater, *J. Geophys. Res.-Atmos.*, 99, 16415–16420, doi:10.1029/94jd00786, 1994.
- Moore, R. M., Geen, C. E., and Tait, V. K.: Determination of henry law constants for a suite of naturally-occurring halo-

- generated methanes in seawater, *Chemosphere*, 30, 1183–1191, doi:10.1016/0045-6535(95)00009-w, 1995a.
- Moore, R. M., Tokarczyk, R., Tait, V. K., Poulin, M., and Geen, C. E.: Marine phytoplankton as a natural source of volatile organohalogens, in: *Naturally-produced organohalogens*, edited by: Grimvall, A., and deLeer, E. W. B., Kluwer Academic Publishers, Dordrecht, The Netherlands, 283–294, 1995b.
- Moore, R. M., Webb, M., Tokarczyk, R., and Wever, R.: Bromoperoxidase and iodoperoxidase enzymes and production of halogenated methanes in marine diatom cultures, *J. Geophys. Res.-Oceans*, 101, 20899–20908, doi:10.1029/96jc01248, 1996.
- Moore, R. M. and Groszko, W.: Methyl iodide distribution in the ocean and fluxes to the atmosphere, *J. Geophys. Res.-Oceans*, 104, 11163–11171, doi:10.1029/1998jc900073, 1999.
- Nightingale, P. D., Malin, G., and Liss, P. S.: Production of chloroform and other low-molecular-weight halocarbons by some species of macroalgae, *Limnol. Oceanogr.*, 40, 680–689, 1995.
- Nightingale, P. D., Malin, G., Law, C. S., Watson, A. J., Liss, P. S., Liddicoat, M. I., Boutin, J., and Upstill-Goddard, R. C.: In situ evaluation of air-sea gas exchange parameterizations using novel conservative and volatile tracers, *Global Biogeochem. Cy.*, 14, 373–387, doi:10.1029/1999gb900091, 2000.
- O'Brien, L. M., Harris, N. R. P., Robinson, A. D., Gostlow, B., Warwick, N., Yang, X., and Pyle, J. A.: Bromocarbons in the tropical marine boundary layer at the cape verde observatory - measurements and modelling, *Atmos. Chem. Phys.*, 9, 9083–9099, doi:10.5194/acp-9-9083-2009, 2009.
- O'Dowd, C. D., Jimenez, J. L., Bahreini, R., Flagan, R. C., Seinfeld, J. H., Hameri, K., Pirjola, L., Kulmala, M., Jennings, S. G., and Hoffmann, T.: Marine aerosol formation from biogenic iodine emissions, *Nature*, 417, 632–636, doi:10.1038/nature00775, 2002.
- Pyle, J. A., Warwick, N., Yang, X., Young, P. J., and Zeng, G.: Climate/chemistry feedbacks and biogenic emissions, *Philos. Trans. R. Soc. A-Math. Phys. Eng. Sci.*, 365, 1727–1740, doi:10.1098/rsta.2007.2041, 2007.
- Quack, B. and Wallace, D. W. R.: Air-sea flux of bromoform: Controls, rates, and implications, *Glob. Biogeochem. Cy.*, 17, 1023, doi:10.1029/2002gb001890, 2003.
- Quack, B., Atlas, E., Petrick, G., Stroud, V., Schauffler, S., and Wallace, D. W. R.: Oceanic bromoform sources for the tropical atmosphere, *Geophys. Res. Lett.*, 31, L23S05, doi:10.1029/2004gl020597, 2004.
- Quack, B., Atlas, E., Petrick, G., and Wallace, D. W. R.: Bromoform and dibromomethane above the mauritanian upwelling: Atmospheric distributions and oceanic emissions, *J. Geophys. Res.-Atmos.*, 112, D09312, doi:10.1029/2006jd007614, 2007a.
- Quack, B., Peeken, I., Petrick, G., and Nachtigall, K.: Oceanic distribution and sources of bromoform and dibromomethane in the mauritanian upwelling, *J. Geophys. Res.-Oceans*, 112, C10006, doi:10.1029/2006jc003803, 2007b.
- Richter, U.: Factors influencing methyl iodide production in the ocean and its flux to the atmosphere, PhD thesis, Mathematisch-Naturwissenschaftliche Fakultät der Christian-Albrechts-Universität zu Kiel, Christian-Albrechts-Universität zu Kiel, Kiel, 117 pp., 2004.
- Richter, U. and Wallace, D. W. R.: Production of methyl iodide in the tropical atlantic ocean, *Geophys. Res. Lett.*, 31, L23S03, doi:10.1029/2004gl020779, 2004.
- Saiz-Lopez, A., Plane, J. M. C., Baker, A. R., Carpenter, L. J., von Glasow, R., Martin, J. C. G., McFiggans, G., and Saunders, R. W.: Atmospheric chemistry of iodine, *Chem. Rev.*, 112, 1773–1804, doi:10.1021/cr200029u, 2012.
- Salawitch, R. J., Weisenstein, D. K., Kovalenko, L. J., Sioris, C. E., Wennberg, P. O., Chance, K., Ko, M. K. W., and McLinden, C. A.: Sensitivity of ozone to bromine in the lower stratosphere, *Geophys. Res. Lett.*, 32, L05811, doi:10.1029/2004gl021504, 2005.
- Schall, C., Heumann, K. G., and Kirst, G. O.: Biogenic volatile organoiodine and organobromine hydrocarbons in the atlantic ocean from 42 degrees N to 72 degrees S, *Fresenius J. Anal. Chem.*, 359, 298–305, 1997.
- Schauffler, S. M., Atlas, E. L., Blake, D. R., Flocke, F., Lueb, R. A., Lee-Taylor, J. M., Stroud, V., and Travnicek, W.: Distributions of brominated organic compounds in the troposphere and lower stratosphere, *J. Geophys. Res.-Atmos.*, 104, 21513–21535, 1999.
- Smythe-Wright, D., Boswell, S. M., Breithaupt, P., Davidson, R. D., Dimmer, C. H., and Diaz, L. B. E.: Methyl iodide production in the ocean: Implications for climate change, *Glob. Biogeochem. Cy.*, 20, GB3003, doi:10.1029/2005GB002642, 2006.
- Solomon, S., Garcia, R. R., and Ravishankara, A. R.: On the role of iodine in ozone depletion, *J. Geophys. Res.-Atmos.*, 99, 20491–20499, doi:10.1029/94JD02028, 1994.
- Stemmler, I., Hense, I., Quack, B., and Maier-Reimer, E.: Methyl iodide production in the open ocean, *Biogeosciences Discuss.*, 10, 17549–17595, doi:10.5194/bgd-10-17549-2013, 2013.
- Taylor, B. B., Torrecilla, E., Bernhardt, A., Taylor, M. H., Peeken, I., Rottgers, R., Piera, J., and Bracher, A.: Bio-optical provinces in the eastern atlantic ocean and their biogeographical relevance, *Biogeosciences*, 8, 3609–3629, doi:10.5194/bg-8-3609-2011, 2011.
- Tegtmeier, S., Krüger, K., Quack, B., Atlas, E. L., Pisso, I., Stohl, A., and Yang, X.: Emission and transport of bromocarbons: From the west pacific ocean into the stratosphere, *Atmos. Chem. Phys.*, 12, 10633–10648, doi:10.5194/acp-12-10633-2012, 2012.
- Tegtmeier, S., Krüger, K., Quack, B., Atlas, E., Blake, D. R., Boenisch, H., Engel, A., Hepach, H., Hossaini, R., Navarro, M. A., Raimund, S., Sala, S., Shi, Q., and Ziska, F.: The contribution of oceanic methyl iodide to stratospheric iodine, *Atmos. Chem. Phys.*, 13, 11869–11886, doi:10.5194/acp-13-11869-2013, 2013.
- Tokarczyk, R. and Moore, R. M.: Production of volatile organohalogens by phytoplankton cultures, *Geophys. Res. Lett.*, 21, 285–288, 1994.
- Tomczak, M.: The distribution of water masses at the surface as derived from t-s diagram analysis in the cineca area, *Rapp. Proc. Verb. Reun. Cons. Inst. Expl. Mer.*, 180, 48–49, 1982.
- Tomczak, M. and Godfrey, J. S.: *Regional oceanography: An introduction*, 2 ed., Daya Publishing House, Delhi, 2005.
- Tran, S., Bonsang, B., Gros, V., Peeken, I., Sarda-Estève, R., Bernhardt, A., and Belviso, S.: A survey of carbon monoxide and non-methane hydrocarbons in the arctic ocean during summer 2010, *Biogeosciences*, 10, 1909–1935, doi:10.5194/bg-10-1909-2013, 2013.
- Tsuchiya, M., Talley, L. D., and McCartney, M. S.: An eastern atlantic section from iceland southward across the equator, *Deep-Sea Res.*, 39, 1885–1917, doi:10.1016/0198-0149(92)90004-d, 1992.

- Williams, J., Gros, V., Atlas, E., Maciejczyk, K., Batsaikhan, A., Scholer, H. F., Forster, C., Quack, B., Yassaa, N., Sander, R., and Van Dingenen, R.: Possible evidence for a connection between methyl iodide emissions and saharan dust, *J. Geophys. Res.-Atmos.*, 112, D07302, doi:10.1029/2005jd006702, 2007.
- Yokouchi, Y., Osada, K., Wada, M., Hasebe, F., Agama, M., Murakami, R., Mukai, H., Nojiri, Y., Inuzuka, Y., Toom-Saunty, D., and Fraser, P.: Global distribution and seasonal concentration change of methyl iodide in the atmosphere, *J. Geophys. Res.-Atmos.*, 113, D18311, doi:10.1029/2008JD009861, 2008.
- Yokouchi, Y., Nojiri, Y., Toom-Saunty, D., Fraser, P., Inuzuka, Y., Tanimoto, H., Nara, H., Murakami, R., and Mukai, H.: Long-term variation of atmospheric methyl iodide and its link to global environmental change, *Geophys. Res. Lett.*, 39, L23805, doi:10.1029/2012GL053695, 2012.
- Ziska, F., Quack, B., Abrahamsson, K., Archer, S. D., Atlas, E., Bell, T., Butler, J. H., Carpenter, L. J., Jones, C. E., Harris, N. R. P., Hepach, H., Heumann, K. G., Hughes, C., Kuss, J., Krüger, K., Liss, P., Moore, R. M., Orlikowska, A., Raimund, S., Reeves, C. E., Reifenhäuser, W., Robinson, A. D., Schall, C., Tanhua, T., Tegtmeier, S., Turner, S., Wang, L., Wallace, D., Williams, J., Yamamoto, H., Yvon-Lewis, S., and Yokouchi, Y.: Global sea-to-air flux climatology for bromoform, dibromomethane and methyl iodide, *Atmos. Chem. Phys.*, 13, 8915–8934, doi:10.5194/acp-13-8915-2013, 2013.

7. Manuscript

Impact of the marine atmospheric boundary layer conditions on VSLs abundances in the eastern tropical and subtropical North Atlantic Ocean

S. Fuhlbrügge¹, K. Krüger¹, B. Quack¹, E. Atlas², H. Hepach¹, and F. Ziska¹

[1] GEOMAR Helmholtz-Zentrum für Ozeanforschung Kiel, Kiel, Germany

[2] Rosenstiel School for Marine and Atmospheric Sciences, Miami, Florida, USA

Published in: Atmospheric Chemistry and Physics, 13, 6345-6357, doi:10.5194/acp-13-6345-2013, 2013.



Impact of the marine atmospheric boundary layer conditions on VSLs abundances in the eastern tropical and subtropical North Atlantic Ocean

S. Fuhlbrügge¹, K. Krüger¹, B. Quack¹, E. Atlas², H. Hepach¹, and F. Ziska¹

¹GEOMAR Helmholtz-Zentrum für Ozeanforschung Kiel, Kiel, Germany

²Rosenstiel School for Marine and Atmospheric Sciences, Miami, Florida, USA

Correspondence to: K. Krüger (kkrueger@geomar.de)

Received: 20 November 2012 – Published in Atmos. Chem. Phys. Discuss.: 5 December 2012

Revised: 13 May 2013 – Accepted: 30 May 2013 – Published: 4 July 2013

Abstract. During the DRIVE (Diurnal and Regional Variability of Halogen Emissions) ship campaign we investigated the variability of the halogenated very short-lived substances (VSLs) bromoform (CHBr_3), dibromomethane (CH_2Br_2) and methyl iodide (CH_3I) in the marine atmospheric boundary layer in the eastern tropical and subtropical North Atlantic Ocean during May/June 2010. The highest VSLs mixing ratios were found near the Mauritanian coast and close to Lisbon (Portugal). With backward trajectories we identified predominantly air masses from the open North Atlantic with some coastal influence in the Mauritanian upwelling area, due to the prevailing NW winds. The maximum VSLs mixing ratios above the Mauritanian upwelling were 8.92 ppt for bromoform, 3.14 ppt for dibromomethane and 3.29 ppt for methyl iodide, with an observed maximum range of the daily mean up to 50 % for bromoform, 26 % for dibromomethane and 56 % for methyl iodide. The influence of various meteorological parameters – such as wind, surface air pressure, surface air and surface water temperature, humidity and marine atmospheric boundary layer (MABL) height – on VSLs concentrations and fluxes was investigated. The strongest relationship was found between the MABL height and bromoform, dibromomethane and methyl iodide abundances. Lowest MABL heights above the Mauritanian upwelling area coincide with highest VSLs mixing ratios and vice versa above the open ocean. Significant high anti-correlations confirm this relationship for the whole cruise. We conclude that especially above oceanic upwelling systems, in addition to sea–air fluxes, MABL height variations can influence atmospheric VSLs mixing ratios, occasionally

leading to elevated atmospheric abundances. This may add to the postulated missing VSLs sources in the Mauritanian upwelling region (Quack et al., 2007).

1 Introduction

Natural halogenated very short-lived substances (VSLs) contribute significantly to the halogen content of the troposphere and lower stratosphere (WMO, 2011). On-going environmental changes such as increases in seawater temperature and nutrient supply, as well as decreasing pH, are expected to influence VSLs production in the ocean. Thus, the oceanic emissions of VSLs might change in the future and, in connection with an altering efficiency of the atmospheric upward transport, might lead to significant future changes of the halogen budget of the troposphere/lower stratosphere (Kloster et al., 2007; Pyle et al., 2007; Dessens et al., 2009; Schmitzner et al., 2008; Montzka and Reimann, 2011), as well as changes to the tropospheric oxidation capacity (Hossaini et al., 2012). Within the group of brominated VSLs, bromoform (CHBr_3) and dibromomethane (CH_2Br_2) are the largest natural sources for bromine in the troposphere and stratosphere. In combination with iodine compounds (i.e. methyl iodide, CH_3I), they can alter tropospheric oxidation processes, including ozone depletion (Read et al., 2008). The VSLs have comparably short tropospheric lifetimes (days to months); however, they can be rapidly transported by deep convection, especially in the tropics, to the upper troposphere and lower stratosphere and contribute to ozone depletion

there (Warwick et al., 2006; WMO, 2007, 2011; Tegtmeier et al., 2012, 2013). Previous studies have reported distinctive halocarbon emissions in tropical coastal and shelf water regions due to high biological productivity, i.e. by macro algae, seaweed and phytoplankton (Gschwend et al., 1985; Manley and Dastoor, 1988; Sturges et al., 1992; Moore and Tokarczyk, 1993; Carpenter and Liss, 2000; Quack et al., 2007). Elevated mixing ratios of the compounds have been found within the marine atmospheric boundary layer (MABL) around the Cape Verde Islands with a mean (range) for CHBr_3 of 8 (2.0–43.7) ppt, CH_2Br_2 of 2 (0.7–8.8) ppt and CH_3I of 3 (0.5–31.4) ppt (O'Brien et al., 2009) and in the area of the Mauritanian upwelling with a mean (range) of CHBr_3 around 6 (3–12) ppt (Carpenter et al., 2007; Quack et al., 2007) and CH_2Br_2 of 2.4 (1.75–3.44) ppt by Quack et al. (2007). These mean mixing ratios from the tropical Atlantic Ocean agree well with other tropical oceanic areas (e.g. Atlas et al., 1993; Butler et al., 2007). Quack et al. (2004) suggested regionally enhanced biogenic production in the water column of the Mauritanian upwelling and a high sea-to-air flux of VSLs to be responsible for elevated tropospheric VSLs mixing ratios in this region. However, Carpenter et al. (2007) and Quack et al. (2007) both pointed out that the marine boundary layer height, besides additional potential coastal sources, may affect the tropospheric VSLs mixing ratios as well. The theory of warm offshore air flowing over cool water and creating a stable internal boundary layer, as suggested by Garratt (1990), applies well in the area of the cold Mauritanian upwelling. Here, the sea surface roughness and near surface turbulence reduce each other over the water, while the flow leads to a collapse of turbulence and a very stable stratification of the lowermost atmosphere, as was observed by Vickers et al. (2001) at the coast of the United States and modelled by Skillingstad et al. (2005).

In this study, we present first results from the DRIVE (Diurnal and Regional Variability of Halogen Emissions) ship campaign during May/June 2010, comprising high-resolution meteorological and VSLs measurements. We investigate the meteorological constraints on the VSLs abundances and whether the cold waters upwelled along the Mauritanian coast have a verifiable influence on the atmospheric boundary layer height and therefore on the mixing of air within the lowermost troposphere. The accompanying study by Hepach et al. (2013) investigates the VSLs sources in the ocean and the sea-to-air fluxes in detail.

This paper begins with a short overview of the meteorological conditions during the DRIVE cruise, followed by a data and method description (Sect. 2.1). In Sect. 3 we present results from the meteorological and VSLs measurements and the influence of meteorology and MABL height on the VSLs mixing ratios and emissions. Finally, a summary is given in Sect. 4.

2 Data and methods

2.1 Cruise overview

During May/June 2010 the DRIVE (P399/2-3) campaign examined the formation and emission of halocarbons and reactive inorganic halogen compounds in the eastern tropical and subtropical North Atlantic Ocean (Bange et al., 2011) as part of the SOPRAN (Surface Ocean Processes in the Anthropocene: www.sopran.pangaea.de) project. The main objectives are to investigate the diurnal and regional variability of marine short-lived substances, as well as oceanic influences on the atmosphere.

The ship expedition was carried out on board the German research vessel (R/V) *Poseidon*. The cruise itself was split into two legs: P399/2 (31 May–17 June 2010) from Las Palmas to Las Palmas and P399/3 (19–24 June 2010) from Las Palmas to Vigo, Spain. For diurnal observations, hourly VSLs measurements were performed at six 24 h stations during leg P399/2. Positions and times of the 24 h stations are given in Table 1. The location of the 24 h stations were chosen to cover the nutrient-rich coastal upwelling region near the Mauritanian coast as well as the nutrient-poor regions near the Cape Verde Islands. In addition, 21 atmospheric VSLs samples were taken during the return from the last station in the Mauritanian upwelling region to Las Palmas (Gran Canaria). During the transit leg P399/3, an additional 20 atmospheric air samples were taken. All VSLs measurements were also integrated into the HalOcAt database used for the Ziska et al. (2013) climatology.

2.2 Meteorology and MABL height

Meteorological data have been collected by the automatic on-board weather station of the German Weather Service (DWD): air and water temperatures, wind speed and direction, humidity and air pressure were recorded once per second and are averaged to 10 min means for our analysis. GRAW DFM-06 radiosondes (<http://www.graw.de>) were launched from the working deck of R/V *Poseidon* at about 3 m above sea level during the cruise to profile the atmospheric composition of air temperature (resolution: 0.1 °C; accuracy: < 0.2 °C), relative humidity (resolution: 1 %; accuracy: < 5 %), and wind (wind speed accuracy: < 0.2 m s⁻¹; horizontal position accuracy: < 5 m) (http://www.gematronik.com/fileadmin/media/pdf/GRAW-Brochure_V01.30_en.pdf) from the sea level up to the middle stratosphere (~30 km altitude). At the 24 h stations, the launch frequency was increased from one radiosonde per day at 12:00 UTC to four per day at 00:00, 06:00, 12:00 and 18:00 UTC, amounting to 41 launches for the whole cruise.

The atmospheric boundary layer height is determined using the approaches summarized by Seibert et al. (2000). These methods include practical and theoretical

Table 1. 24 h stations: position and date.

24 h station	Position	Date/Time
1st	17.6° N, 24.0° W	3 June (23:00 UTC)–4 June 2010 (22:00 UTC)
2nd	18.0° N, 21.0° W	6 June (19:00 UTC)–7 June 2010 (17:00 UTC)
3th	18.0° N, 18.0° W	8 June (18:00 UTC)–9 June 2010 (17:00 UTC)
4th	18.5° N, 16.5° W	10 June (12:00 UTC)–11 June 2010 (11:00 UTC)
5th	19.0° N, 16.5° W	11 June (16:00 UTC)–12 June 2010 (15:00 UTC)
6th	20.0° N, 17.25° W	13 June (04:00 UTC)–14 June 2010 (03:00 UTC)

determinations from radiosoundings. The vertical extension of the boundary layer is in general limited aloft by a temperature inversion or a stable layer, or by a significant reduction in air moisture. Two general types of boundary layers exist, the convective boundary layer (CBL), whose stable layer is found between the lower 100 m of the atmosphere and about 3 km height, and the stable boundary layer (SBL), characterized by a surface inversion. In the case of a CBL, it is recommended to take the height of the base of the inversion, increased by half of the inversion layer depth (Stull, 1988). For a SBL we assume the absence of turbulence and vertical mixing (Garratt, 1990) and further declare that the boundary layer stays close to the surface. According to this, we subjectively determined the height of the boundary layer in our study from the temperature and humidity profiles, and additionally from the bulk Richardson number of the following equation (Troen and Mahrt, 1986; Vogelezang and Holtslag, 1996):

$$Ri_B = \frac{gz(\theta_z - \theta_s)}{\theta_s(u^2 + v^2)}. \quad (1)$$

The quantities g and z are the gravitation acceleration and the geometric height. θ_z and θ_s are the virtual potential temperature at the height z and at the surface, and u and v are the zonal and meridional wind components. The virtual potential temperature can be regarded as a stability criterion for the atmosphere, considering the air moisture. It is constant with height for neutral conditions, increases for stable conditions and decreases if the air is statically unstable. To identify the boundary layer height theoretically, a fixed critical bulk Richardson number of $Ri_c = 0.25$ is chosen as a threshold, following Sorensen (1998), where $Ri_B \geq Ri_c$. Due to missing wind data in the lowermost atmosphere during a number of radiosonde launches (failure of GPS sensor), we were not always able to determine Ri_B for the lower boundary layer. Therefore we use the subjectively determined boundary layer height for our investigations and calculate Ri_B to confirm our determined MABL height.

2.3 Air mass origin

For the analysis of the air mass origin, HYSPLIT trajectories (<http://ready.arl.noaa.gov/HYSPLIT.php>), based on NCEP/NCAR Reanalysis 1 (NNR), were calculated online.

The NNR is a first-generation reanalysis from 1948 to the present and has a horizontal resolution of 208 km (T62) and 28 vertical levels (L28) with a model top at about 3 hPa. The data are globally distributed on a 2.5° latitude × 2.5° longitude Gaussian grid with a total of 144 × 73 grid points (Kalnay et al., 1996; Kistler et al., 2001).

2.4 VSLS measurements

A total of 187 air samples were taken on the monkey deck of R/V *Poseidon*, about 10 m above sea level. The air was pressurized up to 2 standard atmospheres in pre-cleaned stainless steel canisters, each with a volume of 2.6 L. The canisters were analysed within three months after the expedition at the Rosenstiel School for Marine and Atmospheric Sciences (RSMAS, Miami, Florida). The stability of the atmospheric samples has been demonstrated during more than 10 years of work with stainless steel canisters. The compounds reported here are typically stable for at least 6 months or more. The precision is estimated as an uncertainty of approximately 5%, obtained from the standard variability during analysis and from examination of multiple samples within the same air mass. The analysis of the gases is performed with gas chromatography/mass spectrometry (GC/MS), while the calibration gases are standardized by gas chromatography with an atomic emission detector (AED) (Schauffler et al., 1999), and the entire standardization procedure was additionally adjusted to the NOAA scale in order to have better comparability to the NOAA measurements at surface stations. The preparation of standard gases is described in Montzka et al. (2003).

Our study concentrates on the atmospheric abundances of three VSLS: methyl iodide with a lifetime of ~4 days (Solomon et al., 1994), bromoform of ~26 days (Ko et al., 2003) and dibromomethane of ~120 days (Ko et al., 2003).

Samples for dissolved halocarbons in sea water were taken from the continuously working pump from the ship's moon pool at a depth of 5 m on a nearly hourly basis at every 24 h station. A purge and trap system attached to a gas chromatograph with mass spectrometric detection in single-ion mode was used for analysis of the samples with a precision within 10% determined from duplicates (Hepach et al., 2013).

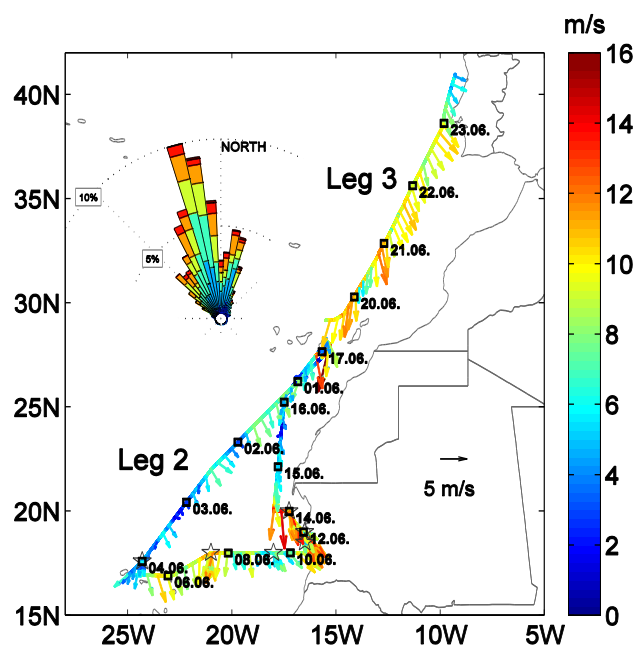


Fig. 1. DRIVE cruise track. In addition, the 3-hourly wind speed [m s^{-1}], direction (10 min averages) and windrose for the whole cruise are shown.

2.5 Sea-to-air flux calculations

Sea-to-air fluxes (F) of methyl iodide, dibromomethane and bromoform were calculated with the air–sea gas transfer coefficient k_w and the air–sea concentration gradient Δc (Heppach et al., 2013):

$$F = k_w \cdot \Delta c \quad (2)$$

The parameterization of Nightingale et al. (2000), based on instantaneous wind speeds (10 min averages) and temperature-dependent Schmidt numbers according to Quack and Wallace (2003), was applied to determine k_w . Δc was calculated from the simultaneous water and air measurements at the 24 h stations.

3 Results

3.1 Meteorology

The cruise was mainly exposed to moderate weather conditions. Contrary to the climatological wind direction of northeasterly trade winds in the subtropics and westerlies north of 30°N during May/June, the mean absolute wind direction was NNW (Fig. 1) with a mean direction of 349° during leg 2 and 344° during leg 3. This caused a predominant influence of air masses with marine background conditions coming from the open North Atlantic Ocean. The mean wind speed during the whole cruise was moderate to fresh for both legs, with $7.4 \text{ m s}^{-1} \pm 2.9 \text{ m s}^{-1}$ during leg 2

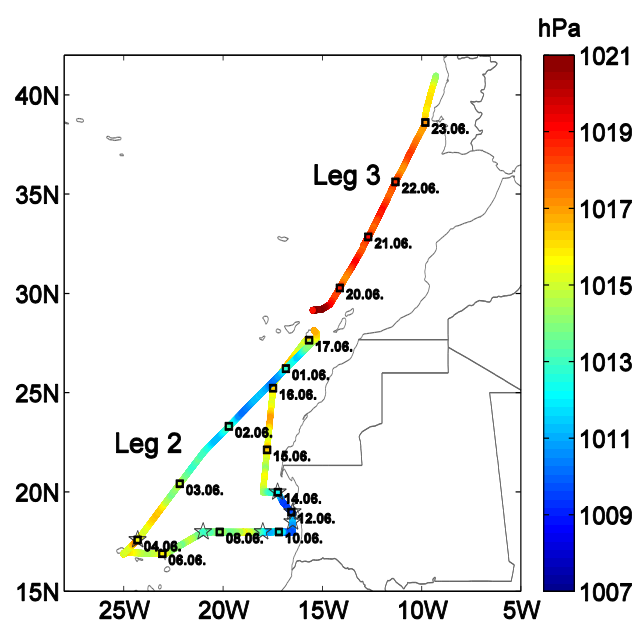


Fig. 2. 10 min average measurements of air pressure [hPa]. The stars indicate position and time of the diurnal stations.

and $9.3 \text{ m s}^{-1} \pm 1.6 \text{ m s}^{-1}$ during leg 3. The total air pressure difference of 13.4 hPa also reflects the moderate and steady weather conditions during the whole cruise with a minimum of 1007.6 hPa on 11 June 2010 close to the Mauritanian coast and a maximum air pressure of 1021 hPa at the beginning of leg 3 on 19 June 2010 close to the Canary Islands (Fig. 2). In addition, typical tropical diurnal variations up to 4 hPa (see also Krüger and Quack, 2012) due to atmospheric tides were observed in this study. The time series of 10 min average measured surface air temperature (T_{SAT}), sea surface temperatures (T_{SST}) and the difference ΔT ($T_{\text{SAT}} - T_{\text{SST}}$) are shown in Fig. 3. The temperature difference is related to the heat flux between atmosphere and ocean and indicates suppressing of convection, turbulence and therefore mixing within the boundary layer for a positive temperature difference (positive heat flux) and enhanced mixing for negative heat flux. As the ship cruise started to the south, the air and water temperatures increased until the maximum air temperature of 25.8°C was recorded directly after the stop at Mindelo (Cape Verde Islands). On 11 June 2010, right after the 4th 24 h station, the ship reached the Mauritanian upwelling region at 18.75°N , 16.5°W . This is noticeable from the abrupt decrease in the water temperature and connected to an increase of the heat flux from the atmosphere to the ocean. After one day, the air temperature also drops, until T_{SAT} and T_{SST} stabilize between 18°C and 20°C (station 5). On 14 June 2010, after the ship has left the last 24 h station, the water temperature increases to about 23.5°C . This increase coincides with a wind speed maximum of about 16 m s^{-1} from the north, indicating transport of water masses from outside the Mauritanian upwelling

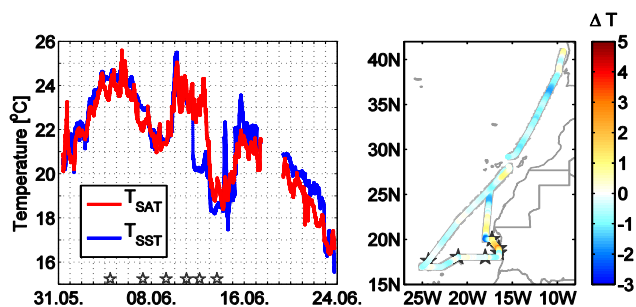


Fig. 3. Left: 10 min average measurements of T_{SAT} and T_{SST} [°C]. The stars indicate position and time of the diurnal stations. Right: the temperature gradient is given in [K].

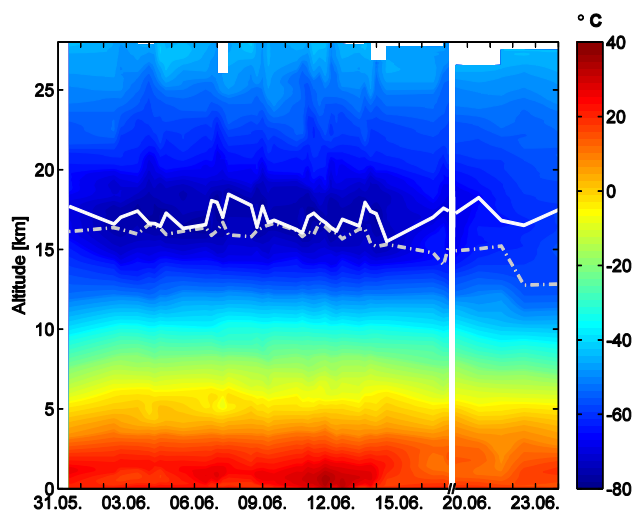


Fig. 4. Air temperature cross sections [°C] from radiosoundings for the whole cruise. Cold point tropopause and lapse rate tropopause are marked by the continuous and the dash-dotted lines, respectively. The measurement gap between leg 2 and 3 is shortened.

towards the ship, until the water temperature drops again to about 18 °C. On 15 June 2010 the ship left the Mauritanian upwelling region, indicated by increasing air and water temperatures until both decreased again while heading northward. A sudden decrease of the water temperature is also observed from 23 to 24 June 2010, as the ship enters the Iberian upwelling (Relvas and Barton, 2002).

3.1.1 Marine atmospheric boundary layer

In the following, we use the radiosonde measurements to analyse the state of the lower atmosphere. Profiles of air temperature along the cruise track are shown in Fig. 4. Lowest temperatures of -80 °C are observed between 2 and 15 June 2010 at 17 km height, indicating tropical air masses south of 25° N during leg 2. Two different tropopause definitions are used to identify the transition between tropical and extra-tropical air masses: the cold point

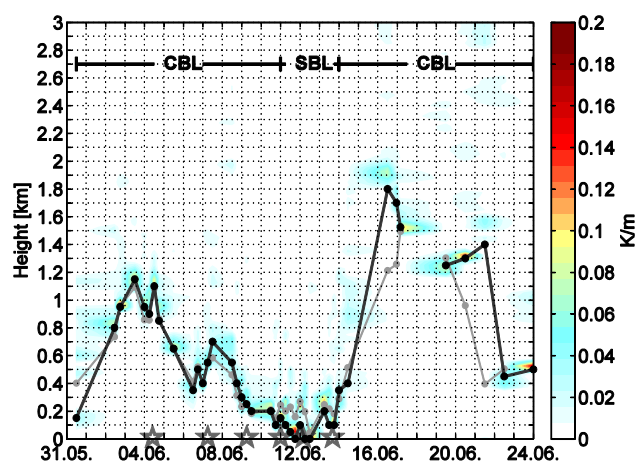


Fig. 5. Virtual potential temperature gradient (colour shading) with derived MABL heights (lines, in km). The black line shows the subjectively determined MABL height from temperature and humidity profiles, and the grey line is determined theoretically (Sect. 2.2). CBL and SBL identify convective and stable boundary layers. The 24 h stations are marked with stars.

tropopause (CPT; Highwood and Hoskins, 1998) and the lapse rate tropopause (LRT, WMO, 1957). During leg 2, the heights of the CPT and LRT are detected between 16 and 17 km altitude. A change of the atmospheric regime is reflected by the decrease of the LRT height to 15 km in contrast to the CPT height after 15 June 2010 at the end of leg 2, as the ship enters the extratropics. The air temperature profiles also reveal typical “trade inversions” (Neiburger et al., 1961) between 1 and 2 km height from the beginning of the cruise until 4 June and from 16 June 2010 until the end of the cruise. Beginning on 4 June 2010, the temperature inversions descend in height, until they migrate, due to cold upwelling deep water (Fig. 3) in the Mauritanian upwelling, to intense surface inversions. The neutral and stable stratification within the lower 3 km of the troposphere, and therefore the upper limit of the atmospheric boundary layer during the cruise, is shown by Fig. 5. The subjectively and theoretically derived MABL heights (see Sect. 2.2) show a good agreement with each other. Differences are found above the Mauritanian upwelling, due to missing near-surface winds for the calculation of the bulk Richardson number, but also at the end of leg 2 and the beginning of leg 3. This may be caused by our fixed Ri_c , which we took for convenience.

Except for the area at and south of the upwelling, observed from 11 to 14 June 2010, where we observed a SBL, the cruise was predominantly characterized by CBLs, without distinct short time or diurnal variations, considering the launch frequencies. Boundary layer heights from the surface up to 400 m at the upwelling area and about 400–2000 m above the open ocean agree with heights derived from trajectory models from previous studies along the Mauritanian coast (Carpenter et al., 2007; Quack et al., 2007). During

Table 2. Observed mixing ratios [in ppt] of bromoform (CHBr_3), dibromomethane (CH_2Br_2), their ratio and methyl iodide (CH_3I) for the whole cruise, open ocean (leg 2 except stations 3–6, and leg 3) and coastal stations (stations 3–6). Given are the mean, the range and the standard deviation values.

	CHBr_3 (ppt)		CH_2Br_2 (ppt)		$\frac{\text{CH}_2\text{Br}_2}{\text{CHBr}_3}$	CH_3I (ppt)	
	Mean (range)	stdv of mean	Mean (range)	stdv of mean		Mean (range)	stdv of mean
Whole cruise	3.75 (0.48–9.9)	2.29	1.85 (0.89–3.14)	0.63	0.69	1.25 (0.51–3.29)	0.56
Open ocean	1.74 (0.48–9.9)	1.34	1.28 (0.89–2.70)	0.31	0.98	0.93 (0.51–2.11)	0.24
Coastal stations	5.60 (4.07–8.92)	1.06	2.37 (1.87–3.14)	0.31	0.43	1.55 (0.90–3.29)	0.62

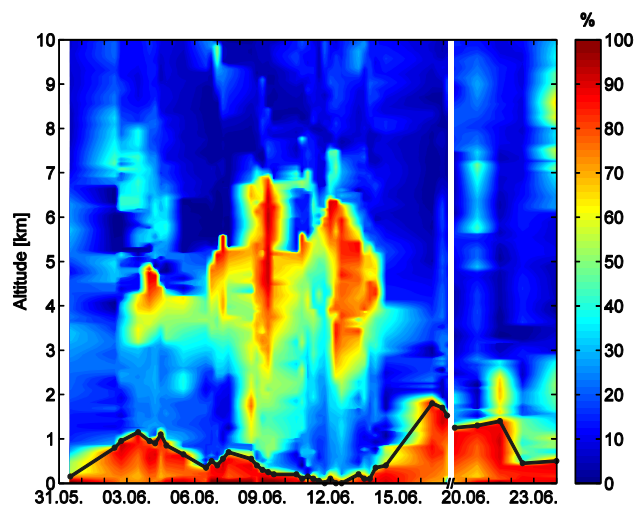


Fig. 6. Relative humidity cross sections [%] from radiosoundings for the whole cruise. The subjectively determined MABL height [km] is marked by the black line. The measurement gap between leg 2 and 3 is shortened.

leg 3 the top of the boundary layer decreases from 1.4 km north of the Canary Islands to about 500 m near the coast of the Iberian Peninsula. The height of the MABL is also well reflected in the profiles of the relative humidity during the whole cruise as shown in Fig. 6. The increase of the surface/lowermost troposphere humidity between 15 and 22 June 2010 (Fig. 6) matches the observed elevation of the negative heat flux (Fig. 3). The height of the atmospheric boundary layer, determined from temperature observations, agrees very well with the surface maximum of relative humidity (Fig. 6). The vertical mixing within the MABL seems to be quite well reflected by the relative humidity observations. Especially the small extension of enhanced relative humidity above the surface of the Mauritanian upwelling from 11 to 12 June 2010 is consistent with the assumption of reduced vertical mixing (turbulence) in this area due to the positive heat flux, leading to a very stable and narrow MABL.

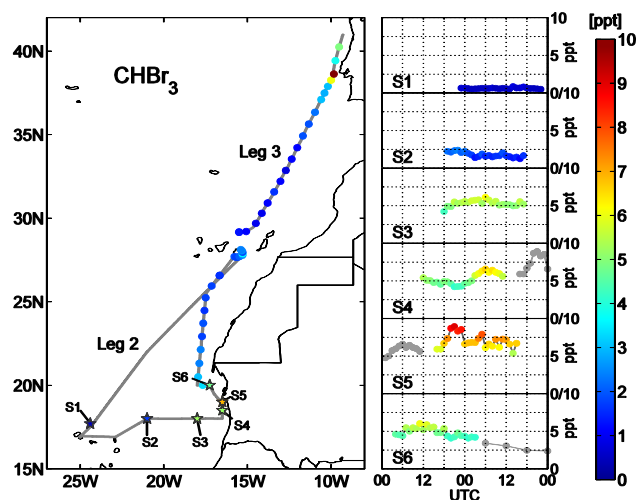


Fig. 7. Bromoform mixing ratios [ppt] measured during the DRIVE ship campaign from 31 May to 24 June 2010. Six 24 h stations (S1–S6) and measurements during transit are colour-coded according to the scale on the right side.

3.2 Atmospheric VSLs variability

The diurnal and regional variations of halogenated trace gas abundances in the MABL have been observed with hourly measurements at six 24 h stations near the Cape Verde Islands and in the Mauritanian upwelling. According to the regional distribution of the diurnal stations (Fig. 1), the first two stations (S1, S2) can be combined to an open ocean cluster. The following 4 diurnal stations are furthermore declared as coastal stations (S3–S6), since they show similar physical and biological characteristics (e.g. salinity and chlorophyll *a*) in the surface water (Hepach et al., 2013). Six-hourly measurements were also taken from 14 June 2010 after the 6th station to the coast of Gran Canaria and during leg 3 (19–23 June 2010). Also along the coast of Gran Canaria (17 June 2010) hourly samples were taken.

An increase of atmospheric mixing ratios from the Cape Verde Islands to the Mauritanian upwelling area is found for all three trace gases: bromoform (Fig. 7), dibromomethane (Fig. 8) and methyl iodide (Fig. 9). Within the open ocean cluster, the mixing ratios ranged 0.48–9.9 ppt

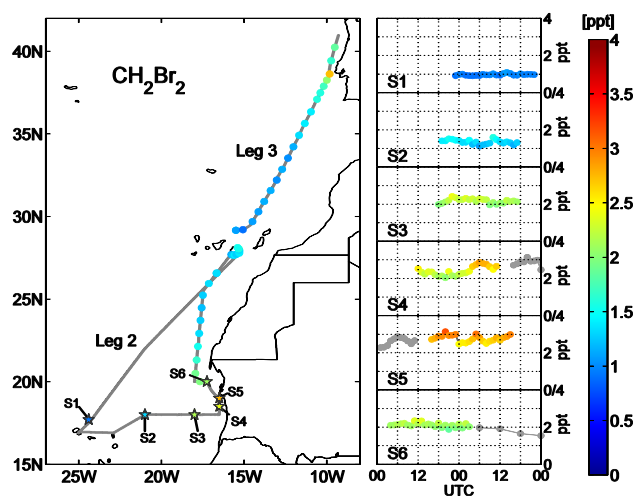


Fig. 8. Dibromomethane mixing ratios [ppt] measured during the DRIVE ship campaign from 31 May to 24 June 2010. Six 24 h stations (S1–S6) and measurements during transit are colour-coded according to the scale on the right side.

with a mean of 1.74 ppt for CHBr_3 , 0.91–1.59 ppt with a mean of 1.28 ppt for CH_2Br_2 , and 0.63–1.32 ppt with a mean of 0.93 ppt for CH_3I . The mixing ratio of CH_2Br_2 and CHBr_3 has often been observed to be around 0.1 in source areas, where the air has been influenced e.g. by fresh coastal emissions (Yokouchi, 2005 and references therein). The ratio increases towards the open ocean due to the different lifetimes of both compounds. A higher value implies an aged air mass and aged emission, while a lower value indicates fresher emissions and air masses. With an overall mean $\text{CH}_2\text{Br}_2/\text{CHBr}_3$ ratio of 1.21 (Table 2) during stations 1 and 2, typical open ocean air masses were observed (Quack et al., 2004; Butler et al., 2007). At the third 24 h station, the bromocarbons increase to 4.22–6.12 ppt for CHBr_3 and 1.96–2.42 ppt for CH_2Br_2 , while CH_3I mixing ratios remain at open ocean values. A mean $\text{CH}_2\text{Br}_2/\text{CHBr}_3$ ratio of 0.41 now indicates fresher emissions. Slightly increased atmospheric mixing ratios of CHBr_3 with 4.21–6.58 ppt and of CH_2Br_2 with 2.04–2.87 ppt, and a $\text{CH}_2\text{Br}_2/\text{CHBr}_3$ ratio of 0.46 are found at the 4th 24 h station. For the first time, the CH_3I mixing ratios show intense variations of 1.11–2.68 ppt at this coastal station. In addition, a diurnal pattern is striking for all three VSLs at this station (S4, Fig. 7). They show a slight decrease from 12:00 UTC to 00:00 UTC followed by an increase from 06:00 UTC to 09:00 UTC on the following day, which coincides with a decrease of the MABL height and the sunrise at about 06:30 UTC. The highest atmospheric mixing ratios for all three VSLs during leg 2 were observed during the 5th station at 19° N and 16.5° W. At this station also the most pronounced variations within one day are observed, with maximum mixing ratios of 8.92 ppt for CHBr_3 , 3.14 ppt for CH_2Br_2 and 3.29 ppt for CH_3I . The extreme minimum of CH_3I at 05:00 UTC appears as an unreliable

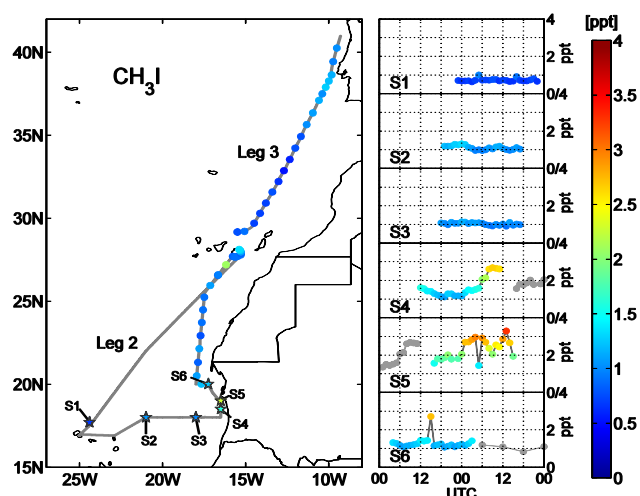


Fig. 9. Methyl iodide mixing ratios [ppt] measured during the DRIVE ship campaign from 31 May to 24 June 2010. Six 24 h stations (S1–S6) and measurements during transit are colour-coded according to the scale on the right side.

outlier due to the high variation of more than 1 ppt within two hours, which is nearly consistent with the whole diurnal variation of CH_3I at station 4. Although this station has the lowest $\text{CH}_2\text{Br}_2/\text{CHBr}_3$ ratio of 0.40 during leg 2, this value is two to three times higher than previously reported ratios of 0.1–0.25 for coastal source regions in the North Atlantic Ocean and the northwest of Tasmania (Carpenter et al., 2003) and tropical islands and the open Pacific Ocean (Yokouchi et al., 2005), suggesting the presence of slightly aged air masses and emissions. While the ship moved away from the Mauritanian coast, southwest of the Banc d'Arguin National Park, the last coastal station (S6) shows an increase of the $\text{CH}_2\text{Br}_2/\text{CHBr}_3$ ratio to 0.44 and a decrease of the trace gas mixing ratios to 4.85 ppt (range: 4.07–6.01 ppt) for bromoform, 2.11 ppt (1.87–2.34 ppt) for dibromomethane and 1.28 ppt (1.07–2.71 ppt) for methyl iodide. The extreme CH_3I maximum at 15:00 UTC appears again as an outlier. A further decrease of the atmospheric abundances is observed up to 22° N. Mixing ratios thereafter remain nearly constant to the Canary Islands, except for methyl iodide, which shows a maximum of 2 ppt southwest of Gran Canaria. Minor variations occur for all three VSLs at the Canarian coast, while the means of 2.29 ppt CHBr_3 , 1.38 ppt CH_2Br_2 and 1.14 ppt CH_3I are in agreement with open ocean values and remain at this level until 35° N. An increase of the brominated halocarbons is observed as the cruise approaches the Portuguese coast. While dibromomethane only reaches 2.70 ppt, bromoform reaches the highest mixing ratio of 9.9 ppt during the whole DRIVE cruise close to Lisbon (Portugal), leading to a ratio of both compounds of 0.27. Raimund et al. (2011) related the increased abundances of halogenated trace gases in the Iberian upwelling system to strong intertidal coastal

Table 3. Correlation coefficients of bromoform (CHBr_3), dibromomethane (CH_2Br_2) and methyl iodide (CH_3I) mixing ratios with wind speed (w_{spd}), wind direction (w_{dir}), surface air pressure (p), surface air temperature (T_{SAT}), sea surface temperature (T_{SST}), temperature difference ($\Delta T = T_{\text{SAT}} - T_{\text{SST}}$), relative humidity (U), and MABL height. Whole cruise (leg 2 and 3) includes $n = 181$ samples for all parameters except MABL height (30 samples), open ocean (leg 2, except stations 3–6 and leg 3) includes $n = 85$ samples for all parameters except MABL height (15 samples) and coastal stations (stations 3–6) include $n = 96$ samples for all parameters except MABL height (15 samples). Bold coefficients have a p value of less than 5 %.

	CHBr_3			CH_2Br_2			CH_3I		
	Whole cruise	Open ocean	Coastal stations	Whole cruise	Open ocean	Coastal stations	Whole cruise	Open ocean	Coastal stations
w_{spd}	0.23	0.23	-0.17	0.27	0.32	-0.05	0.24	0.37	0.06
w_{dir}	-0.49	-0.31	0.04	-0.52	-0.32	-0.18	-0.28	-0.12	-0.01
p	-0.76	-0.01	-0.53	-0.82	-0.11	-0.71	-0.64	-0.33	-0.52
T_{SAT}	-0.04	-0.68	0.42	0.05	-0.67	0.59	0.24	-0.26	0.48
T_{SST}	-0.45	-0.70	-0.04	-0.39	-0.69	0.13	-0.21	-0.24	0.00
ΔT	0.70	0.17	0.64	0.71	0.18	0.63	0.73	-0.13	0.68
U	0.52	0.47	-0.16	0.50	0.58	-0.32	0.21	0.50	-0.38
MABL	-0.81	-0.32	-0.60	-0.82	-0.40	-0.62	-0.64	-0.58	-0.70

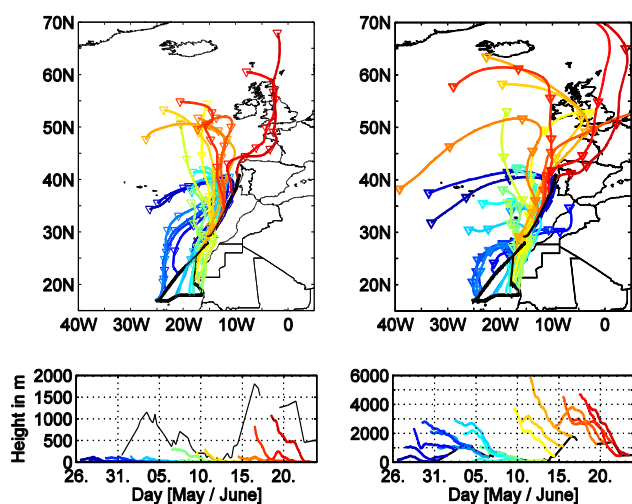


Fig. 10. HYSPLIT 5-day backward trajectories: initiated at the surface (left side) and at the top of the determined marine atmospheric boundary layer (right side) each day at 12:00 UTC. The colours of the trajectories indicate the time when the specific trajectory reached the ships position, e.g. blue at the beginning and red at the end of the cruise. The upper plots show the horizontal and the lower plots the vertical distribution of the trajectories. The black line indicates the height of the MABL. Trajectory and MABL heights are given in [m].

sources and advection of halocarbon-enriched coastal upwelling, but also anthropogenic sources as river outflow are likely (Quack and Wallace, 2003).

3.2.1 Air mass origin

Investigating the air mass history is a good way to reveal potential source regions (Fig. 10). Surface (STs) and boundary layer height trajectories (BLTs) indicate primarily northerly origin of air masses during the cruise. From 31 May to 3 June 2010 the air masses mainly arrive from the Azores.

While the HYSPLIT model projects that the STs do not extend 100 m altitude, the BLTs arise from about 3 km height with little Moroccan influence. A high-pressure system, located between the Azores and the coast of Portugal, deflects the air masses up to 40°N – 50°N , close to the coast of Portugal, and redirects, in combination with the trade winds, the air southwards to the ship. From 6 to 17 June 2010 the light blue, yellow and orange trajectories show a more varying origin, between 30°N and 60°N . Most of the STs descend from heights up to 300 m to the surface 1–2 days before hitting the ship. This air mass descent is typical for a high-pressure system. Reaching the ground, the surface inversions, as described in Sect. 3.1.1, prevent the air masses from ascending. The resulting stable, isolated and very low boundary layer leads to similar origins of offshore STs and BLTs. In the area of the Mauritanian upwelling, from 10 to 15 June 2010, the trajectories also pass the west coast of Mauritania and the western part of West Sahara within the last 24 h; however, the air approaches predominantly from the North Atlantic Ocean between 45°N and 60°N and west of Great Britain. These origins have also been observed in previous measurement campaigns (Quack et al., 2007; Carpenter et al., 2010). In comparison, the BLTs are spatially more widespread over the North Atlantic Ocean, indicating the higher wind speed in the free troposphere. At leg 3 the STs and BLTs have a mid-to polar latitude origin (30°N to 80°N); however, continental influences from northern Europe dominate for the BLTs east of the prime meridian.

3.3 Meteorological constraints on VSLS variability

To distinguish meteorological constraints on the VSLS abundances we correlate meteorological parameters with bromoform, dibromomethane and methyl iodide (Table 3). In the following we highlight the significant correlations. We find a weak but significant correlation between the trace gas abundances and the wind speed for the open ocean and for the whole cruise. In contrast, the wind direction reveals

an overall anti-correlation of -0.5 for the brominated halocarbons and -0.3 for methyl iodide. This means increased VSLS abundances generally coincide with a westerly wind component and reduced abundances coincide with an easterly wind component during the whole cruise. To evaluate land–sea breeze constraints on the trace gas abundances, we take a look to stations 4 and 5. Indeed, both stations show typical land–sea breeze caused diurnal variations in wind speed and direction. The atmospheric abundances reveal significant high correlations of $r = 0.82$ for bromoform, $r = 0.73$ for dibromomethane and 0.82 for methyl iodide with the wind direction at station 4 in contrast to the overall anti-correlation (not shown here). At the 4th station, trace gas abundances increase with an increasing easterly component of the wind, while the abundances decrease with an increasing westerly wind component, related to differences in air mass origin (coastal versus open ocean), as also shown by the trajectories in Fig. 10. At the 5th station, 3-hourly trajectory calculations reveal ground-level air masses with potential coastal and anthropogenic influence along the coast of Western Sahara, with air masses from the open ocean leading to an increase of the dibromomethane abundances ($r = -0.55$) in contrast to the variations of bromoform and methyl iodide, which seem more related to local sources (not shown here). Anti-correlations of -0.6 to -0.8 are also found between the air pressure and the trace gases, caused by predominantly higher pressures at higher latitudes, and over open ocean, with lower VSLS abundances and vice versa for the coastal stations 3–6. At these stations, the anti-correlation is further dominated by the atmospheric tides of the air pressure and amounts to -0.5 for bromoform and methyl iodide and even -0.7 for dibromomethane. Whether or not this relation between the 12-hourly oscillations of sea level pressure and the trace gas variations can be generalized should be investigated in more detail in a future study. The relative humidity correlates with the trace gases in the open ocean with $r = 0.5$ to 0.6 and at the coastal stations with $r = -0.2$ to -0.4 (Table 3). The vertical distribution of the relative humidity has been a good indicator for mixing in and thickness of the MABL (Sect. 3.1.1), which may point to an additional correlation between the surface relative humidity and the VSLS abundances reflected by the high correlation for the whole cruise. However, over the upwelling areas this relationship does not hold. The cold upwelling water creates a positive ΔT and a negative sensible heat flux that suppresses convection and leads to a low relative humidity, which is in contrast to the VSLS abundances. This would explain the reversed correlation above the upwelling. The VSLS abundances are significantly anti-correlated with SAT and SST variations in the open ocean and correlated with SAT in the coastal upwelling. The sensible heat flux, reflected by the temperature difference ΔT ($T_{\text{SAT}} - T_{\text{SST}}$), correlates with r values of at least 0.7 for all trace gases during the whole cruise and at least 0.6 at the coastal stations. The combination of higher air and lower water tempera-

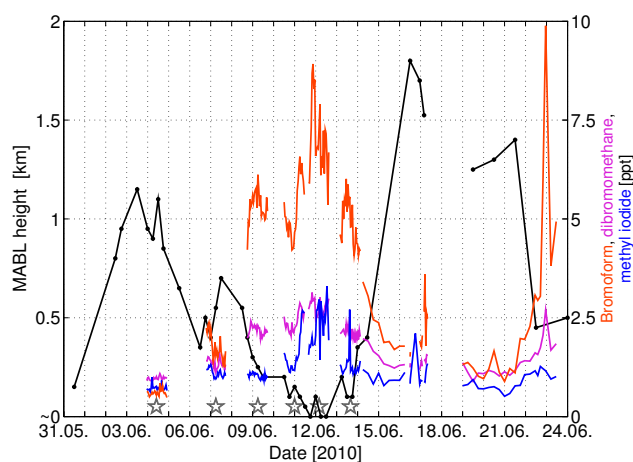


Fig. 11. Comparison of MABL height (left scale, in km) with bromoform, dibromomethane and methyl iodide mixing ratios (right scale, in ppt).

tures coincides with increased trace gas abundances and vice versa, although this is inappropriate for evaporation. This shows that from surface relative humidity one cannot simply infer VSLS abundances or even the MABL height. The temperature difference ΔT further affects the atmospheric stability near the surface. The cold upwelling water at the Mauritanian upwelling converges with warm air from the African coast (Sect. 3.2.1) and creates a negative sensible heat flux between air and water, which cools the near-surface air layer. As a result, surface inversions, or at least a stable stratification of the lower atmosphere, are formed, which suppresses the vertical movement of air. The resulting reduced volume of air that is available for mixing leads to a low MABL height. An anti-correlation of -0.74 between ΔT and the MABL height at the coastal stations confirms this (not shown here). A comparison of bromoform, dibromomethane and methyl iodide with the MABL height during the whole cruise is shown in Fig. 11. Higher VSLS concentrations obviously coincide with a lower MABL height and vice versa. During leg 2 the highest mixing ratios are observed while the MABL height stays between the surface and 500 m in the area of the Mauritanian upwelling (stations 3–6). On the other hand, low mixing ratios measured over the open ocean coincide with a high boundary layer top. The transit towards Vigo (Spain) also shows a decrease of the MABL height and an increase of the three VSLS mixing ratios close to the Iberian coast. In contrast to the other meteorological parameters we derive anti-correlations between the atmospheric trace gas abundances and the MABL height for all regions, reflecting the distinct connection between these variables. The linear correlations of bromoform, dibromomethane and methyl iodide with the MABL height for the whole cruise are represented in Fig. 12a–c. Bromoform, with $r = -0.81$, and dibromomethane, with $r = -0.82$, show the

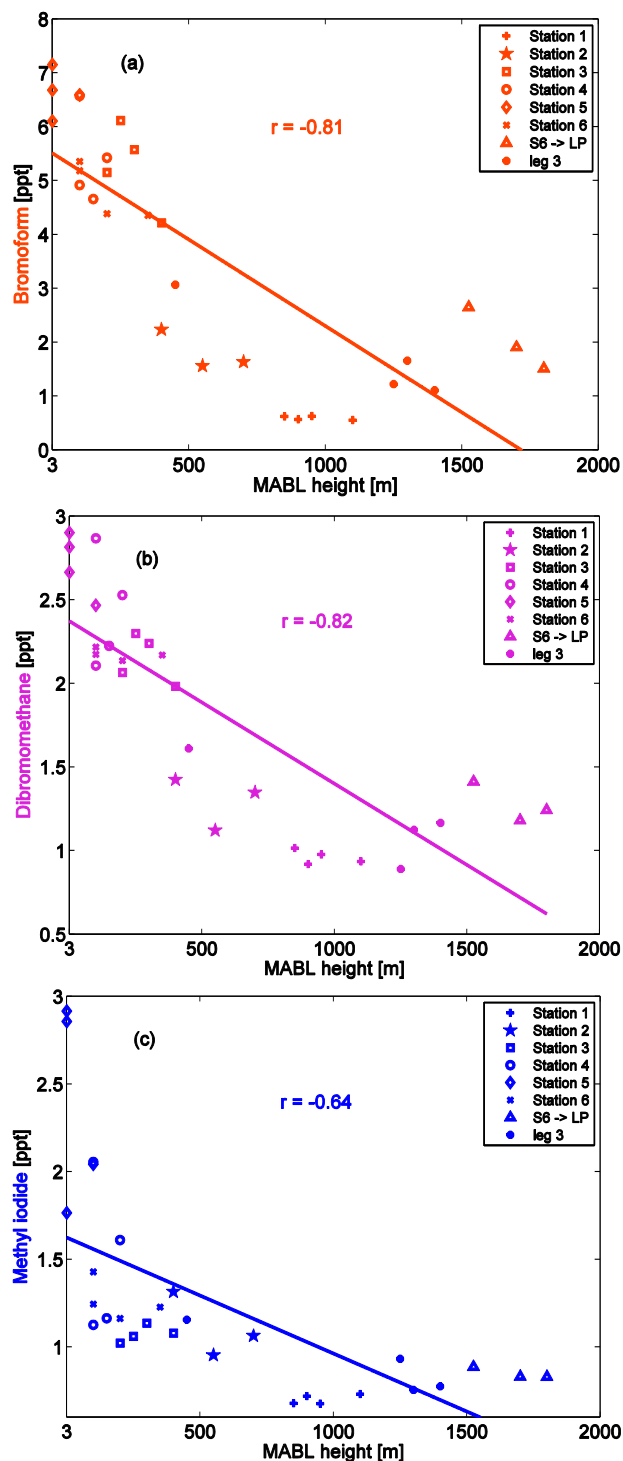


Fig. 12. Correlation between MABL height [m] and (a) bromoform, (b) dibromomethane and (c) methyl iodide abundances [ppt] for the whole cruise. The different markers reflect the different locations: leg 2 including stations 1–6, the transit between station 6 and Las Palmas, and leg 3. The according p values are less than 1 % for all three correlations, with each including 30 samples.

highest anti-correlations. Although the anti-correlation of methyl iodide, $r = -0.64$, is not as high as for the brominated halocarbons, it is significant at the 99 % level.

3.4 Correlations of meteorological parameters and atmospheric abundances with VSLs fluxes

The sea-to-air fluxes, which are calculated depending on wind speed and the concentration gradient Δc between sea water and air (Sect. 2.1), show significant correlations with wind speed and anti-correlations with MABL height (Table 4). The inverse relationship of atmospheric VSLs to MABL height as described in Sect. 3.3 should lead to lower sea-to-air fluxes, F , as lower MABL heights lead to higher atmospheric mixing ratios, decreasing the concentration gradient, Δc (Eq. 2). However, higher sea-to-air fluxes are observed in the lower MABL height areas for dibromomethane and bromoform, with an accordingly positive relationship of F to ΔT (Table 4). This is due to elevated sea water production of brominated VSLs in the cold waters, leading to a large increase in the concentration gradient, which masks the flux suppression by the higher atmospheric mixing ratios (Hepach et al., 2013). Also the elevated atmospheric mixing ratios of methyl iodide have no effect on the fluxes, because methyl iodide is strongly supersaturated in the sea surface water throughout the entire cruise. On the other hand, the observed sea-to-air fluxes reveal correlations with the atmospheric VSLs abundances (Table 5), showing that MABL height and sea-to-air fluxes in combination add to the VSLs variations in the atmosphere. The detailed analysis of the sea-to-air fluxes, their driving factors, such as the sea water concentrations, and their influences on the atmospheric VSLs abundances are discussed in detail in Hepach et al. (2013).

4 Summary

The diurnal and regional variability of atmospheric VSLs has been investigated during the DRIVE ship campaign in May/June 2010 in the eastern tropical and subtropical North Atlantic Ocean. Additionally, we analyse meteorological influences on the observed VSLs mixing ratios using simultaneous high-resolution data. VSLs measurements were conducted hourly at six 24 h stations and during passage from the coast of Mauritania to Vigo (Spain), resulting in a total of 187 atmospheric VSLs measurements during DRIVE. We concentrated our investigation on three trace gases: bromoform, dibromomethane and methyl iodide. Higher mean VSLs mixing ratios were found over the Mauritanian upwelling region (5.60 ppt, 2.37 ppt and 1.50 ppt for bromoform, dibromomethane and methyl iodide, respectively) than over the open ocean (1.74 ppt, 1.28 ppt and 0.93 ppt for bromoform, dibromomethane and methyl iodide, respectively). The upwelling region also shows diurnal variations of the VSLs with highest fluctuations between maximum and minimum

Table 4. Correlation coefficients of bromoform (CHBr_3), dibromomethane (CH_2Br_2) and methyl iodide (CH_3I) fluxes with wind speed (w_{spd}), wind direction (w_{dir}), surface air pressure (p), surface air temperature (T_{SAT}), sea surface temperature (T_{SST}), temperature difference ($\Delta T = T_{\text{SAT}} - T_{\text{SST}}$), relative humidity (U), and MABL height. Whole cruise (leg 2 and 3) includes $n = 109$ samples for all parameters except MABL height (21 samples), open ocean (leg 2 except stations 3–6 and leg 3) includes $n = 37$ samples for all parameters except MABL height (8 samples) and coastal stations (stations 3–6) include $n = 70$ samples for all parameters except MABL height (13 samples). Bold coefficients have a p value of less than 5 %.

	CHBr_3 flux			CH_2Br_2 flux			CH_3I flux		
	Whole cruise	Open ocean	Coastal stations	Whole cruise	Open ocean	Coastal stations	Whole cruise	Open ocean	Coastal stations
w_{spd}	0.37	0.19	0.48	0.54	0.84	0.71	0.54	0.52	0.61
w_{dir}	-0.37	0	0.06	-0.51	0.09	-0.13	0.07	-0.04	0.07
p	-0.67	-0.10	-0.57	-0.81	-0.71	-0.73	-0.08	-0.30	-0.14
T_{SAT}	-0.08	-0.13	0.15	-0.06	-0.75	0.27	-0.20	-0.4	-0.21
T_{SST}	-0.54	-0.29	-0.31	-0.51	-0.84	-0.17	-0.24	-0.55	-0.36
ΔT	0.76	0.35	0.67	0.75	-0.15	0.63	0.12	0.18	0.22
U	-0.04	-0.14	-0.43	-0.02	0.65	-0.61	-0.08	0.21	-0.27
MABL	-0.58	0.26	-0.58	-0.68	-0.93	-0.68	-0.27	-0.12	-0.59

Table 5. Correlation coefficients of bromoform (CHBr_3), dibromomethane (CH_2Br_2) and methyl iodide (CH_3I) fluxes with according mixing ratios. Whole cruise (leg 2 and 3) includes $n = 109$ samples, open ocean (leg 2 except stations 3–6 and leg 3) includes $n = 37$ samples and coastal stations (stations 3–6) include $n = 70$ samples. Bold coefficients have a p value of less than 5 %.

	CHBr_3 flux			CH_2Br_2 flux			CH_3I flux		
	Whole cruise	Open ocean	Coastal stations	Whole cruise	Open ocean	Coastal stations	Whole cruise	Open ocean	Coastal stations
CHBr_3 mixing ratio	0.58	-0.20	0.33	0.68	0.60	0.39	-0.08	0.22	-0.16
CH_2Br_2 mixing ratio	0.61	-0.05	0.40	0.71	0.56	0.49	-0.04	0.33	-0.08
CH_3I mixing ratio	0.62	-0.09	0.50	0.66	0.62	0.51	0.09	0.21	0.12

of 3.57 ppt for bromoform, 0.83 ppt for dibromomethane and 1.85 ppt for methyl iodide. A strong coastal gradient of the VSLs is also observed towards Lisbon (Portugal), where we detect the highest bromoform mixing ratio of the whole cruise of 9.8 ppt.

The air mass origin is investigated by 5-day backward trajectories starting at the surface and at the top of the determined marine atmospheric boundary layer. We identify a predominantly North Atlantic origin of the air due to the prevailing NW winds during the whole cruise, with minor coastal influence at the Mauritanian upwelling area.

To distinguish atmospheric constraints on the VSLs we compare several meteorological parameters with the trace gas abundances. Although we do not find an overall relationship with the wind, we detect a significant correlation between VSLs abundance and easterly wind direction changes ($r > 0.7$) at the 4th station, northwest of Nouakchott (Mauritania), which is linked to land–sea breeze influence. We find a strong anti-correlation between air–sea surface temperature difference and MABL height, derived from radiosoundings. The MABL heights are dependent on the location, as we determine heights from surface level to only 400 m in the upwelling region and between 400 and 1700 m over the open ocean. In the Mauritanian upwelling a stable boundary layer leads to stable atmospheric conditions near the surface, due to warm air flowing over cold upwelling water, suppressing the mixing of air. In the open ocean part of the cruise, the top of the MABL is limited by trade in-

versions. Overall a significant anti-correlation between the VSLs mixing ratios and the marine atmospheric boundary layer height is found. With correlation coefficients of $r = -0.81$ for bromoform, $r = -0.82$ for dibromomethane and $r = -0.64$ for methyl iodide, the MABL height appears to have a significant influence on the trace gas mixing ratios. This relationship may help explain observed events in the tropical eastern Atlantic with increased atmospheric VSLs mixing ratios in the Mauritanian upwelling. Whether this influence can also be found in different seasons or other oceanic regions should be addressed in future studies. Of particular interest would be to investigate other oceanic upwelling regions, which are expected to also have high VSLs sources as the Mauritanian upwelling/Cape Verde Islands region does.

Acknowledgements. We thank the authorities of Cape Verde, Mauritania, Portugal and Spain for the permissions to work in their territorial waters. We acknowledge the NOAA Air Resources Laboratory (ARL) for the provision of NCEP reanalysis data and the HYSPLIT transport and dispersion model used in this publication. We thank S. Tegtmeier for helpful comments and M. Toohey for proofreading. We acknowledge the support of the captain and crew of R/V *Poseidon* as well as Hermann Bange, chief scientist of P399 legs 2 and 3. We also thank the 3 anonymous reviewers and the editor Bill Sturges for the helpful comments. Financial support for this study was provided by the BMBF grant SOPRAN II FKZ 03F0611A. This work also contributes to European Union's

Seventh Framework Programme FP7/2007–2013 under grant agreement no. 226224 – SHIVA.

The service charges for this open access publication have been covered by a Research Centre of the Helmholtz Association.

Edited by: W. T. Sturges

References

- Atlas, E., Pollock, W., Greenberg, J., Heidt, L., and Thompson, A.: Alkyl nitrates, nonmethane hydrocarbons, and halocarbon gases over the equatorial Pacific Ocean during SAGA-3, *J. Geophys. Res.-Atmos.*, 98, 16933–16947, doi:10.1029/93JD01005, 1993.
- Bange, H., Atlas, E., Bahlmann, E., Baker, A., Bracher, A., Cianca, A., Dengler, M., Fuhlbrügge, S., Großmann, K., Hepach, H., Lavrič, J., Löscher, C., Krüger, K., Orlikowska, A., Peeken, I., Quack, B., Schafstall, J., Steinhoff, T., Williams, J., and Witke, F.: FS Poseidon cruise report P399 legs 2 and 3, 74, IFM-GEOMAR, Kiel, Germany, 2011.
- Butler, J., King, D., Lobert, J., Montzka, S., Yvon-Lewis, S., Hall, B., Warwick, N., Mondeel, D., Aydin, M., and Elkins, J.: Oceanic distributions and emissions of short-lived halocarbons, *Global Biogeochem. Cy.*, 21, doi:10.1029/2006GB002732, 2007.
- Carpenter, L. and Liss, P.: On temperate sources of bromoform and other reactive organic bromine gases, *J. Geophys. Res.-Atmos.*, 105, 20539–20547, doi:10.1029/2000JD900242, 2000.
- Carpenter, L., Liss, P., and Penkett, S.: Marine organohalogens in the atmosphere over the Atlantic and Southern Oceans, *J. Geophys. Res.-Atmos.*, 108, 4256, doi:10.1029/2002JD002769, 2003.
- Carpenter, L., Wevill, D., Hopkins, J., Dunk, R., Jones, C., Hornsby, K., and McQuaid, J.: Bromoform in tropical Atlantic air from 25 degrees N to 25 degrees S, *Geophys. Res. Lett.*, 34, L11810, doi:10.1029/2007GL029893, 2007.
- Carpenter, L., Fleming, Z., Read, K., Lee, J., Moller, S., Hopkins, J., Purvis, R., Lewis, A., Muller, K., Heinold, B., Herrmann, H., Fomba, K., van Pinxteren, D., Muller, C., Tegen, I., Wiedensohler, A., Muller, T., Niedermeier, N., Achterberg, E., Patey, M., Kozlova, E., Heimann, M., Heard, D., Plane, J., Mahajan, A., Oetjen, H., Ingham, T., Stone, D., Whalley, L., Evans, M., Pilling, M., Leigh, R., Monks, P., Karunaharan, A., Vaughan, S., Arnold, S., Tschirner, J., Pöhler, D., Friess, U., Holla, R., Mendes, L., Lopez, H., Faria, B., Manning, A., and Wallace, D.: Seasonal characteristics of tropical marine boundary layer air measured at the Cape Verde Atmospheric Observatory, *J. Atmos. Chem.*, 67, 87–140, doi:10.1007/s10874-011-9206-1, 2010.
- Dessens, O., Zeng, G., Warwick, N., and Pyle, J.: Short-lived bromine compounds in the lower stratosphere; impact of climate change on ozone, *Atmospheric Science Letters*, 10, 201–206, doi:10.1002/asl.236, 2009.
- Garratt, J.: The internal boundary-layer – a review, *Bound.-Lay. Meteorol.*, 50, 171–203, doi:10.1007/BF00120524, 1990.
- Gschwend, P., Macfarlane, J., and Newman, K.: Volatile halogenated organic-compounds released to seawater from temperate marine macroalgae, *Science*, 227, 1033–1035, doi:10.1126/science.227.4690.1033, 1985.
- Hepach, H., Quack B., Ziska F., Fuhlbrügge, S., Atlas, E. L., Peeken, I., Krüger, K., and Wallace, D. W. R.: Drivers of diel and regional variations of halocarbon emissions from the tropical North East Atlantic, in preparation, 2013.
- Highwood, E. and Hoskins, B.: The tropical tropopause, *Q. J. Roy. Meteorol. Soc.*, 124, 1579–1604, doi:10.1256/smsqj.54910, 1998.
- Hossaini, R., Chipperfield, M., Dhomse, S., Ordonez, C., Saiz-Lopez, A., Abraham, N., Archibald, A., Braesicke, P., Telford, P., Warwick, N., Yang, X., and Pyle, J.: Modelling future changes to the stratospheric source gas injection of biogenic bromocarbons, *Geophys. Res. Lett.*, 39, L20813, doi:10.1029/2012GL053401, 2012.
- Kalnay, E., Kanamitsu, M., Kistler, R., Collins, W., Deaven, D., Gandin, L., Iredell, M., Saha, S., White, G., Woollen, J., Zhu, Y., Chelliah, M., Ebisuzaki, W., Higgins, W., Janowiak, J., Mo, K., Ropelewski, C., Wang, J., Leetmaa, A., Reynolds, R., Jenne, R., and Joseph, D.: The NCEP/NCAR 40-year reanalysis project, *B. Am. Meteorol. Soc.*, 77, 437–471, doi:10.1175/1520-0477(1996)077<0437:TNYRP>2.0.CO;2, 1996.
- Kistler, R., Kalnay, E., Collins, W., Saha, S., White, G., Woollen, J., Chelliah, M., Ebisuzaki, W., Kanamitsu, M., Kousky, V., van den Dool, H., Jenne, R., and Fiorino, M.: The NCEP-NCAR 50-year reanalysis: Monthly means CD-ROM and documentation, *B. Am. Meteorol. Soc.*, 82, 247–267, doi:10.1175/1520-0477(2001)082<0247:TNNYRM>2.3.CO;2, 2001.
- Kloster, S., Six, K., Feichter, J., Maier-Reimer, E., Roeckner, E., Wetzell, P., Stier, P., and Esch, M.: Response of dimethylsulfide (DMS) in the ocean and atmosphere to global warming, *J. Geophys. Res.-Biogeosci.*, 112, G03005, doi:10.1029/2006JG000224, 2007.
- Ko, M. K. W., Poulet, G., and Blake, D. R.: Very short-lived halogen and sulfur substances, Scientific assessment of ozone depletion: 2002, Global Ozone Research and Monitoring Project. Report No. 47, Chapter 2, World Meteorological Organization, Geneva, 2003.
- Krüger, K. and Quack, B.: Introduction to special issue: the Trans-Brom Sonne expedition in the tropical West Pacific, *Atmos. Chem. Phys. Discuss.*, 12, 1401–1418, doi:10.5194/acpd-12-1401-2012, 2012.
- Manley, S. and Dastoor, M.: Methyl-iodide (CH₃I) production by kelp and associated microbes, *Marine Biol.*, 98, 477–482, doi:10.1007/BF00391538, 1988.
- Montzka, S. A. and Reimann, S.: Ozone-depleting substances and related chemicals, Scientific Assessment of Ozone Depletion: 2010, Global Ozone Research and Monitoring Project – Report No. 52, Geneva, Switzerland, 2011.
- Moore, R. and Tokarczyk, R.: Volatile biogenic halocarbons in the northwest Atlantic, *Global Biogeochem. Cy.*, 7, 195–210, doi:10.1029/92GB02653, 1993.
- Neiburger, M., Johnson, D., and Chien, C.: Studies of the structure of the atmosphere over the Eastern Pacific Ocean in summer: I. The inversion over the Eastern North Pacific Ocean, 1, Univ. of Calif., Publications in Meteorology, 94 pp., 1961.
- Nightingale, P., Malin, G., Law, C., Watson, A., Liss, P., Liddicoat, M., Boutin, J., and Upstill-Goddard, R.: In situ evaluation of air-sea gas exchange parameterizations using novel conservative and volatile tracers, *Global Biogeochem. Cy.*, 14, 373–387, doi:10.1029/1999GB900091, 2000.

- O'Brien, L., Harris, N., Robinson, A., Gostlow, B., Warwick, N., Yang, X., and Pyle, J.: Bromocarbons in the tropical marine boundary layer at the Cape Verde Observatory – measurements and modelling, *Atmos. Chem. Phys.*, 9, 9083–9099, doi:10.5194/acp-9-9083-2009, 2009.
- Pyle, J., Warwick, N., Yang, X., Young, P., and Zeng, G.: Climate/chemistry feedbacks and biogenic emissions, *Phil. Trans. Roy. Soc. a-Mathematical Phys. Eng. Sci.*, 365, 1727–1740, doi:10.1098/rsta.2007.2041, 2007.
- Quack, B. and Wallace, D.: Air-sea flux of bromoform: Controls, rates, and implications, *Global Biogeochem. Cy.*, 17, 1023, doi:10.1029/2002GB001890, 2003.
- Quack, B., Atlas, E., Petrick, G., Stroud, V., Schauffler, S., and Wallace, D.: Oceanic bromoform sources for the tropical atmosphere, *Geophys. Res. Lett.*, 31, L23S05, doi:10.1029/2004GL020597, 2004.
- Quack, B., Atlas, E., Petrick, G., and Wallace, D.: Bromoform and dibromomethane above the Mauritanian upwelling: Atmospheric distributions and oceanic emissions, *J. Geophys. Res.-Atmos.*, 112, D09312, doi:10.1029/2006JD007614, 2007.
- Raimund, S., Quack, B., Bozec, Y., Vernet, M., Rossi, V., Garçon, V., Morel, Y., and Morin, P.: Sources of short-lived bromocarbons in the Iberian upwelling system, *Biogeosciences*, 8, 1551–1564, doi:10.5194/bg-8-1551-2011, 2011.
- Read, K., Mahajan, A., Carpenter, L., Evans, M., Faria, B., Heard, D., Hopkins, J., Lee, J., Moller, S., Lewis, A., Mendes, L., McQuaid, J., Oetjen, H., Saiz-Lopez, A., Pilling, M., and Plane, J.: Extensive halogen-mediated ozone destruction over the tropical Atlantic Ocean, *Nature*, 453, 1232–1235, doi:10.1038/nature07035, 2008.
- Relvas, P., and Barton, E.: Mesoscale patterns in the Cape Sao Vicente (Iberian Peninsula) upwelling region, *J. Geophys. Res.-Ocean.*, 107, 3164, doi:10.1029/2000JC000456, 2002.
- Schmittner, A., Oeschles, A., Matthews, H., and Galbraith, E.: Future changes in climate, ocean circulation, ecosystems, and biogeochemical cycling simulated for a business-as-usual CO₂ emission scenario until year 4000 AD, *Global Biogeochem. Cy.*, 22, GB1013, doi:10.1029/2007GB002953, 2008.
- Seibert, P., Beyrich, F., Gryning, S., Joffre, S., Rasmussen, A., and Tercier, P.: Review and intercomparison of operational methods for the determination of the mixing height, *Atmos. Environ.*, 34, 1001–1027, doi:10.1016/S1352-2310(99)00349-0, 2000.
- Skylingstad, E., Samelson, R., Mahrt, L., and Barbour, P.: A numerical Modeling study of warm offshore flow over cool water, *Mont. Weather Rev.*, 133, 345–361, doi:10.1175/MWR-2845.1, 2005.
- Solomon, S., Garcia, R., and Ravishankara, A.: On the role of iodine in ozone depletion, *J. Geophys. Res.-Atmos.*, 99, 20491–20499, doi:10.1029/94JD02028, 1994.
- Sorensen, J.: Sensitivity of the DERMA long-range gaussian dispersion model to meteorological input and diffusion parameters, *Atmos. Environ.*, 32, 4195–4206, doi:10.1016/S1352-2310(98)00178-2, 1998.
- Stull, R.: An Introduction to Boundary Layer Meteorology, Kluwer Academic Publishers, Dordrecht, the Netherlands, 1988.
- Sturges, W., Cota, G., and Buckley, P.: Bromoform emission from arctic ice algae, *Nature*, 358, 660–662, doi:10.1038/358660a0, 1992.
- Tegtmeier, S., Krüger, K., Quack, B., Atlas, E. L., Pisso, I., Stohl, A., and Yang, X.: Emission and transport of bromocarbons: from the West Pacific ocean into the stratosphere, *Atmos. Chem. Phys.*, 12, 10633–10648, doi:10.5194/acp-12-10633-2012, 2012.
- Tegtmeier, S., Krüger, K., Quack, B., Atlas, E., Blake, D. R., Boenisch, H., Engel, A., Hepach, H., Hossaini, R., Navarro, M. A., Raimund, S., Sala, S., Shi, Q., and Ziska, F.: The contribution of oceanic methyl iodide to stratospheric iodine, *Atmos. Chem. Phys. Discuss.*, 13, 11427–11471, doi:10.5194/acpd-13-11427-2013, 2013.
- Troen, I., and Mahrt, L.: A simple-model of the atmospheric boundary-layer: Sensitivity to surface evaporation, *Bound.-Lay. Meteorol.*, 37, 129–148, doi:10.1007/BF00122760, 1986.
- Vickers, D., Mahrt, L., Sun, J., and Crawford, T.: Structure of offshore flow, *Mon. Weather Rev.*, 129, 1251–1258, doi:10.1175/1520-0493(2001)129<1251:SOOF>2.0.CO;2, 2001.
- Vogelezang, D., and Holtslag, A.: Evaluation and model impacts of alternative boundary-layer height formulations, *Bound.-Lay. Meteorol.*, 81, 245–269, doi:10.1007/BF02430331, 1996.
- Warwick, N., Pyle, J., Carver, G., Yang, X., Savage, N., O'Connor, F., and Cox, R.: Global modeling of biogenic bromocarbons, *J. Geophys. Res.-Atmos.*, 111, D244305, doi:10.1029/2006JD007264, 2006.
- WMO: Definition of the thermal tropopause, *WMO Bulletin*, 136–137, 1957.
- WMO: Scientific Assessment of Ozone Depletion: 2006, Geneva, Switzerland, 572, 2007.
- WMO: Scientific Assessment of Ozone Depletion: 2010, World Meteorological Organization, Geneva, 2011.
- Yokouchi, Y., Hasebe, F., Fujiwara, M., Takashima, H., Shiotani, M., Nishi, N., Kanaya, Y., Hashimoto, S., Fraser, P., Toom-Sauntry, D., Mukai, H., and Nojiri, Y.: Correlations and emission ratios among bromoform, dibromochloromethane, and dibromomethane in the atmosphere, *J. Geophys. Res.-Atmos.*, 110, D23309, doi:10.1029/2005JD006303, 2005.
- Ziska, F., Quack, B., Abrahamsson, K., Archer, S. D., Atlas, E., Bell, T., Butler, J. H., Carpenter, L. J., Jones, C. E., Harris, N. R. P., Hepach, H., Heumann, K. G., Hughes, C., Kuss, J., Krüger, K., Liss, P., Moore, R. M., Orlikowska, A., Raimund, S., Reeves, C. E., Reifenhäuser, W., Robinson, A. D., Schall, C., Tanhua, T., Tegtmeier, S., Turner, S., Wang, L., Wallace, D., Williams, J., Yamamoto, H., Yvon-Lewis, S., and Yokouchi, Y.: Global sea-to-air flux climatology for bromoform, dibromomethane and methyl iodide, *Atmos. Chem. Phys. Discuss.*, 13, 5601–5648, doi:10.5194/acpd-13-5601-2013, 2013.

X. Danksagung

Meiner Betreuerin Dr. Birgit Quack gilt mein größter Dank. Sie gab mir die Gelegenheit dieses spannende und zugleich herausfordernde Thema zu bearbeiten, sowie an Konferenzen und Forschungsreisen teilzunehmen, die meinen wissenschaftlichen und weltlichen Geist füllten. Ich bekam die Möglichkeit viele interessante Menschen unterschiedlicher Nationalitäten kennenzulernen und mit ihnen zu arbeiten. Danke dir auch für den sprachlichen Feinschliff meiner Texte, den vielen Ideen, der Hilfe meine komplexen Gedankengänge zu ordnen, der „Fairness-Brille“ und den Anstoß über den Tellerrand zu gucken. Zugleich möchte ich Prof. Dr. Arne Körtzinger danken, dass er die große Verantwortung übernommen hat mein Doktorvater zu sein und zusammen mit Prof. Dr. Christa Marandino wertvolle Ideen und Ratschläge zur Erstellung dieser Thesis und der Manuskripte gegeben hat. Und danke auch, dass ihr euch die Zeit nehmt diese Thesis zu lesen und zu bewerten.

Meine Arbeitsgruppe fluktuierte stark in den nun 4.5 Jahren in denen ich promoviere. Zum festen Kern gehört Helmke, der ich für wissenschaftliche Diskussionen und Ideenbeiträge aber auch für lustige Abende beispielsweise im Kino zur Sneak danke. Natürlich gehören auch die Meteorologen Susi, Steffen und Kicki zur Arbeitsgruppe, die aus einem anderen Blickwinkel Ratschläge und Verbesserungsvorschläge gaben. Susi, danke dir nochmal speziell für deinen Input und Zeit, die du in diese Thesis und die Manuskripte gesteckt hast.

Danke auch an die HPA für schöne MATLAB-Diskussionen, Freizeitgestaltungen wie Picknicken, Nudeln selber machen, Rodeln oder Plätzchen backen. Ich habe die Zeit sehr genossen und danke euch für eure Hilfe in allen Lebenslagen. Danke der CH-Abteilung für nette Kaffeerunden, Container packen, Diskussionen, Abteilungstreffen, Betriebsausflüge,..., es war schön mit euch zu arbeiten.

Mein Umzug nach Barmstedt hatte leider zur Folge, dass ich meinen Schreibtischplatz in der HPA verloren habe. Ich wurde aber liebevoll bei den Herren Björn und Tobi aufgenommen. Mittlerweile habe ich diesen Platz auch nicht mehr, aber alles Schöne hat mal ein Ende.

Ich bin ebenfalls dankbar für jede private Veränderung der letzten 4.5 Jahre, die auch meine Arbeit beeinflusst haben, beginnend mit dem Kennenlernen und Heiraten meines Mannes, der Geburt unserer Tochter Elizabeth Hedwig, ihr wachsen und gedeihen, der Bau unseres gemeinsamen Heimes und auch der Umzug aus Kiel.

Meine Freunde haben sich trotz Wegzugs in ein Dorf im Grünen nicht abschrecken lassen, uns regelmäßig zu besuchen. Ich weiß, ich habe euch vernachlässigt und ich hoffe, dass sich das in Zukunft ändern wird. Danke auch meinen neuen Nachbarn für die Unterstützung, die Kleine zu Sitten

oder einfach nur ein offenes Ohr zu haben und dabei einen Cappuccino zu trinken oder den Kleinen beim Spielen zu beobachten. Danke dir Wiebke fürs Lesen und Korrigieren der Thesis.

Ich danke meiner Familie für motivierende Worte und Interesse an meiner Arbeit. Meinem Mann sei an dieser Stelle besonders gedankt. Ich kann es nicht besser in Worte fassen: „Bis zum Mond und wieder zurück“.

Und nun freue ich mich auf unseren Nachwuchs und einen neuen Lebensabschnitt.

XI. Curriculum Vitae

Personal

Name: Franziska Ziska (née Wittke)
Current address: Eichhörnchenweg 34, 25355 Barmstedt
Birth date: January 4th 1985 (Rostock)
Nationality: German
Family status: married
Children: two daughters (born on November 28th 2012 and on January 1st 2015)

Education

02/2010 – 11/2014 PhD thesis at the Christian Albrecht University zu Kiel, Germany under the supervision of Dr. Birgit Quack and Prof. Arne Körtzinger
01/2009 – 09/2009 Diploma thesis: “Air-sea interaction and trace gas emissions in coastal upwelling regions”, certificate: Diploma
10/2004 – 01/2009 Study of Maritime Meteorology at Christian Albrecht University, Kiel, Germany; minor subjects: Oceanography, Chemistry
08/1995 – 04/2004 Ernst-Moritz-Arndt Secondary School, certificate: Abitur

Professional Education

05/2008 – 01/2010 Student Assistant, Marine Biogeochemistry Res. Div., of IFM-GEOMAR, Kiel; Measurements of trace gases (nitrous oxide, methane and dimethylsulfide) with a gas chromatograph (FPD (purge and trap) and ECD (headspace)); writing an input program in MATLAB for the MEMENTO database
01/2007 – 10/2007 Employment at WetterWelt GmbH, Kiel: Weather forecast and analyses for sailors

Conference

05/2014 CCMI (chemistry-climate model initiative) Workshop Lancaster (United Kingdom)
04/2014 EGU (European Geosciences Union) General Assembly in Vienna (Austria)
03/2014 6th SOPRAN Annual Meeting in Bremen (Germany)
05/2012 SOLAS Open Science Conference in Seattle (United States)

03/2012	4 th SOPRAN Annual Meeting in Kiel (Germany)
09/2011	Sino-German Summerschool in Quindao (China)
07/2011	Annual SHIVA Meeting in Leeds (England)
01/2011	SHIVA Steering committee Workshop in Kiel (Germany)
11/2010	Transbrom Sonne Workshop in Kiel (Germany)
03/2010	3 rd SOPRAN Annual Meeting in Hamburg (Germany)
05/2005 - 2010	Attendances at the annual Students Meteorology Conference (StuMeTa) in Bonn, Hannover, Leipzig, Kiel, Karlsruhe (Germany)
02/2006 and 03/2007	Extreme Weather Conferences in Hamburg (Germany)
09/2007	German-Austrian-Swiss Meteorology Conference (DACH) in Hamburg (Germany)

Participation in Ship/Field Campaigns

11/2011	R/V Sonne Cruise, SHIVA, investigation of the impact from different halogens on stratospheric ozone in the South China Sea; Sampling air measurements of over 50 trace gases including a range of halocarbons (CH ₃ I, CHBr ₃ etc.), Sampling and measurements of N ₂ O and CH ₄
06/2010	R/V Poseidon cruise P399 leg 2&3, DRIVE, investigation of diurnal and regional variability of halogen emissions in the upwelling area off Mauretania: Sampling air measurements of over 50 trace gases including a range of halocarbons (CH ₃ I, CHBr ₃ etc.), alkanes, and DMS; radio sounding
04/2010	Field campaign in Chile, embedded in the SFB 574 (Collaborative Research Center (SFB) 574, Volatiles and Fluids in Subduction Zones), installation and repairing seismic instruments around the volcanos Iaiima and Villarica
10/2009	R/V Sonne Cruise, TransBrom, investigation of trace gas emissions in the tropical western Pacific through different biogeochemical regimes and their stratospheric contribution: Sampling and measurements of DMS, DMSP, DMSO, N ₂ O, and CH ₄
06/2008	R/V Heincke cruise 290, 2 nd SOPRAN Mesocosm Study, Baltic Sea Ocean acidification experiments with floating mesocosms in the Baltic Sea, Sampling and measurements of DMS
06/2008, 02/2009	R/V Littorina, monthly sampling trips to the IFM GEOMAR time series station Bokins Eck (Eckernförde Bay): Collecting samples for N ₂ O, CH ₄ , DMS, O ₂ , nutrients

Publications

Ziska F., Quack B., Abrahamsson K., Archer, S. D., Atlas, E., Bell, T., Butler, J. H., Carpenter, L. J., Jones, C. E., Harris, N. R. P., Hepach, H., Heumann, K. G., Hughes, C., Kuss, J., Krüger, K., Liss, P., Moore, R. M., Orlikowska, A., Raimund, S., Reeves, C. E., Reifenhäuser, W., Robinson, A. D., Schall, C., Tanhua, T., Tegtmeier, S., Turner, S., Wang, L., Wallace, D., Williams, J., Yamamoto, H., Yvon-Lewis, S. and Yokouchi, Y.: Global sea-to-air flux climatology of bromoform, dibromomethane and methyl iodide, *Atmos. Chem. Phys.*, 13, 8915-8934, 10.5194/acp-13-8915-2013, 2013.

Ziska F., Quack B., Tegtmeier S. and Krüger K., Future emissions of halocarbons based on CMIP 5 model output fields, *in prep.*

Tegtmeier, S., Ziska F., Pisso, I., Quack B., Velders, G., Krüger, K.: Oceanic bromine emissions weighted by their ozone depletion potential, *Atmos. Chem. Phys.*, 2014, *in prep.*

Hepach, H., Quack, B., Ziska, F., Fuhlbrügge, S., Atlas, E., Krüger, K., Peeken, I., and Wallace, D. W. R.: Drivers of diel and regional variations of halocarbon emissions from the tropical North East Atlantic, *Atmos. Chem. Phys.*, 14, 1255-1275, 10.5194/acp-14-1255-2014, 2014.

Hossaini, R., Mantle H., Chipperfield, M. P., Montzka, S. A., Hamer, P., Ziska, F., Quack, B., Krüger, K., Tegtmeier, S., Atlas, E., Sala, S., Engel, A., Bönisch, H., Keber, T., Oram, D., Millis, G., Ordóñez, C., Saiz-Lopez, A., Warwick, N., Liang, Q., Feng, W., Moore, E., Miller, B. R., Marécal, V., Richards, N. A. D., Dorf, M., and Pfeilsticker, K.: Evaluating global emission inventories of biogenic bromocarbons, *Atmos. Chem. Phys.*, 13, 11819-11838, 10.5194/acp-13-11819-2013, 2013.

Tegtmeier S., Krüger, K., Quack, B., Atlas, E., Blake, D. R., Bönisch, H., Engel, A., Hepach, H., Hossaini, R., Navarro M. A., Raimund, S., Sala, S., Shi, Q., and Ziska, F.: The contribution of oceanic methyl iodide to stratospheric iodine, *Atmos. Chem. Phys.*, 13, 11869-11886, 10.5194/acp-13-11869-2013, 2013.

Fuhlbrügge, S., Krüger, K., Quack, B., Atlas, E., Hepach, H., and Ziska, F.: Impact of the marine atmospheric boundary layer conditions on VSLs abundances in the eastern tropical and subtropical North Atlantic Ocean, *Atmos. Chem. Phys.*, 13, 6345-6357, 10.5194/acp-13-6345-2013, 2013.

F. Wittke, A. Kock, H. W. Bange, Nitrous oxide emissions from the upwelling area off Mauretania, GEOPHYSICAL RESEARCH LETTERS, VOL. 37, L12601, doi:1029/2010GL042442, 2010

“Air Sea Interaction and Tracer Gas Emissions on Coastal Upwelling Regions”, Diploma thesis, IFM-GEOMAR, 2009

XII. Eidesstattliche Erklärung

Hiermit erkläre ich, dass ich die von mir vorgelegte Dissertation – abgesehen von der Beratung durch meinen Betreuer – selbstständig und ohne Zuhilfenahme unerlaubte Hilfsmittel angefertigt habe. Alle benutzten Quellen und Hilfsmittel habe ich vollständig angegeben und die Zusammenarbeit mit anderen Wissenschaftlern habe ich kenntlich gemacht. Zudem versichere ich, dass diese Arbeit unter Einhaltung der Regeln guter wissenschaftlicher Praxis der Deutschen Forschungsgesellschaft verfasst wurde, und dass sie nach Form und Inhalt meine eigene Arbeit ist. Weder diese noch eine ähnliche Arbeit wurden an einer anderen Abteilung oder Hochschule im Rahmen eines Prüfungsverfahrens vorgelegt, veröffentlicht oder zur Veröffentlichung vorgelegt. Dies ist mein erstes und einziges Promotionsverfahren.

Kiel, den 14. Oktober 2014

(Franziska Ziska)

